In this Issue

Highlights from this issue of *A&R* | **By Lara C. Pullen, PhD**

Changes in Systemic Sclerosis–Related Interstitial Lung Disease

In this issue, Kim et al (p. 316) report that patients undergoing immunosuppressive treatment for systemic sclerosis–related interstitial lung disease (SSc-ILD) were able to successfully transition from both ground-glass and lung fibrosis ILD patterns to a normal lung pattern. This was true for patients who received cyclophosphamide (CYC) for 1 year, followed by placebo for an additional year, and for those who received treatment with mycophenolate mofetil (MMF) for 2 years.

The investigators performed baseline and follow-up high-resolution computed tomography scans in 47 patients in the CYC group and 50 patients in the MMF group. They identified a mean net improvement from lung fibrosis to a normal lung pattern of 21% in the CYC group and 19% in the MMF group. Mean improvement from a ground-glass pattern to a normal lung pattern was 30% and 28% in these groups, respectively. Researchers observed mean improvement
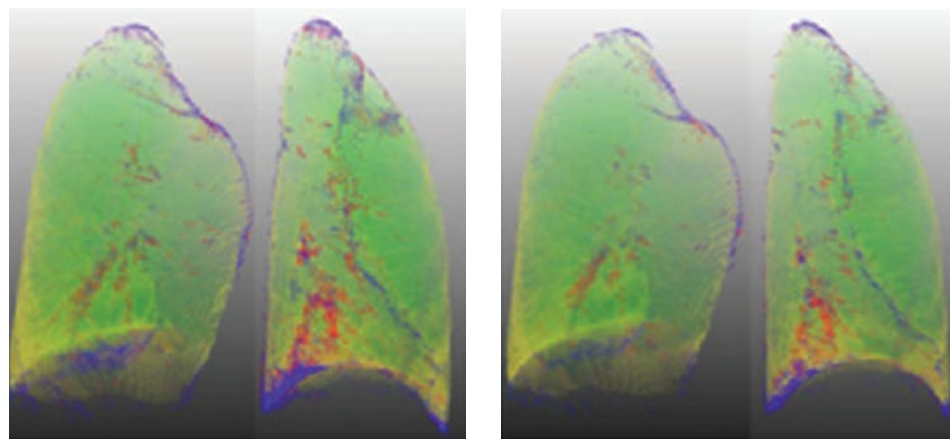
p. 316

Figure 1. Three-dimensional rendering of coronal images showing normal lung pattern (green), quantitative lung fibrosis (blue and red), and a ground-glass pattern (yellow).

from lung fibrosis to a ground-glass pattern of 5% and 0.5%, respectively.

This study revealed several baseline characteristics that were significantly associated with favorable transitions from a ground-glass pattern to a normal pattern (less dyspnea and female sex) and from lung fibrosis to a normal pattern (less restriction, worse skin scores, and female sex). The authors propose that these transitions to a more normalized lung pattern be examined for insights into the underlying pathobiology of treatment response.

Anakinra for the Treatment of Pediatric Secondary Hemophagocytic Lymphohistiocytosis

Rheumatologists use the recombinant human interleukin-1 (IL-1) receptor antagonist anakinra to effectively treat systemic juvenile idiopathic arthritis (JIA). **In this issue, Eloseily et al (p. 326)** report that anakinra appears to be effective in treating pediatric patients with non–malignancy-associated secondary hemophagocytic lymphohistiocytosis (HLH)/ macrophage activation syndrome (MAS). They found that anakinra was particularly effective when it was given early in the disease course and when administered to patients with an underlying rheumatic disease.

The investigators used electronic medical records to identify 44 patients with secondary HLH/MAS who were being treated with anakinra. They found that the median duration of hospitalization

p. 326

was 15 days and the overall mortality rate was 27%. The mean pretreatment serum ferritin level was 33,316 ng/ml, which decreased by 57% to 14,435 ng/ml within 15 days of the start of anakinra treatment.

Early initiation of anakinra (within 5 days of hospitalization) was associated with reduced mortality. In contrast, thrombocytopenia and *STXBP2* mutations were both associated with increased mortality. Looking more specifically at the underlying diagnosis of the patients, the researchers deemed those with systemic JIA to have the lowest mortality rate (no deaths in the 13 patients in the study). In contrast, those with an underlying hematologic malignancy had the highest mortality rate (all 3 patients in the study).

Analysis of Drug Spending for Biologic Antirheumatic Drugs

In this issue, McCormick et al (p. 234) report that postmarket drug price changes are solely responsible for most of the recent spending growth in biologic disease-modifying antirheumatic drugs (DMARDs).

The investigators studied Medicare and Medicaid data and found that spending on 10 biologic DMARDS more than doubled between 2012 and 2016, with the annual spending on public-payer claims growing from $3.8 billion to $8.6 billion.

The researchers also report median drug price increases of 51% in Medicare Part D (mean 54%) and 8% in Medicare Part B (mean 21%). Adjusting for general inflation, they found that unit price increases alone accounted for 57% of the 5-year, $3 billion spending increase in Part D. This stands in contrast to 37% of the spending increase that was the result of increased uptake.

Even accounting for time-varying rebates, the researchers determined that prices were still responsible for 54% of increased spending. These hikes are critical since patients pay a portion of the pre-rebate (list) price for biologic DMARDs. As prices rise, their out-of-pocket costs to rise alongside, especially under Part D. The authors conclude by suggesting that policy interventions targeting price increases may be able to mitigate financial burdens for public payers and biologic DMARD recipients, particularly those under Medicare Part D plans.

Autoantibodies Provide Insights into Rheumatoid Arthritis

In this issue, 2 articles shed light on the role of autoantibodies and the evolution of rheumatoid arthritis (RA). Kelmenson et al (p. 251)

describe results from their analysis of patients with RA, which suggest that the differences in patterns of elevations of autoantibody isotypes have implications for understanding pathophysiology. Zheng et al (p. 262) report that disordered protein structure within autoantigens is a potentially unifying features for reactivity with RA autoantibodies.

The patterns described by Kelmenson and colleagues may provide insights into which factors drive initial autoantibody elevations as opposed to which factors drive later increases in autoantibody levels and the transition to clinically apparent RA. This is one of the largest cohort studies to date, and it shows that levels of IgG anti–citrullinated protein antibodies (ACPAs) are elevated earlier in pre–RA diagnosis than levels of the other autoantibody subtypes.

When the researchers compared cases to controls, they found that autoantibody levels were elevated prior to a diagnosis of RA a mean of 17.9 years for IgG ACPA, 14.2 years for IgA–rheumatoid factor (RF), 7.2 years for IgM-RF, 6.2 years for IgA ACPA, and 5.0 years for both IgM ACPA and IgG-RF. They found a similar relationship for positive or negative autoantibody status, with cases first showing positivity for IgG ACPA 1.9 years pre-RA and for IgA-RF 1.7 years pre-RA, followed by the other isotypes. When the investigators examined post-RA diagnosis samples, they found that only IgA ACPA positivity was significantly increased. All of the autoantibody levels, however, demonstrated an early initial elevation, a period of stability, and then an increase immediately before RA diagnosis.

The researchers found a pre–RA diagnosis endotype of early elevation of autoantibodies to be associated with increased use of biologic therapy, and a higher prevalence of sicca symptoms and lung disease post–RA diagnosis. They conclude that in some individuals IgA-related processes may be important to transitioning to clinically apparent RA, and that the patterns of elevations of autoantibody
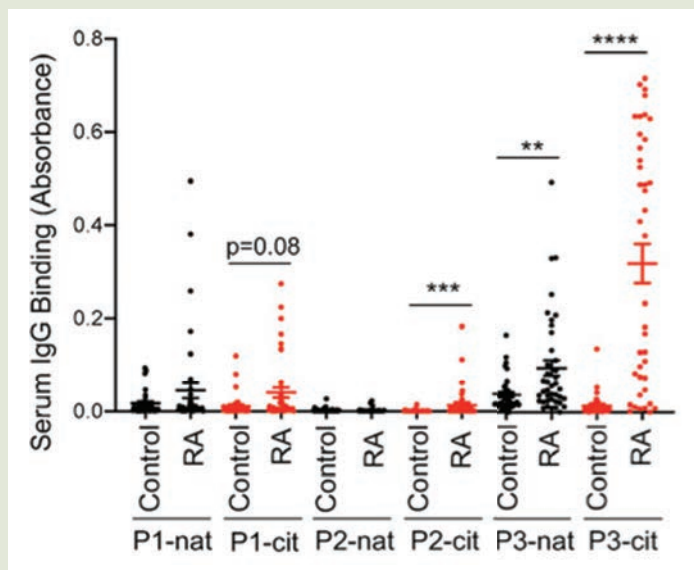

Figure 1. Results in RA patients versus controls were compared.

isotypes may shed light on how pre-RA endotypes may influence post-RA phenotypes.

Zheng and colleagues used a high-density peptide array and 4 serogroups of RA to identify novel features of RA autoantibody reactivity. They found that cyclic citrullinated peptide (CCP)–positive RF+ patients had high citrulline-specific IgG binding to array peptides, and CCP+RF− and CCP−RF+ patients had modest citrulline-specific IgG binding. All RA groups had low homocitrulline-specific binding, and CCP+RF+ patients had moderate IgG binding to native peptides. IgG from CCP+RF+ patients targeted citrulline-containing IgG-derived peptides, suggesting that common epitopes exist for ACPAs and RF.

Overall, however, researchers found that the highest IgG binding was not specific to protein identity, but characterized by an affinity for citrulline-containing peptides, especially if citrulline was adjacent to glycine or serine, motifs also present in proteins endogenously citrullinated in the rheumatoid joint. Such highly bound peptides had multiple features that were predictive of a disordered protein structure.
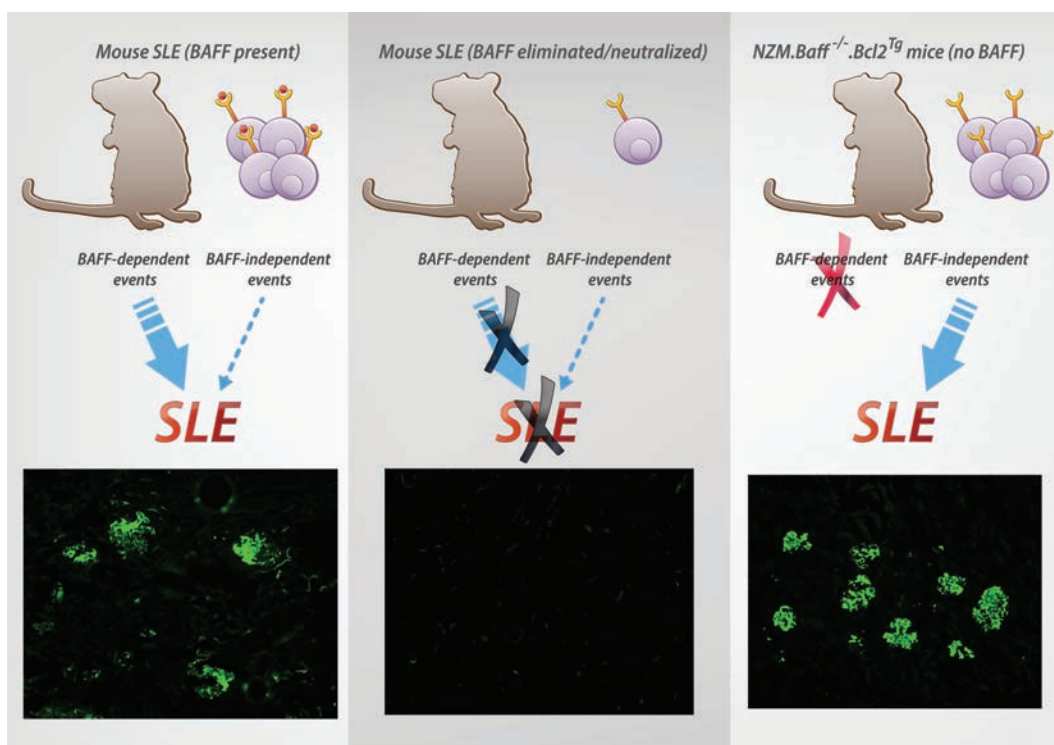
Clinical Connections

Development of Murine Systemic Lupus Erythematosus in the Absence of BAFF

CORRESPONDENCE
William Stohl, MD, PhD: stohl@usc.edu

KEY POINTS

- B cells are reduced in NZM.*Baff*^{−/−} mice but are restored in NZM.*Baff*^{−/−}.*Bcl2*[Tg] mice.

- NZM.*Baff*^{−/−}.*Bcl2*[Tg] mice develop SLE despite the absence of BAFF.

- Reintroduction of the *Baff* gene in NZM.*Baff*^{−/−}.*Bcl2*[Tg] mice accelerates disease, indicating that these mice remain sensitive to the "SLE-genic" property of BAFF.

- NZM.*Baff*^{−/−}.*Bcl2*[Tg] mice may be a valuable murine model for be BAFF-independent SLE.

SUMMARY

BAFF is a vital B cell survival and differentiation factor. Genetic elimination of the *Baff* gene or pharmacologic neutralization of BAFF prevents or ameliorates lupus in mouse models. In contrast, pharmacologic neutralization of BAFF has been far less effective in human subjects, with many systemic lupus erythematosus (SLE) patients failing to achieve a meaningful clinical response. By inference, BAFF-independent pathways contribute importantly to human SLE. Stohl et al developed a murine model in which SLE develops in a BAFF-independent manner by introducing into BAFF-deficient NZM 2328 mice a *Bcl2* transgene (Tg) expressed only in B cells (NZM.*Baff*^{−/−}.*Bcl2*[Tg] mice). In these mice, survival of B cells does not depend upon BAFF-triggered signals. NZM.*Baff*^{−/−}.*Bcl2*[Tg] mice developed full-blown serologic, histologic, and clinical SLE despite the lifelong absence of BAFF. Importantly, these mice remained responsive to BAFF, since reintroduction of the *Baff* gene further accelerated the course of disease. Accordingly, NZM.*Baff*^{−/−}.*Bcl2*[Tg] mice may serve as a valuable and powerful murine model for the study of BAFF-independent SLE and the interplay between BAFF-dependent and BAFF-independent pathogenic pathways.

Role of Interferon-γ–Producing Th1 Cells in a Murine Model of Type I Interferon–Independent Autoinflammation Resulting From DNase II Deficiency

CORRESPONDENCE
Ann Marshak-Rothstein, PhD: ann.rothstein@umassmed.edu
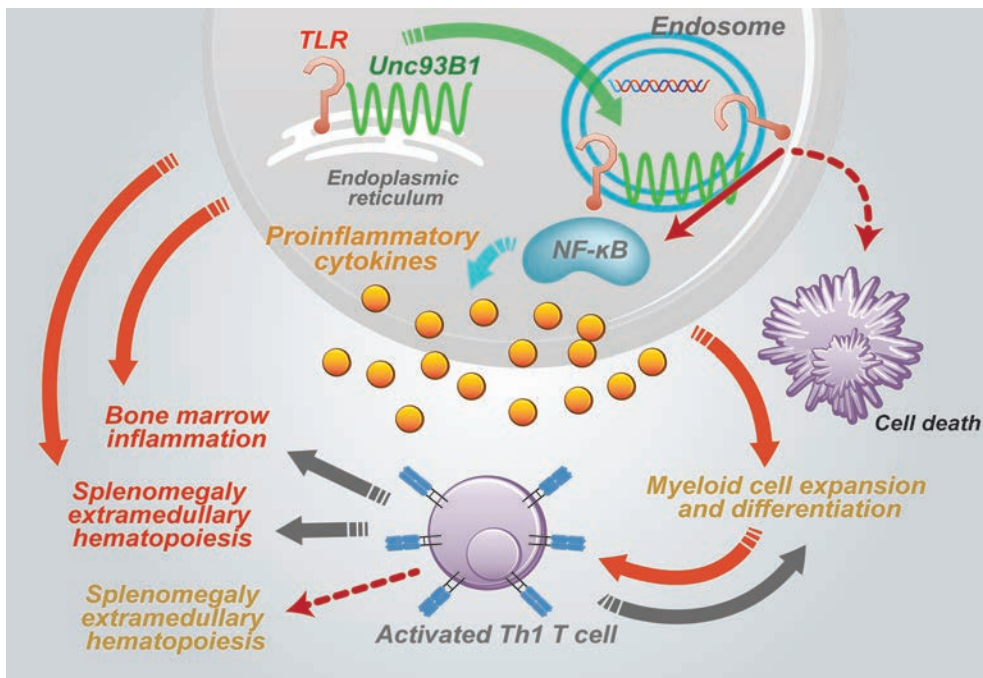
KEY POINTS

- Mice lacking *DNase II* and *Ifnar* recapitulate the clinical manifestations of patients with loss-of-function mutations in DNase II.

- The immune abnormalities of these mice depend on Unc93B1, a chaperone protein for endosomal nucleic acid-sensing TLRs.

- TLR activation in DKO mice leads to the expansion of an unusual IFNγ-producing CD4+ T cell subset.

- IFNγ-producing T cells can transfer autoinflammation to naive recipients.

SUMMARY

Mutations that reduce the function of DNase II and Trex1 (DNase III) lead to the accumulation of undegraded DNA and occur in some patients with autoinflammatory diseases. These conditions are also associated with the elevated expression of type I interferon (IFN)–inducible genes. Such interferonopathies are linked to the activation of the cytosolic DNA–sensing pathway dependent on stimulator of IFN genes (STING) and the production of type I IFNs. DNase II–deficiency in mice is embryonically lethal but can be rescued by loss of expression of the type I IFN receptor (*Ifnar*). *DNase II*$^{-/-}$ × *Ifnar*$^{-/-}$ double-knockout (DKO) mice develop an autoinflammatory condition that recapitulates many of the clinical manifestations of patients with reduced function mutations in DNase II, such as inflammatory arthritis dependent on STING and immune cell abnormalities that depend on another class of nucleic acid sensors, the endosomal Toll-like receptors (TLRs). TLR-driven manifestations include anemia, lymphopenia, extramedullary hematopoiesis, myeloid activation and expansion, and liver fibrosis. As in other diseases driven by TLR overactivation, the remaining T cells include an unusual subset that produce high levels of type II IFN (IFNγ). Notably, CD4+ T cells can independently transfer autoinflammation to healthy mice. These data support the need for targeting both aberrantly activated antigen-presenting cells and aberrantly activated T cells to more effectively treat these patient populations.

Arthritis & Rheumatology

An Official Journal of the American College of Rheumatology
www.arthritisrheum.org and wileyonlinelibrary.com

Arthritis & Rheumatology

An Official Journal of the American College of Rheumatology
www.arthritisrheum.org and wileyonlinelibrary.com

Cover image: The figure on the cover is a magnetic resonance image (sagittal, fat-suppressed pulse sequence) of the knee of a subject in the Multicenter Osteoarthritis Study with painful osteoarthritis. Cartilage loss (especially in the patella and trochlea), bone marrow lesions with cysts, bone attrition (trochlea), and synovitis are seen. This issue of *Arthritis & Rheumatology* features the 2019 American College of Rheumatology/Arthritis Foundation guideline for the management of osteoarthritis of the hand, hip, and knee (Kolasinski et al, pages 220–233). Image courtesy of David Felson, MD, MPH.

AMERICAN COLLEGE
of RHEUMATOLOGY
Empowering Rheumatology Professionals

EDITORIAL

Scrutinizing the Frustrating Cost of Drugs: How Rebates and Step Therapy Inflate Medicare Part D Prices—and Possible Reforms

Angus B. Worthing

In this issue of *Arthritis & Rheumatology*, McCormick and colleagues report their findings on how biologic disease-modifying antirheumatic drug (DMARD) prices increased in Medicare and Medicaid from 2012 to 2016 (1). These novel data are gleaned from the Center for Medicare and Medicaid Services' Drug Spending Dashboard, which began publicizing year-over-year price changes on May 15, 2018 (2). At that time, health policy advocates like myself perused the Dashboard and saw an alarming trend. Biologic DMARD prices appeared to be rising faster in Medicare Part D (the distribution system for drugs self-administered by patients) than in Medicare Part B (drugs received by patients in an office or infusion center). The source of increases in drug prices could not be determined with certainty, though, as data were lacking on how rebates might lower costs in Part D. The current article by McCormick et al is the first to confirm what many had suspected. Using data from the nonpartisan Congressional Budget Office to subtract an average rebate discount for each biologic DMARD in Medicare Part D, the authors found that the prices of biologic DMARDs indeed rose faster in Part D compared to Part B. This editorial examines the complicated drug distribution systems for biologic DMARDs and what may have caused the tremendous price increases observed.

What the data show

From 2012 to 2016, prices of biologic DMARDs increased by a mean of 45% in Medicare Part D after rebates were applied and by a mean of 21% in Medicare Part B. (Medicaid prices also rose in a trend similar to Part D). Although these data are limited by the use of average rebates instead of individual rebates for each drug, the results are unsurprising and can be explained by comparing the incentive structure within the systems. Analysis of the Part D drug distribution system suggests that rebates paid through intermediaries not only drive prices up but are also used to dictate step therapy formularies. Successful drug price reforms will need to address rebates and step therapy, and individual advocacy could encourage such action.

Prices and incentives in Medicare Part B versus Part D

In Medicare Part B, the mean price of drugs is calculated on a quarterly basis based on sales negotiated between buyers (hospitals, clinics, infusion centers, and group purchasing organizations) and commercial sellers (generally private pharmaceutical distributors). Providers administer the drugs and then recoup the mean price plus a 4.3% markup for storage, handling, scheduling, coordination, and other services. Since reimbursement is capped at 4.3% above the mean sales price, buyers attempt to negotiate the largest possible discount below the mean. Discounts are generally reflected in the next quarter's mean price.

In Medicare Part D, drug prices are generally negotiated by pharmacy benefits managers (PBMs) directly with manufacturers, and although Medicare publishes those prices, they are discounted by rebates paid by manufacturers to PBMs and plans. Medicaid has a similar system, but rebates are generally higher, with a floor of at least 23%, and are paid to both federal and state governments. Since PBMs, as McCormick and colleagues state, "retain a percentage of the negotiated rebates as compensation," the arrangement provides PBMs an incentive to negotiate high rebates rather than low list prices. "Higher list prices," they state, "can achieve higher rebates." In order to afford higher rebates and minimize the reduction of their net price, manufacturers are prompted to raise list prices—as if any prompting were necessary—with American drug manufacturers surely sharing the blame here.

Angus B. Worthing, MD: Arthritis and Rheumatism Associates, PC, Washington, DC.

At the time this editorial was submitted and accepted, Dr. Worthing was the Chair of the American College of Rheumatology Government Affairs Committee; however, this editorial was not written in that capacity, and the views and positions expressed are his own and do not necessarily reflect those of the American College of Rheumatology.

So, the system worked as one would expect: Part B drug prices rose more slowly because Part B drug price negotiators (rheumatologists and clinics buying drugs through distributors) were motivated to maximize discounts to obtain the lowest possible mean sales price of Part B drugs, while Part D price negotiators were motivated to maximize rebates that *increase* Part D list prices.

Rebates, PBMs, and step therapy

How exactly does the distribution system for self-administered biologic DMARDs work? Because prices are already so high, drug manufacturers must maximize insurance coverage in order to sell their medications, and PBMs offer preferred coverage status in step therapy formularies to the drug that offers the highest rebate (3). PBMs then keep a portion of the rebates as profit. It appears that the total rebate amount consists of the product of the drug's list price multiplied by the discount percentage and the number of doses sold (i.e., market share), and can also include other fees. Garnering a competitive rebate may therefore be a challenge for new drugs entering the marketplace, such as biosimilars, which lack significant market share and may try to compete by lowering list prices (4). Finally, there is a lack of clarity about the amount of each rebate and how much of it is passed through from PBMs to payers and patients. PBMs use that lack of transparency to profit from charging insurance plans more than the negotiated price at the pharmacy, which is a practice also known as spread pricing.

Rebates and step therapy can prevent patients from accessing effective treatment. In a recent American College of Rheumatology Simple Tasks survey of US adult rheumatology patients, half of those receiving treatment reported being subjected to step therapy (5). An Arthritis Foundation survey showed that step therapy was stopped in 39% of patients because the drugs were ineffective and in 20% of patients due to worsening disease activity. Nearly 25% of patients were required to repeat step therapy after switching insurance carriers (6).

In rheumatoid arthritis (RA), step therapy is associated with a 19% lower odds of treatment effectiveness (likely from lack of adherence to therapy), increased utilization of glucocorticoids and nonsteroidal antiinflammatory drugs, and risk of serious infection (7). Also, since patient cost-sharing is based on list prices and not the net negotiated price, the higher list prices provoked by the rebate system increase patients' out-of-pocket costs. This helps explain why nearly 60% of rheumatology patients report problems affording medications or treatments (5).

In Medicare specifically, step therapy is allowed in Part D but not in Part B (except in Medicare Advantage plans starting in 2019), and this important difference between Part B and Part D explains how Part D rebates, linked with step therapy, may be the main reason that biologic DMARD prices rose more in Part D compared to the open formulary system in Part B. Patient cost-sharing is also relatively higher in Part D compared to Part B due to specialty tier-

ing and lack of secondary insurance to cover patient costs (though a low income subsidy is available), and these high costs interrupt biologic DMARD treatment of patients under Medicare Part D (8).

These points all raise the question Senator Lamar Alexander (Republican, Tennessee) asked of witnesses from pharmaceutical companies and PBMs during a hearing on October 17, 2017 about drug prices (9): "Why not just eliminate rebates?"

Potential solutions for costs, prices, and access

Successful reforms to reduce the cost of drugs for Americans with RA while maintaining or improving access to treatments should involve the following: 1) regulating and changing the role of PBMs, 2) reducing the use of utilization management such as step therapy, and 3) reducing prices through direct government negotiation and improved competition (e.g., biosimilars).

The first step for reforming the role of PBMs is to improve transparency. In late 2018, patients were given the right to find out from their pharmacist when it is less expensive to pay for prescriptions via cash instead of using their insurance (with PBM cost-sharing). This was an important first step, but finding out exactly how much of the rebates go to PBMs and how much to plans and patients will help buyers to make more informed decisions.

If buyers become aware of how much PBMs profit from these secretive arrangements (in the way Ohio's Attorney General recently discovered excessive profits of more than $200 million in Medicaid in 2017 [10]), coupled with how much step therapy limits patients' access to treatments, it could encourage alternative arrangements. For example, Caterpillar, Inc. claims to have saved millions on its employees' medications after "firing the middleman," though the company apparently excludes access to some drugs. Other companies save money on prescription costs by hiring "transparent" PBMs that charge a flat fee (11).

The Department of Health and Human Services (HHS) recently considered eliminating Medicare Part D rebates for PBMs and setting up a pathway for rebates to pass through to patients, but the plan was rescinded before being implemented. The plan's introductory section (12) noted, "Though proponents of the current system describe rebates as discounts that lower drug costs, HHS believes that rebates have proven to be ineffective at and counterproductive to putting downward pressure on drug prices. Indeed, rebates may be harming Federal health care programs by increasing list prices, preventing competition to lower drug prices, discouraging the use of lower-cost brand or generic drugs, and skewing the formulas used to determine pharmacy reimbursement or Medicaid rebates."

Current ideas in Washington, DC

Presently, the US Congress and the Trump administration are considering several common sense reforms related to PBM transparency, rebates, patient cost-sharing, and ways to reduce drug prices throughout Medicare and the commercial markets. Notable

efforts regarding transparency and PBM payments in various different legislative bills would direct HHS to maintain and improve the Drug Pricing Dashboard used by McCormick and colleagues (13) and direct the Federal Trade Commission to investigate anticompetitive actions by PBMs (14). Most significantly, these efforts would force PBMs to disclose the amount earned from rebates and other income, pass all rebates to insurance plans, and stop engaging in spread pricing, while also garnering transparent payments for their services (15). Legislation that directly addresses patients' access to drugs could cap the yearly amount of patient cost-sharing in Medicare Part D (16) and force plans to allow exemptions to step therapy when the "preferred" medication is contraindicated, or expected to cause side effects or disability, or reduce adherence (17).

The White House and key Congressional leaders have proposed ways to directly lower drug prices by negotiating with manufacturers to reduce prices according to prices from an index of selected foreign countries (18,19), or to force manufacturers to reimburse Medicare if prices outpace inflation (16). Indirect ways to lower drug prices include encouraging the use of biosimilars though increased reimbursement in Medicare Part B (16).

It is impossible to predict which, if any, of these initiatives will be enacted, but elected officials face intense political pressure due to the high costs borne by patients and companies and the rationing of treatment via step therapy mandated by non-medical personnel.

What can individuals do to improve patient access to antirheumatic treatments?

Although we live in a time of government gridlock and extreme partisanship, American politicians will work together across party lines when prompted by their constituents. Readers of *Arthritis & Rheumatology* are sophisticated, frustrated, and capable of moving the needle in this debate. Action items include: 1) inform colleagues and patients about how rebates to PBMs dictate step therapy formularies, prompt manufacturers to raise their already too-high list prices, and that those high prices impose higher patient cost-sharing; 2) encourage your elected officials by phone, e-mail, or social media to address these problems; and 3) learn what your elected officials and candidates are saying about drug prices and vote accordingly if you are eligible to vote.

REFERENCES

1. McCormick N, Wallace ZS, Sacks CA, Hsu J, Choi HK. Decomposition analysis of spending and price trends for biologic antirheumatic drugs in Medicare and Medicaid. Arthritis Rheumatol 2022;72:234–41.

2. Centers for Medicare & Medicaid Services. CMS unveils enhanced "drug dashboards" to increase transparency on drug prices. May 2018. URL: https://www.cms.gov/newsroom/press-releases/cms-unveils-enhanced-drug-dashboards-increase-transparency-drug-prices.

3. Wapner J. Understanding the hidden villain of big pharma: pharmacy benefit managers. March 2017. URL: http://www.newsweek.com/big-pharma-villain-pbm-569980.

4. Bridges SL Jr, White DW, Worthing AB, Gravallese EM, O'Dell JR, Nola K, et al, on behalf of the American College of Rheumatology. The science behind biosimilars: entering a new era of biologic therapy. Arthritis Rheumatol 2018;70:334–44.

5. American College of Rheumatology. Press release: national patient survey highlights healthcare challenges for the 1 in 4 Americans living with rheumatic disease. September 2019. URL: https://www.rheumatology.org/About-Us/Newsroom/Press-Releases/ID/1038/fbclid/IwAR3Q4ShRf7mp3YJKKNCd1nYV5uWAuXCQvfo8adJk3KBVnRyzP7-mJUBkSMQ.

6. Lakhanpal S, Palmer AM. Instead of "fail first," put patients first. October 2017. URL: https://thehill.com/blogs/congress-blog/healthcare/356313-instead-of-fail-first-put-patients-first.

7. Boytsov N, Zhang X, Evans KA, Johnson BH. Impact of plan–level access restrictions on effectiveness of biologics among patients with rheumatoid or psoriatic arthritis. Pharmacoecon Open 2019. E-pub ahead of print.

8. Doshi JA, Hu T, Li P, Pettit AR, Yu X, Blum M. Specialty tier-level cost sharing and biologic agent use in the Medicare Part D initial coverage period among beneficiaries with rheumatoid arthritis. Arthritis Care Res (Hoboken) 2016;68:1624–30.

9. Committee on Health, Education, Labor and Pensions. The cost of prescription drugs: how the drug delivery system affects what patients pay. Part II. Washington (DC): US Government Publishing House; 2019. p. 53. URL: https://www.govinfo.gov/content/pkg/CHRG-115shrg27277/pdf/CHRG-115shrg27277.pdf.

10. Candisky C. State accuses pharmacy middlemen of "driving up costs." July 2018. URL: https://gatehousenews.com/sideeffects/side-effects-state-accuses-pharmacy-middlemen-driving-costs/.

11. Weinberg N, Langreth R. Drug costs too high? Fire the middleman. March 2017. URL: https://www.bloomberg.com/news/articles/2017-03-03/drug-costs-too-high-fire-the-middleman.

12. US Department of Health and Human Services. Fraud and abuse: removal of safe harbor protection for rebates involving prescription pharmaceuticals and creation of new safe harbor protection for certain point-of-sale reductions in price on prescription pharmaceuticals and certain pharmacy benefit manager service fees. Federal Register 2019:84:2343. URL: https://www.govinfo.gov/content/pkg/FR-2019-02-06/pdf/2019-01026.pdf.

13. US 116th Congress (2019–2020). S.709: Prescription Drug Pricing Dashboard Act. URL: https://www.congress.gov/bill/116th-congress/senate-bill/709/text.

14. US 116th Congress (2019–2020). H.R.2376: Prescription Pricing for the People Act of 2019. URL: https://www.congress.gov/bill/116th-congress/house-bill/2376.

15. US 116th Congress (2019–2020). S.1895: Lower Health Care Costs Act. URL: https://www.congress.gov/bill/116th-congress/senate-bill/1895.

16. Grassley, Wyden introduce major prescription drug pricing reform to lower costs for Americans. July 2019. URL: https://www.grassley.senate.gov/news/news-releases/grassley-wyden-introduce-major-prescription-drug-pricing-reform-lower-costs.

17. US United States. 116th Congress (2019–2020). H.R.2279/S.2546: Safe Step Act. URL: https://www.congress.gov/bill/116th-congress/house-bill/2279/text.

18. Center for Medicare and Medicaid Services. Medicare programs: international pricing index model for Medicare Part B drugs (CMS-5528-ANPRM). URL: https://www.regulations.gov/document?D=CMS-2018-0132-0001.

19. Goodnough A. Pelosi energizes battle to lower drug prices. The New York Times. September 2019. URL: https://www.nytimes.com/2019/09/10/us/politics/pelosi-trump-drug-prices.html.

AMERICAN COLLEGE
of RHEUMATOLOGY
Empowering Rheumatology Professionals

EDITORIAL

To "Lump" or to "Split" in Macrophage Activation Syndrome and Hemophagocytic Lymphohistiocytosis

Sarah Nikiforow[1] and Nancy Berliner[2] (iD)

The question "To lump or to split?" does not carry the same undertones as Hamlet's searching query but does have far-reaching ramifications for patients and clinicians riding cytokine storms. In this issue of *Arthritis & Rheumatology*, Eloseily and colleagues report their findings from a retrospective analysis of 44 patients with macrophage activation syndrome (MAS) or secondary hemophagocytic lymphohistiocytosis (HLH) who were exposed to the interleukin-1 (IL-1) receptor antagonist anakinra at any time in their treatment course (1). The authors conclude that early use of anakinra may be beneficial in pediatric patients with secondary HLH without an associated malignancy. However, with a cohort that includes patients with underlying systemic juvenile idiopathic arthritis (JIA), malignancy, infection, or at least 10 other potential triggers, should we be "lumpers" or "splitters" in applying these data to a given patient? We posit that patients with MAS, those with other secondary HLH, those with macrophage activation–like syndrome in sepsis, those with cytokine release syndrome (CRS) following chimeric antigen receptor T cell therapy, and those with other hyperinflammatory syndromes still need individualized approaches to therapy.

Nomenclature and diagnostic classification in this field are not clear, which complicates interpretation of the existing data. MAS (or MAS/HLH) is classically referred to as a subset of HLH (characterized by fever, hyperferritinemia, pancytopenia, organomegaly, liver dysfunction, and coagulopathy) that occurs with underlying systemic autoimmune disease but in the absence of inherited homozygous familial HLH–associated mutations or malignancy. Differentiating among a flare of an underlying rheumatic condition, sepsis following immunosuppressive therapy, or MAS has always been difficult. Recently, high circulating levels of IL-18 were identified as a distinguishing factor of MAS compared to systemic JIA, infection-associated HLH, or familial HLH, and introduction of a mutation in *NLRC4* resulting in inflammasome hyperactivity was found to elicit an MAS-like syndrome in mice (2).

Clinical trials using IL-18 binding proteins have demonstrated the safety of this strategy and early signs of efficacy in patients with adult-onset Still's disease (AOSD), and therefore this therapy may potentially bear fruit in patients with MAS (3). Neopterin levels are postulated to differentiate an MAS flare from inflammatory activity in active-phase systemic JIA, and the heavy-chain subunit of ferritin may indicate more severe hematologic involvement and development of MAS (4,5). However, heterozygosity for genetic mutations or hypomorphic variants in T cell and natural killer cell cytolytic, microtubule, and vesicle transport pathways typically associated with familial HLH (e.g., *PRF1*, *UNC13D*, and *STXBP2*) are increasingly described in patients with secondary HLH and MAS (6,7). This implies some shared genetic predisposition and further impedes diagnostic distinction. Finally, targetable cytokines such as IL-1, interferon-γ (IFNγ), and IL-6 may be differentially expressed in familial HLH, secondary HLH, and MAS, and it is unclear how relevant these differences are for predicting therapeutic response (8,9).

Moving to the real-world clinical setting, cytokine levels and genetic sequencing data are often not available in real time to guide diagnosis and management. Several classification systems have evolved based on readily available data. Initially, diagnostic criteria proposed for the HLH-1994 trial were used to diagnose MAS, although patients with systemic rheumatic diseases were specifically excluded from both the HLH-1994 and HLH-2004 cohorts (10,11). Attempts at developing classification schema specific to MAS include recent consensus guidelines to distinguish active systemic JIA from evolution to MAS, suggestions for MAS criteria in juvenile systemic lupus erythematosus (SLE), and a set of criteria for MAS in patients with AOSD. These schema emphasize degrees of hyperferritinemia, thrombocytopenia, lactate dehydrogenase (LDH) elevation, hypertriglyceridemia, coagulopathies, and liver dysfunction, but there is extensive overlap with typical HLH diagnostic parameters (12–14). In developing the HScore, which was designed to distinguish reactive hemophagocytic syndromes in adults, Fardet et al included only 16 patients (5%) with either SLE or AOSD (15). Most relevant to this current discussion, the MH score, designed to distinguish MAS from familial HLH, was validated as a

[1]Sarah Nikiforow, MD, PhD: Dana-Farber Cancer Institute, Boston, Massachusetts; [2]Nancy Berliner, MD: Brigham and Women's Hospital, Boston, Massachusetts.

No potential conflicts of interest relevant to this article were reported.

Address correspondence to Nancy Berliner, MD, 75 Francis Street, Boston, MA 02115. E-mail: nberliner@bwh.harvard.edu.

means to determine need for further functional and genetic testing, since it emphasizes age, degree of cytopenias, splenomegaly, and coagulopathy as distinguishing factors (16).

If the etiologies and diagnostic criteria for various inflammatory syndromes are overlapping, where does that leave clinicians regarding therapeutic decisions? The approaches utilized in the HLH-1994 and HLH-2004 trials based on etoposide and dexamethasone therapy for "familial/genetic" or refractory "secondary" disease have yielded 5-year survival rates following hematopoietic stem cell transplantation of 66% in pediatric patients without malignancies or underlying chronic rheumatic diseases. This approach remains the standard in these 2 clinical settings. In adults with secondary HLH, well-recognized prognostic factors are presence of malignancy (negative prognostic factor), underlying autoimmune disorders (positive prognostic factor), and for both adults and children, severe thrombocytopenia at diagnosis (negative prognostic factor) and rapidity of the ferritin response (positive prognostic factor) (17–22). In MAS complicating systemic JIA and SLE, historical survival rates range from 65% to 95%, and the therapeutic options employed range widely, from frequent steroid use to cyclosporine in 60–74% of patients, intravenous immunoglobulin in 33–68%, anakinra in 33–42%, and etoposide chemotherapy in 32–50%, emphasizing the fact that there are no validated evidence-based treatment guidelines in MAS (23–25). In patients with systemic JIA, blockade of tumor necrosis factor (etanercept, infliximab), CD20 (rituximab), IL-6 (tocilizumab), CTLA-4 (abatacept), and, alternately, IL-1 (canakinumab), and even plasmapheresis, have been used in addition to anakinra. However, studies of patients with SLE-associated MAS do not include significant anakinra use. One center's approach to SLE-associated MAS focused primarily on mycophenolate and azathioprine, highlighting different treatment patterns across the MAS field and for different rheumatic disease entities (26,27).

To date, some data have been presented to substantiate the use of anakinra in MAS. Anakinra is a modified human IL-1 receptor antagonist protein that blocks IL-1α and β signaling, a key proinflammatory cytokine pathway. In a literature review of 35 pediatric patients with MAS and systemic JIA or other autoinflammatory diseases, 33 achieved remission during anakinra therapy (28). In addition, there are case reports of successful anakinra therapy in patients with MAS and AOSD (28).

This is the backdrop of the findings discussed in the report by Eloseily et al (1). The authors report on 44 pediatric patients (median age 10 years) who received anakinra and whose diagnosis was identified by International Classification of Diseases, Ninth Revision (ICD-9) code 288.4 or ICD-10 code D76.1 indicating "hemophagocytic syndromes." Patients were confirmed, by genetic sequencing, to not have homozygosity for familial HLH mutations. The authors rightly emphasize the diagnostic challenge: 95% of patients met the MAS/systemic JIA criteria, 70–75% met the classic HLH criteria, 66% had an Hscore of >90,

and 27% fit the MH score criteria. Identified triggers were heterogeneous, with 3 patients having malignancies (which we posit comprise an entirely separate category), 13 having systemic JIA, 5 having SLE, 2 having mixed connective tissue disease, and individual patients each having a variety of other diagnoses, including gastroparesis, uveitis with spondyloarthritis, Sjögren's disease, vasculitis, Crohn's disease, sarcoidosis, antiphospholipid antibody syndrome, and mitochondrial disorder. Ten patients (23%) had an unknown trigger, meaning that 36% of the patients reported did not have an identifiable rheumatic disease. Presence of concurrent infections was high. Main findings in this cohort were an overall survival rate of 73%, high mortality in patients with malignancy (survival 0%), lowest mortality in patients with MAS/systemic JIA (survival 100%), higher mortality with severe thrombocytopenia and presence of the *STXBP2* mutation, and a salutary effect of earlier initiation of anakinra ($P = 0.046$).

At first blush, these results might be taken as a sweeping endorsement of early use of anakinra in MAS and secondary HLH, and indeed, the authors suggest that all patients with secondary HLH should be initially treated with anakinra. However, limitations of the study and the aforementioned heterogeneity of hyperinflammatory disorders supports the notion that we should remain "splitters" rather than "lumpers" for now. Interpretation must remain nuanced. This analysis, like any retrospective study, is subject to severe selection bias by the treating clinicians. Critically ill patients may have preferentially received cytotoxic therapies and would not have been included in the study despite having MAS or secondary HLH. In a retrospective study that includes only those patients treated with anakinra, one may fail to identify a population of patients who might actually experience harm by receiving anakinra therapy first, to the exclusion of other therapies. In several studies and anecdotally in our institutional practice, cytotoxic chemotherapy was/is preferred over biologic agents in patients with evidence of more severe inflammatory activity. In 1 study of 162 adult patients (without clear indication of who had an underlying rheumatic disease diagnosis), use of etoposide as a first-line agent was associated with better outcomes—albeit 46% of these patients had an underlying malignancy (18,24,29).

In their report, Eloseily et al contribute positive data on the safety of anakinra and its efficacy in the initial treatment of MAS arising in systemic JIA. However, their data do not support a carte blanche approach to hyperinflammatory syndromes, including other secondary HLH with or without malignancy and/or genetic drivers. Personalized approaches to the evaluation of patients with MAS, those with secondary HLH, those with CRS, and even those with severe sepsis that are based on clinical parameters, such as the C-reactive protein, LDH, and ferritin levels, as well as cytokine levels and presence of genetic drivers are being explored (29,30). We may get to the point where rapid assessment of pathologic effectors and affected genetic pathways will guide precision therapy in choosing between IL-1, IL-18, IL-6, or IFNγ blockade or

cytotoxic therapies, but for now we are left with vigilant clinical assessment and frequent reevaluation of therapy (31). Such a complex decision tree and multidisciplinary approach was proposed for adult patients with HLH, involving a breakdown of secondary/nongenetic HLH by cause (i.e., infection, malignancy, autoimmune/inflammatory diseases, or "drug-induced" [following CAR T cell therapy, bispecific T cell engagers, or checkpoint inhibitors]). Distinct initial treatment algorithms have been suggested for each specific cause—notably, including an algorithm for use of anakinra in the treatment of MAS/HLH (32).

Thus, the support for anakinra as a first-line treatment for MAS/HLH, and particularly in patients with systemic JIA–associated MAS, is increasing, as are data for early intervention in general once a diagnosis of MAS or HLH is made. However, early anakinra therapy should be extended to treatment of other forms of secondary HLH only with extreme caution. Specifically, the authors' suggestion that cytotoxic therapy should be considered only after administration of anakinra therapy may be a dangerous approach for some patients. We must continue to recognize the heterogeneity of secondary HLH and develop thoughtful therapeutic algorithms that would distinguish among the broad range of etiologies to determine safe and efficacious therapies for this life-threatening disease.

AUTHOR CONTRIBUTIONS

Drs. Nikiforow and Berliner drafted the article, revised it critically for important intellectual content, and approved the final version to be published.

REFERENCES

1. Eloseily EM, Weiser P, Crayne CB, Haines H, Mannion ML, Stoll ML, et al. Benefit of anakinra in treating pediatric secondary hemophagocytic lymphohistiocytosis. Arthritis Rheumatol 2020;72:326–34.

2. Weiss ES, Girard-Guyonvarc'h C, Holzinger D, de Jesus AA, Tariq Z, Picarsic J, et al. Interleukin-18 diagnostically distinguishes and pathogenically promotes human and murine macrophage activation syndrome. Blood 2018;131:1442–55.

3. Gabay C, Fautrel B, Rech J, Spertini F, Feist E, Kötter I, et al. Open-label, multicentre, dose-escalating phase II clinical trial on the safety and efficacy of tadekinig alfa (IL-18BP) in adult-onset Still's disease. Ann Rheum Dis 2018;77:840–7.

4. Takakura M, Shimizu M, Irabu H, Sakumura N, Inoue N, Mizuta M, et al. Comparison of serum biomarkers for the diagnosis of macrophage activation syndrome complicating systemic juvenile idiopathic arthritis. Clin Immunol 2019;208:108252.

5. Ruscitti P, Cipriani P, Di Benedetto P, Liakouli V, Berardicurti O, Carubbi F, et al. H-ferritin and proinflammatory cytokines are increased in the bone marrow of patients affected by macrophage activation syndrome. Clin Exp Immunol 2018;191:220–8.

6. Kaufman KM, Linghu B, Szustakowski JD, Husami A, Yang F, Zhang K, et al. Whole-exome sequencing reveals overlap between macrophage activation syndrome in systemic juvenile idiopathic arthritis and familial hemophagocytic lymphohistiocytosis. Arthritis Rheumatol 2014;66:3486–95.

7. Chinn IK, Eckstein OS, Peckham-Gregory EC, Goldberg BR, Forbes LR, Nicholas SK, et al. Genetic and mechanistic diversity in pediatric hemophagocytic lymphohistiocytosis. Blood 2018;132:89–100.

8. Prencipe G, Caiello I, Pascarella A, Grom AA, Bracaglia C, Chatel L, et al. Neutralization of IFN-γ reverts clinical and laboratory features in a mouse model of macrophage activation syndrome. J Allergy Clin Immunol 2018;141:1439–49.

9. Cifaldi L, Prencipe G, Caiello I, Bracaglia C, Locatelli F, De Benedetti F, et al. Inhibition of natural killer cell cytotoxicity by interleukin-6: implications for the pathogenesis of macrophage activation syndrome. Arthritis Rheumatol 2015;67:3037–46.

10. Trottestam H, Horne A, Aricò M, Egeler RM, Filipovich AH, Gadner H, et al. Chemoimmunotherapy for hemophagocytic lymphohistiocytosis: long-term results of the HLH-94 treatment protocol. Blood 2011;118:4577–84.

11. Bergsten E, Horne A, Aricó M, Astigarraga I, Egeler RM, Filipovich AH, et al. Confirmed efficacy of etoposide and dexamethasone in HLH treatment: long-term results of the cooperative HLH-2004 study. Blood 2017;130:2728–38.

12. Ravelli A, Minoia F, Davì S, Horne A, Bovis F, Pistorio A, et al, on behalf of the Paediatric Rheumatology International Trials Organisation, Childhood Arthritis and Rheumatology Research Alliance, Pediatric Rheumatology Collaborative Study Group, and Histiocyte Society. 2016 classification criteria for macrophage activation syndrome complicating systemic juvenile idiopathic arthritis: a European League Against Rheumatism/American College of Rheumatology/Paediatric Rheumatology International Trials Organisation collaborative initiative. Arthritis Rheumatol 2016;68:566–76.

13. Parodi A, Davì S, Pringe AB, Pistorio A, Ruperto N, Magni-Manzoni S, et al. Macrophage activation syndrome in juvenile systemic lupus erythematosus: a multinational multicenter study of thirty-eight patients. Arthritis Rheum 2009;60:3388–99.

14. Ahn SS, Yoo BW, Jung SM, Lee SW, Park YB, Song JJ. Application of the 2016 EULAR/ACR/PRINTO classification criteria for macrophage activation syndrome in patients with adult-onset Still disease. J Rheumatol 2017;44:996–1003.

15. Fardet L, Galicier L, Lambotte O, Marzac C, Aumont C, Chahwan D, et al. Development and validation of the HScore, a score for the diagnosis of reactive hemophagocytic syndrome. Arthritis Rheumatol 2014;66:2613–20.

16. Minoia F, Bovis F, Davì S, Insalaco A, Lehmberg K, Shenoi S, et al, on behalf of the Pediatric Rheumatology International Trials Organization, the Childhood Arthritis and Rheumatology Research Alliance, the Pediatric Rheumatology Collaborative Study Group, and the Histiocyte Society. Development and initial validation of the macrophage activation syndrome/primary hemophagocytic lymphohistiocytosis score, a diagnostic tool that differentiates primary hemophagocytic lymphohistiocytosis from macrophage activation syndrome. J Pediatr 2017;189:72–8.

17. Schram AM, Comstock P, Campo M, Gorovets D, Mullally A, Bodio K, et al. Haemophagocytic lymphohistiocytosis in adults: a multicentre case series over 7 years. Br J Haematol 2016;172:412–9.

18. Arca M, Fardet L, Galicier L, Rivière S, Marzac C, Aumont C, et al. Prognostic factors of early death in a cohort of 162 adult haemophagocytic syndrome: impact of triggering disease and early treatment with etoposide. Br J Haematol 2015;168:63–8.

19. Brito-Zerón P, Kostov B, Moral-Moral P, Martínez-Zapico A, Díaz-Pedroche C, Fraile G, et al. Prognostic factors of death in 151 adults with hemophagocytic syndrome: etiopathogenically driven analysis. Mayo Clin Proc Innov Qual Outcomes 2018;2:267–76.

20. Ramos-Casals M, Brito-Zerón P, López-Guillermo A, Khamashta MA, Bosch X. Adult haemophagocytic syndrome. Lancet 2014;383:1503–16.

21. Lin TF, Ferlic-Stark LL, Allen CE, Kozinetz CA, McClain KL. Rate of decline of ferritin in patients with hemophagocytic lymphohistiocytosis

as a prognostic variable for mortality. Pediatr Blood Cancer 2011; 56:154–5.

22. Koh KN, Im HJ, Chung NG, Cho B, Kang HJ, Shin HY, et al. Clinical features, genetics, and outcome of pediatric patients with hemophagocytic lymphohistiocytosis in Korea: report of a nationwide survey from Korea Histiocytosis Working Party. Eur J Haematol 2015;94:51–9.

23. Aytaç S, Batu ED, Ünal Ş, Bilginer Y, Çetin M, Tuncer M, et al. Macrophage activation syndrome in children with systemic juvenile idiopathic arthritis and systemic lupus erythematosus. Rheumatology Int 2016;36:1421–9.

24. Minoia F, Davì S, Horne A, Demirkaya E, Bovis F, Li C, et al, on behalf of the Pediatric Rheumatology International Trials Organization, Childhood Arthritis and Rheumatology Research Alliance, Pediatric Rheumatology Collaborative Study Group, and Histiocyte Society. Clinical features, treatment, and outcome of macrophage activation syndrome complicating systemic juvenile idiopathic arthritis: a multinational, multicenter study of 362 patients. Arthritis Rheumatol 2014;66:3160–9.

25. Boom V, Anton J, Lahdenne P, Quartier P, Ravelli A, Wulffraat NM, et al. Evidence-based diagnosis and treatment of macrophage activation syndrome in systemic juvenile idiopathic arthritis. Pediatr Rheumatol Online J 2015;13:55.

26. Borgia RE, Gerstein M, Levy DM, Silverman ED, Hiraki LT. Features, treatment, and outcomes of macrophage activation syndrome in childhood-onset systemic lupus erythematosus. Arthritis Rheumatol 2018;70:616–24.

27. Gavand PE, Serio I, Arnaud L, Costedoat-Chalumeau N, Carvelli J, Dossier A, et al. Clinical spectrum and therapeutic management of systemic lupus erythematosus-associated macrophage activation syndrome: a study of 103 episodes of 89 adult patients. Autoimmun Rev 2017;16:743–9.

28. Sönmez HE, Demir S, Bilginer Y, Özen S. Anakinra treatment in macrophage activation syndrome: a single center experience and systemic review of literature. Clin Rheumatol 2018;37:3329–35.

29. Minoia F, Davì S, Horne A, Bovis F, Demirkaya E, Akikusa J, et al, on behalf of the Pediatric Rheumatology International Trials Organization, Childhood Arthritis and Rheumatology Research Alliance, Pediatric Rheumatology Collaborative Study Group, and Histiocyte Society. Dissecting the heterogeneity of macrophage activation syndrome complicating systemic juvenile idiopathic arthritis. J Rheumatol 2015;42:994–1001.

30. Kumar B, Aleem S, Saleh H, Petts J, Ballas ZK. A personalized diagnostic and treatment approach for macrophage activation syndrome and secondary hemophagocytic lymphohistiocytosis in adults. J Clin Immunol 2017;37:638–43.

31. Behrens EM, Koretzky GA. Cytokine storm syndrome: looking toward the precision medicine era [review]. Arthritis Rheumatol 2017;69:1135–43.

32. La Rosée P, Horne A, Hines M, von Bahr Greenwood T, Machowicz R, Berliner N, et al. Recommendations for the management of hemophagocytic lymphohistiocytosis in adults. Blood 2019;133:2465–77.

AMERICAN COLLEGE
of RHEUMATOLOGY
Empowering Rheumatology Professionals

REVIEW

Innately Adaptive or Truly Autoimmune: Is There Something Unique About Systemic Juvenile Idiopathic Arthritis?

Christoph Kessel,[1] Christian M. Hedrich,[2] [iD] and Dirk Foell[1] [iD]

Systemic juvenile idiopathic arthritis (JIA) is a form of arthritis in childhood that is initially dominated by innate immunity–driven systemic inflammation and is thus considered a polygenic autoinflammatory disease. However, systemic JIA can progress toward an adaptive immunity–driven afebrile arthritis. Based on this observation of biphasic disease progression, a "window of opportunity" for optimal, individualized and target-directed treatment has been proposed. This hypothesis requires testing, and in this review we summarize current evidence regarding molecular factors that may contribute to the progression from an initially predominantly autoinflammatory disease phenotype to autoimmune arthritis. We consider the involvement of innately adaptive γδ T cells and natural killer T cells that express γδ or αβ T cell receptors but cannot be classified as either purely innate or adaptive cells, versus classic B and T lymphocytes in this continuum. Finally, we discuss our understanding of how and why some primarily autoinflammatory conditions can progress toward autoimmune-mediated disorders over the disease course while others do not and how this knowledge may be used to offer individualized treatment.

Introduction

The concept of autoinflammation was proposed 20 years ago with the characterization of genetic alterations that cause monogenic hereditary fever syndromes (1). Today, at least 8 categories of autoinflammatory diseases have been defined: interleukin-1β (IL-1β) activation disorders (inflammasomopathies), NF-κB activation syndromes, protein misfolding disorders, complement regulatory diseases, cytokine signaling disturbances, macrophage activation syndromes (MAS), ubiquitination disorders, and type I interferonopathies (2). Following the historical definition, autoinflammatory disorders are characterized by seemingly unprovoked episodes of systemic or organ-specific inflammation in the absence of high-titer autoantibodies or self-reactive lymphocyte populations. In a conceptual divide, autoimmunity has historically been seen as the consequence of (isolated) adaptive immune dysregulation. This divide has also been applied to polygenic/multifactorial disorders, in which the absence of disease-causing mutations in single genes makes it challenging to identify molecular pathways.

Today, advances in understanding polygenic autoinflammatory Still's disease or systemic juvenile idiopathic arthritis (JIA) can provide new insights into the complex bidirectional interplay between innate and adaptive immunity (Figure 1).

Systemic JIA in the conceptual divide of autoinflammation versus autoimmunity

Systemic JIA is the childhood counterpart to adult-onset Still's disease (AOSD) and is usually considered a prototypic polygenic autoinflammatory disease (3,4). Approximately 10% of chronic idiopathic arthritis cases occurring during childhood can be classified as systemic JIA. Although the name implies that the disease is a systemic variant of JIA, and regardless of systemic JIA being classified as one of 7 JIA subtypes according to the International League of Associations for Rheumatology (5), recent studies indicate that systemic JIA is fundamentally different from other forms of JIA. Indeed, its unique genetic architecture manifests in a distinct clinical spectrum, indicating that the underlying

Figure 1. Examples of polygenic arthritic disorders with differing degrees of autoinflammation and/or autoimmunity. Arthritic conditions can be dominated by innate immune mechanisms (systemic juvenile idiopathic arthritis [sJIA] and adult-onset Still's disease [AOSD] at onset, gout) or adaptive immune mechanisms (polyarticular JIA [poly-JIA] or oligoarticular JIA [oligo-JIA], rheumatoid arthritis [RA], and systemic JIA and AOSD in the course of disease progression), with or without B cell activation and autoantibody expression, or resemble mixed-pattern diseases (psoriatic arthritis [PsA] and ankylosing spondylitis [AS]). HLA associations are indicated for diseases for which they have been identified. NK = natural killer; anti–IL-1 = anti–interleukin-1; anti–IL-1R = anti–IL-1 receptor; anti-TNF = anti–tumor necrosis factor.

pathomechanistic pathways significantly differ from those in other JIA subtypes (6).

Early in the disease course the clinical presentation of systemic JIA is dominated by "autoinflammatory features" resembling a classic fever syndrome. Common symptoms comprise quotidian spiking fevers accompanied by erythematous rash, while arthritis may be minimal or even absent. Further, hepatosplenomegaly, lymphadenopathy, and/or serositis are clinical hallmarks of the disease that separate systemic JIA from other JIA subtypes (3). During the systemic inflammatory phase, systemic JIA can be complicated by MAS, a severe hyperinflammatory condition characterized by a "cytokine storm" that can result in multiple organ failure with significant mortality. More recently, an association of systemic JIA with pulmonary arterial hypertension, interstitial lung disease, and alveolar proteinosis as severe and mostly fatal complications, potentially resulting from uncontrolled systemic disease activity and inflammation, has been recognized (7).

Disease courses in systemic JIA can be monophasic and self-limiting, polycyclic, or persistent and, if inadequately or not treated, systemic JIA can progress to a disease mainly characterized by aggressive/destructive arthritis, a feature more typical of autoimmune conditions. Indeed, though no specific autoantibodies have yet been detected, a genetic association of systemic JIA with the major histocompatibility complex (MHC) class II–specific

allele HLA–DRB1*11 (8) as well as alterations in adaptive immune cell signatures (9), including a skewed ratio of Th1 and Th17 cells (10) and increased serum levels of IL-17A (11), suggest an autoimmune component to systemic JIA (12,13).

Further evidence indicative of a close interplay between innate and adaptive immune responses is provided by treatment responses. While traditional systemic JIA therapy was limited to steroidal and nonsteroidal antiinflammatory drugs, current treatment regimens mainly rely on drugs interfering with either IL-1 or IL-6 signaling. Therapeutic IL-1 blockade significantly improves disease outcomes (14) and seems particularly effective when initiated as first-line therapy during the systemic disease phase (15–17). In contrast, children with established polyarthritis are less likely to respond to treatment with recombinant IL-1 receptor antagonist (IL-1Ra; anakinra) (18,19). Current clinical trial results suggest that these patients may benefit from therapeutic IL-6R blockade (tocilizumab) instead (20). However, a true head-to-head comparison of drugs interfering with either IL-1 or IL-6 signaling is still lacking.

Taken together, differential response to treatment as well as genetic and immunologic findings suggest that dysbalanced expression of innate molecules may link autoinflammation with autoimmunity in systemic JIA and finally drive autoimmune arthritis on the basis of an initial autoinflammatory disease context (11,12).

Mechanisms linking autoinflammation and autoimmunity in systemic JIA

Role of inflammasome dysregulation in autoinflammation in systemic JIA. A key observation from the investigation of monogenetic autoinflammatory diseases is their strong association with mutations in genes encoding for proteins involved in inflammasome assembly. Inflammasomes are cytoplasmic multiprotein complexes that can sense a wide range of pathogen-associated molecular patterns or damage-associated molecular patterns (DAMPs) (21). Activation of NOD-like receptors (NLRs), NLRP3 (or cryopyrin), NLRP1, NLRC4, or AIM2 (absent in melanoma 2), mediate conformational changes, some of which allow for interaction with an inflammasome adaptor protein, ASC, through pyrin domains (21). Once assembled, ASC binds procaspase 1 through its caspase recruitment domain and assists in assembly and caspase 1 activation, which, in turn, cleaves inactive proIL-1β and proIL-18 and activates the cytosolic protein gasdermin D (GSDMD) (22). Cleaved GSDMD forms pores in the plasma membrane, which induces pyroptotic cell death and permits the release of mature IL-1β and IL-18 to the extracellular space (23). Prototypic autoinflammatory diseases, such as familial Mediterranean fever (FMF) and cryopyrin-associated periodic syndrome (CAPS), are associated with mutations in *MEFV* (encoding pyrin) or *NLRP3*. Aberrant inflammasome activation results in excessive IL-1β and/or IL-18 processing. Consequently, drugs such as colchicine, as specific inhibitors of the pyrin inflammasome, can interfere with cytokine release and thus alleviate clinical symptoms of systemic inflammation in affected individuals (24).

Though a large proportion of patients with systemic JIA benefit from IL-1–blocking therapy, to our knowledge gain-of-function inflammasome polymorphisms in systemic JIA have not been reported, and it remains difficult to measure/quantify increased IL-1 expression as a key autoinflammatory factor. Several studies, including the seminal one by Pascual et al introducing the concept of IL-1 blockade in systemic JIA (14), failed to demonstrate elevated IL-1β levels in patient sera (11) or whole blood (25). Stimulation of ex vivo–isolated monocytes or whole blood using designated pattern-recognition receptor (PRR) ligands, such as lipopolysaccharide and others (www.tollgene.org), did not reveal increased IL-1 release when compared to controls (25,26) or demonstrate decreased cytokine secretion, possibly due to an intermediate regulatory/antiinflammatory (M2) phenotype of circulating systemic JIA monocytes (26). However, complex stimulation conditions using patient sera can induce IL-1–specific gene signatures as well as IL-1β release from healthy donor peripheral blood mononuclear cells (PBMCs) (14). Furthermore, at the level of transcription or translation, both monocytes and neutrophils from patients exhibited increased IL-1β expression (27,28) or protein accumulation over time (25,26). This may be caused by decreased expression of the IL-1–inhibiting aryl hydrocarbon receptor in systemic JIA cells (25). In response to prolonged stimulation (24 hours) by a strong stimulant such as phorbol myristate acetate (PMA)/ionomycin, this can result in enhanced cytokine release from patient cells when compared to controls (14). Gene expression studies of neutrophils from patients with systemic JIA further indicated overexpression of inflammasome components such as *AIM2* and *NLRC4* (27,28).

In contrast to limited detection of circulating IL-1 in systemic JIA, several studies have demonstrated massive overexpression of the IL-1 family member IL-18 (29–31). However, while the role of IL-18 as a systemic JIA biomarker is well established (29,31) and recent studies suggest that IL-18 is a critical driver of MAS (31,32), its cellular sources as well as expression control in systemic JIA remain poorly understood. IL-18 is expressed by a wide range of tissues, including cells of the myeloid lineage but also epithelial cells, and (in contrast to IL-1) IL-18 messenger RNA (mRNA) expression and translation into its propeptide appear to be constitutive (33). However, beyond constitutive expression, a recent murine study (34) and human data from our laboratory (35) indicate that type I interferon (IFN) signaling plays a vital role in controlling IL-18 expression.

Dysregulation of IFN expression and signaling. In the context of systemic JIA, impaired expression of IFNs and altered IFN signaling is usually associated with the type II IFN, IFNγ. IFNγ is predominantly produced by adaptive immune cells, namely Th1 CD4+ lymphocytes, but also by natural killer (NK) and CD8+ T cells. The role of these cells, particularly in MAS, has been extensively discussed elsewhere (31,32,36). More recently, observations on gene expression levels in response to IL-1 inhibition and data on the control of IL-18 by the IFN family suggested a previously underestimated role of the type I IFNs IFNα and IFNβ, another arm of the innate immune system, in the pathogenesis of systemic JIA. Type I IFNs are produced by a multitude of cells and tissues. Their main cellular sources, however, are plasmacytoid dendritic cells, which produce type I IFNs in response to viral infections (37).

Physiologically, type I IFN expression is induced by viral DNA or RNA, which is sensed by PRRs such as endosomal Toll-like receptor 3 (TLR-3), TLR-7, TLR-8, and/or TLR-9. In addition to TLRs, cytosolic sensors for DNA and RNA, such as the retinoic acid–inducible gene 1–like receptors as well as AIM2-like receptors, induce type I IFN expression (38). Cyclic GMP-AMP synthase has been identified as a cytosolic PRR that detects DNA and leads to the production of cyclic GMP-AMP (39,40). Activation of TLRs or cytosolic nucleotide sensors triggers IFN expression, which in turn mediates phosphorylation of transcription factors initiating the expression of IFN-stimulated genes (ISGs). Indeed, transcription levels of selected ISGs in blood cells can be used as a complementary biomarker to generate an IFN signature (38,41). In fact, while even in type I interferonopathies high-sensitivity assays, such as digital enzyme-linked immunosorbent assays, are required in order to produce measurable (fg/ml) serum levels

of IFNα (41), most patients display an IFN signature at the mRNA level in PBMCs (41,42).

Interestingly, though systemic JIA is not readily associated with type I IFN expression and signaling, blockade of IL-1 signaling induces a type I IFN signature in patients with systemic JIA, independent of the clinical response to IL-1 blockade (19). Similar observations regarding the relationship of IL-1 blockade in systemic JIA and type I IFN expression were obtained from a recent study assessing IFN signatures in a variety of pediatric inflammatory conditions (42). At the cellular level, transcriptome analysis of systemic JIA neutrophils reveals—among other genes—an up-regulation of transcripts associated with type I IFN signaling (27). Monocytes from patients with systemic JIA exhibit defective STAT1 phosphorylation downstream of IFNα or IFNγ stimulation, while expressing higher transcript levels of suppressor of cytokine signaling 1 (SOCS-1), an inhibitor of IFN signaling (43). In patients responsive to IL-1 blockade, SOCS-1 levels decrease while STAT1 levels increase. The opposite was observed in individuals whose disease failed to respond to IL-1 blockade, suggesting that response to cytokine-blocking therapy is associated with effects on type I IFN signaling pathways that may in turn result in increased pSTAT1/IFN responses (43). However, as type I IFNs have not yet been mechanistically linked with systemic JIA, it is debatable whether the effects observed are primarily or secondarily associated with disease. Proinflammatory IL-1 and type I IFNs are key players in 2 types of inflammatory responses, which can efficiently counterregulate each other (44). Thus, increased type I IFN expression following IL-1 blockade, but also tumor necrosis factor blockade (45,46), may just reflect the presence of feedback loops induced by cytokine blockade (42). Nonetheless, it has been speculated that the decreased ability of systemic JIA monocytes to respond to IFNγ and IFNα may set the stage for the excessive IL-1β activity evident in the disease (43).

DAMPs and the relevance of sterile inflammation. A hallmark of systemic JIA and other autoinflammatory diseases is the highly increased secretion of myeloid cell–derived S100 proteins. S100A8/A9 and S100A12 are present in the cytoplasm of monocytes and granulocytes and play an incompletely understood role in the homeostasis of these phagocytes (47). Serum levels of S100A8/A9 and S100A12 strongly correlate with peripheral blood neutrophil counts, and neutrophils from patients with systemic JIA exhibit elevated inflammatory gene expression, including inflammasome components and *S100A8* and *S100A12* (27,28). Furthermore, these cells exhibited enhanced PMA-induced S100A8/A9 release compared to controls (27).

When released during the activation of the innate immune system or in the context of tissue damage, S100 proteins function as DAMPs and recruit to PRRs (48,49). In systemic JIA and other autoinflammatory diseases, dysregulation of alternative secretory pathways may furthermore contribute to disease pathogenesis and lead to hypersecretion of S100 proteins (47). Thus, in the absence of infectious pathogens, S100 proteins can generate a sterile inflammatory environment and initiate downstream proinflammatory effects on innate immune cells that feed into amplifying loops, which may perpetuate disease (47). Along these lines, depletion of S100A8/A9 from systemic JIA patient serum or prevention of the Ca^{2+}/Zn^{2+}-induced inflammatory complex formation by S100A12 reduces the release of IL-1 and other inflammatory cytokines from the immune cells (whole blood or monocytes) of patients with systemic JIA or controls (48,50).

Innate molecules fueling adaptive immunity. Apart from driving innate immune responses, IL-1β and IL-18 can play a prominent role in shaping adaptive immune responses. In fact, IL-18 was initially described as an IFNγ-inducing factor (51), since it can induce IFNγ expression from NK cells and Th1 lymphocytes, while blocking regulatory IL-10 expression in the Th1 compartment (52). IL-1β is involved in the differentiation of Th17 cells (53) and IFNγ/IL-17–coexpressing T lymphocytes (54). Furthermore, IL-1β strongly suppresses T cell–derived IL-10 expression and promotes IFNγ production in human Th17 cells, thus influencing the balance between proinflammatory and antiinflammatory cellular functions (55,56). However, human IL-1–mediated Th17 differentiation in particular also requires IL-23 and T cell receptor (TCR) engagement (57). The presence of IL-6, which is also massively overexpressed in systemic JIA, however, appears to be of secondary importance (53). Apart from its vital role in Th cell differentiation, IL-1R signaling stabilizes cytokine transcripts to enable productive and rapid effector functions across effector Th1, Th2, and Th17 lymphocyte subsets (58). Independent from T cells, IL-1β can also enhance B cell proliferation and antibody production, while IL-18 promotes self-reactive antibody responses (59).

However, despite strong effects of IL-1 and IL-18 on T cell differentiation and activity, evidence of altered CD4+ T cell function in systemic JIA or AOSD remains scarce. While some studies suggest increased numbers of Th1 and Th17 cells in systemic JIA (10) and AOSD (60,61), other studies indicate that this may be, if at all present, just a trend (9,11,62). Controversial data on Th1 and Th17 cell numbers furthermore reflect uncertainty regarding a stimulating autoantigen, despite the association with MHC class II variant HLA–DRB1*11 (8). Indeed, Th cell subsets in systemic JIA may rather benefit from increased IL-1R signaling, which can stabilize the effector functions of CD4+ T cells by stabilizing cytokine transcripts, and thus may allow for rapid response to nonspecific stimulation in cell culture and flow cytometry assays (58).

In addition to the potential involvement of classic adaptive immune cells in the pathogenesis of systemic JIA, recent studies highlight a role of innately adaptive cells bridging innate and adaptive immune responses (63), such as γδ T cells or invariant NKT (iNKT) cells (Figure 2). In patients with systemic JIA, iNKT cell numbers are greatly increased (9), while peripheral γδ T cell counts, particularly during active disease, remain reduced compared to those in healthy individuals (9,11,62). This finding may
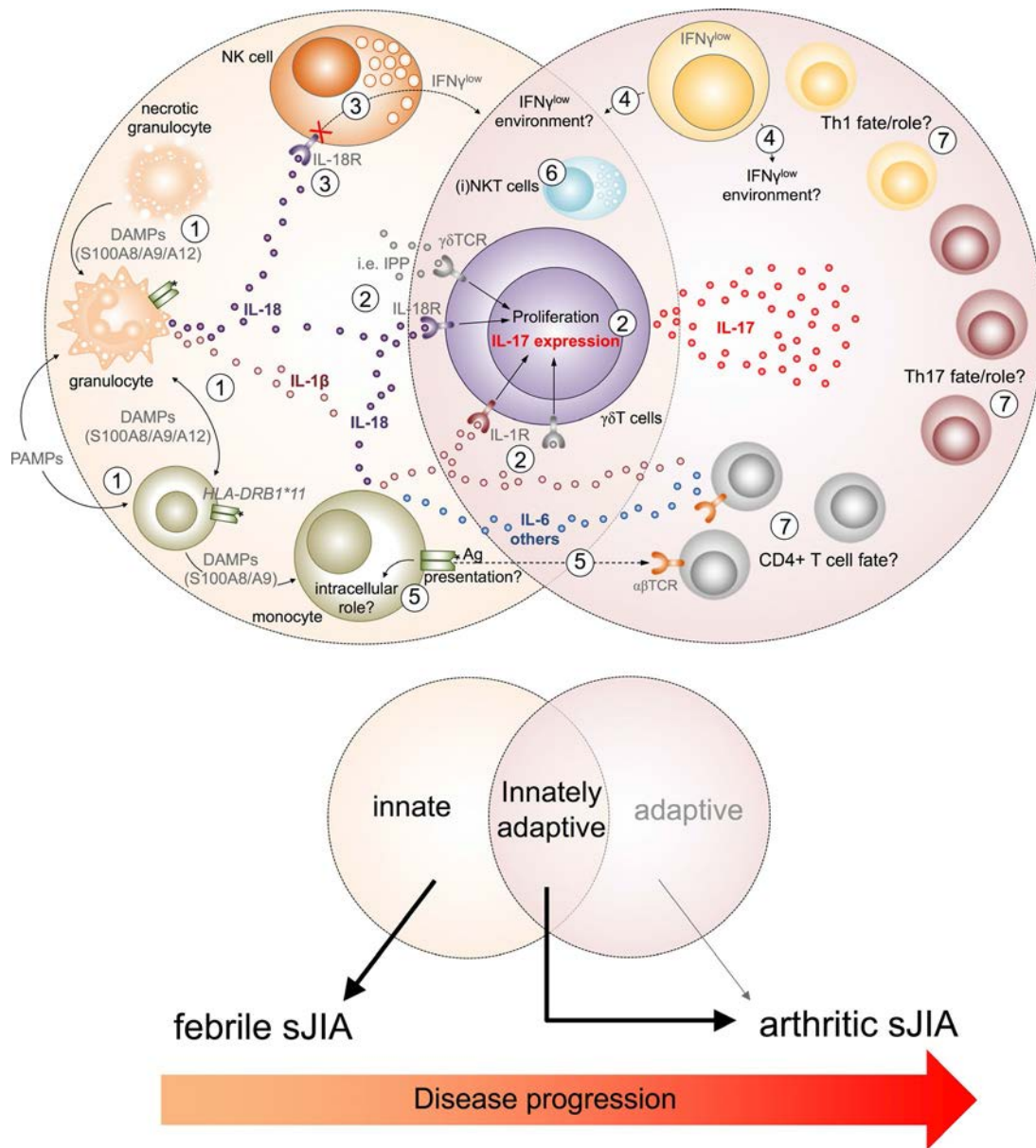
Figure 2. Innately adaptive or truly autoimmune: a pathophysiologic model for disease progression in systemic juvenile idiopathic arthritis (sJIA). Innate immune cells, such as myeloid cells (granulocytes, monocytes) and natural killer (NK) cells, are relevant during the acute febrile phase of systemic JIA. 1) Myeloid cells release interleukin-1 (IL-1) family cytokines (IL-1β, IL-18) and other proinflammatory cytokines which can either be triggered by infection (pathogen-associated molecular patterns [PAMPs]) or result from pattern-recognition receptor activation by damage-associated molecular patterns (DAMPs) released from stressed or necrotic cells. 2) Together with γδ T cell receptor (γδ TCR) activation by endogenous ligands (i.e., isopentenyl pyrophosphate [IPP]) or bacterial ligands, IL-1 and IL-18 can trigger IL-17 expression from γδ T cells, while 3) IL-18 fails to trigger interferon-γ (IFNγ) expression from NK cells due to a defective IL-18 receptor (IL-18R). 4) Similarly, systemic JIA Th1 cells express only low levels of IFNγ. Both cell types may contribute to hypophysiologic IFNγ levels, potentially promoting IL-17 expression in disease. Although a genetic association or alterations in frequencies have been reported, the pathomechanistic roles of 5) HLA-DRB1*11 (whether antigen [Ag] presentation or intracellular function) or 6) invariant NKT (iNKT) and 7) CD4+ T cells in disease progression are yet largely unclear. Thus, current data imply that innately adaptive immune cells bridging innate and adaptive immunity rather than classic B or T lymphocytes play a central role in promoting disease progression in systemic JIA.

be explained by the recruitment of cells from the peripheral circulation to sites of inflammation (11,62). Immunologic changes in both cell subsets have been identified to be a primary predictor of JIA (9). The γδ T cells, but not Th17 lymphocytes, from patients with systemic JIA express increased levels of IL-17, which cor-

roborates findings in a murine model of systemic JIA (64). Importantly, IL-1β is critically involved in IL-17 expression from both γδ T and iNKT cells (11,65,66). In this context, it is noteworthy that mice lacking endogenous IL-1Ra expression develop spontaneous IL-17–driven arthritis (67,68). In this model, γδ T cells serve as

a main source of IL-17 in inflamed joints, but require CD4+ T cells for tissue homing (69). Concurrent reduction in circulating γδ T and IL-17/IFNγ double-expressing CD4+ T cells in patients with systemic JIA experiencing a flare compared to patients with disease in remission or healthy controls (11) may indicate that this observation is also relevant in humans. Once it occurs in the joint, inflammatory Th cell activation can occur independent of conventional TCR signaling (70). Thinking along such lines may also explain recent findings in patients with oligoarticular or polyarticular JIA, in whom an IL-17 signature in synovial fluid is driven by a whole potpourri of contributors comprising γδ T lymphocytes and receptor-negative innate lymphoid cells, but also CD4+ and CD8+ lymphocytes (71).

Importantly, γδ T cell expansion, but also iNKT cell activation, can be driven by IL-18. Both cell types, in contrast to CD4+ T cells, express high levels of IL-18R (11,65,72). It has been demonstrated in both humans (35) and mice (34) that type I IFN signaling is associated with the production of IL-18. Thus, it can be speculated that tilting the IL-1/type I IFN balance toward increasing IFN signaling in response to IL-1 blockade (19,42) may benefit IL-18–associated effects on innate and adaptive immune cells. Indeed, full restoration of the type I IFN/IL-1 balance inhibits autoimmunity in NOD mice (73).

Last, S100 proteins may also play a central role in this context. While IL-1, IL-6, and IL-18 may certainly be the main autoinflammation–related effector molecules promoting adaptive immune cell differentiation and activation in systemic JIA, these effector cytokines are part of an S100 protein–induced sterile inflammatory environment that promotes Th17 (74) and γδ T17 cell (11) development or directly induces autoreactive IL-17–expressing CD8+ T cells (75).

Adaptive immunity in other autoinflammatory disease: fact or fake news?

Key pathophysiologic features of monogenic and polygenic autoinflammatory diseases are either inflammasome dysregulation leading to uncontrolled IL-1 and/or IL-18 release or molecular defects resulting in altered type I IFN responses. While involvement of innate immune mechanisms in B cell– and T cell–driven autoimmunity is well accepted, the fate of these adaptive immune cells in autoinflammation and related cytokine expression seems, apart from in systemic JIA, far less clear or investigated.

About a decade ago, 2 seminal reports were published back-to-back in a single issue of *Immunity* (76,77). A study of 2 mutant *Nlrp3*-knockin mouse strains modeling CAPS showed that the systemic inflammatory phenotype required an intact inflammasome but was only partially dependent on IL-1β and was independent of T cells (77). The second study suggested that a mutation in the *Nlrp3* gene leading to murine CAPS resulted in massive IL-1β production, augmenting Th17 differentiation and resulting in a Th17 cytokine–dominant immune response. The authors reasoned that the investigated *Nlrp3* mutation results in inflammasome hyper-

activation and consequently, Th17-mediated immunopathology in autoinflammation (76). Corresponding to these murine data, untreated CAPS patients have elevated serum IL-17 levels and increased Th17 cell numbers compared to healthy controls (78). Both were reversed in response to anti–IL-1 treatment. Similarly, TLR stimulation of monocyte-derived dendritic cells from CAPS patients triggered enhanced secretion of IL-1β and IL-23, which normalized after the introduction of anti–IL-1 treatment, suggesting a central role of IL-1β in Th17 differentiation in human inflammatory conditions (78). Recent data on the IL-1/IL-23–induced differentiation and activation of human T cells even in the absence of TCR engagement or costimulatory signals support this notion (53,70).

Elevated serum IL-17 levels and increased numbers of Th17 cells also occur in patients with FMF. Part of the increased secretion of IL-17 was shown to be related to the deleterious homozygous *MEFV* p.M694V genotype (79). Another study suggested Th1 polarization in FMF patients, which could be driven by elevated IL-12 and IL-18 levels in FMF patient serum (80). Finally, in Schnitzler syndrome, a polygenic autoinflammatory condition in adults, systemic overproduction of IL-1β translates into a profound loss of antiinflammatory Th17 cell functionalities, which can be reversed by IL-1–blocking treatment (56).

From autoinflammation to autoimmunity: Is there something unique about systemic JIA?

Evidence of the activation of innately or classic adaptive immune cells in autoinflammatory diseases apart from systemic JIA is scarce, albeit the cytokine environment and pathologically activated innate immune cells should have full potential to prime and activate lymphocytes. Thus, it is worth exploring whether specific mechanisms that can either promote or counteract "spillover" of inflammation may be uniquely involved in the pathogenesis of systemic JIA.

The immunoregulatory cytokine IL-10 can limit both the duration and the intensity of PRR signaling in innate immune cells, which also affects inflammasome-dependent IL-1 and IL-18 release (81). Indeed, IL-10 regulates the inflammasome-driven augmentation of inflammatory arthritis and joint destruction (82). In fact, 2 independent studies in systemic JIA cohorts showed increased prevalence of *IL10* promoter haplotypes that encode for low IL-10 expression (83,84). Recently, cell-specific IL-10 defects were observed in patients with systemic JIA and in a murine disease model, resulting in insufficient IL-10 production to counterbalance proinflammatory cytokines (85).

While the relevance of decreased IL-10 expression due to genetic variations can be debated, since recent single-nucleotide polymorphism genotype data from the 9 case–control populations of the International Childhood Arthritis Genetics systemic JIA collection could not reproduce this association (86), data on IFNγ as another potential regulatory factor in systemic JIA appear more consistent. Reduced serum and plasma levels

of IFNγ and CXCL9, a surrogate for IFNγ signaling, have been described in systemic JIA compared to healthy controls (11,87), and decreased IFNγ-induced transcriptional signatures in systemic JIA monocytes have been reported (19,88), suggesting limited in vivo IFNγ exposure. Defective IFNγ release has been observed in NK cells from patients with systemic JIA (87,89), while Th1 cells, although increased in numbers in the peripheral blood of patients with active disease (10,11), show a notable decrease in intracellular IFNγ expression, which is partly corrected in response to IL-1 blockade (11). Furthermore, mice deficient in IFNγ develop systemic JIA–like disease in response to inflammatory challenge with Freund's complete adjuvant (64,87). Surprisingly, iNKT cells from IFNγ$^{-/-}$ animals promote arthritis rather than protect against inflammation (90). Similarly, iNKT cells in rheumatoid arthritis synovial fluid have been shown to express only low levels of IFNγ (90), consistent with the hypothesis that active arthritis is correlated with a decreased cellular ability to produce this cytokine. Thus, aberrantly low IFNγ levels in concert with a dysbalanced innate immune cell–derived proinflammatory cytokine environment in systemic JIA may contribute to the progression to an autoimmune phenotype with a prominent role for IL-17 (91) (Figure 2). As no such findings have yet been reported for other autoinflammatory conditions, this may indeed be unique to systemic JIA.

To date, the dichotomy of this very limited role of IFNγ in the arthritis of systemic JIA, compared to its prominent role in MAS, is not understood. MAS develops in ~10–20% of patients with systemic JIA and resembles a severe hyperinflammatory condition characterized by a catastrophic cytokine storm resulting in multiple organ failure and high mortality (for review, see ref. 36). In contrast to systemic JIA, IFNγ as well as IFNγ-induced chemokines are markedly elevated during MAS (92), and IFNγ neutralization can revert clinical and laboratory features of MAS in a preclinical murine model (93). Furthermore, in a pilot open-label single-arm international study (ClinicalTrials.gov identifier: NCT03311854), therapeutic IFNγ neutralization proved effective in controlling MAS (94). What causes low IFNγ expression during active systemic JIA and whether a disturbed IL-18/IFNγ axis can set the stage for fulminant IFNγ expression and signaling during MAS are intriguing questions for future research.

Getting it right for patients: translating molecular complexity into therapeutic strategies

In the absence of formally approved drugs for the treatment of the majority of (ultra)rare autoinflammatory or autoimmune diseases, there is no shortage of recommendations for the treatment of more common polygenic chronic inflammatory diseases. In the current "treat-to-target" era, medical care focuses on the achievement of remission or low disease activity (95,96).

However, in many patients with systemic JIA, treatment responses could be better if effective therapies were established earlier. Precise definition of relevant subgroups and introduction

of tailored preventative strategies and/or treatments are the most important and pressing challenges for translational research. Understanding inflammatory mechanisms that drive autoimmunity, especially during early disease progression, gave rise to the "window of opportunity" paradigm (12). This strategy promises the potential to prevent the onset of clinically manifest chronic autoimmune/inflammatory disease in susceptible individuals. Moreover, future use of biologic signatures to steer treat-to-target therapies based on the involvement of autoinflammation and/or autoimmunity will allow for disease phenotype– and/or stage-specific individualized precision medicine. Finally, predictive (demographic, clinical, genetic, serologic, etc.) markers may allow for early intervention in susceptible individuals that can prevent the development of chronic autoimmune/inflammatory disease. However, finding the right balance between overtreatment and undertreatment means moving along very thin lines. Without doubt, getting it right for the patient will only be possible if we break down dogmatic barriers dividing immune dysregulation underlying inflammatory disease into antipodes of autoimmunity or autoinflammation. Potentially, innately adaptive cell populations and the molecules involved in their complex interplay with both innate and adaptive immunity should be considered for molecular characterization of disease stages and patient subpopulations, and they may even offer attractive targets for future therapies.

AUTHOR CONTRIBUTIONS

All authors drafted the article, revised it critically for important intellectual content, and approved the final version to be published.

REFERENCES

1. McDermott MF, Aksentijevich I, Galon J, McDermott EM, Ogunkolade BW, Centola M, et al. Germline mutations in the extracellular domains of the 55 kDa TNF receptor, TNFR1, define a family of dominantly inherited autoinflammatory syndromes. Cell 1999;97: 133–44.

2. Manthiram K, Zhou Q, Aksentijevich I, Kastner DL. The monogenic autoinflammatory diseases define new pathways in human innate immunity and inflammation. Nat Immunol 2017;18:832–42.

3. Pardeo M, Bracaglia C, De Benedetti F. Systemic juvenile idiopathic arthritis: new insights into pathogenesis and cytokine directed therapies. Best Pract Res Clin Rheumatol 2017;31:505–16.

4. Nirmala N, Brachat A, Feist E, Blank N, Specker C, Witt M, et al. Gene-expression analysis of adult-onset Still's disease and systemic juvenile idiopathic arthritis is consistent with a continuum of a single disease entity. Pediatr Rheumatol Online J 2015;13:50.

5. Petty RE, Southwood TR, Manners P, Baum J, Glass DN, Goldenberg J, et al. International League of Associations for Rheumatology classification of juvenile idiopathic arthritis: second revision, Edmonton, 2001. J Rheumatol 2004;31:390–2.

6. Ombrello MJ, Arthur VL, Remmers EF, Hinks A, Tachmazidou I, Grom AA, et al. Genetic architecture distinguishes systemic juvenile idiopathic arthritis from other forms of juvenile idiopathic arthritis: clinical and therapeutic implications. Ann Rheum Dis 2017;76: 906–13.

7. Kimura Y, Weiss JE, Haroldson KL, Lee T, Punaro M, Oliveira S, et al. Pulmonary hypertension and other potentially fatal pulmonary

complications in systemic juvenile idiopathic arthritis. Arthritis Care Res (Hoboken) 2013;65:745–52.

8. Ombrello MJ, Remmers EF, Tachmazidou I, Grom A, Foell D, Haas JP, et al, and the International Childhood Arthritis Genetics (INCHARGE) Consortium. HLA-DRB1*11 and variants of the MHC class II locus are strong risk factors for systemic juvenile idiopathic arthritis. Proc Natl Acad Sci U S A 2015;112:15970–5.

9. Van Nieuwenhove E, Lagou V, Van Eyck L, Dooley J, Bodenhofer U, Roca C, et al. Machine learning identifies an immunological pattern associated with multiple juvenile idiopathic arthritis subtypes. Ann Rheum Dis 2019;78:617–28.

10. Omoyinmi E, Hamaoui R, Pesenacker A, Nistala K, Moncrieffe H, Ursu S, et al. Th1 and Th17 cell subpopulations are enriched in the peripheral blood of patients with systemic juvenile idiopathic arthritis. Rheumatology (Oxford) 2012;51:1881–6.

11. Kessel C, Lippitz K, Weinhage T, Hinze C, Wittkowski H, Holzinger D, et al. Proinflammatory cytokine environments can drive interleukin-17 overexpression by γ/δ T cells in systemic juvenile idiopathic arthritis. Arthritis Rheumatol 2017;69:1480–94.

12. Nigrovic PA. Is there a window of opportunity for treatment of systemic juvenile idiopathic arthritis? [review]. Arthritis Rheumatol 2014;66:1405–13.

13. Nigrovic PA. Autoinflammation and autoimmunity in systemic juvenile idiopathic arthritis. Proc Natl Acad Sci U S A 2015;112:15785–6.

14. Pascual V, Allantaz F, Arce E, Punaro M, Bancereau J. Role of interleukin-1 (IL-1) in the pathogenesis of systemic onset juvenile idiopathic arthritis and clinical response to IL-1 blockade. J Exp Med 2005;201:1479–86.

15. Nigrovic PA, Mannion M, Prince FH, Zeft A, Rabinovich CE, van Rossum MA, et al. Anakinra as first-line disease-modifying therapy in systemic juvenile idiopathic arthritis: report of forty-six patients from an international multicenter series. Arthritis Rheum 2011;63:545–55.

16. Vastert SJ, de Jager W, Noordman BJ, Holzinger D, Kuis W, Prakken BJ, et al. Effectiveness of first-line treatment with recombinant interleukin-1 receptor antagonist in steroid-naive patients with new-onset systemic juvenile idiopathic arthritis: results of a prospective cohort study. Arthritis Rheumatol 2014;66:1034–43.

17. Ter Haar NM, van Dijkhuizen EH, Swart JF, van Royen-Kerkhof A, el Idrissi A, Leek AP, et al. Treatment to target using recombinant interleukin-1 receptor antagonist as first-line monotherapy in new-onset systemic juvenile idiopathic arthritis: results from a five-year follow-up study. Arthritis Rheumatol 2019;71:1163–73.

18. Gattorno M, Piccini A, Lasigliè D, Tassi S, Brisca G, Carta S, et al. The pattern of response to anti–interleukin-1 treatment distinguishes two subsets of patients with systemic-onset juvenile idiopathic arthritis. Arthritis Rheum 2008;58:1505–15.

19. Quartier P, Allantaz F, Cimaz R, Pillet P, Messiaen C, Bardin C, et al. A multicentre, randomised, double-blind, placebo-controlled trial with the interleukin-1 receptor antagonist anakinra in patients with systemic-onset juvenile idiopathic arthritis (ANAJIS trial). Ann Rheum Dis 2011;70:747–54.

20. De Benedetti F, Brunner HI, Ruperto N, Kenwright A, Wright S, Calvo I, et al. Randomized trial of tocilizumab in systemic juvenile idiopathic arthritis. N Engl J Med 2012;367:2385–95.

21. Shaw PJ, McDermott MF, Kanneganti TD. Inflammasomes and autoimmunity. Trends Mol Med 2011;17:57–64.

22. Man SM, Karki R, Kanneganti TD. Molecular mechanisms and functions of pyroptosis, inflammatory caspases and inflammasomes in infectious diseases. Immunol Rev 2017;277:61–75.

23. Evavold CL, Ruan J, Tan Y, Xia S, Wu H, Kagan JC. The pore-forming protein gasdermin D regulates interleukin-1 secretion from living macrophages. Immunity 2018;48:35–44.

24. Van Gorp H, Saavedra PH, de Vasconcelos NM, Van Opdenbosch N, Vande Walle L, Matusiak M, et al. Familial Mediterranean fever mutations lift the obligatory requirement for microtubules in Pyrin inflammasome activation. Proc Natl Acad Sci U S A 2016;113:14384–9.

25. Cepika AM, Banchereau R, Segura E, Ohouo M, Cantarel B, Goller K, et al. A multidimensional blood stimulation assay reveals immune alterations underlying systemic juvenile idiopathic arthritis. J Exp Med 2017;214:3449–66.

26. Macaubas C, Nguyen KD, Peck A, Buckingham J, Deshpande C, Wong E, et al. Alternative activation in systemic juvenile idiopathic arthritis monocytes. Clin Immunol 2012;142:362–72.

27. Brown RA, Henderlight M, Do T, Yasin S, Grom AA, DeLay M, et al. Neutrophils from children with systemic juvenile idiopathic arthritis exhibit persistent proinflammatory activation despite long-standing clinically inactive disease. Front Immunol 2018;9:2995.

28. Ter Haar NM, Tak T, Mokry M, Scholman RC, Meerding JM, de Jager W, et al. Reversal of sepsis-like features of neutrophils by interleukin-1 blockade in patients with systemic-onset juvenile idiopathic arthritis. Arthritis Rheumatol 2018;70:943–56.

29. Shimizu M, Nakagishi Y, Inoue N, Mizuta M, Ko G, Saikawa Y, et al. Interleukin-18 for predicting the development of macrophage activation syndrome in systemic juvenile idiopathic arthritis. Clin Immunol 2015;160:277–81.

30. De Jager W, Hoppenreijs EP, Wulffraat NM, Wedderburn LR, Kuis W, Prakken BJ. Blood and synovial fluid cytokine signatures in patients with juvenile idiopathic arthritis: a cross-sectional study. Ann Rheum Dis 2007;66:589–98.

31. Weiss ES, Girard-Guyonvarc'h C, Holzinger D, de Jesus AA, Tariq Z, Picarsic J, et al. Interleukin-18 diagnostically distinguishes and pathogenically promotes human and murine macrophage activation syndrome. Blood 2018;131:1442–55.

32. Girard-Guyonvarc'h C, Palomo J, Martin P, Rodriguez E, Troccaz S, Palmer G, et al. Unopposed IL-18 signaling leads to severe TLR9-induced macrophage activation syndrome in mice. Blood 2018;131:1430–41.

33. Dinarello CA. Overview of the IL-1 family in innate inflammation and acquired immunity. Immunol Rev 2018;281:8–27.

34. Zhu Q, Kanneganti TD. Distinct regulatory mechanisms control proinflammatory cytokines IL-18 and IL-1β. J Immunol 2017;198:4210–5.

35. Verweyen E, Holzinger D, Weinhage T, Hinze C, Wittkowski H, Pickkers P, et al. Synergistic TLR/IFNα/β-signaling facilitates escape of IL-18 expression from endotoxin tolerance. Am J Respir Crit Care Med 2019. E-pub ahead of print.

36. Grom AA, Horne A, De Benedetti F. Macrophage activation syndrome in the era of biologic therapy [review]. Nat Rev Rheumatol 2016;12:259–68.

37. Swiecki M, Colonna M. The multifaceted biology of plasmacytoid dendritic cells. Nat Rev Immunol 2015;15:471–85.

38. Banchereau R, Cepika AM, Banchereau J, Pascual V. Understanding human autoimmunity and autoinflammation through transcriptomics. Annu Rev Immunol 2017;35:337–70.

39. Sun L, Wu J, Du F, Chen X, Chen ZJ. Cyclic GMP-AMP synthase is a cytosolic DNA sensor that activates the type I interferon pathway. Science 2013;339:786–91.

40. Wu J, Sun L, Chen X, Du F, Shi H, Chen C, et al. Cyclic GMP-AMP is an endogenous second messenger in innate immune signaling by cytosolic DNA. Science 2013;339:826–30.

41. Rodero MP, Decalf J, Bondet V, Hunt D, Rice GI, Werneke S, et al. Detection of interferon α protein reveals differential levels and cellular sources in disease. J Exp Med 2017;214:1547–55.

42. Rice GI, Melki I, Frémond ML, Briggs TA, Rodero MP, Kitabayashi N, et al. Assessment of type I interferon signaling in pediatric inflammatory disease. J Clin Immunol 2017;37:123–32.

43. Macaubas C, Wong E, Zhang Y, Nguyen KD, Lee J, Milojevic D, et al. Altered signaling in systemic juvenile idiopathic arthritis monocytes. Clin Immunol 2016;163:66–74.

44. Mayer-Barber KD, Yan B. Clash of the cytokine titans: counter-regulation of interleukin-1 and type I interferon-mediated inflammatory responses. Cell Mol Immunol 2017;14:22–35.

45. Conrad C, Di Domizio J, Mylonas A, Belkhodja C, Demaria O, Navarini A, et al. Paradoxical psoriasis—unabated type I IFN production induced by TNF blockade [abstract]. Cytokine 2015;76:66.

46. Palucka AK, Blanck JP, Bennett L, Pascual V, Banchereau J. Cross-regulation of TNF and IFN-α in autoimmune diseases. Proc Natl Acad Sci U S A 2005;102:3372–7.

47. Kessel C, Holzinger D, Foell D. Phagocyte-derived S100 proteins in autoinflammation: putative role in pathogenesis and usefulness as biomarkers [review]. Clin Immunol 2013;147:229–41.

48. Kessel C, Fuehner S, Zell J, Zimmermann B, Drewianka S, Brockmeyer S, et al. Calcium and zinc tune autoinflammatory Toll-like receptor 4 signaling by S100A12 [letter]. J Allergy Clin Immunol 2018;142:1370–3.

49. Vogl T, Stratis A, Wixler V, Völler T, Thurainayagam S, Jorch SK, et al. Autoinhibitory regulation of S100A8/S100A9 alarmin activity locally restricts sterile inflammation. J Clin Invest 2018;128:1852–66.

50. Frosch M, Ahlmann M, Vogl T, Wittkowski H, Wulffraat N, Foell D, et al. The myeloid-related proteins 8 and 14 complex, a novel ligand of Toll-like receptor 4, and interleukin-1β form a positive feedback mechanism in systemic-onset juvenile idiopathic arthritis. Arthritis Rheum 2009;60:883–91.

51. Nakamura K, Okamura H, Wada M, Nagata K, Tamura T. Endotoxin-induced serum factor that stimulates γ interferon production. Infect Immun 1989;57:590–5.

52. Blom L, Poulsen LK. IL-1 family members IL-18 and IL-33 upregulate the inflammatory potential of differentiated human Th1 and Th2 cultures. J Immunol 2012;189:4331–7.

53. Revu S, Wu J, Henkel M, Rittenhouse N, Menk A, Delgoffe GM, et al. IL-23 and IL-1β drive human Th17 cell differentiation and metabolic reprogramming in absence of CD28 costimulation. Cell Rep 2018;22:2642–53.

54. Uchiyama R, Yonehara S, Taniguchi S, Ishido S, Ishii KJ, Tsutsui H. Inflammasome and Fas-mediated IL-1β contributes to Th17/Th1 cell induction in pathogenic bacterial infection in vivo. J Immunol 2017;199:1122–30.

55. Zielinski CE, Mele F, Aschenbrenner D, Jarrossay D, Ronchi F, Gattorno M, et al. Pathogen-induced human TH17 cells produce IFN-γ or IL-10 and are regulated by IL-1β. Nature 2012;484:514–8.

56. Noster R, de Koning HD, Maier E, Prelog M, Lainka E, Zielinski CE. Dysregulation of proinflammatory versus anti-inflammatory human T_H17 cell functionalities in the autoinflammatory Schnitzler syndrome. J Allerg Clin Immunol 2016;138:1161–9.

57. Boniface K, Blom B, Liu YJ, de Waal Malefyt R. From interleukin-23 to T-helper 17 cells: human T-helper cell differentiation revisited. Immunol Rev 2008;226:132–46.

58. Jain A, Song R, Wakeland EK, Pasare C. T cell-intrinsic IL-1R signaling licenses effector cytokine production by memory CD4 T cells. Nat Commun 2018;9:3185.

59. Enoksson SL, Grasset EK, Hägglöf T, Mattsson N, Kaiser Y, Gabrielsson S, et al. The inflammatory cytokine IL-18 induces self-reactive innate antibody responses regulated by natural killer T cells. Proc Natl Acad Sci U S A 2011;108:E1399–407.

60. Chen DY, Chen YM, Lan JL, Lin CC, Chen HH, Hsieh CW. Potential role of Th17 cells in the pathogenesis of adult-onset Still's disease. Rheumatology (Oxford) 2010;49:2305–12.

61. Chen DY, Lan JL, Lin FJ, Hsieh TY, Wen MC. Predominance of Th1 cytokine in peripheral blood and pathological tissues of patients with active untreated adult onset Still's disease. Ann Rheum Dis 2004;63:1300–6.

62. Macaubas C, Nguyen K, Deshpande C, Phillips C, Peck A, Lee T, et al. Distribution of circulating cells in systemic juvenile idiopathic arthritis across disease activity states. Clin Immunol 2010;134:206–16.

63. Ferreira LM. γδ T cells: innately adaptive immune cells? Int Rev Immunol 2013;32:223–48.

64. Avau A, Mitera T, Put S, Put K, Brisse E, Filtjens J, et al. Systemic juvenile idiopathic arthritis–like syndrome in mice following stimulation of the immune system with Freund's complete adjuvant: regulation by interferon-γ. Arthritis Rheumatol 2014;66:1340–51.

65. Lalor SJ, Dungan LS, Sutton CE, Basdeo SA, Fletcher JM, Mills KH. Caspase-1-processed cytokines IL-1β and IL-18 promote IL-17 production by γδ and CD4 T cells that mediate autoimmunity. J Immunol 2011;186:5738–48.

66. Moreira-Teixeira L, Resende M, Coffre M, Devergne O, Herbeuval JP, Hermine O, et al. Proinflammatory environment dictates the IL-17-producing capacity of human invariant NKT cells. J Immunol 2011;186:5758–65.

67. Horai R, Nakajima A, Habiro K, Kotani M, Nakae S, Matsuki T, et al. TNF-α is crucial for the development of autoimmune arthritis in IL-1 receptor antagonist-deficient mice. J Clin Invest 2004;114:1603–11.

68. Ikeda S, Saijo S, Murayama MA, Shimizu K, Akitsu A, Iwakura Y. Excess IL-1 signaling enhances the development of Th17 cells by downregulating TGF-β-induced Foxp3 expression. J Immunol 2014;192:1449–58.

69. Akitsu A, Ishigame H, Kakuta S, Chung SH, Ikeda S, Shimizu K, et al. IL-1 receptor antagonist-deficient mice develop autoimmune arthritis due to intrinsic activation of IL-17-producing CCR68(+)Vγ6(+)γδ T cells. Nat Commun 2015;6:7464.

70. Ferguson ID, Griffin P, Michel JJ, Yano H, Gaffen SL, Mueller RG, et al. T cell receptor-independent, CD31/IL-17A-driven inflammatory axis shapes synovitis in juvenile idiopathic arthritis. Front Immunol 2018;9:1802.

71. Rosser EC, Lom H, Bending D, Duurland CL, Bajaj-Elliott M, Wedderburn LR. Innate lymphoid cells and T cells contribute to the interleukin-17A signature detected in the synovial fluid of patients with juvenile idiopathic arthritis. Arthritis Rheumatol 2019;71:460–7.

72. Lind SM, Kuylenstierna C, Moll M, Jordö ED, Winqvist O, Lundeberg L, et al. IL-18 skews the invariant NKT-cell population via autoreactive activation in atopic eczema. Eur J Immunol 2009;39:2293–301.

73. Rahman MJ, Rodrigues KB, Quiel JA, Liu Y, Bhargava V, Zhao Y, et al. Restoration of the type I IFN-IL-1 balance through targeted blockade of PTGER4 inhibits autoimmunity in NOD mice. JCI Insight 2018;3:97843.

74. Reinhardt K, Foell D, Vogl T, Mezger M, Wittkowski H, Fend F, et al. Monocyte-induced development of Th17 cells and the release of S100 proteins are involved in the pathogenesis of graft-versus-host disease. J Immunol 2014;193:3355–65.

75. Loser K, Vogl T, Voskort M, Lueken A, Kupas V, Nacken W, et al. The Toll-like receptor 4 ligands Mrp8 and Mrp14 are crucial in the development of autoreactive CD8+ T cells. Nat Med 2010;16:713–7.

76. Meng G, Zhang F, Fuss I, Kitani A, Strober W. A mutation in the Nlrp3 gene causing inflammasome hyperactivation potentiates Th17 cell-dominant immune responses. Immunity 2009;30:860–74.

77. Brydges SD, Mueller JL, McGeough MD, Pena CA, Misaghi A, Gandhi C, et al. Inflammasome-mediated disease animal models reveal roles for innate but not adaptive immunity. Immunity 2009;30:875–87.

78. Lasigliè D, Traggiai E, Federici S, Alessio M, Buoncompagni A, Accogli A, et al. Role of IL-1 β in the development of human T(H)17 cells: lesson from NLPR3 mutated patients. PLoS One 2011;6:e20014.

79. Ovadia A, Livneh A, Feld O, Ben-Zvi I, Kukuy E, Kivity S, et al. T helper 17 polarization in familial Mediterranean fever. Genes Immun 2013;14:212–6.

80. Simsek I, Pay S, Pekel A, Dinc A, Musabak U, Erdem H, et al. Serum proinflammatory cytokines directing T helper 1 polarization in patients with familial Mediterranean fever. Rheumatol Int 2007;27:807–11.

81. Gurung P, Li B, Subbarao Malireddi RK, Lamkanfi M, Geiger TL, Kanneganti TD. Chronic TLR stimulation controls NLRP3 inflammasome activation through IL-10 mediated regulation of NLRP3 expression and caspase-8 activation. Sci Rep 2015;5:14488.

82. Greenhill CJ, Jones GW, Nowell MA, Newton Z, Harvey AK, Moideen AN, et al. Interleukin-10 regulates the inflammasome-driven augmentation of inflammatory arthritis and joint destruction. Arthritis Res Ther 2014;16:419.

83. Fife MS, Gutierrez A, Ogilvie EM, Stock CJ, Samuel JM, Thomson W, et al. Novel IL10 gene family associations with systemic juvenile idiopathic arthritis. Arthritis Res Ther 2006;8:R148.

84. Moller JC, Paul D, Ganser G, Range U, Gahr M, Kelsch R, et al. IL10 promoter polymorphisms are associated with systemic onset juvenile idiopathic arthritis (SoJIA). Clin Exp Rheumatol 2010;28:912–8.

85. Imbrechts M, Avau A, Vandenhaute J, Malengier-Devlies B, Put K, Mitera T, et al. Insufficient IL-10 production as a mechanism underlying the pathogenesis of systemic juvenile idiopathic arthritis. J Immunol 2018;201:2654–63.

86. Arthur VL, Shuldiner E, Remmers EF, Hinks A, Grom AA, Foell D, et al. IL1RN variation influences both disease susceptibility and response to recombinant human interleukin-1 receptor antagonist therapy in systemic juvenile idiopathic arthritis. Arthritis Rheumatol 2018;70:1319–30.

87. Put K, Vandenhaute J, Avau A, van Nieuwenhuijze A, Brisse E, Dierckx T, et al. Inflammatory gene expression profile and defective interferon-γ and granzyme K in natural killer cells from systemic juvenile idiopathic arthritis patients. Arthritis Rheumatol 2017;69:213–24.

88. Sikora KA, Fall N, Thornton S, Grom AA. The limited role of interferon-γ in systemic juvenile idiopathic arthritis cannot be explained by cellular hyporesponsiveness. Arthritis Rheum 2012;64:3799–808.

89. De Jager W, Vastert SJ, Beekman JM, Wulffraat NM, Kuis W, Coffer PJ, et al. Defective phosphorylation of interleukin-18 receptor β causes impaired natural killer cell function in systemic-onset juvenile idiopathic arthritis. Arthritis Rheum 2009;60:2782–93.

90. Zhao M, Svensson MN, Venken K, Chawla A, Liang S, Engel I, et al. Altered thymic differentiation and modulation of arthritis by invariant NKT cells expressing mutant ZAP70. Nat Commun 2018;9:2627.

91. Liu L, Okada S, Kong XF, Kreins AY, Cypowyj S, Abhyankar A, et al. Gain-of-function human STAT1 mutations impair IL-17 immunity and underlie chronic mucocutaneous candidiasis. J Exp Med 2011;208:1635–48.

92. Bracaglia C, de Graaf K, Pires Marafon D, Guilhot F, Ferlin W, Prencipe G, et al. Elevated circulating levels of interferon-γ and interferon-γ-induced chemokines characterise patients with macrophage activation syndrome complicating systemic juvenile idiopathic arthritis. Ann Rheum Dis 2017;76:166–72.

93. Prencipe G, Caiello I, Pascarella A, Grom AA, Bracaglia C, Chatel L, et al. Neutralization of IFN-γ reverts clinical and laboratory features in a mouse model of macrophage activation syndrome. J Allergy Clin Immunol 2018;141:1439–49.

94. De Benedetti F, Brogan P, Grom A, Quartier P, Schneider R, De Graaf K, et al. Emapalumab, an interferon γ (Ifn-Y)-blocking monoclonal antibody, in patients with macrophage activation syndrome (MAS) complicating systemic juvenile idiopathic arthritis (SJIA) [abstract]. Ann Rheum Dis 2019;78 Suppl 2:178.

95. Ravelli A, Consolaro A, Horneff G, Laxer RM, Lovell DJ, Wulffraat NM, et al. Treating juvenile idiopathic arthritis to target: recommendations of an international task force. Ann Rheum Dis 2018;77:819–28.

96. Smolen JS. Treat-to-target as an approach in inflammatory arthritis. Curr Opin Rheumatol 2016;28:297–302.

AMERICAN COLLEGE
of RHEUMATOLOGY
Empowering Rheumatology Professionals

2019 American College of Rheumatology/Arthritis Foundation Guideline for the Management of Osteoarthritis of the Hand, Hip, and Knee

Sharon L. Kolasinski,[1] Tuhina Neogi,[2] Marc C. Hochberg,[3] Carol Oatis,[4] Gordon Guyatt,[5] Joel Block,[6] Leigh Callahan,[7] Cindy Copenhaver,[8] Carole Dodge,[9] David Felson,[2] Kathleen Gellar,[10] William F. Harvey,[11] Gillian Hawker,[12] Edward Herzig,[13] C. Kent Kwoh,[14] Amanda E. Nelson,[7] (iD) Jonathan Samuels,[15] Carla Scanzello,[1] Daniel White,[16] Barton Wise,[17] Roy D. Altman,[18] Dana DiRenzo,[19] (iD) Joann Fontanarosa,[20] Gina Giradi,[20] Mariko Ishimori,[21] Devyani Misra,[2] Amit Aakash Shah,[22] Anna K. Shmagel,[23] Louise M. Thoma,[7] Marat Turgunbaev,[22] Amy S. Turner,[22] and James Reston[20]

Objective. To develop an evidence-based guideline for the comprehensive management of osteoarthritis (OA) as a collaboration between the American College of Rheumatology (ACR) and the Arthritis Foundation, updating the 2012 ACR recommendations for the management of hand, hip, and knee OA.

Methods. We identified clinically relevant population, intervention, comparator, outcomes questions and critical outcomes in OA. A Literature Review Team performed a systematic literature review to summarize evidence supporting the benefits and harms of available educational, behavioral, psychosocial, physical, mind-body, and pharmacologic therapies for OA. Grading of Recommendations Assessment, Development and Evaluation methodology was used to rate the quality of the evidence. A Voting Panel, including rheumatologists, an internist, physical and occupational therapists, and patients, achieved consensus on the recommendations.

Results. Based on the available evidence, either strong or conditional recommendations were made for or against the approaches evaluated. Strong recommendations were made for exercise, weight loss in patients with knee and/or hip OA who are overweight or obese, self-efficacy and self-management programs, tai chi, cane use, hand orthoses for first carpometacarpal (CMC) joint OA, tibiofemoral bracing for tibiofemoral knee OA, topical nonsteroidal antiinflammatory drugs (NSAIDs) for knee OA, oral NSAIDs, and intraarticular glucocorticoid injections for knee OA. Conditional recommendations were made for balance exercises, yoga, cognitive behavioral therapy, kinesiotaping for first CMC OA, orthoses for hand joints other than the first CMC joint, patellofemoral bracing for patellofemoral knee OA, acupuncture, thermal modalities, radiofrequency ablation for knee OA, topical NSAIDs, intraarticular steroid injections and chondroitin sulfate for hand OA, topical capsaicin for knee OA, acetaminophen, duloxetine, and tramadol.

Conclusion. This guideline provides direction for clinicians and patients making treatment decisions for the management of OA. Clinicians and patients should engage in shared decision-making that accounts for patients' values, preferences, and comorbidities. These recommendations should not be used to limit or deny access to therapies.

INTRODUCTION

Osteoarthritis (OA) is the most common form of arthritis, affecting an estimated 302 million people worldwide (1–5), and is a leading cause of disability among older adults. The knees, hips, and hands are the most commonly affected appendicular joints. OA is characterized by pathology involving the whole joint, including cartilage degradation, bone remodeling, osteophyte formation, and synovial inflammation, leading to pain, stiffness, swelling, and loss of normal joint function.

As OA spans decades of a patient's life, patients with OA are likely to be treated with a number of different pharmaceutical and nonpharmaceutical interventions, often in combination. This report provides recommendations to guide patients and clinicians in choosing among the available treatments. Certain principles of management apply to all patients with OA (see Comprehensive Management of OA below and Figure 1). Some recommendations are specific to a particular joint (e.g., hip, knee, patellofemoral joint, first carpometacarpal joint [CMC]) or particular patient populations (e.g., those with erosive OA).

METHODS

This guideline, from the American College of Rheumatology (ACR) and the Arthritis Foundation (AF), follows the ACR guideline development process (https://www.rheumatology.org/Practice-Quality/Clinical-Support/Clinical-Practice-Guidelines), using the Grading of Recommendations Assessment, Development and Evaluation (GRADE) methodology to rate the quality of the available evidence and to develop the recommendations (6). ACR

policy guided management of conflicts of interest and disclosures (https://www.rheumatology.org/Practice-Quality/Clinical-Support/Clinical-Practice-Guidelines/Osteoarthritis). A full description of the methods is presented in Supplementary Appendix 1 (on the *Arthritis & Rheumatology* web site at http://onlinelibrary.wiley.com/doi/10.1002/art.41142/abstract).

Briefly, this work involved 5 teams: 1) a Core Leadership Team that supervised and coordinated the project and drafted the clinical/population, intervention, comparator, outcomes (PICO) questions that served as the basis for the evidence report and manuscript; 2) a Literature Review Team that completed the literature screening and data abstraction and produced the Evidence Report (Supplementary Appendix 2, http://onlinelibrary.wiley.com/doi/10.1002/art.41142/abstract); 3) an Expert Panel that had input into scoping and clinical/PICO question development; 4) a Patient Panel; and 5) an interprofessional Voting Panel that included rheumatologists, an internist, physical and occupational therapists, and patients (Supplementary Appendix 3, http://onlinelibrary.wiley.com/doi/10.1002/art.41142/abstract).

This guideline included an initial literature review limited to English-language publications from inception of the databases to October 15, 2017, with updated searches conducted on August 1, 2018 and relevant papers included. Studies published after August 1, 2018 were not evaluated for this guideline. Supplementary Appendix 4 (http://onlinelibrary.wiley.com/doi/10.1002/art.41142/abstract) shows search terms used and databases reviewed, and Supplementary Appendix 5 (http://onlinelibrary.wiley.com/doi/10.1002/art.41142/abstract) highlights the study selection process. The guideline evidence base results from our own systematic review of randomized

[1]Sharon L. Kolasinski, MD, FACP, FACR, Carla Scanzello, MD: University of Pennsylvania School of Medicine, Philadelphia; [2]Tuhina Neogi, MD, PhD, FRCPC, David Felson, MD, MPH, Devyani Misra, MD, MSc: Boston University School of Medicine, Boston, Massachusetts; [3]Marc C. Hochberg, MD, MPH, MACP, MACR: University of Maryland School of Medicine and Veterans Affairs Maryland Health Care System, Baltimore; [4]Carol Oatis, PT, PhD: Arcadia University, Glenside, Pennsylvania; [5]Gordon Guyatt, MD, MSc: McMaster University, Hamilton, Ontario, Canada; [6]Joel Block, MD: Rush University Medical Center, Chicago, Illinois; [7]Leigh Callahan, PhD, Amanda E. Nelson, MD, MSCR, RhMSUS, Louise M. Thoma, PT, DPT, PhD: University of North Carolina School of Medicine, Chapel Hill; [8]Cindy Copenhaver, LMT: South Holland Recreational Services, University of Chicago, and Ingalls Memorial Hospital, Thornton, Illinois; [9]Carole Dodge, OT, CHT: University of Michigan Medical Center, Ann Arbor; [10]Kathleen Gellar: Watchung, New Jersey; [11]William F. Harvey, MD, MSc, FACR: Tufts Medical Center, Boston, Massachusetts; [12]Gillian Hawker, MD, MSc: University of Toronto, Toronto, Ontario, Canada; [13]Edward Herzig, MD: Fairfield, Ohio; [14]C. Kent Kwoh, MD: University of Arizona College of Medicine, Tucson; [15]Jonathan Samuels, MD: New York University Langone Medical Center, New York, New York; [16]Daniel White, PT, ScD: University of Delaware, Newark; [17]Barton Wise, MD, PhD: University of California, Davis, [18]Roy D. Altman, MD: Ronald Reagan UCLA Medical Center, Los Angeles, California; [19]Dana DiRenzo, MD: Johns Hopkins University School of Medicine, Baltimore, Maryland; [20]Joann Fontanarosa, PhD, Gina Giradi, James Reston, PhD, MPH: ECRI Institute, Plymouth Meeting, Pennsylvania; [21]Mariko Ishimori, MD: Cedars Sinai Medical Center, Los Angeles, California; [22]Amit Aakash Shah, MD, MPH, Marat Turgunbaev, MD, MPH, Amy S. Turner: American College of Rheumatology, Atlanta, Georgia; [23]Anna K. Shmagel, MD, MS: University of Minnesota, Minneapolis.

Figure 1. Recommended therapies for the management of osteoarthritis (OA). Strongly and conditionally recommended approaches to management of hand, knee, and/or hip OA are shown. No hierarchy within categories is implied in the figure, with the recognition that the various options may be used (and reused) at various times during the course of a particular patient's disease. * = Exercise for knee and hip OA could include walking, strengthening, neuromuscular training, and aquatic exercise, with no hierarchy of one over another. Exercise is associated with better outcomes when supervised. ** = Knee brace recommendations: tibiofemoral (TF) brace for TF OA (strongly recommended), patellofemoral (PF) brace for PF OA (conditionally recommended). *** = Hand orthosis recommendations: first carpometacarpal (CMC) joint neoprene or rigid orthoses for first CMC joint OA (strongly recommended), orthoses for joints of the hand other than the first CMC joint (conditionally recommended). RFA = radiofrequency ablation; NSAIDs = nonsteroidal antiinflammatory drugs; IA = intraarticular.

controlled trials (RCTs), rather than focusing on systematic reviews and meta-analyses published by others, as was done for the 2012 ACR recommendations for the use of nonpharmacologic and pharmacologic therapies in hand, hip, and knee OA (7). Systematic reviews of observational studies published by others were included if, in the opinion of the Voting Panel, they added critical information for the formulation of a recommendation: for example, related to adverse effects that may not be seen in shorter-duration RCTs. Subsequent updates of this guideline will consider studies included here and new RCTs published since completion of the literature review for the current publication.

Although RCTs are considered the gold standard for evaluation, a number of limitations of RCTs proved particularly important in the formulation of the final recommendations: possible publication bias (favoring publication of positive results), inadequate blinding, and inadequate provision of active comparators and appropriate sham alternatives. Further, short-duration RCTs cannot provide adequate prognostic information when applied to a complex disease such as OA, in which pathophysiologic processes are slowly progressive over decades.

We focused on management options that are available in the US and, for pharmacologic therapies, we additionally focused on agents that are available in pharmaceutical-grade formulations, thus eliminating most nutraceuticals. We limited our review to the English-language literature. We reviewed www.clinicaltrials.gov to identify phase 2 and 3 trials that may be far enough along to be US Food and Drug Administration (FDA)–approved and available by the time this guideline was published.

A hierarchy of outcome measures assessing pain and function in OA was developed based on the published literature (8,9). This hierarchy is detailed in Supplementary Appendix 1 (http://onlinelibrary.wiley.com/doi/10.1002/art.41142/abstract).

Using GRADE, a recommendation can be either in favor of or against the proposed intervention and either strong or conditional (10,11). The strength of the recommendation is based on a 70% consensus among the Voting Panel members. Much of the evidence proved indirect (did not specifically address the PICO question as written) and of low-to-moderate quality (12,13). The Voting Panel made *strong recommendations* when it inferred compelling evidence of efficacy and that benefits clearly outweighed harms and burdens. Thus, a strong recommendation means that the Voting Panel was confident that the desirable effects of following the recommendation outweigh potential undesirable effects (or vice versa), so the course of action would apply to all or almost all patients, and only a small proportion of patients would not want to follow the recommendation.

The Voting Panel made *conditional recommendations* when the quality of the evidence proved low or very low and/

or the balance of benefits versus harms and burdens was sufficiently close that shared decision-making between the patient and the clinician would be particularly important. Conditional recommendations are those for which the majority of informed patients would choose to follow the recommended course of action, but some would not (14,15). Thus, conditional recommendations are particularly value- and preference-sensitive and always warrant a full shared decision-making approach involving a complete and clear explication of benefits, harms, and burdens in language and in a context that patients understand (16). Where recommendations are made regarding a particular approach, details and references regarding that approach can be found in the Evidence Report (Supplementary Appendix 2, http://onlinelibrary.wiley.com/doi/10.1002/art.41142/abstract).

RESULTS/RECOMMENDATIONS

Comprehensive management of OA

A comprehensive plan for the management of OA in an individual patient may include educational, behavioral, psychosocial, and physical interventions, as well as topical, oral, and intraarticular medications. Recommendations assume appropriate application of physical, psychological, and/or pharmacologic therapies by an appropriate provider. Goals of management and principles for implementing those goals have broad applicability across patients. However, for some patients at some time points, a single physical, psychosocial, mind-body, or pharmacologic intervention may be adequate to control symptoms; for others, multiple interventions may be used in sequence or in combination. Which interventions and the order in which interventions are used will vary among patients. An overview of a general approach to management of OA is outlined in Figure 1 for recommended options, but no specific hierarchy of one option over another is implied other than on the basis of strength of the recommendation. Figure 2 summarizes the approaches that were not recommended.

Treatment decisions should take the personal beliefs and preferences of the patient, as well as the patient's medical status, into consideration. This guideline applies to patients with OA with no specific contraindications to the recommended therapies. However, each patient should be assessed for the presence of medical conditions, such as hypertension, cardiovascular disease, heart failure, gastrointestinal bleeding risk, chronic kidney disease, or other comorbidities, that might have an impact on their risk of side effects from certain pharmacologic agents, as well as injuries, disease severity, surgical history, and access to and availability of services (transportation, distance, ability to take time off work, cost, insurance coverage) that might have an impact on the choice of physical, psychological, and mind-body approaches. It is assumed that such an assessment
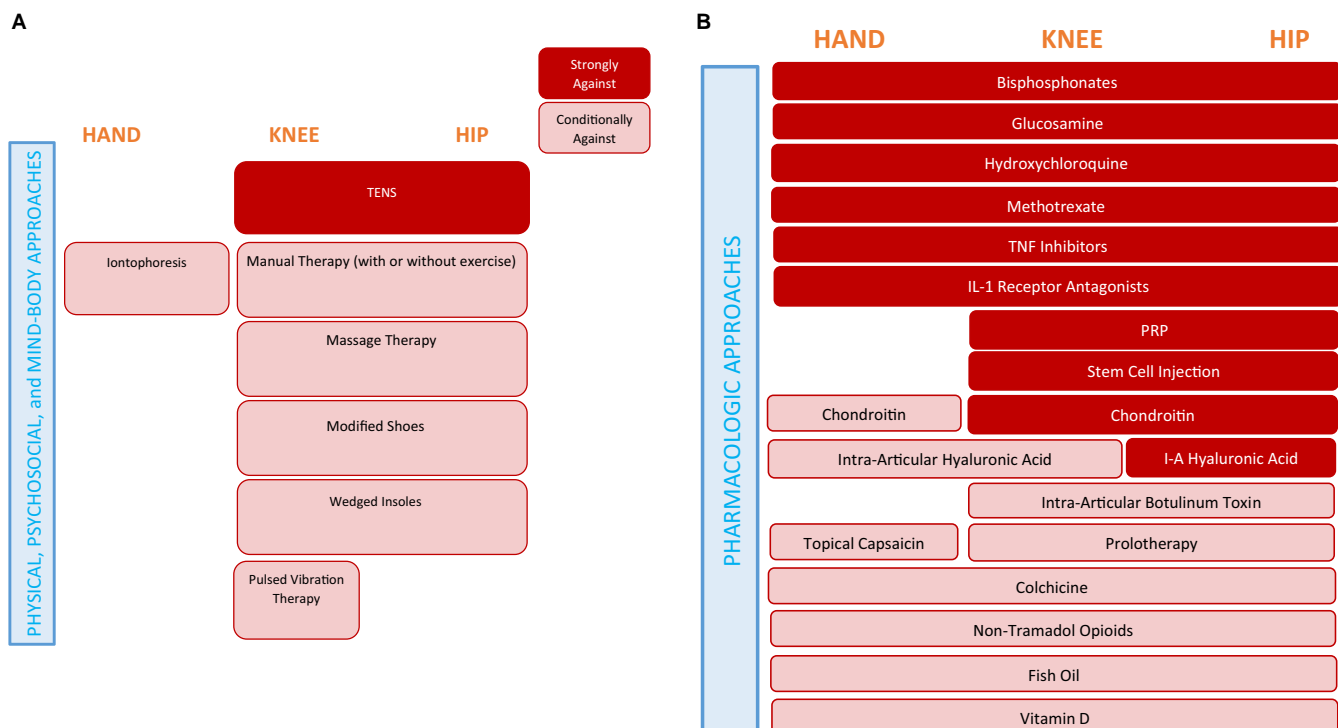
Figure 2. Therapies recommended *against* (physical, psychosocial, and mind-body approaches [**A**] and pharmacologic approaches [**B**]) in the management of hand, knee, and/or hip osteoarthritis. No hierarchy within categories is implied in the figure. TENS = transcutaneous electrical nerve stimulation; TNF = tumor necrosis factor; IL-1 = interleukin-1; PRP = platelet-rich plasma; IA = intraarticular.

will be performed prior to finalization of an individual treatment plan. When choosing among pharmacologic therapies, management should begin with treatments with the least systemic exposure or toxicity.

Patients may experience a variety of additional symptoms as a result of the pain and functional limitations arising from OA and/or comorbidities. These include mood disorders, such as depression and anxiety, altered sleep, chronic widespread pain, and impaired coping skills. The Patient Panel noted that the broader impact of OA on these comorbidities is of particular importance when choosing among treatment options and best addressed by a multimodal treatment plan, rather than one that is limited to the prescription of a single medication. Measures aimed at improving mood, reducing stress, addressing insomnia, managing weight, and enhancing fitness may improve the patient's overall well-being and OA treatment success. Indeed, interventions that have proven beneficial in the management of chronic pain may prove useful in OA (17) even when data specific to patients with OA are limited.

Unless otherwise specified, recommendations regarding physical, psychosocial, and mind-body approaches assume that the patient will be adding the intervention to usual care. For the purposes of this guideline, usual care includes the use of maximally recommended or safely tolerated doses of over-the-counter oral nonsteroidal antiinflammatory drugs (NSAIDs) and/or acetaminophen, as has generally been explicitly permitted in clinical trials of nonpharmacologic interventions.

Physical, psychosocial, and mind-body approaches (Table 1)

During the GRADE analysis, clinical trials involving physical modalities and mind-body approaches were often designated as yielding low-quality evidence because blinding with regard to the active treatment was not always possible. This contributed to a preponderance of conditional recommendations for physical modalities and mind-body approaches. The delivery of instruction by physical and occupational therapists is helpful, and often essential, for the appropriate initiation and maintenance of exercise as a part of OA management. In addition to exercise, physical and occupational therapists often incorporate self-efficacy and self-management training, thermal therapies, and instruction in use of and fitting of splints and braces in their practices. Most patients with OA are likely to experience benefit from referral to physical therapy and/or occupational therapy at various times during the course of their disease.

Exercise is strongly recommended for patients with knee, hip, and/or hand OA.

Though exercise is strongly recommended for all OA patients, there is considerably more evidence for the use of exercise in the treatment of knee and hip OA than for hand OA, and the variety of exercise options studied is far greater. While patients and providers seek recommendations on the "best" exercise and the ideal dosage (duration, intensity, and frequency), current evidence

Table 1. Recommendations for physical, psychosocial, and mind-body approaches for the management of osteoarthritis of the hand, knee, and hip

Intervention	Joint		
	Hand	**Knee**	**Hip**
Exercise			
Balance training			
Weight loss			
Self-efficacy and self-management programs			
Tai chi			
Yoga			
Cognitive behavioral therapy			
Cane			
Tibiofemoral knee braces		(Tibiofemoral)	
Patellofemoral braces		(Patellofemoral)	
Kinesiotaping	(First carpometacarpal)		
Hand orthosis	(First carpometacarpal)		
Hand orthosis	(Other joints)		
Modified shoes			
Lateral and medial wedged insoles			
Acupuncture			
Thermal interventions			
Paraffin			
Radiofrequency ablation			
Massage therapy			
Manual therapy with/without exercise			
Iontophoresis	(First carpometacarpal)		
Pulsed vibration therapy			
Transcutaneous electrical nerve stimulation			

Strongly recommended	
Conditionally recommended	
Strongly recommended against	
Conditionally recommended against	
No recommendation	

is insufficient to recommend specific exercise prescriptions. Broad recommendations suggesting one form of exercise over another are based largely on expert opinion. A substantial body of literature (see Evidence Report, Supplementary Appendix 2 [http://onlinelibrary.wiley.com/doi/10.1002/art.41142/abstract]) supports a wide range of appropriate exercise options and suggests that the vast majority of OA patients can participate in, and benefit from with regard to pain and function, some form of exercise. Exercise recommendations to patients should focus on the patient's preferences and access, both of which may be important barriers to participation. If a patient does not find a certain form of exercise acceptable or cannot afford to participate or arrange transportation to participate, he or she is not likely to get any benefit from the suggestion to pursue that exercise.

In the majority of studies that assessed the role of aerobic exercise in the management of OA, walking was the most common form of exercise evaluated, either on a treadmill or as supervised, community-based, indoor fitness walking. Other studies used supervised group cycling on stationary bicycles. Strengthening exercises have included the use of isokinetic weight machines, resistance exercise training with and without props such as elastic bands, and isometric exercise. Neuromuscular training has been developed to address muscle weakness, reduced sensorimotor control, and functional instability specifically seen with knee OA, with a series of dynamic maneuvers of increased complexity. Aquatic exercise often encompasses aspects of aerobic fitness exercises and exercises for enhancing joint range of motion, in a low-impact environment.

A specific hierarchy of these various forms of exercise could not be discerned from the literature. Patient participants on the Patient and Voting Panels raised the concern that patients who are in pain might be hesitant to participate in exercise. There is no uniformly accepted level of pain at which a patient should or should not exercise, and a common-sense approach of shared decision-making between the treating clinician and the patient regarding when to initiate an exercise program is advisable. However, clinical trials of exercise for OA include patients with pain and functional limitations due to OA, and improvements in OA-specific outcomes have been demonstrated; thus, results are likely to be generalizable to most patients with pain due to OA.

Although there is currently insufficient evidence to recommend one form of exercise over another, patients will likely benefit from advice that is as specific as possible, rather than simple encouragement to exercise. Given the wide range of evidence-based exercise interventions shown to effectively improve pain and function in OA, all patients should be encouraged to consider some form of exercise as a central part of their treatment plan. Individual preferences, access, and affordability are likely to play a role in what works best for an individual patient. Overall, exercise programs are more effective if supervised, often by physical therapists and sometimes in a class setting, rather than when performed by the individual at home. They also tend to be more effective when combined with self-efficacy and self-management interventions or weight loss programs.

Few studies have employed monitoring devices or pre- and postintervention assessment of cardiovascular or musculoskeletal fitness, so targets using these devices or assessments are not available. Future research is essential to establish specific exercise guidelines that will direct the patient and provider toward more individualized exercise prescriptions.

Balance exercises are conditionally recommended for patients with knee and/or hip OA.

Balance exercises include those that improve the ability to control and stabilize body position (American Physical Therapy Association: http://www.apta.org/BalanceFalls/). Although one might expect balance exercises to help reduce the risk of falls in patients with OA, RCTs to date have not addressed this outcome in this population, and the low quality of evidence addressing the use of balance exercises necessitates only a conditional recommendation for balance exercises.

Weight loss is strongly recommended for patients with knee and/or hip OA who are overweight or obese.

A dose-response has been noted with regard to the amount of weight loss that will result in symptom or functional improvement in patients with OA (18). A loss of ≥5% of body weight can be associated with changes in clinical and mechanistic outcomes. Furthermore, clinically important benefits continue to increase with weight loss of 5–10%, 10–20%, and >20% of body weight. The efficacy of weight loss for OA symptom management is enhanced by use of a concomitant exercise program.

Self-efficacy and self-management programs are strongly recommended for patients with knee, hip, and/or hand OA.

Although effect sizes are generally small, the benefits of participation in self-efficacy and self-management programs are consistent across studies, and risks are minimal. These programs use a multidisciplinary group–based format combining sessions on skill-building (goal-setting, problem-solving, positive thinking), education about the disease and about medication effects and side effects, joint protection measures, and fitness and exercise goals and approaches. Health educators, National Commission for Certification Services–certified fitness instructors, nurses, physical therapists, occupational therapists, physicians, and patient peers may lead the sessions, which can be held in person or online. In the studies reviewed, sessions generally occurred 3 times weekly, but varied from 2 to 6 times weekly.

Tai chi is strongly recommended for patients with knee and/or hip OA.

Tai chi is a traditional Chinese mind-body practice that combines meditation with slow, gentle, graceful movements, deep diaphragmatic breathing, and relaxation. The efficacy of tai chi may

reflect the holistic impact of this mind-body practice on strength, balance, and fall prevention, as well as on depression and self-efficacy.

Yoga is conditionally recommended for patients with knee OA.

Yoga is a mind-body practice with origins in ancient Indian philosophy and typically combines physical postures, breathing techniques, and meditation or relaxation (National Center for Complementary and Integrative Health [NCCIH]: https://nccih.nih.gov/health/yoga). Though far less well studied than tai chi, yoga may be helpful in OA through a similar blend of physical and psychosocial factors. Due to lack of data, no recommendation can be made regarding use of yoga to help manage symptoms of hip OA. Other mind-body practices could not be assessed due to insufficient evidence, as well as a lack of standard definitions of certain interventions (hypnosis, qi gong).

Cognitive behavioral therapy (CBT) is conditionally recommended for patients with knee, hip, and/or hand OA.

There is a well-established body of literature (19,20) supporting the use of CBT in chronic pain conditions, and CBT may have relevance for the management of OA. Trials have demonstrated improvement in pain, health-related quality of life, negative mood, fatigue, functional capacity, and disability in conditions other than OA. In OA, limited evidence suggests that CBT may reduce pain (21). Further research is needed to establish whether or not benefits in OA are related to alteration in mood, sleep, coping, or other factors that may co-occur with, result from, or be a part of the experience of OA (22).

Cane use is strongly recommended for patients with knee and/or hip OA in whom disease in 1 or more joints is causing a sufficiently large impact on ambulation, joint stability, or pain to warrant use of an assistive device.

Tibiofemoral knee braces are strongly recommended for patients with knee OA in whom disease in 1 or both knees is causing a sufficiently large impact on ambulation, joint stability, or pain to warrant use of an assistive device, and who are able to tolerate the associated inconvenience and burden associated with bracing.

Patellofemoral braces are conditionally recommended for patients with patellofemoral knee OA in whom disease in 1 or both knees is causing a sufficiently large impact on ambulation, joint stability, or pain to warrant use of an assistive device.

The recommendation is conditional due to the variability in results across published trials and the difficulty some patients will have in tolerating the inconvenience and burden of these braces. Optimal management with knee bracing is likely to require that clinicians are familiar with the various types of braces and where

they are available and have expertise in fitting the braces. Patient Voting Panel members strongly emphasized the importance of coordination of care between primary care providers, specialists, and providers of braces.

Kinesiotaping is conditionally recommended for patients with knee and/or first CMC joint OA.

Kinesiotaping permits range of motion of the joint to which it is applied, in contrast to a brace, which maintains the joint in a fixed position. Published studies have examined various products and methods of application, and blinding with regard to use is not possible, thereby limiting the quality of the evidence.

Hand orthoses are strongly recommended for patients with first CMC joint OA.

Hand orthoses are conditionally recommended for patients with OA in other joints of the hand.

A variety of mechanical supports are available, including digital orthoses, ring splints, and rigid or neoprene orthoses, some of which are intended for specifically affected joints (e.g., first CMC joint, individual digits, wrist) and some of which support the entire hand. In addition, gloves may offer benefit by providing warmth and compression to the joints of the hand. Data are insufficient to recommend one type of orthosis over another for use in the hand. Patients considering these interventions will likely benefit from evaluation by an occupational therapist.

Modified shoes are conditionally recommended *against* in patients with knee and/or hip OA.

Modifications to shoes can be intended to alter the biomechanics of the lower extremities and the gait. While optimal footwear is likely to be of considerable importance for those with knee and/or hip OA, the available studies do not define the best type of footwear to improve specific outcomes for knee or hip OA.

Lateral and medial wedged insoles are conditionally recommended *against* in patients with knee and/or hip OA.

The currently available literature does not demonstrate clear efficacy of lateral or medial wedged insoles.

Acupuncture is conditionally recommended for patients with knee, hip, and/or hand OA.

Although a large number of trials have addressed the use of acupuncture for OA, its efficacy remains a subject of controversy. Issues related to the use of appropriate blinding, the validity of sham controls, sample size, effect size, and prior expectations have arisen with regard to this literature. Variability in the results of RCTs and meta-analyses is likely driven, in part, by differences in the type of controls and the intensity of the control

interventions used. In addition, the benefits of acupuncture result from the large contextual effect plus small differences in outcomes between "true" and "sham" acupuncture. The latter is of the same magnitude as the effect of full-dose acetaminophen versus placebo. The greatest number of positive trials with the largest effect sizes have been carried out in knee OA. Positive trials and meta-analyses have also been published in a variety of other painful conditions and have indicated that acupuncture is effective for analgesia. While the "true" magnitude of effect is difficult to discern, the risk of harm is minor, resulting in the Voting Panel providing a conditional recommendation.

Thermal interventions (locally applied heat or cold) are conditionally recommended for patients with knee, hip, and/or hand OA.

The method of delivery of thermal interventions varies considerably in published reports, including moist heat, diathermy (electrically delivered heat), ultrasound, and hot and cold packs. Studies using diathermy or ultrasound were more likely to be sham controlled than those using other heat delivery modalities. The heterogeneity of modalities and short duration of benefit for these interventions led to the conditional recommendation.

Paraffin, an additional method of heat therapy for the hands, is conditionally recommended for patients with hand OA.

Radiofrequency ablation is conditionally recommended for patients with knee OA.

A number of studies have demonstrated potential analgesic benefits with various ablation techniques but, because of the heterogeneity of techniques and controls used and lack of long-term safety data, this recommendation is conditional.

Massage therapy is conditionally recommended *against* in patients with knee and/or hip OA.

Massage therapy encompasses a number of techniques aimed at affecting muscle and other soft tissue (NCCIH: https://nccih.nih.gov/health/massage/massageintroduction.htm#hed2). Studies addressing massage have suffered from high risk of bias, have included small numbers of patients, and have not demonstrated benefit for OA-specific outcomes. Patient participants on the Patient and Voting Panels noted that some studies have shown positive outcomes and minimal risk and felt strongly that massage therapy was beneficial for symptom management (23). However, based on the available evidence regarding OA specifically, a conditional recommendation against the use of massage for reduction of OA symptoms is made, though the Voting Panel acknowledged that massage may have other benefits.

Manual therapy with exercise is conditionally recommended *against* over exercise alone in patients with knee and/or hip OA.

Manual therapy techniques may include manual lymphatic drainage, manual traction, massage, mobilization/manipulation, and passive range of motion and are always used in conjunction with exercise (http://guidetoptpractice.apta.org/content/1/SEC38.extract). A limited number of studies have addressed manual therapy added to exercise versus exercise alone in hip and knee OA. Although manual therapy can be of benefit for certain conditions, such as chronic low back pain, limited data in OA show little additional benefit over exercise alone for managing OA symptoms.

Iontophoresis is conditionally recommended *against* in patients with first CMC joint OA.

There are no published RCTs evaluating iontophoresis for OA in any anatomic location.

Pulsed vibration therapy is conditionally recommended *against* in patients with knee OA.

Few trials have addressed pulsed vibration therapy, and in the absence of adequate data, we conditionally recommend against its use.

Transcutaneous electrical stimulation (TENS) is strongly recommended *against* in patients with knee and/or hip OA.

Studies examining the use of TENS have been of low quality with small size and variable controls, making comparisons across trials difficult. Studies have demonstrated a lack of benefit for knee OA.

Pharmacologic management (Table 2)

RCTs of pharmacologic agents may be subject to a variety of limitations, including generalizability of their findings across patients. Publication bias may reduce the likelihood that negative trials will become part of the published literature. Statistically significant findings may represent benefits so small that they are not clinically important to patients. We have highlighted these considerations where relevant.

Topical NSAIDs are strongly recommended for patients with knee OA and conditionally recommended for patients with hand OA.

In keeping with the principle that medications with the least systemic exposure (i.e., local therapy) are preferable, topical NSAIDs should be considered prior to use of oral NSAIDs (24). Practical considerations (e.g., frequent hand washing) and the lack of direct evidence of efficacy in the hand lead to a conditional recommendation for use of topical NSAIDs in hand OA. In hip OA, the depth of the joint beneath the skin surface suggests that topical NSAIDs are unlikely to

Table 2. Recommendations for the pharmacologic management of osteoarthritis of the hand, knee, and hip

Intervention	Joint		
	Hand	**Knee**	**Hip**
Topical nonsteroidal antiinflammatory drugs	Conditionally recommended	Strongly recommended	No recommendation
Topical capsaicin	Conditionally recommended against	Conditionally recommended	No recommendation
Oral nonsteroidal antiinflammatory drugs	Strongly recommended	Strongly recommended	Strongly recommended
Intraarticular glucocorticoid injection	Conditionally recommended	Strongly recommended	Strongly recommended
Ultrasound-guided intraarticular glucocorticoid injection	No recommendation	No recommendation	Strongly recommended
Intraarticular glucocorticoid injection compared to other injections	Conditionally recommended	Conditionally recommended	Conditionally recommended
Acetaminophen	Conditionally recommended	Conditionally recommended	Conditionally recommended
Duloxetine	Conditionally recommended	Conditionally recommended	Conditionally recommended
Tramadol	Conditionally recommended	Conditionally recommended	Conditionally recommended
Non-tramadol opioids	Conditionally recommended against	Conditionally recommended against	Conditionally recommended against
Colchicine	Conditionally recommended against	Conditionally recommended against	Conditionally recommended against
Fish oil	Conditionally recommended against	Conditionally recommended against	Conditionally recommended against
Vitamin D	Conditionally recommended against	Conditionally recommended against	Conditionally recommended against
Bisphosphonates	Strongly recommended against	Strongly recommended against	Strongly recommended against
Glucosamine	Strongly recommended against	Strongly recommended against	Strongly recommended against
Chondroitin sulfate	Conditionally recommended	Strongly recommended against	Strongly recommended against
Hydroxychloroquine	Strongly recommended against	Strongly recommended against	Strongly recommended against
Methotrexate	Strongly recommended against	Strongly recommended against	Strongly recommended against
Intraarticular hyaluronic acid injection	(First carpometacarpal) Conditionally recommended against	Conditionally recommended against	Conditionally recommended against
Intraarticular botulinum toxin	No recommendation	Conditionally recommended against	Conditionally recommended against
Prolotherapy	No recommendation	Conditionally recommended against	Conditionally recommended against
Platelet-rich plasma	No recommendation	Strongly recommended against	Strongly recommended against
Stem cell injection	No recommendation	Strongly recommended against	Strongly recommended against
Biologics (tumor necrosis factor inhibitors, interleukin-1 receptor antagonists)	Strongly recommended against	Strongly recommended against	Strongly recommended against

Strongly recommended
Conditionally recommended
Strongly recommended against
Conditionally recommended against
No recommendation

confer benefit, and thus, the Voting Panel did not examine use in hip OA.

Topical capsaicin is conditionally recommended for patients with knee OA and conditionally recommended *against* in patients with hand OA.

Topical capsaicin is conditionally recommended for treatment of knee OA due to small effect sizes and wide confidence intervals in the available literature. We conditionally recommend against the use of topical capsaicin in hand OA because of a lack of direct evidence to support use, as well as a potentially increased risk of contamination of the eye with use of topical capsaicin to treat hand OA. In hip OA, the depth of the joint beneath the skin surface suggests that topical capsaicin is unlikely to have a meaningful effect, and thus, the Voting Panel did not examine use of topical capsaicin in hip OA. Insufficient data exists to make recommendations about the use of topical lidocaine preparations in OA.

Oral NSAIDs are strongly recommended for patients with knee, hip, and/or hand OA.

Oral NSAIDs remain the mainstay of the pharmacologic management of OA, and their use is strongly recommended. A large number of trials have established their short-term efficacy. Oral NSAIDs are the initial oral medication of choice in the treatment of OA, regardless of anatomic location, and are recommended over all other available oral medications.

While this guideline did not address the relative merits of different NSAIDs, there is evidence suggesting that certain agents may have more favorable side effect profiles than others (25–27). Clinical considerations aimed at risk mitigation for the safe use of NSAIDs, such as appropriate patient selection, regular monitoring for the development of potential adverse gastrointestinal, cardiovascular, and renal side effects and potential drug interactions, were not specifically included in the GRADE process for the formulation of recommendations. Doses should be as low as possible, and NSAID treatment should be continued for as short a time as possible.

Intraarticular glucocorticoid injections are strongly recommended for patients with knee and/or hip OA and conditionally recommended for patients with hand OA.

Trials of intraarticular glucocorticoid injections have demonstrated short-term efficacy in knee OA. Intraarticular glucocorticoid injection is conditionally, rather than strongly, recommended for hand OA given the lack of evidence specific to this anatomic location. There are insufficient data to judge the choice of short-acting over long-acting preparations or the use of low rather than high doses. A recent report (28) raised the possibility that specific steroid preparations or a certain frequency of steroid injections may contribute to cartilage loss, but the Voting Panel was uncertain of the clinical significance of this finding, particularly since

change in cartilage thickness was not associated with a worsening in pain, functioning, or other radiographic features.

Ultrasound guidance for intraarticular glucocorticoid injection is strongly recommended for injection into hip joints.

When available, ultrasound guidance for steroid injection may help ensure accurate drug delivery into the joint, but is not required for knee and hand joints. However, imaging guidance for injection into hip joints is strongly recommended.

Intraarticular glucocorticoid injections versus other injections are conditionally recommended for patients with knee, hip, and/or hand OA.

In OA generally, intraarticular glucocorticoid injection is conditionally recommended over other forms of intraarticular injection, including hyaluronic acid preparations. Head-to-head comparisons are few, but the evidence for efficacy of glucocorticoid injections is of considerably higher quality than that for other agents.

Acetaminophen is conditionally recommended for patients with knee, hip, and/or hand OA.

In clinical trials, the effect sizes for acetaminophen are very small, suggesting that few of those treated experience important benefit, and meta-analysis has suggested that use of acetaminophen as monotherapy may be ineffective (29). Longer-term treatment is no better than treatment with placebo for most individuals. Members of the Patient Panel noted that, for most individuals, acetaminophen is ineffective. For those with limited pharmacologic options due to intolerance of or contraindications to the use of NSAIDs, acetaminophen may be appropriate for short-term and episodic use. Regular monitoring for hepatotoxicity is required for patients who receive acetaminophen on a regular basis, particularly at the recommended maximum dosage of 3 gm daily in divided doses.

Duloxetine is conditionally recommended for patients with knee, hip, and/or hand OA.

While studied primarily in the knee, the effects of duloxetine may plausibly be expected to be similar for OA of the hip or hand. While a variety of centrally acting agents (e.g., pregabalin, gabapentin, selective serotonin reuptake inhibitors, serotonin norepinephrine reuptake inhibitors, and tricyclic antidepressants) have been used in the management of chronic pain, only duloxetine has adequate evidence on which to base recommendations for use in OA. However, in considering all the ways in which OA may be affecting an individual patient, shared decision-making between the physician and patient may include consideration of any of these agents. Considering the utility of these agents in pain management generally, their use may be an appropriate target of future investigations specific to OA. Evidence suggests that duloxetine has efficacy in the treatment of OA when used alone or in combination with NSAIDs; however, there are issues regarding tolerability and side effects. No recommendations were made for the other centrally acting agents due to lack of direct studies of relevance in OA.

Tramadol is conditionally recommended for patients with knee, hip, and/or OA.

Recent work has highlighted the very modest level of beneficial effects in the long-term (3 months to 1 year) management of non-cancer pain with opioids (30). Nonetheless, there are circumstances in which tramadol or other opioids may be appropriate in the treatment of OA, including when patients may have contraindications to NSAIDs, find other therapies ineffective, or have no available surgical options. Patient Panel input demonstrated a high level of understanding concerning addiction potential, but also included an appreciation for the role of these agents when other pharmacologic and physical options have been ineffective. However, RCT evidence addressing the use of tramadol and other opioids for periods longer than 1 year is not available. Clinical trials have demonstrated some symptomatic efficacy, though concerns regarding potential adverse effects remain. If an opioid is being considered, tramadol is conditionally recommended over non-tramadol opioids.

Non-tramadol opioids are conditionally recommended *against* in patients with knee, hand, and/or hip OA with the recognition that they may be used under certain circumstances, particularly when alternatives have been exhausted.

As noted above, evidence suggests very modest benefits of long-term opioid therapy and a high risk of toxicity and dependence. Use of the lowest possible doses for the shortest possible length of time is prudent, particularly since a recent systematic review and meta-analysis suggests that less pain relief occurs during longer trials in the treatment of non-cancer chronic pain (30).

Colchicine is conditionally recommended *against* in patients with knee, hip, and/or hand OA.

Two very small studies have suggested analgesic benefit of colchicine in OA, but the quality of the data was low. In addition, potential adverse effects, as well as drug interactions, may occur with use of colchicine.

Fish oil is conditionally recommended *against* in patients with knee, hip, and/or hand OA.

Fish oil is the most commonly used dietary supplement in the US (31). Despite its popularity, only 1 published trial has addressed its potential role in OA. This study failed to show efficacy of a higher dose of fish oil over a lower dose.

Vitamin D is conditionally recommended *against* in patients with knee, hip, and/or hand OA.

A number of trials in OA demonstrated small effect sizes with vitamin D treatment, while others have shown no benefit and pooling data across studies yielded null results. In addition, limited

and questionable health benefits from vitamin D supplementation have been suggested in other contexts (32,33).

Bisphosphonates are strongly recommended *against* in patients with knee, hip, and/or hand OA.

Though a single small study of an oral bisphosphonate suggested a potential analgesic benefit in OA, the preponderance of data shows no improvement in pain or functional outcomes.

Glucosamine is strongly recommended *against* in patients with knee, hip, and/or hand OA.

Pharmaceutical-grade preparations of glucosamine are available and have been studied in multiple trials. However, discrepancies in efficacy reported in studies that were industry sponsored as opposed to publicly funded have raised serious concerns about publication bias (34,35). In addition, there is a lack of a clear biologic understanding of how efficacy would vary with the type of salt studied. The data that were deemed to have the lowest risk of bias fail to show any important benefits over placebo. These recommendations represent a change from the prior conditional recommendation against the use of glucosamine. The weight of the evidence indicates a lack of efficacy and large placebo effects. Nonetheless, glucosamine remains among the most commonly used dietary supplements in the US (31), and clinicians should be aware that many patients perceive that glucosamine is efficacious. Patients also often perceive that different glucosamine formulas are associated with different degrees of efficacy and seek advice on brands and manufacturers. The potential toxicity of glucosamine is low, though some patients exposed to glucosamine may show elevations in serum glucose levels (36).

Chondroitin sulfate is strongly recommended *against* in patients with knee and/or hip OA as are combination products that include glucosamine and chondroitin sulfate, but is conditionally recommended for patients with hand OA.

A single trial suggested analgesic efficacy of chondroitin sulfate, without evidence of harm, in hand OA.

Hydroxychloroquine is strongly recommended *against* in patients with knee, hip, and/or hand OA.

Well-designed RCTs of hydroxychloroquine, conducted in the subset of patients with erosive hand OA, have demonstrated no efficacy.

Methotrexate is strongly recommended *against* in patients with knee, hip, and/or hand OA.

Well-designed RCTs of methotrexate, conducted in the subset of patients with erosive hand OA, have demonstrated no efficacy.

Intraarticular hyaluronic acid injections are conditionally recommended *against* in patients with knee and/or first CMC joint OA and strongly recommended *against* in patients with hip OA.

In prior systematic reviews, apparent benefits of hyaluronic acid injections in OA have been reported. These reviews have not, however, taken into account the risk of bias of the individual primary studies. Our review showed that benefit was restricted to the studies with higher risk of bias: when limited to trials with low risk of bias, meta-analysis has shown that the effect size of hyaluronic acid injections compared to saline injections approaches zero (37). The finding that best evidence fails to establish a benefit, and that harm may be associated with these injections, motivated the recommendation against use of this treatment.

Many providers want the option of using hyaluronic acid injections when glucocorticoid injections or other interventions fail to adequately control local joint symptoms. In clinical practice, the choice to use hyaluronic acid injections in the knee OA patient who has had an inadequate response to nonpharmacologic therapies, topical and oral NSAIDs, and intraarticular steroids may be viewed more favorably than offering no intervention, particularly given the impact of the contextual effects of intraarticular hyaluronic acid injections (38). The conditional recommendation against is consistent with the use of hyaluronic acid injections, in the context of shared decision-making that recognizes the limited evidence of benefit of this treatment, when other alternatives have been exhausted or failed to provide satisfactory benefit. The conditional recommendation against is not intended to influence insurance coverage decisions.

In contrast, the evidence of lack of benefit is of higher quality with respect to hyaluronic acid injection in the hip. We therefore strongly recommend against hyaluronic acid injections in hip OA.

Intraarticular botulinum toxin injections are conditionally recommended *against* in patients with knee and/or hip OA.

The small number of trials of intraarticular botulinum toxin treatment in knee or hip OA suggest a lack of efficacy. This treatment has not been evaluated in hand OA and, therefore, no recommendation is made with regard to OA of the hand.

Prolotherapy is conditionally recommended *against* in patients with knee and/or hip OA.

A limited number of trials involving a small number of participants have shown small effect sizes of prolotherapy in knee or hip OA. However, injection schedules, injection sites, and comparators have varied substantially between trials. This treatment has not been evaluated in hand OA and, therefore, no recommendation is made with regard to OA of the hand.

Platelet-rich plasma treatment is strongly recommended *against* in patients with knee and/or hip OA.

In contrast to intraarticular therapies discussed above, there is concern regarding the heterogeneity and lack of standardization in available preparations of platelet-rich plasma, as well as techniques used, making it difficult to identify exactly what is being injected. This treatment has not been evaluated in hand OA and, therefore, no recommendation is made with regard to OA of the hand.

Stem cell injections are strongly recommended *against* in patients with knee and/or hip OA.

There is concern regarding the heterogeneity and lack of standardization in available preparations of stem cell injections, as well as techniques used. This treatment has not been evaluated in hand OA and, therefore, no recommendation is made with regard to OA of the hand.

Tumor necrosis factor inhibitors and interleukin-1 receptor antagonists are strongly recommended *against* in patients with knee, hip, and/or hand OA.

Tumor necrosis factor inhibitors and interleukin-1 receptor antagonists have been studied in trials using both subcutaneous and intraarticular routes of administration. Efficacy has not been demonstrated, including in erosive hand OA. Therefore, given their known risks of toxicity, we strongly recommended against their use for any form of OA.

Initial observations addressing the use of anti–nerve growth factor (anti-NGF) agents suggest that significant analgesic benefits may occur but that incompletely explained important safety issues may arise. A small subset of patients treated with these agents had rapid joint destruction leading to early joint replacement. The FDA temporarily halted clinical trials of anti-NGF as a result, but trials have since resumed, with ongoing collection of longer-term efficacy and safety data. As none of these agents were approved for use by the FDA and the longer-term data were not available at the time of the literature review and Voting Panel meeting, we are unable to make recommendations regarding the use of anti-NGF therapy.

DISCUSSION

These 2019 ACR/AF recommendations for the management of OA are based on the best available evidence of benefit, safety, and tolerability of physical, educational, behavioral, psychosocial, mind-body, and pharmacologic interventions, as well as the consensus judgment of clinical experts. The GRADE approach used provided a comprehensive, explicit, and transparent methodology for developing recommendations for OA management. The choice of any single or group of interventions may vary over the course of the disease or with patient and provider preferences, and is optimally arrived at through shared decision-making.

The Voting Panel made strong recommendations for patients to participate in a regular, ongoing exercise program. The literature provides support for choice from a broad menu of exercises for patients with OA. The effectiveness of an exercise program is enhanced when patient preferences and access to exercise programs are considered, as well as when they are supervised or coupled with self-efficacy, self-management, and weight loss programs. Strong recommendations were also made for weight loss in patients with knee and/or hip OA who are overweight or obese, self-efficacy and self-management programs, tai chi, cane use, first CMC joint orthoses, tibiofemoral bracing, topical NSAIDs for knee OA and oral NSAIDs for hand, knee, and/or hip OA, and intraarticular glucocorticoid injections for knee and/or hip OA. The Voting Panel made conditional recommendations for balance exercises, yoga, CBT, kinesiotaping, orthoses for hand joints other than the first CMC, patellofemoral bracing, acupuncture, thermal modalities, radiofrequency ablation, topical NSAIDs, intraarticular steroid injections and chondroitin sulfate for hand OA, topical capsaicin for knee OA, acetaminophen, duloxetine, and tramadol. The recommendations provide an array of options for a comprehensive approach for optimal management of OA encompassing the use of educational, physical, behavioral, psychosocial, mind-body, and pharmacologic interventions. The availability, accessibility, and affordability of some of these interventions vary, but in many communities the AF, as well as local hospitals and other health-related agencies, offer free self-efficacy and self-management programs.

For some patients with more limited disease in whom medication is required, topical NSAIDs represent an appropriate first choice. For others, particularly with hip OA or polyarticular involvement, oral NSAIDs are more appropriate. The appropriate use of other oral agents, particularly acetaminophen and opioids, will continue to evolve (39–41).

Despite the many options available, some patients may continue to experience inadequate symptom control; others will experience adverse effects from the available interventions. Clinicians treating patients in these circumstances should choose interventions with a low risk of harm, but both clinicians and patients may be dissatisfied with the options and unsure of how to choose among them. There are controversies in interpretation of the evidence, particularly with regard to the use of glucosamine and chondroitin, acupuncture, and intraarticular hyaluronic acid injections. Nonetheless, the process of updating treatment guidelines permits scrutiny of the state of the literature and identification of critical gaps in our knowledge about best practices. Further, it highlights the need for ongoing, appropriately funded, high-quality clinical research, as well as development of new treatment modalities, to address the human and economic impact of the most common form of arthritis.

No effective disease-modifying agents for OA have yet been identified though phase 2 and 3 trials are underway, and, for the time being, preventive strategies focus on weight management and injury prevention. Development of more effective therapies that

permit a sophisticated and individualized approach to the patient with OA await the outcome of future investigation. Important directions for research include gaining a more comprehensive understanding of the optimal types of exercises and the modifications that should be used based on disease location and severity, study of the intensity of exercise that would be optimal for a given individual (https://health.gov/paguidelines/second-edition/report.aspx), defining optimal footwear for patients with knee and hip OA and understanding the interaction between footwear and exercise, conducting rigorous RCTs for physical modality options in hand OA, assessing a broader array of outcomes, including fall prevention, assessing optimal use of oral, topical, and injectable agents alone and in combination, obtaining a better understanding of the role of integrative medicine, including massage, herbal products, medical marijuana, and additional mind-body interventions, and exploring agents with novel mechanisms of action for prevention and treatment.

In conclusion, optimal management requires a comprehensive, multimodal approach to treating patients with hand, hip, and/or knee OA offered in the context of shared decision-making with patients, to choose the safest and most effective treatment possible. A large research agenda remains to be addressed, with a need for more options with greater efficacy for the millions of people worldwide with osteoarthritis.

Addendum. Therapies that were approved after the original systematic literature review are not included in these recommendations.

ACKNOWLEDGMENTS

REFERENCES

1. Cisternas MG, Murphy L, Sacks JJ, Solomon DH, Pasta DJ, Helmick CG. Alternative methods for defining osteoarthritis and the impact on estimating prevalence in a US population-based survey. Arthritis Care Res (Hoboken) 2016;68:574–80.

2. GBD 2015 DALYs and HALE Collaborators. Global, regional, and national disability-adjusted life-years (DALYs) for 315 diseases and injuries and healthy life expectancy (HALE), 1990–2015: a systematic analysis for the Global Burden of Disease Study 2015. Lancet 2016;388:P1603–58.

3. Murphy L, Schwartz TA, Helmick CG, Renner JB, Tudor G, Koch G, et al. Lifetime risk of symptomatic knee osteoarthritis. Arthritis Rheum 2008;59:1207–13.

4. Murphy LB, Helmick CG, Schwartz TA, Renner JB, Tudor G, Koch GG, et al. One in four people may develop symptomatic hip osteoarthritis in his or her lifetime. Osteoarthritis Cartilage 2010;18:1372–9.

5. Qin J, Barbour KE, Murphy LB, Nelson AE, Schwartz TA, Helmick CG, et al. Lifetime risk of symptomatic hand osteoarthritis: the Johnston County Osteoarthritis Project. Arthritis Rheumatol 2017;69:1204–12.

6. Guyatt GH, Oxman AD, Vist GE, Kunz R, Falck-Ytter Y, Alonso-Coello P, et al. GRADE: an emerging consensus on rating quality of evidence and strength of recommendations. BMJ 2008;336:924–6.

7. Hochberg MC, Altman RD, April KT, Benkhalti M, Guyatt G, McGowan J, et al. American College of Rheumatology 2012 recommendations for the use of nonpharmacologic and pharmacologic therapies in osteoarthritis of the hand, hip, and knee. Arthritis Care Res (Hoboken) 2012;64:465–74.

8. Dobson F, Hinman RS, Hall M, Marshall CJ, Sayer T, Anderson C, et al. Reliability and measurement error of the Osteoarthritis Research Society International (OARSI) recommended performance-based tests of physical function in people with hip and knee osteoarthritis. Osteoarthritis Cartilage 2017;25:1792–6.

9. Juhl C, Lund H, Roos EM, Zhang W, Christensen R. A hierarchy of patient-reported outcomes for meta-analysis of knee osteoarthritis trials: empirical evidence from a survey of high impact journals [review]. Arthritis 2012;2012:136245.

10. Guyatt GH, Oxman AD, Kunz R, Falck-Ytter Y, Vist GE, Liberati A, et al, for the GRADE Working Group. Going from evidence to recommendations. BMJ 2008;336:1049–51.

11. Guyatt GH, Oxman AD, Kunz R, Vist GE, Falck-Ytter Y, Schünemann HJ, for the GRADE Working Group. What is "quality of evidence" and why is it important to clinicians? BMJ 2008;336:995–8.

12. Alonso-Coello P, Schünemann HJ, Moberg J, Brignardello-Petersen R, Akl EA, Davoli M, et al. GRADE Evidence to Decision (EtD) frameworks: a systematic and transparent approach to making well informed healthcare choices. 1. Introduction. BMJ 2016;353:i2016.

13. Neumann I, Santesso N, Akl EA, Rind DM, Vandvik PO, Alonso-Coello P, et al. A guide for health professionals to interpret and use recommendations in guidelines developed with the GRADE approach. J Clin Epidemiol 2016;72:45–55.

14. Andrews J, Guyatt G, Oxman AD, Alderson P, Dahm P, Falck-Ytter Y, et al. GRADE guidelines: 14. Going from evidence to recommendations: the significance and presentation of recommendations. J Clin Epidemiol 2013;66:719–25.

15. Andrews JC, Schünemann HJ, Oxman AD, Pottie K, Meerpohl JJ, Coello PA, et al. GRADE guidelines: 15. Going from evidence to recommendation—determinants of a recommendation's direction and strength. J Clin Epidemiol 2013;66:726–35.

16. Elwyn G, Frosch D, Thomson R, Joseph-Williams N, Lloyd A, Kinnersley P, et al. Shared decision making: a model for clinical practice. J Gen Intern Med 2012;27:1361–7.

17. Skelly AC, Chou R, Dettori JR, Turner JA, Friedly JL, Rundell SD, et al, for the Agency for Healthcare Research and Quality. Noninvasive nonpharmacological treatment for chronic pain: a systematic review. 2018. URL: https://effectivehealthcare.ahrq.gov/sites/default/files/pdf/nonpharma-chronic-pain-cer-209.pdf.

18. Messier SP, Resnik AE, Beavers DP, Mihalko SL, Miller GD, Nicklas BJ, et al. Intentional weight loss in overweight and obese patients with knee osteoarthritis: is more better? Arthritis Care Res (Hoboken) 2018;70:1569–75.

19. Bernardy K, Klose P, Welsch P, Häuser W. Efficacy, acceptability and safety of cognitive behavioural therapies in fibromyalgia syndrome: a systematic review and meta-analysis of randomized controlled trials. Eur J Pain 2018;22:242–60.

20. Hajihasani A, Rouhani M, Salavati M, Hedayati R, Kahlaee AH. The influence of cognitive behavioral therapy on pain, quality of life, and depression in patients receiving physical therapy for chronic low back pain: a systematic review. PM R 2019;11:167–76.

21. Ismail A, Moore C, Alshishani N, Yaseen K, Alshehri MA. Cognitive behavioural therapy and pain coping skills training for osteoarthritis knee pain management: a systematic review. J Phys Ther Sci 2017;29:2228–35.

22. Eberly L, Richter D, Comerci G, Ocksrider J, Mercer D, Mlady G, et al. Psychosocial and demographic factors influencing pain scores of patients with knee osteoarthritis. PLoS One 2018;13:e0195075.

23. Perlman AI, Ali A, Njike VY, Hom D, Davidi A, Gould-Fogerite S, et al. Massage therapy for osteoarthritis of the knee: a randomized dose-finding trial. PLoS One 2012;7:e30248.

24. Rannou F, Pelletier JP, Martel-Pelletier J. Efficacy and safety of topical NSAIDs in the management of osteoarthritis: evidence from real-life setting trials and surveys. Semin Arthritis Rheum 2016;45 Suppl:S18–21.

25. Chan FK, Ching JY, Tse YK, Lam K, Wong GL, Ng SC, et al. Gastrointestinal safety of celecoxib versus naproxen in patients with cardiothrombotic diseases and arthritis after upper gastrointestinal bleeding (CONCERN): an industry-independent, double-blind, double-dummy, randomised trial. Lancet 2017;389:2375–82.

26. Nissen SE, Yeomans ND, Solomon DH, Lüscher TF, Libby P, Husni ME, et al, for the PRECISION Trial Investigators. Cardiovascular safety of celecoxib, naproxen, or ibuprofen for arthritis. N Engl J Med 2016;375:2519–29.

27. Solomon DH, Husni ME, Libby PA, Yeomans ND, Lincoff AM, Lüscher TF, et al. The risk of major NSAID toxicity with celecoxib, ibuprofen, or naproxen: a secondary analysis of the PRECISION trial. Am J Med 2017;130:1415–22.

28. McAlindon TE, LaValley MP, Harvey WF, Price LL, Driban JB, Zhang M, et al. Effect of intra-articular triamcinolone vs saline on knee cartilage volume and pain in patients with knee osteoarthritis: a randomized clinical trial. JAMA 2017;317:1967–75.

29. Da Costa BR, Reichenbach S, Keller N, Nartey L, Wandel S, Juni P, et al. Effectiveness of non-steroidal anti-inflammatory drugs for the treatment of pain in knee and hip osteoarthritis: a network meta-analysis. Lancet 2017;390:e21–33.

30. Busse JW, Wang L, Kamaleldin M, Craigie S, Riva JJ, Montoya L, et al. Opioids for chronic noncancer pain: a systematic review and meta-analysis. JAMA 2018;320:2448–60.

31. Clarke TC, Black LI, Stussman BJ, Barnes PM, Nahin RL. Trends in the use of complementary health approaches among adults: United States, 2002–2012. Natl Health Stat Report 2015;1–16.

32. Ong JS, Gharahkhani P, An J, Law MH, Whiteman DC, Neale RE, et al. Vitamin D and overall cancer risk and cancer mortality: a Mendelian randomization study. Hum Mol Genet 2018;27:4315–22.

33. Pilz S, Verheyen N, Grübler MR, Tomaschitz A, März W. Vitamin D and cardiovascular disease prevention. Nat Rev Cardiol 2016;13:404–17.

34. Runhaar J, Rozendaal RM, van Middelkoop M, Bijlsma HJ, Doherty M, Dziedzic KS, et al. Subgroup analyses of the effectiveness of oral glucosamine for knee and hip osteoarthritis: a systematic review and individual patient data meta-analysis from the OA trial bank. Ann Rheum Dis 2017;76:1862–9.

35. Wandel S, Jüni P, Tendal B, Nüesch E, Villiger PM, Welton NJ, et al. Effects of glucosamine, chondroitin, or placebo in patients with osteoarthritis of hip or knee: network meta-analysis. BMJ 2010;341:c4675.

36. Biggee BA, Blinn CM, Nuite M, Silbert JE, McAlindon TE. Effects of oral glucosamine sulphate on serum glucose and insulin during an oral glucose tolerance test of subjects with osteoarthritis. Ann Rheum Dis 2007;66:260–2.

37. Rutjes AW, Jüni P, da Costa BR, Trelle S, Nüesch E, Reichenbach S. Viscosupplementation for osteoarthritis of the knee: a systematic review and meta-analysis. Ann Intern Med 2011;157:180–91.

38. Zhang W, Doherty M. Efficacy paradox and proportional contextual effect (PCE). Clin Immunol 2018;186:82–6.

39. Rubin R. Limits on opioid prescribing leave patients with chronic pain vulnerable. JAMA 2019;321:2059–62.

40. Zeng C, Dubreuil M, LaRochelle MR, Lu N, Wei J, Choi HK, et al. Association of tramadol with all-cause mortality among patients with osteoarthritis. JAMA 2019;321:969–82.

41. Leopoldino AO, Machado GC, Ferreira PH, Pinheiro MB, Day R, McLachlan AJ, et al. Paracetamol versus placebo for knee and hip osteoarthritis. Cochrane Database Syst Rev 2019;2: CD013273.

AMERICAN COLLEGE
of RHEUMATOLOGY
Empowering Rheumatology Professionals

Decomposition Analysis of Spending and Price Trends for Biologic Antirheumatic Drugs in Medicare and Medicaid

Natalie McCormick,[1] (iD) Zachary S. Wallace,[2] (iD) Chana A. Sacks,[2] John Hsu,[2] and Hyon K. Choi[1] (iD)

Objective. Billions of public dollars are spent each year on biologic disease-modifying antirheumatic drugs (DMARDs), but the drivers of recent increases in biologic DMARD spending are unclear. This study was undertaken to characterize changes in total spending and unit prices for biologic DMARDs in Medicare and Medicaid programs and quantified the major sources of these spending increases.

Methods. We accessed drug spending data from years 2012–2016, covering all Medicare Part B (fee-for-service), Medicare Part D, and Medicaid enrollees. After calculating 5-year changes in total spending and unit prices for each biologic DMARD as well as in aggregate, we performed standard decomposition analyses to isolate 4 sources of spending growth: drug prices, uptake (number of recipients), treatment intensity (mean number of doses per claim), and treatment duration (annual number of claims per recipient), both excluding and including time-varying rebates.

Results. From 2012 to 2016, annual spending on public-payer claims for the 10 biologic DMARDs included in this study more than doubled ($3.8 billion to $8.6 billion), with median drug price increases of 51% in Medicare Part D (mean 54%) and 8% in Medicare Part B (mean 21%). With adjustment for general inflation, unit price increases alone accounted for 57% of the 5-year, $3.0 billion spending increase in Part D, while 37% of the spending increase was from increased uptake. Accounting for time-varying rebates, prices were still responsible for 54% of increased spending. Unit prices and spending were lower under Medicaid than under Medicare Part D, though temporal trends and contributors were similar.

Conclusion. Postmarket drug price changes alone account for the majority of the recent spending growth in biologic DMARDs. Policy interventions targeting price increases, particularly those under Medicare Part D plans, may help mitigate financial burdens for public payers and biologic DMARD recipients.

INTRODUCTION

Over the past 2 decades since biologic disease-modifying antirheumatic drugs (DMARDs) were first approved by the Federal Drug Administration (FDA), they have improved the health and productivity of many patients with moderate-to-severe rheumatoid arthritis (RA), psoriasis/psoriatic arthritis, ankylosing spondylitis, lupus, systemic vasculitis, and other rheumatic and autoimmune diseases (1–7), which together affect more than 1 million Medicare beneficiaries (8–10). However, due to their high prices ($22,000–44,000 per patient annually [11]) and placement in specialty tiers with high levels of cost-sharing, biologic DMARDs pose substantial financial burdens for patients and taxpayers. For example, a

recent analysis of acquisition costs showed that 3 biologic agents (adalimumab, etanercept, and infliximab) ranked among the top 5 prescription medications in the US for greatest total spending (12).

With annual prescription drug spending exceeding $333 billion dollars (13), the US is in the midst of active public debate about approaches to mitigate the high cost of prescription drugs for patients and payers. These approaches include moving some drugs from Medicare Part B to Part D (14) and passing manufacturers' rebates through to beneficiaries at the point of sale (15). Biologic DMARDs, which are covered by Medicare as a medical and pharmacy benefit (Parts B and D, respectively), are a prime target for such measures due to the high levels of spending associated with these medications. Recent reports documented

increases in total spending and per-person treatment costs for biologic DMARDs but could not differentiate between various sources of growth (12,16). Specifically, detailed decompositions that separate spending growth into changes in price, recipient numbers, and treatment intensity are important to understand spending changes and their implications (17). Thus, we used national-level Medicare and Medicaid data to decompose growth in spending between 2012 and 2016 for the biologic DMARDs used in the treatment of rheumatic diseases.

PATIENTS AND METHODS

Data source. Data were obtained from the Medicare and Medicaid Drug Spending Dashboards published from 2012 through 2016 by the Centers for Medicare and Medicaid Services (CMS) (18). These data sets contain aggregated, nonidentifiable, national-level data on outpatient prescription medications. Part D files were derived from Prescription Drug Event claims for Medicare beneficiaries enrolled in Part D, including standalone prescription drug plans and Medicare Advantage plans (19). Approximately 70% of all Medicare beneficiaries are enrolled in a Part D plan; this included 31.9 million individuals in 2012 and 41.2 million in 2016 (a 5-year increase of 29%) (20). Part B files include administrative claims data on non–self-administered drugs prescribed to Medicare beneficiaries with fee-for-service plans (32.9 million individuals in 2012 and 33.7 million in 2016 [20]) (21). Medicaid files contain data for outpatient drugs paid for by state Medicaid agencies (22). As our analysis was based on aggregated data and involved no patient health records, it was exempt from institutional review board approval.

Study data. We included all biologic DMARDs approved by the FDA for the treatment of 1 or more rheumatic diseases through December 2014 (Supplementary Table 1, available on the *Arthritis & Rheumatology* web site at http://onlinelibrary.wiley.com/doi/10.1002/art.41138/abstract). We required this inclusion criterion in order to have at least 2 full years of follow-up data; for example, we excluded secukinumab, which was approved by the FDA in 2015. Similarly, for drugs (or formulations) newly approved during the period, we only assessed trends for individual drugs during years in which these medications were approved for the entire 12 months. For example, for intravenous golimumab, which was approved in July 2013, we assessed the trend from 2014 to 2016. Since the data sets did not contain information on disease indication, we excluded rituximab from our primary analysis as it is commonly used in the treatment of lymphoma and spending for this indication may differ from spending for the treatment of rheumatic diseases.

Variable and data extraction. For each drug and calendar year, we extracted data on total spending, recipients, doses, claims, and average number of doses per claim and per recipient over the year. From these variables, we calculated the drug unit price (average cost per dose) for each biologic DMARD. Total

spending included amounts paid by Medicare, federal and state Medicaid programs, beneficiaries (as deductible, coinsurance, or copayment), and third parties (e.g., supplemental Part B insurance plans). For Medicare Part D and Medicaid, total spending included the ingredient cost, dispensing fees, and sales tax.

CMS defined total recipients as the total number of Medicare Part D or Part B fee-for-service beneficiaries who received the drug each year; this information was not reported for Medicaid. Total doses reported by CMS were the total number of doses dispensed and were weighted to account for variation in strength and dosage form. For self-administered drugs, a single dose was the amount in a prefilled syringe or injector pen. Dosage quantities and frequencies for each drug are listed in Supplementary Table 1, available on the *Arthritis & Rheumatology* web site at http://onlinelibrary.wiley.com/doi/10.1002/art.41138/abstract. While the data sets did not contain information on disease indication or prescriber specialty, claims data stratified by prescriber specialty were available for a subset of the Medicare files, which included ~40% of Part B spending data and 80% of Part D spending for 2016 (23,24). We used these data to assess the proportion of costs from claims submitted by rheumatologists, dermatologists, and gastroenterologists.

Statistical analysis. After adjusting all spending amounts to 2016 dollars using general inflation rates obtained from the US Bureau of Labor Statistics Consumer Price Index (25), we calculated 5-year changes in total spending and drug price (our primary end point) for each biologic DMARD as well as in aggregate. We then analyzed changes in the average number of doses and cost per claim, number of recipients dispensed each drug, and claims per recipient in each calendar year.

As increases in spending (ΔC) can result from increases in prices (ΔP), volume (ΔV; e.g. number of recipients, treatment intensity), or both ($\Delta C = \Delta P \times \Delta V$), we used standard decomposition methods to determine the major drivers of the expected 5-year spending increases. These methods, used previously to assess changes in outpatient and drug expenditures (26–30), isolate the impact of each driver (or effect) by estimating the change in spending from the change in one effect, while holding other effects constant. For each biologic DMARD, we considered 1 price effect (specifically, change in price per dose) and 3 volume effects: number of recipients (V_a); number of claims per recipient (V_b), which reflects the duration of treatment; and number of doses per claim (V_c), which reflects the intensity of treatment. The product of the 3 volume effects ($\Delta V_a \times \Delta V_b \times \Delta V_c$) equaled the change in total number of doses dispensed.

Though price effects are usually the product of changes in individual drug prices and in use of lower-cost generic medications (31), the latter was not applicable to this analysis of biologic agents, given the absence of generic drugs in this class. We determined the absolute and percentage contribution of these effects toward the increase in spending for each biologic DMARD, as well

Table 1. Annual spending and utilization for biologic DMARDs covered under Medicare Part D*

Biologic DMARD	Total spending in 2016, dollars	No. of recipients in 2016	Change from 2012					
			Total spending, %	Total spending, rebate-adjusted, %†	No. of recipients, %	No. of doses per claim, %	Drug prices, %	Drug prices, rebate-adjusted, %†
Adalimumab SC (injector pen)	1,638,715,583	48,164	261	237	80	0	84	72
Etanercept SC	1,572,038,339	47,795	107	93	11	–1	88	75
Adalimumab SC (prefilled syringe)	490,135,622	15,477	107	93	11	1	84	72
Ustekinumab SC	264,877,321	6,616	401	367	249	4	37	28
Abatacept SC‡	185,560,929	6,916	72	66	19	–3	31	26
Certolizumab SC	160,787,675	5,903	172	154	61	6	51	41
Golimumab SC	111,914,458	3,549	124	109	11	18	49	39
Infliximab IV	68,074,955	2,407	110	96	37	19	20	12
Tocilizumab (IV or SC)§	61,489,157	3,499	142	134	60	–34	100	93
Abatacept IV	22,475,179	1,162	99	85	24	–8	54	44
Anakinra SC	10,858,651	388	142	126	11	11	87	74
Belimumab IV	8,612,441	388	385	352	304	–10	3	–4
Golimumab IV‡	5,836,741	292	149	141	70	–1	17	13
All	4,670,514,740	–	177	159	–	–	51¶	41¶

* Percent changes are 5-year changes from year 2012, unless otherwise indicated. IV = intravenous.
† Average annual rebate percentages were extrapolated from those reported by the Congressional Budget Office for brand name specialty drugs for the years 2010 (2.6%) and 2015 (10.5%). Extrapolated annual percentages were 5.8% (2012), 7.3% (2013), 8.9% (2014), and 12.1% (2016).
‡ Three-year changes in spending and dosage volume were calculated since no data were available for 2012, and limited data were available for 2013.
§ Three-year changes in spending and dosage volume were calculated since the subcutaneous (SC) formulation of tocilizumab was not approved until October 2013.
¶ Median change across all biologic disease-modifying antirheumatic drugs (DMARDs) covered under Medicare Part D.

as in aggregate, employing formulas adapted from those used by the US Congressional Budget Office (CBO) (26). Since Medicaid data files do not contain information on number of recipients (22), we defined volume effects for biologic DMARDs covered under Medicaid simply as the total number of doses dispensed.

Rebate adjustment. The spending amounts represent actual program spending and directly impact beneficiary out-of-pocket spending, which were our main outcomes of interest. These amounts do not include Medicare Part D rebates from manufacturers to either pharmacy benefit managers (PBMs) or Part D plans (there are no such point-of-sale rebates in Part B). For Medicaid, the drug rebate amounts are based on statutory formulas, and the minimum basic rebate for biologic DMARDs, which Medicaid classifies as single-source innovator drugs, is 23.1% (32). Manufacturers pay the Medicaid drug rebates on a quarterly basis, with the rebate split between the states and the federal government (32). Therefore, we conducted our analyses including the Medicaid rebates (as these decrease public spending), but both excluded and included consideration of the Medicare Part D rebates.

As CMS is prohibited from publicly disclosing the rebates paid for specific drugs, rebate amounts for each year of study were extrapolated from the average rebates for brand name specialty drugs reported by the CBO for years 2010 (2.6% and 42.1% for Medicare Part D and Medicaid, respectively) and 2015 (10.5% and 50% for Medicare Part D and Medicaid, respectively) (33). The extrapolated Medicare Part D rebate percentages were 5.8% in 2012, 7.3% in 2013, 8.9% in 2014, and 12.1% in 2016, and the corresponding statutory Medicaid rebates (basic and inflation rebates combined) were 45.2% in 2012, 46.7% in 2013, 48.3% in 2014, and 51.6% in 2016. The CBO was granted access to confidential data from years 2010–2015 on the rebates paid to Part D plans and statutory Medicaid rebates for individual drugs, which they used to determine the average rebates for brand name drugs in each program. Thus, we applied the same rebate amount to each biologic DMARD.

Sensitivity analysis. Evidence suggests that higher-than-average rebates may be negotiated for brand name specialty drugs available from multiple manufacturers, with the possible inclusion of biologic DMARDs. Thus, to account for this uncertainty and lack of transparency surrounding rebates, we repeated our Medicare Part D analysis using larger time-varying rebate amounts, as employed in previous analyses of Medicare drug spending (34,35), though not specific to specialty brand name drugs. These ranged from 20% (in 2012) to 30% (in 2016). We also reassessed spending trends and contributors with rituximab included. Furthermore, we separately assessed spending trends and contributors for tofacitinib, an oral medication that was the only targeted synthetic DMARD approved by the FDA during the study period (approved for RA in November 2012).

RESULTS

Ten biologic DMARDs met inclusion criteria and were included in the main study cohort: abatacept, anakinra, adalimumab, belimumab, certolizumab, etanercept, golimumab, infliximab, tocilizumab, and ustekinumab (Supplementary Table 1, available on the *Arthritis & Rheumatology* web site at http://onlinelibrary.wiley.com/doi/10.1002/art.41138/abstract). From 2012 to 2016, annual spending on Medicare and Medicaid claims for these 10 biologic DMARDs increased by $4.8 billion (from $3.8 billion in 2012 to $8.6 billion in 2016, a 126% increase). Biologic DMARD price increases alone were responsible for $2.5 billion of this $4.8 billion rise in spending. By program, total annual spending increased by 177% in Medicare Part D, 80% in Medicare Part B, and 204% in Medicaid. The majority of 2016 Medicare claims were for prescriptions from rheumatologists, except for ustekinumab (71% from dermatologists) and rituximab (Supplementary Table 2, available on the *Arthritis & Rheumatology* web site at http://onlinelibrary.wiley.com/doi/10.1002/art.41138/abstract).

Medicare Part D spending on biologic DMARDs. Reported Medicare Part D spending increased by $3.0 billion over the 5 years examined in this study. Biologic DMARDs with the biggest increases included adalimumab ($1.5 billion increase), etanercept ($813 million), ustekinumab ($211 million), and abatacept ($197 million). When time-varying manufacturers' rebates were applied, the 5-year increase in Part D spending still exceeded $2.5 billion. Prices for most biologic DMARDs increased substantially over the period, with a median list price increase of 51% (mean 54%) and rebate-adjusted median price increase of 41% (mean 45%) (Table 1). With controlling for increases in dosage volume, drug price increases accounted for 57% of the 5-year increase in aggregate inflation-adjusted spending within Part D (Figure 1). Growth in the number of recipients accounted for 37% of total spending, while annual number of claims per recipient accounted for 6%. After CBO-reported time-varying rebates were applied, prices were still responsible for 54% of the aggregate Part D spending increase (Figure 1); when larger time-varying rebate amounts (20–30% of the list price) were applied, unit price hikes still accounted for half of the 5-year 142% spending increase (Supplementary Figure 1, available on the *Arthritis & Rheumatology* web site at http://onlinelibrary.wiley.com/doi/10.1002/art.41138/abstract).

For most individual Medicare Part D drugs, drug prices accounted for ≥50% of the increase in spending (Figure 1). Adalimumab and etanercept, 2 of the oldest biologic DMARDs, were prescribed to the largest numbers of Part D beneficiaries (>47,000 in 2016) and had the biggest 5-year price increases: 84% for adalimumab and 88% for etanercept (72% and 75%, respectively, with rebate adjustments) (Table 1). Total annual spending on the oral targeted synthetic DMARD, tofacitinib, increased by $175 million from 2013 to 2016. Forty-eight percent of this increase was from
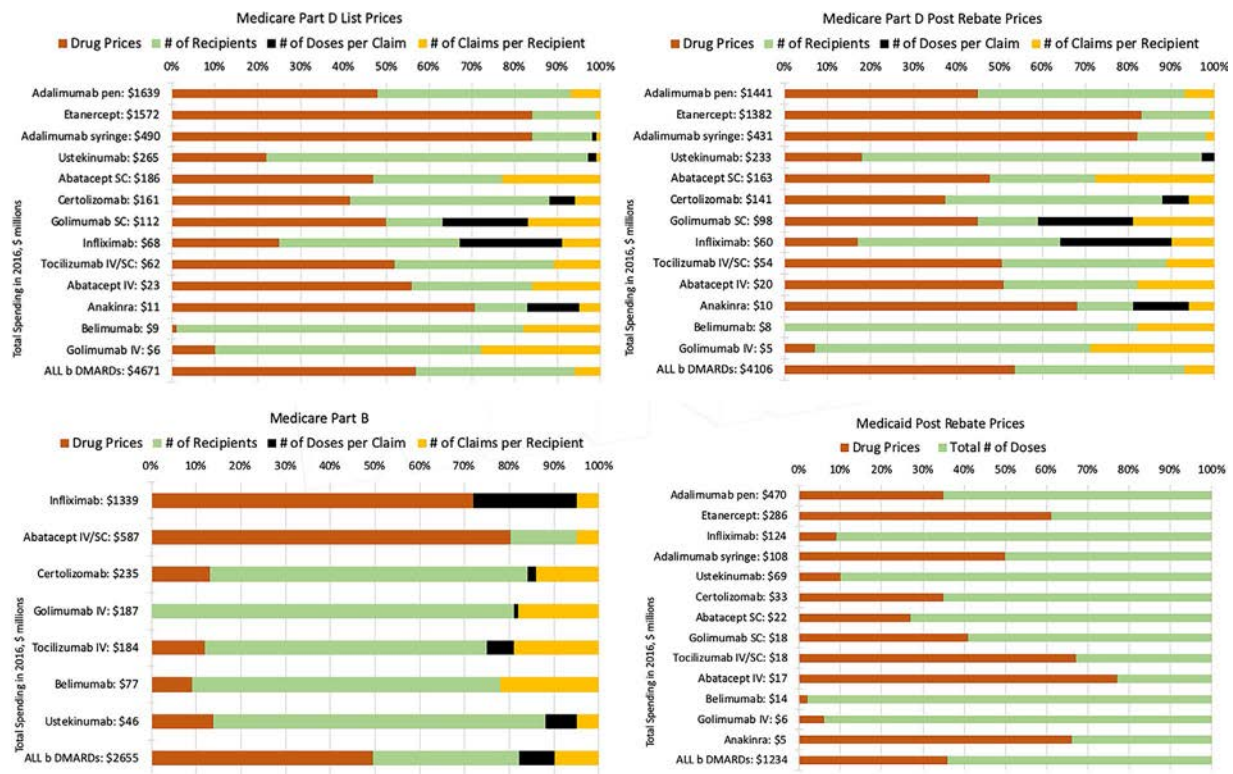
Figure 1. Component proportion of biologic disease-modifying antirheumatic drug (bDMARD) spending increases from 2012 to 2016 (ranked by 2016 spending), by public program. SC = subcutaneous; IV = intravenous.

an increased number of recipients, with increases in drug price and number of claims per recipient each responsible for 25% of this overall increase.

Medicare Part B spending on biologic DMARDs. In Medicare Part B, total annual spending increased by $1.2 billion from years 2012 to 2016, with abatacept and infliximab as the biggest contributors to this increase ($300 million and $284 million increases, respectively). Compared to Medicare Part D, drug price increases for biologic DMARDs covered under Part B were much lower (median change 8%; mean 21%) (Table 2).

Yet, drug price increases accounted for 50% of the increase in aggregate Part B spending, while growth in recipient numbers contributed 33%, number of claims per person contributed 10%, and changes in treatment intensity (number of doses per claim) contributed 8%. The majority of spending growth for the 2 oldest Part B drugs included in our primary analysis (abatacept and infliximab) was due to price increases (81% and 72% of spending growth, respectively), whereas for the 5 newer drugs (golimumab, ustekinumab, tocilizumab, certolizumab, and belimumab), number of recipients was the main driver of spending growth (63–81%) (Figure 1). When rituximab was

Table 2. Annual spending and utilization for biologic DMARDs covered under Medicare Part B fee-for-service program*

Biologic DMARD	Total spending in 2016, dollars	No. of recipients in 2016	Change from 2012			
			Total spending, %	No. of recipients, %	No. of doses per claim, %	Drug prices, %
Infliximab IV	1,338,726,191	58,397	27	−2	6	20
Abatacept (IV or SC)	586,532,893	22,879	104	11	0	79
Certolizumab SC†	235,364,173	11,953	93	60	1	8
Golimumab IV†	186,707,915	10,521	195	144	1	0
Tocilizumab IV	184,202,071	11,167	102	56	4	8
Belimumab IV	76,797,133	2,922	124	84	−6	8
Ustekinumab SC	46,408,889	1,752	379	235	10	21
All	2,654,874,949	–	80	–	–	8‡

* Percent changes are 5-year changes from year 2012, unless otherwise indicated. See Table 1 for definitions.
† Three-year changes in spending and dosage volume were calculated since no data were available for the years 2012 and 2013.
‡ Median change across all biologic DMARDs covered under Medicare Part B.

included, the 5-year increase in Part B spending exceeded $1.3 billion, with 64% from unit price increases, 30% from numbers of recipients, and 6% from numbers of doses per claim. Unlike abatacept, whose total spending increase was predominantly driven by the 79% increase in its unit price, infliximab and rituximab exhibited a different pattern, with modest increases in unit price (20% and 18%, respectively) and even smaller changes in dosage volume (6% increase for infliximab and 6% decrease for rituximab) (Table 2).

Medicaid spending. As shown in Supplementary Table 3 (available on the *Arthritis & Rheumatology* web site at http://onlinelibrary.wiley.com/doi/10.1002/art.41138/abstract), prices and total spending amounts were numerically lower under Medicaid compared to Medicare Part D, but temporal trends were similar. With controlling for changes in dosage volume, drug price increases were responsible for 36% of total spending growth within Medicaid (Figure 1).

DISCUSSION

This study of Medicare and Medicaid data shows that spending on biologic DMARDs more than doubled between 2012 and 2016, reaching $8.6 billion in 2016. Postmarket drug price increases alone (e.g., increases in the prices of drugs already being marketed) accounted for the majority of the increase in total annual spending (i.e., $2.5 billion of the $4.8 billion increase), after adjustment for changes in numbers of recipients and treatment intensity. Moreover, the drug price increases were more prominent in Medicare Part D than in Part B. These detailed decomposition data suggest policy interventions targeting price increases, particularly under Part D plans, may help alleviate financial burdens for patients and taxpayers.

Drug spending growth may be attributable to a range of factors, each with different potential implications for the value of the spending and for the viability of policy interventions aimed at mitigating financial concerns. For example, biologic DMARD spending growth attributable to increases in recipient numbers could be desirable to the extent that it reflects better adherence to effective treatments or reductions in underuse. For drugs that gained new indications during the study period (e.g., ustekinumab for psoriatic arthritis), the increased number of recipients in part reflects patients switching from a therapy that may have been less effective or poorly tolerated to one from which they may have greater benefit. In other scenarios (e.g., belimumab for systemic lupus erythematosus), the increased number of recipients reflects patients' gaining access to biologic treatment for the first time. Alternatively, some growth in the number of drug recipients could reflect overtreatment, e.g., early use of biologic agents versus older nonbiologic DMARDs that might offer greater value (36), or even extension of treatment to those with more questionable indications.

The prominent biologic DMARD cost increases observed in this study, which were substantially greater under Medicare Part D than Part B, even when accounting for rebates, represent a growing burden to taxpayers and beneficiaries. The magnitude of these increases is independent from any assessment of value. Our findings are consistent with recent reports on US wholesale drug expenditures, in which spending on adalimumab and etanercept increased by 180% and 61%, respectively, from 2012 to 2016 (12,37). Similarly, total spending and out-of-pocket costs for biologic agents increased among ~14,000 privately insured RA patients in the US (38). It might be expected that the price increases would be lower in Medicare Part D than in Part B, given the ability to negotiate prices in Part D. However, these negotiations may not necessarily result in lower price increases since PBMs, who negotiate on behalf of Part D plans, retain a percentage of the negotiated rebates as compensation (39), and because higher list prices can achieve higher rebates. While these rebates accrue for insurance plans and PBMs (40), they do not directly impact Part D beneficiaries' out-of-pocket costs, which are driven by pre-rebate (list) prices. Thus, many patients end up paying higher out-of-pocket costs when the list price increases, creating financial barriers to use and adherence (41–43).

Furthermore, this greater accumulation of out-of-pocket costs can also increase government spending by pushing more beneficiaries into the catastrophic coverage phase (44), in which Medicare itself pays 80% of prescription costs. As the patient cost sharing burden for biologic agents tends to be greater under Medicare Part D (45,46), ongoing shifts from Part B to Part D could further exacerbate these concerns.

The recent introduction of biosimilars could foster more competition and lower prices in theory, but as of August 2019, only 2 of 9 FDA-approved DMARD biosimilars (infliximab-dyyb and infliximab-abda) were marketed in the US. The DMARD markets also are potentially more complicated than basic theory may suggest. For example, adalimumab and etanercept, 2 of the earliest approved drugs to market, also experienced some of the largest relative price increases, even as the number of other approved biologic DMARDs increased.

A limitation of this analysis was our reliance on aggregated data, which were more current and standardized than raw data, but prevented us from assessing trends in treatment indications that might be possible with individual-level data. The aggregated data set, however, did include all biologic DMARD claims processed for the entire Medicare Part D and Part B fee-for-service populations (as opposed to the portions of data examined previously) and allowed us to examine the spending trends overall and by component. While we could not incorporate proprietary data on individual drug-specific manufacturers' rebates, applying time-varying manufacturers' rebates of ≤30% did not meaningfully impact our findings. Furthermore, our rebate-adjusted findings expand on a recent analysis (47) that showed little impact from

the incorporation of manufacturers' rebates and other discounts for adalimumab and etanercept when assessing their price hikes from 2009 to 2015.

Fundamentally, there is a lack of transparency surrounding the rebates paid for specific drugs and even classes of drugs. While rebates for brand name specialty drugs tend to be smaller than for nonspecialty drugs on the whole (e.g., 10.5% versus 28.4% of the list price, respectively, in 2015 [33]), this varies by class. Reports suggest rebates are higher for specialty drugs that are available from multiple manufacturers (e.g., insulin [40,47] and hepatitis C therapies [40]), wherein insurance plans have more negotiating power compared to specialty drugs with limited competition or those in protected classes such as antineoplastic agents (40,47,48). It is difficult to speculate about the rebates for biologic DMARDs, though a third-party analysis of selected biologic DMARDs (47) suggests they may be relatively low, with total price discounts for etanercept, abatacept, and adalimumab (inclusive of rebates, concessions given to wholesalers and distributors, and other discounts) averaging around 20%. As such, while rebate pass-through at the point of sale (or similar proposals wherein rebates are converted to discounts off the list price) may help lower out-of-pocket costs for patients prescribed highly rebated medications (40), those taking biologic DMARDs may reap fewer benefits. We echo notions that a multifaceted approach (40,49) is needed to control prescription drug spending and out-of-pocket costs, and potentially one that eliminates specialty tiers (50), changes how PBMs are compensated (40), and increases pricing transparency (49,50).

In conclusion, postmarket drug price changes alone accounted for the majority of recent multibillion-dollar increases in biologic DMARD spending. Policy interventions that target price increases, particularly under Medicare Part D plans, may help lessen financial burdens for taxpayers and elderly and disabled biologic DMARD recipients alike.

AUTHOR CONTRIBUTIONS

All authors were involved in drafting the article or revising it critically for important intellectual content, and all authors approved the final version to be published. Dr. McCormick had full access to all of the data in the study and takes responsibility for the integrity of the data and the accuracy of the data analysis.
Study conception and design. McCormick, Hsu, Choi.
Acquisition of data. Wallace, Sacks, Choi.
Analysis and interpretation of data. McCormick, Wallace, Sacks, Hsu, Choi.

REFERENCES

1. Ruiz Garcia V, Burls A, Cabello JB, Vela Casasempere P, Bort-Marti S, Bernal JA. Certolizumab pegol (CDP870) for rheumatoid arthritis in adults. Cochrane Database Syst Rev 2017;9:CD007649.

2. Singh JA, Hossain A, Tanjong Ghogomu E, Mudano AS, Tugwell P, Wells GA. Biologic or tofacitinib monotherapy for rheumatoid arthritis in people with traditional disease-modifying anti-rheumatic drug (DMARD) failure: a Cochrane Systematic Review and network meta-analysis (NMA). Cochrane Database Syst Rev 2016;11:CD012437.

3. Rahman P, Puig L, Gottlieb AB, Kavanaugh A, McInnes IB, Ritchlin C, et al. Ustekinumab treatment and improvement of physical function and health-related quality of life in patients with psoriatic arthritis. Arthritis Care Res (Hoboken) 2016;68:1812–22.

4. Hassan RI, Gaffo AL. Rituximab in ANCA-associated vasculitis [review]. Curr Rheumatol Rep 2017;19:6.

5. Olofsson T, Petersson IF, Eriksson JK, Englund M, Nilsson JA, Geborek P, et al, for the ARTIS Study Group. Predictors of work disability after start of anti-TNF therapy in a national cohort of Swedish patients with rheumatoid arthritis: does early anti-TNF therapy bring patients back to work? Ann Rheum Dis 2017;76:1245–52.

6. Kristensen LE, Englund M, Neovius M, Askling J, Jacobsson LT, Petersson IF. Long-term work disability in patients with psoriatic arthritis treated with anti-tumour necrosis factor: a population-based regional Swedish cohort study. Ann Rheum Dis 2013;72:1675–9.

7. Kristensen LE, Petersson IF, Geborek P, Jöud A, Saxne T, Jacobsson LT, et al. Sick leave in patients with ankylosing spondylitis before and after anti-TNF therapy: a population-based cohort study. Rheumatology (Oxford) 2012;51:243–9.

8. Li S, Molony JT, Peng Y, Nieman KM, Gilbertson DT. Prevalence of rheumatoid arthritis and associated comorbidities in the 2011–2015 Medicare population [abstract]. Arthritis Rheumatol 2017;69 Suppl 10. URL: https://acrabstracts.org/abstract/prevalence-of-rheumatoid-arthritis-and-associated-comorbidities-in-the-2011-2015-medicare-population/.

9. Li S, Gong T, Peng Y, Nieman K, Gilbertson D. Prevalence of systemic lupus erythematosus (SLE) and associated comorbidities in the 2011–2015 Medicare population [abstract]. Arthritis Rheumatol 2018;70 Suppl 10. URL: https://acrabstracts.org/abstract/prevalence-of-systemic-lupus-erythematosus-sle-and-associated-comorbidities-in-the-2011-2015-medicare-population/.

10. Hutfless SM, Wang P. Su1850: inflammatory bowel disease rates in the United States Medicare population [abstract]. Gastroenterology 2018;154 Suppl 1:S-606.

11. Institute for Clinical and Economic Review (ICER), for New England Comparative Effectiveness Public Advisory Council. Targeted immune modulators for rheumatoid arthritis: effectiveness & value. April 2017. URL: https://icer-review.org/wp-content/uploads/2016/08/NE_CEPAC_RA_Evidence_Report_FINAL_040717.pdf.

12. Schumock GT, Li EC, Wiest MD, Suda KJ, Stubbings J, Matusiak LM, et al. National trends in prescription drug expenditures and projections for 2017. Am J Health Syst Pharm 2017;74:1158–73.

13. US Department of Health and Human Services. National health expenditure accounts: methodology paper, 2017. Definitions, sources, and methods. URL: https://www.cms.gov/Research-Statistics-Data-and-Systems/Statistics-Trends-and-Reports/NationalHealthExpendData/downloads/dsm-17.pdf.

14. President Donald J. Trump's blueprint to lower drug prices. May 2018. URL: https://www.whitehouse.gov/briefings-statements/president-donald-j-trumps-blueprint-lower-drug-prices/.

15. Trump administration proposes to lower drug costs by targeting back-door rebates and encouraging direct discounts to patients. January 2019. URL: https://www.hhs.gov/about/news/2019/01/31/trump-administration-proposes-to-lower-drug-costs-by-targeting-backdoor-rebates-and-encouraging-direct-discounts-to-patients.html.

16. San-Juan-Rodriguez A, Prokopovich MV, Shrank WH, Good CB, Hernandez I. Assessment of price changes of existing tumor necrosis factor inhibitors after the market entry of competitors. JAMA Intern Med 2019;179:713–6.

17. Starr M, Dominiak L, Aizcorbe A. Decomposing growth in spending finds annual cost of treatment contributed most to spending growth, 1980–2006. Health Aff (Millwood) 2014;33:823–31.

18. Centers for Medicare & Medicaid Services. CMS drug spending. URL: https://www.cms.gov/Research-Statistics-Data-and-Systems/Statistics-Trends-and-Reports/Information-on-Prescription-Drugs/index.html.

19. Centers for Medicare & Medicaid Services. Medicare Part D Drug Spending Dashboard & data. URL: https://www.cms.gov/Research-Statistics-Data-and-Systems/Statistics-Trends-and-Reports/Information-on-Prescription-Drugs/MedicarePartD.html.

20. Centers for Medicare & Medicaid Services. Research, statistics, data & systems. URL: https://www.cms.gov/Research-Statistics-Data-and-Systems/Research-Statistics-Data-and-Systems.html.

21. Centers for Medicare & Medicaid Services. Medicare Part B Drug Spending Dashboard. URL: https://www.cms.gov/Research-Statistics-Data-and-Systems/Statistics-Trends-and-Reports/Information-on-Prescription-Drugs/MedicarePartB.html.

22. Centers for Medicare & Medicaid Services. Medicaid Drug Spending Dashboard. URL: https://www.cms.gov/Research-Statistics-Data-and-Systems/Statistics-Trends-and-Reports/Information-on-Prescription-Drugs/Medicaid.html.

23. Centers for Medicare & Medicaid Services. Medicare provider utilization and payment data: 2016 Part D prescriber. URL: https://data.cms.gov/Medicare-Part-D/Medicare-Provider-Utilization-and-Payment-Data-201/yvpj-pmj2.

24. Centers for Medicare & Medicaid Services. Medicare provider utilization and payment data: physician and other supplier PUF CY2016. 2015. URL: https://data.cms.gov/Medicare-Physician-Supplier/Medicare-Provider-Utilization-and-Payment-Data-Phy/utc4-f9xp.

25. US Bureau of Labor Statistics. Consumer Price Index. URL: https://www.bls.gov/cpi/.

26. Congressional Budget Office. Background paper: factors underlying the growth in Medicare's spending for physicians' services. June 2007. URL: https://www.cbo.gov/publication/18726.

27. Bundorf MK, Royalty A, Baker LC. Health care cost growth among the privately insured. Health Aff (Millwood) 2009;28:1294–304.

28. Wu J, Yue N, Xu W. Increasing anti-infective drug expenditure in Tianjin, China: a decomposition analysis. Value Health Reg Issues 2013;2:37–42.

29. Soppi A, Heino P, Kurko T, Maljanen T, Saastamoinen L, Aaltonen K. Growth of diabetes drug expenditure decomposed—a nationwide analysis. Health Policy 2018;122:1326–32.

30. Morgan SG. Quantifying components of drug expenditure inflation: the British Columbia seniors' drug benefit plan. Health Serv Res 2002;37:1243–66.

31. Morgan S. Drug spending in Canada: recent trends and causes. Med Care 2004;42:635–42.

32. Medicaid. Medicaid drug rebate program. URL: https://www.medicaid.gov/medicaid/prescription-drugs/medicaid-drug-rebate-program/index.html.

33. Anderson-Cook A, Maeda J, Nelson L, for the Congressional Budget Office. Prices for and spending on specialty drugs in Medicare Part D and Medicaid: an in-depth analysis. March 2019. URL: https://www.cbo.gov/publication/55011.

34. Hwang TJ, Jain N, Lauffenburger JC, Vokinger KN, Kesselheim AS. Analysis of proposed Medicare Part B to Part D shift with associated changes in total spending and patient cost-sharing for prescription drugs. JAMA Intern Med 2019;179:374–80.

35. Venker B, Stephenson KB, Gellad WF. Assessment of spending in Medicare Part D if medication prices from the Department of Veterans Affairs were used. JAMA Intern Med 2019;179:431–3.

36. Bansback N, Phibbs CS, Sun H, O'Dell JR, Brophy M, Keystone EC, et al. Triple therapy versus biologic therapy for active rheumatoid arthritis: a cost-effectiveness analysis. Ann Intern Med 2017;167:8–16.

37. Schumock GT, Li EC, Suda KJ, Matusiak LM, Hunkler RJ, Vermeulen LC, et al. National trends in prescription drug expenditures and projections for 2014. Am J Health Syst Pharm 2014;71:482–99.

38. Atzinger CB, Guo JJ. Biologic disease-modifying antirheumatic drugs in a national, privately insured population: utilization, expenditures, and price trends. Am Health Drug Benefits 2017;10:27–36.

39. Bai G, Sen AP, Anderson GF. Pharmacy benefit managers, brand-name drug prices, and patient cost sharing. Ann Intern Med 2018;168:436–7.

40. Dusetzina SB, Bach PB. Prescription drugs-list price, net price, and the rebate caught in the middle. JAMA 2019;321:1563–4.

41. Doshi JA, Hu T, Li P, Pettit AR, Yu X, Blum M. Specialty tier-level cost sharing and biologic agent use in the Medicare Part D initial coverage period among beneficiaries with rheumatoid arthritis. Arthritis Care Res (Hoboken) 2016;68:1624–30.

42. Heidari P, Cross W, Crawford K. Do out-of-pocket costs affect medication adherence in adults with rheumatoid arthritis? A systematic review. Semin Arthritis Rheum 2018;48:12–21.

43. Hsu J, Price M, Huang J, Brand R, Fung V, Hui R, et al. Unintended consequences of caps on Medicare drug benefits. N Engl J Med 2006;354:2349–59.

44. Dusetzina SB, Conti RM, Yu NL, Bach PB. Association of prescription drug price rebates in Medicare Part D with patient out-of-pocket and federal spending. JAMA Intern Med 2017;177:1185–8.

45. Yazdany J, Tonner C, Schmajuk G. Use and spending for biologic disease-modifying antirheumatic drugs for rheumatoid arthritis among US Medicare beneficiaries. Arthritis Care Res (Hoboken) 2015;67:1210–8.

46. Zhang J, Xie F, Delzell E, Chen L, Kilgore ML, Yun H, et al. Trends in the use of biologic agents among rheumatoid arthritis patients enrolled in the US Medicare program. Arthritis Care Res (Hoboken) 2013;65:1743–51.

47. Langreth R, Keller M, Cannon C. Decoding big pharma's secret drug pricing practices. June 2016. URL: https://www.bloomberg.com/graphics/2016-drug-prices/.

48. Azar AM II, US Department of Health and Human Services. Remarks on drug pricing blueprint. May 2018. URL: https://www.hhs.gov/about/leadership/secretary/speeches/2018-speeches/remarks-on-drug-pricing-blueprint.html.

49. Daniel H, for the Health and Public Policy Committee of the American College of Physicians. Stemming the escalating cost of prescription drugs: a position paper of the American College of Physicians. Ann Intern Med 2016;165:50–2.

50. American College of Rheumatology. 2019 ACR health policy statements. URL: https://www.rheumatology.org/Portals/0/Files/ACR-Health-Policy-Statements.pdf.

AMERICAN COLLEGE
of RHEUMATOLOGY
Empowering Rheumatology Professionals

Comprehensive Profiling of the Rheumatoid Arthritis Antibody Repertoire

Ken C. Lo,[1] [ID] Eric Sullivan,[1] Ryan M. Bannen,[1] Huiyan Jin,[1] Mark Rowe,[1] Hanying Li,[1] Richard S. Pinapati,[1] Adam J. Cartwright,[1] John C. Tan,[1] Jigar Patel,[1] Edward C. Keystone,[2] and Katherine A. Siminovitch[3]

Objective. Autoantibodies against citrullinated proteins are found in 64–89% of rheumatoid arthritis (RA) patients, with 88–99% specificity. This study was undertaken to create an unbiased, comprehensive profile of serum antibodies against the human proteome, including the citrullinome and the homocitrullinome, in RA patients, using a high-density peptide array.

Methods. Our high-density peptide array, consisting of >4.6 million peptides, contained the entire annotated human proteome. The 20,246 proteins were represented as overlapping 16-mer peptides. In addition to native peptides, citrullinated and homocitrullinated peptides were included, as substitutions for arginine and lysine, and provided a comprehensive screen against all possible epitopes. Twenty-six serum samples (from 8 controls and 18 RA patients) were profiled on the high-density peptide array. Using RA-specific epitopes, we constructed an 8-epitope diagnostic biomarker on a Gyrolab xPlore instrument with a cohort of 92 serum samples (from 29 controls and 63 RA patients). The diagnostic biomarker was further validated with an independent cohort of 181 serum samples (from 54 controls and 127 RA patients).

Results. In the initial cohort the diagnostic performance of the 8-epitope biomarker yielded 96.6% specificity and 92.1% sensitivity. The overall diagnostic performance in the validation cohort was 94.4% specificity and 85% sensitivity. In both cohorts, the performance of the 8-epitope diagnostic biomarker compared favorably against the Abnova cyclic citrullinated peptide 2 (CCP2) assay. Using data from the peptide array, we identified novel RA-specific epitopes and formed the basis of a new RA diagnostic assay.

Conclusion. Comprehensive antibody profiling using a high-density peptide array not only identified novel RA-specific epitopes but also allowed us to construct a novel diagnostic biomarker that is as specific as and more sensitive than the Abnova CCP2 assay.

INTRODUCTION

Rheumatoid arthritis (RA) is a progressive autoimmune disease characterized by inflammation and progressive erosion of joint cartilage and bone tissue. In the seminal works by Schellekens et al (1) and Shi et al (2), antibodies against citrullinated and homocitrullinated proteins were isolated from RA patients and are thought to contribute to RA pathogenesis. Anti–citrullinated protein antibody (ACPA) blood tests were then developed, and ACPA status was included in the American College of Rheumatology (ACR)/European League Against Rheumatism (EULAR) 2010 classification criteria for RA (3). ACPA-positive subsets of RA patients typically have a more aggressive disease course (4), thereby making early diagnosis critical for early intervention to minimize joint erosion and maintain subsequent joint motility for RA patients.

Increasingly, serum profiling using either protein or peptide arrays is becoming commonplace in the study of various diseases. Notable examples include systemic lupus erythematosus, infectious diseases, cancer, and RA (5–11). While protein arrays may have the advantage of retaining native 3-dimensional conformation, complete conversion of arginine and lysine to citrulline and homocitrulline in recombinant proteins remains a challenge. Peptide arrays, however, can circumvent these problems by incorporating the necessary monomer during the peptide synthesis process. In the case of peptide arrays synthesized using maskless array synthesis, photoprotected citrulline and homocitrulline were added to the catalog of canonical amino acids used during the synthesis process. Substitution of arginine and lysine with citrulline and homocitrulline, respectively, is accomplished during the array design process, and incorporation efficiency is limited only by the efficiency of the coupling reaction. Thus, citrulline-specific antibody reactivity detected on the peptide array is not conflated by the incomplete conversion of arginine to citrulline in the case of enzymatic conversion.

Antibody binding to its cognate antigen is achieved through noncovalent interactions between the complementarity-determining regions of the antibody against conformation adopted by the antigen. While structural studies have illustrated the importance of key residues at the interfaces, it is unclear what proportion of the human antibody repertoire recognizes epitopes derived from conformation adopted by contiguous amino acids (linear epitopes) and discontinuous amino acid stretches (conformational epitopes) (12,13), especially in the context of RA. To our knowledge, an unbiased and comprehensive profile of serum antibodies in RA serum samples against the entire human proteome, including the citrullinome and the homocitrullinome, has not been reported in the literature. Using this comprehensive serum antibody profile, novel epitopes that are RA specific can be used to develop future diagnostic, prognostic, and theranostic assays.

MATERIALS AND METHODS

Peptide array design, synthesis, and processing. Peptide array design, synthesis, and processing were performed as described in the study by Yan et al (14). The peptide array included >4.6 million peptides and contained the entire annotated human proteome. The 20,246 proteins were represented as overlapping 16-mer peptides.

Data analysis. All analyses were performed in the R statistical programming environment, version 3.2.3 (www.cran.r-project.org) using an R package "RNGdat" that was developed in-house. Briefly, raw array signal intensities were spatially corrected via a 2-dimensional loess smoother (15) and background was corrected by deconvolution (16). A 1-sided Kolmogorov-Smirnov test was used to assess whether the signal within an 8-mer sliding window centered on a specific probe was above the sampled background (17). A signal intensity exceeding 2^{12} (or 4,096) fluorescence units with a sliding window significance of 0.05 was used to categorize significant antibody reactivity. An epitope was defined as ≥2 contiguous probes with significant reactivity.

Hierarchical clustering was performed on log-transformed array signal intensities using peptide probe intensities belonging to significant epitopes in ≥3 samples within the 26 serum samples profiled on the whole proteome array, using the R package "hclust." Hierarchical clustering was performed separately for citrullinated, homocitrullinated, and native peptide probes.

All data graphics were created using the R package "ggplot2," version 2.2.1, and any additional statistical analyses were conducted in R (including central tendency such as the mean). For additional information, please refer to R documentation. Data are available in the Gene Expression Omnibus database (https://www.ncbi.nlm.nih.gov/geo/query/acc.cgi?acc=GSE136052).

Gyros miniature immunoassay. Peptides were obtained from Lifetein (www.lifetein.com) and synthesized with C-terminal amidation and biotinylation via the side chain of the C-terminal lysine. The Gyros 3-step Capture Analyte Detect (CAD) assay was carried out according to the manufacturer's instructions. During the capture phase of the 3-step CAD assay, 1 μM peptide in 1× phosphate buffered saline–Tween was used. Serum samples were diluted to 10% in 1× HNmax buffer. Alexa Fluor 647–conjugated goat anti–human Fc secondary antibody (1 mg/ml stock) was diluted to 3.6 µg/ml in 1× Rexxip F buffer. Quantification of signal intensity was performed with Gyrolab Evaluator software using signal at the 5% photomultiplier tube scan setting.

After signal extraction, signal specific to citrullinated or homocitrullinated peptide was converted to a ratio against the native peptide, which we termed the "signal-to-noise" ratio. For signal not specific to citrullinated or homocitrullinated peptides, the ratio was calculated against a no-peptide control.

Cyclic citrullinated peptide 2 (CCP2) assay. A CCP2 IgG enzyme-linked immunosorbent assay kit was purchased from Abnova (www.abnova.com). The assay was conducted according to the manufacturer's instructions with one deviation: at step 8, the reaction after adding chromogenic substrate solution was stopped after 5 minutes. The resulting colorimetric intensity was measured at 450 nm using a BioTek Synergy 2 Multi-Mode Microplate Reader.

Patients and healthy controls. Serum samples were obtained from healthy individuals and patients with RA who fulfilled the ACR/EULAR 2010 classification criteria. Samples obtained at the outpatient clinic of the Rheumatology Division at Mount Sinai Hospital were collected after obtaining appropriate informed consent and in accordance with the Institutional Review Board. Commercial serum samples were purchased from Discovery

Life Sciences. Samples were obtained under Institutional Review Board–approved protocols.

RESULTS

RA antibody reactome. The comprehensive human proteome profiling of antibody reactivity against native, citrullinated, and homocitrullinated linear peptide probes undertaken in this study represents the first unbiased portrait of the RA serum antibody repertoire, which we term the "RA antibody reactome". The frequency of significant antibody reactivity (defined in Materials and Methods) is shown in Figure 1. The peptide probes detected at high frequency (≥50%) in RA samples and control samples are listed in Supplementary Table 1, available on the *Arthritis & Rheumatology* web site at http://onlinelibrary.wiley.com/doi/10.1002/art.41089/abstract. Overall, antibody reactivity against citrullinated peptide probes was detected at high frequency within the cohort of 18 RA serum samples, as shown by the preponderance of bars in Figure 1 exceeding 50%, throughout the proteome. A total of 14,953 citrullinated peptide probes (1.1% of total citrullinated probes) had significant reactivity at high frequency in RA samples and could potentially represent diagnostic biomarkers

(Supplementary Table 1). This was in contrast to antibody reactivity for native and homocitrullinated peptide probes, which was observed at substantially lower frequencies (Figure 1). Only 10 native and 2 homocitrullinated peptide probes showed significant reactivity in >50% of the RA samples (Supplementary Table 1).

When a group comparison was made between all RA samples (including both ACPA-positive and ACPA-negative patients) and control samples, the mean number of peptide probes with significant reactivity was not significantly different for native or homocitrullinated peptide probes ($P = 0.997$ for both) (Supplementary Figure 1, available on the *Arthritis & Rheumatology* web site at http://onlinelibrary.wiley.com/doi/10.1002/art.41089/abstract). In contrast, a difference was detected for citrullinated peptide probes ($P = 0.020$) (Supplementary Figure 1). Interestingly, antibody reactivity against native peptide probes was observed for control samples, which is consistent with the findings of Nagele et al (18). Unexpectedly, reactivity against citrullinated and homocitrullinated peptide probes was also observed for control samples and was not restricted to specific individuals. In fact, 2 homocitrullinated peptide probes showed reactivity in up to 50% of controls but were absent in RA samples (Supplementary Table 1).
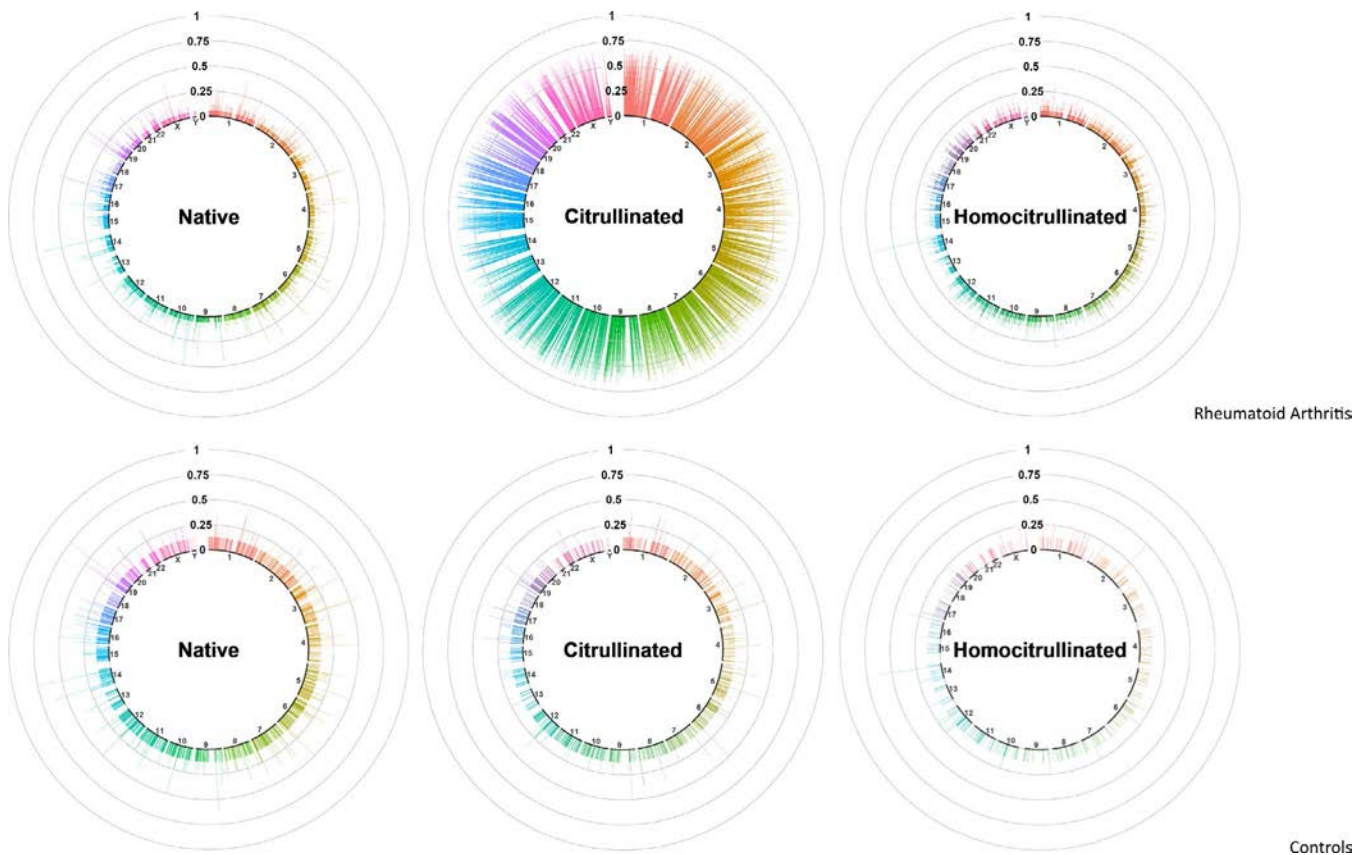
Figure 1. Map of the rheumatoid arthritis (RA) antibody reactome for native peptides, citrullinated peptides, and homocitrullinated peptides in RA samples (top) and control samples (bottom). Peptides are organized by their chromosomal locations. The height of the bar indicates the proportion of samples for which significant antibody reactivity was detected on a high-density peptide array. To facilitate visualization, all peptides are color coded and grouped by their chromosome. Color figure can be viewed in the online issue, which is available at http://onlinelibrary.wiley.com/doi/10.1002/art.41089/abstract.
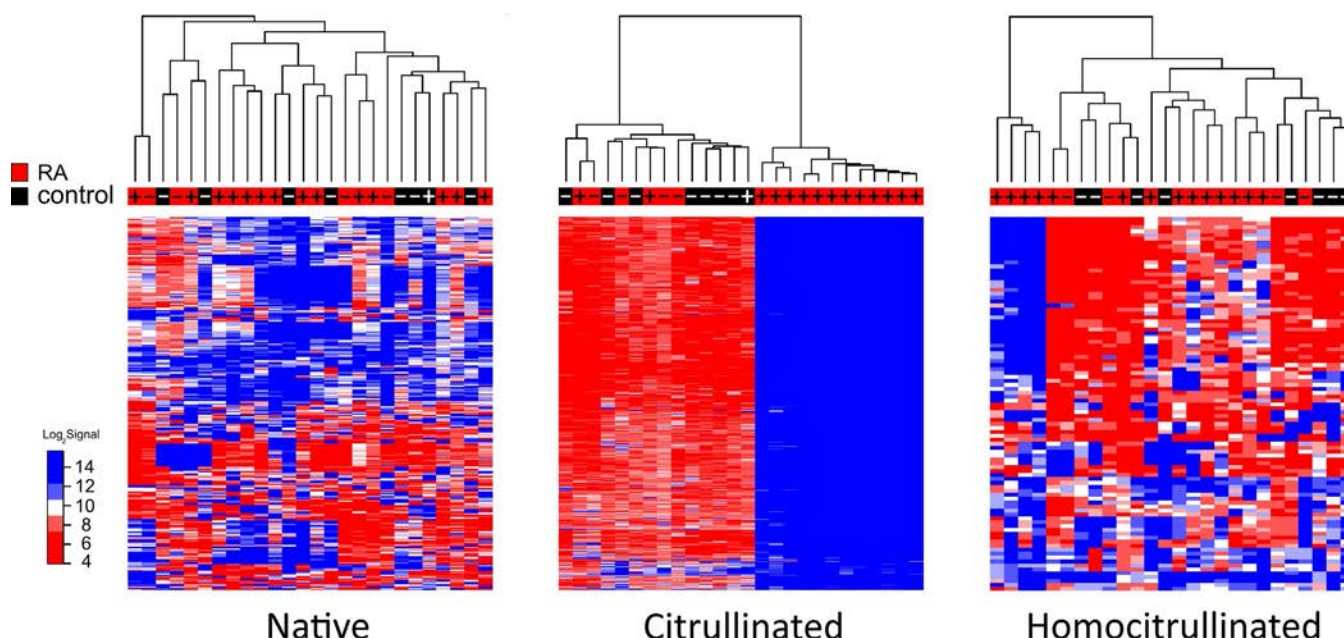
Figure 2. Heatmaps of log-transformed array signals derived from a high-density peptide array for native, citrullinated, and homocitrullinated peptides in rheumatoid arthritis (RA) and control samples. Red indicates low signals; blue indicates high signals. Peptides are organized in rows, and serum samples are organized in columns. Plus signs indicate cyclic citrullinated peptide 2 (CCP2) positivity; minus signs indicate CCP2 negativity.

Within the RA antibody reactome, hierarchical clustering analysis (as described in Materials and Methods) showed that 12 of 18 RA samples had consistent peptide level reactivity against citrullinated peptide probes and readily formed a group of RA patients distinct from controls (Figure 2). In contrast, antibody reactivity against native peptide probes did not show any ability to distinguish between RA and control samples (Figure 2). Interestingly, strong reactivity against homocitrullinated peptide probes was seen in 4 RA samples, although those individuals also showed reactivity against citrullinated peptide probes and did not constitute a homocitrulline-positive/citrulline-negative subgroup (Figure 2).

Miniature immunoassay validation of peptide array findings in RA sera. Due to the overlapping nature of the linear peptide array, antibody reactivity against a linear epitope is expected to be represented by signals from multiple contiguous peptide probes. As such, significant signals observed in contiguous peptide probes are summarized as "composite epitopes" since some of these composite epitopes contain multiple citrulline residues. As these composite epitopes may have potential implications for RA prognosis or diagnosis and are the bases of current diagnostic assays, citrullinated composite epitopes frequently observed in RA samples are listed in Table 1. These frequently occurring composite epitopes against citrullinated peptide probes ranged from 20 amino acids (2 contiguous peptides) to as long as 44 amino acids (7 contiguous peptides) in size, with a mean size of 26.7 amino acids.

While the array detected antibody reactivity against citrullinated peptide probes in proteins previously reported to be associated with RA, such as filaggrin and fibrin (UniProt IDs P20930, P02671, and P02675) (Supplementary Table 1), many of the proteins detected had not previously been reported to be associated with RA. As an illustrative example, we conducted a PubMed search of the proteins listed in Table 1 with the search term "rheumatoid arthritis" (Supplementary Table 2, available on the *Arthritis & Rheumatology* web site at http://onlinelibrary.wiley.com/doi/10.1002/art.41089/abstract). Eleven of the 25 proteins yielded no results. Additionally, for many of the proteins, a connection with RA was established through either association studies or gene expression analysis but not by the detection of ACPAs against these proteins. These proteins may represent novel targets for further investigation. However, epitopes against homocitrullinated and native peptides occurring at 50% frequency were not seen exclusively in RA serum samples (Supplementary Table 1).

To verify antibody reactivity findings for frequently occurring composite epitopes, we used a Gyrolab xPlore miniature immunoassay instrument. The Gyrolab instrument uses microfluidics to carry out an automated miniature enzyme-linked immunosorbent assay. In some instances, frequently occurring composite epitopes are broken into multiple peptides depending on the length of the region due to peptide synthesis limitations. An illustrative example is shown in Figure 3A, where the peptide sequence N′-CNTCIYTEGWKCMAG-R/citrulline-GTCIAKENELCS-C′, corresponding to positions 29–56 of the protein prostate and testis expressed protein 4 (P0C8F1) and comprising 4 contiguous

Table 1. Citrullinated composite epitopes most frequently associated with RA in the high-density peptide array*

UniProt ID	Protein	Start position	End position	Mean proportion of RA patients with reactivity
Q99470	SDF-2	65	92	0.64
P01185	AVP	13	36	0.64
Q9HCQ7	NPVF	37	60	0.63
P0DJI8	SAA1	49	72	0.61
P0DJI9	SAA2	49	72	0.61
Q9UMX5	NENF	69	112	0.58
Q9P0M4	IL-17C	41	68	0.58
Q8WXF3	RLN-3	89	128	0.57
P49913	FALL-39	105	132	0.57
P0C8F1	PATE-4	29	68	0.57
P78380	OLR-1	217	260	0.57
Q9NP84	TNFRSF12A	29	52	0.56
P01574	IFNβ1	121	144	0.56
P32970	CD70	153	176	0.56
A8K4G0	UNQ2530/PRO6029	53	76	0.56
Q9NPH9	IL-26	21	48	0.56
Q69YU5	C12orf73	33	56	0.56
Q8NET1	DEFB108B	13	32	0.56
Q30KQ7	DEFB113	33	52	0.56
Q8NHW4	CCL4L2	61	80	0.56
Q99731	CCL19	57	76	0.56
Q96NZ9	PRAP1	69	96	0.56
P35542	SAA4	49	68	0.56
Q9BQY6	WFDC-6	57	76	0.56
Q9NYY1	IL-20	41	64	0.56

* Start and end positions refer to the first and last positions of the peptides found within the composite epitopes. RA = rheumatoid arthritis; SDF-2 = stromal cell–derived factor 2; AVP = arginine vasopressin; NPVF = neuropeptide VF precursor; SAA1 = serum amyloid A1; NENF = neudesin neurotrophic factor; IL-17C = interleukin-17C; RLN-3 = relaxin 3; FALL-39 = cathelicidin antimicrobial peptide; PATE-4 = prostate and testis expressed protein 4; OLR-1 = oxidized low-density lipoprotein receptor 1; TNFRSF12A = tumor necrosis factor receptor superfamily member 12A; IFNβ1 = interferon-β1; UNQ2530/PRO6029 = CMRF35-like molecule 7; DEFB108B = β-defensin 108B; PRAP-1= proline-rich acidic protein 1; WFDC-6 = WAP 4-disulfide core domain protein 6.

peptide probes on the array, was synthesized commercially as a single peptide with C-terminal biotinylation via a terminal lysine residue. In all 8 samples shown in Figure 3 (4 control samples and 4 RA samples), little to no detectable antibody reactivity was observed for the native peptides on the array. This finding is consistent with the integrated signal obtained from the Gyrolab instrument. In contrast, 3 of the 4 RA samples showed strong reactivity on the array (Figure 3A), as well as when analyzed using the Gyrolab instrument (Figure 3B), for the citrullinated peptides within this epitope. A compilation of all validation experiments is shown in Supplementary Figures 2 and 3, available on the *Arthritis & Rheumatology* web site at http://onlinelibrary.wiley.com/doi/10.1002/art.41089/abstract.

While the overall concordance between the signal generated from the Gyrolab instrument and our peptide array is high, due to differences in surface properties between the peptide array surface and the Gyrolab streptavidin-coated beads, as well as the interaction kinetics differences between the 2 platforms, signal between the 2 technologies cannot be quantitatively reproduced perfectly (i.e., by regression coefficients and R^2 values). However, a qualitative assessment comparing the array signal and the Gyro-lab instrument output for the 13 epitopes in the validation experiment showed concordance 86.4% of the time.

Construction of a novel RA diagnostic biomarker. Given the large number of frequently occurring citrullinated composite epitopes, as shown in Table 1, and peptides, as shown in Supplementary Table 1, we explored the possibility of constructing a novel RA diagnostic biomarker based on data derived from the peptide array using the Gyrolab xPlore instrument. Peptides were chosen based on the minimum number needed to non-redundantly identify RA samples versus controls, and epitope sequences are listed in Supplementary Table 3, available on the *Arthritis & Rheumatology* web site at http://onlinelibrary.wiley.com/doi/10.1002/art.41089/abstract. In some instances, peptides were chosen to maximize the number of RA samples identified and were not necessarily picked from the frequently occurring citrullinated composite epitopes listed in Table 1.

Using a signal threshold set at >95% specificity, signal-to-noise ratios for each epitope derived from the Gyrolab xPlore instrument are categorized as positive or negative. Overall diagnostic performance of an 8-epitope biomarker was assessed
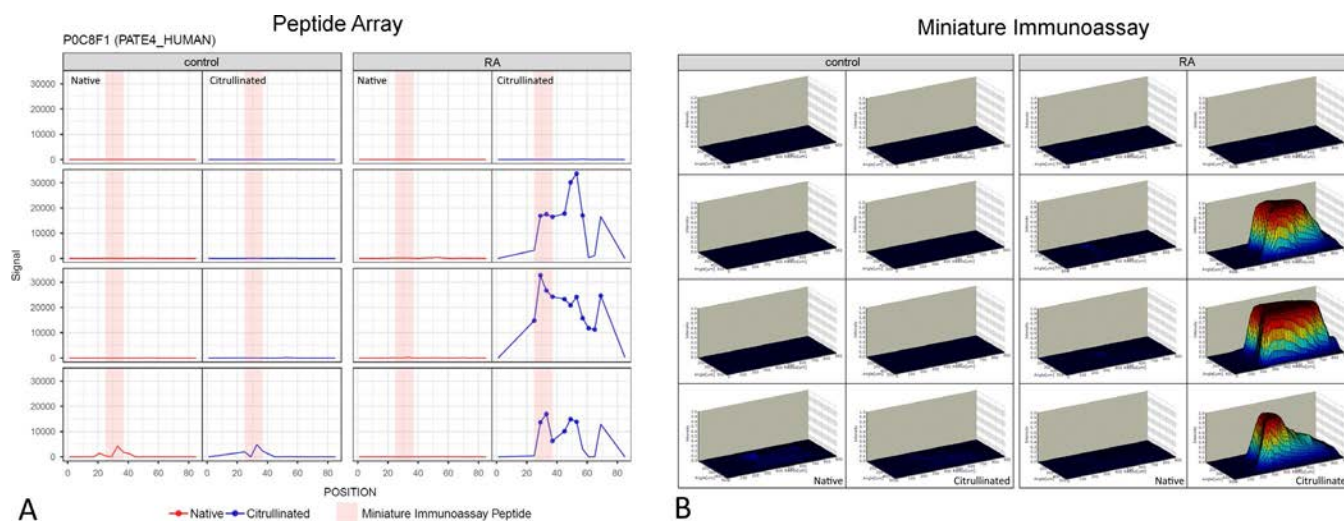
Figure 3. Side-by-side comparison of the fluorescence signal derived from a high-density peptide array and results of a Gyros miniature immunoassay. **A**, Peptide array signals for native and citrullinated peptides for prostate and testis expressed protein 4 (PATE-4) in 4 representative control samples and 4 representative rheumatoid arthritis (RA) samples. Pink shading shows the epitope (sequences N′-CNTCIYTEGWKCMAG-R/citrulline-GTCIAKENELCS-C′) that was included in subsequent validation studies. **B**, Gyros immunoassay signal histograms for the same samples as in **A**. Strong reactivity with the citrullinated peptides within this epitope was seen for 3 of the 4 RA samples on both the array and the miniature immunoassay. Color figure can be viewed in the online issue, which is available at http://onlinelibrary. wiley.com/doi/10.1002/art.41089/abstract.

in the initial cohort of 92 samples (from 29 controls and 63 RA patients) (Figure 4A), yielding 96.6% specificity and 92.1% sensitivity. For comparison, the same cohort was tested using a commercially available CCP2 assay, which yielded 96.6% specificity and 68.3% sensitivity.

In order to validate the diagnostic performance of our 8-epitope biomarker, an independent cohort of 181 serum samples (from 54 controls and 127 RA patients) was obtained from a commercial source (Bioconversant) (Supplementary Table 4, available on the *Arthritis & Rheumatology* web site at http://online library.wiley.com/doi/10.1002/art.41089/abstract), and the diagnostic performance of our 8-epitope biomarker was tested on the Gyrolab xPlore instrument. The overall diagnostic performance in the validation cohort was 94.4% specificity and 85% sensitivity. In contrast, the CCP2 assay resulted in 96.3% specificity and 53.5% sensitivity. A comparison of the diagnostic performance results for the CCP2 assay and our 8-epitope biomarker for both the initial and validation cohorts is shown in Table 2.

DISCUSSION

To our knowledge, an unbiased and comprehensive profile of antibodies against the entire human proteome, including the citrullinome and the homocitrullinome, in RA serum samples has not been reported in the literature. As has been shown previously, antibodies against citrullinated epitopes are readily seen in RA serum samples and characterize ACPA-positive RA patients (1). However, when screening was extended to the proteome, CCP2-negative RA patients also showed antibody reactivity against cit-

rullinated peptides, at a frequency 2.5 times greater than controls, indicating that CCP2-negative RA patients are not necessarily lacking ACPA (19,20). To provide context, CCP2-negative RA patients showed significant reactivity at ~2 orders of magnitude lower than CCP2-positive RA patients (data not shown).

While a proteome-scale survey allows for an unbiased view, it was not clear whether expanding the exploration landscape would be helpful in identifying novel epitopes and proteins potentially important to understanding RA biology. Notably, the data presented in Figures 1 and 2 show extensive antibody reactivity against the citrullinated proteome. While we observed reactivity against citrullinated peptides in proteins known to be associated with RA, such as filaggrin, fibrin, RA33, tenascin-C, and peptidylarginine deiminase type 4 (PAD4), the majority of the reactivity reported in Supplementary Table 1 has not previously been reported in the literature. To illustrate this, a PubMed search of the proteins listed in Table 1 yielded 0 results for 11 of the 25 proteins. Moreover, in the majority of the cases, establishment of an association with RA did not involve observing ACPAs against these proteins. Thus, it seems likely that there is still a large amount of unexplored territory in terms of identifying ACPA epitopes in RA.

Recent evidence (8,21) has demonstrated an ACPA preference for binding to citrulline–glycine motifs in linear peptides. Additionally, work involving recombinant human PAD2 and PAD4 has shown substrate preference for peptides containing a citrulline–glycine motif, in addition to other surrounding residues (for review, see ref. 22). As shown in Supplementary Table 1, we observed that most (99.8%) of the citrullinated peptides with reactivity occurring in >50% of the RA samples contained a citrulline–glycine

Initial Cohort (92)

A

Validation Cohort (181)

B
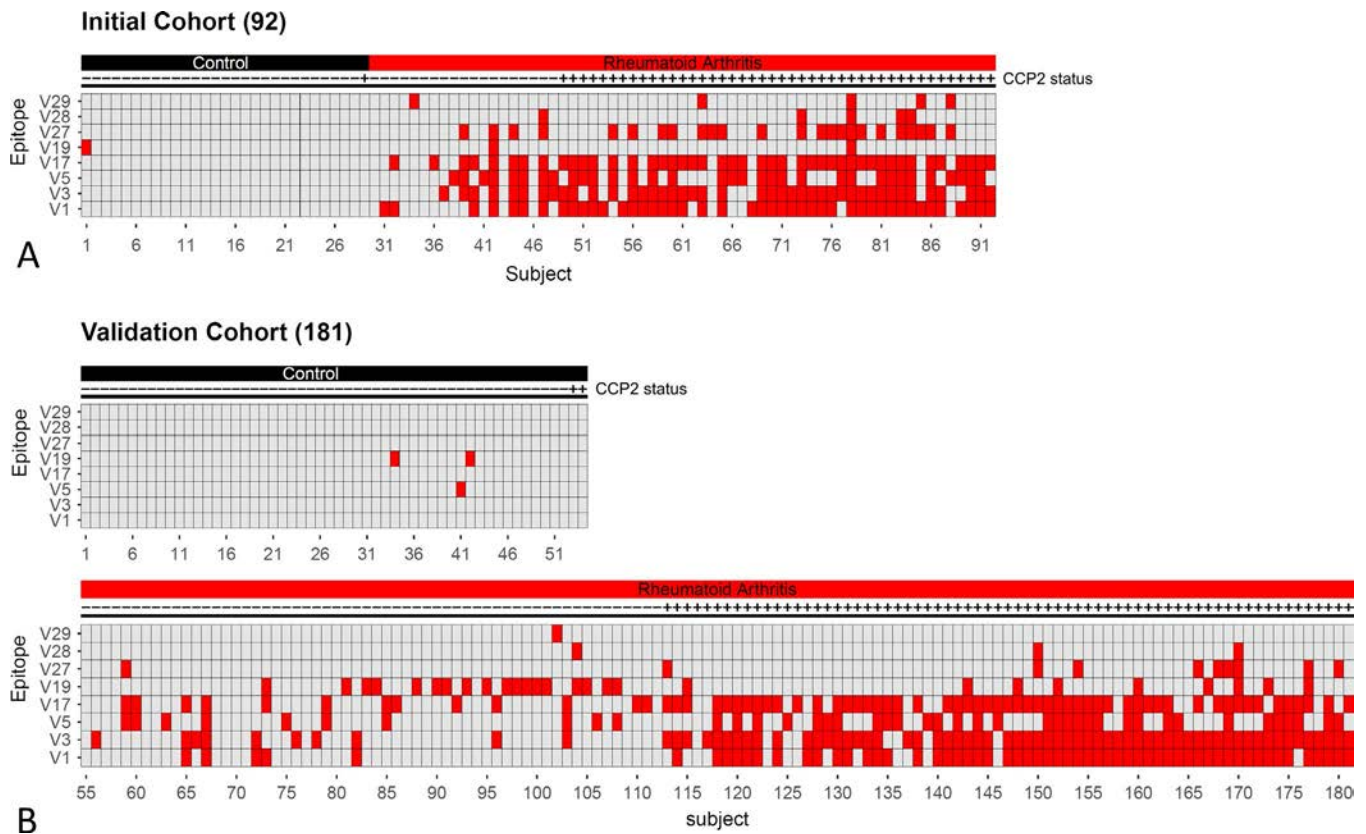
Figure 4. Performance of an 8-epitope rheumatoid arthritis (RA) diagnostic biomarker, assessed on a Gyrolab xPlore instrument. **A**, Results for the initial expanded cohort of 92 samples (from 29 controls and 63 RA patients). **B**, Results for the independent validation cohort of 181 samples (from 54 controls and 127 RA patients). Red indicates positivity; gray indicates negativity. CCP2 = cyclic citrullinated peptide 2. Color figure can be viewed in the online issue, which is available at http://onlinelibrary.wiley.com/doi/10.1002/art.41089/abstract.

motif. However, 30 of the peptide sequences did not contain citrulline–glycine. Additionally, we observed statistical enrichment of motifs that do not contain citrulline–glycine in specific RA samples (data not shown). Clearly, additional exploration is needed to understand what other motifs may be important to ACPA binding. As a continuation of this work, we plan on exploring the whole proteome peptide array data, as well as performing systematic

substitution analysis for specific epitopes to identify critical binding residues in a more comprehensive manner in the future.

Relative to ACPA reactivity, antibody reactivity against homocitrullinated epitopes (anti–carbamylated protein [anti-CarP]) was seen less frequently in this cohort, which is consistent with the findings of a seminal study by Shi et al (2). Interestingly, 4 of 18 RA serum samples in our whole-proteome array studies showed

Table 2. Comparison of the diagnostic performance of the CCP2 assay and an 8-epitope biomarker for the initial and validation cohorts*

	No. of controls	No. of RA patients	Specificity (TN/N)*	Sensitivity (TP/P)†
Initial cohort				
CCP2 assay	29	63	0.966 (28/29)	0.683 (43/63)
8-epitope biomarker	29	63	0.966 (28/29)	0.921 (58/63)
Validation cohort				
CCP2 assay	54	127	0.963 (52/54)	0.535 (68/127)
8-epitope biomarker	54	127	0.944 (51/54)	0.850 (108/127)

* TN represents the number of controls determined to be negative (not have rheumatoid arthritis [RA]) by the cyclic citrullinated peptide 2 (CCP2) assay or 8-epitope biomarker. N represents the number of controls who were negative (did not have RA) according to the American College of Rheumatology (ACR)/European League Against Rheumatism (EULAR) 2010 classification criteria.
† TP represents the number of RA patients determined to be positive (have RA) by the CCP2 assay or 8-epitope biomarker. P represents the number of RA patients who were positive (had RA) according to the ACR/EULAR 2010 classification criteria.

extensive anti-CarP antibody reactivity (Figure 2B); however, these individuals also showed ACPA reactivity and did not constitute an anti-CarP–positive and ACPA-negative subgroup of RA patients. This is also consistent with observations reported in a comprehensive meta-analysis by Verheul et al (23), in which the majority of anti-CarP–positive patients were also ACPA positive.

Overall signal between the peptide array and Gyrolab instrument was comparable despite differences in surface chemistry, interaction kinetics, and incubation temperatures between the 2 platforms. Linear regression coefficients for signal log ratios of citrullinated and homocitrullinated versus native peptides varied from 0.32 to 0.78 and were epitope dependent. Peptide array signals had a higher dynamic range, as saturation effects were observed in the Gyrolab instrument, coupled with regression coefficients being less than 1 in all epitopes (Supplementary Figures 2 and 3, available on the *Arthritis & Rheumatology* web site at http://onlinelibrary.wiley.com/doi/10.1002/art.41089/abstract). Based on these differences, treating array signal qualitatively yielded better concordance. When qualitative calls were compared between the 2 platforms, the overall concordance rate was 86.4%.

While there is much debate as to the relative proportion of human antibodies binding linear epitopes versus conformational, or discontinuous, epitopes (9,10), we explored the question of whether a comprehensive, whole-proteome screen of linear epitopes can be potentially informative for RA diagnosis. After mining the RA antibody reactome data from peptide arrays, candidate epitopes were screened using a Gyros instrument with traditionally synthesized peptides to avoid potentially spurious findings that are peptide-array specific. When 8 epitopes were combined, the overall diagnostic performance of our biomarker was 96.6% specificity and 92.1% sensitivity in our initial 92-sample cohort. To serve as a direct comparison, a CCP2 assay was performed and yielded 96.6% specificity and 68.3% sensitivity. In addition to identifying all serum samples that were CCP2-positive, the 8-epitope diagnostic biomarker identified 14 CCP2-negative RA samples. As shown in previous studies (17,18), the CCP2 assay does not identify all ACPA-positive individuals with RA, and additional epitopes can be used to improve sensitivity. By mining the peptide array data, we were able to find a novel 8-epitope biomarker for an RA diagnostic blood test that outperforms the CCP2 assay in terms of sensitivity while being comparable in terms of specificity. Finally, in order to assess the robustness of the 8-epitope biomarker, we further validated the diagnostic performance with an independent, commercially purchased cohort of 181 serum samples. The 8-epitope biomarker identified all but 1 CCP2-positive RA sample while additionally identifying 40 CCP2-negative RA samples. Overall, validation performance was 94.4% specific and 85% sensitive.

There are some notable limitations to our study (1). A previous study by Blachère et al (24) suggested that intermittent citrullination may offer a more diverse assortment of citrullinated epitopes in fibrinogen. Due to the nature of our peptide synthesis technology, substitution of citrulline for arginine and homocitrulline for lysine was complete. While this approach may be superior from an experimental perspective, whether it is physiologically relevant requires additional investigation (2). There is no assurance that short linear peptides can adopt native protein confirmation. Recently, we have shown that linear peptides can adopt the necessary conformation needed for protein binding to occur (25). However, whether this conformation resembles the native protein confirmation and to what extent is unknown (3).

During the development of the 8-epitope biomarker, we intentionally acquired 2 different cohorts of serum samples. The initial cohort (29 controls and 63 RA patients), of which a small number (8 controls and 18 RA patients) were profiled on the whole-proteome peptide array, was used for whole-proteome testing and biomarker development. The validation cohort (54 controls and 127 RA patients) was used specifically to test biomarker performance. The separation was intended to avoid a well-known statistical problem with high-throughput screening technologies, such as the peptide array, known as "the curse of dimensionality," where analysis of multiple analytes far exceeds the number of samples profiled. Given the similarities between the initial and validation cohorts in terms of the performance of the 8-epitope biomarker, it is unlikely that our 8-epitope biomarker is a spurious finding. However, given the small number of samples (i.e., 273 samples total) and the lack of other disease controls, additional confirmation would be prudent. Finally, it is unclear what the diagnostic performance of our 8-epitope biomarker would be in early RA or pre-RA cohorts since they were not tested in this instance. As demonstrated by our 8-epitope diagnostic biomarker, it is evident that whole-proteome profiling of linear epitopes has potential utility in revealing novel insights for disease prognosis and diagnosis.

AUTHOR CONTRIBUTIONS

All authors were involved in drafting the article or revising it critically for important intellectual content, and all authors approved the final version to be published. Dr. Lo had full access to all of the data in the study and takes responsibility for the integrity of the data and the accuracy of the data analysis.
Study conception and design. Lo, Bannen, Pinapati, Patel, Keystone, Siminovitch.
Acquisition of data. Lo, Sullivan, Jin, Rowe, Li, Cartwright.
Analysis and interpretation of data. Lo, Tan.

ROLE OF THE STUDY SPONSOR

ADDITIONAL DISCLOSURES

REFERENCES

1. Schellekens GA, de Jong BA, van den Hoogen FH, van de Putte LB, van Venrooij WJ. Citrulline is an essential constituent of antigenic determinants recognized by rheumatoid arthritis-specific autoantibodies. J Clin Invest 1998;101:273–81.

2. Shi J, Knevel R, Suwannalai P, van der Linden MP, Janssen GM, van Veelen PA, et al. Autoantibodies recognizing carbamylated proteins are present in sera of patients with rheumatoid arthritis and predict joint damage. Proc Natl Acad Sci U S A 2011;108:17372–7.

3. Aletaha D, Neogi T, Silman AJ, Funovits J, Felson DT, Bingham CO III, et al. 2010 rheumatoid arthritis classification criteria: an American College of Rheumatology/European League Against Rheumatism collaborative initiative. Arthritis Rheum 2010;62:2569–81.

4. Van der Helm-van Mil AH, Verpoort KN, Breedveld FC, Toes RE, Huizinga TW. Antibodies to citrullinated proteins and differences in clinical progression of rheumatoid arthritis. Arthritis Res Ther 2005;7:R949–58.

5. Frostegård J, Hellström C, Nilsson P, Frostegård AG, Ajeganova S. Autoantibody profiling reveals four protein candidate autoantigens associated with systemic lupus erythematosus. Lupus 2018;27:1670–78.

6. Ewaisha R, Panicker G, Maranian P, Unger ER, Anderson KS. Serum immune profiling for early detection of cervical disease. Theranostics 2017;7:3814–23.

7. Pin E, Henjes F, Hong MG, Wiklund F, Magnusson P, Bjartell A, et al. Identification of a novel autoimmune peptide epitope of prostein in prostate cancer. J Proteome Res 2017;16:204–16.

8. Steen J, Forsström B, Sahlström P, Odowd V, Israelsson L, Krishnamurthy A, et al. Recognition of amino acid motifs, rather than specific proteins, by human plasma cell–derived monoclonal antibodies to posttranslationally modified proteins in rheumatoid arthritis. Arthritis Rheumatol 2019;71:196–209.

9. Fernandes-Cerqueira C, Ossipova E, Gunasekera S, Hansson M, Mathsson L, Catrina AI, et al. Targeting of anti-citrullinated protein/peptide antibodies in rheumatoid arthritis using peptides mimicking endogenously citrullinated fibrinogen antigens. Arthritis Res Ther 2015;17:155.

10. Hueber W, Kidd BA, Tomooka BH, Lee BJ, Bruce B, Fries JF, et al. Antigen microarray profiling of autoantibodies in rheumatoid arthritis. Arthritis Rheum 2005;52:2645–55.

11. Mathsson L, Hansson M, Israelsson L, Harwanegg C, Nystrand M, Klareskog L, et al. A multiplex microarray for the detection of rheumatoid arthritis-associated autoantibodies [abstract]. Ann Rheum Dis 2011;70:A66.

12. Forsström B, Axnäs BB, Rockberg J, Danielsson H, Bohlin A, Uhlen M, et al. Dissecting antibodies with regards to linear and conformational epitopes. PLoS One 2015;10:e0121673.

13. Zhang J, Zhao X, Sun P, Gao B, Ma Z. Conformational B-cell epitopes prediction from sequences using cost-sensitive ensemble classifiers and spatial clustering. Biomed Res Int 2014;2014:689219.

14. Yan Y, Sun N, Wang H, Kobayashi M, Ladd JJ, Long JP, et al. Whole genome-derived tiled peptide arrays detect prediagnostic autoantibody signatures in non-small-cell lung cancer. Cancer Res 2019;79:1549–57.

15. Cleveland WS, Grosse E, Shyu WM. Local regression models. In: Chambers JM, Hastie TJ, editors. Statistical models in S. Boca Raton (FL): Chapman & Hall/CRC; 1991.

16. Bolstad BM. Low level analysis of high-density oligonucleotide array data: background, normalization and summarization [dissertation]. Berkeley: University of California, Berkeley; 2004.

17. Scacheri PC, Crawford GE, Davis S. Statistics for ChIP-chip and DNase hypersensitivity experiments on NimbleGen arrays. Methods Enzymol 2006;411:270–82.

18. Nagele EP, Han M, Acharya NK, DeMarshall C, Kosciuk MC, Nagele RG. Natural IgG autoantibodies are abundant and ubiquitous in human sera, and their number is influenced by age, gender, and disease. PLoS One 2013;8:e60726.

19. Rönnelid J, Hansson M, Mathsson-Alm L, Cornillet M, Reed E, Jakobsson PJ, et al. Anticitrullinated protein/peptide antibody multiplexing defines an extended group of ACPA-positive rheumatoid arthritis patients with distinct genetic and environmental determinants. Ann Rheum Dis 2018;77:203–11.

20. Van Heemst J, Trouw LA, Nogueira L, van Steenbergen HW, van der Helm-van Mil AH, Allaart CF, et al. An investigation of the added value of an ACPA multiplex assay in an early rheumatoid arthritis setting. Arthritis Res Ther 2015;17:276.

21. Trier NH, Holm BE, Hansen PR, Slot O, Locht H, Houen G. Specificity of anti-citrullinated protein antibodies in rheumatoid arthritis. Antibodies 2019;8:37.

22. Hensen SM, Pruijn GJ. Methods for the detection of peptidylarginine deiminase (PAD) activity and protein citrullination. Mol Cell Proteomics 2014;13:388–96.

23. Verheul MK, Böhringer S, van Delft MA, Jones JD, Rigby WF, Gan RW, et al. Triple positivity for anti–citrullinated protein autoantibodies, rheumatoid factor, and anti–carbamylated protein antibodies conferring high specificity for rheumatoid arthritis: implications for very early identification of at-risk individuals. Arthritis Rheumatol 2018;70:1721–31.

24. Blachère NE, Parveen S, Frank MO, Dill BD, Molina H, Orange DE. High-titer rheumatoid arthritis antibodies preferentially bind fibrinogen citrullinated by peptidylarginine deiminase 4. Arthritis Rheumatol 2017;69:986–95.

25. Lyamichev VI, Goodrich LE, Sullivan EH, Bannen RM, Benz J, Albert TJ, et al. Stepwise evolution improves identification of diverse peptides binding to a protein target. Sci Rep 2017;7:12116.

AMERICAN COLLEGE
of RHEUMATOLOGY
Empowering Rheumatology Professionals

Timing of Elevations of Autoantibody Isotypes Prior to Diagnosis of Rheumatoid Arthritis

Lindsay B. Kelmenson,[1] Brandie D. Wagner,[1] Bryan K. McNair,[1] Ashley Frazer-Abel,[1] M. Kristen Demoruelle,[1] Dylan T. Bergstedt,[1] Marie L. Feser,[1] Laura K. Moss,[1] Mark C. Parish,[1] Elizabeth A. Mewshaw,[2] Ted R. Mikuls,[3] (iD) Jess D. Edison,[2] V. Michael Holers,[1] and Kevin D. Deane[1] (iD)

Objective. To evaluate patterns of elevations of isotypes of rheumatoid factor (RF) and anti–citrullinated protein antibodies (ACPAs) pre–rheumatoid arthritis (RA) diagnosis and post–RA diagnosis.

Methods. Using the Department of Defense Serum Repository we identified 214 RA cases and 210 matched controls. Up to 3 pre–RA diagnosis and 1 post–RA diagnosis serum samples per subject were tested for RF and for IgA, IgG, and IgM ACPAs. The timing and trajectories of elevations of autoantibodies were evaluated.

Results. Autoantibody levels were elevated in cases versus controls a mean of 17.9 years before RA diagnosis for IgG ACPA, 14.2 years for IgA-RF, 7.2 years for IgM-RF, 6.2 years for IgA ACPA, and 5.0 years for both IgM ACPA and IgG-RF ($P < 0.01$ for all comparisons). There were similar relationships for positive or negative autoantibody status, with cases first showing positivity for IgG ACPA 1.9 years pre-RA and for IgA-RF 1.7 years pre-RA, followed by the other isotypes. Only IgA ACPA positivity was significantly increased in post–RA diagnosis samples (19% 0–2 years pre-RA versus 39% >2 years post–RA diagnosis; $P = 0.04$). All autoantibody levels demonstrated an early initial elevation, a period of stability, then an increase immediately before RA diagnosis. A pre-RA endotype of early elevation of autoantibodies was associated with increased use of biologic therapy, and a higher prevalence of sicca symptoms and lung disease post–RA diagnosis.

Conclusion. Differences in patterns of elevations of autoantibody isotypes have implications for understanding the pathophysiology of RA development. These include understanding what factors drive initial autoantibody elevations compared to what factors (including mucosal) drive later increases in autoantibody levels and a transition to clinically apparent RA, and how pre-RA endotypes may influence post–RA diagnosis phenotypes.

INTRODUCTION

Serum levels of autoantibodies including rheumatoid factor (RF), anti–citrullinated protein antibodies (ACPAs), and other autoantibodies (e.g., antibodies to carbamylated proteins), as well as systemic inflammation, have been shown to be abnormal prior to the development of clinically identifiable synovitis and a diagnosis of rheumatoid arthritis (RA) (1–11). Importantly, the discovery of this pre–RA diagnosis period has led to an improved understanding of the natural history and pathogenesis of RA, as well as provided rationale for strategies for prevention (12).

Elevations of serum autoantibody levels prior to the onset of clinically apparent synovitis also suggest that autoantibodies may initially be generated outside of the joints and potentially related to mucosal processes (13). Findings supporting an important role for these processes in the early development of RA include elevations

[1]Lindsay B. Kelmenson, MD, MSCS, Brandie D. Wagner, PhD, Bryan K. McNair, MS, Ashley Frazer-Abel, PhD, M. Kristen Demoruelle, MD, Dylan T. Bergstedt, BS, Marie L. Feser, MSPH, Laura K. Moss, BS, Mark C. Parish, BS, V. Michael Holers, MD, Kevin D. Deane, MD, PhD: University of Colorado Denver Anschutz Medical Campus; [2]Elizabeth A. Mewshaw, MSN, Jess D. Edison, MD: Walter Reed National Military Medical Center, Bethesda, Maryland; [3]Ted R. Mikuls, MD, MSPH: University of Nebraska, Omaha.

of serum levels of IgA-RF and IgA ACPA isotypes pre–RA diagnosis (9,14), and lung abnormalities in some individuals before they develop RA (15,16). Furthermore, cross-sectional studies of subjects at risk of future RA have demonstrated elevations of serum levels of IgA ACPA and IgA-RF (17), and IgA-producing plasmablast expansion (18). In addition, epidemiologic studies have linked a risk of RA with factors, such as exposure to tobacco smoke, that can drive mucosal inflammation (19).

The purpose of the present study was to evaluate serum levels of RF and ACPA isotypes pre– and post–RA diagnosis using multiple serial samples from a new large and well-characterized cohort of subjects with RA and matched controls obtained from the US military. Our findings highlight the timing and trajectories of elevations of autoantibody isotype levels in RA development, with a focus on the relationships between IgG and IgA isotypes.

PATIENTS AND METHODS

Study subjects. A case–control study was performed using samples from the Department of Defense Serum Repository (DoDSR) from individuals pre– and post–RA diagnosis and controls. The DoDSR is part of a program to monitor the health of US military personnel, and samples are collected at enlistment, deployment, and approximately every other year of service (20). For research purposes, the DoDSR can be used to identify individuals who develop incident RA with the availability of longitudinally collected prediagnosis data and samples.

For this study, candidate RA cases were initially identified based on documentation in the medical record of at least 2 International Classification of Diseases (ICD) codes consistent with RA over time, and at least 1 rheumatologist encounter. Medical records for each candidate case were subsequently evaluated at Walter Reed National Military Medical Center by a rheumatologist and an experienced clinical rheumatology nurse with training in research methodologies, and 346 RA cases were identified, all of whom satisfied the American College of Rheumatology (ACR) 1987 classification criteria for RA (21) or were diagnosed as having RA by a rheumatologist. Notably, none of these 346 cases were included in an earlier evaluation of 83 individuals with RA in the DoDSR by our group (3,5,6,22,23). Up to 4 DoDSR samples for each case were selected, including 3 samples obtained pre–RA diagnosis, and 1 sample obtained post–RA diagnosis. Up to 4 controls were identified per case, excluding individuals with a diagnosis of RA or inflammatory arthritis, and matched to cases based on age (at the time of RA diagnosis for their matched cases), sex, race, region of enlistment, and duration of sample storage. When fewer samples were available from controls than cases, controls were matched by the overall time span covered by the samples (i.e., oldest to newest) rather than the total number of serum samples.

This analysis included a subset of 214 RA cases who were diagnosed as having RA between 1995 and 2012, with 212 (99%)

meeting the ACR 1987 RA classification criteria. The 2 remaining cases were diagnosed as having RA by a board-certified rheumatologist. This subset of cases was selected because they had a clear date of RA diagnosis available from chart review, sufficient clinical information available to evaluate the clinical course of their RA postdiagnosis, and 2 or more prediagnosis serum samples as well as a postdiagnosis sample with adequate volume available for autoantibody testing. Notably, the 214 RA cases selected for analysis did not differ from the 132 remaining RA cases in terms of age at diagnosis, sex, race, smoking status, or ACPA positivity postdiagnosis (data not shown). We also analyzed a subset of 210 matched controls. The number of controls was fewer than the 214 RA cases because 4 controls were removed from the analysis since after initial selection and prior to autoantibody testing, they lacked sufficient information to exclude inflammatory arthritis.

Clinical data for each case were identified based on review of medical reports and ICD codes, and abstracted onto a standardized form by personnel who were blinded with regard to autoantibody status. Data included demographic characteristics, date of RA diagnosis and symptom onset, comorbidities including ocular/oral dryness, lung disease, use of disease-modifying antirheumatic drugs, radiographic erosions, family history of RA (unavailable for controls), and smoking status (never versus ever). Race/ethnicity was categorized as non-Hispanic white, African American, or other, with the "other" category including Asian, Hispanic, and Native American. Material for genetic studies was not available.

Ethical considerations. The study protocol was approved by the appropriate regulatory bodies at the DoDSR and Walter Reed National Military Medical Center as well as by the Colorado Multiple Institutional Review Board.

Autoantibody assays. Serum was tested in a blinded manner at Exsera BioLabs at the University of Colorado. To provide a comparison with clinically available ACPA assays, we tested serum for anti–cyclic citrullinated peptide 3.1 (CCP3.1) (IgG/A). In addition, we tested IgA-, IgG-, and IgM-RF (assays were supplied by Inova Diagnostics). IgA, IgG, and IgM ACPA isotype levels were measured with kits using the same antigen plate as the commercial CCP3.1 assay but that are only available in the isotype-specific assay for research (Inova Diagnostics). For each assay, serum was tested in duplicate and levels were determined using a standard curve. The final level for analyses was determined from the mean of the 2 wells. For all isotype assays, the mean difference between wells was <15%.

Determination of autoantibody positivity. We randomly selected 156 (~75%) of the 210 DoDSR controls and used their last available sample to set cutoff points for each antibody that was present in <2% of these controls. A subset of 54 controls (25%) was used to compare rates of positivity to those in cases. Of note, there were no significant differences between these 156

controls and the 214 cases with regard to age, sex, or race; furthermore, there were no significant differences between the sets of 156 controls and 54 controls with regard to age, sex, race, or autoantibody levels (see Supplementary Table 1, available on the *Arthritis & Rheumatology* web site at http://onlinelibrary.wiley.com/doi/10.1002/art.41091/abstract). For the CCP3.1 assay, we used a cutoff level of ≥20 units for positivity, which is the manufacturer's suggested cutoff and is commonly used in general clinical practice.

Statistical analysis. For descriptive analyses, continuous data were analyzed by *t*-test, and categorical data were analyzed by chi-square test. For analyses of autoantibodies as continuous outcomes, levels were log (base 2) transformed, and values

outside of the limit of detection for each assay were randomly imputed within a window around the limit to avoid truncation. To examine the timing of elevation of the isotype levels, a mixed-model analysis was performed for each autoantibody isotype. Time was included as a continuous variable and modeled using cubic B-splines that were allowed to vary by group with internal knots placed at the tertiles and boundary knots placed at the extremes (24). The model included a random subject intercept and slope, which were assumed to have a multivariate normal distribution. Cholesky decomposition was used to constrain the covariance matrix of the random effects to be positive-definite. Isotype levels were compared at 1-month intervals to identify the time at which levels differed significantly ($P < 0.05$) between cases

Table 1. Characteristics of the RA cases and controls*

Characteristic	RA cases (n = 214)	Controls (n = 210)†	*P*
Samples			
Number tested, mean (range)	4 (3–4)	3 (2–4)	–
Pre–RA diagnosis	3 (2–3)	–	
Post–RA diagnosis	1 (1–1)	–	
Time span of pre-RA diagnosis samples, mean ± SD (range) years	−5.1 ± 5.7 (−22.8 to −0.1)	–	–
Time span of post–RA diagnosis samples, mean ± SD (range) years	1.3 ± 0.9 (0.1–5.6)	–	–
Time span, oldest to newest sample, mean ± SD years	12.8 ± 5.6	12.3 ± 5.4	0.39
Age at time of diagnosis, mean ± SD	37 ± 7.9	37 ± 7.9	1.0
Female, %	48	48	1.0
Non-Hispanic white, %	58	55	0.93
Ever smoker, %‡	32	23	0.06
Autoantibody positivity post–RA diagnosis, no. (%)			
CCP3.1	162 (76)	2 (4)	<0.01
IgA-RF	86 (40)	1 (2)	<0.01
IgG-RF	35 (16)	0 (0)	<0.01
IgM-RF	112 (52)	2 (4)	<0.01
IgA ACPA	56 (26)	0 (0)	<0.01
IgG ACPA	150 (70)	1 (2)	<0.01
IgM ACPA	52 (24)	0 (0)	<0.01
Any RF isotype positive	129 (60)	3 (6)	<0.01
Any ACPA isotype positive	151 (71)	1 (2)	<0.01
Any RF or ACPA isotype positive	174 (81)	4 (7)	<0.01
No RF or ACPA isotype positive	40 (19)	50 (93)	<0.01
Only RF isotype positive	23 (11)	3 (6)	<0.01
Only ACPA isotype positive	45 (21)	1 (2)	<0.01
Both ACPA and RF isotype positive	106 (50)	0 (0)	<0.01
Follow-up time post–RA diagnosis by medical record review, mean ± SD years§	6.9 (3.6)	7.2 (4.4)	0.54
RA medications (ever used), %			
MTX	87	–	–
Anti-TNF inhibitor	73	–	–
Radiographic erosions, %	45	–	–
Self-reported first-degree relative with RA, %¶	16	–	–

* MTX = methotrexate; anti-TNF = anti–tumor necrosis factor.
† A total of 210 controls were available for analyses. They were split into 2 groups. Group 1 consisted of 156 controls (~75%) and group 2 consisted of 54 controls (~25%). The last available sample for the controls in group 1 was used to set cutoff levels for positivity for rheumatoid factor (RF) and anti–citrullinated protein antibody (ACPA) isotypes. The prevalence rates of positivity for the different autoantibody isotypes was then compared in group 2. Demographic characteristics are for the entire group (n = 210). Autoantibody positivity rates are for group 2 (n = 54) and were obtained using their last available sample. Additional comparisons between the 2 groups of controls are presented in Supplementary Table 1, available on the *Arthritis & Rheumatology* web site at http://onlinelibrary.wiley.com/doi/10.1002/art.41091/abstract.
‡ Data on smoking were missing for 5 (2%) of 214 cases and 89 (42%) of 210 controls.
§ For cases, this follow-up time refers to the time post–rheumatoid arthritis (RA) diagnosis that charts were available for review. For controls, it refers to the time between the age they were at the time their matched case was diagnosed as having RA and final chart information available for review.
¶ Defined as a parent, sibling, or child with RA. This information was not available for controls.

and controls. Comparisons were adjusted for multiple testing using a step-down Holm-simulated method to control the family-wise Type I error rate. Of note, a matched nested random effect was evaluated and did not change the results; as such, analyses of autoantibody levels do not include matched pair analyses.

Additionally, a proportional hazards frailty model was used to compare differences in time to first positivity using dichotomous outcomes for each isotype within cases (25). This model took into account left censorship, and only included those cases whose status changed from negative to positive for the isotype of interest. Comparisons between survival curves were reported as hazard ratios (95% confidence intervals) and accounted for within-patient correlation, and Kaplan-Meier plots were generated. Contingency tables and chi-square testing were used to evaluate fluctuations in autoantibody positivity across the pre– and post–RA diagnosis periods.

Finally, estimated subject-specific autoantibody trajectories as levels from the mixed models were evaluated in an unsupervised random forest with 10,000 trees to estimate a proximity matrix. Partition around medoids clustering was performed on the matrix and a silhouette plot was used to identify the number of clusters, which we defined as "endotypes" or subtypes of a condition with distinct pathophysiologic mechanisms based on biomarker patterns rather than clinically observable phenotypes (e.g., sex) (26). The mixed-effects model was applied to each isotype, allowing for different B-spline between clusters, and compared between cases and controls. All analyses were performed using SAS version 9.4 (SAS Institute) or SPSS version 25 (IBM).

RESULTS

Cases and controls. Study subjects included 214 RA cases and 210 controls (Table 1). Overall, cases were similar to controls in age, sex, and race, although cases had a nonsignificant increase in ever smoking compared to controls (32% versus 23%; $P = 0.06$).

Timing of elevations of autoantibody isotype levels in cases compared to controls. In the mixed models, IgA-RF levels in cases diverged significantly from those in controls 14.2 years prior to RA diagnosis (Figure 1A). This divergence was qualitatively earlier than the divergence for IgG-RF, which occurred 5.0 years prior to RA diagnosis (Figure 1B). IgM-RF levels diverged between cases and controls 7.2 years prior to RA diagnosis (data not shown).

For ACPA, IgG levels in cases diverged significantly from those in controls 17.9 years prior to RA diagnosis. This divergence was qualitatively earlier than the divergence at 6.2 years prior to RA diagnosis that was observed for IgA ACPA (Figures 1C and D). IgM ACPA levels diverged between cases and controls 5.0 years prior to RA diagnosis (data not shown).

Notably, the divergence times identified using the mixed models described above can only be compared in a qualitative manner. Therefore, we additionally used analytic approaches that evaluated the differences between cases and controls on a subject level to quantitatively compare the timing of divergence of autoantibody levels between cases and controls. In these analyses, the sequence of divergence was similar to that seen in the mixed models and was as follows, from earliest to latest divergence from controls pre-RA diagnosis: IgG ACPA, IgA-RF, IgM-RF, IgA ACPA, IgM ACPA, and IgG-RF ($P < 0.01$ for all comparisons) (Supplementary Figure 1, available on the *Arthritis & Rheumatology* web site at http://onlinelibrary.wiley.com/doi/10.1002/art.41091/abstract). There was no significant difference in the overall levels of autoantibodies based on smoking status (Supplementary Figure 2, available on the *Arthritis & Rheumatology* web site at http://onlinelibrary.wiley.com/doi/10.1002/art.41091/abstract). Furthermore, there was no significant difference in the timing of autoantibody levels diverging from controls for any isotype based on smoking status (data not shown).

Survival models to evaluate the relative timing of autoantibody positivity prior to RA diagnosis. To complement the analyses of autoantibody levels, we performed survival analyses to evaluate the relative timing of earliest positivity of each autoantibody isotype, adjusting for age, sex, and smoking status. In these analyses, the time of first positivity for IgG ACPA was earliest, at a median of 1.9 years prior to diagnosis, followed by the other autoantibodies closer to diagnosis (Table 2). The cumulative probability for a positive test by autoantibody isotype is shown in Supplementary Figures 3 and 4, available on the *Arthritis & Rheumatology* web site at http://onlinelibrary.wiley.com/doi/10.1002/art.41091/abstract.

Fluctuations in autoantibody levels and positivity pre– and post–RA diagnosis. To evaluate changes in autoantibody positivity in periods pre– and post–RA diagnosis, we analyzed positivity rates 0–2 years prior to RA diagnosis, 0–2 years immediately post–RA diagnosis, and >2 years post–RA diagnosis, using a single sample from each case per time interval. There were no significant changes across these time periods in the prevalence of positivity for IgA-RF, IgM-RF, or IgG-RF, or for IgM ACPA or IgG ACPA (Table 3). However, the prevalence of positivity for IgA ACPA increased: 18.9% 0–2 years pre-RA, 23.4% 0–2 years post–RA diagnosis, and 38.5% >2 years post–RA diagnosis ($P = 0.04$) (Table 3). There were no significant differences between those who developed IgA ACPA across these time periods in sex, age at diagnosis of RA, medication use, or smoking history (data not shown).

In addition, subject-specific plots indicated that between-subject variability over time was similar for IgA-RF and IgM-RF (variance 0.001 for both) (Supplementary Figure 5, available on the
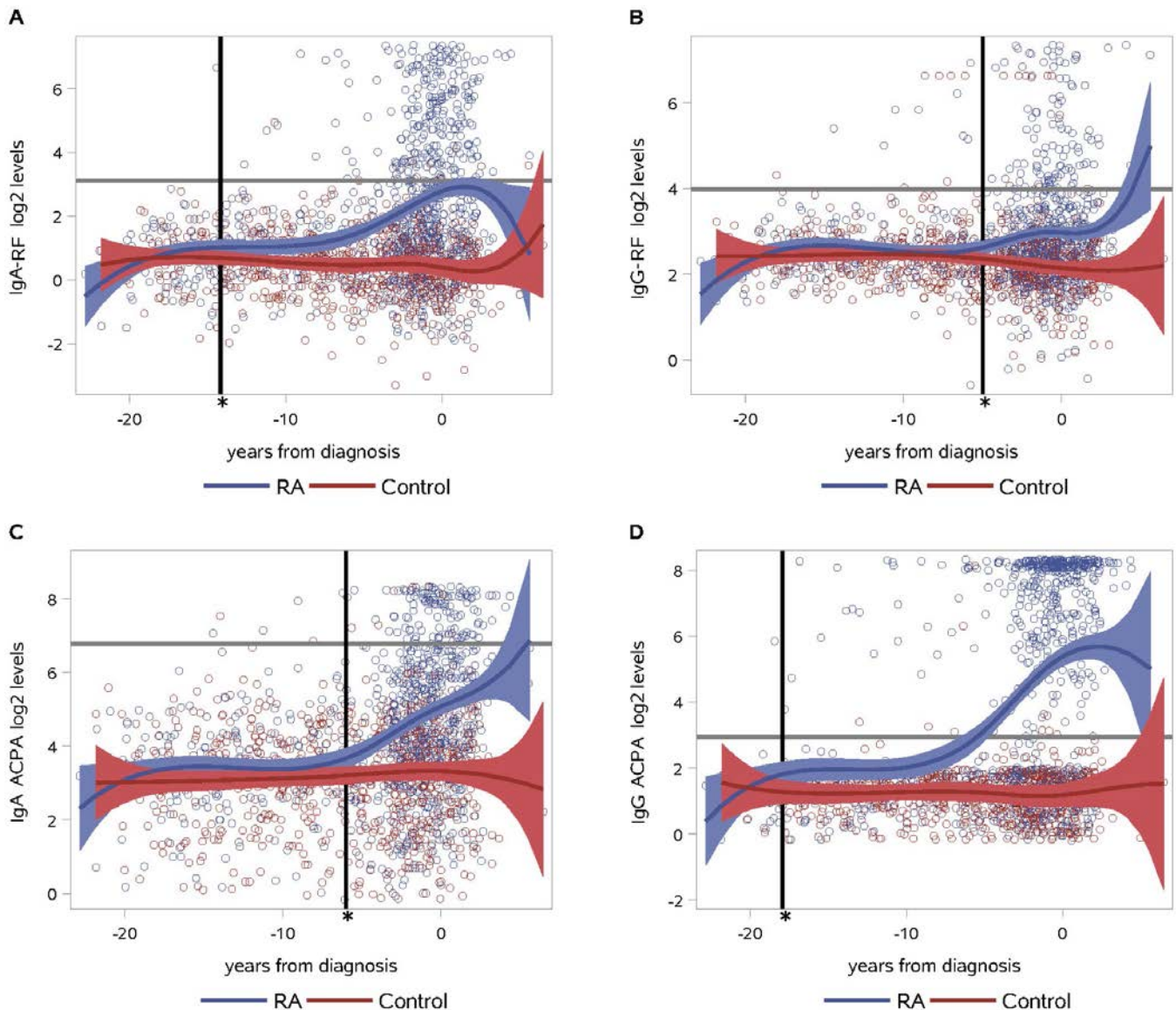
Figure 1. IgA rheumatoid factor (IgA-RF), IgG-RF, IgA anti–citrullinated protein antibody (ACPA), and IgG ACPA levels in rheumatoid arthritis (RA) cases and controls. **A** and **B**, Mixed model estimates of levels of IgA-RF (**A**) and IgG-RF (**B**) in RA patients and controls. Levels of IgA-RF diverged significantly between cases and controls 14.2 years prior to RA diagnosis (mean ± SEM $\log_2$ level 1.02 ± 0.12 IU in cases versus 0.69 ± 0.11 IU in controls; $P < 0.05$). Levels of IgG-RF diverged significantly between cases and controls 5.0 years prior to RA diagnosis (mean ± SEM $\log_2$ level 2.62 ± 0.08 IU in cases versus 2.36 ± 0.07 IU in controls; $P < 0.05$). IgM-RF levels in RA cases diverged from those in controls 7.2 years prior to RA diagnosis (data not shown). **C** and **D**, Mixed model estimates of levels of IgA ACPA (**C**) and IgG ACPA (**D**) in RA patients and controls. Levels of IgA ACPA diverged significantly between cases and controls 6.2 years prior to RA diagnosis (mean ± SEM $\log_2$ levels 3.67 ± 0.14 units in cases versus 3.20 ± 0.12 units in controls; $P < 0.05$). Levels of IgG ACPA diverged significantly between cases and controls 17.9 years prior to RA diagnosis (mean ± SEM $\log_2$ levels 1.81 ± 0.19 units in RA cases versus 1.28 ± 0.19 units in controls; $P < 0.05$). IgM ACPA levels in RA cases diverged from those in controls 5.0 years prior to RA diagnosis (data not shown). Horizontal lines and shading show the mean ± SD; circles represent individual subjects. The gray horizontal lines represent the cutoff for positivity determined in 156 controls. Vertical lines indicate the time point at which values diverged between cases and controls. * = $P < 0.05$.

Arthritis & Rheumatology web site at http://onlinelibrary.wiley.com/ doi/10.1002/art.41091/abstract). In contrast, there was greater between-subject variability for IgA ACPA compared to IgG ACPA (variance 0.03 versus 0.001). Additional findings regarding the variability of autoantibody positivity in cases and controls where "reversion" of autoantibody positivity was defined as positivity in one

sample followed by negativity in the next sample are presented in Supplementary Table 2, available on the *Arthritis & Rheumatology* web site at http://onlinelibrary.wiley.com/doi/10.1002/art.41091/ abstract. In summary, these analyses showed that reversion was least common for IgG ACPA (19%) and most common for IgG-RF (49%). Furthermore, a subset of cases were negative for a

Table 2. Timing of autoantibody isotype positivity in RA cases prior to RA diagnosis*

Autoantibody isotype	Time between first positive sample and RA diagnosis, median (IQR) years	Unadjusted HR (95% CI)	P	Adjusted HR (95% CI)†	P
IgG ACPA	1.92 (1.35–2.65)	Referent	–	Referent	–
IgA-RF	1.74 (1.12–2.57)	1.72 (1.17–2.53)	<0.01	1.71 (1.16–2.53)	<0.01
IgM-RF	1.66 (0.83–2.29)	1.55 (1.10–2.19)	<0.01	1.59 (1.13–2.24)	0.01
IgM ACPA	1.59 (0.78–2.1)	1.934 (1.19–3.14)	0.01	1.974 (1.22–3.21)	0.01
IgG-RF	1.37 (0.57–2.23)	2.82 (1.51–5.26)	<0.01	2.83 (1.52–5.29)	<0.01
IgA ACPA	1.35 (0.83–2.56)	2.81 (1.66–4.75)	<0.01	2.83 (1.68–4.77)	<0.01

* The cutoff for positivity for each autoantibody was defined as the level at which <2% of 156 controls were considered positive. IQR = interquartile range; 95% CI = 95% confidence interval; IgA-RF = IgA rheumatoid factor.
† Adjusted for age at rheumatoid arthritis (RA) diagnosis, sex, and smoking history. A hazard ratio (HR) >1 indicates that the duration of autoantibody positivity was shorter (i.e., the first positive sample was obtained closer to RA diagnosis) than that for the referent autoantibody isotype IgG anti–citrullinated protein antibody (ACPA).

particular isotype post–RA diagnosis yet had been positive pre-RA. The lowest rate of reversion to a negative finding post–RA diagnosis was for IgG ACPA (12%), and the highest was for IgG-RF (49%).

Endotype evaluation. Cluster analysis identified 2 endotypes based on subjects with similar trajectories of autoantibody level elevations in the pre-RA period (Figure 2). An "early endotype" was characterized by autoantibody levels rising early in the pre-RA period. In contrast, a "late endotype" was characterized by autoantibody levels rising closer to RA diagnosis. There were no significant differences between the 2 endotypes with regard to age at RA diagnosis, year of diagnosis, history of smoking, or prevalence of erosive disease assessed by review of radiologic reports from throughout the duration of follow-up post–RA diagnosis (Table 4). However, the early endotype group included more female subjects (55% versus 39%; P = 0.02), and also had a longer mean duration of follow-up post–RA diagnosis (7.4 years versus 6.3 years; P = 0.03). Post–RA diagnosis, patients with the early endotype also more frequently exhibited sicca symptoms (35% versus 19%; P = 0.04), lung disease (15% versus 4%; P = 0.01), and use of anti–tumor necrosis factor (anti-TNF) inhibitors (81% versus 64%; P = 0.01). The patients with the early endotype were also posi-

tive for a higher mean number of RF and ACPA isotypes post–RA diagnosis (2.9 versus 1.6; P < 0.01). Notably, while the timing of autoantibody elevations was different between the endotypes, the overall relationships between isotypes remained similar to those seen in other analyses, with IgG ACPA levels elevated earliest.

DISCUSSION

In one of the largest cohorts studied to date, we have shown that IgG ACPA levels are elevated earlier pre–RA diagnosis than levels of the other autoantibody isotypes, and there is an initial early elevation of autoantibody levels, followed by a period of stability, and then an increase in levels immediately prior to a diagnosis of RA. We also demonstrated that rates of positivity of IgA ACPA significantly increased post–RA diagnosis, and that there appear to be 2 endotypes of autoantibody trajectories pre–RA diagnosis that are associated with differences in post–RA diagnosis phenotypes.

Our a priori hypothesis for this study was that IgA ACPA levels would be elevated earlier than IgG ACPA levels pre–RA diagnosis; however, this was not the observed outcome. Furthermore, in published studies, IgG ACPA has been shown

Table 3. Changes in autoantibody positivity in the periods before and after RA diagnosis*

	0–2 years prior to RA diagnosis	0–2 years after RA diagnosis	>2 years after RA diagnosis
IgA-RF positive	41	39	5
IgM-RF positive	53	52	55
IgG-RF positive	19	16	18
IgA ACPA positive†	19	23	39
IgM ACPA positive	25	25	23
IgG ACPA positive	67	68	80
CCP3.1 positive	73	75	82
Number of subjects	206	175	39
Time from diagnosis to when sample was obtained, mean ± SD years	−0.7 ± 0.5	1.0 ± 0.5	2.6 ± 0.8

* Each interval contains only 1 sample per subject; if more than 1 sample per subject was available in an interval, the sample obtained closest to the middle of the interval was selected for analysis; however, not all subjects had a sample available in each time interval. Except where indicated otherwise, values are the percentage of subjects. RA = rheumatoid arthritis; IgA-RF = IgA rheumatoid factor; ACPA = anti–citrullinated protein antibody.
† P = 0.04 for the comparison of percentages of positivity across the 3 time intervals, by chi-square analysis of contingency tables.
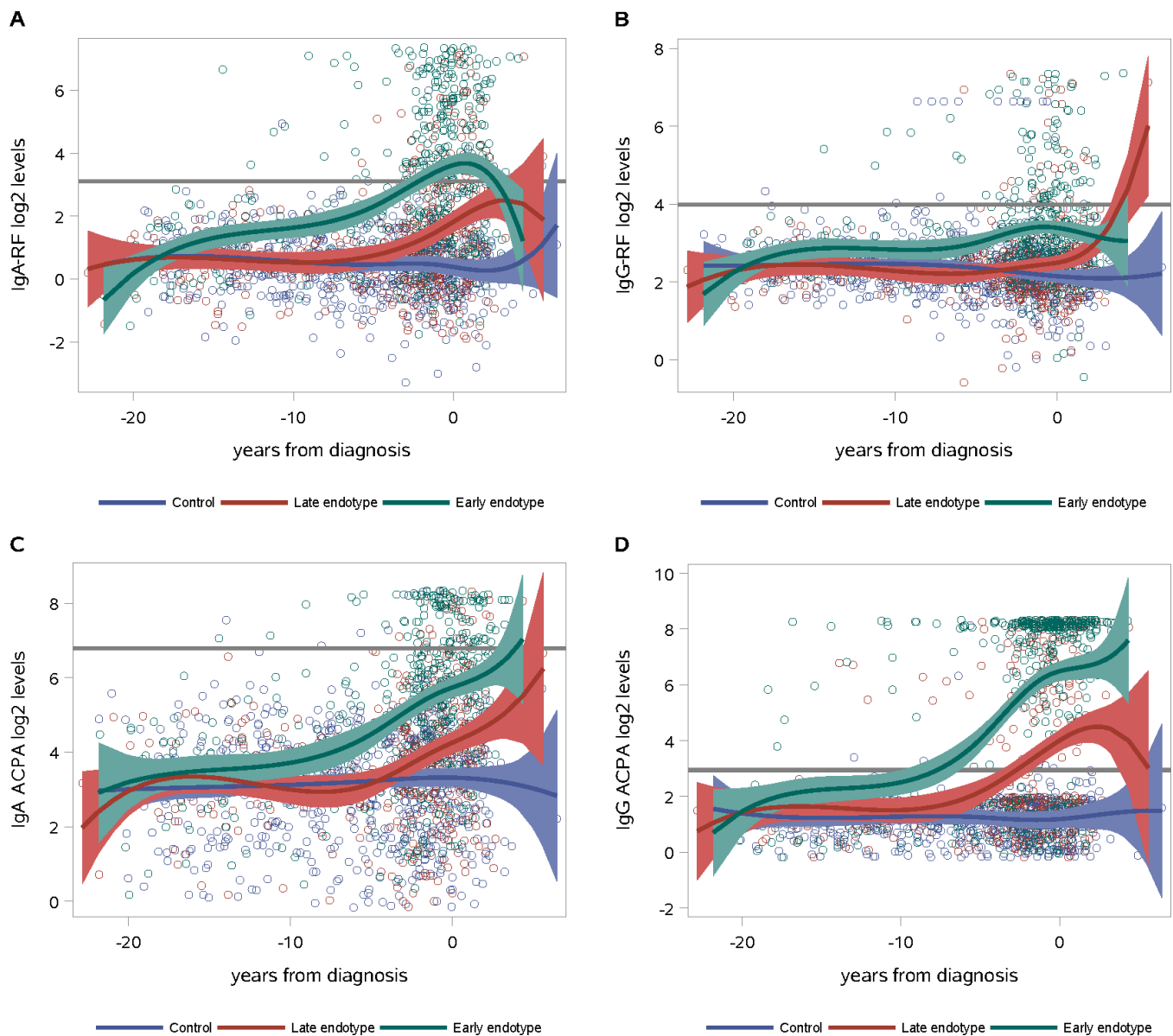
Figure 2. Identification of 2 endotypes among rheumatoid arthritis (RA) cases based on trajectories of autoantibody isotypes. **A** and **B**, Levels of IgA rheumatoid factor (IgA-RF) (**A**) and IgG-RF (**B**) in controls, RA cases with the late endotype, and RA cases with the early endotype. **C** and **D**, Levels of IgA anti–citrullinated protein antibody (ACPA) (**C**) and IgG ACPA (**D**) in controls, RA cases with the late endotype, and RA cases with the early endotype. In RA cases with the early endotype (n = 116), IgA-RF, IgG-RF, IgA ACPA, and IgG ACPA autoantibody levels began to increase compared to those in controls early in the pre-RA period. In RA cases with the late endotype (n = 98), IgA-RF, IgG-RF, IgA ACPA, and IgG ACPA autoantibody levels increased compared to those in controls just proximal to the diagnosis of RA. IgM-RF and IgM ACPA trajectories are not pictured but were within the range of IgG and IgA autoantibodies for each endotype. Horizontal lines and shading show the mean ± SD; circles represent individual subjects. The gray horizontal lines represent the cutoff for positivity determined in 156 controls.

to be elevated pre-RA in more individuals than IgA ACPA, similar to our findings in the present study (9). Taken together, these findings suggest that IgG ACPA is indeed systemically elevated earlier than IgA ACPA pre–RA diagnosis. This finding may suggest that for ACPA, IgA processes are not the earliest drivers of autoimmunity.

However, several lines of evidence suggest that IgA and potentially mucosal responses are important in the evolution of RA, and in particular in the transition from pre-RA to clinically apparent

RA. First, several cross-sectional studies of first-degree relatives (FDRs) of RA patients have shown a higher prevalence of IgA ACPA than IgG ACPA (17,27), although one study showed higher rates of positivity for IgG ACPA than for IgA ACPA among FDRs and non-FDR healthy controls (28). While mixed, these results may support the notion that IgA-RF and IgA ACPA levels are higher due to "natural" mucosal-related autoimmunity in individuals who do not develop RA—and perhaps in a T cell–independent manner (29). In contrast, in individuals who progress to RA, certain factors

Table 4. Characteristics of 2 RA endotypes with different autoantibody isotype patterns prior to RA diagnosis*

Characteristic	Early endotype (n = 116)	Late endotype (n = 98)	P
Duration of clinical follow-up available after RA diagnosis, mean ± SD years	7.4 ± 3.8	6.3 ± 3.20	0.03
Age, mean ± SD years	37.5 ± 8.5	36.2 ± 7.2	0.24
Female	55	39	0.02
Ever smoker	32	32	0.97
Current smoker	19	14	0.36
Radiographic erosions†	47	41	0.33
Lung disease	15	4	0.01
Dry eyes or mouth	32	19	0.04
Self-reported first-degree relative with RA‡	18	14	0.29
Body mass index			0.75
Normal	21	22	
Overweight	47	46	
Obese	33	32	
Medications (ever used)			
Glucocorticoids	81	77	0.42
Methotrexate	91	83	0.06
Leflunomide	16	8	0.07
Anti-TNF inhibitors	81	64	0.01
Rituximab	7	8	0.73
RA nodules	8	7	0.86
No. of antibodies positive after RA diagnosis, mean ± SD	2.9 ± 1.7	1.6 ± 1.6	<0.01
Time from RA diagnosis to when serum sample was obtained, mean ± SD years	1.4 ± 0.9	1.1 ± 0.9	0.05

* Except where indicated otherwise, values are the percentage of patients. Anti-TNF = anti–tumor necrosis factor.
† Erosions were assessed by chart review of all available follow-up data for the rheumatoid arthritis (RA) cases; there was no significant difference in the numbers of subjects who had radiographs performed, or the timing of radiographs, between endotypes.
‡ Defined as a parent, sibling, or child with RA.

may lead to more pathogenic immune responses, including early transition to IgG that may be facilitated through the presence of the shared epitope (4).

Second, in the cases studied herein we may have missed earlier elevations of IgA ACPA related to the greater fluctuations in IgA ACPA levels than in IgG ACPA levels (Supplementary Figure 5, available on the *Arthritis & Rheumatology* web site at http://onlinelibrary.wiley.com/doi/10.1002/art.41091/abstract). This variability may be due in part to a shorter circulating half-life of IgA versus IgG (~5 days versus ~21 days) that could make it difficult to capture persistent elevation or positivity of IgA until higher levels are sustained (30).

Third, prior work from our group has demonstrated that IgA ACPA is present in sputum, but may not be simultaneously detected in the blood (31,32). As such, our observation herein that IgG ACPA was elevated in the blood before IgA ACPA could mean that IgG more efficiently transfers from a mucosal surface to the circulation and is therefore detected earlier (33).

Fourth, for ACPA and RF, we measured total IgA. However, there are subtypes of IgA, including its secretory form, that may be more indicative of direct mucosal generation, although bone marrow or other sites of generation of IgA are also possible (34–36); future studies should evaluate these subtypes further. Finally, while IgA is the dominant antibody response at most mucosal sites, certain sites such as the cervico-vaginal tract can generate IgG locally

(37), raising the possibility that even the early presence of serum IgG may be indicative of mucosal responses.

There are additional factors that suggest that mucosal processes play an important role in RA development. In particular, RF and ACPA appear to be separate yet synergistic systems in RA, with distinct processes that drive the development of each autoantibody lineage (38–40). It is also known that these autoantibodies may be generated in the joints of individuals with established RA (41), although it is not yet fully understood how and where RF and ACPA are generated pre–RA diagnosis when presumably there is no synovitis. However, earlier elevation of IgA-RF levels compared to IgM-RF and IgG-RF levels suggests that RF may initially be generated due to mucosal responses. In addition, the later elevations of IgA ACPA compared to IgG ACPA, and in particular the increased prevalence of IgA ACPA positivity in the pre– to post–RA diagnosis periods, suggest that IgA ACPA generation could represent mucosal processes that facilitate a transition to clinically apparent synovitis. This latter concept is supported in other studies by the finding of circulating IgA ACPA plasmablasts in early RA (42), as well as by findings in an animal model of inflammatory arthritis where a systemic autoimmune response is initiated through subcutaneous immunization yet there is a requirement for mucosal interactions with bacteria for the development of arthritis (43). Future studies can expand on these issues including by evaluating mucosal interventions that are applied after the initial development

of RA-related autoimmunity and which could halt propagation of immunity and a transition to synovitis.

In our longitudinal analyses of samples, we saw pre–RA diagnosis increases in the levels of all autoantibody isotypes in the cases compared to the controls; for example, IgG ACPA levels in cases diverged from those in controls ~17 years prior to diagnosis (Figure 1). However, when autoantibodies were evaluated as positive or negative, the times of elevation were much closer to the time of diagnosis (Table 2). This supports the notion that autoantibody positivity as defined by a cutoff value can be useful for predicting near-term onset of clinically apparent RA. Indeed, positivity for ACPA and RF is being used in RA prevention trials that have the expectation of near-term development of clinically apparent RA (12). However, when autoantibody levels were evaluated, there was still a period of many years during which the levels remained relatively low yet still higher than those seen in controls. Importantly, for many cases, this level would be considered negative using standard cutoff values for RF or ACPA (Figure 1). Others have suggested that there are "two hits" in the evolution of RA, where there is an initial break in tolerance and early generation of autoantibodies, followed by a later expansion of autoimmunity and transition to clinically apparent RA (5,40,44), and the findings of the present study strongly support this concept. The factors associated with the initial increase in autoantibody levels and then later expansion closer to the onset of clinically apparent RA need further evaluation.

Also of interest was our finding that there were fluctuations in autoantibody positivity within cases pre– and post–RA diagnosis (Table 3 and Supplementary Table 2, available on the *Arthritis & Rheumatology* web site at http://onlinelibrary.wiley.com/doi/10.1002/art.41091/abstract). Fluctuation in autoantibody positivity post–RA diagnosis is not a novel finding, although less is known about the positive/negative states across the transition from pre– to post–RA diagnosis (45). The findings postdiagnosis are somewhat limited in that the mean time of collection of post–RA diagnosis samples was ~1.3 years after diagnosis, and we did not have serial post–RA diagnosis samples for each individual. However, these results are consistent with the concept that there is continued evolution of autoantibodies across the span of RA development, although the factors that contribute to it (e.g., genetic, environmental, medication, etc.) need to be evaluated in the future.

There is an emerging understanding that in individuals with established RA there can be a variety of "endotypes" defined by a variety of features, including autoantibodies, that may have different clinical outcomes and response to therapy (46). Consistent with this idea, we uniquely identified that there were early and late endotypes among cases based on the temporal pattern of elevations of autoantibody isotype levels pre–RA diagnosis. This was an observational study and there were differences in the duration of post–RA diagnosis follow-up between endotypes. As such, conclusions regarding the relationship between these endotypes

and clinical outcomes are limited. However, the differences in TNF inhibitor use and extraarticular disease and similarities in erosive disease suggest there are underlying differences in disease pathogenesis between these endotypes. In addition, in prior work using a different and smaller cohort of subjects (n = 83) we found that an older age at RA diagnosis was significantly associated with a longer duration of autoantibody positivity pre–RA diagnosis (22). In this new cohort, we did not observe a significant relationship between age and duration of autoantibody positivity pre–RA diagnosis. However, the mean age at RA diagnosis was nonsignificantly higher for the patients with the early endotype versus those with the late endotype (37.5 years versus 36.2 years), suggesting that there may be a similar effect of age on duration of autoantibody elevation pre–RA diagnosis. Age, genetic factors, inflammatory pathways, or other unmeasured variables that may also explain the differences between these endotypes will need further investigation (9,27).

There are several additional caveats. This is one of the largest sample sets to date evaluated throughout the development of RA; however, we performed multiple analyses, many resulting in novel findings, and therefore we welcome replication in additional studies. The military cohort may also represent a more severe form of RA than is seen in other populations given that the age at RA diagnosis was younger than in other RA cohorts (~37 years versus 50–60 years in other studies) (47), there was a high post–RA diagnosis rate of RF and ACPA positivity, and a high percentage of individuals were treated with biologic agents. In addition, the percentage of patients who were men (~50%) was higher than the typical ~30% seen in other RA cohorts (47). Our selection of cases who predominantly met the ACR 1987 criteria may have led to the identification of more severe phenotypes. Furthermore, some of these issues may be inherent to the US military, whose members are typically young and predominantly male, and a higher use of biologic agents may be attributed to access to health care and the individual's desire to maintain active military status. However, given that our analyses were adjusted for sex and age, it is likely that these findings are still generalizable to patients with seropositive RA.

Furthermore, 67% of the samples were obtained 0–5 years pre–RA diagnosis. More than 85% of autoantibody-positive samples were obtained in that 0–5-year window; therefore, we believe that the analyses and findings regarding timing of elevations of autoantibody levels are robust; however, this may limit our understanding of the behaviors of autoantibodies in earlier time periods. In addition, because of potential delays in individuals seeking medical attention for joint symptoms, the actual time of onset of clinically apparent synovitis may be earlier than the date of diagnosis, leading to a potential overestimation of the time between autoantibody elevation and onset of synovitis. However, in the present study the median duration of symptoms attributed to RA was <6 months prior to diagnosis, and so we suspect this issue is not a major confounder. These latter points can be addressed in prospective studies with more frequent sample analyses as well as joint evaluations.

The inherent properties of each of the autoantibody isotypes may also differ, which could lead to differences in the ability to identify elevations in autoantibody levels. For example, IgA affinity may be lower than IgG affinity, and therefore serum levels may be more difficult to detect. However, the approaches that we have taken using the same assays and cutoff values for positivity, and the fact we observed a similar sequence of isotypes when examining both levels and dichotomous outcomes, strengthen our conclusions regarding the timing of elevations of autoantibody levels. Finally, for ACPA testing we used an antigen plate that is proprietary and therefore the specific antigens are unknown; therefore, the evolution of autoantibody isotypes and fine specificities pre– and post–RA diagnosis should be evaluated further in future studies (5,28).

In conclusion, there are differences in RF and ACPA isotype patterns during RA development. These findings have implications for understanding the pathophysiology of disease development.

ACKNOWLEDGMENTS

AUTHOR CONTRIBUTIONS

All authors were involved in drafting the article or revising it critically for important intellectual content, and all authors approved the final version to be published. Dr. Deane had full access to all of the data in the study and takes responsibility for the integrity of the data and the accuracy of the data analysis.
Study conception and design. Kelmenson, Demoruelle, Bergstedt, Feser, Moss, Mewshaw, Mikuls, Edison, Holers, Deane.
Acquisition of data. Kelmenson, Frazer-Abel, Bergstedt, Feser, Moss, Parish, Mewshaw, Mikuls, Edison, Holers, Deane.
Analysis and interpretation of data. Kelmenson, Wagner, McNair, Frazer-Abel, Bergstedt, Feser, Moss, Parish, Mewshaw, Mikuls, Edison, Holers, Deane.

REFERENCES

1. Rantapää-Dahlqvist S, de Jong BA, Berglin E, Hallmans G, Wadell G, Stenlund H, et al. Antibodies against cyclic citrullinated peptide and IgA rheumatoid factor predict the development of rheumatoid arthritis. Arthritis Rheum 2003;48:2741–9.

2. Nielen MM, van Schaardenburg D, Reesink HW, van de Stadt RJ, van der Horst-Bruinsma IE, de Koning MH, et al. Specific autoantibodies precede the symptoms of rheumatoid arthritis: a study of serial measurements in blood donors. Arthritis Rheum 2004;50:380–6.

3. Deane KD, O'Donnell CI, Hueber W, Majka DS, Lazar AA, Derber LA, et al. The number of elevated cytokines and chemokines in preclinical seropositive rheumatoid arthritis predicts time to diagnosis in an age-dependent manner. Arthritis Rheum 2010;62:3161–72.

4. Rakieh C, Nam JL, Hunt L, Hensor EM, Das S, Bissell LA, et al. Predicting the development of clinical arthritis in anti-CCP positive individuals with non-specific musculoskeletal symptoms: a prospective observational cohort study. Ann Rheum Dis 2015;74:1659–66.

5. Sokolove J, Bromberg R, Deane KD, Lahey LJ, Derber LA, Chandra PE, et al. Autoantibody epitope spreading in the pre-clinical phase predicts progression to rheumatoid arthritis. PLoS One 2012;7:e35296.

6. Kolfenbach JR, Deane KD, Derber LA, O'Donnell CI, Gilliland WR, Edison JD, et al. Autoimmunity to peptidyl arginine deiminase type 4 precedes clinical onset of rheumatoid arthritis. Arthritis Rheum 2010;62:2633–9.

7. Shi J, van de Stadt LA, Levarht EW, Huizinga TW, Hamann D, van Schaardenburg D, et al. Anti-carbamylated protein (anti-CarP) antibodies precede the onset of rheumatoid arthritis. Ann Rheum Dis 2014;73:780–3.

8. Gan RW, Trouw LA, Shi J, Toes RE, Huizinga TW, Demoruelle MK, et al. Anti-carbamylated protein antibodies are present prior to rheumatoid arthritis and are associated with its future diagnosis. J Rheumatol 2015;42:572–9.

9. Kokkonen H, Mullazehi M, Berglin E, Hallmans G, Wadell G, Rönnelid J, et al. Antibodies of IgG, IgA and IgM isotypes against cyclic citrullinated peptide precede the development of rheumatoid arthritis. Arthritis Res Ther 2011;13:R13.

10. Deane KD, Demoruelle MK, Kelmenson LB, Kuhn KA, Norris JM, Holers VM. Genetic and environmental risk factors for rheumatoid arthritis. Best Pract Res Clin Rheumatol 2017;31:3–18.

11. Catrina AI, Svensson CI, Malmström V, Schett G, Klareskog L. Mechanisms leading from systemic autoimmunity to joint-specific disease in rheumatoid arthritis. Nat Rev Rheumatol 2017;13: 79–86.

12. Deane KD, Striebich CC, Holers VM. Prevention of rheumatoid arthritis: now is the time, but how to proceed? [editorial] Arthritis Rheumatol 2017;69:873–7.

13. Holers VM, Demoruelle MK, Kuhn KA, Buckner JH, Robinson WH, Okamoto Y, et al. Rheumatoid arthritis and the mucosal origins hypothesis: protection turns to destruction [review]. Nat Rev Rheumatol 2018;14:542–57.

14. Brink M, Hansson M, Mathsson-Alm L, Wijayatunga P, Verheul MK, Trouw LA, et al. Rheumatoid factor isotypes in relation to antibodies against citrullinated peptides and carbamylated proteins before the onset of rheumatoid arthritis. Arthritis Res Ther 2016; 18:43.

15. Fischer A, Solomon JJ, du Bois RM, Deane KD, Olson AL, Fernandez-Perez ER, et al. Lung disease with anti-CCP antibodies but not rheumatoid arthritis or connective tissue disease. Respir Med 2012;106:1040–7.

16. Demoruelle MK, Weisman MH, Simonian PL, Lynch DA, Sachs PB, Pedraza IF, et al. Airways abnormalities and rheumatoid arthritis–related autoantibodies in subjects without arthritis: early injury or initiating site of autoimmunity? Arthritis Rheum 2012;64:1756–61.

17. Barra L, Scinocca M, Saunders S, Bhayana R, Rohekar S, Racapé M, et al. Anti–citrullinated protein antibodies in unaffected first-degree relatives of rheumatoid arthritis patients. Arthritis Rheum 2013;65:1439–47.

18. Kinslow JD, Blum LK, Deane KD, Demoruelle MK, Okamoto Y, Parish MC, et al. Elevated IgA plasmablast levels in subjects at risk of developing rheumatoid arthritis. Arthritis Rheumatol 2016;68:2372–83.

19. Sparks JA, Karlson EW. The roles of cigarette smoking and the lung in the transitions between phases of preclinical rheumatoid arthritis. Curr Rheumatol Rep 2016;18:15.

20. Perdue CL, Eick-Cost AA, Rubertone MV. A brief description of the operation of the DoD Serum Repository. Mil Med 2015;180 Suppl: 10–2.

21. Arnett FC, Edworthy SM, Bloch DA, McShane DJ, Fries JF, Cooper NS, et al. The American Rheumatism Association 1987 revised cri-

teria for the classification of rheumatoid arthritis. Arthritis Rheum 1988;31:315–24.

22. Majka DS, Deane KD, Parrish LA, Lazar AA, Barón AE, Walker CW, et al. Duration of preclinical rheumatoid arthritis-related autoantibody positivity increases in subjects with older age at time of disease diagnosis. Ann Rheum Dis 2008;67:801–7.

23. Demoruelle MK, Parish MC, Derber LA, Kolfenbach JR, Hughes-Austin JM, Weisman MH, et al. Performance of anti–cyclic citrullinated peptide assays differs in subjects at increased risk of rheumatoid arthritis and subjects with established disease. Arthritis Rheum 2013;65:2243–52.

24. Hastie T, Tibshirani R, Friedman J. The elements of statistical learning: data mining, inference, and prediction. 1st ed. New York: Springer-Verlag; 2001.

25. Ripatti S, Palmgren J. Estimation of multivariate frailty models using penalized partial likelihood. Biometrics 2000;56:1016–22.

26. Agache I, Akdis CA. Endotypes of allergic diseases and asthma: an important step in building blocks for the future of precision medicine. Allergol Int 2016;65:243–52.

27. Ärlestig L, Mullazehi M, Kokkonen H, Rocklöv J, Rönnelid J, Dahlqvist SR. Antibodies against cyclic citrullinated peptides of IgG, IgA and IgM isotype and rheumatoid factor of IgM and IgA isotype are increased in unaffected members of multicase rheumatoid arthritis families from northern Sweden. Ann Rheum Dis 2012;71:825–9.

28. Ioan-Facsinay A, Willemze A, Robinson DB, Peschken CA, Markland J, van der Woude D, et al. Marked differences in fine specificity and isotype usage of the anti–citrullinated protein antibody in health and disease. Arthritis Rheum 2008;58:3000–8.

29. Bessa J, Bachmann MF. T cell-dependent and -independent IgA responses: role of TLR signalling. Immunol Invest 2010;39:407–28.

30. Fagarasan S, Honjo T. Intestinal IgA synthesis: regulation of front-line body defences. Nat Rev Immunol 2003;3:63–72.

31. Willis VC, Demoruelle MK, Derber LA, Chartier-Logan CJ, Parish MC, Pedraza IF, et al. Sputum autoantibodies in patients with established rheumatoid arthritis and subjects at risk of future clinically apparent disease. Arthritis Rheum 2013;65:2545–54.

32. Demoruelle MK, Harrall KK, Ho L, Purmalek MM, Seto NL, Rothfuss HM, et al. Anti–citrullinated protein antibodies are associated with neutrophil extracellular traps in the sputum in relatives of rheumatoid arthritis patients. Arthritis Rheumatol 2017;69:1165–75.

33. Schroeder HW Jr, Cavacini L. Structure and function of immunoglobulins. J Allergy Clin Immunol 2010;125 Suppl 2:S41–52.

34. Hansen IS, Baeten DL, den Dunnen J. The inflammatory function of human IgA. Cell Mol Life Sci 2019;76:1041–55.

35. Roos K, Martinsson K, Ziegelasch M, Sommarin Y, Svärd A, Skogh T, et al. Circulating secretory IgA antibodies against cyclic citrullinated peptides in early rheumatoid arthritis associate with inflammatory activity and smoking. Arthritis Res Ther 2016;18:119.

36. Van Delft MA, van der Woude D, Toes RE, Trouw LA. Secretory form of rheumatoid arthritis–associated autoantibodies in serum are mainly of the IgM isotype, suggesting a continuous reactivation of autoantibody responses at mucosal surfaces [letter]. Ann Rheum Dis 2019;78:146–8.

37. Mestecky J, Moldoveanu Z, Russell MW. Immunologic uniqueness of the genital tract: challenge for vaccine development. Am J Reprod Immunol 2005;53:208–14.

38. Lu DR, McDavid AN, Kongpachith S, Lingampalli N, Glanville J, Ju CH, et al. T cell–dependent affinity maturation and innate immune pathways differentially drive autoreactive B cell responses in rheumatoid arthritis. Arthritis Rheumatol 2018;70:1732–44.

39. Ursum J, Bos WH, van de Stadt RJ, Dijkmans BA, van Schaardenburg D. Different properties of ACPA and IgM-RF derived from a large dataset: further evidence of two distinct autoantibody systems. Arthritis Res Ther 2009;11:R75.

40. Sokolove J, Johnson DS, Lahey LJ, Wagner CA, Cheng D, Thiele GM, et al. Rheumatoid factor as a potentiator of anti–citrullinated protein antibody–mediated inflammation in rheumatoid arthritis. Arthritis Rheumatol 2014;66:813–21.

41. Humby F, Bombardieri M, Manzo A, Kelly S, Blades MC, Kirkham B, et al. Ectopic lymphoid structures support ongoing production of class-switched autoantibodies in rheumatoid synovium. PLoS Med 2009;6:e1.

42. Elliott SE, Kongpachith S, Lingampalli N, Adamska JZ, Cannon BJ, Mao R, et al. Affinity maturation drives epitope spreading and generation of proinflammatory anti–citrullinated protein antibodies in rheumatoid arthritis. Arthritis Rheumatol 2018;70:1946–58.

43. Jubair WK, Hendrickson JD, Severs EL, Schulz HM, Adhikari S, Ir D, et al. Modulation of inflammatory arthritis in mice by gut microbiota through mucosal inflammation and autoantibody generation. Arthritis Rheumatol 2018;70:1220–33.

44. Scherer HU, Huizinga TW, Krönke G, Schett G, Toes RE. The B cell response to citrullinated antigens in the development of rheumatoid arthritis. Nat Rev Rheumatol 2018;14:157–69.

45. Barra L, Bykerk V, Pope JE, Haraoui BP, Hitchon CA, Thorne JC, et al. Anticitrullinated protein antibodies and rheumatoid factor fluctuate in early inflammatory arthritis and do not predict clinical outcomes. J Rheumatol 2013;40:1259–67.

46. Derksen VF, Ajeganova S, Trouw LA, van der Helm-van Mil AH, Hafström I, Huizinga TW, et al. Rheumatoid arthritis phenotype at presentation differs depending on the number of autoantibodies present. Ann Rheum Dis 2017;76:716–20.

47. Gabriel SE, Crowson CS, O'Fallon WM. The epidemiology of rheumatoid arthritis in Rochester, Minnesota, 1955–1985. Arthritis Rheum 1999;42:415–20.

AMERICAN COLLEGE
of RHEUMATOLOGY
Empowering Rheumatology Professionals

Disordered Antigens and Epitope Overlap Between Anti–Citrullinated Protein Antibodies and Rheumatoid Factor in Rheumatoid Arthritis

Zihao Zheng,[1] Aisha M. Mergaert,[1] Lauren M. Fahmy,[1] Mandar Bawadekar,[1] Caitlyn L. Holmes,[1] Irene M. Ong,[2] Alan J. Bridges,[3] Michael A. Newton,[1] and Miriam A. Shelef[3] iD

Objective. Anti–citrullinated protein antibodies (ACPAs) and rheumatoid factor (RF) are commonly present in rheumatoid arthritis (RA) without a clear rationale for their coexistence. Moreover, autoantibodies develop against proteins with different posttranslational modifications and native proteins without obvious unifying characteristics of the antigens. We undertook this study to broadly evaluate autoantibody binding in seronegative and seropositive RA to identify novel features of reactivity.

Methods. An array was created using a total of 172,828 native peptides, citrulline-containing peptides, and homocitrulline-containing peptides derived primarily from proteins citrullinated in the rheumatoid joint. IgG and IgM binding to peptides were compared between cyclic citrullinated peptide (CCP)–positive RF+, CCP+RF–, CCP–RF+, and CCP–RF– serum from RA patients (n = 48) and controls (n = 12). IgG-bound and endogenously citrullinated peptides were analyzed for amino acid patterns and predictors of intrinsic disorder, i.e., unstable 3-dimensional structure. Binding to IgG-derived peptides was specifically evaluated. Enzyme-linked immunosorbent assay confirmed key results.

Results. Broadly, CCP+RF+ patients had high citrulline-specific IgG binding to array peptides and CCP+RF– and CCP–RF+ patients had modest citrulline-specific IgG binding (median Z scores 3.02, 1.42, and 0.75, respectively; $P < 0.0001$). All RA groups had low homocitrulline-specific binding. CCP+RF+ patients had moderate IgG binding to native peptides (median Z score 2.38; $P < 0.0001$). The highest IgG binding was to citrulline-containing peptides, irrespective of protein identity, especially if citrulline was adjacent to glycine or serine, motifs also seen in endogenous citrullination in the rheumatoid joint. Highly bound peptides had multiple features predictive of disorder. IgG from CCP+RF+ patients targeted citrulline-containing IgG-derived peptides.

Conclusion. Disordered antigens, which are frequently citrullinated, and common epitopes for ACPAs and RF are potentially unifying features for RA autoantibodies.

INTRODUCTION

In rheumatoid arthritis (RA), autoantibodies are both pathologic (1–3) and diagnostic (4). Patients with RA produce a variety of anti–citrullinated protein antibodies (ACPAs) with overlapping

reactivity (5–8) that underlie the diagnostic anti–cyclic citrullinated peptide (anti-CCP) antibody tests. They also generate rheumatoid factor (RF), antibodies of any isotype that bind to the Fc portion of IgG, which is also used for diagnosis. In RA, autoantibodies that target homocitrulline, known as anti-homocitrullinated

[1]Zihao Zheng, BS, Aisha M. Mergaert, BA, Lauren M. Fahmy, BS, Mandar Bawadekar, PhD (current address: Invenra, Inc., Madison, Wisconsin), Caitlyn L. Holmes, BS, Michael A. Newton, PhD: University of Wisconsin–Madison; [2]Irene M. Ong, PhD: University of Wisconsin–Madison and University of Wisconsin Carbone Comprehensive Cancer Center; [3]Alan J. Bridges, MD, Miriam A. Shelef, MD, PhD: University of Wisconsin–Madison and William S. Middleton Memorial Veterans Hospital.

Dr. Bawadekar owns stock or stock options in Invenra, Inc. No other disclosures relevant to this article were reported.

Address correspondence to Miriam A. Shelef, MD, PhD, 4130 Medical Foundation Centennial Building, 1685 Highland Avenue, Madison, WI 53705. E-mail: mshelef@medicine.wisc.edu.

Submitted for publication March 29, 2018; accepted in revised form August 6, 2019.

protein antibodies (AHCPAs) or anti–carbamylated protein antibodies, are produced (9). There appears to be some cross-reactivity between AHCPAs and ACPAs (7, 10–12), but this issue has not been completely resolved. Moreover, RA patients produce autoantibodies against malondialdehyde-acetaldehyde adducted proteins (13) and acetylated proteins (14), suggesting that autoantibodies in RA may primarily bind posttranslationally modified proteins (15). However, native proteins can also be targeted in RA (16–18), and autoantibodies against posttranslationally modified proteins often coexist with RF. It remains unclear why these seemingly unrelated antigens are targeted in RA.

Although the majority of patients with RA generate ACPAs and RF, ~25% are seronegative for both CCP and RF (19). RA patients who are seronegative may lack autoantibodies in general or common autoantibodies for this subset simply may not have been discovered yet. Additionally, some patients are seropositive for only RF or CCP. Little is known about autoantibody reactivity in patients who are positive for one but not both of these antibodies. However, an understanding of autoantibodies in these groups could shed light on the spectrum of disease in RA. In this study, we used a high-density peptide array to evaluate autoantibodies against citrulline-containing peptides, homocitrulline-containing peptides, and native peptides in seropositive and seronegative patients in order to identify unifying and novel features of autoantibody reactivity in RA.

MATERIALS AND METHODS

Human subjects. Human subject research was carried out in compliance with the Helsinki Declaration and was approved by the University of Wisconsin Institutional Review Board. Serum from age- and sex-matched controls and RA patients were selected from the University of Wisconsin (UW) Rheumatology Biorepository as described previously (20,21). Briefly, RA patients were identified based on having ≥2 outpatient visits within 24 months at which RA-associated International Classification of Diseases codes were used (22), or 1 visit and a positive CCP test result. RA diagnosis was confirmed by manual review of the 3 most recent progress notes from a rheumatologist. Anti-CCP was assessed by generation II anti-CCP or anti-CCP3 enzyme-linked immunosorbent assay (ELISA) (Inova), and RF was assessed by latex or polystyrene agglutination in the UW clinical laboratory. RA patients were included in the following groups if CCP and/or RF titers were negative or were >2 times the upper limit of normal: CCP+RF+, CCP–RF+, CCP+RF–, and CCP–RF–. Controls were excluded if they had any of the following as determined by verbal screening and manual review of the medical record: RA, lupus, Sjögren's syndrome, scleroderma, multiple sclerosis, type 1 diabetes mellitus, psoriasis, spondyloarthropathy, inflammatory bowel disease, or hematologic malignancy. A total of 48 RA patients and 12 controls were included in array studies, and 40 CCP+RF+ RA patients and 40 controls were included in confirmatory ELISAs.

High-density peptide array. Twelve–amino acid peptides from 224 UniProt sequences (see Supplementary Table 1, on the *Arthritis & Rheumatology* web site at http://onlinelibrary.wiley.com/doi/10.1002/art.41074/abstract) for 122 unique proteins (including variants) were tiled at a 1–amino acid interval to generate an array (Roche NimbleGen), as previously described (23). The majority of selected proteins were previously found to contain ≥1 citrulline in the rheumatoid joint (24–26), with some family members of the proteins included as well as a few known targets of ACPAs (3,8,27). Peptides containing arginine or lysine were included as native peptides and as peptides with all arginines replaced with citrullines or all lysines replaced with homocitrullines. Redundant peptides (found in >1 protein) were included once. Peptides from 5 proteins were included in duplicate. Each chip contained 12 copies of the array, which included 172,828 peptides: 35,459 citrulline-containing peptides, 41,608 homocitrulline-containing peptides, and 95,761 native peptides. Sera were sent to Roche NimbleGen for processing in order to apply to the array for analysis to detect IgA, IgM, and IgG that bound to each peptide (23), with sera diluted 1:100 in binding buffer (0.01M Tris HCl [pH 7.4], 1% alkali-soluble casein, 0.05% Tween 20). Six serum samples were run in duplicate on different chips. Roche NimbleGen provided raw signal intensities and a key for placing redundant peptides into the appropriate proteins.

ELISA. High-binding ELISA plates (Costar 3590; Corning) were coated with 5 μg/ml of streptavidin (Thermo Scientific) in phosphate buffered saline (PBS), incubated overnight at 4°C, washed 3 times with 0.2% Tween 20 in PBS (wash buffer), and incubated overnight at 4°C with 20 μg/ml of C-terminal biotinylated peptides (Peptide 2.0) in PBS. Peptides were EIFDSRGNPTVEK-biotin and EIFDScitGNPTVEK-biotin derived from α-enolase, and VFPLAPCSRSTSK-biotin, VFPLAPCScitSTSK-biotin, KPREEQYNSTYRK-biotin, KPcitEEQYNSTYcitK-biotin, FLYSRLTVDKSRK-biotin, and FLYScitLTVDKScitK-biotin derived from IgG heavy chain. Next, at room temperature, plates were washed 3 times, blocked with 5% nonfat dry milk for 2 hours, incubated for 2 hours with serum diluted 1:100 in wash buffer with 5% milk, washed 4 times, incubated for 2 hours with horseradish peroxidase–conjugated goat anti-human IgG (SouthernBiotech) diluted 1:5,000 in wash buffer with 5% milk, washed 3 times, developed with 3,3′,5,5′-tetramethylbenzidine, and read at 450 nm with 540 nm correction. Absorbance values were normalized to blank wells and sample-specific uncoated wells. Positive results were in the linear range.

Statistical analysis. Computations on peptide array data were performed using built-in functions and custom scripts within the R system for statistical computing (28). Raw intensity levels were transformed using a double logarithm (log[log(x)]) to stabilize variation and improve sensitivity (29).

Comparisons between RA patients and control subjects were conducted using a novel distribution analysis that considers all quantitative scores and does not threshold to identify "positive" peptides. First, for the signal intensity of each peptide or peptide-matched pair (i.e., signal from citrulline-containing peptide minus signal from corresponding arginine-containing peptide), we computed the Student's t statistic to measure differential abundance between an RA group and controls. We converted each t statistic to a Z score, which is essentially the number of standard deviations for the RA group from controls, using the probability integral transform, and then presented each set of Z scores as an empirical cumulative distribution function (ecdf).

Statistical significance was determined by sample-label permutation followed by repeated regeneration of Z score ecdfs; a measure of distributional distance was computed each time between the synthetic ecdf and the null integrated bell curve (>10,000 permuted data sets). The same inference results were obtained for different distance measures: mean difference, Kullback-Leibler divergence, and Hellinger distance. Using the Monte Carlo testing on sets of peptides, we could infer large-scale differential antibody abundance between RA and control groups, while respecting potential dependencies between abundance measures in the same subject without heavy multiple-comparison penalties associated with single-peptide

testing. Comparisons between ELISA data and array data or between the proportion of arginine or lysine and average binding were made using distance covariance (30). ELISA data were compared between groups using a Mann-Whitney test or Wilcoxon's matched pairs signed rank test, with P values less than 0.05 considered significant.

RESULTS

Broad evaluation of autoantibody binding in RA. A peptide array was designed with overlapping peptides primarily from proteins with ≥1 citrulline detected in the rheumatoid joint (24–26), including native peptides, peptides with all arginines replaced by citrullines, and peptides with all lysines replaced by homocitrullines. Sera from controls and RA patients, categorized into CCP+RF+, CCP+RF−, CCP−RF+, and CCP−RF− groups, were subjected to the array in order to quantify IgM and IgG binding to each peptide. As shown in Supplementary Table 2 (http://onlinelibrary.wiley.com/doi/10.1002/art.41074/abstract), subjects were similar across groups. Additionally, the array methodology was accurate and reproducible as determined by cluster analysis, duplicate sample analysis, duplicate peptide analysis, and confirmatory ELISA (Supplementary Figures 1 and 2, http://onlinelibrary.wiley.com/doi/10.1002/art.41074/abstract).
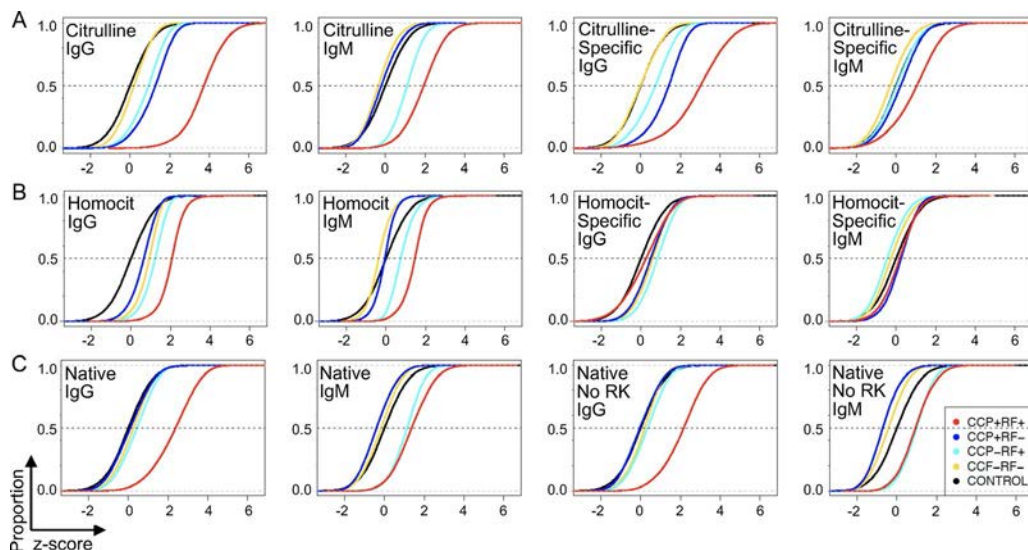
Figure 1. Broad patterns of antibody reactivity against peptides in rheumatoid arthritis (RA). IgG and IgM binding were measured in all samples for each peptide and the Z score for each peptide calculated for each RA group (cyclic citrullinated peptide–positive [CCP+] rheumatoid factor–positive [RF+], CCP+RF−, CCP−RF+, and CCP−RF−), compared to controls. The proportion of Z scores less than the specific Z value was graphed as an empirical cumulative distribution function (ecdf) plot. The median Z score for each RA group is where its ecdf curve crosses the dotted line at 0.5. Statistical significance was assessed by permutation analysis. **A**, Citrulline-containing peptides and citrulline-specific binding (binding values for citrulline-containing peptides minus corresponding arginine-containing peptides) (n = 35,459 peptides or peptide pairs). **B**, Homocitrulline (homocit)–containing peptides and homocitrulline-specific binding (binding values for homocitrulline-containing peptides minus corresponding lysine-containing peptides) (n = 41,608 peptides or peptide pairs). **C**, All native peptides and native peptides excluding peptides with arginine or lysine (n = 95,761 native peptides, n = 18,694 native peptides without arginine or lysine). For all panels, n = 12 samples per group; $P < 0.0001$ for all comparisons despite some small visual differences (except citrulline-specific IgM binding for CCP−RF+ versus control, which was not significant).

Following these confirmatory tests, we evaluated general antibody binding patterns in the 4 RA groups, first focusing on citrulline. As expected, CCP+RF+ patients had very high IgG binding to citrulline-containing peptides (Figure 1A). CCP+RF− and CCP−RF+ groups showed modest IgG binding. For IgM, the CCP+RF+ group had high binding to citrulline-containing peptides, with modest binding in the CCP−RF+ group. We next quantified citrulline-specific binding (binding to citrulline-containing peptides minus corresponding arginine-containing peptides) and found very high citrulline-specific IgG binding in the CCP+RF+ patients and modest citrulline-specific IgG binding in CCP−RF+ and CCP+RF− groups. For IgM, there was modest citrulline-specific binding in the CCP+RF+ group. We also performed similar analyses of IgA binding (Supplementary Figure 3, http://onlinelibrary.wiley.com/doi/10.1002/art.41074/abstract). Although there appeared to be a small increase in citrulline-specific IgA binding in CCP+RF+ subjects, we could detect only low IgA binding in general, limiting our analyses. Notably, similar to most studies evaluating antibody binding in RA, in CCP+RF+ patients we could not determine how much detected binding was direct binding of Ig to citrulline-containing peptides versus indirect binding of RF to IgG that was bound to citrulline-containing peptides.

We next evaluated reactivity with homocitrulline-containing peptides (Figure 1B). CCP+RF+ subjects showed increased IgG binding to homocitrulline-containing peptides, with small increases in binding for the other 3 groups. For IgM binding, the CCP+RF+ group had an increase in binding, with a small increase in the CCP−RF+ group. Overall, there was low homocitrulline-specific IgM and IgG binding in all RA groups (i.e., binding to homocitrulline-containing peptides minus corresponding lysine-containing peptides).

Finally, we assessed binding to native peptides (Figure 1C). Moderate binding of IgG to native peptides in the CCP+RF+ group was observed, as well as modest IgM binding to native peptides in both RF+ groups. To reduce the possibility of cross-reactivity with citrulline- and homocitrulline-containing peptides, antibody binding to native peptides that did not contain arginine or lysine was assessed. Again, we observed moderate IgG binding to native peptides only in the CCP+RF+ group and modest IgM binding in both RF+ groups.

Collectively, these data suggest that citrulline is a major driver of autoantibody reactivity in our RA patients who were positive for both RF and CCP, as expected, with little specific reactivity against homocitrulline and moderate binding to native peptides. Moreover, seronegative subjects had little antibody binding in general, and RA patients with seropositivity for only RF or only CCP showed intermediate binding, primarily with citrulline.

A dominant target of IgG in RA is citrulline, irrespective of protein identity, particularly if citrulline is adjacent to glycine or serine. We next evaluated whether peptides from specific proteins were preferentially targeted in RA. We identified peptides bound by IgG at a level 10 times
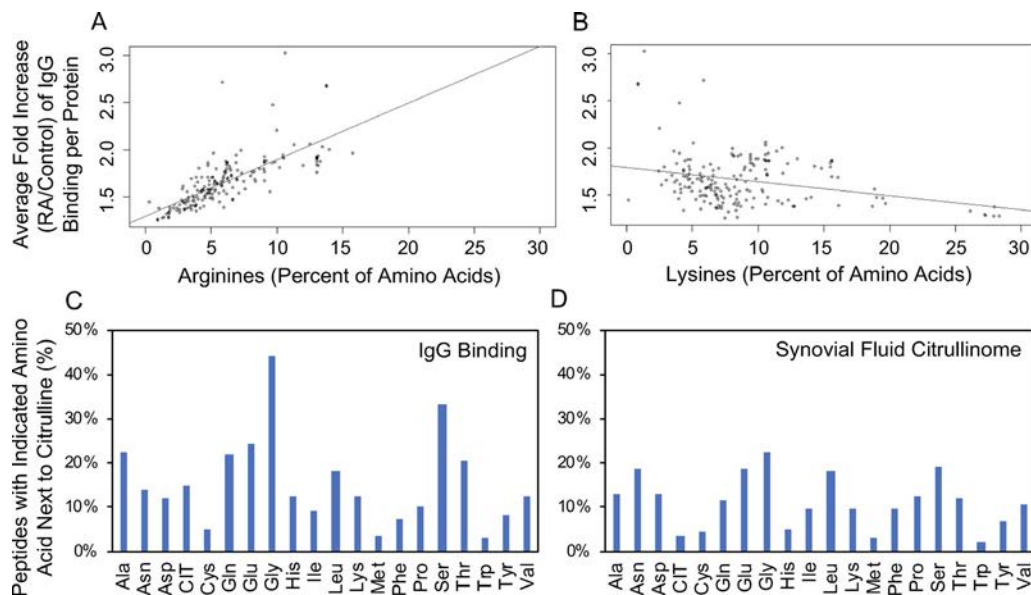
Figure 2. Amino acids that correlated with increased IgG binding in rheumatoid arthritis (RA). **A**, The average fold increase in IgG binding for RA versus control sera was determined for each peptide (including native, citrulline-containing, and homocitrulline-containing peptides) and was then averaged for each protein to generate the average fold increase of IgG binding per protein. The percentage of amino acids in each protein encoded as arginine was then compared to the average fold increase of IgG binding per protein (r = 0.74, P < 0.0001, by Pearson's correlation). **B**, The average fold increase of IgG binding per protein was compared to the percentage of amino acids in each protein encoded as lysine. **C**, The percentage of peptides that contain each indicated amino acid next to citrulline was determined for all citrulline-containing peptides for which there was >10 times more IgG binding in RA compared to control. **D**, The percentage of peptides that contain each indicated amino acid next to citrulline was determined for citrulline-containing peptides reported in the rheumatoid joint. Color figure can be viewed in the online issue, which is available at http://onlinelibrary.wiley.com/doi/10.1002/art.41074/abstract.

greater in RA than in controls (Supplementary Table 3, http://onlinelibrary.wiley.com/doi/10.1002/art.41074/abstract) and found that every protein whose peptides were included in the array had ≥1 peptide that met this criterion. Moreover, every peptide with >10 times increased binding in RA (9,098 unique peptides) contained citrulline except for 2 native peptides from fibrinogen, which lacked arginine. Some proteins had more peptides highly bound by IgG than others. Given the high reactivity with citrulline overall in our subjects (Figure 1), we determined whether the amount of arginine in a protein (citrullines in our array) correlated with the level of IgG binding for its peptides. We assessed the fold increase in IgG binding for each peptide in the RA group versus controls. We then averaged the fold increase in IgG binding for all peptides in each protein and compared this average to the percent of amino acids in each protein encoded as arginine. There was a strong correlation between the proportion of encoded arginines and the binding of serum IgG in RA (Figure 2A). In contrast, there was no positive correlation between the proportion of encoded lysines and the binding of IgG in RA (Figure 2B). Taken together, these data suggest that a major determinant of IgG binding in RA is citrulline, not protein identity, similar to findings on monoclonal antibodies derived from patients with RA (7).

We then determined whether there was a motif related to high IgG binding in our RA sera. Using MEME software (31) and the highly bound citrulline-containing peptides mentioned above, no strong motifs could be identified. Rather, certain amino acids appeared frequently in multiple minimal motifs. Thus, we verified how often each amino acid was adjacent to citrulline in the highly bound peptides. Some amino acids, most strikingly glycine and serine, were frequently next to citrulline in highly bound peptides (Figure 2C), suggesting either a preference for antibody development against citrullines next to these amino acids or preferred citrullination of arginines next to these amino acids. Of note, these amino acids were not simply more commonly encoded next to arginine, since the lowest bound citrulline-containing peptides by IgG did not have a high frequency of glycine or serine next to citrulline.

To differentiate between antibody development and citrullination preference, we evaluated 451 citrulline-containing peptides detected in rheumatoid synovial fluid (24–26) and determined the percentage of peptides that contained each amino acid next to citrulline. The citrullinome peptides differed

Table 1. Native peptides (without arginine or lysine) with >2 times higher IgG binding in rheumatoid arthritis sera than in control sera

Protein	Peptides (distance from disorder, no. of amino acids)	Disordered amino acids/total amino acids (%)
Apolipoprotein B-100	IPDFDVDLGTIL (23), VGINGEANLDFL (8), GINGEANLDFLN (9), INGEANLDFLNI (10), NGEANLDFLNIP (11)	371/4,563 (8)
Ceruloplasmin	SSTVTPTLPGET (0)	183/1,065 (17)
Collagen α2 (I) chain	SGGGYDFGYDGD (0)	471/1,366 (34)
Complement C4a/b	PMPQAPALWIET (1), EANEDYEDYEYD (0), QLNDFLQEYGTQ (0), LNDFLQEYGTQG (0)	219/1,744 (13)
Complement C5	DLGCGAGGGLNN (0), LGCGAGGGLNNA (0), GCGAGGGLNNAN (0), CGAGGGLNNANV (0)	217/1,676 (13)
Complement C7	INNDFNYEFYNS (3), NNDFNYEFYNST (2), INNNPEFLQLAE (16)	88/843 (10)
Complement C8 α chain	DAQSVYDASYYG (24), GISSEFYDNAND (3), ISSEFYDNANDL (2), SSEFYDNANDLL (1)	115/584 (20)
Complement factor B	ETIEGVDAEDGH (0)	24/764 (3)
Coronin-1A	YPPTAGPDPALT (22)	52/461 (11)
Fibrinogen γ chain	CEIDGSGNGWTV (67), GDAFDGFDFGDD (98), DAFDGFDFGDDP (97), AFDGFDFGDDPS (96), FDGFDFGDDPSD (95)	63/453 (14)
Fibronectin	TSLSAQWTPPNV (15)	487/2,386 (20)
High mobility group protein B1	EDEEDEEDEEEE (0), EDEEDEEEEEDE (0), EDEEEEEDEEDE (0), EDEEDEDEEEDD (0)	74/215 (34)
High mobility group protein B2	EDEDEEEEDEDE (0)	70/209 (33)
Histone H2A	GGVLPNIHPELL (4)	87/372 (23)
IgM heavy chain	SILTVSEEEWNT (8)	54/453 (12)
Inter-α trypsin inhibitor heavy chain H4	APPATSNPDPAV (0)	268/930 (29)
Myeloid cell nuclear differentiation antigen	SSVSDFNQNFEV (52)	143/407 (35)
Plasminogen	QGEPLDDYVNTQ (13)	35/810 (4)
Tenascin	VEWDPLDIAFET (9), LDGPSGLVTANI (2)	486/2,201 (22)
Vinculin	DDYEPELLLMPS (0)	294/1,134 (26)
Zinc α2–glycoprotein	DIVEYYNDSNGS (36), VVVAVPPQDTAP (16), VVAVPPQDTAPY (15), VAVPPQDTAPYS (14), AVPPQDTAPYSC (13), VPPQDTAPYSCH (12)	17/298 (6)

from the array peptides in that the citrullinome included all peptides with detected endogenous citrullines, whereas the highly bound array peptides were derived from a subset of proteins identified in the citrullinome with all arginines replaced by citrullines. We found that the overall pattern of amino acids frequently found next to endogenous citrulline was roughly similar to the pattern of amino acids frequently found next to citrulline in highly bound peptides (Figure 2D). Again, both glycine and serine were commonly next to citrulline. Taken together, these data suggest that arginine next to serine or glycine is frequently citrullinated and frequently targeted by IgG in RA.

Multiple features of intrinsic structural disorder in peptides bound by IgG in RA. Given the moderate binding of native peptides observed in our RA subjects, we further evaluated these peptides. We identified native peptides that were >2 times more highly bound by IgG in RA patients as compared to controls, excluding peptides with arginine or lysine to reduce potential effects from cross-reactivity with citrulline- or homocitrulline-containing peptides. As shown in Table 1, a total of 49 peptides met these criteria. Interestingly, several of the proteins from which the peptides were derived were related to complement. Additionally, many of the

peptides contained repeated amino acids or repeated short motifs, hallmarks of intrinsically disordered regions of proteins, i.e., regions that lack stable 3-dimensional structure. We were intrigued by this observation, since arginine-glycine and arginine-serine, which we determined were minimal motifs for both citrullination and autoantibody binding in RA (Figure 2), are found in intrinsically disordered regions of proteins (32,33). Thus, we verified whether bound native peptides were located in disordered regions by identifying regions of predicted disorder in the parent proteins, using the Protein DisOrder prediction System (PrDOS) (34). Thirty-five percent of the native peptides that were bound >2 times more in RA patients than in controls were predicted to be within disordered regions. In contrast, only 18% of the 49 native peptides with the least binding in RA were in disordered regions.

We also calculated the median distance from disorder for the 49 highest binding and lowest binding native peptides, resulting in 4 and 32 amino acids, respectively ($P = 0.0003$). Finally, PrDOS predicted that 67% of the 100 highest bound citrulline-containing peptides were in regions of disorder compared to only 38% of the lowest bound citrulline-containing peptides, with median distances from disorder of 0 and 12 amino acids, respectively ($P < 0.0001$).
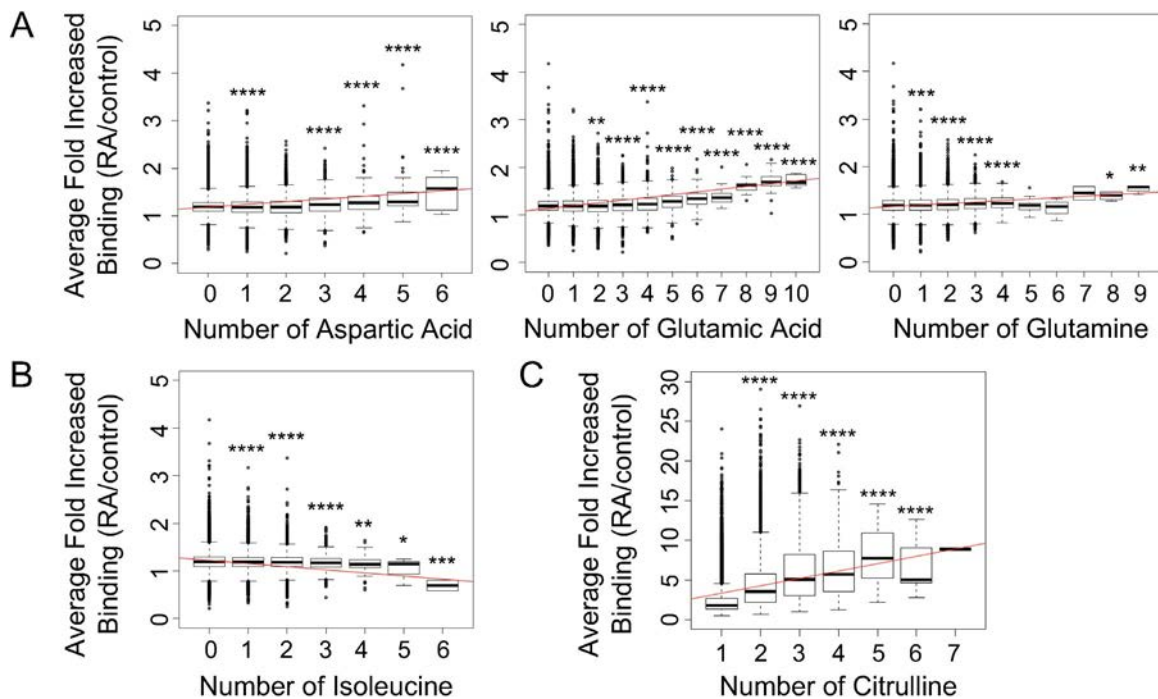
Figure 3. IgG in rheumatoid arthritis (RA) targets peptides with amino acids associated with intrinsic disorder. Peptides were grouped by the number of specific amino acids present, and the average fold increase in binding for all RA patients compared to controls was plotted for each peptide group. Results are shown for amino acids in native peptides (n = 95,761) that demonstrated a real increase (**A**) or reduction (**B**) in IgG binding or a real increase in IgG binding for citrulline-containing peptides (**C**) (n = 35,459) with an increasing number of that amino acid, in RA patients (n = 48) compared to controls (n = 12). The difference in binding for each peptide group was compared to peptides in which that amino acid was not present (i.e., the 0 group), or in the case of citrulline-containing peptides, compared to a single citrulline present (i.e., the 1 group). Data are presented as box plots, where the boxes represent the 25th to 75th percentiles, the lines within the boxes represent the median, and the lines outside the boxes represent the 10th and 90th percentiles. * = $P < 0.05$; ** = $P < 0.01$; *** = $P < 0.001$; **** = $P < 0.0001$, by t-test. Color figure can be viewed in the online issue, which is available at http://onlinelibrary.wiley.com/doi/10.1002/art.41074/abstract.

Intrinsically disordered regions also tend to contain arginine, glycine, lysine, glutamine, serine, glutamic acid, aspartic acid, and proline (32,35). To evaluate whether specific amino acids in peptides correlated with IgG binding in RA, we quantified the average binding of IgG in RA patients versus controls for native peptides with different amounts of each amino acid. We found that with increased representation of most amino acids in peptides, there was no real change in IgG binding in RA. However, higher IgG binding to peptides in RA was observed with increasing numbers of aspartic acid, glutamic acid, and glutamine (Figure 3A). Smaller increases in IgG binding in RA were seen with increasing numbers of glycine or proline (data not shown). Interestingly, increasing representation of isoleucine, which is associated with ordered protein regions (35), was associated with reduced IgG binding in RA (Figure 3B). We performed a similar analysis with citrulline-containing peptides. We found a dramatic increase in IgG binding in RA patients, compared to controls, with increasing citrulline content (Figure 3C), which vastly overshadowed the effects of any other amino acid. Considered together, these data suggest that peptides in regions of intrinsic structural disorder are targeted in RA.

IgG binding of citrulline-containing peptides derived from IgG in patients with CCP+RF+ RA. One of the most well-known antigens in RA is the Fc portion of IgG, the target of RF. Native peptides derived from IgG heavy chain were not identified as bound by IgG >2 times more in RA patients than in controls (Table 1), potentially because known RF epitopes are discontinuous (36) and not included in our array, or because bound epitopes contain arginine or lysine, which were excluded from the analysis. Therefore, we examined the recognition of peptides derived from IgG more closely. RF+ patients showed modest IgM binding to all peptide types derived from the constant region of IgG1 heavy chain (Figure 4A), with similar binding to peptides derived
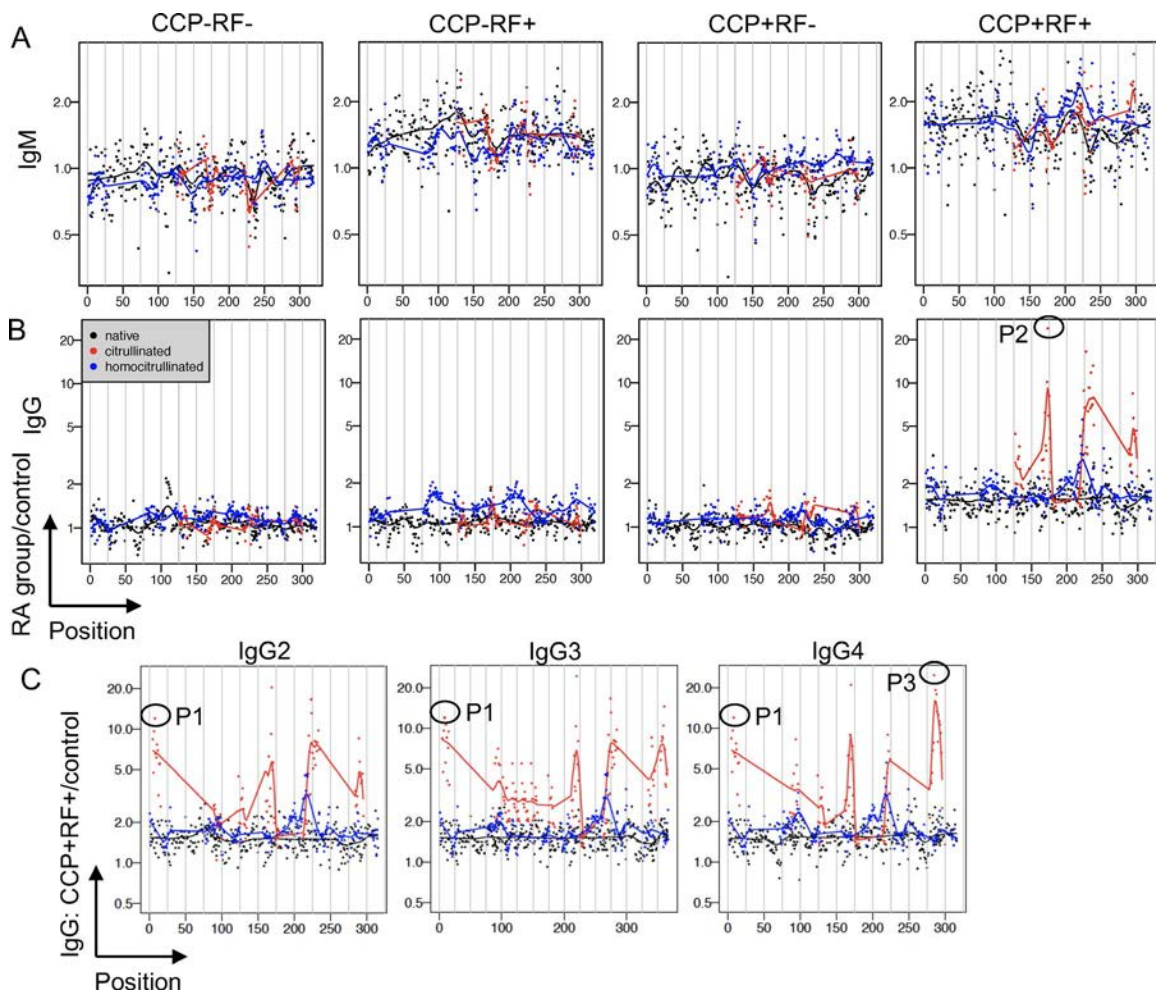
Figure 4. In RA, IgM binds IgG-derived peptides at a low level, and IgG binds primarily citrulline-containing IgG peptides at a high level. **A** and **B**, Binding of IgM (**A**) and IgG (**B**) in RA patients, in relation to controls, is shown for each peptide according to its position in the constant region of IgG1. RA patients were categorized as CCP–RF–, CCP–RF+, CCP+RF–, and CCP+RF+ (n = 12 per group). **C**, IgG binding in CCP+RF+ RA patients, in relation to controls, is shown for each peptide of the constant regions of IgG2, IgG3, and IgG4 (n = 12). Peptides (native and citrulline-containing versions) circled in **B** and **C** were evaluated by enzyme-linked immunosorbent assay as described in Figure 5. See Figure 1 for definitions.
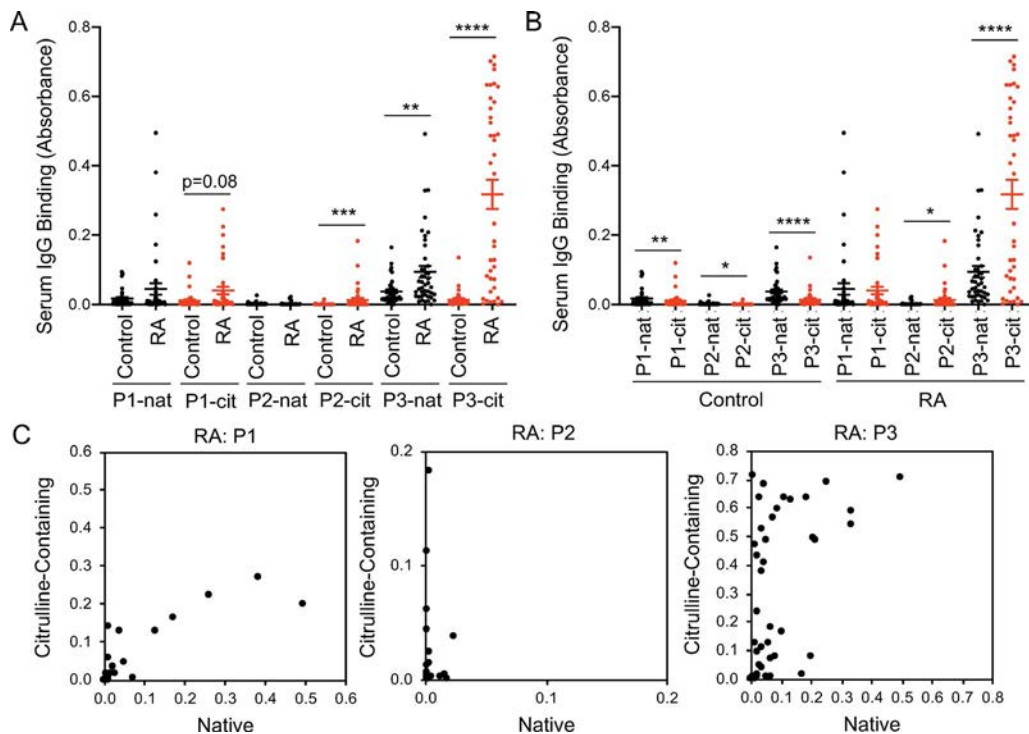
Figure 5. IgG binds to citrulline-containing peptides of IgG in RA. Peptides (native [nat] and citrulline-containing [cit] versions) circled in Figure 4 were used in an enzyme-linked immunosorbent assay to detect IgG binding in CCP+RF+ RA patient sera (n = 40) and control sera (n = 40). **A**, Results in RA patients versus controls were compared. **B**, Results for native versus citrulline-containing peptides were compared. **C**, For each subject, IgG binding is shown for the citrulline-containing peptide versus the native peptide. * = $P < 0.05$; ** = $P < 0.01$; *** = $P < 0.001$; **** = $P < 0.0001$, by Mann-Whitney test (**A**) or Wilcoxon's matched pairs signed rank test (**B**). See Figure 1 for other definitions. Color figure can be viewed in the online issue, which is available at http://onlinelibrary.wiley.com/doi/10.1002/art.41074/abstract.

from IgG2, IgG3, and IgG4 (data not shown). IgG binding in CCP–RF+ RA patients compared to controls was modestly greater for homocitrulline-containing than citrulline-containing or native peptides derived from IgG1 ($P < 0.0001$; Figure 4B), similar to IgG2, IgG3, and IgG4 (data not shown). More dramatically, the CCP+RF+ group demonstrated very high IgG binding predominantly to citrulline-containing peptides in the constant region of IgG1 (Figure 4B), with similar results for peptides derived from IgG2, IgG3, and IgG4 (Figure 4C).

Next, we selected 3 highly bound IgG-derived peptides with strong sequence homology across IgG isoforms and quantified IgG binding to those peptides by ELISA using a larger number of subjects. For 1 native and 2 citrulline-containing peptides, CCP+RF+ sera showed increased IgG binding compared to controls (Figure 5A). For the 1 native peptide with increased IgG binding in CCP+RF+ sera, binding to the citrulline-containing peptide was >3 times greater than the native version in RA (Figure 5B). Additionally, for individual RA patients, IgG binding to 2 of the 3 IgG-derived peptides appeared to favor citrulline (Figure 5C). Interestingly, although there was overall low binding to IgG-derived peptides in controls, controls had slightly higher binding to native peptides than citrulline-containing peptides (Figure 5B). Collectively, these data suggest that IgG can target citrulline-containing peptides of

IgG in RA, identifying epitopes that could be bound by an antibody defined as an ACPA or an RF.

DISCUSSION

Using a high-density peptide array and 4 serogroups of RA, we revealed interesting features of RA autoantibody reactivity. First, and not surprisingly, we found that citrulline was a dominant autoantibody target in the polyclonal repertoire of RA. The highest level of IgG binding in RA was to citrulline-containing peptides, and the encoded arginine content (citrullines on our array) directly correlated with average peptide IgG binding for each protein. Also, ≥1 citrulline-containing peptide from every protein on the array was bound by IgG. These findings are consistent with a similar lack of protein specificity reported for monoclonal autoantibodies in RA using a different set of peptide antigens (7), as well as with observations that ACPAs are cross-reactive (5–8) and recognize citrulline largely independently of surrounding peptides (37). Thus, our data support the theory that citrulline itself is a major driver of IgG reactivity in RA.

Our evaluation of homocitrulline reactivity revealed primarily nonspecific homocitrulline binding, and none of the peptides that were most highly bound by IgG contained homocitrulline. These

results suggest that homocitrulline may not be targeted to as great an extent as citrulline, consistent with the finding that AHCPAs have lower avidity than ACPAs (38). However, any homocitrulline-specific binding dependent on a nearby citrulline or other modified amino acid would not have been detected, since our peptides contained either citrulline or homocitrulline, but not both. Additionally, if homocitrulline-containing epitopes are primarily discontinuous, they would not have been detected using our array of linear peptides. However, homocitrulline-containing peptides were bound by rheumatoid monoclonal antibodies using a similar array (7). Also, homocitrullination increases structural disorder (39) and thus increases the likelihood of linear epitopes. Importantly, homocitrulline reactivity may change over time in subjects (7), causing variability among studies. Future experiments with additional subjects, modifications, and time points may clarify this issue.

We also observed moderate IgG binding to native peptides in CCP+RF+ patients. Unlike IgM binding, which was increased against native peptides in both RF+ groups, moderate IgG binding of native peptides was absent in CCP–RF+ patients and was thus unlikely due to promiscuity of RF. Furthermore, the IgG binding was unlikely due to cross-reactivity against citrulline- and homocitrulline-containing peptides, given a similar increase in IgG binding in CCP+RF+ patients when peptides with arginine or lysine were excluded. IgG binding to native peptides could be due to an unknown endogenous posttranslational modification resulting in cross-reactivity with native peptides in the array. For example, increased glutamic acid, which can mimic phosphoserine, was associated with increased IgG binding to native peptides in our array (Figure 3). If rheumatoid autoantibodies target phosphoserine in vivo, we might have simply detected cross-reactivity with glutamic acid with our array peptides. Alternatively, autoantibodies in RA may commonly target a host of native antigens as part of a polyclonal response and/or polyreactive autoantibodies.

Upon further characterization of citrulline reactivity in our experiments, we detected a preference for glycine or serine next to citrulline in highly bound peptides as well as next to endogenous citrullines in the rheumatoid joint, suggesting that these amino acid pairs may be commonly targeted by autoantibodies due to their common presence in antigens. There were some differences between the patterns of amino acids next to citrulline in the citrullinome and highly bound peptides that could reflect differences in the efficacy of major histocompatibility complex, B cell, or T cell receptor binding, other factors in generating an immune response, or simply sample size. However, our findings related to glycine are consistent with the findings of others. The presence of glycine next to citrulline has been observed in the citrullinome of 30 human tissues (40), in motifs targeted by the citrullinating peptidylarginine deiminases 2 and 4 (41–43), and in autoantibody binding in RA (7,44,45). The preference for citrullination of or IgG binding to peptides with citrulline next to serine has not been previously described. Perhaps the unique features of our subject groups, analyses, or array allowed for this novel finding.

Interestingly, arginine-serine and arginine-glycine-glycine repeats are commonly found in disordered regions of proteins (32,33). Moreover, disordered regions of proteins are citrullinated to a higher degree than ordered regions, and citrullination increases disorder (39). Taken together, these observations suggest that disorder, citrullination, and the highest affinity autoantibodies in RA are profoundly linked.

We obtained additional evidence that autoantibodies in RA target regions of intrinsic disorder. Native and citrulline-containing peptides bound by IgG in RA were more likely to be found in regions of disorder than poorly bound peptides. Moreover, increased content of amino acids associated with intrinsic disorder (32,35) correlated with increased IgG binding in RA. Similarly, in lupus, approximately one-third of characteristic autoantigens contain stretches of charged amino acids (46), which is common in disordered regions, and nuclear autoantigens are often disordered proteins (47). Furthermore, although many examples of structured epitopes exist, epitopes predicted to be within regions of disorder were slightly more likely to be recognized by antibodies, compared to epitopes in ordered regions in a wide range of normal and pathologic conditions (48,49). We were unable to directly compare the binding in disordered versus ordered regions, since ordered epitopes are often discontinuous and thus were not present on our array. However, our findings provide a body of evidence that autoantibodies in RA bind intrinsically disordered regions, which are frequently citrullinated (39), a concept that has potential importance regarding to the basis of autoantibody development in RA. Of note, it has been hypothesized that repetition and charge lead to autoantibody reactivity (50). However, in RA, the charge may not be the driving factor as charge is reduced with citrullination. Perhaps disorder is the main driver due to the high degree of accessibility of intrinsically disordered regions of proteins (51) or due to bound DNA or RNA activating Toll-like receptors.

Since the binding of citrulline-containing and native peptides was predominantly seen in CCP+RF+ RA, many of our findings related to targeting disordered regions may predominantly apply to this group. However, our subject selection also allowed for an evaluation of antibody binding in seronegative RA and in RA patients positive for only CCP or RF. Despite our evaluation of 178,828 peptides, seronegative patients showed little binding to citrulline-containing or native peptides, suggesting minimal autoantibody presence. Interestingly, IgG binding to homocitrulline-containing peptides was greater in CCP–RF– patients than controls, suggesting that homocitrulline could be the basis for an improved diagnostic test for seronegative RA. However, despite using multiple models, we have not yet identified any peptides predictive of an RA diagnosis in seronegative patients. At least a subset of seronegative RA may be truly seronegative, lacking autoantibodies in general. An absence of autoantibodies in seronegative disease might suggest a different disease pathophysiology than seropositive disease, given evidence that RF and ACPAs are pathologic (1,2). Alternatively, RA may exist on a continuum.

In support of this idea, we observed that levels of citrulline-specific IgG in CCP+RF– and CCP–RF+ disease fell between levels in CCP+RF+ and CCP–RF– disease. Future studies with even larger arrays that are not limited by protein selection bias or by linear epitopes, or perhaps arrays incorporating additional posttranslational modifications, combinations of posttranslational modifications, or full-length proteins, may resolve these issues.

Our final observation was that IgG from CCP+RF+ sera targets citrulline-containing peptides of IgG. This finding raises the possibility that IgG-RF (IgG that binds IgG) could also be an ACPA, making citrullinated IgG, which has been reported in humans (24,26,52), a linchpin connecting ACPAs and RF in RA. IgM did not preferentially target citrulline-containing peptides of IgG. IgM-RF, which also occurs in healthy individuals, may arise independently of citrulline due to smoking or pathogens, whereas the development of IgG-RF, which requires a break in tolerance and T cell help, may be driven by targeting citrulline, like other ACPAs (53). However, it is not known whether the IgG we detected originally developed against citrullinated IgG, or whether the observed targeting of citrulline-containing IgG peptides was due to cross-reactivity of ACPAs. Also, not all IgG that bound IgG-derived peptides targeted citrulline (Figure 5), potentially indicating different mechanisms for the break in tolerance for generating IgG-RF (53). Finally, despite having a unique name for its autoantibody, IgG may be similar to other proteins in RA, with native epitopes targeted, but less so than citrulline-containing epitopes. It will be important for future work to clearly define the reactivity of RF in RA and diseases with RF that do not have a citrulline bias, in order to shed light on disease pathophysiology as well as to fully understand and optimize RF-based diagnostic tests.

In summary, using the 4 serogroups of RA and a high-density peptide array, we demonstrated very strong autoantibody targeting of citrulline, particularly if adjacent to glycine or serine, as well as a moderate binding to native peptides primarily in CCP+RF+ RA and very little antibody binding in seronegative disease. Furthermore, we identified disorder as a feature of IgG-targeted peptides and epitope overlap between ACPAs and RF.

AUTHOR CONTRIBUTIONS

All authors were involved in drafting the article or revising it critically for important intellectual content, and all authors approved the final version to be published. Dr. Shelef had full access to all of the data in the study and takes responsibility for the integrity of the data and the accuracy of the data analysis.
Study conception and design. Bridges, Shelef.
Acquisition of data. Mergaert, Fahmy, Bawadekar, Shelef.
Analysis and interpretation of data. Zheng, Mergaert, Fahmy, Bawadekar, Holmes, Ong, Bridges, Newton, Shelef.

ADDITIONAL DISCLOSURES

After these experiments were completed, but before manuscript submission, author Bawadekar became employed by Invenra, Inc.

REFERENCES

1. Engdahl C, Bang H, Dietel K, Lang SC, Harre U, Schett G. Periarticular bone loss in arthritis is induced by autoantibodies against citrullinated vimentin. J Bone Miner Res 2017;32:1681–91.

2. Mathsson L, Lampa J, Mullazehi M, Rönnelid J. Immune complexes from RA synovial fluid induce FcγRIIa dependent and rheumatoid factor correlated production of tumour necrosis factor-α by peripheral blood mononuclear cells. Arthritis Res Ther 2006;8:R64.

3. Uysal H, Bockermann R, Nandakumar KS, Sehnert B, Bajtner E, Engström A, et al. Structure and pathogenicity of antibodies specific for citrullinated collagen type II in experimental arthritis. J Exp Med 2009;206:449–62.

4. Aletaha D, Neogi T, Silman AJ, Funovits J, Felson DT, Bingham CO III, et al. 2010 rheumatoid arthritis classification criteria: an American College of Rheumatology/European League Against Rheumatism collaborative initiative. Arthritis Rheum 2010;62:2569–81.

5. Ioan-Facsinay A, el-Bannoudi H, Scherer HU, van der Woude D, Ménard HA, Lora M, et al. Anti-cyclic citrullinated peptide antibodies are a collection of anti-citrullinated protein antibodies and contain overlapping and non-overlapping reactivities. Ann Rheum Dis 2011;70:188–93.

6. Titcombe PJ, Wigerblad G, Sippl N, Zhang N, Shmagel AK, Sahlström P, et al. Pathogenic citrulline-multispecific B cell receptor clades in rheumatoid arthritis. Arthritis Rheumatol 2018;70:1933–45.

7. Steen J, Forsström B, Sahlström P, Odowd V, Israelsson L, Krishnamurthy A, et al. Recognition of amino acid motifs, rather than specific proteins, by human plasma cell–derived monoclonal antibodies to posttranslationally modified proteins in rheumatoid arthritis. Arthritis Rheumatol 2019;71:196–209.

8. Liang B, Ge C, Lönnblom E, Lin X, Feng H, Xiao L, et al. The autoantibody response to cyclic citrullinated collagen type II peptides in rheumatoid arthritis. Rheumatology (Oxford) 2019;58:1623–33.

9. Shi J, Knevel R, Suwannalai P, van der Linden MP, Janssen GM, van Veelen PA, et al. Autoantibodies recognizing carbamylated proteins are present in sera of patients with RA and predict joint damage. Proc Natl Acad Sci U S A 2011;108:17372–7.

10. Scinocca M, Bell DA, Racapé M, Joseph R, Shaw G, McCormick JK, et al. Antihomocitrullinated fibrinogen antibodies are specific to RA and frequently bind citrullinated proteins/peptides. J Rheumatol 2014;41:270–9.

11. Reed E, Jiang X, Kharlamova N, Ytterberg AJ, Catrina AI, Israelsson L, et al. Antibodies to carbamylated α-enolase epitopes in RA also bind citrullinated epitopes and are largely indistinct from anti-citrullinated protein antibodies. Arthritis Res Ther 2016;18:96.

12. Turunen S, Hannonen P, Koivula MK, Risteli L, Risteli J. Separate and overlapping specificities in rheumatoid arthritis antibodies binding to citrulline- and homocitrulline-containing peptides related to type I and II collagen telopeptides. Arthritis Res Ther 2015;17:2.

13. Thiele GM, Duryee MJ, Anderson DR, Klassen LW, Mohring SM, Young KA, et al. Malondialdehyde-acetaldehyde adducts and anti–malondialdehyde-acetaldehyde antibodies in rheumatoid arthritis. Arthritis Rheumatol 2015;67:645–55.

14. Juarez M, Bang H, Hammar F, Reimer U, Dyke B, Sahbudin I, et al. Identification of novel antiacetylated vimentin antibodies in patients with early inflammatory arthritis. Ann Rheum Dis 2016;75:1099–107.

15. Darrah E, Andrade F. Citrullination, and carbamylation, and malondialdehyde-acetaldehyde! Oh my! Entering the forest of autoantigen modifications in RA [editorial]. Arthritis Rheumatol 2015;67:604–8.

16. Hueber W, Kidd BA, Tomooka BH, Lee BJ, Bruce B, Fries JF, et al. Antigen microarray profiling of autoantibodies in rheumatoid arthritis. Arthritis Rheum 2005;52:2645–55.

17. Konig MF, Giles JT, Nigrovic PA, Andrade F. Antibodies to native and citrullinated RA33 (hnRNP A2/B1) challenge citrullination as the inciting principle underlying loss of tolerance in RA. Ann Rheum Dis 2016;75:2022–8.

18. Demoruelle MK, Bowers E, Lahey LJ, Sokolove J, Purmalek M, Seto NL, et al. Antibody responses to citrullinated and noncitrullinated antigens in the sputum of subjects with rheumatoid arthritis and subjects at risk for development of rheumatoid arthritis. Arthritis Rheumatol 2018;70:516–27.

19. Barra L, Pope JE, Orav JE, Boire G, Haraoui B, Hitchon C, et al. Prognosis of seronegative patients in a large prospective cohort of patients with early inflammatory arthritis. J Rheumatol 2014;41:2361–9.

20. Rebernick R, Fahmy L, Glover C, Bawadekar M, Shim D, Holmes CL, et al. DNA area and NETosis analysis (DANA): a high-throughput method to quantify neutrophil extracellular traps in fluorescent microscope images. Biol Proced Online 2018;20:7.

21. Holmes CL, Peyton CG, Bier AM, Donlon TZ, Osman F, Bartels CM, et al. Reduced IgG titers against pertussis in rheumatoid arthritis: evidence for a citrulline-biased immune response and medication effects. PLoS One 2019;14:e0217221.

22. Katz JN, Barrett J, Liang MH, Bacon AM, Kaplan H, Kieval RI, et al. Sensitivity and positive predictive value of Medicare Part B physician claims for rheumatologic diagnoses and procedures. Arthritis Rheum 1997;40:1594–600.

23. Bailey AL, Buechler CR, Matson DR, Peterson EJ, Brunner KG, Mohns MS, et al. Pegivirus avoids immune recognition but does not attenuate acute-phase disease in a macaque model of HIV infection. PLoS Pathog 2017;13:e1006692.

24. Wang F, Chen FF, Gao WB, Wang HY, Zhao NW, Xu M, et al. Identification of citrullinated peptides in the synovial fluid of patients with rheumatoid arthritis using LC-MALDI-TOF/TOF. Clin Rheumatol 2016; 35:2185–94.

25. Van Beers JJ, Schwarte CM, Stammen-Vogelzangs J, Oosterink E, Božič B, Pruijn GJ. The rheumatoid arthritis synovial fluid citrullinome reveals novel citrullinated epitopes in apolipoprotein E, myeloid nuclear differentiation antigen, and β-actin. Arthritis Rheum 2013;65:69–80.

26. Tutturen AE, Fleckenstein B, de Souza GA. Assessing the citrullinome in rheumatoid arthritis synovial fluid with and without enrichment of citrullinated peptides. J Proteome Res 2014;13:2867–73.

27. Nogueira L, Sebbag M, Vincent C, Arnaud M, Fournié B, Cantagrel A, et al. Performance of two ELISAs for antifilaggrin autoantibodies, using either affinity purified or deiminated recombinant human filaggrin, in the diagnosis of rheumatoid arthritis. Ann Rheum Dis 2001;60:882–7.

28. Gentleman R, Ihaka R. R: a language and environment for statistical computing. 2017. URL: https://www.R-project.org/.

29. Bartlett MS. The use of transformations. Biometrics 1947;3:39–52.

30. Székely GJ, Rizzo ML, Bakirov NK. Measuring and testing dependence by correlation of distances. Ann Stat 2007;35:2769–94.

31. Bailey TL, Elkan C. Fitting a mixture model by expectation maximization to discover motifs in biopolymers. Proc Int Conf Intell Syst Mol Biol 1994;2:28–36.

32. Castello A, Fischer B, Eichelbaum K, Horos R, Beckmann BM, Strein C, et al. Insights into RNA biology from an atlas of mammalian mRNA-binding proteins. Cell 2012;149:1393–406.

33. Haynes C, Iakoucheva LM. Serine/arginine-rich splicing factors belong to a class of intrinsically disordered proteins. Nucleic Acids Res 2006;34:305–12.

34. Ishida T, Kinoshita K. PrDOS: prediction of disordered protein regions from amino acid sequence. Nucleic Acids Res 2007;35:W460–4.

35. Uversky VN. The alphabet of intrinsic disorder. II. Various roles of glutamic acid in ordered and intrinsically disordered proteins [review]. Intrinsically Disord Proteins 2013;1:e24684.

36. Artandi SE, Calame KL, Morrison SL, Bonagura VR. Monoclonal IgM rheumatoid factors bind IgG at a discontinuous epitope comprised of amino acid loops from heavy-chain constant-region domains 2 and 3. Proc Natl Acad Sci U S A 1992;89:94–8.

37. Ge C, Xu B, Liang B, Lönnblom E, Lundström SL, Zubarev RA, et al. Structural basis of cross-reactivity of anti–citrullinated protein antibodies. Arthritis Rheumatol 2019;71:210–21.

38. Van Delft MA, Verheul MK, Burgers LE, Rantapää-Dahlqvist S, van der Helm-van Mil AH, Huizinga TW, et al. The anti-carbamylated protein antibody response is of overall low avidity despite extensive isotype switching. Rheumatology (Oxford) 2018;57:1583–91.

39. Tarcsa E, Marekov LN, Mei G, Melino G, Lee SC, Steinert PM. Protein unfolding by peptidylarginine deiminase: substrate specificity and structural relationships of the natural substrates trichohyalin and filaggrin. J Biol Chem 1996;271:30709–16.

40. Lee CY, Wang D, Wilhelm M, Zolg DP, Schmidt T, Schnatbaum K, et al. Mining the human tissue proteome for protein citrullination. Mol Cell Proteomics 2018;17:1378–91.

41. Haag S, Schneider N, Mason DE, Tuncel J, Andersson IE, Peters EC, et al. Identification of new citrulline-specific autoantibodies, which bind to human arthritic cartilage, by mass spectrometric analysis of citrullinated type II collagen. Arthritis Rheumatol 2014;66:1440–9.

42. Tanikawa C, Ueda K, Suzuki A, Iida A, Nakamura R, Atsuta N, et al. Citrullination of RGG motifs in FET proteins by PAD4 regulates protein aggregation and ALS susceptibility. Cell Rep 2018;22: 1473–83.

43. Assohou-Luty C, Raijmakers R, Benckhuijsen WE, Stammen-Vogelzangs J, de Ru A, van Veelen PA, et al. The human peptidyl-arginine deiminases type 2 and type 4 have distinct substrate specificities. Biochim Biophys Acta 2014;1844:829–36.

44. Burkhardt H, Koller T, Engström Å, Nandakumar KS, Turnay J, Kraetsch HG, et al. Epitope-specific recognition of type II collagen by rheumatoid arthritis antibodies is shared with recognition by antibodies that are arthritogenic in collagen-induced arthritis in the mouse. Arthritis Rheum 2002;46:2339–48.

45. Szarka E, Aradi P, Huber K, Pozsgay J, Végh L, Magyar A, et al. Affinity purification and comparative biosensor analysis of citrulline-peptide-specific antibodies in rheumatoid arthritis. Int J Mol Sci 2018;19:E326.

46. Brendel V, Dohlman J, Blaisdell BE, Karlin S. Very long charge runs in systemic lupus erythematosus-associated autoantigens. Proc Natl Acad Sci U S A 1991;88:1536–40.

47. Carl PL, Temple BR, Cohen PL. Most nuclear systemic autoantigens are extremely disordered proteins: implications for the etiology of systemic autoimmunity. Arthritis Res Ther 2005;7:R1360–74.

48. MacRaild CA, Richards JS, Anders RF, Norton RS. Antibody recognition of disordered antigens. Structure 2016;24:148–57.

49. Guy AJ, Irani V, MacRaild CA, Anders RF, Norton RS, Beeson JG, et al. Insights into the immunological properties of intrinsically disordered malaria proteins using proteome scale predictions. PLoS One 2015;10:e0141729.

50. Plotz PH. The autoantibody repertoire: searching for order. Nat Rev Immunol 2003;3:73–8.

51. Wright PE, Dyson HJ. Intrinsically disordered proteins in cellular signalling and regulation. Nat Rev Mol Cell Biol 2015;16:18–29.

52. Hutchinson D, Clarke A, Heesom K, Murphy D, Eggleton P. Carbamylation/citrullination of IgG Fc in bronchiectasis, established RA with bronchiectasis and RA smokers: a potential risk factor for disease. ERJ Open Res 2017;3:00018–2017.

53. Shelef MA. New relationships for old autoantibodies in rheumatoid arthritis [editorial]. Arthritis Rheumatol 2019;71:1396–1399.

Five-Year Outcome of Operative and Nonoperative Management of Meniscal Tear in Persons Older Than Forty-Five Years

Jeffrey N. Katz,[1] [iD] Swastina Shrestha,[1] Elena Losina,[1] [iD] Morgan H. Jones,[2] Robert G. Marx,[3] Lisa A. Mandl,[3] Bruce A. Levy,[4] Lindsey A. MacFarlane,[1] [iD] Kurt P. Spindler,[2] Genevieve S. Silva,[1] METEOR Investigators, and Jamie E. Collins[1] [iD]

Objective. To determine the 5-year outcome of treatment for meniscal tear in osteoarthritis.

Methods. We examined 5-year follow-up data from the Meniscal Tear in Osteoarthritis Research trial (METEOR) of physical therapy versus arthroscopic partial meniscectomy. We performed primary intent-to-treat (ITT) and secondary as-treated analyses. The primary outcome measure was the Knee Injury and Osteoarthritis Outcome Score (KOOS) pain scale; total knee replacement (TKR) was a secondary outcome measure. We used piecewise linear mixed models to describe change in KOOS pain. We calculated 5-year cumulative TKR incidence and used a Cox model to estimate hazard ratios (HRs) for TKR, with 95% confidence intervals (95% CIs).

Results. Three hundred fifty-one participants were randomized. In the ITT analysis, the KOOS pain scores were ~46 (scale of 0 [no pain] to 100 [most pain]) at baseline in both groups. Pain scores improved substantially in both groups over the first 3 months, continued to improve through the next 24 months (to ~18 in each group), and were stable at 24–60 months. Results of the as-treated analyses of the KOOS pain score were similar. Twenty-five participants (7.1% [95% CI 4.4–9.8%]) underwent TKR over 5 years. In the ITT model, the HR for TKR was 2.0 (95% CI 0.8–4.9) for subjects randomized to the arthroscopic partial meniscectomy group, compared to those randomized to the physical therapy group. In the as-treated analysis, the HR for TKR was 4.9 (95% CI 1.1–20.9) for subjects ultimately treated with arthroscopic partial meniscectomy, compared to those treated nonoperatively.

Conclusion. Pain improved considerably in both groups over 60 months. While ITT analysis revealed no statistically significant differences following TKR, greater frequency of TKR in those undergoing arthroscopic partial meniscectomy merits further study.

INTRODUCTION

Knee pain in the setting of meniscal tear and damage to cartilage, bone, and other intraarticular knee structures is common in middle-aged and older adults. Patients with these findings are typically treated nonoperatively with medications, physical therapy, and corticosteroid injections. When these measures fail, patients are often offered arthroscopic partial meniscectomy as a surgical option.

Several randomized controlled trials (RCTs) have addressed the short-term (1–2 years) outcomes of nonoperative and surgical treatments for meniscal tear in this patient population (1–8).

These trials demonstrated clinically important improvements in pain and function from baseline to 1–2 years of follow-up in patients receiving nonoperative treatment and those undergoing surgical treatment. In intent-to-treat (ITT) analyses, one trial showed an advantage of arthroscopic partial meniscectomy over physical therapy (6,7), while several other trials did not reveal clinically important differences in the outcomes of these 2 strategies (1–5). In some trials, as-treated analyses were also performed, in which participants randomized to treatment with physical therapy who then elected to have an arthroscopic partial meniscectomy were analyzed within the arthroscopic partial meniscectomy group (1–3). These as-treated analyses suggest a benefit in crossing over to arthroscopic partial meniscectomy among those not responding to physical therapy (1–3). In summary, the literature suggests that, regardless of treatment, middle-aged and older patients presenting with knee pain, osteoarthritis (OA) changes, and meniscal tear are likely, on average, to improve considerably over a 1–2-year period. These short-term trials indicate that nonoperative therapy is a sensible initial treatment strategy. Arthroscopic partial meniscectomy appears to be effective in those who do not respond to initial physical therapy (9).

Relatively little is known about the effects of treatment on outcomes beyond 1–2 years in patients with meniscal tear and OA changes. To address this gap in the literature, we used data from the 5-year follow-up of patients who participated in the Meniscal Tear in Osteoarthritis Research (METEOR) trial to evaluate the effect of treatment on pain, functional status, and frequency of total knee replacement (TKR) over 5 years of follow-up.

PATIENTS AND METHODS

Study population and design. This study was a longitudinal 5-year follow-up of participants in the METEOR trial, a multicenter RCT. The METEOR investigators are listed in Appendix A. Participants were at least 45 years of age and had knee pain for at least 1 month, which was diagnosed by their treating physician to be due to a meniscal tear. Additional inclusion criteria were evidence of meniscal tear and either one or more cartilage defects seen on magnetic resonance imaging (MRI), or the presence of osteophytes or joint space narrowing on radiography. We excluded individuals with greater than 50% joint space narrowing. This criterion is often used to define Kellgren/Lawrence (K/L) grade 4 on radiographs, as the precise definition of K/L grade 4 has not been established (10,11). Full details are reported elsewhere (1,12).

Participants were randomized 1:1 to undergo either a standardized, strengthening-based, 12-week physical therapy regimen or arthroscopic partial meniscectomy followed by the physical therapy regimen. Participating surgeons performed arthroscopic partial meniscectomy in a standardized manner, with resection of the tear to achieve a stable edge and no osteochondral drilling.

Groups for analysis. We adopted an ITT approach for the primary analysis, in which all subjects were analyzed in their assigned group at randomization, regardless of the treatment(s) they actually received. Because some subjects randomized to receive physical therapy later underwent an arthroscopic partial meniscectomy over the follow-up period, we also performed an as-treated analysis in which we categorized participants into 3 groups: randomized to and underwent an arthroscopic partial meniscectomy; randomized to physical therapy without crossover to arthroscopic partial meniscectomy; and randomized to physical therapy with crossover to arthroscopic partial meniscectomy. Ten subjects were randomized to arthroscopic partial meniscectomy but did not undergo the procedure. This group was too small to examine meaningfully and was excluded from the as-treated analysis.

Outcome measures. Participants completed questionnaires prior to randomization, at 3 and 6 months postrandomization, and every 6 months thereafter through 60 months of follow-up. The primary outcome measure for this analysis was the Knee Injury and Osteoarthritis Outcome Score (KOOS) pain scale (13,14), which was assessed in each follow-up questionnaire. The KOOS pain scale consists of 9 items that ask about the severity of pain related to a range of activities. We transformed the score to a 0–100 scale, with 100 representing the most pain and 0 representing no pain. We used the KOOS pain scale rather than the Western Ontario and McMaster Universities Osteoarthritis Index (WOMAC) pain scale (15) as the primary outcome measure because the WOMAC pain scale asks about pain with largely sedentary activities, while the KOOS pain scale includes the WOMAC pain items and 4 additional items regarding knee pain with bending, straightening, twisting, or pivoting, and knee pain frequency. A secondary outcome measure was the WOMAC functional status scale (15), which is also scored on a scale of 0–100, with 100 representing worst functional status.

We evaluated the occurrence of TKR in the index knee in all participants as an additional outcome measure. Participants were asked about TKR in the questionnaires, and we examined the medical records of each subject to verify that they received TKR. Since the procedures could have occurred at a different hospital from the one at which the subject was enrolled in the METEOR trial, we used both self-reported and medical record review data. If the date of the TKR procedure was self-reported by the participant in the questionnaire with only the month and year, we assigned the first day of the reported month as the TKR date. In subjects undergoing TKR of the index knee, any data collected following the date of TKR were not included in our analyses.

Baseline covariates. We collected data on several baseline factors, including age, sex, body mass index (BMI), K/L grade, musculoskeletal comorbidity index (painful sites other than the index knee) (16), 5-item mental health index (17), and baseline measures of the primary and secondary outcome metrics.

Statistical analysis. We conducted the statistical analyses in 2 parts: evaluation of pain and function, and evaluation of TKR rates. Our principal analyses used an ITT approach and secondary analyses used an as-treated approach. Hazard ratios (HRs) with 95% confidence intervals (95% CIs) were calculated.

Pain and function. We used descriptive statistics and a piecewise linear mixed model to describe the trend in the KOOS pain and WOMAC function outcome over time. Piecewise linear models, or spline models, describe nonlinear trends well when the mean change in response varies over some duration (18). Points at which the slope changes are referred to as knots. We evaluated models with knots at 3, 6, 12, 24, 36, and 48 months, and chose the final model based on the goodness of fit assessed by the Bayesian Information Criterion (BIC) (18). These models were adjusted for baseline age, BMI, sex, musculoskeletal comorbidity index, and mental health index. We included covariate-by-time interactions for treatment group, baseline K/L grade, and treatment group and K/L grade. These interactions show whether the trend in outcomes over time differs by each level of covariate.

We used pattern mixture models to investigate the potential effect of dropout on longitudinal estimates of self-reported outcomes. Pattern mixture modeling is a technique used to account for potentially informative dropouts; the models stratify the population by the pattern of dropout and then separately model each group (19). The final estimate is a weighted average of these patterns. We stratified the population into 3 mutually exclusive groups: subjects undergoing TKR prior to 60 months, study completers (defined as participants who completed either the 48-, 54-, or 60-month questionnaire), and study noncompleters (those who did not complete questionnaires at 48, 54, or 60 months and who did not have TKR). This analysis assesses whether the trend in outcome over time is different for different dropout groups (suggesting that dropout may be not at random), and evaluates whether these potentially not-at-random dropouts bias the overall estimate of longitudinal pain and function trajectory.

While we incorporated pre-TKR KOOS pain scores in the longitudinal model, we did not follow up these subjects post-TKR. To address the concern that subjects dropping out of the study to undergo TKR may have worse pain and not be missing at random, we performed a sensitivity analysis to examine the effect of TKR dropout on the KOOS pain score across the 2 randomized groups. First, we performed multiple imputation under a missing-at-random assumption, using baseline covariates associated with outcomes and observed KOOS pain values. Next, we assumed that subjects dropping out to undergo TKR would have worse KOOS pain values than predicted by the multiple imputation model (i.e., a not-at-random dropout mechanism). We increased the attributed KOOS pain in subjects who dropped out to undergo TKR by either 33% or 50% at all time points. We chose these increases in pain score based on the results of the pattern mixture models suggesting that TKR dropouts had worse pain and function and because they are clinically plausible. We then fit a mixed-effects model on

the imputed data set with knots at 3, 12, and 24 months to estimate the effect of treatment groups on KOOS pain scores.

Total knee replacement. We calculated the 5-year cumulative incidence of TKR overall and stratified by the 2 randomized groups. In a secondary, as-treated analysis, we stratified by the 3 treatment groups (randomized to and underwent arthroscopic partial meniscectomy; randomized to and underwent physical therapy; randomized to physical therapy and crossed over to arthroscopic partial meniscectomy). We fit Cox proportional hazard models to evaluate the association between group (randomized group in the primary analysis, and underwent arthroscopic partial meniscectomy versus did not undergo arthroscopic partial meniscectomy in the as-treated analysis) and time to TKR, adjusting for baseline covariates including K/L grade. We examined associations between model residuals and time to confirm the proportional hazards assumption.

RESULTS

Three hundred fifty-one participants were randomized to undergo arthroscopic partial meniscectomy (n = 174) or physical therapy (n = 177). These subjects were included in the ITT analyses. In the as-treated analyses, we excluded the 10 random-

Table 1. Characteristics of the patients in the 2 randomized meniscal tear treatment groups*

	Physical therapy	Arthroscopic partial meniscectomy
Age, mean ± SD years (n)	57.2 ± 6.7 (177)	58.6 ± 7.9 (174)
Body mass index, mean ± SD (n)	30.2 ± 6.1 (168)	30.2 ± 6.2 (164)
KOOS pain, mean ± SD (n)	47.4 ± 16.2 (175)	46.4 ± 16.1 (172)
WOMAC function, mean ± SD (n)	37.6 ± 18.2 (176)	37.5 ± 18.2 (173)
MHI-5 index, mean ± SD (n)	73.6 ± 14.2 (176)	74.8 ± 12.8 (171)
Sex		
Male	75 (42)	75 (43)
Female	102 (58)	99 (57)
Race		
White	145 (82)	151 (87)
Black	19 (11)	15 (9)
Hispanic	5 (3)	2 (1)
Other or missing	8 (5)	6 (3)
Index knee		
Left	106 (60)	96 (55)
Right	71 (40)	78 (45)
Kellgren/Lawrence grade		
0 (normal)	14 (8)	14 (8)
1 (questionable osteophyte)	43 (24)	33 (19)
2 (definite osteophyte)	59 (33)	69 (40)
3 (<50% joint space narrowing)	61 (34)	58 (33)

* Except where indicated otherwise, values are the number (%). KOOS = Knee Injury and Osteoarthritis Outcome Score; WOMAC = Western Ontario and McMaster Universities Osteoarthritis Index; MHI-5 = 5-item mental health index.

ized to receive arthroscopic partial meniscectomy who never underwent surgery. The as-treated groups included 164 subjects randomized to and receiving arthroscopic partial meniscectomy, 109 randomized to receive physical therapy who did not cross over to arthroscopic partial meniscectomy, and 68 who were randomized to receive physical therapy and crossed over to arthroscopic partial meniscectomy. Seventy-nine percent of crossovers occurred in the first 6 months following randomization, 12% between 6 and 12 months, and 9% after 12 months.

Baseline features. Participants in the 2 randomized groups were similar in age (mean 57.2 years and 58.6 years in the 2 groups), sex (~43% male in each group), BMI (~30 in each group), and K/L grade (approximately one-third of subjects in each group had K/L grade 3 radiographs). The mean KOOS pain score at baseline was 47.4 and 46.4 in the 2 groups (Table 1). The baseline characteristics of the as-treated groups are shown in Supplementary Table 1, available on the *Arthritis & Rheumatology* web site at http://onlinelibrary.wiley.com/doi/10.1002/art.41082/abstract.

Subject retention. Among the 351 participants in the primary analysis cohort, 4 subjects (1%) died, 25 (7%) underwent TKR, 65 (19%) discontinued participation over 5 years, and 18 (5%) were lost to follow-up. In both the arthroscopic partial meniscectomy and physical therapy groups, 66% of participants completed at least 9 of the 12 questionnaires. Detailed data on questionnaire

completion by time point are presented in Supplementary Table 2 (http://onlinelibrary.wiley.com/doi/10.1002/art.41082/abstract).

KOOS pain. The unadjusted data on KOOS pain over the 60-month follow-up period in the 2 randomized groups are shown in Figure 1. We evaluated piecewise linear mixed models with knots at 3, 6, 12, 24, 36, and 48 months. The best fit based on BIC (18) was the model with knots at 3, 12, and 24 months (Figure 2), defining 4 distinct pain slopes: baseline to 3 months, 3–12 months, 12–24 months, and 24–60 months.

The slope for the first 3 months for those randomized to undergo arthroscopic partial meniscectomy was −7.4 points/month, while the slope for those randomized to receive physical therapy was −5.90 points/month. The slope for the 3–12-month period was −0.41 in the arthroscopic partial meniscectomy group and −0.96 in the physical therapy group. For the 12–24-month period, the slopes were −0.29 and −0.18 in the arthroscopic partial meniscectomy and physical therapy groups, respectively, while the slopes for the 24–60-month period were 0.038 and 0.027 in the arthroscopic partial meniscectomy and physical therapy groups, respectively. The interaction effect between randomization group and time on the degree of KOOS pain was statistically significant, due largely to less robust improvement in the physical therapy group in months 0–3. The effect of randomized group on pain did not change significantly after adjustment for age, BMI, sex, K/L grade, musculoskeletal index, and mental health index.
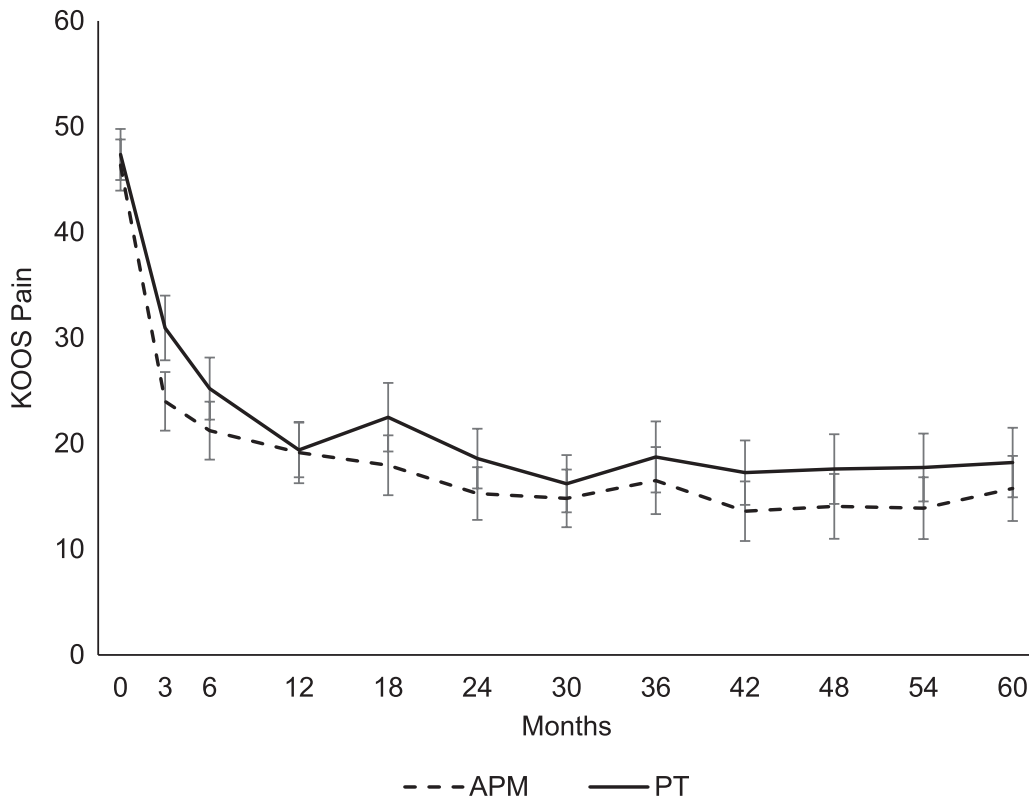
Figure 1. Crude KOOS Pain Scores in the two randomized groups over time.
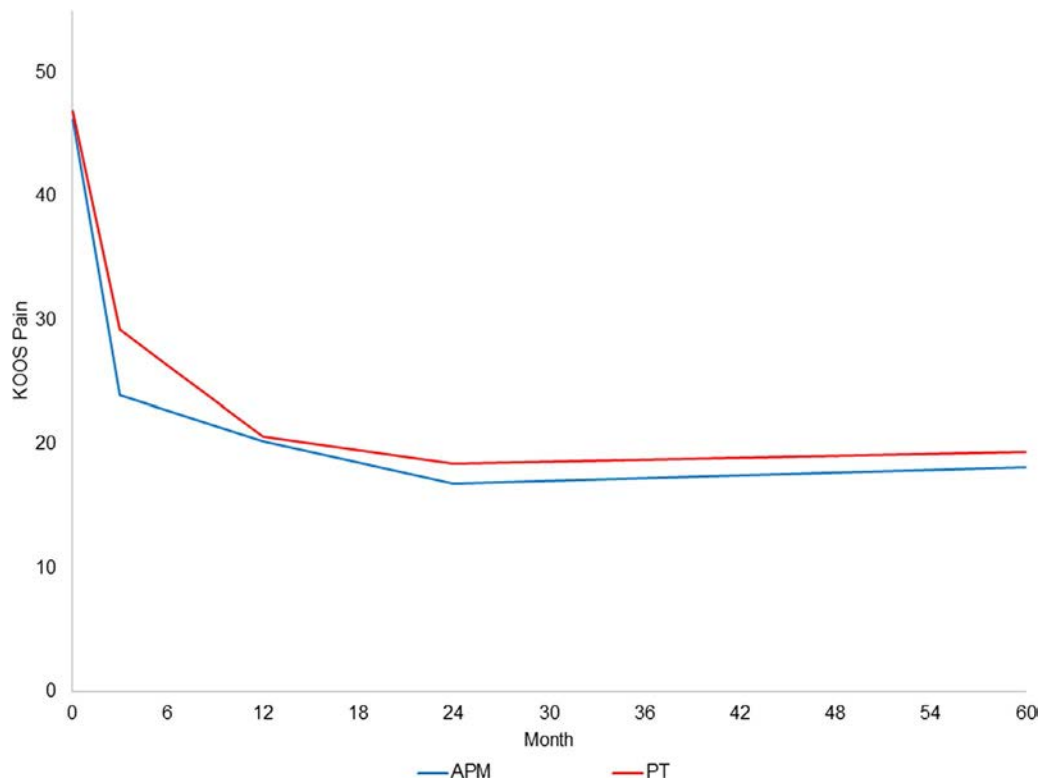
Figure 2. Piecewise linear mixed model of KOOS pain scores in subjects randomized to undergo arthroscopic partial meniscectomy or physical therapy. Slopes are estimated in 4 time periods: 0–3 months, 3–12 months, 12–24 months, and 24–60 months. See Figure 1 for definitions.

The crude, unadjusted data on KOOS pain in the as-treated group is shown in Supplementary Figure 1, http://onlinelibrary.wiley.com/doi/10.1002/art.41082/abstract, and the piecewise linear model with knots at 3, 12, and 24 months in the as-treated groups is shown in Supplementary Figure 2 (http://onlinelibrary.wiley.com/doi/10.1002/art.41082/abstract). These as-treated analyses highlight the less rapid improvement in pain from baseline to 3 months in the group that crossed over from physical therapy to arthroscopic partial meniscectomy. By 12 months, pain scores in all 3 of the as-treated groups were similar.

The pattern mixture models separately modeled each dropout pattern and indicated that participants ultimately undergoing TKR started with the highest KOOS pain scores and experienced the slowest improvement in pain over the first 3 months postrandomization. The TKR group improved from 50 to 41 points, on average; the noncompleters improved from 48 to 28, on average; and the study completers improved from 46 to 22, on average (Figure 3). The overall combined estimate using the pattern mixture model approach was similar to the combined estimate obtained using the piecewise linear mixed model (Figure 3). The similarity in these estimates reflects that only 7% of the subjects underwent TKR.

In the sensitivity analysis, we imputed KOOS pain scores for subjects who dropped out, and then increased the KOOS pain scores by 33% in one model and by 50% in a second model,

for those who dropped out due to TKR (see Supplementary Figures 3 and 4, http://onlinelibrary.wiley.com/doi/10.1002/art.41082/abstract). The effect of treatment group on the KOOS pain score over time in these models changed little compared with the original piecewise mixed model that used data without imputation (Figure 2).

WOMAC function. Results of analyses of WOMAC function scores were largely similar to those of KOOS pain scores, with substantial improvements in the first year in both randomized groups. Improvements achieved in the first year were largely maintained in the 2 randomized groups over the 5-year follow-up (Supplementary Figure 5, http://onlinelibrary.wiley.com/doi/10.1002/art.41082/abstract).

Total knee replacement. Twenty-five participants (7.1% [95% CI 4.4–9.8]) underwent TKR of the index knee over the course of follow-up. From an ITT perspective, 9.2% (95% CI 4.9–13.5) of those randomized to the arthroscopic partial meniscectomy group underwent TKR, as compared with 5.1% (95% CI 1.9–8.3) of those randomized to the physical therapy group (Figure 4A). The ITT Cox regression model included K/L grade and randomized group. TKR occurred more often in those randomized to undergo arthroscopic partial meniscectomy than in those randomized to undergo physical therapy (HR 2.0 [95% CI
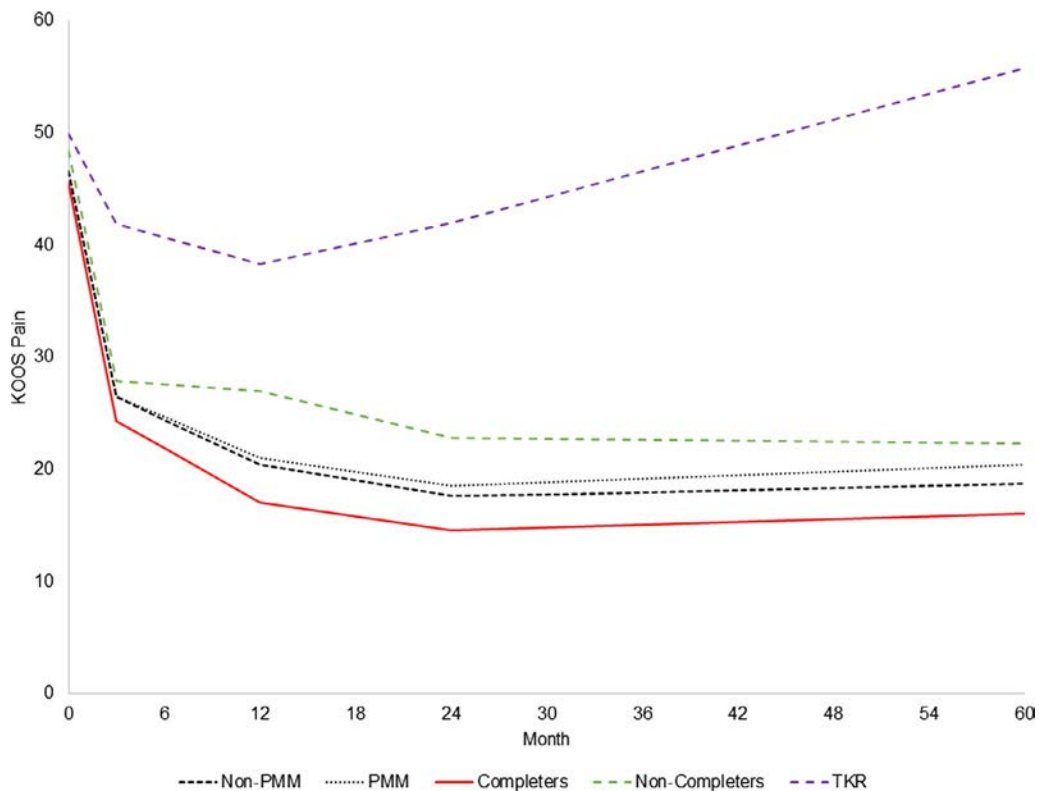
Figure 3. Estimated Knee Injury and Osteoarthritis Outcome Score (KOOS) pain scores in 3 groups: those who had total knee replacement (TKR), those who dropped out of the study for reasons other than TKR (noncompleters), and those who completed the study (completers). The pattern mixture model (PMM) shows the weighted average of the TKR, noncompleter, and completer groups. The non-PMM trace shows the results of the piecewise linear mixed model. The PMM and non-PMM traces are very similar (since only 7% of subjects had TKR). Slopes for the TKR and noncompleter groups were generated from data obtained before subjects in these groups left the cohort.

0.84–4.9]). The model also showed that subjects with K/L grade 3 radiographs had greater risk of TKR than those with K/L grade 0–2 radiographs (HR 3.0 [95% CI 1.3–6.9]). As the 95% CIs suggest, the TKR risk in this ITT model did not reach statistical significance ($P = 0.11$).

From an as-treated perspective, TKRs were performed in 1.8% of subjects treated with physical therapy alone (95% CI 0–4.4), 9.8% of those treated with arthroscopic partial meniscectomy alone (95% CI 5.2–14.3), and 10.3% of those who crossed over from physical therapy to arthroscopic partial meniscectomy (95% CI 3.1–17.5) (Figure 4B). In the as-treated analysis, with adjustment for K/L grade, the HR of TKR was greater in those who underwent arthroscopic partial meniscectomy (either immediate or crossover) than in those treated with only physical therapy (HR 4.9 [95% CI 1.1–20.9]).

DISCUSSION

We found that participants in the METEOR trial experienced considerable pain relief in the first year, which was maintained over 5 years. These generally favorable results were observed in subjects randomized to the arthroscopic partial meniscectomy group and those randomized to the nonoperative therapy group. TKR

rates were generally low (7.1% in the whole cohort), and greater among those who were randomized to undergo arthroscopic partial meniscectomy. As-treated analyses also documented favorable 5-year outcomes regardless of treatment received, with greater TKR risk in those treated with arthroscopic partial meniscectomy.

Our findings are consistent with those of Herrlin et al, who conducted a smaller single-center trial of arthroscopic partial meniscectomy with physical therapy versus physical therapy alone (3). Those authors followed up the subjects for up to 5 years and observed considerable improvement in pain and function in both the arthroscopic partial meniscectomy and physical therapy groups, with improvement sustained over 5 years. Herrlin and colleagues observed, as we did, that those randomized to undergo physical therapy who crossed over to arthroscopic partial meniscectomy had 5-year outcomes similar to those randomized to undergo arthroscopic partial meniscectomy. These findings are also consistent with cohort data that show favorable long-term pain outcomes of arthroscopic partial meniscectomy (20,21). There are relatively few studies of outcomes of nonoperative therapy beyond 1–2 years.

The less robust reduction in pain over the first 3 months in the physical therapy group in the ITT analysis reflects that some subjects randomized to undergo physical therapy crossed over to arthroscopic partial meniscectomy due to the persistence of pain
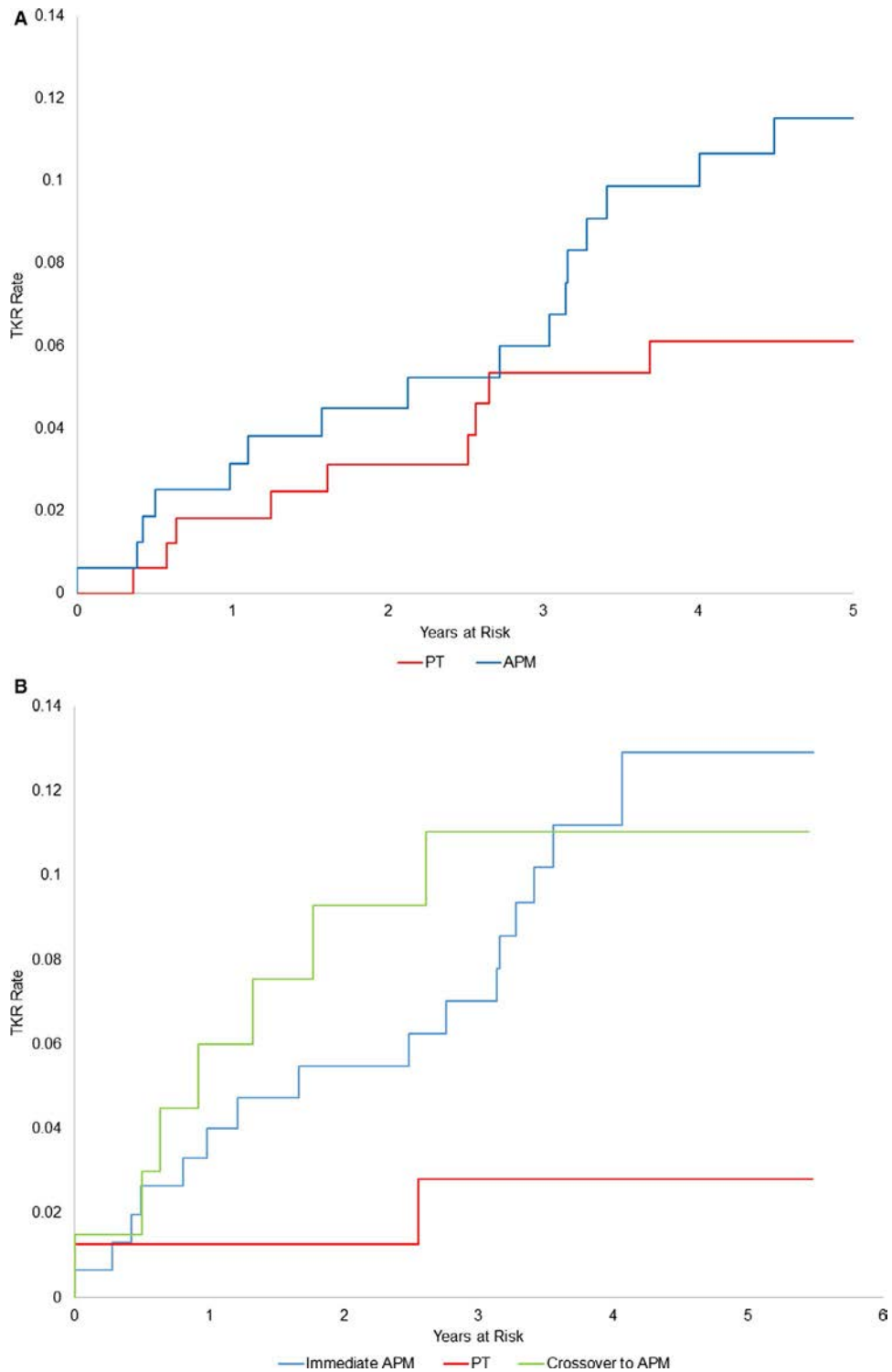
Figure 4. Kaplan-Meier plots of time to total knee replacement (TKR) in 2 intent-to-treat groups and in 3 as-treated groups. **A**, Subjects randomized to undergo arthroscopic partial meniscectomy and those randomized to undergo physical therapy. **B**, Subjects randomized to and receiving arthroscopic partial meniscectomy, those randomized to undergo physical therapy only, and those randomized to undergo physical therapy and crossing over to arthroscopic partial meniscectomy. See Figure 1 for other definitions.

in the first several months. By 12 months, pain levels in subjects who crossed over to arthroscopic partial meniscectomy were similar to pain levels in those who underwent immediate arthroscopic partial meniscectomy.

The greater likelihood of TKR in those who ultimately underwent arthroscopic partial meniscectomy merits comment. The as-treated analysis suggested a 5-fold increased TKR risk among those exposed to arthroscopic partial meniscectomy

over the follow-up period, as compared to those treated non-operatively. The ITT analysis of the 5-year TKR risk in the 2 randomized groups showed a 2-fold increased hazard of TKR among those randomized to undergo arthroscopic partial meniscectomy, though this HR was not statistically significant. Our analyses of TKR use were adjusted for baseline K/L grade, suggesting that the findings are not due to greater radiographic severity prior to arthroscopic partial meniscectomy. The group that crossed over had severe symptoms at baseline and physical therapy was unsuccessful. These factors may underlie the decision to ultimately undergo TKR. Arthroscopic partial meniscectomy may be associated with greater progression of OA, and increased risk of TKR on that basis. Our analyses of 18-month progression in MRI-documented cartilage damage support this hypothesis (22). Finally, subjects who undergo arthroscopic partial meniscectomy become more familiar and comfortable with the process of undergoing surgical therapy and may be more inclined to undergo TKR. These potential explanations require further examination.

We acknowledge several limitations of the present study. Participants enrolled in the METEOR trial may not be representative of the larger population of persons with degenerative meniscal tear, as just 26% of eligible participants agreed to participate in the METEOR trial (1). Of the participants in the trial, 30% crossed over from physical therapy to arthroscopic partial meniscectomy, and dropout was substantial over 5 years, potentially disturbing the matching of baseline characteristics across randomized groups. Because of these postrandomization events, we performed both an ITT analysis and an as-treated analysis to address potential selection bias with adjustment for potential confounders. We recognize that unmeasured variables could create residual confounding. While losses to follow-up occurred at a similar rate across the randomized groups, the rate of dropout due to TKR differed. We used pattern mixture models and multiple imputation to account for potentially informative dropouts due to TKR. Finally, we acknowledge that the pre-TKR pain scores may have been recorded up to 6 months before the TKR and thus may have underestimated actual pain levels at the time of surgery.

In summary, patients in the METEOR cohort experienced, on average, substantial symptom relief in the first year following treatment, which was maintained over 5 years, with a relatively low cumulative incidence of TKR (7.1%). These findings provide reassurance that both strategies—early treatment with arthroscopic partial meniscectomy and physical therapy with the opportunity for delayed arthroscopic partial meniscectomy—are associated with generally favorable outcomes in middle-aged and older persons presenting with knee pain, OA changes, and degenerative meniscal tear. While we did not observe statistically significant differences in TKR use in the ITT analysis, the greater TKR utilization observed in those undergoing arthroscopic partial meniscectomy merits further study.

AUTHOR CONTRIBUTIONS

All authors were involved in drafting the article or revising it critically for important intellectual content, and all authors approved the final version to be published. Dr. Katz had full access to all of the data in the study and takes responsibility for the integrity of the data and the accuracy of the data analysis.
Study conception and design. Katz, Losina, Jones, Marx, Mandl, Levy, MacFarlane, Spindler, Collins.
Acquisition of data. Katz, Jones, Marx, Mandl, Levy, Spindler, Collins.
Analysis and interpretation of data. Katz, Shrestha, Losina, Jones, Marx, Mandl, Levy, MacFarlane, Spindler, Silva, Collins.

REFERENCES

1. Katz JN, Brophy RH, Chaisson CE, de Chaves L, Cole BJ, Dahm DL, et al. Surgery versus physical therapy for a meniscal tear and osteoarthritis. N Engl J Med 2013;368:1675–84.

2. Herrlin S, Hållander M, Wange P, Weidenhielm L, Werner S. Arthroscopic or conservative treatment of degenerative medial meniscal tears: a prospective randomised trial. Knee Surg Sports Traumatol Arthrosc 2007;15:393–401.

3. Herrlin SV, Wange PO, Lapidus G, Hållander M, Werner S, Weidenhielm L. Is arthroscopic surgery beneficial in treating non-traumatic, degenerative medial meniscal tears? A five year follow-up. Knee Surg Sports Traumatol Arthrosc 2013;21:358–64.

4. Kise NJ, Risberg MA, Stensrud S, Ranstam J, Engebretsen L, Roos EM. Exercise therapy versus arthroscopic partial meniscectomy for degenerative meniscal tear in middle aged patients: randomised controlled trial with two year follow-up. BMJ 2016;354:i3740.

5. Yim JH, Seon JK, Song EK, Choi JI, Kim MC, Lee KB, et al. A comparative study of meniscectomy and nonoperative treatment for degenerative horizontal tears of the medial meniscus. Am J Sports Med 2013;41:1565–70.

6. Gauffin H, Sonesson S, Meunier A, Magnusson H, Kvist J. Knee arthroscopic surgery in middle-aged patients with meniscal symptoms: a 3-year follow-up of a prospective, randomized study. Am J Sports Med 2017;45:2077–84.

7. Gauffin H, Tagesson S, Meunier A, Magnusson H, Kvist J. Knee arthroscopic surgery is beneficial to middle-aged patients with meniscal symptoms: a prospective, randomised, single-blinded study. Osteoarthritis Cartilage 2014;22:1808–16.

8. Van de Graaf VA, Noorduyn JC, Willigenburg NW, Butter IK, de Gast A, Mol BW, et al. Effect of early surgery vs physical therapy on knee function among patients with nonobstructive meniscal tears: the ESCAPE randomized clinical trial. JAMA 2018;320:1328–37.

9. Katz JN, Wright J, Spindler KP, Mandl LA, Safran-Norton C, Reinke EK, et al. Predictors and outcomes of crossover to surgery from physical therapy for meniscal tear and osteoarthritis: a randomized trial comparing physical therapy and surgery. J Bone Joint Surg Am 2016;98:1890–6.

10. Spector TD, Cooper C. Radiographic assessment of osteoarthritis in population studies: whither Kellgren and Lawrence? [editorial]. Osteoarthritis Cartilage 1993;1:203–6.

11. Kellgren JH, Lawrence JS. Radiological assessment of osteoarthrosis. Ann Rheum Dis 1957;16:494–502.

12. Katz JN, Chaisson CE, Cole B, Guermazi A, Hunter DJ, Jones M, et al. The MeTeOR trial (Meniscal Tear in Osteoarthritis Research): rationale and design features. Contemp Clin Trials 2012;33:1189–96.

13. Roos EM, Roos HP, Ekdahl C, Lohmander LS. Knee injury and Osteoarthritis Outcome Score (KOOS): validation of a Swedish version. Scandinavian J Med Sci Sports 1998;8:439–48.

14. Roos EM, Roos HP, Lohmander LS, Ekdahl C, Beynnon BD. Knee injury and Osteoarthritis Outcome Score (KOOS): development of a self-administered outcome measure. J Orthop Sports Phys Ther 1998;28:88–96.

15. Bellamy N, Buchanan WW, Goldsmith CH, Campbell J, Stitt LW. Validation study of WOMAC: a health status instrument for measuring clinically important patient relevant outcomes to antirheumatic drug therapy in patients with osteoarthritis of the hip or knee. J Rheumatol 1988;15:1833–40.

16. Katz JN, Wright EA, Baron JA, Losina E. Development and validation of an index of musculoskeletal functional limitations. BMC Musculoskelet Disord 2009;10:62.

17. Berwick DM, Murphy JM, Goldman PA, Ware JE Jr, Barsky AJ, Weinstein MC. Performance of a five-item mental health screening test. Med Care 1991;29:169–76.

18. Fitzmaurice GM, Laird NM, Ware JH. Applied longitudinal analysis. 2nd ed. Hoboken, NJ: Wiley; 2011.

19. Little RJ. A class of pattern-mixture models for normal incomplete data. Biometrika 1994;81:471–83.

20. Higuchi H, Kimura M, Shirakura K, Terauchi M, Takagishi K. Factors affecting long-term results after arthroscopic partial meniscectomy. Clin Orthop Relat Res 2000;161–8.

21. Schimmer RC, Brülhart KB, Duff C, Glinz W. Arthroscopic partial meniscectomy: a 12-year follow-up and two-step evaluation of the long-term course. Arthroscopy 1998;14:136–42.

22. Collins JE, Losina E, Marx RG, Guermazi A, Jarraya M, Jones MH, et al. Early MRI-based changes in patients with meniscal tear and osteoarthritis. Arthritis Care Res (Hoboken) doi: http://online library.wiley.com/doi/10.1002/acr.23891/abstract. E-pub ahead of print.

APPENDIX A: THE METEOR INVESTIGATORS

METEOR investigators, in addition to the authors, are as follows: Drs. Robert Brophy, Brian J. Cole, Michael J. Stuart, Matthew J. Matava, Rick W. Wright, and Clare E. Safran-Norton.

AMERICAN COLLEGE
of RHEUMATOLOGY
Empowering Rheumatology Professionals

Population-Specific Patterns of Epigenetic Defects in the B Cell Lineage in Patients With Systemic Lupus Erythematosus

Megan E. Breitbach,[1] [iD] Ryne C. Ramaker,[2] [iD] Kevin Roberts,[3] Robert P. Kimberly,[4] and Devin Absher[3] [iD]

Objective. To determine the stage of B cell development at which a systemic lupus erythematosus (SLE)–associated DNA methylation signature originates in African American (AA) and European American (EA) subjects, and to assess whether epigenetic defects in B cell development patterns could be predictive of SLE status in individual and mixed immune cell populations.

Methods. B cells from AA patients (n = 31) and EA patients (n = 49) with or without SLE were sorted using fluorescence-activated cell sorting into 5 B cell subsets. DNA methylation, measured at ~460,000 CpG sites, was interrogated in each subset. Enrichment analysis of transcription factor interaction at SLE-associated methylation sites was performed. A random forests algorithm was used to identify an epigenetic signature of SLE in the B cell subsets, which was then validated in an independent cohort of AA and EA patients and healthy controls.

Results. Regression analysis across all B cell stages resulted in identification of 60 CpGs that reached genome-wide significance for SLE-associated methylation differences ($P \leq 1.07 \times 10^{-7}$). Interrogation of ethnicity-specific CpGs associated with SLE revealed a hypomethylated pattern that was enriched for interferon (IFN)–regulated genes and binding of EBF1 in AA patients (each $P < 0.001$). AA patients with SLE could be distinguished from healthy controls when the predictive model developed with the transitional B cell subset was applied to other B cell subsets (mean receiver operating characteristic [ROC] area under the curve [AUC] 0.98), and when applied to CD19+ pan–B cells (mean ROC AUC 0.95) and CD4+ pan–T cells (mean ROC AUC 0.97) from the independent validation cohort.

Conclusion. These results indicate that SLE-specific methylation patterns are ethnicity dependent. A pattern of epigenetic changes near IFN-regulated genes early in B cell development is a hallmark of SLE in AA female subjects. EBF1 binding sites are highly enriched for significant methylation changes, implying that this may be a potential regulator of SLE-associated epigenetic changes.

INTRODUCTION

Systemic lupus erythematosus (SLE) is a complex autoimmune disease that is characterized by a dysregulated immune system leading to chronic inflammation, and the underlying mechanisms of pathogenesis and effective treatments remain elusive (1,2). African American (AA) women are the population most at risk for developing SLE, and they also have the most severe SLE-associated symptoms, often including acute and irreversible organ damage (3–8). The majority of SLE genomic studies to date have focused on European and Asian ethnicities but have left out this most at-risk population (9). We therefore focused on AA female subjects in this study.

A commonly cited hypothesis regarding the origin of SLE is that an environmental trigger, such as an infection or drug exposure, elicits T lymphocytes (T cells) to recognize self antigens and induce B lymphocytes (B cells) to produce autoantibodies (10). B cells play an essential role in adaptive immunity through their ability to produce and present antigens, proinflammatory cytokines, and costimulatory factors to T cells. Dysregulation of B cell function, signaling, or development can lead to excessive autoantibody production and B cell hyperactivity (11).

Epigenetic dysregulation of B cell differentiation may be an important mechanism underlying the pathogenesis of SLE, as we know the epigenome plays a significant role in the etiology of several autoimmune diseases, but the exact nature of the relationship has not been established (12–14). Studies of associations between DNA methylation and SLE reveal widespread hypomethylation of CpGs within interferon (IFN)–related genes in SLE patients relative to controls in European and Asian populations (12,15–18). Yet, population-specific risk loci have recently been identified, and therefore different ethnic populations must be studied independently to fully understand the genetic mechanisms of SLE (19,20).

Our study was designed to analyze whole-genome DNA methylation data from B cell subsets in a cohort of female patients with or without SLE to ascertain the stage of B cell development at which aberrant epigenetic patterns arise and to identify a multivariate epigenetic signature of SLE. To accomplish these tasks, we sorted B cell subsets from AA female patients with SLE (n = 24) and those without SLE (n = 25), as well as B cell subsets from European American (EA) female patients with SLE (n = 18) and those without SLE (n = 13). The B cell subsets analyzed included transitional, naive, unswitched, switched, and IgD–/CD27– double-negative B cells. We used regression analysis to test for associations between single CpGs within each B cell subset and SLE. Regression analysis was also used to identify ethnicity-specific SLE-associated CpGs across B cell types. The single CpGs showing the strongest association were used in machine-learning approaches to build a multivariate model of SLE. The models were tested across ethnicity groups in an independent validation cohort of AA and EA subjects, in which both CD19+ pan–B cells and CD4+ pan–T cells were tested to determine whether this signature could be predictive of SLE status in broader cell populations.

Our results demonstrate that epigenetic defects in female AA patients with SLE are already present in immature B cells emerging from bone marrow (transitional B cells), whereas epigenetic defects in EA female patients with SLE appear to develop later during B cell development. We observed that AA-specific CpG sites associated with SLE are enriched for IFN-regulated genes and are located near EBF1 regulatory sites, and that AA-specific SLE-associated CpGs are predictive of SLE status in mixed immune cell populations from AA female subjects.

PATIENTS AND METHODS

Discovery set participants. The discovery cohort was obtained through recruitment to the rheumatology outpatient clinic at the University of Alabama at Birmingham (UAB). Patients' blood samples were collected following provision of informed consent and in compliance with the UAB Institutional Review Board. A total of 80 blood samples were used,

among which 49 samples were from patients of self-reported AA ancestry and 31 were from patients of self-reported EA ancestry (see Supplementary Table 1, available on the *Arthritis & Rheumatology* web site at http://onlinelibrary.wiley.com/doi/10.1002/art.41083/abstract). Age, sex, self-reported ethnicity, and smoking status were recorded for each subject regardless of SLE status. Additional clinical data were obtained from SLE patients, including the following: the SLE Disease Activity Index (SLEDAI) score (determined using the American College of Rheumatology guidelines [21]), flare status, body mass index, presence and stage of nephritis, creatinine level, proteinuria, glucose level, and prednisone usage and dose (Supplementary Table 1).

Validation set. For validation, methylation data in sorted CD19+ pan–B cells and CD4+ pan–T cells were obtained from an independent cohort of AA and EA subjects in the outpatient rheumatology clinic at UAB; this cohort has been previously described in detail in a study by Absher et al (12) (characteristics of both cohorts are listed in Supplementary Table 1 [http://onlinelibrary.wiley.com/doi/10.1002/art.41083/abstract]). The independent validation cohort consisted of 45 AA female subjects (23 with SLE, 22 healthy controls) and 24 EA female subjects (11 with SLE, 13 healthy controls). CD4+ pan–T cells were sorted from all 45 samples from the AA subjects and all 23 samples from the EA subjects. CD19+ pan–B cells were sorted from 43 samples from the AA subjects and all 24 samples from the EA subjects.

Cell and DNA isolation. Individual B cell subsets from the discovery cohort were sorted using flow cytometry. Antibodies particular to lineage-specific cell surface receptors were used to separate 5 individual B cell subsets. The number of samples in the discovery set extracted for a specific cell type ranged from 42 samples (for IgD–/CD27– double-negative B cells) to 72 samples (for naive B cells) (see Supplementary Figure 1, available on the *Arthritis & Rheumatology* web site at http://onlinelibrary.wiley.com/doi/10.1002/art.41083/abstract). Cells were then lysed and DNA was extracted using Qiagen DNeasy kits according to the manufacturer's protocol.

Methylation450 assays, quality control, and batch normalization. The Infinium HumanMethylation450 array (Illumina) was used for measurement of DNA methylation levels. In total, 500 ng of each sample was bisulfite converted (Zymo EZ DNA), amplified, hybridized, and imaged. Raw data intensity files were processed using GenomeStudio. CpG probes with detection P values of >0.01 and those affected by common variants were filtered out. ComBat was used to correct for batch effects, in which a single array (12 samples) was used to describe a batch. Infinium chemistry corrections were performed to correct for differences between probe types. Genome-wide data methylation

analysis was then performed using the R statistical suite (version 3.5.1).

Regression analysis. Multivariate linear regression was performed to identify CpG methylation changes associated with SLE status, both independent of and dependent on self-reported ethnicity. A simpler model was performed first for the interrogation of single CpGs associated with SLE status, incorporating age and smoking status as covariates (Equation 1), calculated as follows:

$$\beta \sim \text{Age} + \text{Smoking} + \text{Ethnicity} + \text{SLE}$$

A second, more complex model was then performed for the discovery of CpGs associated with the interaction of SLE status and ethnicity, including age, sex, self-reported ethnicity, and smoking status as covariates (Equation 2), calculated as follows:

$$\beta \sim \text{Age} + \text{Smoking} + \text{Ethnicity} + \text{SLE} + \text{Ethnicity} \times \text{SLE}$$

Both models were performed on samples from AA and EA female subjects across all 5 B cell lineages, resulting in a total of 10 regression models in this stage of analysis.

Predictive modeling. Random forests (RFs) regression was performed on the transitional B cell samples from AA female subjects (n = 38), since that was the first B cell stage for which aberrant methylation associated with SLE status was detected. We tested various P value cutoffs for association with SLE ($P = 5 \times 10^{-2}$ to 5×10^{-6}) resulting from multivariate linear regression, as well as various variance cutoffs (ranging from 0.02 to 0.1), with m-try parameters ranging from 1 to 20 and 1,000 trees. RF regression analyses were carried out using the RandomForest package in R (22). For each iteration, a random sample comprising 25 samples was used for the training set, and the remaining samples were used as the test set. Using the same approach, multivariate linear regression using L1 penalized log partial likelihood (LASSO) was performed via the glmnet package in R (23). Three-fold cross-validation using an alpha parameter of 1 was performed to find the optimal lambda value. The lambda value plus 1SD, and an alpha of 1, was then used to build the model. Ridge regression using samples from AA female subjects was performed in a manner similar to LASSO, with the only difference being that the alpha parameter was 0 instead of 1.

An optimal prediction cutoff value for separation of SLE from controls was determined for the model based on the training set, and this optimal value was used to calculate the misclassification percentage in the test set. Model prediction accuracy was assessed in individual B cell lineages from EA and AA patients in the discovery set, as well as in CD19+ pan–B cells and CD4+ pan–T cells from the independent data set of EA and AA subjects. The mean receiver operating characteristic (ROC) area under the curve (AUC) was used to assess the model's sensitivity and specificity in each of the test sets described, in addition to the misclassification percentage as

defined based on the optimal prediction cutoff from the training set. Top-performing classifiers from each RF model were determined based on their Gini coefficient, a function unique to the RF algorithm that assigns the coefficient based on ability to accurately separate cases from controls during the model training phase, so that the higher the coefficient, the better the CpG is at separating SLE cases from controls in the model.

RF, LASSO, and Ridge regression analyses were also performed on sorted B cell samples from all EA subjects combined, using one-third of the samples (n = 24) for the training set and the rest as a test set. The same P value cutoffs and m-try values tested in the modeling using AA samples were applied in the modeling using EA samples. Modeling was performed using the switched B cell stage, since that was the B cell stage for which substantial differences in methylation associated with SLE status was detected in EA samples. The top-performing model was then determined using the same approach as was used for analysis of AA samples.

Transcription factor enrichment. GM12878 chromatin immunoprecipitation sequencing (ChIP-seq) from the ENCODE data portal was used for genome-wide interrogation of transcription factor binding sites (TFBS) (24). Using BEDtools, intersection between the Methyl450 annotation file and the ChIP-seq bed file was performed (25). Permutation testing was then carried out to allow for the determination of whether specific transcription factors showing binding within 500 bp of the top CpGs were enriched compared to all other sites assayed. Orthogonal analysis was conducted on the top TFBS enriched using ChIP-seq data. Position frequency matrices for the most enriched transcription factors were obtained from JASPAR, and the FIMO package within the MEME suite was used for analysis of motifs within 500 bp of the CpGs of interest (26–28). Permutation testing allowed us to determine whether top CpGs were enriched for a specific binding motif compared to the other sites assayed.

RESULTS

Altered CpG methylation in immature B cells from SLE patients. To identify loci at which DNA methylation levels were associated with SLE, we performed epigenome-wide regression analysis in sorted B cells for which we found statistically significant methylation differences in SLE patients compared to controls (see Supplementary Figures 2A–E and Supplementary Table 2, available on the *Arthritis & Rheumatology* web site at http://onlinelibrary.wiley.com/doi/10.1002/art.41083/abstract). Across all 5 B cell subsets, we found 60 CpGs that reached genome-wide significance for methylation differences in SLE patients compared to controls ($P \leq 1.07 \times 10^{-7}$), among which 13 occurred in transitional B cells, which was the earliest B cell stage assayed, indicating that epigenetic defects in SLE patients are already present as immature B cells emerge from the bone marrow.

The most significant CpGs were found in multiple genes, particularly near IFN-regulated genes (Figure 1). The top SLE-associated CpGs from regression analyses of transitional B cells displayed a distinct hypomethylation pattern within AA patients with SLE compared to controls, which was less apparent in EA patients with SLE and controls (Figure 2).

The epigenetic defects observed indicated that those individuals carrying severe epigenetic defects tended to carry severe defects across all of the significant CpGs, and that those with mild defects tended to carry mild defects across all loci, suggesting that the epigenetic pattern behaves as a correlated module, rather than a set of independent, heterogeneous effects at each CpG.

Further interrogation revealed that methylation specifically within the top 15 CpGs (based on transitional B cell regression analyses) was highly correlated in AA patients with SLE and in AA controls, but there was a clear negative correlation between the 2 groups, indicating that the strong differences in methylation at these sites were correlated with the presence of SLE in AA subjects, a trend that was not seen in EA subjects (see Supplementary Figures 3 and 4, available on the *Arthritis & Rheumatology* web site at http://onlinelibrary.wiley.com/doi/10.1002/art.41083/abstract).

To further examine the population-specific nature of these epigenetic defects, we ran additional regression models using an interaction term between SLE and ethnicity. The results revealed numerous sites across all 5 B cell subsets that approached and/or reached genome-wide significance for methylation differences in SLE patients compared to controls (see Supplementary Figures 5A–E, available on the *Arthritis & Rheumatology* web site at http://onlinelibrary.wiley.com/doi/10.1002/art.41083/

abstract). Most of those top CpGs resulted from regression analyses of early (transitional and naive) B cells and were near IFN-regulated genes. The highest AA-dependent SLE association (at cg17980508; $P = 1.12 \times 10^{-9}$) originated from transitional B cells and was located near the IFI44L gene (see Supplementary Table 3, available on the *Arthritis & Rheumatology* web site at http://onlinelibrary.wiley.com/doi/10.1002/art.41083/abstract). The highest EA-dependent SLE association (at cg13710613; $P = 8.13 \times 10^{-8}$) originated from naive B cells and was located near the EHMT1 gene (see Supplementary Table 4, available on the *Arthritis & Rheumatology* web site at http://onlinelibrary.wiley.com/doi/10.1002/art.41083/abstract).

Analysis of methylation at top individual AA- and EA-specific sites (cg17980508, cg21549285, and cg13710613) across B cell development in both AA and EA patients and controls revealed that methylation differences strongly distinguished AA patients with SLE, but not EA patients with SLE, from controls (see Supplementary Figures 6, 7, and 8, available on the *Arthritis & Rheumatology* web site at http://onlinelibrary.wiley.com/doi/10.1002/art.41083/abstract). We observed that the difference in the percentage of methylation between AA patients and controls was broader earlier during B cell development and decreased in later B cell stages, further suggesting that aberrant hypomethylation occurs at the earliest stages of B cell development in SLE patients of AA ancestry.

Evidence of DNA methylation patterns in transitional B cells as a predictor of SLE status in AA female subjects. The modular nature of the epigenetic defects observed in immature B cells from SLE patients suggested that a multivariate predictive model could be used to distinguish
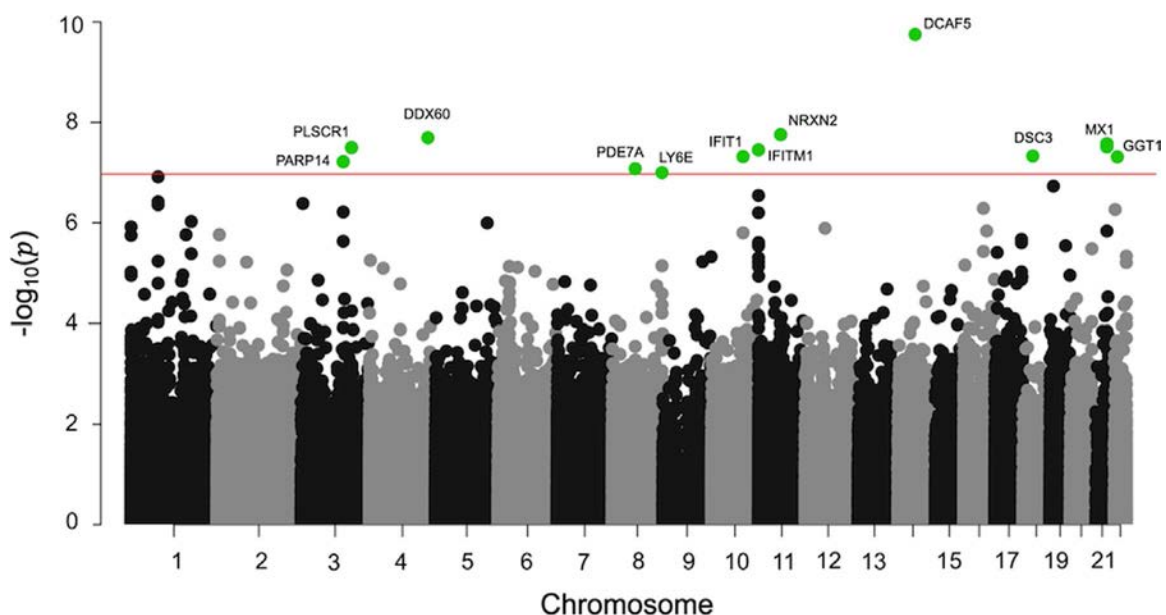
Figure 1. Manhattan plots of regression P values ($-\log_{10}$) are shown for the association of multiple CpGs across the genome with systemic lupus erythematosus in transitional B cells. Significant CpGs (green symbols) are indicated according to a P value cutoff for genome-wide significance of $P = 1.07 \times 10^{-7}$ (horizontal red line).
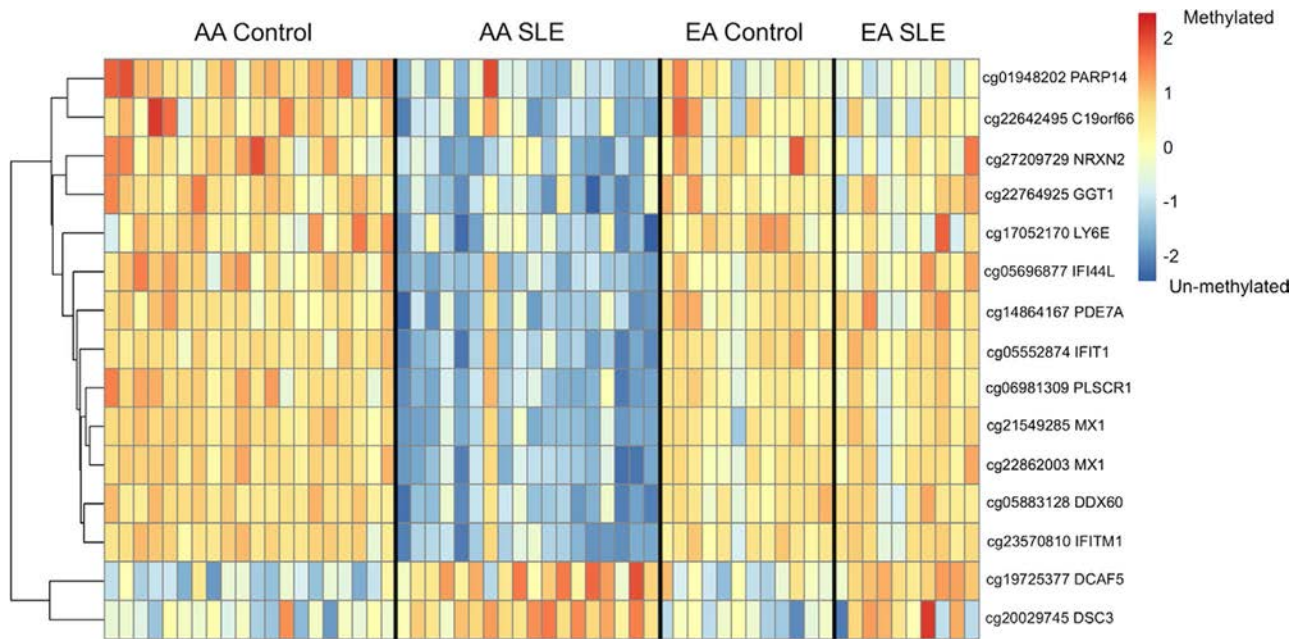
Figure 2. Heatmaps of the methylation status are shown for the top 15 CpGs associated with systemic lupus erythematosus (SLE) (based on *P* value) in transitional B cells. Each column represents an individual subject, grouped by ethnicity (African American [AA] or European American [EA]) and disease status (SLE or control). Each row shows a top SLE-associated CpG (interferon-regulated gene), with color scale based on methylation status. Hierarchical clustering of CpGs resulted in groupings that were representative of the methylation change in SLE patients compared to controls.

patients from controls, and that a machine-learning optimization approach would identify the most informative genes that carry these aberrant epigenetic states. We tested multiple machine-learning approaches using methylation levels in transitional B cells, the B cell developmental stage for which the largest difference in methylation between patients and controls was observed, to predict SLE in AA subjects. The mean ROC AUCs across the discovery and validation cohorts for AA female

subjects was highest for the top-performing ridge regression model (cutoff $P = 1 \times 10^{-4}$, mean ROC AUC 0.97), and yet the mean standard error (MSE) was lowest in the RF regression model (MSE 0.02) (see Supplementary Table 5, available on the *Arthritis & Rheumatology* web site at http://onlinelibrary.wiley.com/doi/10.1002/art.41083/abstract).

When performance of the RF regression model for SLE prediction was tested across individual B cell subsets, the
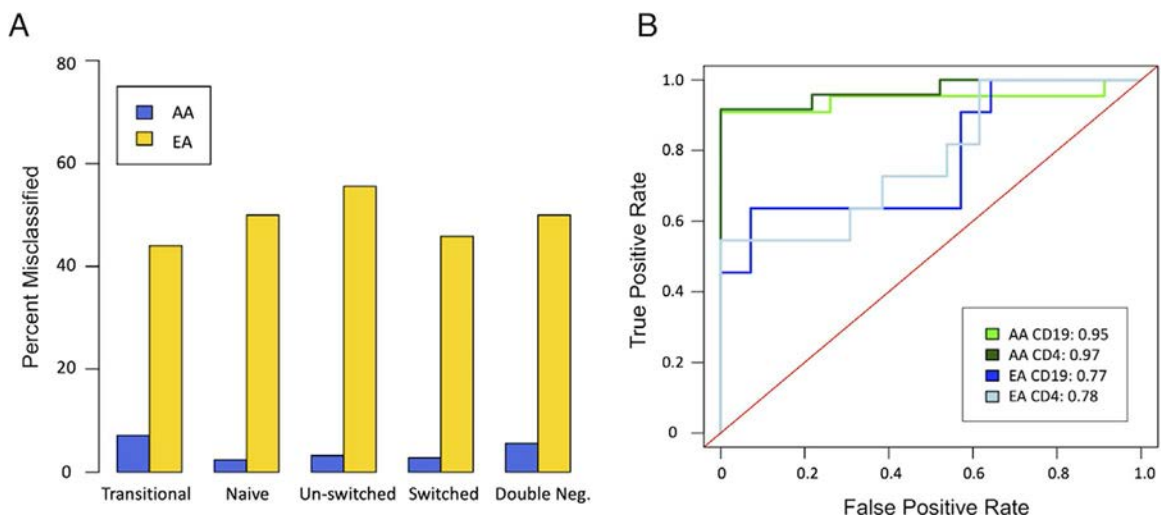
Figure 3. Machine learning in transitional B cells identifies an epigenetic signature that can predict SLE in AA subjects. Performance of the random forests regression model for prediction of SLE using transitional B cells was assessed in AA and EA female subjects according to misclassification percentages across B cell stages (**A**) and according to validation receiver operating characteristic curves for CD19+ pan–B cells and CD4+ pan–T cells (**B**). Neg. = negative (see Figure 2 for other definitions).

model performed well in B cells from AA subjects at both the early stages and later stages of B cell development (mean ROC AUC 0.98, misclassification errors in 2% of naive B cells, 3% of unswitched B cells, 3% of switched B cells, and 6% of double-negative B cells). Applying the same model to EA B cell stages produced poor predictive success, indicating that the AA SLE signature is distinct from that in EA (Figure 3A). For validation, we tested each model's ability to distinguish SLE patients from controls using previously published data on broader cell populations, comprising CD4+ pan–T cells and CD19+ pan–B cells. The top AA-specific RF regression model accurately predicted SLE status in AA subjects, with mean ROC AUCs of 0.967 and 0.945 for CD4+ pan–T cells and CD19+ pan–B cells, respectively (Figure 3B).

Unlike pure regression analysis, for which top results are often within correlated regions of the genome, RF regression results present unique and highly predictive sites across the genome. Most of our top predictors (based on Gini coefficients of importance) were associated with various genes scattered throughout the genome (see Supplementary Table 6, available on the *Arthritis & Rheumatology* web site at http://onlinelibrary.wiley.com/doi/10.1002/art.41083/abstract). The top predictor, cg07839457, was near the transcription start site of NLRC5. Methylation analysis at cg07839457 across the stages of B cell development revealed perpetuation of the hypomethylated state in AA patients with SLE compared to controls, but not in EA patients with SLE compared to controls (see Supplementary Figure 9, available on the *Arthritis & Rheumatology* web site at http://onlinelibrary.wiley.com/doi/10.1002/art.41083/abstract). Further interrogation of the methylation status at other highly predictive sites in transitional B cells revealed consistent hypomethylation in SLE cases for almost every CpG regardless of the SLEDAI score.

In EA subjects, the optimal data reduction method for predictive modeling utilized a cutoff P value of 1×10^{-4} for CpGs associated with SLE status, which was dependent on EA ethnicity in the switched B cell subset. This model modestly distinguished EA patients with SLE from controls, with <45% misclassification error across all B cell subsets, and proved to have poor performance in AA B cells, resulting in misclassification percentages ranging from 42% to 68% across the 5 B cell stages assayed (Figure 4A).

With regard to its performance in the validation cohort, the top EA-specific model had mean ROC AUCs of 0.571 and 0.755 for CD19+ pan–B cells and CD4+ pan–T cells, respectively (Figure 4B). For mixed immune cells from AA subjects in the validation cohort, the model performance was much lower, showing mean ROC AUCs of 0.539 and 0.537 for CD19+ pan–B cells and CD4+ pan–T cells, respectively. Predictors in the top EA-specific RF regression model had Gini coefficients ranging from 0.299 to 0.009 (see Supplementary Table 7, available on the *Arthritis & Rheumatology* web site at http://onlinelibrary.wiley.com/doi/10.1002/art.41083/abstract). There was a lack of methylation differences between SLE patient samples and controls in the EA population (see Supplementary Figure 10, available on the *Arthritis & Rheumatology* web site at http://onlinelibrary.wiley.com/doi/10.1002/art.41083/abstract), in contrast to predictors in the AA population, for which severe differences in methylation were observed.

Enrichment for EBF1 binding in SLE-associated CpGs near IFN-regulated genes. To determine whether the CpGs significantly associated with SLE based on methylation status resided in regulatory regions of the genome, we performed an enrichment test of TFBS status near the top 100 CpGs showing an association with SLE (based on P value), revealing enrichment
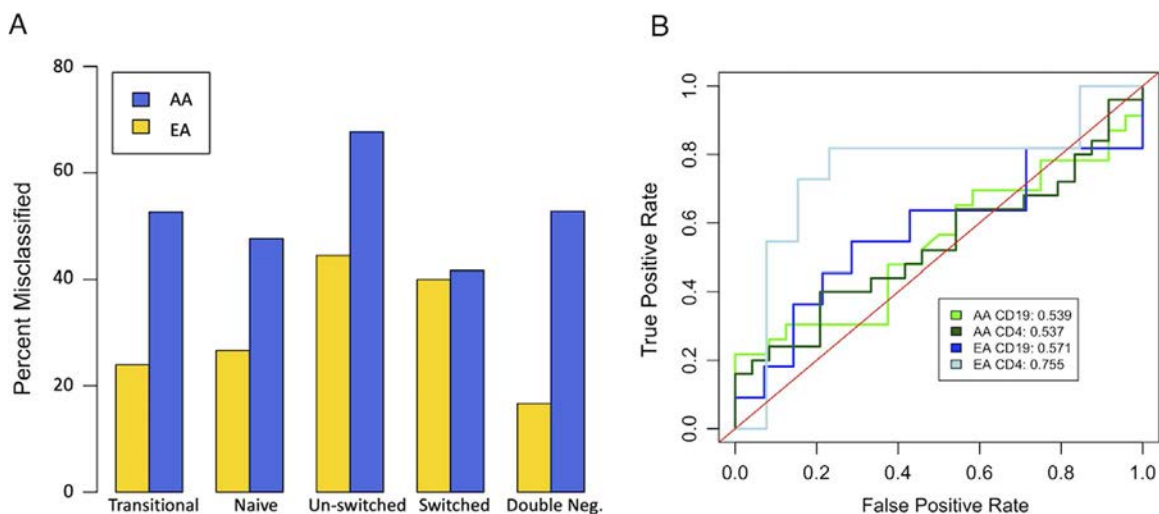
Figure 4. Machine learning in switched B cells modestly predicts SLE in EA subjects. Performance of the random forests regression model for prediction of SLE using switched B cells was assessed in AA and EA female subjects according to misclassification percentages across B cell stages (**A**) and according to validation receiver operating characteristic curves for CD19+ pan–B cells and CD4+ pan–T cells (**B**). Neg. = negative (see Figure 2 for other definitions).

for POLR2A, EBF1, CHD1, WRNIP1, MTA3, STAT3, and IZKF1. A similar analysis of the ethnicity-specific SLE-associated sites identified enrichment of CpGs in binding sites for POLR2A ($P < 5 \times 10^{-4}$), EBF1 ($P < 8 \times 10^{-4}$), POU2F2 ($P < 3.27 \times 10^{-1}$), and RELA ($P < 4.46 \times 10^{-1}$) (Figure 5).

Among the most enriched transcription factors, EBF1 is of particular interest, as it is a pioneer transcription factor essential for B cell development (29). Further interrogation of EBF1 binding using a bioinformatics-based approach to identify EBF1 motifs (5′-TCCCNNGGGA-3′) within the DNA sequence surrounding those top SLE-associated CpGs strengthened this hypothesis, as hypermethylated sites significantly associated with SLE in transitional B cells were enriched for EBF1 motifs. Among the top 100 SLE-associated population-specific CpGs (based on P value), 36 were near (±250 bp) an EBF1 binding motif, which was much greater than expected based on analysis of EBF1 motifs near CpGs on a random subset of 100,000 CpGs covered by the Methyl450 array ($P < 0.015$). Genes associated with CpGs near both an EBF1 ChIP-seq peak and an EBF1 motif included IFN-regulated genes (NLRC5, IFITM1) and HCP5, among others, further strengthening the hypothesis that EBF1 regulation is actively involved in the biologic processes of SLE.
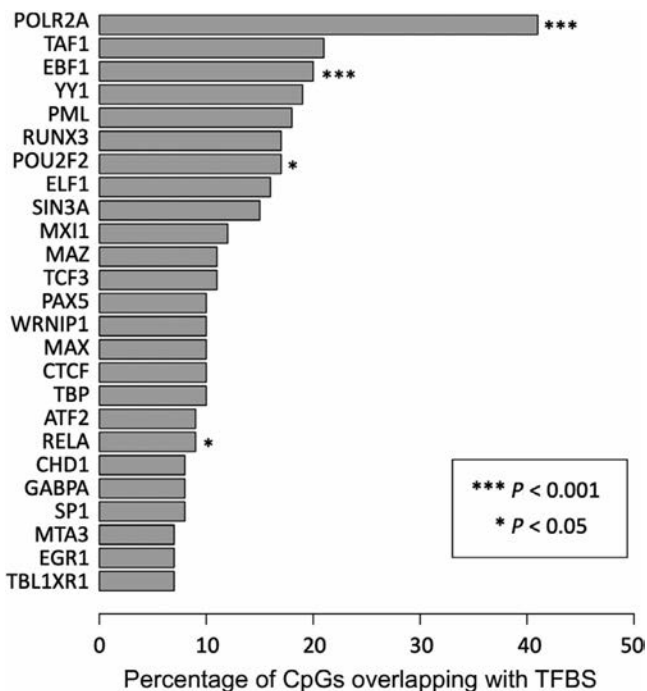
Figure 5. Systemic lupus erythematosus (SLE)–associated CpGs are enriched for EBF1 binding. Transcription factor enrichment within the top 100 ethnicity-dependent SLE-associated CpGs was determined using ENCODE chromatin immunoprecipitation–sequencing data. Transcription factors that were statistically significantly more enriched compared to the rest of the CpGs assayed are indicated (empirical P values marked by asterisks). TFBS = transcription factor binding sites.

DISCUSSION

In this study, we used various statistical and machine-learning methods to better understand the biologic changes that occur throughout B cell development in SLE patients and to discern any differences in these effects between AA and EA subjects. Our initial analysis was focused on following up previous studies that performed linear regression analysis in mixed cell populations. To identify CpG methylation differences associated with SLE status, we first implemented a simple regression model for SLE status across all 5 purified B cell subsets within our cohort, regardless of ethnicity. Several CpGs reached genome-wide significance ($P = .07 \times 10^{-7}$) for SLE-associated methylation differences across B cell subsets, including many that had been previously found to be associated with the disease (12–14,16,30–32). We showed that CpGs near IFN-regulated genes are hypomethylated in AA patients with SLE from the earliest circulating B cell stage, indicating that B cells might be epigenetically "primed" for an aberrant immune response prior to maturation in SLE patients of AA ancestry. When analyzing EA patients with SLE, we observed methylation changes in mature B cell stages, revealing potential differences in etiology between these 2 ethnicities. These epigenetic differences may explain the differences in disease presentation and severity between the ethnic groups as well.

Epidemiology studies have revealed that SLE risk and burden are significantly higher in AA women compared to other affected populations, which could potentially be explained by the more severe epigenetic signature observed in AA female patients with SLE in the present study. To further interrogate the ethnicity-specific methylation changes, we also performed a more complex regression model to identify ethnicity-specific SLE-associated CpGs. We noted that many genes associated with our top AA-specific CpGs (based on P value) are IFN-regulated and/or have previously been associated with SLE in other cohorts of various ancestral background (10,33,34). However, the same observation was not made for EA-specific CpGs.

The observed high level of within-patient correlation across genes suggests that there is a modular epigenetic defect in SLE patients, prompting us to build multivariate predictive models of disease using machine-learning optimization. Our AA-specific predictor was extremely effective at distinguishing SLE patients from controls, with high sensitivity and specificity (mean ROC AUC 0.94). Of the 34 CpGs used in the top-performing AA SLE prediction model, 7 had a statistically significant association with SLE ($P < 1.07 \times 10^{-7}$) and were near 6 different IFN-related genes, providing ancillary evidence that IFN plays a major role in SLE biology. A CpG at the transcription start site of NLRC5, and near a TFBS for EBF1 among multiple other transcription factors, had the highest predictive power for SLE status (Gini coefficient 0.461).

NLRC5 is 1 of 22 NLR family proteins, is highly expressed in the cytoplasm and nucleus of lymphocytes, and is a known regulator of major histocompatibility complex (MHC) class molecules

(35,36). In an analysis by Coit et al assessing genome-wide methylation in naive CD8+ T cells, hypomethylation at this same site near NLRC5 was observed (13). We hypothesize that hypomethylation in SLE patients at this site might alter regulation of MHC class I molecules in response to up-regulated IFN expression, which is characteristic of SLE. The next highest predictor (Gini coefficient 0.453) is near IFIT1, an IFN-stimulated gene that activates the innate immune system in response to inflammatory stimulation (37). IFIT1 not only contains known risk alleles for SLE, but also has been repeatedly noted for having both decreased methylation and increased expression in SLE patients compared to controls (16,37,38).

A CpG near the 5′–untranslated region of MX1 (cg21549285) was also within the top predictors. This site is near a TFBS for RUNX3, MAX, and STAT3, and is characterized by hypomethylation across B cell development in AA cases compared to controls. MX1 is activated by IFIT1, another top gene from our analysis, indicating that our model successfully identified biologically relevant relationships between CpGs to build a superior predictive model of disease. MX1 is downstream in the type I IFN pathway and is an important component of the early innate immune system, as it plays a role in the IFN-induced antiviral response against various viruses, but its role in response to IFN stimulation in the absence of virus has yet to be determined (39–41). MX1 hypomethylation, increased RNA expression, and higher protein concentrations are consistently observed in SLE patients (20,42–44). Multiple CpGs associated with MX1 were observed to be highly associated with SLE status in this analysis, and methylation at 2 MX1 CpGs revealed almost perfect separation of AA patients with SLE from controls, leading us to hypothesize that a targeted assay for MX1 methylation would be fruitful in diagnosing SLE.

To assess whether SLE-associated CpG sites were in regulatory regions of the genome, we interrogated TFBS near those regions using publicly available ChIP-seq data. We identified an increased number of binding sites for POL2RA, EBF1, POU2F2, and RELA in the top SLE-associated CpGs compared to all other CpG sites assayed. Of particular interest is the enrichment of EBF1 interaction at highly associated IFN sites, as this transcription factor is known as a pioneer transcription factor, especially in the B cell lineage (29). Through a distinct DNA binding domain at the N-terminus, EBF1 binds DNA as a homodimer at a palindromic recognition site consisting of 18 bp (5′-TCCCNNGGGA-3′) stabilized by an α–α motif, referred to as a zinc knuckle (45). EBF1 operates as an epigenetic regulator that induces demethylation, nucleosome remodeling, and active chromatin modifications to target genes (46). Binding sites for EBF1 that are poorly methylated are enriched for enhancer sites that undergo transcription factor–mediated changes in methylation (29).

A limitation to ChIP-sequencing is the inability to distinguish between direct and indirect protein–DNA interactions. To supplement the EBF1 enrichment observed in ChIP-seq data, we performed a motif enrichment analysis of the top 100 SLE-associated CpGs, in which we observed an increased occurrence of EBF1 motifs ($P < 0.015$) within 500 bp of the top 100 CpGs associated with SLE status in comparison to the rest of the CpG sites assayed. From these observations, we hypothesize that EBF1 plays a role in the immune response through regulation of IFN-regulated gene expression. A possible mechanism in which this might occur is that hypomethylation at or near the EBF1 motif of IFN-regulated genes, as frequently observed in our data, increases chromatin accessibility at those regions, allowing for higher affinity of EBF1 binding. This would allow for increased expression of downstream genes involved in the IFN pathway and dysregulation of the immune response in AA patients with SLE. ChIP–polymerase chain reaction experimentation in conjunction with methylation analysis in patient-derived B cells allowing for interrogation of the methylation status at EBF1 binding regions should be performed to further investigate this hypothesis.

Thus, we have identified an aberrant epigenetic signature that developed early in B cell development in AA patients with SLE. This observation is consistent with the findings from a recently published study in which an SLE-specific epigenetic signature was identified in a cohort of AA female subjects, with epigenetic defects found in the resting naive B cell stage and persisting throughout B cell development (42). Many genes highly associated with SLE in our cohort were enriched for IFN regulation, such as MX1, IFI44L, USP18, and IFITM1, indicating that B cells might be epigenetically "primed" for an aberrant immune response to IFN stimulation in AA patients with SLE. We also found that the AA-specific SLE signature defined herein was enriched for EBF1 interaction and served as an effective multivariate predictor of disease when validated in mixed immune cell populations from AA, but not EA, female patients with SLE and healthy controls, indicating epigenetic differences between the 2 populations with respect to disease.

A limitation of this study is the lack of genetic variant analysis. The presence of an SLE-related epigenetic signature, with a population-specific severity, could indicate either a shared set of methylQTLs in each of the genes that are only carried by AA patients with SLE, or alternatively, a defective signaling pathway that leads to correlated epigenetic effects at multiple genes. Given that the effects are seen at many unlinked genes and given the unlikelihood of shared genetic variants at each of these unlinked genes among AA patients with SLE, the former hypothesis is more likely. To add confirmation to this hypothesis, we analyzed the P values for CpGs within genes with known AA-specific SLE genetic associations and found a lack of association with methylation and SLE status for those sites (47,48). If known SLE-related genetic risk factors were drivers of epigenetic effects, we would expect an overlap between these loci.

In addition, another limitation of this study was the number of EA patients included. The vast difference in methylation (effect size) observed in AA patients compared to controls allowed for the

determination of several CpGs highly associated with SLE status, and yet the observed effect size was much lower in EA patients compared to controls. While our EA sample size should have been sufficient to detect effects (if they exist) similar to those seen in AA patients, power calculations indicate that our study was well powered to detect an effect size of 0.09 (i.e., a 9% change in methylation). We also point out that many of the AA patients with SLE in our cohort were affected by nephritis, whereas none of the EA patients with SLE had nephritis, which raises the question as to whether nephritis contributes to the population-specific SLE signatures. Additional regression analyses identified a lack of overlap between SLE-associated CpGs specific to nephritis and the CpGs determined to be associated with SLE and specific to either population (see Supplementary Table 8, available on the *Arthritis & Rheumatology* web site at http://onlinelibrary.wiley.com/doi/10.1002/art.41083/abstract).

Despite the limitations addressed, this study was the first to interrogate genome-wide methylation across individual B cell developmental stages in both AA and EA patients with SLE. Overall, the epigenetic patterns appeared to be different between AA and EA patients, suggesting that there are some mechanistic differences in etiology that may be related to the different clinical paths that these patient populations experience.

AUTHOR CONTRIBUTIONS

All authors were involved in drafting the article or revising it critically for important intellectual content, and all authors approved the final version to be published. Dr. Absher had full access to all of the data in the study and takes responsibility for the integrity of the data and the accuracy of the data analysis.

Study conception and design. Breitbach, Kimberly, Absher.
Acquisition of data. Roberts, Kimberly, Absher.
Analysis and interpretation of data. Breitbach, Ramaker, Absher.

REFERENCES

1. Rekvig OP. Systemic lupus erythematosus: definitions, contexts, conflicts, enigmas. Front Immunol 2018;9:387.

2. Morawski PA, Bolland S. Expanding the B cell-centric view of systemic lupus erythematosus. Trends Immunol 2017;38:373–82.

3. Yen EY, Shaheen M, Woo JM, Mercer N, Li N, McCurdy DK, et al. 46-year trends in systemic lupus erythematosus mortality in the United States, 1968 to 2013: a nationwide population-based study. Ann Intern Med 2017;167:777–85.

4. Bentham J, Morris DL, Graham DS, Pinder CL, Tombleson P, Behrens TW, et al. Genetic association analyses implicate aberrant regulation of innate and adaptive immunity genes in the pathogenesis of systemic lupus erythematosus. Nat Genet 2015;47:1457–64.

5. Centers for Disease Control and Prevention. Lupus. URL: www.cdc.gov/lupus/facts/detailed.html.

6. Pons-Estel GJ, Alarcón GS, Scofield L, Reinlib L, Cooper GS. Understanding the epidemiology and progression of systemic lupus erythematosus. Semin Arthritis Rheum 2010;39:257–68.

7. Somers EC, Marder W, Cagnoli P, Lewis EE, DeGuire P, Gordon C, et al. Population-based incidence and prevalence of systemic lupus erythematosus. Arthritis Rheumatol 2014;66:369–78.

8. Lewis MJ, Jawad AS. The effect of ethnicity and genetic ancestry on the epidemiology, clinical features and outcome of systemic lupus erythematosus. Rheumatology (Oxford) 2017;56 Suppl 1:i67–77.

9. Iwamoto T, Dorschner J, Jolly M, Huang X, Niewold TB. Associations between type I interferon and antiphospholipid antibody status differ between ancestral backgrounds. Lupus Sci Med 2018;5:e000246.

10. Wu H, Zeng J, Yin J, Peng Q, Zhao M, Lu Q. Organ-specific biomarkers in lupus. Autoimmun Rev 2017;16:391–7.

11. De S, Barnes BJ. B cell transcription factors: potential new therapeutic targets for SLE. Clin Immunol 2014;152:140–51.

12. Absher DM, Li X, Waite LL, Gibson A, Roberts K, Edberg J, et al. Genome-wide DNA methylation analysis of systemic lupus erythematosus reveals persistent hypomethylation of interferon genes and compositional changes to CD4+ T-cell populations. PLoS Genet 2013;9:e1003678.

13. Coit P, Jeffries M, Altorok N, Dozmorov MG, Koelsch KA, Wren JD, et al. Genome-wide DNA methylation study suggests epigenetic accessibility and transcriptional poising of interferon-regulated genes in naïve CD4+ T cells from lupus patients. J Autoimmun 2013;43:78–84.

14. Jeffries M, Dozmorov M, Tang Y, Merrill JT, Wren JD, Sawalha AH. Genome-wide DNA methylation patterns in CD4+ T cells from patients with systemic lupus erythematosus. Epigenetics 2011;6:593–601.

15. Chen S, Pu W, Guo S, Jin L, He D, Wang J. Genome-wide DNA methylation profiles reveal common epigenetic patterns of interferon-related genes in multiple autoimmune diseases. Front Genet 2019;10:223.

16. Coit P, Yalavarthi S, Ognenovski M, Zhao W, Hasni S, Wren JD, et al. Epigenome profiling reveals significant DNA demethylation of interferon signature genes in lupus neutrophils. J Autoimmun 2015;58:59–66.

17. Mok A, Solomon O, Nayak RR, Coit P, Quach HL, Nititham J, et al. Genome-wide profiling identifies associations between lupus nephritis and differential methylation of genes regulating tissue hypoxia and type 1 interferon responses. Lupus Sci Med 2016;3:e000183.

18. Yeung KS, Chung BH, Choufani S, Mok MY, Wong WL, Mak CC, et al. Genome-wide DNA methylation analysis of Chinese patients with systemic lupus erythematosus identified hypomethylation in genes related to the type I interferon pathway. PLoS One 2017;12:e0169553.

19. Langefeld CD, Ainsworth HC, Cunninghame Graham DS, Kelly JA, Comeau ME, Marion MC, et al. Transancestral mapping and genetic load in systemic lupus erythematosus. Nat Commun 2017;8:16021.

20. Coit P, Ognenovski M, Gensterblum E, Maksimowicz-McKinnon K, Wren JD, Sawalha AH. Ethnicity-specific epigenetic variation in naive CD4+ T cells and the susceptibility to autoimmunity. Epigenetics Chromatin 2015;8:49.

21. Bombardier C, Gladman DD, Urowitz MB, Caron D, Chang DH, and the Committee on Prognosis Studies in SLE. Derivation of the SLEDAI: a disease activity index for lupus patients. Arthritis Rheum 1992;35:630–40.

22. Breiman L. Random forests. Mach Learn 2001;45:5–32.

23. Friedman J, Hastie T, Tibshirani R. Regularization paths for generalized linear models via coordinate descent. J Stat Softw 2010;33:1–22.

24. Davis CA, Hitz BC, Sloan CA, Chan ET, Davidson JM, Gabdank I, et al. The Encyclopedia of DNA Elements (ENCODE): data portal update. Nucleic Acids Res 2018;46:D794–801.

25. Quinlan AR, Hall IM. BEDTools: a flexible suite of utilities for comparing genomic features. Bioinformatics 2010;26:841–2.

26. Bailey TL, Boden M, Buske FA, Frith M, Grant CE, Clementi L, et al. MEME Suite: tools for motif discovery and searching. Nucleic Acids Res 2009;37:W202–8.

27. Grant CE, Bailey TL, Noble WS. FIMO: scanning for occurrences of a given motif. Bioinformatics 2011;27:1017–8.

28. Khan A, Fornes O, Stigliani A, Gheorghe M, Castro-Mondragon JA, van der Lee R, et al. JASPAR 2018: update of the open-access database of transcription factor binding profiles and its web framework. Nucleic Acids Res 2018;46:D260–6.

29. Li R, Cauchy P, Ramamoorthy S, Boller S, Chavez L, Grosschedl R. Dynamic EBF1 occupancy directs sequential epigenetic and transcriptional events in B-cell programming. Genes Dev 2018;32:96–111.

30. Park SH, Kang K, Giannopoulou E, Qiao Y, Kang K, Kim G, et al. Type I interferons and the cytokine TNF cooperatively reprogram the macrophage epigenome to promote inflammatory activation. Nat Immunol 2017;18:1104–16.

31. Lugar PL, Love C, Grammer AC, Dave SS, Lipsky PE. Molecular characterization of circulating plasma cells in patients with active systemic lupus erythematosus. PLoS One 2012;7:e44362.

32. Wahadat MJ, Bodewes IL, Maria NI, van Helden-Meeuwsen CG, van Dijk-Hummelman A, Steenwijk EC, et al. Type I IFN signature in childhood-onset systemic lupus erythematosus: a conspiracy of DNA- and RNA-sensing receptors? Arthritis Res Ther 2018;20:4.

33. Bing PF, Xia W, Wang L, Zhang YH, Lei SF, Deng FY. Common marker genes identified from various sample types for systemic lupus erythematosus. PLoS One 2016;11:e0156234.

34. Mohan C, Putterman C. Genetics and pathogenesis of systemic lupus erythematosus and lupus nephritis. Nat Rev Nephrol 2015;11: 329–41.

35. Meissner TB, Li A, Biswas A, Lee KH, Liu YJ, Bayir E, et al. NLR family member NLRC5 is a transcriptional regulator of MHC class I genes. Proc Natl Acad Sci U S A 2010;107:13794–9.

36. Kobayashi KS, van den Elsen PJ. NLRC5: a key regulator of MHC class I-dependent immune responses. Nat Rev Immunol 2012;12:813–20.

37. McDermott JE, Vartanian KB, Mitchell H, Stevens SL, Sanfilippo A, Stenzel-Poore MP. Identification and validation of IFIT1 as an important innate immune bottleneck. PLoS One 2012;7:e36465.

38. Ye S, Pang H, Gu YY, Hua J, Chen XG, Bao CD, et al. Protein interaction for an interferon-inducible systemic lupus associated gene, IFIT1. Rheumatology (Oxford) 2003;42:1155–63.

39. Melén K, Ronni T, Lotta T, Julkunen I. Enzymatic characterization of interferon-induced antiviral GTPases murine Mx1 and human MxA proteins. J Biol Chem 1994;269:2009–15.

40. Nakayama M, Nagata K, Kato A, Ishihama A. Interferon-inducible mouse Mx1 protein that confers resistance to influenza virus is GTPase. J Biol Chem 1991;266:21404–8.

41. Haller O, Kochs G. Human MxA protein: an interferon-induced dynamin-like GTPase with broad antiviral activity. J Interferon Cytokine Res 2011;31:79–87.

42. Scharer CD, Blalock EL, Mi T, Barwick BG, Jenks SA, Deguchi T, et al. Epigenetic programming underpins B cell dysfunction in human SLE. Nat Immunol 2019;20:1071–82.

43. Shimizu Y, Yasuda S, Kimura T, Nishio S, Kono M, Ohmura K, et al. Interferon-inducible Mx1 protein is highly expressed in renal tissues from treatment-naive lupus nephritis, but not in those under immunosuppressive treatment. Mod Rheumatol 2018;28:661–9.

44. Watanabe S, Imaizumi T, Tsuruga K, Aizawa T, Ito T, Matsumiya T, et al. Glomerular expression of myxovirus resistance protein 1 in human mesangial cells: possible activation of innate immunity in the pathogenesis of lupus nephritis. Nephrology (Carlton) 2013;18:833–7.

45. Treiber N, Treiber T, Zocher G, Grosschedl R. Structure of an Ebf1: DNA complex reveals unusual DNA recognition and structural homology with Rel proteins. Genes Dev 2010;24:2270–5.

46. Vilagos B, Hoffmann M, Souabni A, Sun Q, Werner B, Medvedovic J, et al. Essential role of EBF1 in the generation and function of distinct mature B cell types. J Exp Med 2012;209:775–92.

47. Ghodke-Puranik Y, Imgruet M, Dorschner JM, Shrestha P, McCoy K, Kelly JA, et al. Novel genetic associations with interferon in systemic lupus erythematosus identified by replication and fine-mapping of trait-stratified genome-wide screen. Cytokine 2019. E-pub ahead of print.

48. Kariuki SN, Franek BS, Kumar AA, Arrington J, Mikolaitis RA, Utset TO, et al. Trait-stratified genome-wide association study identifies novel and diverse genetic associations with serologic and cytokine phenotypes in systemic lupus erythematosus. Arthritis Res Ther 2010;12:R151.

AMERICAN COLLEGE
of RHEUMATOLOGY
Empowering Rheumatology Professionals

Development of Murine Systemic Lupus Erythematosus in the Absence of BAFF

William Stohl,[1] [iD] Ning Yu,[1] Samantha Chalmers,[2] Chaim Putterman,[2] and Chaim O. Jacob[1]

Objective. To determine whether systemic lupus erythematosus (SLE) can develop in the absence of BAFF in an SLE-prone host.

Methods. Starting with C57BL/6 mice that express a human *BCL2* transgene (Tg) in their B cells (thereby rendering B cell survival largely independent of BAFF-triggered signals), we introgressed this Tg into NZM 2328 mice genetically deficient in BAFF (NZM.*Baff*$^{-/-}$) to generate NZM.*Baff*$^{-/-}$.*Bcl2*^{Tg} mice. Expression of human Bcl-2 and lymphocyte profiles were assessed by fluorescence-activated cell sorting, and serologic profiles were determined by enzyme-linked immunosorbent assay. Immunofluorescence and histologic analyses were performed to assess renal immunopathologic features in the mice, and clinical disease was assessed according to the outcomes of severe proteinuria and death.

Results. In comparison to their non-Tg NZM.*Baff*$^{-/-}$ littermates (n ≥ 7), NZM.*Baff*$^{-/-}$.*Bcl2*^{Tg} mice (n ≥ 8) overexpressed Bcl-2 in their B cells and developed significantly increased percentages and numbers of B cells and plasma cells, serum levels of IgG autoantibodies, glomerular deposition of IgG and C3, and severity of glomerular and tubulointerstitial inflammation, culminating in severe proteinuria and death (all $P < 0.05$ versus NZM.*Baff*$^{-/-}$ littermates). The time course for development of SLE-like features in NZM.*Baff*$^{-/-}$.*Bcl2*^{Tg} mice was more rapid than has been previously observed in NZM 2328 wild-type mice (median age at death 4.5 months versus 7.5 months). NZM.*Baff*$^{-/-}$.*Bcl2*^{Tg} mice remained responsive to BAFF, since reintroduction of the *Baff* gene into these mice further accelerated the course of disease (median age at death 3 months).

Conclusion. The role of BAFF in the development of SLE-like disease may be dispensable as long as B cell survival is preserved via a BAFF-independent pathway. This may help explain the limited and variable clinical success with BAFF antagonists in human SLE. Thus, NZM.*Baff*$^{-/-}$.*Bcl2*^{Tg} mice may serve as a powerful murine model for the study of BAFF-independent SLE.

INTRODUCTION

One of the classic hallmarks of systemic lupus erythematosus (SLE) is B cell hyperactivity. Studies in murine SLE have conclusively demonstrated that B cells are an indispensable component of disease development, in that otherwise SLE-prone MRL.*lpr/lpr* or NZM 2328 (NZM) mice fail to develop SLE when genetically rendered B cell deficient (1,2).

BAFF (also known as B lymphocyte stimulator [BLyS]) is a vital survival and differentiation factor for B cells (3–6). In non–SLE-prone mice, antagonism of BAFF results in considerable, albeit subtotal, reduction in the number of B cells (7), and genetic

disruption of the *Baff* gene results in even greater, albeit still subtotal, reduction in B cells (8). Comparable observations have been made in SLE-prone mice, in which pharmacologic neutralization with either of 2 BAFF antagonists or genetic elimination of BAFF leading to substantial (subtotal) reduction in the number of B cells have been tested with clinical efficacy (9–11).

In human SLE, treatment with any of 4 different BAFF antagonists also results in subtotal reduction in the number of circulating B cells (12–16). However, clinical efficacy has not always been achieved. Whereas the primary end point was met in each of the 4 phase III clinical trials with the anti-BAFF monoclonal antibody (mAb) belimumab in patients with SLE (17–20), the phase II trials

in SLE with either blisibimod or atacicept did not achieve their primary end point (13,21), and only 1 of the 2 phase III trials with tabalumab met its primary end point (15,16). Even treatment with belimumab, which is approved by the US Food and Drug Administration for the treatment of SLE (for review, see ref. 22), failed to elicit a clinical response in >40% of subjects in the phase II or phase III SLE clinical trials (17,18,20,23).

The heterogeneity in clinical response to BAFF antagonism raises the possibility that incomplete B cell depletion may be a contributing factor to the clinical resistance to BAFF antagonist therapy in some patients; that is, pathogenic B cells that survive pharmacologic neutralization of BAFF may continue to promote disease in some patients. Accordingly, the degree of (pathogenic) B cell depletion induced by a BAFF antagonist may be sufficient to ameliorate disease activity in some SLE patients, whereas the degree of (pathogenic) B cell depletion induced by the same BAFF antagonist may be insufficient to ameliorate disease activity in other SLE patients.

To test whether an SLE-prone host otherwise clinically responsive to BAFF elimination would remain clinically responsive if B cells are preserved in the face of elimination of BAFF, we turned to a murine model of SLE in which mouse B cells harbor a human *BCL2* transgene (Tg). In such mice, survival of B cells, which constitutively overexpress Bcl-2, largely does not depend on BAFF-triggered signals (24,25).

Accordingly, we introgressed the *BCL2* Tg into NZM mice genetically deficient in BAFF (NZM.*Baff*^{-/-}) (11), to generate NZM.*Baff*^{-/-}.*Bcl2*[Tg] mice. Our studies demonstrate that these mice, despite the life-long absence of BAFF, develop the immunologic, pathologic, and clinical features of SLE over a time course even more rapid than that seen in NZM wild-type (WT) mice. Thus, BAFF is a dispensable factor in the development of SLE-like disease in NZM mice under conditions in which B cell survival is preserved via a BAFF-independent pathway. By inference, some SLE patients may be inherently resistant to BAFF-directed therapies by virtue of the fact that they have pathogenic B cells whose survival is independent of BAFF. Therefore, NZM.*Baff*^{-/-}.*Bcl2*[Tg] mice may serve as a powerful murine model in the study of this BAFF-independent component of SLE.

MATERIALS AND METHODS

Mice. All reported studies in mice were approved by the University of Southern California Institutional Animal Care and Use Committee. NZM WT and NZM.*Baff*^{-/-} mice (11) were maintained in a single specific pathogen–free room. B6.Cg-Tg(BCL2)22Wehi/J mice (on a C57BL/6 background and bearing a human *BCL2* Tg expressed only in B-lineage cells) (B6.*Bcl2*[Tg]) (26) were obtained from The Jackson Laboratory and housed in the same specific pathogen–free room. NZM.*Baff*^{-/-}.*Bcl2*[Tg] mice were generated by introgressing the *Bcl2*[Tg] genotype from B6.*Bcl2*[Tg] mice into NZM.*Baff*^{-/-} mice using a marker-assisted selection proto-

col (27,28) with 47 microsatellite markers. These markers were chosen to include those regions identified as susceptibility loci in NZM mice (29). The N7 backcross generation was fully congenic. NZM.*Baff*^{+/-}.*Bcl2*[Tg] and non-Tg NZM.*Baff*^{+/-} littermate mice were generated by mating NZM.*Baff*^{-/-}.*Bcl2*[Tg] mice with NZM WT (*Baff*^{+/+}) mice. Results are reported for female mice only.

For the purpose of identifying Foxp3+ Treg cells in NZM WT mice, NZM[foxp3-gfp] mice were generated by introgressing the *Foxp3-gfp* knockin genotype from B6[foxp3-gfp] mice (obtained from Dr. Song Guo Zheng, Ohio State University Medical Center, Columbus) into NZM WT mice. For the purpose of identifying Foxp3+ cells in NZM.*Baff*^{-/-}.*Bcl2*[Tg] mice, NZM[foxp3-gfp] mice were first crossed with NZM.*Baff*^{-/-} mice to generate NZM[foxp3-gfp].*Baff*^{-/-} mice. The *Bcl2*[Tg] genotype was then introgressed from B6.*Bcl2*[Tg] mice into NZM-[foxp3-gfp].*Baff*^{-/-} mice, to yield NZM[foxp3-gfp].*Baff*^{-/-}.*Bcl2*[Tg] mice.

Cell surface staining. Spleen mononuclear cells were stained with combinations of fluorochrome-conjugated mAb specific for CD1d, CD3, CD4, CD8, CD19, CD44, CD62L, CD69, CD138, soluble IgD, or soluble IgM (from BioLegend or BD Biosciences) to identify total B cells (CD19+), follicular (FO) B cells (CD3–CD19+IgM^{low}IgD^{high}), marginal zone (MZ) B cells (CD3–CD19+IgM^{high}IgD^{low}CD1d^{high}), plasma cells (CD3–CD138+CD19^{low/–}), total CD4+ T cells, total CD8+ T cells, activated memory T cells (CD4+CD44^{high}CD62L^{low}), and recently activated CD4+ T cells (CD4+CD69+). Data were analyzed with FlowJo software (version 7.6.1; Tree Star).

Intracellular staining for Bcl-2. Spleen mononuclear cells were first stained for surface CD3 and CD19, as described above. Following treatment with Fix/Perm buffer (BioLegend), the cells were stained for intracellular Bcl-2 using phycoerythrin-conjugated anti-human Bcl-2 mAb or isotype control mAb (BioLegend) and analyzed as described above.

Serum levels of total IgG and IgG autoantibodies. Serum levels of total IgG and IgG autoantibodies were determined by enzyme-linked immunosorbent assay (2). Autoantibody optical density (OD) values were normalized to the mean OD value of serum from 5-month-old MRL-*lpr* mice, the latter arbitrarily assigned a value of 100 units/ml.

Kidney histology. Sections of formalin-fixed kidneys were stained with hematoxylin and eosin and assessed by light microscopy for histologic features (30).

Kidney immunofluorescence analysis. Sections of snap-frozen kidneys were stained for IgG or C3 deposition using fluorescein isothiocyanate–conjugated goat F(ab′)₂ fragment anti-mouse IgG or C3 antibodies (MP Biomedicals) (2).

Assessment of clinical disease. Mice were monitored for the development of severe proteinuria or death; each outcome was recorded separately. To assess proteinuria, reagent strips

for urinary protein (Albustix; Bayer) were dipped in mouse urine, and the extent of proteinuria was assigned a score (on a scale of 0–4) by visual color comparison to the supplied standard color key. Severe proteinuria was defined as ≥3+ on 2 consecutive examinations, either prior to natural death or at the time of euthanasia. Since the death of some NZM.*Baff*+/−.*Bcl2*Tg mice was very precipitous and resulted in the absence, at the moribund state, of assessment of proteinuria (which, presumably, would have been severe), severe clinical disease in these mice was defined as development of either severe proteinuria or death.

Assessment of in vitro Treg cell function. T responder cells (CD4+Foxp3−) from NZM*foxp3-gfp* WT mice and Treg cells (CD4+Foxp3+) from NZM*foxp3-gfp* WT or NZM*foxp3-gfp*.*Baff*−/−.*Bcl2*Tg mice were isolated by fluorescence-activated cell sorting of spleen CD4+ T cells. T responder cells were stained with the proliferation dye eFluor 670 (eBioscience), and then stimulated with anti-CD3 mAb (0.025 mg/ml; BioLegend) and with irradiated B6 WT mouse non–T cells (30 Gy, 1:1 ratio) in the presence of graded ratios of Treg cells. On day 3, cells were harvested, and the division index (DI) (total number of T responder cell divisions divided by original number of T responder cells), the proliferation index (PI) (total number of T responder cell divisions divided by number of T responder cells undergoing at least 1 division), and percentage

of dividing cells (number of T responder cells undergoing at least 1 division divided by original number of T responder cells) were evaluated using a FACSCalibur (BD Biosciences). Results are expressed as the percentage suppression, calculated as (value in cultures with T responder cells only − value in cultures with T responder cells and Treg cells) divided by value in cultures with T responder cells only.

In vitro responsiveness of B cells to BAFF. Spleen B cells were isolated using an autoMACS separator with anti-mouse CD19 microbeads (Miltenyi). To assess B cell survival, B cells were cultured (2 × 10^5/0.2 ml) in triplicate in 96-well flat-bottomed plates in RPMI 1640 medium–10% fetal calf serum, with or without the addition of exogenous recombinant BAFF (100 ng/ml; R&D Systems). The viability of the cells was determined at 48 hours of culture, by staining with annexin V and propidium iodide (BioLegend).

Statistical analysis. All analyses were performed using SigmaStat software (SPSS). Parametric testing for comparisons between 2 groups was performed using unpaired *t*-tests, and comparisons among 3 or more groups were performed using one-way analysis of variance (ANOVA). When the data were not normally distributed or the equal variance test was
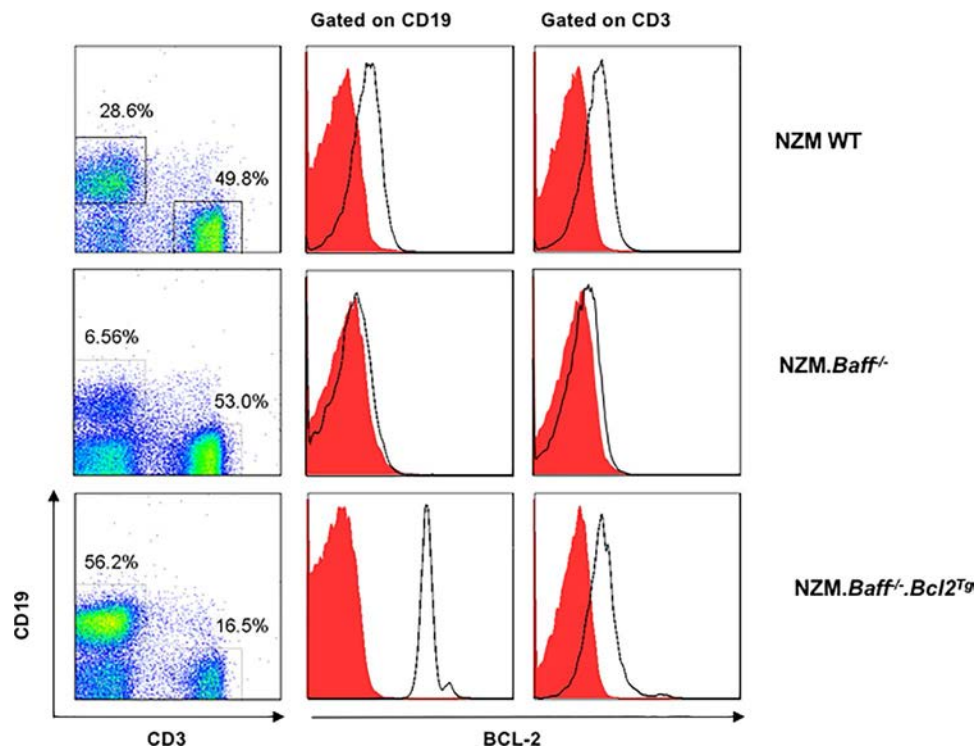
Figure 1. Selective overexpression of Bcl-2 in B cells from NZM.*Baff*−/−.*Bcl2*Tg mice. Spleen cells from NZM 2328 wild-type (WT), NZM.*Baff*−/−, and NZM.*Baff*−/−.*Bcl2*Tg mice were stained for surface CD19 and CD3 expression and then for intracellular Bcl-2. Left, Dot plots illustrate CD19 versus CD3 staining. Values are the percentage of CD19+ and CD3+ cells. Center and right, Histograms illustrate intracellular Bcl-2 staining in CD19+ cells (center) and CD3+ cells (right). Open areas outlined by black lines indicate staining with anti–Bcl-2, and solid red-filled areas indicate staining with the isotype control. Color figure can be viewed in the online issue, which is available at http://onlinelibrary.wiley.com/doi/10.1002/art.41097/abstract.

not satisfied, nonparametric testing was performed using Mann-Whitney rank sum tests for comparison of 2 groups, and Kruskal-Wallis one-way ANOVA tests on ranks for comparison of 3 or more groups. Survival data were analyzed by the log-rank test.

RESULTS

Selective overexpression of Bcl-2 in NZM.*Baff*$^{-/-}$.*Bcl2*^{Tg} mouse B cells. To confirm at the protein level that Bcl-2 is selectively overexpressed in the B cells of NZM.*Baff*$^{-/-}$.*Bcl2*^{Tg} mice, B
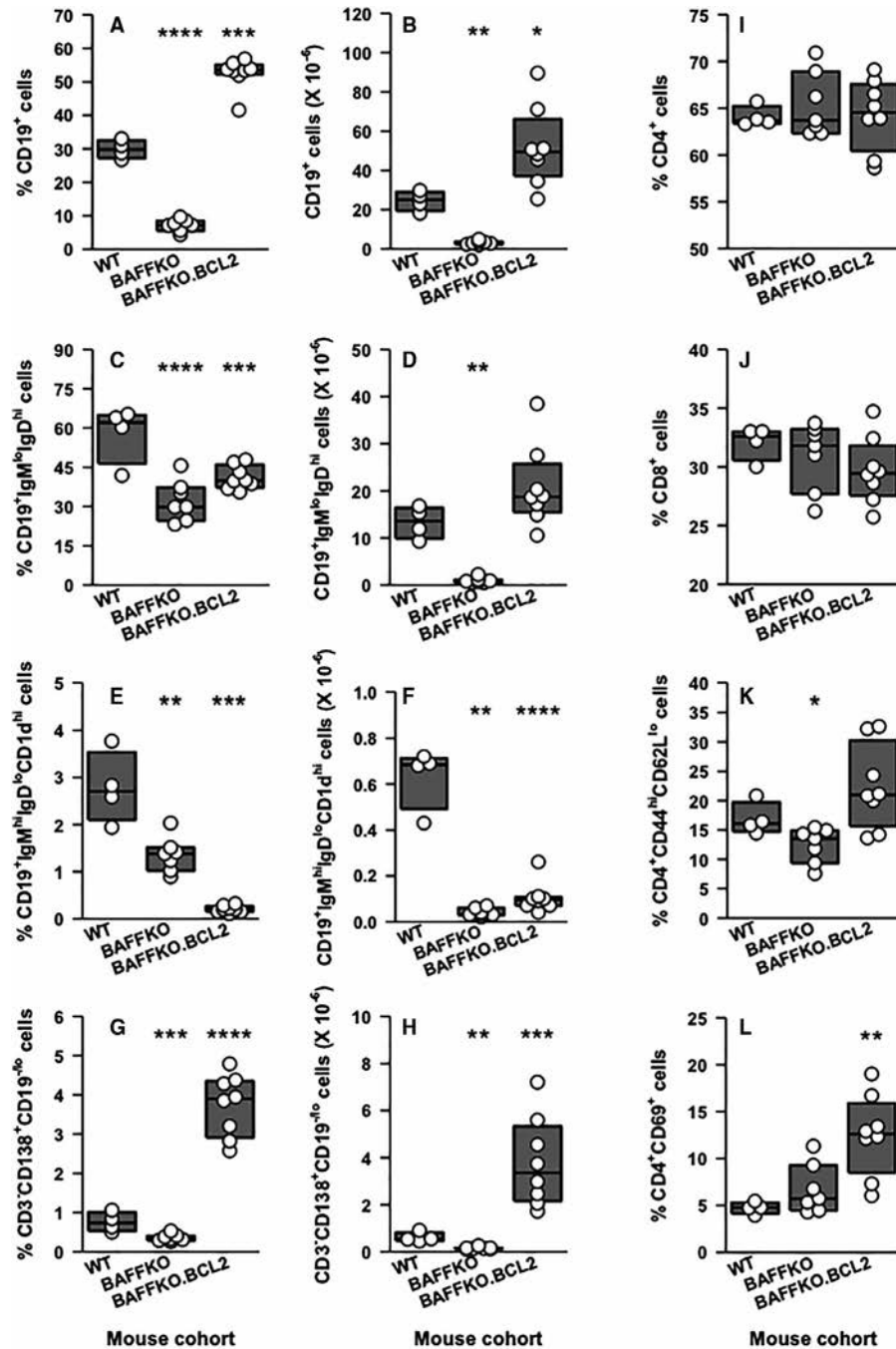
Figure 2. Spleen lymphocyte profiles. Plots show the distributions of spleen total B cells (CD19+) (**A** and **B**), follicular B cells (CD19+IgM^{high}IgD^{low}) (**C** and **D**), marginal zone B cells (CD19+IgM^{high}IgD^{low}CD1d^{high}) (**E** and **F**), plasma cells (CD3−CD138+CD19$^{-/low}$) (**G** and **H**), CD4+ T cells (**I**), CD8+ T cells (**J**), CD4+ activated memory T cells (CD4+CD44^{high}CD62L^{low}) (**K**), and CD4+ recently activated T cells (CD4+CD69+) (**L**) from 2-month-old NZM 2328 wild-type (WT) mice (n = 4), NZM.*Baff*$^{-/-}$ (BAFFKO) mice (n = 7), and NZM.*Baff*$^{-/-}$.*Bcl2*^{Tg} (BAFFKO.BCL2) mice (n = 8). Results are expressed as the percentage based on numbers of total spleen mononuclear cells (**A** and **G**), total B cells (**C** and **E**), total T cells (**I** and **J**), or total CD4+ T cells (**K** and **L**) or as the absolute number (**B**, **D**, **F**, and **H**). Each circle represents an individual mouse. Composite results are presented as box plots, where the lines inside the box indicate the median, and the outer borders indicate the 25th and 75th percentiles. * = $P \leq 0.05$; ** = $P \leq 0.01$; *** = $P \leq 0.005$; **** = $P \leq 0.001$ versus WT mice.

cells (CD19+) and T cells (CD3+) from NZM WT, NZM.$Baff^{-/-}$, and NZM.$Baff^{-/-}$.$Bcl2^{Tg}$ mice were analyzed for intracellular expression of Bcl-2. Expression of Bcl-2 in NZM WT mouse B cells was similar to that in NZM WT mouse T cells (Figure 1). Expression of Bcl-2 in B and T cells from NZM.$Baff^{-/-}$ mice was lower than that in the corresponding cells from NZM WT mice, whereas, conversely, Bcl-2 expression was previously reported to be increased in C57BL/6 mice bearing a $Baff$ transgene (31). In contrast, in NZM.$Baff^{-/-}$.$Bcl2^{Tg}$ mice, expression of Bcl-2 in T cells was similar to that in NZM WT mouse T cells, but expression of Bcl-2 in B cells was greatly increased compared to that in B cells from NZM WT mice.

B-lineage cell profiles. In non–SLE-prone mice, BAFF deficiency results in dramatic reductions in the number of B cells at or beyond the T2 stage, including FO B cells and MZ B cells (7,8). Introduction of a *BCL2* Tg into the B cells of such BAFF-deficient mice restores all B cells other than MZ B cells (24). We observed a similar pattern in NZM mice. Consistent with our previous observations (11), NZM.$Baff^{-/-}$ mice at age 2 months harbored decreased percentages and numbers of total B cells (CD19+), FO B cells (CD19+IgM^{low}IgD^{high}), and MZ B cells (CD19+IgM^{high}IgD^{low}CD1d^{high}) as compared to those in age-matched NZM WT mice. In NZM.$Baff^{-/-}$.$Bcl2^{Tg}$ littermates of the NZM.$Baff^{-/-}$ mice, the percentages and numbers of total B cells and FO B cells were restored to at least the levels seen in WT mice, whereas essentially no restorative effect on the MZ B cell population was observed (Figures 2A–F).

Consistent with the reductions in mature B cells, we previously documented that NZM.$Baff^{-/-}$ mice harbor fewer plasma cells than do NZM WT mice (30). Accordingly, 2-month-old NZM.$Baff^{-/-}$ mice harbored decreased percentages and numbers of plasma cells compared to age-matched NZM WT mice. Strikingly, the percentages and absolute numbers of CD3–CD138+CD19$^{low/-}$ plasma cells in the NZM.$Baff^{-/-}$.$Bcl2^{Tg}$ littermates of the NZM.$Baff^{-/-}$ mice surpassed the levels seen in WT mice (Figures 2G and H).

T cell profiles. As opposed to the stark differences in the distribution of spleen B-lineage cells across the 3 mouse cohorts, no differences were noted in the percentages of CD4+ and CD8+ T cells within the total spleen T cell population (Figures 2I and J). Nevertheless, differences in activated CD4+ T cell subsets were noted. Within the CD4+ T cell subset, the percentages of activated memory T cells (CD4+CD44^{high}CD62L^{low}) were reduced in NZM.$Baff^{-/-}$ mice but were restored in their NZM.$Baff^{-/-}$.$Bcl2^{Tg}$ littermates (Figure 2K). Moreover, the percentages of recently activated T cells (CD4+CD69+) within the CD4+ T cell subset were similar between NZM WT and NZM.$Baff^{-/-}$ mice, whereas they were increased in NZM.$Baff^{-/-}$.$Bcl2^{Tg}$ mice (Figure 2L).

Serologic profiles. BAFF deficiency in non–SLE-prone mice not only leads to marked reductions in mature B cells but also leads to marked reductions in baseline serum Ig levels and Ig

responses to T cell–dependent and T cell–independent antigens (7,8). We previously demonstrated that, compared to NZM WT mice, the serum levels of total IgG and some IgG autoantibodies in NZM.$Baff^{-/-}$ mice are substantially reduced through age 6 months, although the levels "catch up" by ages 7–9 months (11). Consistent with the increases in B cells, plasma cells, and activated CD4+ T cells, serum levels of total IgG and IgG autoantibodies were significantly higher in 2-month-old NZM.$Baff^{-/-}$.$Bcl2^{Tg}$ mice than in their NZM.$Baff^{-/-}$ littermates (Figure 3). Serum levels of IgG antichromatin and IgG anti–double-stranded DNA continued to
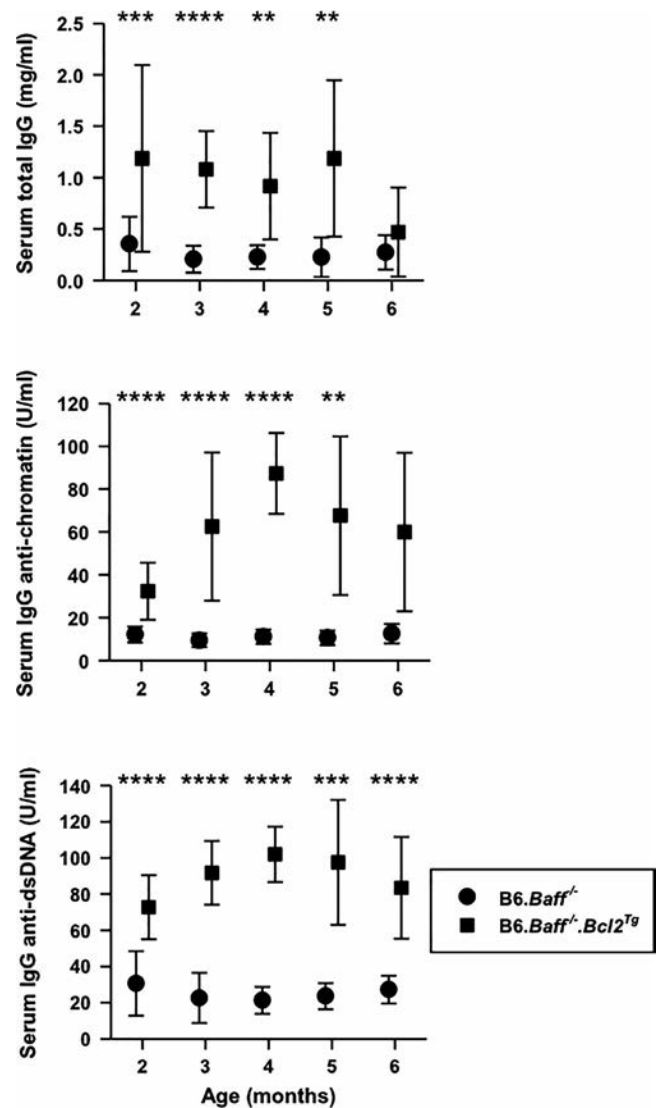
Figure 3. Serologic profiles. Blood samples were obtained longitudinally from NZM.$Baff^{-/-}$.$Bcl2^{Tg}$ mice (n = 18) and NZM.$Baff^{-/-}$ littermate mice (n = 12) at the indicated ages. Serum levels of total IgG (top), IgG antichromatin (middle), and IgG anti–double-stranded DNA (anti-dsDNA) (bottom) were determined. Results are the mean ± SD. Due to accelerated mortality among NZM.$Baff^{-/-}$.$Bcl2^{Tg}$ mice, blood was collected from 9 NZM.$Baff^{-/-}$.$Bcl2^{Tg}$ mice at age 4 months, 7 NZM.$Baff^{-/-}$.$Bcl2^{Tg}$ mice at age 5 months, and 4 NZM.$Baff^{-/-}$.$Bcl2^{Tg}$ mice at age 6 months. ** = $P \leq 0.01$; *** = $P \leq 0.005$; **** = $P \leq 0.001$ between the 2 groups.
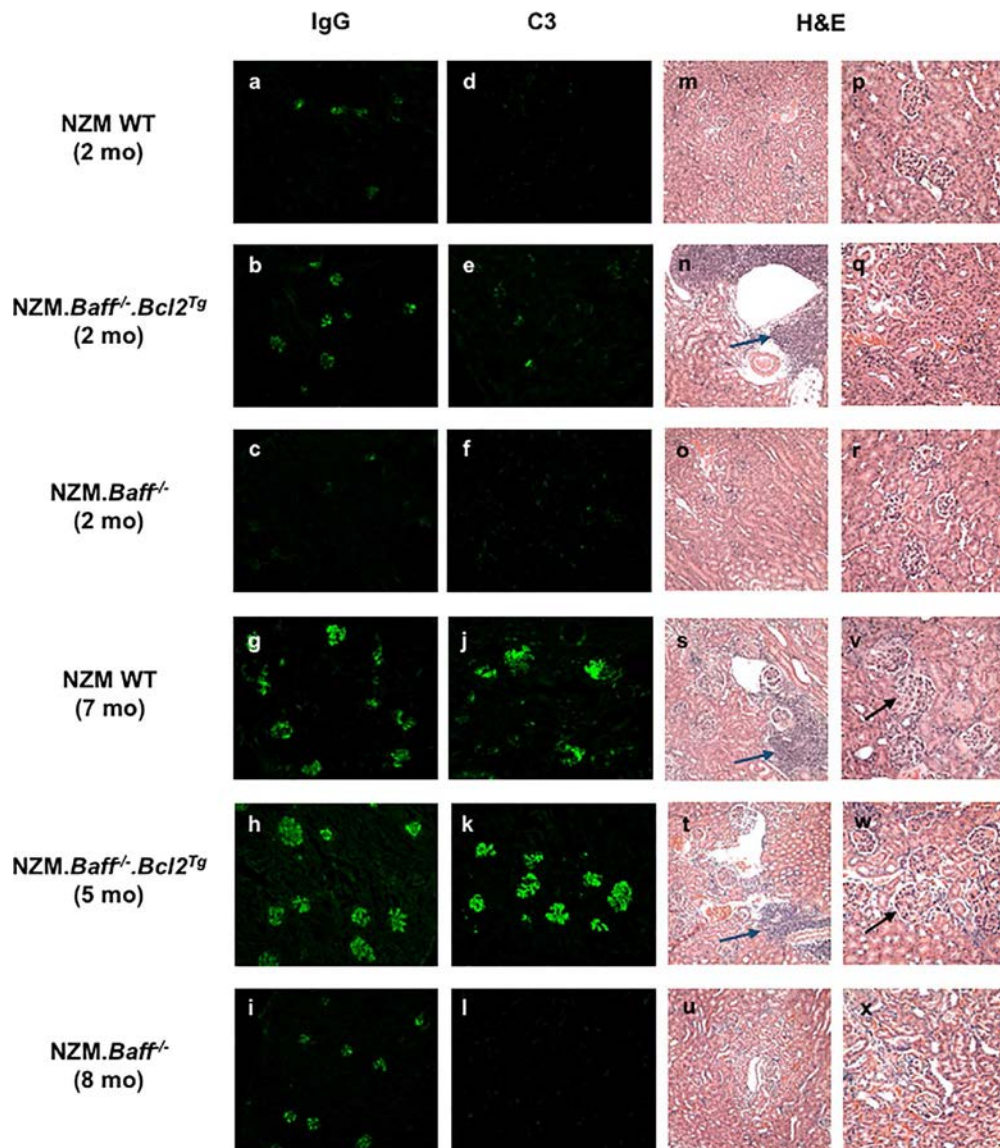
Figure 4. Renal immunopathology. Kidney sections from NZM 2328 wild-type (WT) mice (**a**, **d**, **g**, **j**, **m**, **p**, **s**, and **v**), NZM.*Baff*$^{-/-}$.*Bcl2*^{Tg} mice (**b**, **e**, **h**, **k**, **n**, **q**, **t**, and **w**), and NZM.*Baff*$^{-/-}$ mice (**c**, **f**, **i**, **l**, **o**, **r**, **u**, and **x**) at the indicated ages (in months [mo]) were stained for IgG or C3 immunofluorescence analyses or stained with hematoxylin and eosin (H&E) for histologic evaluation. **Blue arrows** indicate interstitial/perivascular infiltrates, and **black arrows** indicate swollen/hypercellular glomeruli. In immunofluorescence micrographs (left and right panels), original magnification × 100. In H&E-stained micrographs, original magnification × 200 in left panels, × 400 in right panels.

rise in NZM.*Baff*$^{-/-}$.*Bcl2*^{Tg} mice through age 4 months, and the declines in serum total IgG and IgG autoantibody levels at ages 5–6 months was reflective of the premature death (discussed in more detail below) of those mice that harbored high serum levels of total IgG and IgG autoantibodies at earlier time points.

Glomerular IgG and C3 deposition. NZM WT mice develop considerable glomerular deposition of IgG and C3 by age 6 months, with such deposition being substantially reduced in NZM.*Baff*$^{-/-}$ mice (11). To assess the age at onset of glomerular IgG and C3 deposition, we first examined the mice at age 2 months. At this young age, glomerular deposition of IgG was already evident in each of the 8 NZM.*Baff*$^{-/-}$.*Bcl2*^{Tg}

mice examined. In contrast, glomerular IgG deposition was detected in none of the 7 NZM.*Baff*$^{-/-}$ littermate mice examined and in only 1 of the 4 age-matched control NZM WT mice examined (Figures 4a–c).

Glomerular deposition of C3 lagged behind glomerular deposition of IgG in 2-month-old mice, with unequivocal deposition observed in 1 of the 8 NZM.*Baff*$^{-/-}$.*Bcl2*^{Tg} mice examined and in none of the 7 NZM.*Baff*$^{-/-}$ littermate mice examined and none of the 4 age-matched control NZM WT mice examined (Figures 4d–f).

In older mice (ages 5–7 months), the disparity between NZM.*Baff*$^{-/-}$.*Bcl2*^{Tg} and NZM.*Baff*$^{-/-}$ mice was more apparent. Glomerular deposition of both IgG and C3 in each of the 5
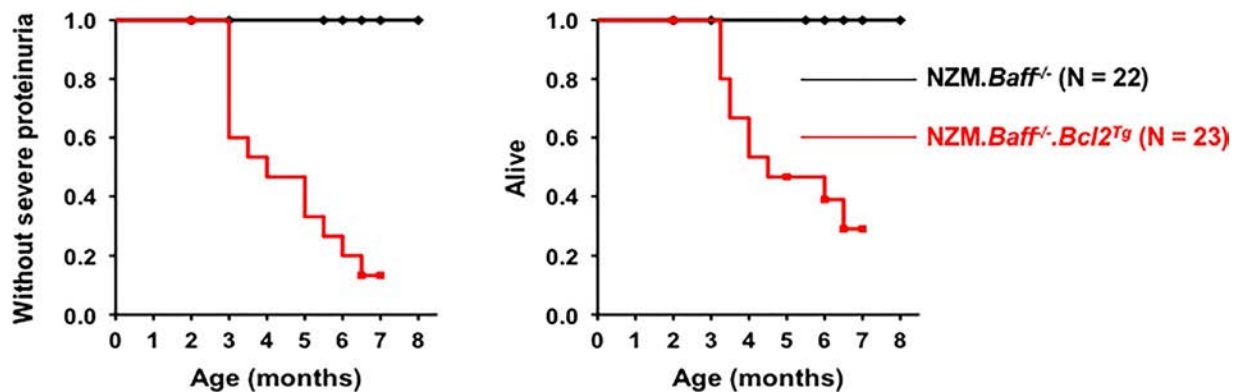
Figure 5. Clinical disease. NZM.*Baff*$^{-/-}$ mie (n = 22) and NZM.*Baff*$^{-/-}$.*Bcl2*^{Tg} mice (n = 23) were monitored up to age 8 months for the development of severe proteinuria (left) and survival (right). Data are plotted as the fraction of mice over time that did not develop severe proteinuria or that remained alive. Diamonds and squares indicate censored data. Color figure can be viewed in the online issue, which is available at http://onlinelibrary.wiley.com/doi/10.1002/art.41097/abstract.

NZM.*Baff*$^{-/-}$.*Bcl2*^{Tg} mice examined at ages 5–7 months was at least as robust as that in age-matched NZM WT mice. In contrast, glomerular deposition of IgG in NZM.*Baff*$^{-/-}$ mice was considerably weaker, with such deposition not being detectable in 4 of the 12 mice examined at ages 5.5–8 months and being only weakly detectable in 6 of these mice. Moreover, no glomerular deposition of C3 was detected in any of these 12 NZM.*Baff*$^{-/-}$ mice (Figures 4g–l).

Renal histopathologic features. When mice were examined for renal histopathologic features at age 2 months, occasional interstitial/perivascular infiltrates were observed in a minority of the NZM.*Baff*$^{-/-}$.*Bcl2*^{Tg} mice. No such infiltrates were appreciable in NZM.*Baff*$^{-/-}$ littermate mice or in age-matched control NZM WT mice. Glomeruli appeared normal in all 2-month-old mice studied, including NZM.*Baff*$^{-/-}$.*Bcl2*^{Tg} mice (Figures 4m–r).

In contrast, marked glomerular swelling and hypercellularity, along with widespread interstitial/perivascular infiltrates, were the rule in NZM.*Baff*$^{-/-}$.*Bcl2*^{Tg} mice by age 5 months. These pathologic changes were at least as severe as those in 7-month-old NZM WT mice. Conversely, evaluation of kidney sections from NZM.*Baff*$^{-/-}$ mice as old as age 8 months revealed no appreciable histologic disease (Figures 4s–x).

Clinical disease. We have previously shown that NZM WT mice start to develop severe proteinuria at ages 5–6 months, with 50% of the mice being affected by age 7 months and ≥90% being affected by age 10 months. In contrast, development of severe proteinuria in NZM.*Baff*$^{-/-}$ mice is markedly attenuated, with no mice being affected at age 8 months, and only 20% being affected by age 12 months (11). Consistent with this latter observation, NZM.*Baff*$^{-/-}$ mice in the present study failed to manifest severe proteinuria by age 8 months (the oldest age at which the mice were euthanized). In sharp contrast, development of severe

proteinuria among NZM.*Baff*$^{-/-}$.*Bcl2*^{Tg} mice was appreciable as early as age 3 months, with 50% of the mice being affected by age 4 months (*P* < 0.001 in comparison to NZM.*Baff*$^{-/-}$ mice) (Figure 5).

Mortality patterns paralleled the proteinuria patterns. We previously reported that NZM WT mice begin dying at age 6 months, with 50% dying at ages 7–8 months and 90% dying at ages 10–11 months, whereas all NZM.*Baff*$^{-/-}$ mice remained alive at age 9 months, with only 10% dying at age 12 months (11). In the present study, all NZM.*Baff*$^{-/-}$ mice remained alive through age 8 months, whereas NZM.*Baff*$^{-/-}$.*Bcl2*^{Tg} mice died as early as age 3 months, with 50% dying at age 4.5 months (Figure 5). In other words, full-blown (accelerated) SLE-like clinical disease developed even in the life-long absence of BAFF.

Relative decrease in Treg cell numbers in NZM.*Baff*$^{-/-}$.*Bcl2*^{Tg} mice. Given the importance of Treg cells to immune homeostasis and the prevention of autoimmunity in general (32) and the suppression of SLE specifically (33), the accelerated onset of disease in NZM.*Baff*$^{-/-}$.*Bcl2*^{Tg} mice raised the possibility that Treg cell numbers and/or function were altered in NZM.*Baff*$^{-/-}$.*Bcl2*^{Tg} mice relative to that in NZM WT mice. To address this possibility, we generated NZM WT and NZM.*Baff*$^{-/-}$.*Bcl2*^{Tg} mice that bore a *Foxp3-gfp* knockin genotype (NZM$^{foxp3-gfp}$ and NZM$^{foxp3-gfp}$.*Baff*$^{-/-}$.*Bcl2*^{Tg} mice, respectively), thereby permitting not only identification of Foxp3+ (Treg) cells but also elucidation of their functional capacities.

As observed with NZM WT and NZM.*Baff*$^{-/-}$.*Bcl2*^{Tg} mice not bearing the *Foxp3-gfp* knockin genotype, B cells (CD19+) were greatly expanded in NZM$^{foxp3-gfp}$.*Baff*$^{-/-}$.*Bcl2*^{Tg} mice relative to that in NZM$^{foxp3-gfp}$ mice (see Supplementary Figure 1A, available on the *Arthritis & Rheumatology* web site at http://onlinelibrary.wiley.com/doi/10.1002/art.41097/abstract). In contrast, these mice harbored similar numbers of CD3+ cells, CD4+, and Foxp3+ cells. Whereas the slopes of the regression lines for Foxp3+ cells compared to CD3+ cells and for Foxp3+ cells compared to CD4+ cells
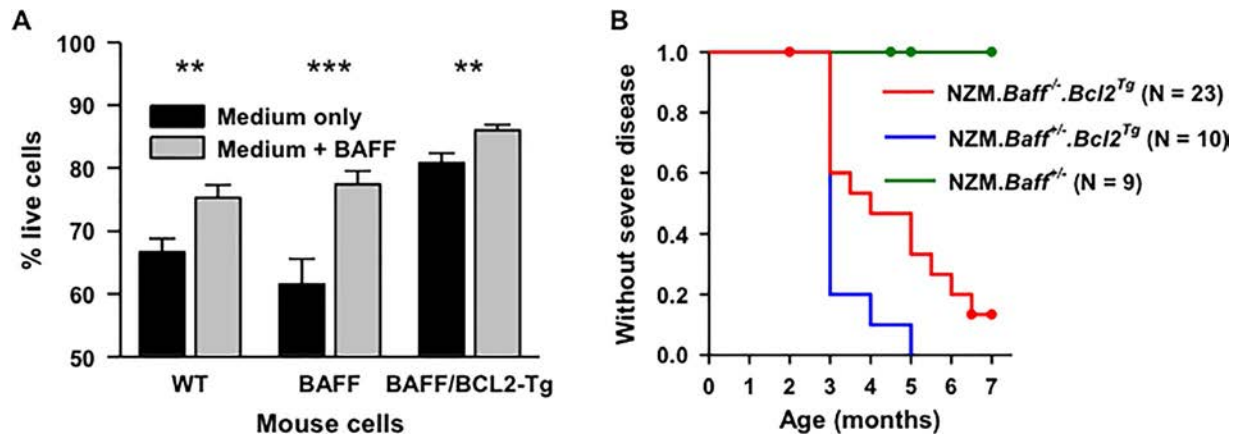
Figure 6. Responsiveness of NZM.*Baff*$^{-/-}$.*Bcl2*^{Tg} mice to BAFF. **A**, Spleen B cells from from NZM 2328 wild-type (WT), NZM.*Baff*$^{-/-}$, and NZM.*Baff*$^{-/-}$.*Bcl2*^{Tg} mice were cultured in medium only or in medium along with exogenous recombinant BAFF (100 ng/ml), and viability of the cells was determined at 48 hours by identifying those cells that did not stain with annexin V and propidium iodide. Results are the mean ± SD percentage of live cells from a representative experiment. ** = $P \leq 0.01$; *** = $P \leq 0.005$. **B**, NZM.*Baff*$^{-/-}$.*Bcl2*^{Tg} mice (n = 23), NZM.*Baff*$^{+/-}$.*Bcl2*^{Tg} mice (n = 10), and NZM.*Baff*$^{+/-}$ mice (n = 9) were monitored up to age 8 months for the development of severe clinical disease (severe proteinuria or death). Data are plotted as the fraction of mice over time that did not develop severe clinical disease. Circles indicate censored data. Color figure can be viewed in the online issue, which is available at http://onlinelibrary.wiley.com/doi/10.1002/art.41097/abstract.

were close in NZM$^{foxp3-gfp}$ and NZM$^{foxp3-gfp}$.*Baff*$^{-/-}$.*Bcl2*^{Tg} mice (0.057 versus 0.116, respectively and 0.086 versus 0.110, respectively), the slope for Foxp3+ cells compared to CD19+ cells was much shallower in NZM$^{foxp3-gfp}$.*Baff*$^{-/-}$.*Bcl2*^{Tg} mice than in NZM$^{foxp3-gfp}$ mice (0.0185 versus 0.0779) (see Supplementary Figure 1B [http://online library.wiley.com/doi/10.1002/art.41097/abstract]), pointing to a relative inability of NZM$^{foxp3-gfp}$.*Baff*$^{-/-}$.*Bcl2*^{Tg} mice to generate Treg cells in response to the degree of B cell expansion.

To determine whether Treg cell function was also altered in NZM$^{foxp3-gfp}$.*Baff*$^{-/-}$.*Bcl2*^{Tg} mice, we tested Treg cells from NZM$^{foxp3-gfp}$ and NZM$^{foxp3-gfp}$.*Baff*$^{-/-}$.*Bcl2*^{Tg} mice for in vitro suppressor activity against NZM$^{foxp3-gfp}$ WT mouse T responder cells. Regardless of whether suppression was assessed according to the DI, PI, or percentage of cells that underwent division, the in vitro suppressor activity of NZM$^{foxp3-gfp}$.*Baff*$^{-/-}$.*Bcl2*^{Tg} mouse Treg cells was virtually identical to that exhibited by NZM$^{foxp3-gfp}$ WT mouse Treg cells (see Supplementary Figure 1C [http://online library.wiley.com/doi/10.1002/art.41097/abstract]).

Sensitivity of NZM.*Baff*$^{-/-}$.*Bcl2*^{Tg} mice to restoration of BAFF. The fact that full-blown (accelerated) SLE-like clinical disease developed in BAFF-deficient NZM.*Baff*$^{-/-}$.*Bcl2*^{Tg} mice raised the possibility that the disease in these mice might be insensitive to BAFF; that is, the constitutive overexpression of Bcl-2 in the B cells of these mice may have maximally stimulated their inherent autoimmune diathesis and rendered them unresponsive to further BAFF-generated "autoimmunogenic" signals.

To determine whether B cells from NZM.*Baff*$^{-/-}$.*Bcl2*^{Tg} mice remained responsive to BAFF, we cultured B cells from NZM WT, NZM.*Baff*$^{-/-}$, and NZM.*Baff*$^{-/-}$.*Bcl2*^{Tg} mice in the absence or presence of exogenous BAFF. In all cases, survival of B cells was

enhanced when BAFF was added to the cultures (Figure 6A). Not surprisingly, survival of B cells from NZM.*Baff*$^{-/-}$.*Bcl2*^{Tg} mice, by virtue of their overexpression of Bcl-2, was greater than that of B cells from either NZM WT or NZM.*Baff*$^{-/-}$ mice regardless of whether or not exogenous BAFF was present.

To establish that restoration of BAFF to NZM.*Baff*$^{-/-}$.*Bcl2*^{Tg} mice would also have an in vivo effect, these mice were mated to BAFF-sufficient NZM WT (*Baff*$^{+/+}$) mice. All resulting offspring were genetically *Baff*$^{+/-}$, with each pup having a 50% chance of bearing the *BCL2* Tg.

Ten NZM.*Baff*$^{+/-}$.*Bcl2*^{Tg} mice and 9 littermate non-Tg NZM.*Baff*$^{+/-}$ mice were generated. In stark contrast to non-Tg NZM.*Baff*$^{+/-}$ mice that remained clinically healthy for their entire 8-month observation period, NZM.*Baff*$^{+/-}$.*Bcl2*^{Tg} mice developed clinical disease very quickly. Eight NZM.*Baff*$^{+/-}$.*Bcl2*^{Tg} mice were either dead or moribund by age 3 months, and the other 2 mice succumbed by age 4 months and age 5 months, respectively ($P < 0.001$ in comparison to non-Tg NZM.*Baff*$^{+/-}$ mice). Importantly, development of clinical disease in NZM.*Baff*$^{+/-}$.*Bcl2*^{Tg} mice was more robust than that in NZM.*Baff*$^{-/-}$.*Bcl2*^{Tg} mice, in that only 40% of the latter had developed severe clinical disease by age 3 months, of which 13% continued to remain free of severe proteinuria even at age 6.5 months ($P = 0.02$) (Figure 6B).

DISCUSSION

Not only does pharmacologic neutralization of BAFF or its genetic elimination effectively treat "natural" SLE in SLE-prone mice (9–11), but also their life-long deficiency of BAFF protects against the development of interferon-α (IFNα)–accelerated disease (2), and short-term neutralization of BAFF with TACI-Ig at the time of

IFNα challenge delays IFNα-accelerated disease (34). Thus, even the explosive disease promoted by IFNα is highly sensitive to BAFF elimination/neutralization. Notwithstanding this profound sensitivity of SLE disease to loss of BAFF, we have herein documented that full-blown SLE can develop in a BAFF-deficient SLE-prone host in which B survival is not critically dependent on BAFF.

Given that NZM.$Baff^{-/-}$.$Bcl2^{Tg}$ mice harbor more B cells, plasma cells, and activated CD4+ T cells than do NZM WT mice, it may not be surprising that development of serologic autoimmunity, renal immunopathologic features, and clinical disease is accelerated in these mice compared to that in BAFF-sufficient NZM WT mice. The blunted expansion of Treg cells relative to the degree of B cell expansion in NZM.$Baff^{-/-}$.$Bcl2^{Tg}$ mice as compared to that in NZM WT mice, consistent with a role for BAFF in promoting Treg cells (35), may be a contributing factor. B cell expansion may be more limited (and, hence, disease onset may be delayed) in NZM WT mice compared to NZM.$Baff^{-/-}$.$Bcl2^{Tg}$ mice, due to the relative abundance of Treg cells in NZM WT mice. In any case, the early expansions of B cells, recently activated CD4+ T cells, and activated memory CD4+ T cells in NZM.$Baff^{-/-}$.$Bcl2^{Tg}$ mice parallel similar expansions in other genetically modified NZM mice that develop accelerated disease, including NZM mice doubly deficient in both tumor necrosis factor receptors, NZM mice doubly deficient in the BAFF receptors BCMA and TACI, and NZM mice deficient in neutrophil cytosolic factor 2 (36–38).

Although our studies do not address the critical quantitative threshold for B cells, plasma cells, and/or activated CD4+ T cells needed for BAFF-independent disease, our studies do raise the plausibility of SLE patients maintaining such threshold levels despite treatment with a BAFF antagonist and, thereby, remaining resistant to BAFF antagonist therapy. BAFF is certainly not the only clinically relevant B cell survival factor, as evidenced by the persistence of substantial numbers of circulating B cells in SLE patients treated with the BAFF antagonists belimumab (12), blisibimod (13), atacicept (14), or tabalumab (15,16). Activities of such non-BAFF B cell survival factors (not neutralized by belimumab) may help explain why ≥39% of SLE patients failed to achieve the predefined clinical response in each of the successful phase III belimumab trials (17–20).

One factor that may importantly contribute to B cell survival in SLE is Bcl-2. Bcl-2 is up-regulated in B cells (and T cells) that infiltrate the tubulointerstitium in human SLE nephritis, and the Bcl-2 inhibitor venetoclax (previously known as ABT-199) prolonged survival and prevented proteinuria and development of tubulointerstitial inflammation in the (NZB × NZW)F1 mouse SLE model (39). The relationship between the degree of up-regulation of Bcl-2 and clinical responsiveness to a BAFF antagonist (i.e., belimumab) in human SLE remains unknown and should be assessed. Of note, acceptable safety and tolerability of venetoclax has been documented in a phase I trial in human SLE (40). Given that restoration of BAFF to NZM.$Baff^{-/-}$.$Bcl2^{Tg}$ mice results in further aggravation of disease, the addition of a Bcl-2 inhibitor might be a useful therapeutic option, especially in SLE patients who are clinically unresponsive to BAFF antagonism.

It must be stressed that the clinical efficacy seen with BAFF antagonists may not solely be attributable to their effects on B cells. In both murine and human SLE, the reduction in B cells following treatment with anti-CD20 mAb is much greater than that following treatment with BAFF antagonists (41–45). However, despite good clinical efficacy with this approach in murine SLE, the 2 phase II/phase III SLE trials with the anti-CD20 mAb rituximab failed to achieve their primary end points (44,45), and the phase III SLE trial with the anti-CD20 mAb ocrelizumab also did not meet its end point (46).

Given that greater levels of B cell depletion do not necessarily translate into better clinical responses, it is possible that the (variable) success of BAFF antagonists in their clinical trials versus the failure of anti-CD20 mAb in their clinical trials may, at least in part, be related to non–B cells. Whereas CD20 (the target of anti-CD20 mAb) is expressed only on B cells (47), BAFF receptors (the targets of BAFF) are expressed not only on B cells but also (weakly) on certain non–B cells as well (48–52). Indeed, we recently demonstrated that BAFF has a B cell–independent effect in experimental autoimmune encephalomyelitis (53), and therefore BAFF may be contributing to SLE not only through its agonist effects on B cells but also through its effects on non–B cells as well. In any case, the present study demonstrates in the NZM murine SLE model that, regardless of the putative non–B cell–mediated contribution of BAFF to SLE, BAFF is a dispensable factor in the processes of disease development as long as B cell survival is preserved via a BAFF-independent pathway. Importantly, the BAFF-independent disease that develops in NZM.$Baff^{-/-}$.$Bcl2^{Tg}$ mice is aggravated by reintroduction of BAFF, thereby showing that SLE disease can be effected via BAFF-independent and BAFF-dependent pathways in the same host.

To our knowledge, NZM.$Baff^{-/-}$.$Bcl2^{Tg}$ mice represent the first and only mouse model of SLE that is fully independent of BAFF. Whereas a large percentage of SLE patients do not clinically respond to BAFF antagonist therapy (13,15–19,21,23), thereby pointing to a substantial BAFF-independent component to human SLE, the clinical responses to BAFF neutralization or elimination are highly robust among commonly utilized murine SLE models (9–11), thereby pointing to a very limited (if any) BAFF-independent component in these models. NZM.$Baff^{-/-}$.$Bcl2^{Tg}$ mice could therefore serve as a valuable model in the investigation of the in vivo BAFF-independent component to SLE.

AUTHOR CONTRIBUTIONS

takes responsibility for the integrity of the data and the accuracy of the data analysis.

Study conception and design. Stohl.

Acquisition of data. Stohl, Yu, Chalmers.

Analysis and interpretation of data. Stohl, Yu, Putterman, Jacob.

REFERENCES

1. Shlomchik MJ, Madaio MP, Ni DH, Trounstein M, Huszar D. The role of B cells in lpr/lpr-induced autoimmunity. J Exp Med 1994;180:1295–306.

2. Jacob N, Guo SH, Mathian A, Koss MN, Gindea S, Putterman C, et al. B cell and BAFF dependence of IFN-α-exaggerated disease in systemic lupus erythematosus-prone NZM 2328 mice. J Immunol 2011;186:4984–93.

3. Thompson JS, Schneider P, Kalled SL, Wang L, Lefevre EA, Cachero TG, et al. BAFF binds to the tumor necrosis factor receptor-like molecule B cell maturation antigen and is important for maintaining the peripheral B cell population. J Exp Med 2000;192:129–35.

4. Do RK, Hatada E, Lee H, Tourigny MR, Hilbert D, Chen-Kiang S. Attenuation of apoptosis underlies B lymphocyte stimulator enhancement of humoral immune response. J Exp Med 2000;192:953–64.

5. Rolink AG, Tschopp J, Schneider P, Melchers F. BAFF is a survival and maturation factor for mouse B cells. Eur J Immunol 2002;32:2004–10.

6. Litinskiy MB, Nardelli B, Hilbert DM, He B, Schaffer A, Casali P, et al. DCs induce CD40-independent immunoglobulin class switching through BLyS and APRIL. Nat Immunol 2002;3:822–9.

7. Gross JA, Dillon SR, Mudri S, Johnston J, Littau A, Roque R, et al. TACI-Ig neutralizes molecules critical for B cell development and autoimmune disease: impaired B cell maturation in mice lacking BLyS. Immunity 2001;15:289–302.

8. Schiemann B, Gommerman JL, Vora K, Cachero TG, Shulga-Morskaya S, Dobles M, et al. An essential role for BAFF in the normal development of B cells through a BCMA-independent pathway. Science 2001;293:2111–4.

9. Gross JA, Johnston J, Mudri S, Enselman R, Dillon SR, Madden K, et al. TACI and BCMA are receptors for a TNF homologue implicated in B-cell autoimmune disease. Nature 2000;404:995–9.

10. Ramanujam M, Wang XB, Huang W, Liu Z, Schiffer L, Tao H, et al. Similarities and differences between selective and nonselective BAFF blockade in murine SLE. J Clin Invest 2006;116:724–34.

11. Jacob CO, Pricop L, Putterman C, Koss MN, Liu Y, Kollaros M, et al. Paucity of clinical disease despite serological autoimmunity and kidney pathology in lupus-prone New Zealand mixed 2328 mice deficient in BAFF. J Immunol 2006;177:2671–80.

12. Stohl W, Hiepe F, Latinis KM, Thomas M, Scheinberg MA, Clarke A, et al. Belimumab reduces autoantibodies, normalizes low complement levels, and reduces select B cell populations in patients with systemic lupus erythematosus. Arthritis Rheum 2012;64:2328–37.

13. Furie RA, Leon G, Thomas M, Petri MA, Chu AD, Hislop C, et al. A phase 2, randomised, placebo-controlled clinical trial of blisibimod, an inhibitor of B cell activating factor, in patients with moderate-to-severe systemic lupus erythematosus, the PEARL-SC study. Ann Rheum Dis 2015;74:1667–75.

14. Dall'Era M, Chakravarty E, Wallace D, Genovese M, Weisman M, Kavanaugh A, et al, and the Merck Serono and ZymoGenetics Atacicept Study Group. Reduced B lymphocyte and immunoglobulin levels after atacicept treatment in patients with systemic lupus erythematosus: results of a multicenter, phase Ib, double-blind, placebo-controlled, dose-escalating trial. Arthritis Rheum 2007;56:4142–50.

15. Isenberg DA, Petri M, Kalunian K, Tanaka Y, Urowitz MB, Hoffman RW, et al. Efficacy and safety of subcutaneous tabalumab in patients with systemic lupus erythematosus: results from ILLUMINATE-1, a 52-week, phase III, multicentre, randomised, double-blind, placebo-controlled study. Ann Rheum Dis 2016;75:323–31.

16. Merrill JT, van Vollenhoven RF, Buyon JP, Furie RA, Stohl W, Morgan-Cox M, et al. Efficacy and safety of subcutaneous tabalumab, a monoclonal antibody to B-cell activating factor, in patients with systemic lupus erythematosus: results from ILLUMINATE-2, a 52-week, phase III, multicentre, randomised, double-blind, placebo-controlled study. Ann Rheum Dis 2016;75:332–40.

17. Navarra SV, Guzmán RM, Gallacher AE, Hall S, Levy RA, Jimenez RE, et al, for the BLISS-52 Study Group. Efficacy and safety of belimumab in patients with active systemic lupus erythematosus: a randomised, placebo-controlled, phase 3 trial. Lancet 2011;377:721–31.

18. Furie R, Petri M, Zamani O, Cervera R, Wallace DJ, Tegzová D, et al. A phase III, randomized, placebo-controlled study of belimumab, a monoclonal antibody that inhibits B lymphocyte stimulator, in patients with systemic lupus erythematosus. Arthritis Rheum 2011;63:3918–30.

19. Stohl W, Schwarting A, Okada M, Scheinberg M, Doria A, Hammer AE, et al. Efficacy and safety of subcutaneous belimumab in systemic lupus erythematosus: a fifty-two–week randomized, double-blind, placebo-controlled study. Arthritis Rheumatol 2017;69:1016–27.

20. Zhang FC, Bae SC, Bass D, Chu M, Egginton S, Gordon D, et al. A pivotal phase III, randomised, placebo-controlled study of belimumab in patients with systemic lupus erythematosus located in China, Japan and South Korea. Ann Rheum Dis 2018;77:355–63.

21. Isenberg D, Gordon C, Licu D, Copt S, Rossi CP, Wofsy D. Efficacy and safety of atacicept for prevention of flares in patients with moderate-to-severe systemic lupus erythematosus (SLE): 52-week data (APRIL-SLE randomised trial). Ann Rheum Dis 2015;74:2006–15.

22. Stohl W, Hilbert DM. The discovery and development of belimumab: the anti-BLyS–lupus connection. Nat Biotechnol 2012;30:69–77.

23. Wallace DJ, Stohl W, Furie RA, Lisse JR, McKay JD, Merrill JT, et al. A phase II, randomized, double-blind, placebo-controlled, dose-ranging study of belimumab in patients with active systemic lupus erythematosus. Arthritis Rheum 2009;6:1168–78.

24. Tardivel A, Tinel A, Lens S, Steiner QG, Sauberli E, Wilson A, et al. The anti-apoptotic factor Bcl-2 can functionally substitute for the B cell survival but not for the marginal zone B cell differentiation activity of BAFF. Eur J Immunol 2004;34:509–18.

25. Sasaki Y, Casola S, Kutok JL, Rajewsky K, Schmidt-Supprian M. TNF family member B cell-activating factor (BAFF) receptor-dependent and -independent roles for BAFF in B cell physiology. J Immunol 2004;173:2245–52.

26. Strasser A, Whittingham S, Vaux DL, Bath ML, Adams JM, Cory S, et al. Enforced BCL2 expression in B-lymphoid cells prolongs antibody responses and elicits autoimmune disease. Proc Natl Acad Sci U S A 1991;88:8661–5.

27. Morel L, Yu Y, Blenman KR, Caldwell RA, Wakeland EK. Production of congenic mouse strains carrying genomic intervals containing SLE-susceptibility genes derived from the SLE-prone NZM2410 strain. Mamm Genome 1996;7:335–9.

28. Markel P, Shu P, Ebeling C, Carlson GA, Nagle DL, Smutko JS, et al. Theoretical and empirical issues for marker-assisted breeding of congenic mouse strains. Nat Genet 1997;17:280–4.

29. Waters ST, Fu SM, Gaskin F, Deshmukh US, Sung SS, Kannapell CC, et al. NZM2328: a new mouse model of systemic lupus erythematosus with unique genetic susceptibility loci. Clin Immunol 2001;100:372–83.

30. Jacob CO, Guo SH, Jacob N, Pawar RD, Putterman C, Quinn WJ III, et al. Dispensability of APRIL to the development of systemic lupus erythematosus in NZM 2328 mice. Arthritis Rheum 2012;64:1610–9.

31. Mackay F, Woodcock SA, Lawton P, Ambrose C, Baetscher M, Schneider P, et al. Mice transgenic for BAFF develop lymphocytic disorders along with autoimmune manifestations. J Exp Med 1999;190:1697–710.

32. Kim JM, Rasmussen JP, Rudensky AY. Regulatory T cells prevent catastrophic autoimmunity throughout the lifespan of mice. Nat Immunol 2007;8:191–7.

33. Scalapino KJ, Tang Q, Bluestone JA, Bonyhadi ML, Daikh DI. Suppression of disease in New Zealand Black/New Zealand White lupus-prone mice by adoptive transfer of ex vivo expanded regulatory T cells. J Immunol 2006;177:1451–9.

34. Liu Z, Bethunaickan R, Huang W, Ramanujam M, Madaio MP, Davidson A. IFN-α confers resistance of systemic lupus erythematosus nephritis to therapy in NZB/W F1 mice. J Immunol 2011;187:1506–13.

35. Walters S, Webster KE, Sutherland A, Gardam S, Groom J, Liuwantara D, et al. Increased CD4+Foxp3+ T cells in BAFF-transgenic mice suppress T cell effector responses. J Immunol 2009;182:793–801.

36. Jacob N, Yang HT, Pricop L, Liu Y, Gao X, Zheng SG, et al. Accelerated pathological and clinical nephritis in systemic lupus erythematosus-prone New Zealand Mixed 2328 mice doubly deficient in TNF receptor 1 and TNF receptor 2 via a Th17-associated pathway. J Immunol 2009;182:2532–41.

37. Jacob CO, Yu N, Sindhava V, Cancro MP, Pawar RD, Putterman C, et al. Differential development of systemic lupus erythematosus in NZM 2328 mice deficient in discrete pairs of BAFF receptors. Arthritis Rheumatol 2015;67:2523–35.

38. Jacob CO, Yu N, Yoo DG, Perez-Zapata LJ, Barbu EA, Kaplan MJ, et al. Haploinsufficiency of NADPH oxidase subunit neutrophil cytosolic factor 2 is sufficient to accelerate full-blown lupus in NZM 2328 mice. Arthritis Rheumatol 2017;69:1647–60.

39. Ko K, Wang J, Perper S, Jiang YL, Yanez D, Kaverina N, et al. Bcl-2 as a therapeutic target in human tubulointerstitial inflammation. Arthritis Rheumatol 2016;68:2740–51.

40. Lu P, Fleischmann R, Curtis C, Ignatenko S, Clarke SH, Desai M, et al. Safety and pharmacodynamics of venetoclax (ABT-199) in a randomized single and multiple ascending dose study in women with systemic lupus erythematosus. Lupus 2018;27:290–302.

41. Ahuja A, Shupe J, Dunn R, Kashgarian M, Kehry MR, Shlomchik MJ. Depletion of B cells in murine lupus: efficacy and resistance. J Immunol 2007;179:3351–61.

42. Bekar KW, Owen T, Dunn R, Ichikawa T, Wang W, Wang R, et al. Prolonged effects of short-term anti-CD20 B cell depletion therapy in murine systemic lupus erythematosus. Arthritis Rheum 2010;62:2443–57.

43. Lin W, Seshasayee D, Lee WP, Caplazi P, McVay S, Suto E, et al. Dual B cell immunotherapy is superior to individual anti-CD20 depletion or BAFF blockade in murine models of spontaneous or accelerated lupus. Arthritis Rheumatol 2015;67:215–24.

44. Merrill JT, Neuwelt CM, Wallace DJ, Shanahan JC, Latinis KM, Oates JC, et al. Efficacy and safety of rituximab in moderately-to-severely active systemic lupus erythematosus: the randomized, double-blind, phase II/III systemic lupus erythematosus evaluation of rituximab trial. Arthritis Rheum 2010;62:222–33.

45. Rovin BH, Furie R, Latinis K, Looney RJ, Fervenza FC, Sanchez-Guerrero J, et al, for the LUNAR Investigator Group. Efficacy and safety of rituximab in patients with active proliferative lupus nephritis: the Lupus Nephritis Assessment with Rituximab study. Arthritis Rheum 2012;64:1215–26.

46. Mysler EF, Spindler AJ, Guzman R, Bijl M, Jayne D, Furie RA, et al. Efficacy and safety of ocrelizumab in active proliferative lupus nephritis: results from a randomized, double-blind, phase III study. Arthritis Rheum 2013;65:2368–79.

47. Reff ME, Carner K, Chambers KS, Chinn PC, Leonard JE, Raab R, et al. Depletion of B cells in vivo by a chimeric mouse human monoclonal antibody to CD20. Blood 1994;83:435–45.

48. Laabi Y, Gras MP, Brouet JC, Berger R, Larsen CJ, Tsapis A. The BCMA gene, preferentially expressed during B lymphoid maturation, is bidirectionally transcribed. Nucleic Acids Res 1994;22:1147–54.

49. Von Bülow GU, Bram RJ. NF-AT activation induced by a CAML-interacting member of the tumor necrosis factor receptor superfamily. Science 1997;278:138–41.

50. Thompson JS, Bixler SA, Qian F, Vora K, Scott ML, Cachero TG, et al. BAFF-R, a newly identified TNF receptor that specifically interacts with BAFF. Science 2001;293:2108–11.

51. Chang SK, Mihalcik SA, Jelinek DF. B lymphocyte stimulator regulates adaptive immune responses by directly promoting dendritic cell maturation. J Immunol 2008;180:7394–403.

52. Chang SK, Arendt BK, Darce JR, Wu X, Jelinek DF. A role for BLyS in the activation of innate immune cells. Blood 2006;108:2687–94.

53. Stohl W, Banfalvi A. B cell-independent contribution of BAFF to murine autoimmune disease. Clin Immunol 2016;172:111–6.

AMERICAN COLLEGE
of RHEUMATOLOGY
Empowering Rheumatology Professionals

Targeting Mechanistic Target of Rapamycin Complex 1 Restricts Proinflammatory T Cell Differentiation and Ameliorates Takayasu Arteritis

Jifeng Zhang,[1] Lei Zhao,[2] Jing Wang,[3] Zhihua Cheng,[4] Mengyao Sun,[4] Jiayi Zhao,[5] Bin Liu,[2] Xiyu Liu,[6] Zhenke Wen,[7] (ID) and Zhibo Li[2] (ID)

Objective. Takayasu arteritis (TAK) is a progressive autoimmune large vessel vasculitis with infiltration of proinflammatory T cells, with a largely unknown etiology. This study was undertaken to explore the involvement of mechanistic target of rapamycin (mTOR) in proinflammatory T cell differentiation and disease progression in TAK.

Methods. Ninety-five patients with TAK, 26 patients with small vessel vasculitis, and 40 healthy donors were enrolled. Naive and memory CD4+ T cells were activated with anti-CD3/CD28 beads and analyzed for lineage differentiation. The mTORC1 activity was determined by quantifying intracellular phospho–S6 kinase 1 and phospho–S6 ribosomal protein. Rapamycin and lentiviral regulatory-associated protein of mTOR short hairpin RNA were used to block mTORC1 activity. Human artery–NSG mouse chimeras representing human TAK were established for targeting mTORC1 in disease treatment.

Results. TAK CD4+ T cells were selectively prepositioned with hyperactivity of mTORC1 ($P < 0.001$), resulting in spontaneous maldifferentiation of Th1 and Th17 cells ($P < 0.001$). Activity of mTORC1^{high} in circulating CD4+ T cells predicted elevated frequencies of proinflammatory T cells and active disease in TAK patients ($P < 0.001$). Blockade of mTORC1 with rapamycin efficiently abrogated the maldifferentiation of Th1 and Th17 cells ($P < 0.01$) and ameliorated vasculitis in humanized TAK chimeras ($P < 0.001$). Inhibition of mTORC1 using RNA interference technology is sufficient to reduce proinflammatory T cell frequencies ($P < 0.01$) and restrict TAK disease progression in vivo ($P < 0.01$).

Conclusion. Our findings indicate that hyperactivity of mTORC1 is a critical cell-intrinsic mechanism underlying spontaneous maldifferentiation of proinflammatory T cells in TAK patients. Targeting mTORC1 is a promising therapeutic strategy against TAK.

INTRODUCTION

Takayasu arteritis (TAK) is a chronic and progressive autoimmune large vessel vasculitis that preferentially targets the aorta and its major branches (1,2). TAK can affect individuals of any ethnicity, but especially affects young Asian women. Its etiology is unknown (1,3). Patients with TAK have a high morbidity rate, and the 5-year incidence of death and vascular complication is nearly 50% among those with high-risk factors (progressive clinical course, thoracic aorta involvement, and retinopathy) (4). Half of all TAK patients will

experience a relapse and vascular complication within 10 years of disease diagnosis (4,5). Meanwhile, the first-line and mainstay treatment of TAK in clinical practice is restricted to nonspecific glucocorticoids (3,6). There are significant gaps between the understanding of disease pathogenesis and the development of therapies for TAK (6).

TAK is a granulomatous arteritis with inflammatory infiltrates composed of T cells and macrophages accumulated in the vessel wall, predominantly in the adventitial layer (2,7). Interleukin-6 (IL-6) and tumor necrosis factor (TNF) are involved in TAK disease progression, reflecting disease activity (8,9). Proinflammatory Th1

No potential conflicts of interest relevant to this article were reported.

Address correspondence to Xiyu Liu, MD, PhD, China-Japan Union Hospital of Jilin University, Department of Thoracic Surgery, Changchun, Jilin 130033, China (e-mail: xiyuliu_jlu@126.com); or to Zhenke Wen, MD, PhD, Soochow University, Institutes of Biology and Medical Sciences, Suzhou, Jiangsu 215123, China (e-mail: zkwen@suda.edu.cn); or to Zhibo Li, MD, PhD, Second Hospital of Jilin University, Department of Cardiovascular Medicine, Changchun, Jilin 130041, China (e-mail: zbli@vip.126.com).

and Th17 cells are dominant infiltrates in the vascular walls, producing interferon (IFN) and IL-17 to drive systemic and vascular manifestations of TAK (7,10,11). Accordingly, Th1 and Th17 cells are expanded in the circulation in TAK patients (10–12). Glucocorticoid treatment suppresses Th1 cytokines but spares Th17 cytokines in patients with TAK (10,13). Alternative therapies for clinical management of TAK are urgently needed. However, cell-intrinsic mechanisms underlying the differentiation of proinflammatory T cells in TAK patients are essentially unknown.

The mechanistic target of rapamycin (mTOR) is a conserved kinase that critically regulates cell differentiation, proliferation, and metabolism (14,15). It forms 2 distinct protein complexes, mTOR complex 1 (mTORC1) and mTORC2 (16). While mTORC1 contains the scaffolding protein regulatory-associated protein of mTOR (RAPTOR) and is sensitive to rapamycin, mTORC2 has another scaffolding protein, rapamycin-insensitive companion of mTOR (RICTOR) and is relatively resistant to rapamycin (17,18). Previous studies have pinpointed a crucial role of mTOR in determining T cell fate (15). For differentiation of Th1 and Th17 cells mTORC1 is critical, and mTORC2 controls the differentiation of Th2 cells (19,20). In patients with autoimmune inflammatory diseases such as rheumatoid arthritis (RA), blocking mTORC1 with rapamycin abrogates the maldifferentiation of proinflammatory Th1 and Th17 cells, reducing the number of synovial tissue resident inflammatory cells (21). Inhibition of mTORC1 also blocks the maldifferentiation of Th1 and Th17 cells in patients with giant cell arteritis (GCA) (19). These findings implicate mTORC1 in the proinflammatory T cell differentiation and disease progression of autoimmune inflammatory diseases.

In the present study, we explored the potential role of mTOR in the spontaneous differentiation of proinflammatory T cells in patients with TAK and evaluated the therapeutic strategy of targeting mTOR using a humanized model representing human TAK. We observed spontaneous maldifferentiation of CD4+ T cells into proinflammatory Th1 and Th17 cells in TAK patients under cytokine-unbiased conditions. This maldifferentiation was licensed by hyperactivity of mTORC1 in CD4+ T cells from TAK patients. In support of this notion, mTORC1 hyperactivity in circulating CD4+ T cells portended expanded proinflammatory T cells and active disease in TAK patients. Inhibition of mTORC1 using rapamycin and RNA interference (RNAi) strategy was sufficient to correct the maldifferentiation of TAK CD4+ T cells and to ameliorate the large vessel vasculitis mediated by immune cells from TAK patients in human artery–NSG mouse chimeras. These findings shed new light on the critical role of mTORC1 in disease progression in TAK patients and provide a novel therapeutic strategy for clinical practice.

MATERIALS AND METHODS

Patients and tissues. The study included 95 patients with TAK, 40 age-matched healthy controls, and 26 patients with the small vessel vasculitis granulomatosis with polyangiitis (GPA) as disease controls. The characteristics of the TAK patients and GPA patients are shown in Supplementary Table 1, available on the *Arthritis & Rheumatology* web site at http://onlinelibrary.wiley.com/doi/10.1002/art.41084/abstract. Human aortic arteries were obtained from patients undergoing aortic surgery. Informed consent was obtained from all participants, and experiments were approved by the Institutional Review Board of the Second Hospital of Jilin University.

Cell isolation and culture. Peripheral blood mononuclear cells (PBMCs) were isolated from healthy individuals and patients by density-gradient centrifugation using Lymphocyte Separation Medium (Corning). Naive and memory CD4+ T cells were purified from PBMCs using an EasySep human naive CD4+ T cell enrichment kit (StemCell Technologies) and Human Memory CD4+ T cell enrichment kit (StemCell Technologies), respectively. The purity of cell populations was consistently >95%. Cells were cultured in RPMI 1640 medium supplemented with 10% fetal bovine serum (ThermoFisher Scientific) plus penicillin—streptomycin–glutamine (ThermoFisher Scientific).

Reagents. The mTORC1 inhibitor rapamycin was purchased from Sigma-Aldrich. Human lentiviral RAPTOR short hairpin RNA (shRNA) and control shRNA were from Santa Cruz Biotechnology. A Human IL-6 Quantikine enzyme-linked immunosorbent assay (ELISA) kit and human TNF Quantikine ELISA kit were obtained from R&D Systems. All reagents were used according to the manufacturer's instructions.

Cell differentiation. CD4+ T cells were stimulated with anti-CD3/CD28 beads (cell-to-bead ratio 2:1; ThermoFisher Scientific) for 4 days, and the lineage-determining transcription factors T-bet, retinoic acid receptor–related orphan nuclear receptor (RORγt), and GATA-3 were then analyzed by flow cytometry. The intracellular cytokines IFNγ, IL-17, and IL-4 were detected in CD4+ T cells by flow cytometry on day 6 after activation with anti-CD3/CD28 beads.

Flow cytometric analysis. CD4+ T cells were fixed with Fix Buffer I (BD Biosciences), permeabilized with Perm Buffer III (BD Biosciences), and stained with the following antibodies: phycoerythrin (PE)–Cy7–conjugated anti-CD45 (clone 2D1; BioLegend), allophycocyanin (APC)–Cy7–conjugated anti-CD3 (clone HIT3a; BioLegend), fluorescein isothiocyanate (FITC)–conjugated anti-CD4 (clone OKT4; BioLegend), PE-conjugated anti–T-bet (clone eBio4B10; ThermoFisher Scientific), APC-conjugated anti-RORγt (clone AFKJS-9; ThermoFisher Scientific), Brilliant Violet 421–conjugated anti–GATA-3 (clone 16E10A23; BioLegend), PE-conjugated anti–phospho–S6 ribosomal protein (anti–phospho-S6RP; Ser[235/236]) (clone D57.2.2E; Cell Signaling), Alexa Fluor 647–conjugated anti–phospho–S6 kinase 1 (anti–phospho-S6K1) (catalog no. sc-377529; Santa Cruz Biotechnology), rabbit anti-RAPTOR

(catalog no. 42-4000; ThermoFisher Scientific) plus Pacific Blue–conjugated anti-rabbit IgG (catalog no. P-10994; ThermoFisher Scientific), and PE-conjugated anti–phospho-Akt (Ser[473]) (catalog no. 5315S; Cell Signaling Technology). For quantification of CD4+ T cells expressing IFNγ, IL-17, or IL-4, cells were pretreated with phorbol myristate acetate (PMA) (50 ng/ml; Tocris) and ionomycin (500 ng/ml; Tocris) plus brefeldin A (5 μg/ml; BioLegend) for 6 hours, fixed, permeabilized, and stained with FITC-conjugated anti-CD4 antibody (clone OKT4; BioLegend), PE-conjugated anti-IFNγ antibody (clone 4S.B3; BioLegend), APC-conjugated anti–IL-17 antibody (clone BL168; BioLegend), and PE–Cy7–conjugated anti-IL-4 antibody (clone MP4-25D2; BioLegend). Cells were stained for 45 minutes at 4°C. Flow cytometry was performed on an LSRII flow cytometer (BD Biosciences). All data were analyzed using FlowJo software (Tree Star).

Immunofluorescence. Expression of human CD3 and IFNγ protein in arterial tissue sections were detected by immunostaining as previously described (19,21). Briefly, frozen sections of arterial tissues were stained with mouse anti-human CD3 antibody (1:100) (clone SPV-T3b; ThermoFisher Scientific) and visualized with Alexa Fluor 594–conjugated anti-mouse IgG (1:200) (catalog no. A-11032; ThermoFisher Scientific). For some experiments, rabbit anti–human IFNγ antibody (1:50) (catalog no. ab9657; Abcam) and Alexa Fluor 488–conjugated anti-rabbit IgG (1:200) (catalog no. A-11034; ThermoFisher Scientific) were used to stain human IFNγ protein in the arterial tissue sections. Images for the stained sections were acquired using an LSM710 confocal microscope (Carl Zeiss) with a Plan neofluar oil objective lens (40×; 1.3 numerical aperture).

Histologic analysis and blinded scoring. Hematoxylin and eosin (H&E) staining of arterial tissue sections was performed using an H&E Stain Kit from Abcam. Adventitial inflammation was graded on a scale of 1–4, where 1 = rare, 2 = multifocal, 3 = coalescing, and 4 = diffuse (22), by a pathologist who was blinded with regard to test sample group.

Real-time polymerase chain reaction (PCR). RNA was extracted using an RNeasy Mini Kit (Qiagen). Complementary DNA (cDNA) was synthesized with a Maxima First Strand cDNA synthesis kit (ThermoFisher Scientific). Quantitative PCR was performed with SYBR Green qPCR Master Mix (ThermoFisher Scientific). Primers were used as previously described (19,21). Gene expression was normalized to 18S ribosomal RNA.

Humanized TAK model. Human artery–NSG mouse chimeras representing human TAK were generated by modifying previously described humanized GCA chimeras (19,23). NSG mice (Biocytogen) were housed in institutional pathogen-free animal facilities and used at the age of 8 weeks. To generate human artery–NSG mouse chimeras, human arterial pieces were engrafted into a subcutaneous pocket on the backs of NSG mice. Buprenorphine (0.125 mg/kg body weight) was used for postsurgical pain control. Human artery–NSG mouse chimeras were intraperitoneally injected with lipopolysaccharide (10 μg/mouse) (Sigma) on day 9 and reconstituted with PBMCs (15×10^6 cells/mouse) from patients with active TAK on day 10. PBMCs (15×10^6 cells/mouse) from healthy donors were injected into chimeras as a control. Chimeras implanted with arterial pieces from the same donor were randomly assigned to control and treatment groups. Chimeras were treated with rapamycin as previously described (21). For some experiments, TAK PBMCs were transfected with RAPTOR shRNA or control shRNA prior to the immune reconstitution of human artery–NSG mouse chimeras. Otherwise, CD4+ T cells were isolated from TAK PBMCs, transfected with RAPTOR shRNA or control shRNA, and injected into the chimeras together with the CD4+ T cell–depleted TAK PBMCs for immune reconstitution. The human arterial grafts were explanted on day 25 for the detection of vasculitis. All animal experiments were approved by the Animal Care and Use Committee of the Second Hospital of Jilin University.

Statistical analysis. Data are presented as the mean ± SEM. Student's t-test was used for comparisons between 2 groups as appropriate, followed by the Bonferroni method to adjust for multiple comparisons. Analysis of variance was used for comparison of more than 2 groups, and multiple comparisons were conducted with Tukey's method. Pearson's correlation analysis was used for testing correlations. Statistical analysis was performed using GraphPad Prism, version 8.0. P values less than 0.05 were considered significant.

RESULTS

Spontaneous maldifferentiation of proinflammatory T cells in TAK patients. To detect the spontaneous differentiation of Th1 and Th17 cells, naive CD4+ T cells from healthy individuals, TAK patients, and GPA patients were stimulated with anti-CD3/CD28 beads. Such naive CD4+ T cells were essentially negative for CD45RA– memory cells, CD45RA+CD95+ TSCM cells and CD45RA+CD28– TEMRA cells (Supplementary Figure 1, available on the *Arthritis & Rheumatology* web site at http://onlinelibrary.wiley.com/doi/10.1002/art.41084/abstract). Compared with healthy donors, naive CD4+ T cells from TAK patients showed multiple folds higher frequencies of T-bet– and RORγ-expressing T cells after activation (Figures 1A–C). Intracellular IFNγ and IL-17 were increased along with T-bet and RORγ in TAK CD4+ T cells (Figures 1A–F). Such maldifferentiations were selective for proinflammatory Th1 and Th17 cells, sparing GATA-3– and IL-4–expressing Th2 cells (Figures 1A–G). Of note, spontaneous
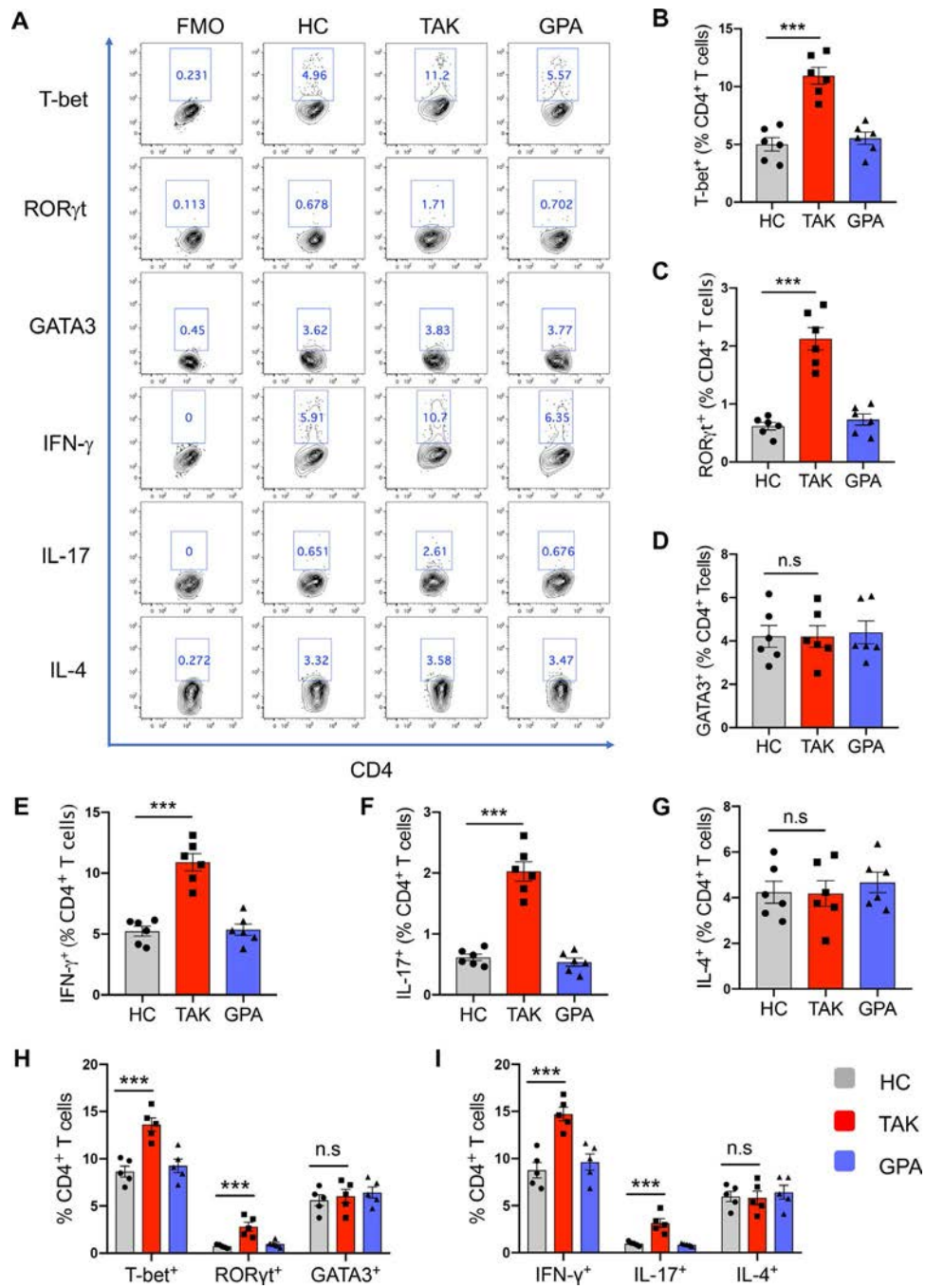
Figure 1. Maldifferentiation of proinflammatory T cells in patients with Takayasu arteritis (TAK). Naive CD4+ T cells or memory CD4+ T cells were isolated from healthy donors, patients with TAK, and patients with granulomatosis with polyangiitis (GPA) and stimulated with anti-CD3/CD28 beads. T cell lineage–determining transcription factors (T-bet, retinoic acid receptor–related orphan nuclear receptor γt [RORγt], and GATA-3) were analyzed on day 4, while intracellular cytokines (interferon-γ [IFNγ], interleukin-17 [IL-17], and IL-4) were detected on day 6. **A**, Proportion of naive CD4+ T cells positive for the indicated transcription factors or intracellular cytokines in healthy controls (HC), patients with TAK, and patients with GPA. Fluorescence Minus One (FMO) was used as a control. Representative results are shown. **B**–**G**, Proportion of naive CD4+ T cells positive for T-bet (**B**), RORγt (**C**), GATA-3 (**D**), IFNγ (**E**), IL-17 (**F**), and IL-4 (**G**) in healthy controls, patients with TAK, and patients with GPA. Bars show the mean ± SEM. Symbols represent individual subjects (n = 6 per group). **H** and **I**, Proportion of memory CD4+ T cells positive for T-bet, RORγt, and GATA-3 (**H**) and for IFNγ, IL-17, and IL-4 (**I**). Bars show the mean ± SEM. Symbols represent individual subjects (n = 5 per group). *** = $P < 0.001$ by analysis of variance with Tukey's test. NS = not significant.

maldifferentiation of Th1 and Th17 cells in TAK patients was not shared by patients with GPA (Figures 1A–G).

When memory CD4+ T cells were isolated from healthy donors, TAK patients, and GPA patients, stimulated with anti-CD3/CD28 beads, and evaluated for cell differentiation, we found results similar to those for naive CD4+ T cells. Memory CD4+ T cells from TAK patients showed higher expression of T-bet, IFNγ, RORγ, and IL-17 than those from healthy individuals and GPA patients, while GATA-3 and IL-4 expression in CD4 T cells were similar (Figures 1H and I). Thus, CD4+ T cells from TAK patients spontaneously differentiate into proinflammatory Th1 and Th17 cells, implicating CD4+ T cell–intrinsic abnormalities in driving TAK pathologic disease progression.

Hyperactivity of mTORC1 in CD4+ T cells from TAK patients. To evaluate mTORC1 activity in CD4+ T cells from TAK patients, naive CD4+ T cells were isolated from healthy donors, TAK patients, and GPA patients and stimulated with anti-CD3/CD28 beads for 3 days, and the levels of phospho-S6K1 and phospho-S6RP, 2 critical targets of mTORC1 signaling, were determined (Figures 2A–D). We found robust phospho-S6K1 and phospho-S6RP expression in TAK CD4+ T cells, while phospho-S6K1 and phospho-S6RP levels were similar and low in CD4+ T cells from healthy donors and GPA patients (Figures 2A–D).

Memory CD4+ T cells were isolated from healthy donors, TAK patients, and GPA patients and stimulated with anti-CD3/CD28 beads for 3 days, and mTORC1 activity was determined. CD4+ T cells from TAK patients also showed enhanced mTORC1 activity, expressing higher levels of phospho-S6K1 and phospho-S6RP (Figure 2E). Taken together, these findings show that CD4+ T cells from TAK patients exert mTORC1 hyperactivity compared with those from healthy donors and patients with small vessel vasculitis, suggesting cell-intrinsic reprogramming of the mTOR pathway in TAK CD4+ T cells.

The hyperactivity of mTOR in TAK CD4+ T cells was restricted to mTORC1. The activity of mTORC2 in TAK CD4+ T cells was indistinguishable from that in healthy and GPA CD4+ T cells (Supplementary Figure 2, available on the *Arthritis & Rheumatology* web site at http://onlinelibrary.wiley.com/doi/10.1002/art.41084/abstract). Expression of RICTOR messenger RNA (mRNA) and phospho-Akt (Ser[473]) protein were generally comparable in CD4+ T cells from TAK patients, GPA patients, and healthy individuals.

Hyperactivity of mTORC1 drives the maldifferentiation of proinflammatory T cells in TAK. To determine the function of mTORC1 hyperactivity in driving spontaneous maldifferentiation of proinflammatory T cells in TAK patients, naive CD4+ T cells were isolated and stimulated with anti-CD3/CD28 beads in the presence or absence of rapamycin. Administration of rapamycin efficiently abrogated the increased expression of
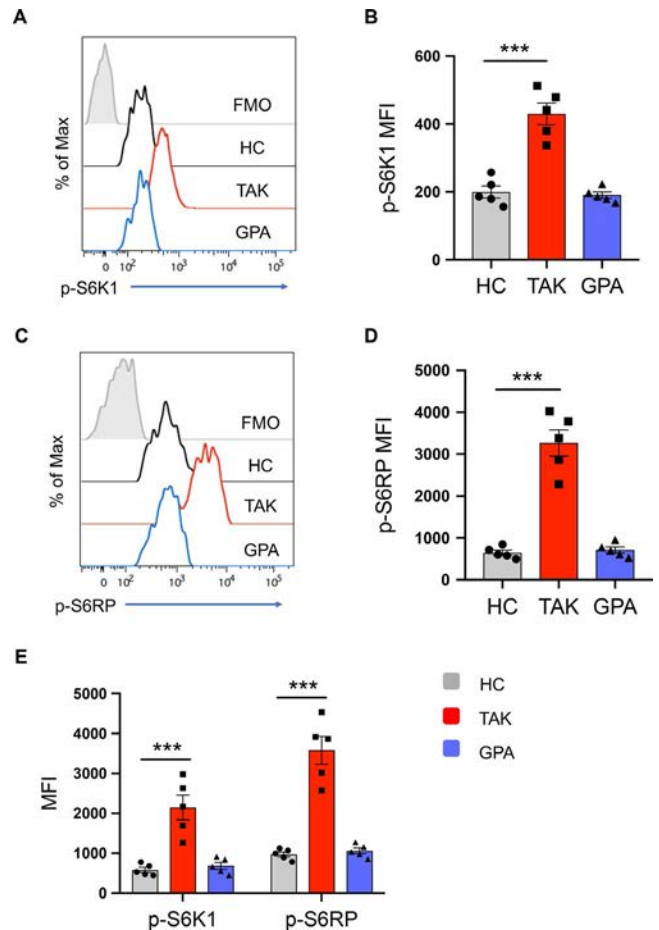
Figure 2. Hyperactivity of mechanistic target of rapamycin complex 1 in CD4+ T cells from patients with Takayasu arteritis (TAK). Naive CD4+ T cells or memory CD4+ T cells were isolated from healthy controls (HC), patients with TAK, and patients with granulomatosis with polyangiitis (GPA) and stimulated with anti-CD3/CD28 beads for 3 days. Phospho–S6 kinase 1 (phospho-S6K1) and phospho–S6 ribosomal protein (phospho-S6RP) levels were determined by flow cytometry. **A** and **C**, Results of flow cytometric analysis of phospho-S6K1 (**A**) and phospho-S6RP (**C**) in naive CD4+ T cells from healthy controls, patients with TAK, and patients with GPA. Representative results are shown. **B** and **D**, Levels of phospho-S6K1 (**B**) and phospho-S6RP (**D**) in naive CD4+ T cells from healthy controls, patients with TAK, and patients with GPA. **E**, Levels of phospho-S6K1 and phospho-S6RP in memory CD4+ T cells from healthy controls, patients with TAK, and patients with GPA. In **B**, **D**, and **E**, bars show the mean ± SEM. Symbols represent individual subjects (n = 5 per group). *** = $P < 0.001$ by analysis of variance with Tukey's test. FMO = Fluorescence Minus One; MFI = mean fluorescence intensity.

T-bet, IFNγ, RORγ, and IL-17 in TAK CD4+ T cells (Figures 3A–D). Further, rapamycin reduced the robust accumulation of Th1 and Th17 cells from memory CD4+ T cells in TAK patients (Figure 3E).

To avoid the nonspecific function of rapamycin, we used RNAi technology to knock down the mTORC1-specific component RAPTOR in TAK CD4+ T cells using lentiviral RAPTOR shRNA (Supplementary Figure 3, available on the
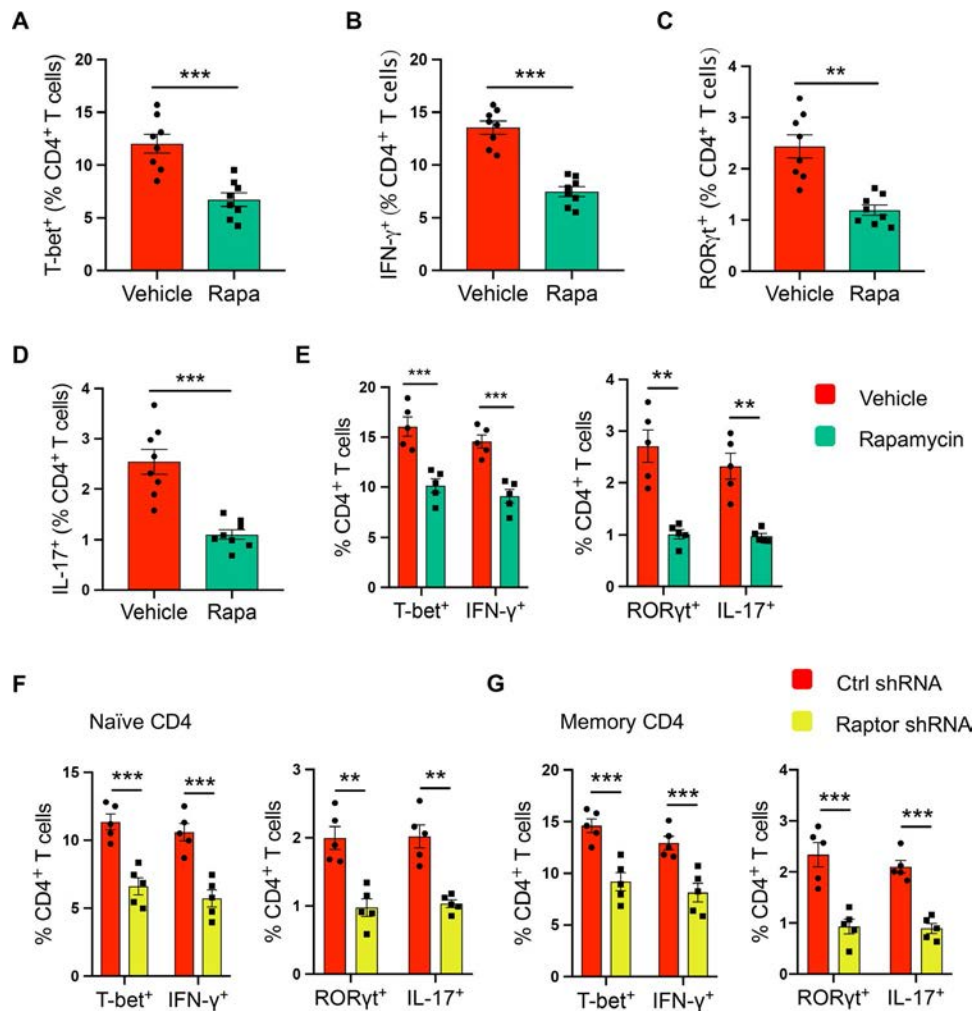
**Figure 3.** Blocking mechanistic target of rapamycin complex 1 corrects the maldifferentiation of CD4+ T cells from patients with Takayasu arteritis (TAK). Naive CD4+ T cells or memory CD4+ T cells were isolated from TAK patients and stimulated with anti-CD3/CD28 beads in the presence or absence of rapamycin (rapa; 10 μm) or isolated from TAK patients and transfected with control short hairpin RNA (shRNA) or regulatory-associated protein of mechanistic target of rapamycin (RAPTOR) shRNA. T cell lineage–determining transcription factors (T-bet and retinoic acid receptor–related orphan nuclear receptor γt [RORγt]) were analyzed on day 4, while intracellular cytokines (interferon-γ [IFNγ] and interleukin-17 [IL-17]) were detected on day 6. **A**–**D**, Proportion of naive CD4+ T cells positive for T-bet (**A**), IFNγ (**B**), RORγt (**C**), and IL-17 (**D**) after treatment with vehicle or rapamycin. **E**, Proportion of memory CD4+ T cells positive for T-bet, IFNγ, RORγt, and IL-17 after treatment with vehicle or rapamycin. **F** and **G**, Proportion of naive CD4+ T cells (**F**) and memory CD4+ T cells (**G**) positive for T-bet, IFNγ, RORγt, and IL-17 after transfection with control shRNA or RAPTOR shRNA. Bars show the mean ± SEM. Symbols represent individual subjects (n = 8 per group in **A**–**D** and 5 per group in **E**–**G**). ** = $P < 0.01$; *** = $P < 0.001$ by Student's paired t-test in **A**–**D**; by Student's paired t-test with Bonferroni correction in **E**–**G**.

Arthritis & Rheumatology web site at http://onlinelibrary.wiley.com/doi/10.1002/art.41084/abstract) and analyzed the subsequent cell differentiation under cytokine-unbiased conditions. RAPTOR knockdown in naive CD4+ T cells from TAK patients effectively reduced the intracellular expression of T-bet, IFNγ, RORγ, and IL-17 upon stimulation (Figure 3F). RAPTOR knockdown in memory CD4+ T cells also abrogated the abnormal expansion of proinflammatory T cells upon activation (Figure 3G).

The mTORC1 was critically involved in the differentiation of proinflammatory T cells but not Th2 cells. Blocking mTORC1 activity using rapamycin and RNAi technology exerted no significant effect on the expression of GATA-3 in TAK CD4+ T cells

(Supplementary Figure 4, available on the *Arthritis & Rheumatology* web site at http://onlinelibrary.wiley.com/doi/10.1002/art.41084/abstract). Taken together, these findings show that CD4+ T cell–intrinsic mTORC1 hyperactivity allows the spontaneous maldifferentiation of proinflammatory T cells in TAK patients.

Correlation of CD4+ T cell–intrinsic mTORC1 activity with proinflammatory T cell expansion and disease progression in TAK patients. To analyze the direct in vivo relevance of mTORC1 hyperactivity and spontaneous maldifferentiation of proinflammatory T cells, we detected CD4+ T cell–intrinsic mTORC1 activity by quantifying phospho-S6RP in

circulating CD4+ T cells and circulating frequencies of Th1 and Th17 cells in patients with TAK. Compared to healthy individuals and GPA patients, phospho-S6RP expression was higher in circulating CD4+ T cells from TAK patients, especially those with active disease (Figures 4A and B). In parallel, circulating frequencies of T-bet– and RORγ–expressing CD4+ T cells were increased in patients with active TAK (Figures 4C and D). Of note, the expression level of phospho-S6RP in circulating CD4+ T cells was closely correlated with the frequencies of T-bet and RORγ-expressing CD4+ T cells in patients with active TAK (Figures 4E and F). In contrast, mTORC1 hyperactivity in CD4+ T cells was not significantly correlated with the circulating frequency of GATA-3–expressing Th2 cells in patients with active TAK (Figure 4G), pinpointing an in

vivo relevance of CD4+ T cell–intrinsic mTORC1 hyperactivity to proinflammatory T cell expansion in TAK patients.

The hyperactivation of mTORC1 in circulating CD4+ T cells was positively associated with a higher erythrocyte sedimentation rate and C-reactive protein levels in TAK patients, predicting an acute-phase TAK in such patients (Figures 4H and I). In essence, hyperactivity of mTORC1 in CD4+ T cells correlates with progressive disease in human TAK.

Establishment of a humanized model of TAK. Humanized murine models are valuable in representing realistic conditions for human patients and have been widely used in translational studies (24,25). While TAK and GCA are both large
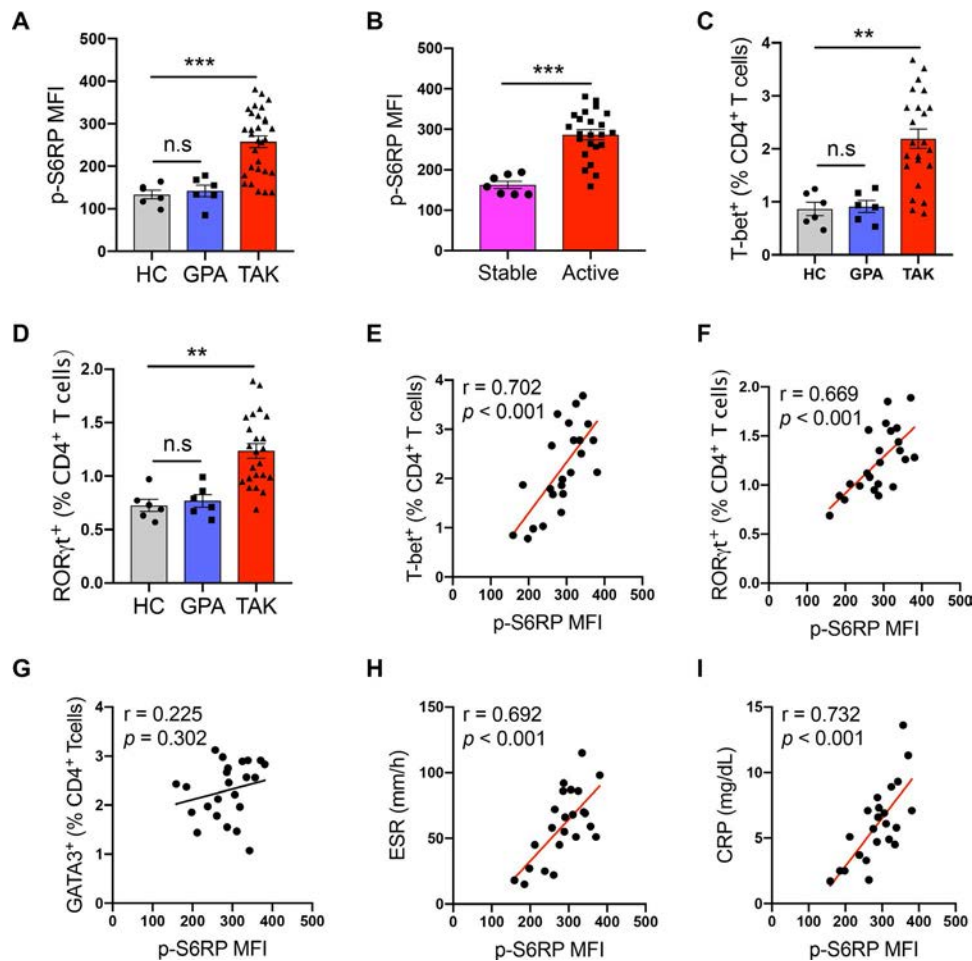
Figure 4. Hyperactivity of mechanistic target of rapamycin complex 1 predicts proinflammatory T cell expansion and active disease in patients with Takayasu arteritis (TAK). **A**, Levels of phospho–S6 ribosomal protein (phospho-S6RP) in circulating CD4+ T cells from healthy controls (HC; n = 6), patients with granulomatosis with polyangiitis (GPA) (n = 6), and patients with TAK (n = 30). **B**, Levels of phospho-S6RP in circulating CD4+ T cells from patients with stable TAK (n = 7) and patients with active TAK (n = 23). **C** and **D**, Frequencies of T-bet–expressing (**C**) and retinoic acid receptor–related orphan nuclear receptor γt (RORγt)–expressing (**D**) circulating CD4+ T cells from healthy controls (n = 6), patients with GPA (n = 6), and patients with active TAK (n = 23). In **A**–**D**, bars show the mean ± SEM. Symbols represent individual subjects. ** = $P < 0.01$; *** = $P < 0.001$ by analysis of variance with Tukey's test in **A**, **C**, and **D**; by Student's unpaired t-test in **B**. NS = not significant. **E**–**I**, Correlation of phospho-S6RP levels in circulating CD4+ T cells with the frequency of T-bet–expressing CD4+ T cells (**E**), the frequency of RORγt–expressing CD4+ T cells (**F**), the frequency of GATA-3–expressing CD4+ T cells (**G**), the erythrocyte sedimentation rate (ESR) (**H**), and the C-reactive protein (CRP) level (**I**) in patients with active TAK (n = 23). Correlations were determined by Pearson's correlation analysis. MFI = mean fluorescence intensity.

vessel arteritis, human artery–NSG mouse chimeras representing human GCA have been well documented for exploring GCA pathogeneses and therapeutics (19,23,26,27), in contrast to the lack of such a model representing human TAK. We modified

human artery–NSG mouse chimeras and generated a humanized large vessel vasculitis model in which inflammation was induced in human arterial tissue by immune cells from patients with active TAK (Supplementary Figure 5, available on the
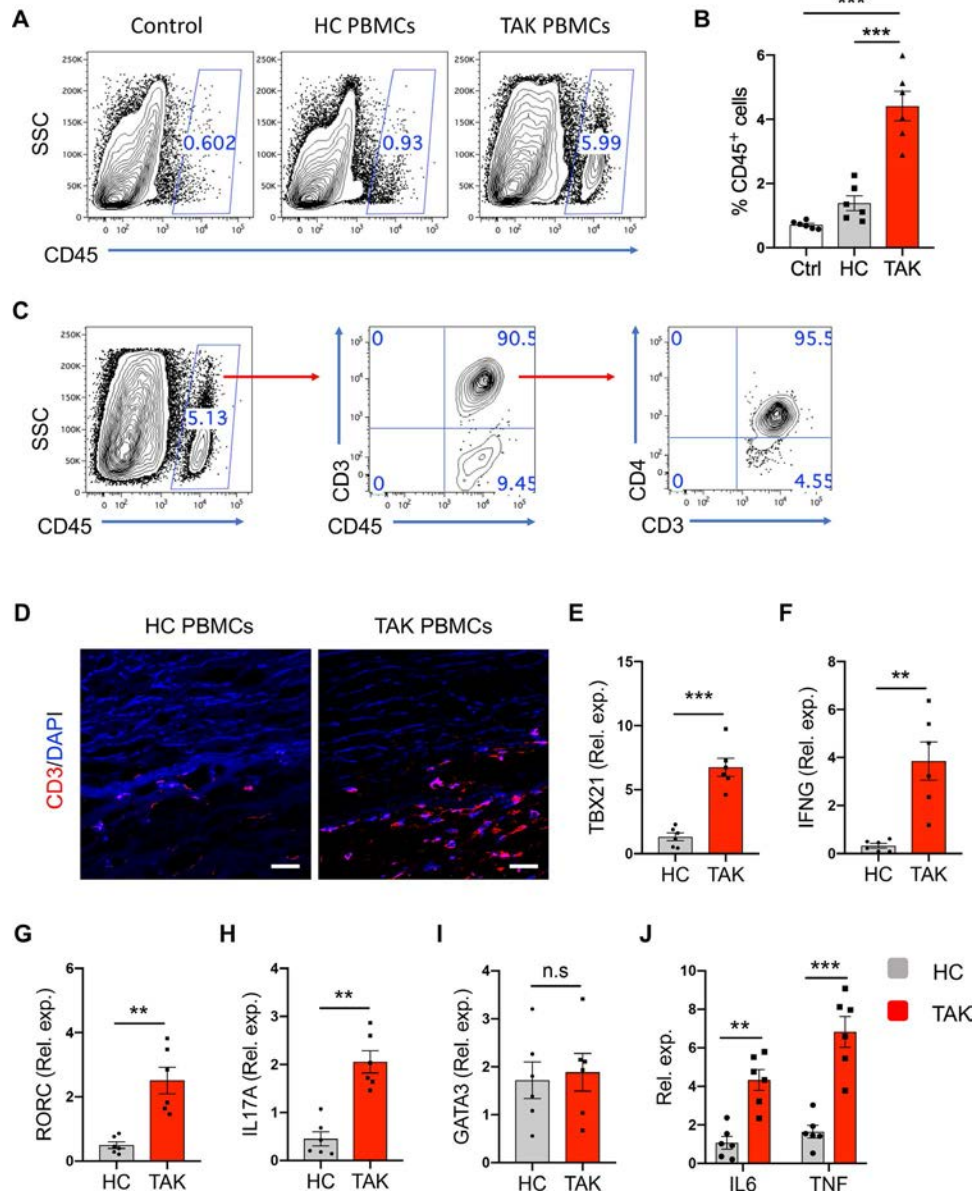
Figure 5. Development of a humanized large vessel vasculitis model mediated by immune cells from patients with Takayasu arteritis (TAK). **A** and **B**, Results of flow cytometric analysis (**A**) and proportion of CD45+ human immune cells (**B**) in human arterial explants from human artery–NSG mouse chimeras without reconstitution with human immune cells (control), human artery–NSG mouse chimeras reconstituted with healthy control (HC) peripheral blood mononuclear cells (PBMCs), and human artery–NSG mouse chimeras reconstituted with TAK PBMCs. In **A**, representative results are shown. Values are the percent of CD45+ cells. In **B**, bars show the mean ± SEM. Symbols represent individual grafts (n = 6 per group). *** = $P < 0.001$ by analysis of variance with Tukey's test. **C**, Quantification of CD3+ and CD4+ cells among tissue-resident CD45+ human immune cells. Representative results from 6 arterial tissues in chimeras reconstituted with TAK PBMCs are shown. Values are the percent of cells. **D**, Immunostaining of human CD3 protein in human arterial tissues from chimeras reconstituted with healthy control or TAK PBMCs. Representative results from 6 grafts are shown. Bars = 20 μm. **E–J**, Transcriptional analysis of the Th1-related genes TBX21 (**E**) and IFNG (**F**), the Th17-related genes RORC (**G**) and IL17A (**H**), the Th2-related gene GATA3 (**I**), and the innate inflammatory genes IL6 and TNF (**J**) in human arterial explants from chimeras reconstituted with healthy control or TAK PBMCs. Bars show the mean ± SEM. Symbols represent individual grafts (n = 6 per group). ** = $P < 0.01$; *** = $P < 0.001$ by Student's paired *t*-test with Bonferroni correction. Rel. exp. = relative expression; NS = not significant.

Arthritis & Rheumatology web site at http://onlinelibrary.wiley.com/doi/10.1002/art.41084/abstract).

When immune-deficient NSG mice were engrafted with human arteries and reconstituted with PBMCs from patients with active TAK, significant inflammatory infiltrates were observed in the human arterial tissue, evidenced by increased frequency of tissue-resident human CD45+ immune cells (Figures 5A and B). While human arterial tissues from chimeras without immune reconstitution, which served as the control group, were negative for human CD45+ inflammatory infiltrates, PBMCs from healthy donors also exerted minimum effect in inducing the inflammatory infiltrates (Figures 5A and B), indicating a selective strong capacity of TAK PBMCs in inducing large vessel vasculitis.

Flow analyses of human grafts showed a significant proportion of CD3+ T cells in the chimeras reconstituted with TAK PBMCs (Figure 5C). Tissue-resident human CD3+ T cells were predominantly CD4+ T cells (Figure 5C). Immunostaining of human grafts showed the adventitial infiltration of CD3+ T cells in chimeras reconstituted with TAK PBMCs (Figure 5D), which was confirmed by H&E staining (Supplementary Figure 6, available on the *Arthritis & Rheumatology* web site at http://onlinelibrary.wiley.com/doi/10.1002/art.41084/abstract). These findings implicate a crucial role of T cells in driving human TAK.

Transcriptional analyses of human grafts revealed higher expression of proinflammatory Th1- and Th17-related genes, including TBX21, IFNG, RORC and IL17A, in chimeras reconstituted with TAK PBMCs than in chimeras reconstituted with healthy PBMCs (Figures 5E–H). GATA-3 mRNA expression in human grafts was similar in the chimeras reconstituted with TAK PBMCs and those reconstituted with healthy PBMCs (Figure 5I). These findings were confirmed by intracellular staining for IFNγ and IL-17 in tissue-resident CD4+ T cells after pretreatment with PMA plus ionomycin (Supplementary Figure 6B), and the immunostaining of IFNγ+CD3+ T cells in the adventitial layer of tissue sections (Supplementary Figure 6C). These results demonstrate a predominant infiltration of proinflammatory Th1 and Th17 cells in the human grafts, mimicking the vascular lesions in TAK patients.

Reconstitution of human artery–NSG mouse chimeras with TAK PBMCs resulted in robust expression of IL6 and TNF in human grafts (Figure 5J), indicating an infiltration of innate lymphocytes such as macrophages in the inflammatory tissue. Again, such proinflammatory gene expression was much lower in the tissue explants from human artery–NSG mouse chimeras injected with healthy PBMCs (Figure 5J). Taken together, these data strongly demonstrate the successful establishment of human artery–NSG mouse chimeras in which human large vessel vasculitis is mediated by immune cells from TAK patients and thus represents human TAK.

Amelioration of large vessel vasculitis in humanized TAK chimeras by targeting mTORC1 in TAK immune cells. To evaluate the therapeutic application of targeting mTORC1 for TAK disease progression, immune cells from TAK patients were transfected with lentiviral RAPTOR shRNA or control shRNA prior to injection into human artery–NSG mouse chimeras, followed by the detection of inflammatory infiltrates using immunostaining, flow cytometry, and quantitative PCR. Additional chimeras were treated with rapamycin in order to evaluate the function of mTORC1 activity in TAK disease progression.

Blockade of mTORC1 activity using RNAi technology and rapamycin efficiently reduced the frequencies of tissue-resident human CD45+ immune cells and CD3+ T cells in arterial grafts (Figures 6A–D). Tissue-resident infiltration of CD3+ T cells was diminished by mTORC1 knockdown of TAK PBMCs (Figure 6B). Accordingly, inflammatory infiltration of the arterial adventitial layer was significantly reduced by mTORC1 knockdown (Figure 6C). In addition, mTORC1 inhibition by rapamycin restricted the tissue infiltration of human CD3+ T cells (Figure 6D). Further, tissue-resident Th1-related and Th17-related genes (TBX21, IFNG, RORC, and IL17A), and innate inflammatory genes (IL6 and TNF), were fundamentally decreased by blocking mTORC1 (Figures 6E–G). The tissue-resident IL-6 and TNF were evidenced by detecting the cytokine levels in tissue lysates with ELISA, showing diminished levels upon mTORC1 inhibition (Supplementary Figure 7A, available on the *Arthritis & Rheumatology* web site at http://onlinelibrary.wiley.com/doi/10.1002/art.41084/abstract). The efficiency of RNAi technology was generally comparable to that of rapamycin in restricting vasculitis (Figures 6A–G), while avoiding unwanted off-target effects (28,29). Both RAPTOR shRNA and rapamycin failed to affect the Th2-related gene GATA3 in human grafts (Figure 6H).

To pursue a CD4+ T cell–specific therapeutic strategy, CD4+ T cells were isolated from TAK PBMCs, transfected with RAPTOR shRNA or control shRNA, and added back with CD4+ T cell–depleted PBMCs for the subsequent immune reconstitution of human artery–NSG mouse chimeras. Application of RNAi technology targeting mTORC1 in CD4+ T cells ameliorated the vasculitis in human grafts (Figures 6I–K and Supplementary Figure 7B). Compared with control shRNA, RAPTOR shRNA transfection of CD4+ T cells diminished the tissue infiltrates of human immune cells (Figure 6I and Supplementary Figure 7B), consistent with reduced tissue-resident CD3+ T cells (Figure 6J) and decreased expression of proinflammatory T cell–related genes (Figure 6K). These findings demonstrate that targeting mTORC1 is an effective strategy in restricting human TAK.

DISCUSSION

TAK is a critical large vessel vasculitis with unknown etiology and poor prognosis (4,5,7). While multiple studies have shown that proinflammatory T cells are a crucial driver of TAK disease progression (10,12), molecular mechanisms underlying spontaneous proinflammatory T cell differentiation are largely unknown. In this study, we identified a critical mechanism for the spontaneous maldifferentiation of proinflammatory T cells in TAK patients.
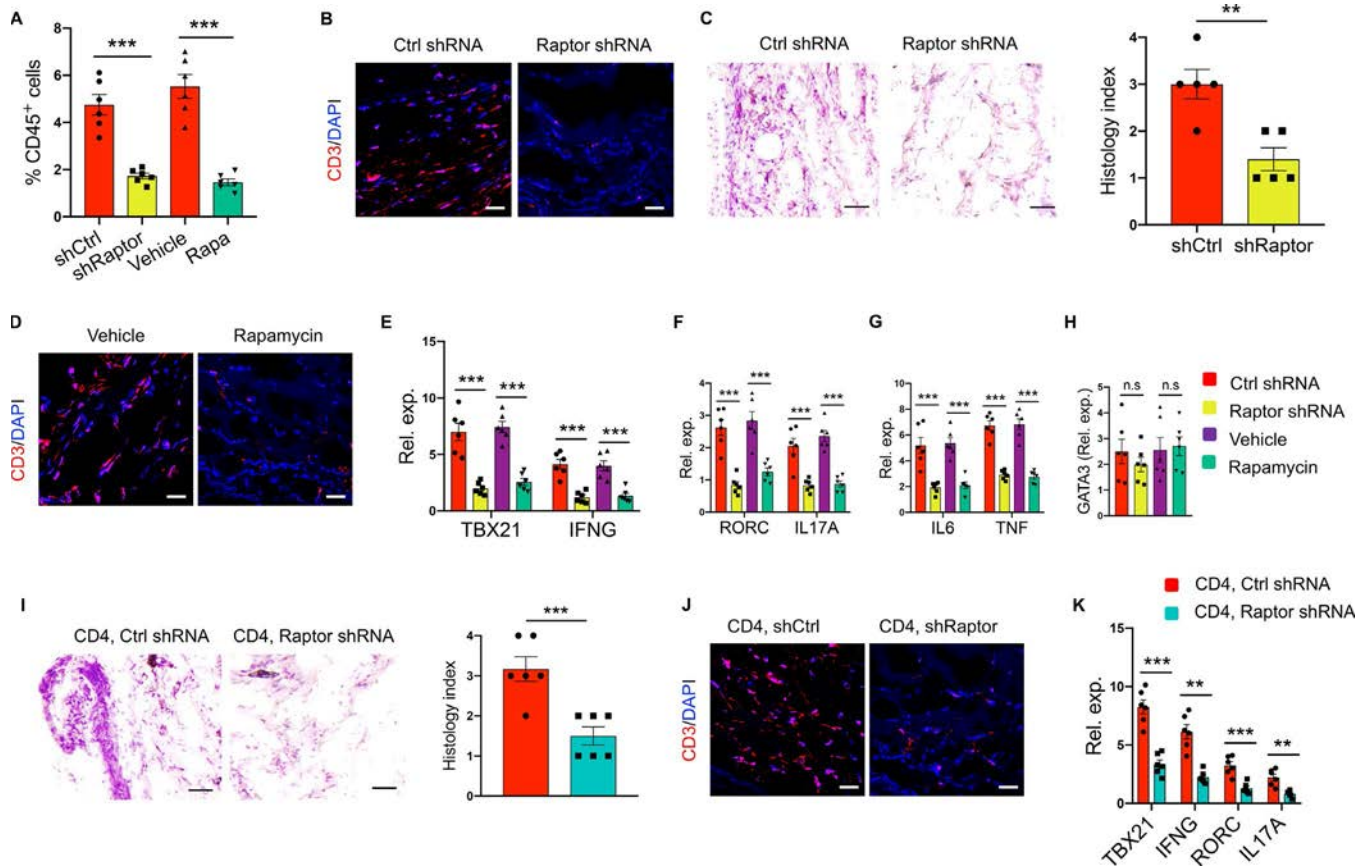
Figure 6. Targeting of mechanistic target of rapamycin complex 1 is sufficient to restrict vasculitis in human TAK. **A**–**H**, Human artery–NSG mouse chimeras were generated and reconstituted with either TAK or healthy control peripheral blood mononuclear cells (PBMCs). For some experiments, TAK PBMCs were transfected with RAPTOR shRNA or control shRNA prior to immune reconstitution of the chimeras. Otherwise, chimeras were treated with rapamycin. Arterial grafts were explanted 2 weeks after immune reconstitution. **A**, Frequencies of CD45+ immune cells in human grafts from chimeras treated as indicated. **B**, Immunostaining for human CD3 in the adventitia of arterial grafts from the chimeras treated as indicated. Bars = 20 μm. **C**, Left, Hematoxylin and eosin (H&E) staining of arterial adventitial tissue from the chimeras treated as indicated. Bars = 50 μm. Right, Histology index for the chimeras treated as indicated. **D**, Immunostaining for human CD3 in the adventitia of arterial grafts from the chimeras treated as indicated. Bars = 20 μm. **E**–**H**, Expression of mRNA for the proinflammatory genes TBX21 and IFNG (**E**), RORC and IL17A (**F**), and IL6 and TNF (**G**) and the Th2-related gene GATA3 (**H**) in human grafts from the chimeras treated as indicated. **I**–**K**, CD4+ T cells from TAK PBMCs were transfected with RAPTOR shRNA or control shRNA and injected into human artery–NSG mouse chimeras for immune reconstitution. **I**, Left, H&E staining of arterial adventitial tissues from the chimeras treated as indicated. Bars = 50 μm. Right, Histology index for the chimeras treated as indicated. **J**, Immunostaining for human CD3 in the adventitia of arterial grafts from the chimeras treated as indicated. Bars = 20 μm. **K**, Quantitative polymerase chain reaction analysis of the proinflammatory genes TBX21, IFNG, RORC, and IL17A in human grafts. In **B**, the left panel of **D**, the left panel of **I**, and **J**, results are representative of 6 grafts. In the left panel of **C**, results are representative of 5 grafts. In **A**, the right panel of **C**, **E**–**H**, the right panel of **I**, and **K**, bars show the mean ± SEM. Symbols represent individual grafts (n = 6 per group in **A**, **E**–**H**, the right panel of **I**, and **K** and 5 per group in the right panel of **C**). ** = $P < 0.01$; *** = $P < 0.001$ by Student's paired t-test with Bonferroni correction in **A** and **K**; by Student's paired t-test in the right panel of **C** and the right panel of **I**; by analysis of variance with Tukey's test in **E**–**H**. Rel. exp. = relative expression; NS = not significant (see Figure 3 for other definitions).

Specifically, CD4+ T cells from TAK patients have cell-intrinsic hyperactivity of mTORC1, driving the spontaneous and selective differentiation of Th1 and Th17 cells. Accordingly, circulating mTORC1^{high}CD4+ T cells predict proinflammatory T cell expansion and active disease in TAK patients. We established a humanized large vessel vasculitis model that represents human TAK, providing an optimal platform for elucidating disease pathogenesis and exploring novel therapeutics. Targeting mTORC1 with rapamycin and RNAi technology was sufficient to limit TAK development.

TAK and GCA are 2 major types of large vessel arteritis, narrowing the aorta and its major branches with or without aneurysm formation (7,30). While TAK mainly affects young individuals, GCA affects patients >50 years old (31). Although often present in different frequencies, both disorders share similar clinical symptoms, signs, and imaging abnormalities (32,33), showing strong similarities and subtle differences in the distribution of arterial disease (34). These findings support an assumption that TAK and GCA may represent skewed phenotypes within the spectrum of

the same disorder. Mechanistically, Th1 and Th17 cells are the major vascular infiltrates for both TAK patients and GCA patients (10,33,35,36). Treatment with glucocorticoids efficiently reduces the tissue infiltration of Th1 cells but not Th17 cells in both vasculitides (10,35,36). Previous studies pinpoint hyperactivity of mTORC1 in CD4+ T cells from GCA patients, permitting the differentiation of Th1 and Th17 cells in such patients (19). Herein, we identify mTORC1 hyperactivity as a cell-intrinsic mechanism of spontaneous maldifferentiation of proinflammatory T cells in TAK patients, mechanistically connecting TAK and GCA, and, at least in part, accounting for their strong similarities in arterial lesions and clinical manifestations.

A master regulator of cell proliferation and differentiation, mTORC1 plays critical roles in autoimmune inflammatory diseases (37–39). Activation of mTORC1 determines T cell fate, promoting the differentiation of Th1 and Th17 cells while inhibiting the differentiation of FoxP3+ Treg cells (20,21,40,41). In addition, mTORC1 controls CD8+ T cell differentiation as CD8+ T cells deficient in mTORC1 activity are resistant to differentiation into effector cells but retain memory cell characteristics (42). Given the crucial functions of Th1 and Th17 cells in autoimmune inflammatory diseases, mTORC1 hyperactivity is widely shared in autoimmune diseases such as GCA, RA, systemic lupus erythematosus (SLE), and multiple sclerosis (19,21,43). The mTORC1^{high} phenomenon in CD4+ T cells from TAK patients reinforces the critical function of mTORC1 in autoimmune inflammatory diseases. Consistent with our findings that blocking mTORC1 activity efficiently ameliorates large vessel vasculitis in humanized TAK chimeras, targeting mTORC1 is also effective in restricting disease progression in RA and SLE (21,44). To avoid the unwanted effects of small chemical molecules, we applied RNAi technology by transfecting immune cells from TAK patients with lentiviral RAPTOR shRNA for to explore therapeutic options using humanized TAK chimeras. Genetic knockdown of mTORC1 in TAK immune cells is sufficient to abrogate TAK vasculitis. Selective knockdown of mTORC1 in CD4+ T cells of TAK patients is also efficient in the treatment of large vessel vasculitis in humanized TAK chimeras. These findings provide novel therapeutic strategies for targeting mTORC1 to control TAK and other autoimmune inflammatory diseases.

While mTORC1 hyperactivation is a central pathway for autoimmune inflammatory diseases (39), this characteristic spares patients with GPA, who have mTORC1 activity similar to that of healthy individuals, indicating the existence of distinct pathologic mechanisms for different autoimmune inflammatory diseases. In support of this notion, CD4+ T cells from patients with psoriatic arthritis also have mTORC1 activity similar to that of healthy individuals and are fundamentally different from RA CD4+ T cells in metabolic reprogramming (21,45). Of interest, although patients with RA and those with SLE both have mTORC1 hyperactivity in CD4+ T cells, protein N-myristoylation is deficient in RA but not

in SLE, leading to AMP-activated protein kinase inactivation and mTORC1 hyperactivity in RA patients (21). Meanwhile, patients with GCA but not those with RA have robust levels of circulating vascular endothelial growth factor, inducing Jagged-1–expressing endothelial niche in the adventitia and Notch-1–mTORC1 activation in CD4+ T cells, which results in the expansion of proinflammatory T cells (19). Those studies assign distinct molecular mechanisms underlying mTORC1 hyperactivity in various autoimmune inflammatory diseases. In this study, while mTORC1 hyperactivity is a critical mechanism underlying the spontaneous maldifferentiation of Th1 and Th17 cells in TAK patients, the precise mechanisms for mTORC1 hyperactivity in TAK CD4+ T cells still remain unclear. Successive studies are required to further the understanding of mTORC1 hyperactivity in TAK patients, which would expand the promising therapeutic targets for clinical practice.

Given the central role of pathogenic CD4+ T cells in TAK, CD4 T cell-intrinsic mechanisms that drive their spontaneous differentiations and functions are relevant for disease treatment. Although previous studies have reported mTORC1 activation in vascular endothelial cells and in activated T effector cells of patients with large vessel vasculitis including TAK (46,47), those studies did not explore the function of mTORC1 in the spontaneous differentiation of CD4+ T cells. To our knowledge, this is the first study to demonstrate spontaneous maldifferentiation of Th1 and Th17 cells using purified naive CD4+ T cells or memory CD4+ T cells from TAK patients. Further, we showed that mTORC1 activity is selectively higher in TAK CD4+ T cells, driving the spontaneous differentiation of proinflammatory T cells in TAK patients. Such findings are previously unknown, implicating a fundamentally reprogrammed mTOR pathway in TAK patients. Finally, we established a new humanized vasculitis model that represents human TAK, providing strong evidence that targeting mTORC1 using small chemical inhibitors or specific genetic knockdown is sufficient to restrict arterial inflammation in vivo.

In essence, patients with TAK have cell-intrinsic mTORC1 hyperactivity in CD4+ T cells, leading to spontaneous maldifferentiation of proinflammatory Th1 and Th17 cells and disease progression. Inhibiting mTORC1 activity is efficient in reducing the maldifferentiation of proinflammatory T cells and in restricting vasculitis in humanized TAK chimeras. Targeted therapeutic strategy by genetic knockdown of mTORC1 works well for TAK treatment in vivo. These findings were obtained with primary cells from TAK patients and humanized chimeras that represent human TAK, reflecting realistic conditions in patients and shedding new light on disease pathogenesis. Targeting mTORC1 could be a promising therapeutic strategy in controlling human TAK in clinical practice.

AUTHOR CONTRIBUTIONS

Study conception and design. X. Liu, Wen, Li.
Acquisition of data. Zhang, L. Zhao, Wang, Cheng, Sun, J. Zhao, B. Liu.
Analysis and interpretation of data. Zhang, L. Zhao, Wang, Cheng, Sun, J. Zhao, B. Liu, X. Liu, Wen, Li.
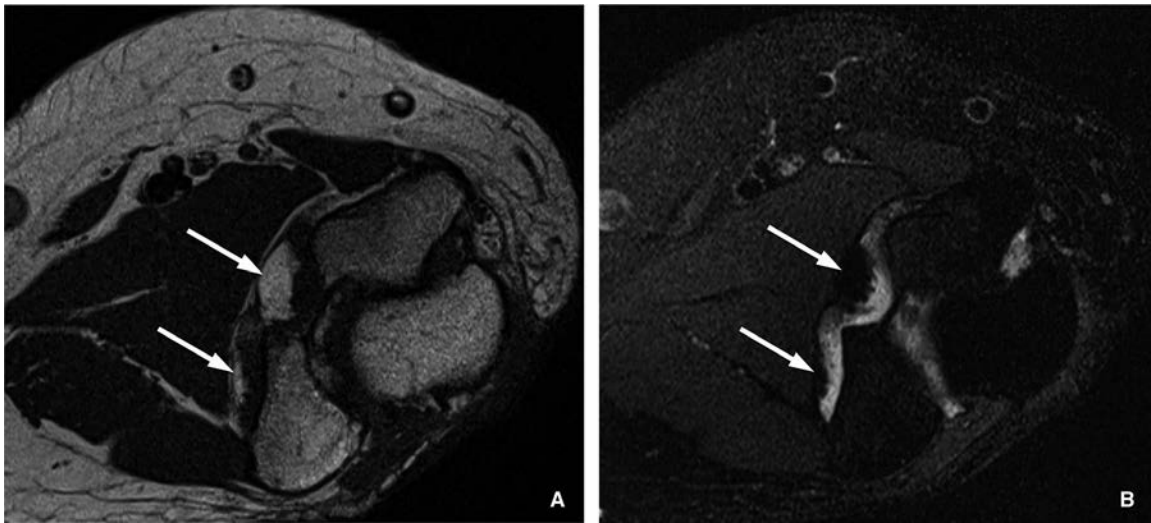
ADDITIONAL DISCLOSURES

REFERENCES

1. Chasset F, Francès C. Cutaneous manifestations of medium- and large-vessel vasculitis. Clin Rev Allergy Immunol 2017;53:452–68.

2. Weyand CM, Goronzy JJ. Immune mechanisms in medium and large-vessel vasculitis. Nat Rev Rheumatol 2013;9:731–40.

3. Kermani TA, Dasgupta B. Current and emerging therapies in large-vessel vasculitis. Rheumatology (Oxford) 2018;57:1513–24.

4. Mirouse A, Biard L, Comarmond C, Lambert M, Mekinian A, Ferfar Y, et al. Overall survival and mortality risk factors in Takayasu's arteritis: a multicenter study of 318 patients. J Autoimmun 2019;96:35–9.

5. Comarmond C, Biard L, Lambert M, Mekinian A, Ferfar Y, Kahn JE, et al. Long-term outcomes and prognostic factors of complications in Takayasu arteritis: a multicenter study of 318 patients. Circulation 2017;136:1114–22.

6. Kim ES, Beckman J. Takayasu arteritis: challenges in diagnosis and management. Heart 2018;104:558–65.

7. Weyand CM, Watanabe R, Zhang H, Akiyama M, Berry GJ, Goronzy JJ. Cytokines, growth factors and proteases in medium and large vessel vasculitis. Clin Immunol 2019. E-pub ahead of print.

8. Tamura N, Maejima Y, Tezuka D, Takamura C, Yoshikawa S, Ashikaga T, et al. Profiles of serum cytokine levels in Takayasu arteritis patients: potential utility as biomarkers for monitoring disease activity. J Cardiol 2017;70:278–85.

9. Yoshifuji H. Pathophysiology of large vessel vasculitis and utility of interleukin-6 inhibition therapy. Mod Rheumatol 2019;29:287–93.

10. Saadoun D, Garrido M, Comarmond C, Desbois AC, Domont F, Savey L, et al. Th1 and Th17 cytokines drive inflammation in Takayasu arteritis. Arthritis Rheumatol 2015;67:1353–60.

11. Savioli B, Abdulahad WH, Brouwer E, Kallenberg CG, de Souza AW. Are cytokines and chemokines suitable biomarkers for Takayasu arteritis? Autoimmun Rev 2017;16:1071–8.

12. Misra DP, Chaurasia S, Misra R. Increased circulating Th17 cells, serum IL-17A, and IL-23 in Takayasu Arteritis. Autoimmune Dis 2016;2016:7841718.

13. Nakaoka Y, Isobe M, Takei S, Tanaka Y, Ishii T, Yokota S, et al. Efficacy and safety of tocilizumab in patients with refractory Takayasu arteritis: results from a randomised, double-blind, placebo-controlled, phase 3 trial in Japan (the TAKT study). Ann Rheum Dis 2018;77:348–54.

14. Waickman AT, Powell JD. MTOR, metabolism, and the regulation of T-cell differentiation and function. Immunol Rev 2012;249:43–58.

15. Chi H. Regulation and function of mTOR signalling in T cell fate decisions. Nat Rev Immunol 2012;12:325–38.

16. Oh WJ, Jacinto E. MTOR complex 2 signaling and functions. Cell Cycle 2011;10:2305–16.

17. Kim LC, Cook RS, Chen J. MTORC1 and mTORC2 in cancer and the tumor microenvironment. Oncogene 2017;36:2191–201.

18. Kennedy BK, Lamming DW. The mechanistic target of rapamycin: the grand conducTOR of metabolism and aging. Cell Metab 2016;23:990–1003.

19. Wen Z, Shen Y, Berry G, Shahram F, Li Y, Watanabe R, et al. The microvascular niche instructs T cells in large vessel vasculitis via the VEGF-Jagged1-Notch pathway. Sci Transl Med 2017;9:eaal3322.

20. Delgoffe GM, Pollizzi KN, Waickman AT, Heikamp E, Meyers DJ, Horton MR, et al. The kinase mTOR regulates the differentiation of helper T cells through the selective activation of signaling by mTORC1 and mTORC2. Nat Immunol 2011;12:295–303.

21. Wen Z, Jin K, Shen Y, Yang Z, Li Y, Wu B, et al. N-myristoyltransferase deficiency impairs activation of kinase AMPK and promotes synovial tissue inflammation. Nat Immunol 2019;20:313–25.

22. Gibson-Corley KN, Olivier AK, Meyerholz DK. Principles for valid histopathologic scoring in research. Vet Pathol 2013;50:1007–15.

23. Watanabe R, Maeda T, Zhang H, Berry GJ, Zeisbrich M, Brockett R, et al. MMP (matrix metalloprotease)-9-producing monocytes enable T cells to invade the vessel wall and cause vasculitis. Circ Res 2018;123:700–15.

24. Bolker JA. Animal models in translational research: Rosetta Stone or stumbling block? Bioessays 2017;39:1700089.

25. McGonigle P, Ruggeri B. Animal models of human disease: challenges in enabling translation. Biochem Pharmacol 2014;87:162–71.

26. Zhang H, Watanabe R, Berry GJ, Vaglio A, Liao YJ, Warrington KJ, et al. Immunoinhibitory checkpoint deficiency in medium and large vessel vasculitis. Proc Natl Acad Sci U S A 2017;114:E970–9.

27. Piggott K, Deng J, Warrington K, Younge B, Kubo JT, Desai M, et al. Blocking the Notch pathway inhibits vascular inflammation in large-vessel vasculitis. Circulation 2011;123:309–18.

28. Finlay DK. N-myristoylation of AMPK controls T cell inflammatory function. Nat Immunol 2019;20:252–4.

29. Schenone M, Dančík V, Wagner BK, Clemons PA. Target identification and mechanism of action in chemical biology and drug discovery. Nat Chem Biol 2013;9:232–40.

30. Sreih AG, Alibaz-Oner F, Kermani TA, Aydin SZ, Cronholm PF, Davis T, et al. Development of a core set of outcome measures for large-vessel vasculitis: report from OMERACT 2016. J Rheumatol 2017;44:1933–7.

31. Carmona FD, Coit P, Saruhan-Direskeneli G, Hernández-Rodríguez J, Cid MC, Solans R, et al. Analysis of the common genetic component of large-vessel vasculitides through a meta-ImmunoChip strategy. Sci Rep 2017;7:43953.

32. Maksimowicz-McKinnon K, Clark TM, Hoffman GS. Takayasu arteritis and giant cell arteritis: a spectrum within the same disease? Medicine (Baltimore) 2009;88:221–6.

33. Kermani TA. Takayasu arteritis and giant cell arteritis: are they a spectrum of the same disease? Int J Rheum Dis 2019;22 Suppl 1:41–8.

34. Grayson PC, Maksimowicz-McKinnon K, Clark TM, Tomasson G, Cuthbertson D, Carette S, et al. Distribution of arterial lesions in Takayasu's arteritis and giant cell arteritis. Ann Rheum Dis 2012;71:1329–34.

35. Deng J, Younge BR, Olshen RA, Goronzy JJ, Weyand CM. Th17 and Th1 T-cell responses in giant cell arteritis. Circulation 2010;121:906–15.

36. Weyand CM, Younge BR, Goronzy JJ. IFN-γ and IL-17: the two faces of T-cell pathology in giant cell arteritis. Curr Opin Rheumatol 2011;23:43–9.

37. Kim J, Guan KL. MTOR as a central hub of nutrient signalling and cell growth. Nat Cell Biol 2019;21:63–71.

38. Martens S. A division of labor in mTORC1 signaling and autophagy. Sci Signal 2018;11:eaav3530.

39. Perl A. MTOR activation is a biomarker and a central pathway to autoimmune disorders, cancer, obesity, and aging. Ann N Y Acad Sci 2015;1346:33–44.

40. Zeng H, Yang K, Cloer C, Neale G, Vogel P, Chi H. MTORC1 couples immune signals and metabolic programming to establish T(reg)-cell function [letter]. Nature 2013;499:485–90.

41. Zeng H, Chi H. MTOR signaling in the differentiation and function of regulatory and effector T cells. Curr Opin Immunol 2017;46:103–11.

42. Pollizzi KN, Patel CH, Sun IH, Oh MH, Waickman AT, Wen J, et al. MTORC1 and mTORC2 selectively regulate CD8+ T cell differentiation. J Clin Invest 2015;125:2090–108.

43. Perl A. Activation of mTOR (mechanistic target of rapamycin) in rheumatic diseases. Nat Rev Rheumatol 2016;12:169–82.

44. Lai ZW, Kelly R, Winans T, Marchena I, Shadakshari A, Yu J, et al. Sirolimus in patients with clinically active systemic lupus erythematosus resistant to, or intolerant of, conventional medications: a single-arm, open-label, phase 1/2 trial. Lancet 2018;391:1186–96.

45. Shen Y, Wen Z, Li Y, Matteson EL, Hong J, Goronzy JJ, et al. Metabolic control of the scaffold protein TKS5 in tissue-invasive, proinflammatory T cells. Nat Immunol 2017;18:1025–34.

46. Maciejewski-Duval A, Comarmond C, Leroyer A, Zaidan M, Le Joncour A, Desbois AC, et al. MTOR pathway activation in large vessel vasculitis. J Autoimmun 2018;94:99–109.

47. Hadjadj J, Canaud G, Mirault T, Samson M, Bruneval P, Régent A, et al, on behalf of the French Vasculitis Study Group. MTOR pathway is activated in endothelial cells from patients with Takayasu arteritis and is modulated by serum immunoglobulin G. Rheumatology (Oxford) 2018;57:1011–20.

Clinical Images: Teenaged boy with lipoma arborescens of the knee and elbow and presumed juvenile idiopathic arthritis

The patient, a 16-year-old boy with severe obesity, presented to the pediatric rheumatology clinic with a 1.5-year history of right knee swelling. Laboratory findings were unremarkable other than mild elevations of inflammation markers (C-reactive protein [CRP] and erythrocyte sedimentation rate). Results of a Lyme screen were negative. Previous magnetic resonance imaging (MRI) of the knee showed a large joint effusion with synovitis and some punctate foci of low signal intensity throughout the synovium, suggesting possible pigmented villonodular synovitis. Physical examination demonstrated a large right knee effusion, guarding with wrist flexion, and reduced elbow extension (assessment for effusions was difficult due to obesity). MRI of the knee showed fronds of lipomatous tissue surrounded by joint fluid that followed fat signal on all pulse sequences, consistent with macroscopic intraarticular fat seen in lipoma arborescens. Synovial biopsy and synovectomy were performed. Histopathologic analysis revealed focal hyperplasia of the synovial lining, dense lymphoplasmacytic inflammation, and diffuse infiltration by mature adipose tissue that reached the synovial lining, consistent with lipoma arborescens. Marked chronic inflammation suggested underlying inflammatory synovitis. MRI of the elbow revealed synovitis with macroscopic intraarticular fat, consistent with lipoma arborescens (**arrows** in **A** and **B**), which is usually monoarticular, affecting the knee; however, it may be associated with inflammatory arthritis (1,2). Given the histopathologic findings, polyarticular involvement, and elevated levels of inflammation markers, underlying juvenile idiopathic arthritis (JIA) was presumed, and naproxen and methotrexate were prescribed. Six weeks later, knee pain and swelling had improved, and the CRP level had decreased. However, the patient was lost to follow-up. After 1 year he returned with large effusions in both knees, unchanged wrist and elbow examination findings, and elevated levels of inflammation markers. These worsening features while the patient was not being treated supported the presumption of underlying JIA. Systemic therapies were restarted. The finding of lipoma arborescens in a child affecting at least 2 joints and associated with JIA is unique.

1. Xue J, Alario AJ, Nelson SD, Wu H. Progressive bilateral lipoma arborescens of the knee complicated by juvenile spondyloarthropathy: a case report and review of the literature. Semin Arthritis Rheum 2013;43:259–63.

2. Bent MA, Varacallo M, Fox EJ, Voss S, Frauenhoffer EE. Lipoma arborescens and coexisting psoriatic arthritis: a case report and review of the literature. JBJS Case Connect 2013;3:e121.

Cody S. Dail, BA
Kelly R. Dietz, MD [iD]
Michael A. Murati, MD [iD]
Colleen K. Correll, MD, MPH [iD]
University of Minnesota Medical School
Minneapolis, MN

44. Lai ZW, Kelly R, Winans T, Marchena I, Shadakshari A, Yu J, et al. Sirolimus in patients with clinically active systemic lupus erythematosus resistant to, or intolerant of, conventional medications: a single-arm, open-label, phase 1/2 trial. Lancet 2018;391:1186–96.

45. Shen Y, Wen Z, Li Y, Matteson EL, Hong J, Goronzy JJ, et al. Metabolic control of the scaffold protein TKS5 in tissue-invasive, proinflammatory T cells. Nat Immunol 2017;18:1025–34.

46. Maciejewski-Duval A, Comarmond C, Leroyer A, Zaidan M, Le Joncour A, Desbois AC, et al. MTOR pathway activation in large vessel vasculitis. J Autoimmun 2018;94:99–109.

47. Hadjadj J, Canaud G, Mirault T, Samson M, Bruneval P, Régent A, et al, on behalf of the French Vasculitis Study Group. MTOR pathway is activated in endothelial cells from patients with Takayasu arteritis and is modulated by serum immunoglobulin G. Rheumatology (Oxford) 2018;57:1011–20.

Clinical Images: Teenaged boy with lipoma arborescens of the knee and elbow and presumed juvenile idiopathic arthritis

The patient, a 16-year-old boy with severe obesity, presented to the pediatric rheumatology clinic with a 1.5-year history of right knee swelling. Laboratory findings were unremarkable other than mild elevations of inflammation markers (C-reactive protein [CRP] and erythrocyte sedimentation rate). Results of a Lyme screen were negative. Previous magnetic resonance imaging (MRI) of the knee showed a large joint effusion with synovitis and some punctate foci of low signal intensity throughout the synovium, suggesting possible pigmented villonodular synovitis. Physical examination demonstrated a large right knee effusion, guarding with wrist flexion, and reduced elbow extension (assessment for effusions was difficult due to obesity). MRI of the knee showed fronds of lipomatous tissue surrounded by joint fluid that followed fat signal on all pulse sequences, consistent with macroscopic intraarticular fat seen in lipoma arborescens. Synovial biopsy and synovectomy were performed. Histopathologic analysis revealed focal hyperplasia of the synovial lining, dense lymphoplasmacytic inflammation, and diffuse infiltration by mature adipose tissue that reached the synovial lining, consistent with lipoma arborescens. Marked chronic inflammation suggested underlying inflammatory synovitis. MRI of the elbow revealed synovitis with macroscopic intraarticular fat, consistent with lipoma arborescens (**arrows** in **A** and **B**), which is usually monoarticular, affecting the knee; however, it may be associated with inflammatory arthritis (1,2). Given the histopathologic findings, polyarticular involvement, and elevated levels of inflammation markers, underlying juvenile idiopathic arthritis (JIA) was presumed, and naproxen and methotrexate were prescribed. Six weeks later, knee pain and swelling had improved, and the CRP level had decreased. However, the patient was lost to follow-up. After 1 year he returned with large effusions in both knees, unchanged wrist and elbow examination findings, and elevated levels of inflammation markers. These worsening features while the patient was not being treated supported the presumption of underlying JIA. Systemic therapies were restarted. The finding of lipoma arborescens in a child affecting at least 2 joints and associated with JIA is unique.
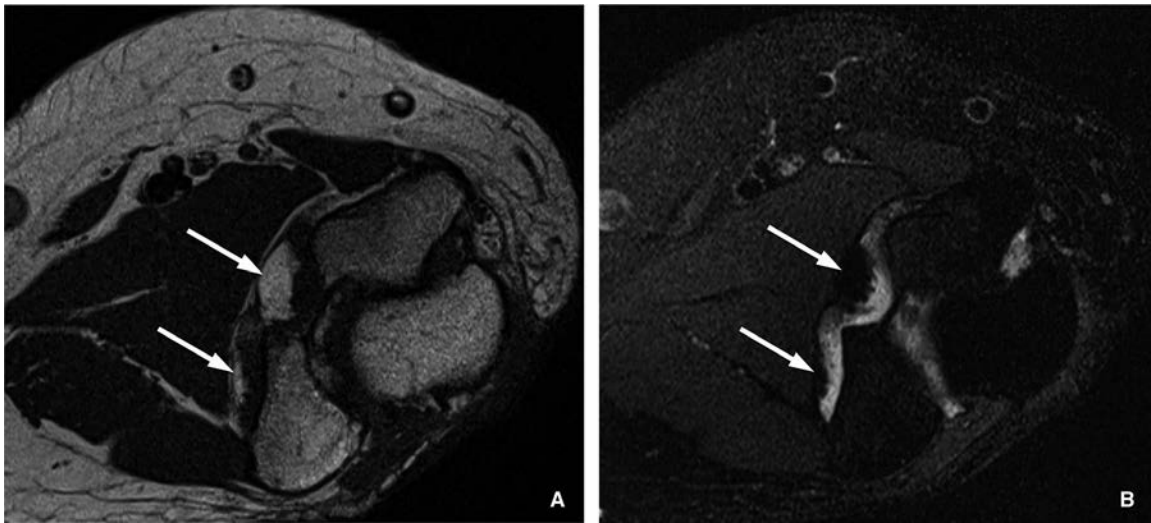
1. Xue J, Alario AJ, Nelson SD, Wu H. Progressive bilateral lipoma arborescens of the knee complicated by juvenile spondyloarthropathy: a case report and review of the literature. Semin Arthritis Rheum 2013;43:259–63.

2. Bent MA, Varacallo M, Fox EJ, Voss S, Frauenhoffer EE. Lipoma arborescens and coexisting psoriatic arthritis: a case report and review of the literature. JBJS Case Connect 2013;3:e121.

Cody S. Dail, BA
Kelly R. Dietz, MD (iD)
Michael A. Murati, MD (iD)
Colleen K. Correll, MD, MPH (iD)
University of Minnesota Medical School
Minneapolis, MN

AMERICAN COLLEGE
of RHEUMATOLOGY
Empowering Rheumatology Professionals

Benefit of Anakinra in Treating Pediatric Secondary Hemophagocytic Lymphohistiocytosis

Esraa M. Eloseily,[1] Peter Weiser,[2] Courtney B. Crayne,[2] Hilary Haines,[2] Melissa L. Mannion,[2] Matthew L. Stoll,[2] Timothy Beukelman,[2] T. Prescott Atkinson,[2] and Randy Q. Cron[2]

Objective. To assess the benefit of the recombinant human interleukin-1 receptor antagonist anakinra in treating pediatric patients with secondary hemophagocytic lymphohistiocytosis (HLH)/macrophage activation syndrome (MAS) associated with rheumatic and nonrheumatic conditions.

Methods. A retrospective chart review of all anakinra-treated patients with secondary HLH/MAS was performed at Children's of Alabama from January 2008 through December 2016. Demographic, clinical, laboratory, and genetic characteristics, outcomes data, and information on concurrent treatments were collected from the records and analyzed using appropriate univariate statistical approaches to assess changes following treatment and associations between patient variables and outcomes.

Results. Forty-four patients with secondary HLH/MAS being treated with anakinra were identified in the electronic medical records. The median duration of hospitalization was 15 days. The mean pretreatment serum ferritin level was 33,316 ng/ml and dropped to 14,435 ng/ml (57% decrease) within 15 days of the start of anakinra treatment. The overall mortality rate in the cohort was 27%. Earlier initiation of anakinra (within 5 days of hospitalization) was associated with reduced mortality ($P = 0.046$), whereas thrombocytopenia (platelet count <100,000/μl) and *STXBP*2 mutations were both associated with increased mortality ($P = 0.008$ and $P = 0.012$, respectively). In considering patients according to their underlying diagnosis, those with systemic juvenile idiopathic arthritis (JIA) had the lowest mortality rate, with no deaths among the 13 systemic JIA patients included in the study ($P = 0.006$). In contrast, those with an underlying hematologic malignancy had the highest mortality rate, at 100% (n = 3).

Conclusion. These findings suggest that anakinra appears to be effective in treating pediatric patients with non–malignancy-associated secondary HLH/MAS, especially when it is given early in the disease course and when administered to patients who have an underlying rheumatic disease.

INTRODUCTION

Secondary hemophagocytic lymphohistiocytosis (HLH) is a life-threatening condition that is diagnosed among severely ill, febrile patients who require hospitalization (1). Familial, or primary, HLH presents in infancy and often is attributed to homozygous or compound heterozygous mutations in lymphocyte cytolytic pathway genes (2). Secondary HLH, also termed macrophage activation syndrome (MAS), when associated with rheumatic disorders (3), affects children and can also affect adults with various disorders. Secondary HLH and MAS can be associated with

heterozygous defects in primary HLH genes, and thus the distinction between primary HLH and secondary HLH/MAS seems to be blurred (4,5). Secondary HLH is often associated with conditions in which chronic immune dysregulation occurs, such as in rheumatic diseases and certain hematologic malignancies. Infectious agents, particularly members of the herpesvirus (*Herpesviridae*) family, may also serve as a trigger to overcome a "threshold" of disease (6). Thus, secondary HLH/MAS is not a diagnosis of exclusion, and many investigators have considered MAS, primary HLH, and secondary HLH to be on the same spectrum of disease (1,2).

Initial symptoms of secondary HLH/MAS are usually non-specific. The cardinal feature is unremitting high fever, although it is not an absolute finding in all cases (7). Other features include hepatomegaly, splenomegaly, central nervous system involvement (e.g., seizures, coma), rash, hepatic dysfunction, pancytopenia, and, ultimately, multiorgan failure (7). Features of disseminated intravascular coagulopathy are often present, and this can be partly explained by the presence of liver dysfunction, fibrinogen consumption, and thrombocytopenia (8). To combat this highly fatal disorder, both primary HLH and secondary HLH are frequently treated with etoposide-based protocols, which are associated with significant toxicity and mortality (9). Alternative therapies that are less toxic and more targeted are currently being explored for secondary HLH/MAS.

In terms of its pathologic origins, secondary HLH/MAS develops as part of a "cytokine storm" (10). The proinflammatory cytokines that have been associated with secondary HLH/MAS include interferon-γ, interleukin-1 (IL-1), IL-6, IL-12, IL-18, and tumor necrosis factor (11). Anakinra is a recombinant human IL-1 receptor antagonist that blocks IL-1 function. While the safety and benefits of IL-1 blockade in the inflammatory process have been demonstrated in many diseases, including in the treatment of systemic juvenile idiopathic arthritis (JIA) and systemic JIA–related MAS (12–15), its role in treating non–systemic JIA–related MAS has not been widely explored. Nevertheless, anakinra has been reported to improve survival in several cases of MAS associated with non–systemic JIA rheumatic disorders (16), including systemic lupus erythematosus (SLE) (14).

In the present study, we retrospectively analyzed the benefit of anakinra in treating a cohort of pediatric patients with secondary HLH/MAS associated with various underlying diseases, including both rheumatic and nonrheumatic conditions. Our findings show that 1) the recombinant human IL-1 receptor antagonist anakinra appears effective in the treatment of pediatric patients who have secondary HLH/MAS in conjunction with non–malignancy-associated diseases, 2) thrombocytopenia is a risk factor for mortality in children with secondary HLH treated with anakinra, 3) the presence of an *STXBP2* heterozygous mutation is a risk factor for mortality in children with secondary HLH treated with anakinra, 4) children with systemic JIA–associated MAS have good outcomes with anakinra therapy, and 5) in the absence of malignancy, early initiation of anakinra therapy for secondary HLH is associated with decreased mortality.

PATIENTS AND METHODS

Patients. An institutional review board–approved retrospective chart review was conducted to identify consecutive pediatric patients with secondary HLH/MAS (defined as International Classification of Diseases, Ninth Revision [ICD-9] code

Table 1. Demographic and clinical characteristics at presentation and outcomes after treatment start in all patients and according to those who survived and those who died*

	Total (n = 44)	Survived (n = 32)	Died (n = 12)	P, survived vs. died†
Male	19 (43)	13 (41)	6 (50)	1
Age, mean ± SD years	10.3 ± 5.7	9.6 ± 5.3	12.3 ± 6.5	0.165
Clinical presentation				
Persistent fever	43 (98)	31 (97)	12 (100)	1
Hepatomegaly	13 (30)	10 (31)	3 (25)	1
Splenomegaly	15 (34)	12 (38)	3 (25)	0.5
Leukopenia <1,000/μl	24 (55)	15 (47)	9 (75)	0.173
Hemoglobin <9 gm/liter	30 (68)	20 (63)	10 (83)	0.282
Platelets <100,000/μl	31 (71)	19 (59)	12 (100)	0.008
Trigylcerides >3 mmoles/liter	30/41 (73)	20/29 (69)	10 (83)	0.456
Fibrinogen <1.5 gm/liter	16/43 (37)	9 (28)	7/11 (64)	0.092
Hemophagocytosis	14/35 (40)	11/26 (42)	3/9 (33)	1
Low NK cell function	13/24 (54)	10/18 (56)	3/6 (50)	1
Elevated sCD25 (>1,105 units/ml)	31/35 (89)	22/24 (92)	9/11 (82)	1
Hepatitis	43 (98)	31 (94)	12 (100)	1
Ferritin level, mean ± SD ng/ml	33,316 ± 56,514	28,480.8 ± 48,582	48,803.8 ± 79,565	0.309
Outcome				
Hospitalization, mean ± SD days	30 ± 40	18 ± 16	62 ± 62	0.0005
Ferritin level				
Within 15 days of start of anakinra, mean ± SD ng/ml	14,435 ± 79,842	1,651 ± 2,967	51,511 ± 157,590	0.075
Change at 15 days, mean ± SD ng/ml	19,256 ± 66,334	−26,830 ± 47,078	+2,707 ± 104,703	0.201
Decrease at 15 days, mean ± SD %	72 ± 62	85 ± 17	35 ± 115	0.0202
Defervescence after anakinra start, mean ± SD days	1.7 ± 1.1	1.6 ± 1	2 ± 1.4	0.297

* Except where indicated otherwise, values are the number (%) of patients. NK = natural killer; sCD25 = soluble interleukin-2 receptor α-chain.
† By *t*-test or Fisher's exact text.

288.4 or ICD-10 code D76.1 in the electronic medical record [EMR]) who were older than age 1 year (to exclude patients with primary HLH) and who were treated with anakinra at Children's of Alabama from January 2008 through December 2016. There were no patients older than age 1 year who were identified as having homozygous HLH mutations.

A diagnosis of secondary HLH or MAS was confirmed using at least 1 of 6 different sets of criteria: the HLH-2004 criteria (9), the HLH-2009 criteria (17), the criteria for SLE-associated MAS (18), the 2016 criteria for systemic JIA–associated MAS (19), the HScore for diagnosis of reactive hemophagocytic syndrome (20), or the MAS/primary HLH (MH) score (21). Data on demographic, clinical, laboratory, and genetic characteristics, concurrent treatments, and outcomes were collected and analyzed using appropriate univariate statistical approaches (as described below).

Tests. Soluble IL-2 receptor α-chain (sCD25) and natural killer (NK) cell function assays were performed at Cincinnati Children's Diagnostic Immunology Laboratory and tested by chromium release assay. Four different effector-to–target cell ratios were analyzed, and normal NK cell function was defined as ≥2.6 lytic units. Genetic analysis for primary HLH–associated genes was performed at Cincinnati Children's Genetics, and results from a subset of these patients have been reported previously (5).

Statistical analysis. Data analysis was performed using SAS software version 9.3, and descriptive statistics were used as appropriate. Patients' demographic, clinical, and laboratory data and the day of starting anakinra treatment were examined against outcome measures (duration of hospital stay, days to defervescence, drop in ferritin level, and mortality) to identify any predictors of outcome. Paired t-tests were used to compare changes in laboratory measurements before and after anakinra treatment. Chi-square analysis and ordinal univariate regression analysis were used to determine the association between patient variables and outcomes. Group comparisons (as shown in Tables 1 and 2) were considered hypothesis-generating, and no adjustment for multiple comparisons was made. Chi-square analyses (as shown in Table 4) were performed to assess correlations with outcomes.

Table 2. HLH genetic testing results*

Test result	Total tested (n = 38)	Survived (n = 28)	Died (n = 10)
No HLH gene mutation	25 (66)	20 (80)	5 (20)
Any HLH heterozygous gene mutation	13 (34)	8 (62)	5 (38)
UNC13D	6 (16)	5 (83)	1 (17)
STXBP2	5 (13)	1 (20)†	4 (80)
PRF1	1 (3)	1 (100)	0
RAB27A	1 (3)	1 (100)	0

* Values are the number (%) of patients. HLH = hemophagocytic lymphohistiocytosis.
† P = 0.012 versus patients who died.

RESULTS

Diagnoses. Forty-four pediatric patients with secondary HLH/MAS treated with anakinra at Children's of Alabama were identified on the basis of ICD-9 and ICD-10 codes in the EMRs over the 9-year span. Forty-two children (95%) met the classification criteria for systemic JIA–associated MAS (see Supplementary Table 1, available on the *Arthritis & Rheumatology* web site at http://onlinelibrary.wiley.com/doi/10.1002/art.41103/abstract). The more restrictive 2004 and 2009 criteria for HLH were met by 70% and 75% of patients, respectively. Applying the HScore for secondary HLH/MAS (selecting a probability score of >90%) identified 66% of patients, and the discriminatory MH score identified only 27% of the patients as not having primary HLH. All patients, including all 8 with SLE or mixed connective tissue disease (MCTD), met the criteria for SLE-associated MAS, but these criteria were not specific to either SLE or MCTD.

The underlying diseases of the secondary HLH cohort were systemic JIA (n = 13), SLE (n = 5), MCTD (n = 3), malignancy/acute lymphoblastic leukemia (n = 3; 2 with pre–B cell and 1 with T cell malignancies), gastroparesis (n = 3, of whom 1 also had systemic JIA), uveitis with spondyloarthritis (n = 2) (both being previously reported [22,23]), other autoimmune conditions (n = 5; Sjögren's disease, vasculitis, Crohn's disease, sarcoidosis, antiphospholipid antibody syndrome), mitochondrial disorder (n = 1), and unknown (n = 10). Thus, 16 (36%) of the patients with secondary HLH did not have an identifiable rheumatic disease. Six (60%) of the 10 patients without any known underlying disease had identified infections, while infections were present in 13 (38%) of the 34 patients with underlying disorders (see Supplementary Table 1, http://onlinelibrary.wiley.com/doi/10.1002/art.41103/abstract). Nine (47%) of the 19 infections that occurred in patients were members of the herpesvirus family.

Demographics and clinical presentation. The cohort as a whole included 25 female patients and 19 male patients, and the mean age was 10 years (range 1–19 years) (Table 1). Clinical presentations in patients with secondary HLH/MAS (using the HScore criteria for HLH diagnosis) included persistent fever in 43 (98%) of 44 patients, hepatomegaly in 13 (30%) of 44 patients, and splenomegaly in 15 (34%) of 44 patients. Laboratory features (among those tested) included leukopenia (leukocytes <1,000/μl) in 24 (55%) of 44 patients, anemia (hemoglobin <9 gm/liter) in 30 (68%) of 44 patients, thrombocytopenia (platelet count <100,000/μl) in 31 (71%) of 44 patients, hypertriglyceridemia (>3 mmoles/liter) in 30 (73%) of 41 patients, hypofibrinogenemia (<1.5 gm/liter) in 16 (44%) of 43 patients, low NK cell function in 13 (54%) of 24 patients, elevated sCD25 level (>1,105 units/ml) in 31 (89%) of 35 patients, and hepatitis (aspartate aminotransferase >30 IU/liter) in 43 (98%) of 44 patients (20). Thirty-five of 44 patients

underwent bone marrow biopsy, of whom 14 (40%) had hemophagocytosis (Table 1).

Treatments other than anakinra that the patients had been receiving either during their secondary HLH/MAS presentation or prior to the secondary HLH/MAS diagnosis are listed in Supplementary Table 2 (available on the *Arthritis & Rheumatology* web site at http://onlinelibrary.wiley.com/doi/10.1002/art.41103/abstract). Concomittant therapies included glucocorticoids (73%), cyclosporin A (25%), intravenous immunoglobulin (9%), etoposide (9%), tocilizumab (5%), and abatacept, rituximab, cyclophosphamide, and plasmapheresis in 1 patient each.

HLH genetics. Genetic testing for 5 of the primary HLH–associated genes (*UNC13D, STXBP2, STX11, PRF1,* and *RAB27A*) was carried out in 38 of the 44 patients. A heterozygous mutation was noted in 13 (34%) of the 38 patients tested (Table 2). Six patients (16%) had a mutation in *UNC13D* (MUNC13-4), and 1 of these patients died. Five of the 6 *UNC13D* mutations resulted in amino acid substitutions (only 1 being considered benign), and 1 was a predicted splice variant. Five patients (13%) had at least 1 *STXBP2* mutation (MUNC18-2) (see Supplementary Table 3, available on the *Arthritis & Rheumatology* web site at http://onlinelibrary.wiley.com/doi/10.1002/art.41103/abstract). Two patients had *STXBP2* amino acid substitutions, and 3 had at least 1 noncoding nucleotide mutation (intron, 3′–untranslated region, and just upstream of the transcription start site), some resulting in splice variants. Four (80%) of the 5 patients with *STXBP2* mutations died. One patient had a perforin gene (*PRF1*) mutation, and 1 other patient had an *RAB27A* mutation; both of these patients survived, and amino acid substitutions were present in the mutation in both patients.

With regard to associations of the demographic and baseline clinical, genetic, and laboratory features of the patients with mortality, thrombocytopenia at a platelet count of <100,000/μl and presence of an *STXBP2* mutation were each associated with increased mortality (*P* = 0.008 and *P* = 0.012, respectively) (Tables 1 and 2). There were no other significant differences in any other measures between the patients who survived and those who died.

Hospital course and mortality. The overall mortality rate in all patients was 27%, and the median duration of hospitalization was 15 days. Presumed causes of mortality are listed in Table 3. Five of 12 patients died with the diagnosis of septic shock, and 6 of 12 patients died with the diagnosis of multiorgan system failure. Six of the 12 patients who died had confirmed systemic infections, and 5 of these patients had positive fungal cultures. Of the 12 patients who died, 11 had been receiving concurrent immunosuppressive therapy, which included glucocorticoids (Table 3). There was no association with the timing of anakinra administration and infection.

The survival rate in patients with rheumatic/autoimmune diseases was 86% (100% in those with systemic JIA and 70% in those with SLE and related conditons), whereas it was 50% in all other patients with secondary HLH, including those with cancer. The survival rate in patients with nonrheumatic conditions or those with non–leukemia-associated conditions was 62%.

Not surprisingly, an earlier start to treatment with anakinra (≤5 days of hospitalization) was associated with a reduction in the frequency of mortality (*P* = 0.046) (Table 4). In considering patients according to the underlying diagnosis, those with systemic JIA had the lowest mortality rate, with no deaths among the 13 patients with systemic JIA included in the study (*P* = 0.006 by chi-square test). In contrast, patients with an underlying malignancy had the highest rate of mortality, at 100% (n = 3). In 2 of these patients, remission was achieved during treatment with dexamethasone, but was complicated

Table 3. Causes of death*

Patient	Diagnosis	Cause of death	Concurrent immunosuppression
16	SLE	Septic shock	IVMP (× 3), CYC
19	SLE/MCTD	MOSF	None
22	EBV	Septic shock	Prednisolone, rituximab
24	EBV	MOSF	IVMP (× 3), dexamethasone, CsA, etoposide
27	HHV6	Fungemia, MOSF	Prednisolone, CsA, dexamethasone, etoposide
32	Sjögren's syndrome	MOSF, septic shock	IVMP (× 3), IVIG, plasmapheresis
34	Crohn's disese	*Clostridium difficile* colitis, septic shock	IVMP (× 3)
35	Pre–B cell ALL/*Esherichia coli*	Septic shock, pancreatitis, MOSF	CsA, dexamethasone, induction chemotherapy
36	T cell ALL	Disseminated *Fusarium* fungal infection (BMT)	Dexamethasone, etoposide
37	Pre–B cell ALL	Disseminated mucormycosis	Dexamethasone
38	TPN-dependent gastroparesis/CMV	*Aspergillus* central line infection, MOSF	IVMP (× 3), CsA, abatacept, tocilizumab
41	Unknown	GVHD, fungemia (after BMT)	Dexamethasone, etoposide, BMT

* SLE = systemic lupus erythematosus; IVMP = intravenous methylprednisolone; CYC = cyclophosphamide; MCTD = mixed connective tissue disease; MOSF = multiorgan system failure; EBV = Epstein-Barr virus; CsA = cyclosporin A; HHV6 = human herpesvirus 6; IVIG = intravenous immunoglobulin; ALL = acute lymphoblastic leukemia; BMT = bone marrow transplantation; TPN = total parenteral nutrition; CMV = cytomegalovirus; GVHD = graft-versus-host disease.

Table 4. Predictive factors correlated with outcomes*

Outcome, predictive factor	P
Increased mortality rate	
Thrombocytopenia	0.025
HScore cell lineage	0.033
STXBP2 mutation	0.004
Decreased mortality rate	
Earlier start to anakinra treatment	0.046
Systemic JIA	0.006
Improvement in ferritin level	
Earlier start to anakinra treatment	0.001

* JIA = juvenile idiopathic arthritis.

by disseminated fungal infection, and 1 patient who was undergoing induction therapy died of multiorgan system failure, presumably attributable to secondary HLH. Nevertheless, 1 of the patients with pre–B cell leukemia (patient 37 in Table 3) had a presenting diagnosis of MAS and was effectively treated with anakinra. It was only on the third bone marrow evaluation of this patient that the leukemia was identified (6 months after presentation, long after the patient had been discharged from the hospital), although there was a heightened concern for the diagnosis of leukemia from the time of presentation. Once the patient had been diagnosed as having leukemia, treatment with anakinra was stopped, and the patient quickly succumbed to infection upon initiation of induction chemotherapy for leukemia.

In comparison, 3 of the 6 patients with an underlying infectious etiology died from septic shock or multiorgan system failure. Of the 28 patients with a rheumatic or autoimmune disease, only 4 (14%) died following anakinra administration. One of these patients, who had underlying Crohn's disease, had confirmed *Clostridium difficile* infection, and the other 3 died of multiorgan system failure and/or septic shock (Table 3).

Four patients who died (3 from systemic fungal infections) also received concurrent etoposide as part of the HLH-04 protocol (10). In terms of timing, 2 patients received the HLH-04 protocol at the time of secondary HLH diagnosis. One patient (patient 24 in Table 3) received anakinra as a last-ditch effort during the last 4 days of her life and 4 months into the diagnosis. The other patient (patient 27 in Table 3) received anakinra 4 days after the HLH-04 protocol, as adjunctive therapy, because the patient's condition dramatically worsened. Another patient (patient 41 in Table 3) received anakinra 1 day after diagnosis and started the HLH-04 protocol the next day. He eventually died 7 months later, following stem cell transplantation. The fourth patient (patient 36 in Table 3) who was receiving etoposide had received the HLH-04 protocol previously, and then the disease relapsed with the emergence of T cell leukemia and secondary HLH. Dexamethsone was started but treatment with etoposide was withheld due to the occurrence of severe cytopenia from recent chemotherapy. Anakinra was added 11 days after hospital admission, and etoposide was added 2 days later. In this retrospective study, all

patients who received etoposide as part of the HLH-04 protocol died.

Thrombocytopenia at any point was also significantly associated with mortality, as all patients who died had platelet counts of <100,000/μl ($P = 0.025$). Having a higher HScore for the cytopenia lineage was also associated with higher mortality ($P = 0.033$).

In terms of a biomarker, the mean pretreatment serum ferritin level was 33,316 ng/ml and dropped to 14,435 ng/ml (57% decrease) within 15 days of the start of anakinra treatment (Table 1). An increased serum ferritin level was closely associated with death ($P = 0.075$), whereas a drop in the ferritin level within 15 days of hospitalization was significantly associated with survival ($P = 0.0202$) (Table 1). Regarding the drop in ferritin level, an earlier start to the anakinra treatment (≤5 days of hospitalization) was associated with a greater drop in ferritin level ($P = 0.001$) (Table 4). Specifically, anakinra given within 5 days of the secondary HLH/MAS diagnosis led to a mean reduction in ferritin level of 90%, compared to a mean reduction of 54% if anakinra was given after the first 5 days of hospitalization. Anakinra given within 3 days of the start of hospitalization did not show further benefits. However, an earlier start to the anakinra treatment was associated with earlier defervescence ($P = 0.004$).

DISCUSSION

The recombinant human IL-1 receptor antagonist anakinra has been shown to be highly effective for the treatment of systemic JIA (12). MAS and systemic JIA flare share many clinical and laboratory features. Moreover, in addition to the 10% risk of developing overt MAS as part of systemic JIA, another 30–40% of systemic JIA patients may have occult or subclinical MAS during a disease flare that can eventually lead to overt MAS (24). This association of MAS with systemic JIA suggested that anakinra would also be a valuable treatment for systemic JIA–associated MAS. There are several reports of dramatically successful use of anakinra in cases of systemic JIA–associated MAS (12,13,15), in addition to its use in other rheumatic conditions such as SLE with or without antiphospholipid antibody syndrome (14,25), acute rheumatic fever, antineutrophil cytoplasmic antibody–positive vasculitis, eosinophilic granulomatosis with polyangiitis, Kawasaki disease (16,26), and autoinflammatory conditions (13).

MAS and severe sepsis also share many clinical and laboratory features, such as elevated serum ferritin levels, hepatic dysfunction, cytopenias, coagulopathy, central nervous system dysfunction (27), tissue hemophagocytosis, and elevated expression of CD163+ macrophages in the reticuloendothelial system (28,29). These shared features are initiated and perpetuated by a cytokine storm in which IL-1 plays a major role (30,31). IL-1 receptor blockade was associated with significant

improvement in survival of patients with sepsis and concurrent hepatobiliary dysfunction/disseminated intravascular coagulation (32), and also in a series of patients with a clinical picture of secondary HLH/sepsis/multiple organ dysfunction syndrome/MAS that occurred in the setting of a variety of rheumatic and nonrheumatic diseases (33). Thus, based on the association of IL-1 signaling pathway dysfunction in these diverse conditions, we were encouraged to use anakinra for treating cases of MAS complicating a variety of rheumatic and nonrheumatic conditions. However, we should acknowledge that our study is limited by its retrospective nature, nonuniform approach to therapy, lack of treatment controls, and variable follow-up period. In particular, selection bias in terms of use of anakinra in those who were less severely ill may have played a role.

In this study, anakinra treatment of pediatric patients with secondary HLH/MAS was associated with improved overall survival (73%) in comparison to that in patients with primary HLH and those with secondary HLH who received etoposide-based protocols (survival rate of 55%, of whom 82% had secondary HLH) (9), perhaps due in part to its more acceptable safety profile relative to chemotherapy. Moreover, the earlier initiation of anakinra (≤5 days of hospitalization) was associated with further reduced mortality in all patients (Table 4). Of note, it worked best in patients with underlying rheumatic conditions, particularly systemic JIA (Table 5), but it has also been shown to be beneficial in other conditions, such as infection-related secondary HLH/MAS (32,33). Patients with an underlying malignancy showed poor survival, regardless of remission status, suggesting that IL-1 blockade may be ineffective in treating patients with a history of cancer and related conditions. Survival rates within this cohort were also lower in those patients who had Epstein-Barr virus (EBV)–induced secondary HLH/MAS, similar to a recent report of 44% survival in a pediatric secondary HLH cohort, with the worst survival in those with both EBV and cytomegalovirus infections (34).

Table 5. Survival based on diagnosis

Diagnosis	No. of patients	Survival rate, no. (%)
Systemic JIA	13	13 (100)*
Malignancy (leukemia)	3	0 (0)
Lupus and related conditions†	10	7 (70)
Infection alone	6	3 (50)
Other/unknown‡	12	9 (75)

* The survival rate in patients with systemic juvenile idiopathic arthritis (JIA) was significantly different compared to the other groups (*P* = 0.006).
† Includes systemic lupus erythematosus (n = 5), mixed connective tissue disease (n = 3), Sjögren's syndrome (n = 1), and antiphospholipid syndrome (n = 1).
‡ Includes gastroparesis (n = 2), spondyloarthritis with uveitis (n = 2), sarcoidosis (n = 1), Crohn's disease (n = 1), mitochondrial disorder (n = 1), undefined vasculitis (n = 1), and unknown (n = 4).

The survival rate in the present study cohort was 73%, in contrast to survival rates of 53% and 65% in other studies (35,36). In a nationwide registry of pediatric patients with HLH in Korea, the 5-year overall survival rate was 68% (38% in the familial group and 81% in the presumed secondary HLH group). The 5-year overall survival rate among 32 patients who underwent allogeneic hematopoietic stem cell transplantation was 64% (37). Similar or even higher mortality rates were reported in adults with secondary HLH (38). This could potentially be explained by the safety profile of anakinra and the avoidance of the need for bone marrow transplantation and the pretransplantation myeloablative regimen, both of which have their own associated significant morbidity and mortality. Nevertheless, if a patient does not have a marked response to high-dose anakinra, then cytotoxic agents are probably warranted. Interestingly, prior to the introduction of anakinra, systemic JIA–related MAS was previously reported to have a mortality rate as high as 28% (39); nevertheless, all of the patients with systemic JIA in our cohort did well, being likely attributable to the use of IL-1 inhibitors (40). In this study, patients with MAS associated with systemic JIA had the best outcome, with 100% survival, while those with secondary HLH associated with malignancy had the worst outcome, with 100% mortality. This is consistent with a reported mortality rate of 85% in adults with hematologic malignancy–associated secondary HLH (41).

In addition to the underlying disease–associated mortality, other features associated with outcomes were explored. In this study, the mean serum level of ferritin within the first 15 days of treatment was higher in patients who died, a difference that approached statistical significance (*P* = 0.075). Moreover, the percentage drop in ferritin level at 15 days was significantly associated with survival (*P* = 0.0202) in this cohort (Table 1). This is in accordance with the findings from other studies, in which the rate of decrease in ferritin concentration was associated with differences in mortality rates in children (42).

A more compelling laboratory feature from the current study was the platelet count. In total, 71% of the patients had clear thrombocytopenia (platelet count <100,000/μl) at presentation, and this was associated with the mortality rate (*P* = 0.008) (Table 1). This is comparable to studies in adult patients, in which disseminated intravascular coagulation (in 40% of cases) was reported to be associated with high mortality rates, especially in patients with severe thrombocytopenia (43). In the current study, thrombocytopenia at any point during hospitalization was also associated with a significantly higher rate of mortality, such that all patients who died had platelet counts of <100,000/μl at some point (*P* = 0.025). Thus, thrombocytopenia in the setting of an inflammatory state that often leads to thrombocytosis is a poor prognostic finding.

In addition to laboratory findings in the peripheral blood, pathologic specimens can be informative in the setting of

secondary HLH/MAS. Hemophagocytosis observed on bone marrow biopsy, although considered a hallmark of secondary HLH, was found in only 14 (40%) of the 35 patients who were tested in the present cohort. Other studies have reported hemophagocytosis in 64% (44) to 84% (45) of patients with secondary HLH/MAS who had a bone marrow aspirate assessed or a reticuloendothelial organ biopsy performed. Our results emphasize the fact that bone marrow hemophagocytosis is not essential for the diagnosis of secondary HLH/MAS, since it might be absent, particularly early on in the disease course (46). Moreover, patients with secondary HLH/MAS are usually critically ill and might not be stable enough to undergo bone marrow biopsy, which might lead to a delay in an urgently needed diagnosis.

Although it is a potential diagnostic tool that has only recently been utilized, HLH genetics were also explored as prognostic factors. Of the 5 HLH genes analyzed, 34% of those tested were found to possess at least 1 heterozygous mutation (Table 2). This is very much in keeping with what has been reported in cohorts of patients with secondary HLH/MAS whose genetic profiles have been explored (4,5). Specifically, in the current cohort, *STXBP2* mutations were found in 5 (13.2%) of the 38 patients who were tested. The highest mortality rate among those with HLH gene mutations was associated with *STXBP2* (*P* = 0.012), as 4 of 5 patients with an *STXBP2* mutation died. These results are similar to those in a study by Cetica et al, who identified 4 patients (14%) with a positive *STXBP2* mutation among patients with HLH who lacked mutations in *PRF1*, *UNC13D*, and *STX11* genes, and of these 4 patients, 2 (50%) died (47).

Taken together, these findings suggest that possessing a heterozygous mutation in *STXBP2* represents a significant risk factor for mortality in the setting of secondary HLH/MAS. Indeed, we previously showed that 1 of these fatality-associated *STXBP2* mutations (c.1298 C>T, p.A433V) (see Supplementary Table 3, http://onlinelibrary.wiley.com/doi/10.1002/art.41103/abstract) acts in a partially dominant-negative manner to inhibit NK cell cytolytic activity (5). *STXBP2* is also important for apical trafficking in epithelial cells, as it is necessary for fusion of vesicles with the plasma membrane, and lack of *STXBP2* function results in villous atrophy and intestinal atresia critical for gut barrier protection (48–50). Perhaps the association of *STXBP2* mutations with enteropathy also puts these patients at greater risk of intestinal border bacterial translocation and sepsis.

In summary, our findings indicate that anakinra (a recombinant human IL-1 receptor antagonist) appears to be effective in the treatment of non–malignancy-related secondary HLH/MAS in children, notably those with systemic JIA, but also in patients with underlying SLE, MCTD, other autoimmune diseases, and/or infections. Anakinra was less effective in treating those with hematologic malignancies and those with *STXBP2* mtuations. Based on these results, we recom-

mend the use of anakinra as a safe and promising treatment for non–malignancy-related secondary HLH/MAS, especially when given early in the disease course. Anakinra is currently being studied in a randomized, double-blind, placebo-controlled trial (ClinicalTrials.gov identifier: NCT02780583) to test its safety and efficacy in the treatment of secondary HLH/MAS in children and adults.

AUTHOR CONTRIBUTIONS

All authors were involved in drafting the article or revising it critically for important intellectual content, and all authors approved the final version to be published. Dr. Cron had full access to all of the data in the study and takes responsibility for the integrity of the data and the accuracy of the data analysis.

Study conception and design. Eloseily, Weiser, Crayne, Haines, Beukelman, Atkinson, Cron.
Acquisition of data. Eloseily, Weiser, Crayne.
Analysis and interpretation of data. Eloseily, Weiser, Crayne, Mannion, Stoll, Beukelman, Cron.

REFERENCES

1. Filipovich AH. The expanding spectrum of hemophagocytic lymphohistiocytosis. Curr Opin Allergy Clin Immunol 2011;11:512–6.
2. Zhang L, Zhou J, Sokol L. Hereditary and acquired hemophagocytic lymphohistiocytosis. Cancer Control 2014;21:301–12.
3. Grom AA. Macrophage activation syndrome and reactive hemophagocytic lymphohistiocytosis: the same entities? Curr Opin Rheumatol 2003;15:587–90.
4. Kaufman KM, Linghu B, Szustakowski JD, Husami A, Yang F, Zhang K, et al. Whole-exome sequencing reveals overlap between macrophage activation syndrome in systemic juvenile idiopathic arthritis and familial hemophagocytic lymphohistiocytosis. Arthritis Rheumatol 2014;66:3486–95.
5. Zhang M, Behrens EM, Atkinson TP, Shakoory B, Grom AA, Cron RQ. Genetic defects in cytolysis in macrophage activation syndrome. Curr Rheumatol Rep 2014;16:439.
6. Strippoli R, Caiello I, De Benedetti F. Reaching the threshold: a multilayer pathogenesis of macrophage activation syndrome. J Rheumatol 2013;40:761–7.
7. Cron RQ, Davi S, Minoia F, Ravelli A. Clinical features and correct diagnosis of macrophage activation syndrome. Expert Rev Clin Immunol 2015;11:1043–53.
8. Minoia F, Davì S, Horne A, Demirkaya E, Bovis F, Li C, et al, on behalf of the Pediatric Rheumatology International Trials Organization, the Childhood Arthritis and Rheumatology Research Alliance, the Pediatric Rheumatology Collaborative Study Group, and the Histiocyte Society. Clinical features, treatment, and outcome of macrophage activation syndrome complicating systemic juvenile idiopathic arthritis: a multinational, multicenter study of 362 patients. Arthritis Rheumatol 2014;66:3160–9.
9. Henter JI, Horne A, Aricó M, Egeler RM, Filipovich AH, Imashuku S, et al. HLH-2004: diagnostic and therapeutic guidelines for hemophagocytic lymphohistiocytosis. Pediatr Blood Cancer 2007;48:124–31.
10. Canna SW, Behrens EM. Making sense of the cytokine storm: a conceptual framework for understanding, diagnosing, and treating hemophagocytic syndromes. Pediatr Clin North Am 2012;59:329–44.
11. Grom AA, Mellins ED. Macrophage activation syndrome: advances towards understanding pathogenesis. Curr Opin Rheumatol 2010;22:561–6.

12. Ravelli A, Grom AA, Behrens EM, Cron RQ. Macrophage activation syndrome as part of systemic juvenile idiopathic arthritis: diagnosis, genetics, pathophysiology and treatment. Genes Immun 2012;13:289–98.

13. Sönmez HE, Demir S, Bilginer Y, Özen S. Anakinra treatment in macrophage activation syndrome: a single center experience and systemic review of literature. Clin Rheumatol 2018;37:3329–35.

14. Aytaç S, Batu ED, Ünal Ş, Bilginer Y, Çetin M, Tuncer M, et al. Macrophage activation syndrome in children with systemic juvenile idiopathic arthritis and systemic lupus erythematosus. Rheumatol Int 2016;36:1421–9.

15. Barut K, Yücel G, Sinoplu AB, Şahin S, Adroviç A, Kasapçopur Ö. Evaluation of macrophage activation syndrome associated with systemic juvenile idiopathic arthritis: single center experience over a one-year period. Turk Pediatri Ars 2015;50:206–10.

16. Miettunen PM, Narendran A, Jayanthan A, Behrens EM, Cron RQ. Successful treatment of severe paediatric rheumatic disease-associated macrophage activation syndrome with interleukin-1 inhibition following conventional immunosuppressive therapy: case series with 12 patients [letter]. Rheumatology (Oxford) 2011;50:417–9.

17. Filipovich AH. Hemophagocytic lymphohistiocytosis (HLH) and related disorders. Hematology Am Soc Hematol Educ Program 2009;127–31.

18. Parodi A, Davì S, Pringe AB, Pistorio A, Ruperto N, Magni-Manzoni S, et al. Macrophage activation syndrome in juvenile systemic lupus erythematosus: a multinational multicenter study of thirty-eight patients. Arthritis Rheum 2009;60:3388–99.

19. Ravelli A, Minoia F, Davì S, Horne A, Bovis F, Pistorio A, et al. 2016 classification criteria for macrophage activation syndrome complicating systemic juvenile idiopathic arthritis: a European League Against Rheumatism/American College of Rheumatology/Paediatric Rheumatology International Trials Organisation collaborative initiative. Arthritis Rheumatol 2016;68:566–76.

20. Fardet L, Galicier L, Lambotte O, Marzac C, Aumont C, Chahwan D, et al. Development and validation of the HScore, a score for the diagnosis of reactive hemophagocytic syndrome. Arthritis Rheumatol 2014;66:2613–20.

21. Minoia F, Bovis F, Davì S, Insalaco A, Lehmberg K, Shenoi S, et al, on behalf of the Pediatric Rheumatology International Trials Organization, the Childhood Arthritis and Rheumatology Research Alliance, the Pediatric Rheumatology Collaborative Study Group, and the Histiocyte Society. Development and initial validation of the macrophage activation syndrome/primary hemophagocytic lymphohistiocytosis score, a diagnostic tool that differentiates primary hemophagocytic lymphohistiocytosis from macrophage activation syndrome. J Pediatr 2017;189:72–8.

22. Cron RQ, Chatham WW. Development of spondyloarthropathy following episodes of macrophage activation syndrome in children with heterozygous mutations in haemophagocytic lymphohistiocytosis-associated genes [letter]. Clin Exp Rheumatol 2016;34:953.

23. Zhang M, Bracaglia C, Prencipe G, Bemrich-Stolz CJ, Beukelman T, Dimmitt RA, et al. A heterozygous RAB27A mutation associated with delayed cytolytic granule polarization and hemophagocytic lymphohistiocytosis. J Immunol 2016;196:2492–503.

24. Behrens EM, Beukelman T, Paessler M, Cron RQ. Occult macrophage activation syndrome in patients with systemic juvenile idiopathic arthritis. J Rheumatol 2007;34:1133–8.

25. Tayer-Shifman OE, Ben-Chetrit E. Refractory macrophage activation syndrome in a patient with SLE and APLA syndrome—successful use of PET-CT and anakinra in its diagnosis and treatment. Mod Rheumatol 2013;25:954–7.

26. Shafferman A, Birmingham JD, Cron RQ. High dose anakinra for treatment of severe neonatal Kawasaki disease: a case report. Pediatr Rheumatol Online J 2014;12:26.

27. Strauss R, Neureiter D, Westenburger B, Wehler M, Kirchner T, Hahn EG. Multifactorial risk analysis of bone marrow histiocytic hyperplasia with hemophagocytosis in critically ill medical patients—a postmortem clinicopathologic analysis. Crit Care Med 2004;32:1316–21.

28. Crayne CB, Albeituni S, Nichols KE, Cron RQ. The immunology of macrophage activation syndrome [review]. Front Immunol 2019;10:119.

29. Schaer DJ, Schaer CA, Schoedon G, Imhof A, Kurrer MO. Hemophagocytic macrophages constitute a major compartment of heme oxygenase expression in sepsis. Eur J Haematol 2006;77:432–6.

30. Dinarello CA. Interleukin-1 in the pathogenesis and treatment of inflammatory diseases. Blood 2011;117:3720–32.

31. Hotchkiss RS, Karl IE. The pathophysiology and treatment of sepsis. N Engl J Med 2003;348:138–50.

32. Shakoory B, Carcillo JA, Chatham WW, Amdur RL, Zhao H, Dinarello CA, et al. Interleukin-1 receptor blockade is associated with reduced mortality in sepsis patients with features of macrophage activation syndrome: reanalysis of a prior phase III trial. Crit Care Med 2016;44:275–81.

33. Rajasekaran S, Kruse K, Kovey K, Davis AT, Hassan NE, Ndika AN, et al. Therapeutic role of anakinra, an interleukin-1 receptor antagonist, in the management of secondary hemophagocytic lymphohistiocytosis/sepsis/multiple organ dysfunction/macrophage activating syndrome in critically ill children. Pediatr Crit Care Med 2014;15:401–8.

34. Dao D, Xoay TD, Galeano BK, Phuc PH, Ouellette Y. Etiologies and clinical outcomes of patients with secondary hemophagocytic lymphohistiocytosis at a tertiary PICU. Pediatr Crit Care Med 2019;20:e311–8.

35. Brito-Zerón P, Kostov B, Moral-Moral P, Martínez-Zapico A, Díaz-Pedroche C, Fraile G, et al, on behalf of the REGHEM-GEAS-SEMI Study Group. Prognostic factors of death in 151 adults with hemophagocytic syndrome: etiopathogenically driven analysis. Mayo Clin Proc Innov Qual Outcomes 2018;2:267–76.

36. Leow EH, Soh SY, Tan AM, Mok YH, Chan MY, Lee JH. Critically ill children with hemophagocytic lymphohistiocytosis: a case series of 14 patients. J Pediatr Hematol Oncol 2017;39:e303–6.

37. Koh KN, Im HJ, Chung NG, Cho B, Kang HJ, Shin HY, et al. Clinical features, genetics, and outcome of pediatric patients with hemophagocytic lymphohistiocytosis in Korea: report of a nationwide survey from Korea Histiocytosis Working Party. Eur J Haematol 2015;94:51–9.

38. Ishii E, Ohga S, Imashuku S, Yasukawa M, Tsuda H, Miura I, et al. Nationwide survey of hemophagocytic lymphohistiocytosis in Japan. Int J Hematol 2007;86:58–65.

39. Sawhney S, Woo P, Murray K. Macrophage activation syndrome: a potentially fatal complication of rheumatic disorders. Arch Dis Child 2001;85:421–6.

40. Stoll ML, Cron RQ. Treatment of juvenile idiopathic arthritis in the biologic age. Rheum Dis Clin North Am 2013;39:751–66.

41. Lorenz F, Klimkowska M, Pawlowicz E, Bulanda Brustad A, Erlanson M, Machaczka M. Clinical characteristics, therapy response, and outcome of 51 adult patients with hematological malignancy-associated hemophagocytic lymphohistiocytosis: a single institution experience. Leuk Lymphoma 2018;59:1840–50.

42. Lin TF, Ferlic-Stark LL, Allen CE, Kozinetz CA, McClain KL. Rate of decline of ferritin in patients with hemophagocytic lymphohistiocytosis as a prognostic variable for mortality. Pediatr Blood Cancer 2011;56:154–5.

43. Stéphan F, Thiolière B, Verdy E, Tulliez M. Role of hemophagocytic histiocytosis in the etiology of thrombocytopenia in patients with sepsis syndrome or septic shock. Clin Infect Dis 1997;25:1159–64.

44. Davì S, Minoia F, Pistorio A, Horne A, Consolaro A, Rosina S, et al. Performance of current guidelines for diagnosis of macrophage activation syndrome complicating systemic juvenile idiopathic arthritis. Arthritis Rheumatol 2014;66:2871–80.

45. Gupta A, Tyrrell P, Valani R, Benseler S, Weitzman S, Abdelhaleem M. The role of the initial bone marrow aspirate in the diagnosis of hemophagocytic lymphohistiocytosis. Pediatr Blood Cancer 2008;51:402–4.

46. Ravelli A. Macrophage activation syndrome. Curr Opin Rheumatol 2002;14:548–52.

47. Cetica V, Santoro A, Gilmour KC, Sieni E, Beutel K, Pende D, et al. STXBP2 mutations in children with familial haemophagocytic lymphohistiocytosis type 5. J Med Genet 2010;47:595–600.

48. Mosa MH, Nicolle O, Maschalidi S, Sepulveda FE, Bidaud-Meynard A, Menche C, et al. Dynamic formation of microvillus inclusions during enterocyte differentiation in Munc18-2-deficient intestinal organoids. Cell Mol Gastroenterol Hepatol 2018;6:477–93.

49. Stepensky P, Bartram J, Barth TF, Lehmberg K, Walther P, Amann K, et al. Persistent defective membrane trafficking in epithelial cells of patients with familial hemophagocytic lymphohistiocytosis type 5 due to STXBP2/MUNC18-2 mutations. Pediatr Blood Cancer 2013;60:1215–22.

50. Vogel GF, van Rijn JM, Krainer IM, Janecke AR, Posovszky C, Cohen M, et al. Disrupted apical exocytosis of cargo vesicles causes enteropathy in FHL5 patients with Munc18-2 mutations. JCI Insight 2017;2:94564.

AMERICAN COLLEGE
of RHEUMATOLOGY
Empowering Rheumatology Professionals

Genetic Deficiency of Interferon-γ Reveals Interferon-γ–Independent Manifestations of Murine Hemophagocytic Lymphohistiocytosis

Thomas N. Burn,[1] Lehn Weaver,[2] Julia E. Rood,[1] Niansheng Chu,[2] Aaron Bodansky,[2] Portia A. Kreiger,[2] and Edward M. Behrens[1] iD

Objective. Familial hemophagocytic lymphohistiocytosis (FHLH) is a complex cytokine storm syndrome caused by genetic abnormalities rendering CD8+ T cells and natural killer cells incapable of cytolytic killing. In murine models of FHLH, interferon-γ (IFNγ) produced by CD8+ T cells has been identified as a critical mediator of disease, and an IFNγ-blocking antibody (emapalumab) has recently been approved by the Food and Drug Administration. However, development of hemophagocytic lymphohistiocytosis (HLH)/macrophage activation syndrome (MAS) in patients who are genetically unresponsive to IFNγ questions the absolute necessity of IFNγ in driving disease. This study was undertaken to determine the necessity of IFNγ in driving HLH.

Methods. IFNγ$^{-/-}$Prf1$^{-/-}$ mice were infected with lymphocytic choriomeningitis virus (LCMV), and HLH immunopathologic features, including survival, weight loss, cytopenias, cytokine profiles, and immune cell phenotypes, were assessed. Mixed bone marrow chimeras were created to determine the immune cell–intrinsic role of IFNγ receptor signaling. CD8+ T cell depletion and interleukin-33 (IL-33)/ST2 blockade were performed using monoclonal antibodies.

Results. LCMV infection of IFNγ$^{-/-}$Prf1$^{-/-}$ mice resulted in severe HLH-like disease. CD8+ T cells and the IL-33/ST2 axis remained essential mediators of disease; however, IFNγ-independent HLH immunopathology correlated with a 10–15-fold increase in neutrophilia ($P < 0.001$) and an altered cytokine milieu dominated by IL-6, IL-1β, and granulocyte–macrophage colony-stimulating factor (GM-CSF) ($P < 0.05$). Furthermore, IFNγ regulated CD8+ T cell expression of GM-CSF and neutrophil survival.

Conclusion. IFNγ is not necessary for the development of fulminant HLH, requiring physicians to consider case-by-case treatment strategies. Use of therapies that target upstream activators of CD8+ T cells, such as IL-33/ST2 signaling, may be more universally applicable treatment options that ameliorate both IFNγ-dependent and -independent manifestations of HLH/MAS.

INTRODUCTION

Hemophagocytic lymphohistiocytosis (HLH) is a life-threatening cytokine storm syndrome, characterized by overabundance and overactivation of CD8+ T cells (1). The genetic abnormalities that underlie familial forms of HLH (FHLH) have been traced to genes involved in the cytolytic capabilities of cytotoxic lymphocytes (2). Currently, the only effective cure for FHLH is bone marrow transplantation. The best characterized

and most frequently identified genetic lesions occur in the perforin gene (*Prf1*) and define a group of patients known as FHL2 patients. The inability to clear antigen through perforin-dependent cytolysis by CD8+ T cells leads to protracted antigen exposure, increased CD8+ T cell proliferation and activation, and exaggerated inflammatory cytokine production, thought to drive immunopathology (3,4).

Studies utilizing the perforin-knockout mouse (Prf1$^{-/-}$) have implicated the excessive production of interferon-γ (IFNγ) by

hyperactive CD8+ T cells as the primary driver of disease (3). Antibody-mediated depletion of CD8+ T cells and antibody-mediated blockade of IFNγ are effective in preventing disease in multiple murine models of FHLH (3,5). Additionally, we have recently identified interleukin-33 (IL-33) signaling through ST2 as an additional upstream activator of CD8+ T cells that is essential in driving CD8+ T cell hyperactivation (6,7). These data have spurred a clinical trial investigating antibody-mediated blockade of IFNγ (emapalumab) in human HLH patients that has recently resulted in approval by the Food and Drug Administration (8).

HLH diagnoses in the absence of obvious genetic lesions in known FHLH genes are defined by a set of clinical criteria, leaving scope for many causative triggers and pathologic effectors (9). Despite the precedence that HLH disease pathogenesis is dependent on IFNγ, several murine models have shown that HLH disease can be driven by alternative cytokines (10,11). Additionally, a number of patients have developed HLH-like or macrophage activation syndrome (MAS)–like disease in the setting of mutations in the IFNγ receptor (IFNγR), rendering them unresponsive to IFNγ (12–14). This suggests that HLH/MAS physiology can result independent of IFNγ, or that IFNγ can signal through an alternative receptor to drive disease in these settings. Other preclinical models of murine HLH in mice that lack IFNγ or a functional IFNγR have not been adequately incorporated into most explanations of disease pathogenesis (15,16).

To query the absolute necessity of IFNγ in driving HLH, we infected IFNγ$^{-/-}$Prf1$^{-/-}$ double-knockout mice with lymphocytic choriomeningitis virus (LCMV). Herein, we demonstrate that LCMV infection is sufficient to drive HLH-like pathology in the absence of IFNγ. LCMV-infected IFNγ$^{-/-}$Prf1$^{-/-}$ double-knockout mice have disease of equal lethality to Prf1$^{-/-}$ mice. A modified qualitative response is highlighted by an altered serum cytokine signature and extensive neutrophilia, reminiscent of that seen in systemic juvenile idiopathic arthritis (JIA)–associated MAS (17). Despite loss of IFNγ production, CD8+ T cells and ST2 signaling remain essential in the pathogenesis of IFNγ-independent HLH-like disease. Additionally, in the absence of IFNγ signaling, CD8+ T cells have heightened granulocyte–macrophage colony-stimulating factor (GM-CSF)–producing capacity, unveiling an unrecognized method of GM-CSF regulation. These results highlight important regulatory roles for IFNγ under inflammatory conditions, which may be informative for diseases in which neutrophilia and/or aberrant GM-CSF production are pathogenic. Furthermore, this study addresses a clinically relevant and underappreciated aspect of HLH biology by defining IFNγ-independent cytokine storm pathology.

MATERIALS AND METHODS

Mice. C57BL/6 (wild-type), perforin-deficient (C57BL/6-Prf1^{tm1Sdz}/J, Prf1$^{-/-}$), IFNγ-deficient (B6.129S7-Ifng^{tm1Ts}/J, IFNγ$^{-/-}$), IFNγR–deficient (B6.129S7-Ifngr1^{tm1Agt}/J, IFNγR$^{-/-}$), and B6-CD45.1(B6.SJL-Ptprc^a Ptprc^b/BoyJ) mice were purchased from

The Jackson Laboratory and bred in our facility. Prf1$^{-/-}$ mice were crossed with IFNγ$^{-/-}$ mice, IFNγR$^{-/-}$ mice, and B6-CD45.1 mice. All animal studies were performed with approval from The Children's Hospital of Philadelphia Institutional Animal Care and Use Committee.

Induction of FHLH. Mice (6–8 weeks old) were infected intraperitoneally with 2 × 10^5 plaque-forming units of LCMV (Armstrong strain) and killed upon development of significant morbidity or weight loss. Peripheral blood cell counts were performed on a Sysmex XT-2000iV Automated Hematology Analyzer in the Translational Core Laboratory at The Children's Hospital of Philadelphia. Serum ferritin (Alpco), soluble CD25 (sCD25; R&D Systems), IL-6, GM-CSF, IL-1β, and IFNγ (BD Biosciences) were measured by enzyme-linked immunosorbent assay. Plaque assay was performed on Vero cells as previously described (18).

Histologic analysis. All slides were stained with hematoxylin and eosin. Images were acquired on an Eclipse 90i microscope (Nikon) using NIS-elements software.

Analysis of human gene expression. The published data set (GEO accession no. GSE26050) (19) was accessed through the National Center for Biotechnology Information Gene Expression Omnibus. The IFNγ gene set (HALLMARK_INTERFERON_GAMMA_RESPONSE) was downloaded from the Molecular Signatures Database (MSigDB; Broad Institute). Hierarchical clustering was performed and heatmaps were created using Morpheus (Broad Institute).

Flow cytometric analysis. Peripheral blood leukocytes, splenocytes, intrahepatic leukocytes, and bone marrow leukocytes were stained with Live/Dead Fixable Viability dye (Life Technologies), anti-CD90.2, CD19, NK1.1, CD11b, Ly6G, Ly6C, CD4, CD8α, CD44, CD62L, CD45.2, and CD45.1 (from BD PharMingen, eBioscience, and BioLegend). H-2D^{b}GP$_{33–41}$ major histocompatibility complex (MHC)–peptide complexes were provided as fluorophore-conjugated tetramers by Dr. E. J. Wherry (University of Pennsylvania). Samples were acquired on a MACSQuant flow cytometer (Miltenyi Biotec) and analyzed using FlowJo software version 10.4.2.

Intracellular cytokine staining. Splenocytes (10^6) were stimulated with 50 ng/ml phorbol myristate acetate (PMA; Sigma), 1 μg/ml ionomycin (Cell Signaling Technology), 2 μg/ml brefeldin A (Sigma), and 2 μM monensin (eBioscience) for 5 hours at 37°C. After staining with Live/Dead viability dye and surface antigens as described above, cells were stained for IFNγ (clone XMG1.2; BD Biosciences) and GM-CSF (clone MP1-22E9; BD Biosciences) using a Cytofix/Cytoperm kit (BD Biosciences).

In vivo antibody and recombinant IFNγ administration. Antibodies were administered to mice intraperitoneally beginning on day 3 after infection and every other day thereafter. Dosing and antibodies used were as follows. For CD8 depletion, 500 μg clone 2.43 (Bio X Cell) and IgG2b isotype control (clone LTF-2; Bio X Cell) were used. ST2 blockade was carried out as previously described using antibody provided by Amgen (20,21). For cytokine blockade, 500 μg anti-IFNγ (clone XMG1.2; Bio X Cell), 200 μg anti–IL-6 receptor (clone15A7; Bio X Cell), 200 μg anti–IL-1β (clone B122; Bio X Cell), 100 μg anti–GM-CSF (clone MP1-22E9; Bio X Cell), and the same dose of respective isotype controls (Bio X Cell) were used. For recombinant IFNγ give-back experiments, 10 μg recombinant IFNγ (PeproTech) was administered to mice every other day beginning either on day 0 or on day 6 after infection.

In vitro CD8+ T cell GM-CSF production assay. Naive (CD44–) CD8+ T cells were enriched from naive IFNγ$^{-/-}$ mice using Naive CD8a+ T cell isolation kits (Miltenyi Biotec). Purity was consistently >90%. Cells were cultured on plate-bound anti-CD3 (2 μg/ml; BioLegend) and anti-CD28 (2 μg/ml; BioLegend) in 96-well flat-bottomed plates with 10 ng/ml recombinant murine IL-12 (PeproTech) and 50 units/ml human IL-2 (PeproTech) for 2 days. Cells were removed from anti-CD3/28 and cultured a further 2 days with IL-2 and IL-12, before being cultured for 1 day with IL-2 alone. CD8+ T cells were restimulated with PMA and ionomycin and stained for intracellular GM-CSF as described above.

Generation of bone marrow chimeras. Host mice (Prf1$^{-/-}$IFNγR$^{+/+}$CD45.1$^{+/+}$ mice) ages 6–8 weeks old were lethally irradiated (950 rad on an X-RAD irradiator). Bone marrow was isolated from donor strains (Prf1$^{-/-}$IFNγR$^{+/+}$CD45.1$^{+/+}$ and Prf1$^{-/-}$IFNγR$^{-/-}$CD45.2$^{+/+}$), mixed 1:1, and 5 × 10^6 bone marrow cells were injected intravenously to host mice 6 hours after irradiation. Chimeras were reconstituted for 8 weeks before LCMV infection.

Apoptosis assay. Bone marrow obtained from chimeric mice on day 10 after infection was incubated at 37°C. Cells were stained for active caspase 3/7 using a Vybrant FAM caspase 3/7 assay kit (ThermoFisher) according to the manufacturer's instructions. Cells were then stained with Live/Dead viability dye and surface antigens as described above.

Statistical analysis. Weight loss data were analyzed with linear mixed-effects models using R (R Core Team, 2014), and *lme4*. Visual inspection of residual plots did not reveal any obvious deviations from homoscedasticity or normality. *P* values were obtained by likelihood ratio tests of the full model with the effect in question against the model without the effect in question. All other data were analyzed in GraphPad Prism 7 using the statistical tests indicated in the figure legends.

RESULTS

Development of HLH-like disease in IFNγ$^{-/-}$Prf1$^{-/-}$ mice. To determine whether IFNγ was necessary for fulminant HLH development in the murine FHL2 model, we generated IFNγ$^{-/-}$Prf1$^{-/-}$ double-knockout mice and evaluated them for HLH clinical characteristics following LCMV infection. IFNγ$^{-/-}$Prf1$^{-/-}$ and Prf1$^{-/-}$ mice experienced equivalent mortality (Figure 1A) and significant weight loss, despite this not being quite as severe in the Prf1$^{-/-}$ mice (Figure 1B). Wild-type and IFNγ$^{-/-}$ mice cleared LCMV (Armstrong strain) (22), displayed no mortality or weight loss, and were used as controls throughout. While IFNγ$^{-/-}$Prf1$^{-/-}$ mice did not experience anemia (Figure 1C), suggesting an IFNγ-dependent effect, both IFNγ$^{-/-}$Prf1$^{-/-}$ and Prf1$^{-/-}$ mice had severe thrombocytopenia (Figure 1D). Interestingly, while leukopenia is a common feature in HLH pathology, IFNγ$^{-/-}$Prf1$^{-/-}$ mice had elevated leukocyte counts (Figure 1E). IFNγ$^{-/-}$Prf1$^{-/-}$ mice had extremely elevated sCD25 levels (Figure 1F), suggesting the presence of highly activated T cells, had serum ferritin levels equivalent to those in Prf1$^{-/-}$ mice (Figure 1G), and had hepatosplenomegaly equivalent to that in Prf1$^{-/-}$ mice (Figures 1H and I). Finally, hemophagocytes were readily identified in the spleens of IFNγ$^{-/-}$Prf1$^{-/-}$ mice (Figure 1J). Given that natural killer cell function is defective by virtue of the absence of perforin, IFNγ$^{-/-}$Prf1$^{-/-}$ mice fulfill 5 criteria required for HLH diagnosis and partially fulfill a sixth in terms of cytopenia (9). Importantly, splenic viral titers did not differ between Prf1$^{-/-}$ and IFNγ$^{-/-}$Prf1$^{-/-}$ mice on day 10 postinfection (Supplementary Figure 1, available on the *Arthritis & Rheumatology* web site at http://onlinelibrary.wiley.com/doi/10.1002/art.41076/abstract).

Unlike genetic deficiency, antibody-mediated blockade of IFNγ protects against most disease features in Prf1$^{-/-}$ mice. We suspected that such blockade is not 100% efficient, explaining this difference. We therefore compared expression of the IFNγ-induced gene MHCII on inflammatory monocytes in Prf1$^{-/-}$ mice treated with anti-IFNγ blocking antibody to that in IFNγ$^{-/-}$Prf1$^{-/-}$ mice. Incomplete IFNγ blockade by antibody was suggested based on incomplete reduction in MHCII expression (Supplementary Figure 2, available on the *Arthritis & Rheumatology* web site at http://onlinelibrary.wiley.com/doi/10.1002/art.41076/abstract). Taken together, these data indicate that many clinical features of HLH pathology can arise independent of IFNγ, and that low level IFNγ signaling correlates with protection against disease.

Extensive neutrophilia in IFNγ$^{-/-}$Prf1$^{-/-}$ mice. Leukocyte counts were extremely high in IFNγ$^{-/-}$Prf1$^{-/-}$ mice compared to Prf1$^{-/-}$ and wild-type/IFNγ$^{-/-}$ controls and were predominantly neutrophils (Figure 2A). Increased numbers of neutrophils were also seen in the spleens and livers of IFNγ$^{-/-}$Prf1$^{-/-}$ mice following LCMV infection (Figures 2B and C and Supplementary Figure 3, available on the *Arthritis & Rheumatology* web site at http://onlinelibrary.wiley.com/doi/10.1002/art.41076/abstract). Histologic analysis of livers from IFNγ$^{-/-}$Prf1$^{-/-}$ mice revealed
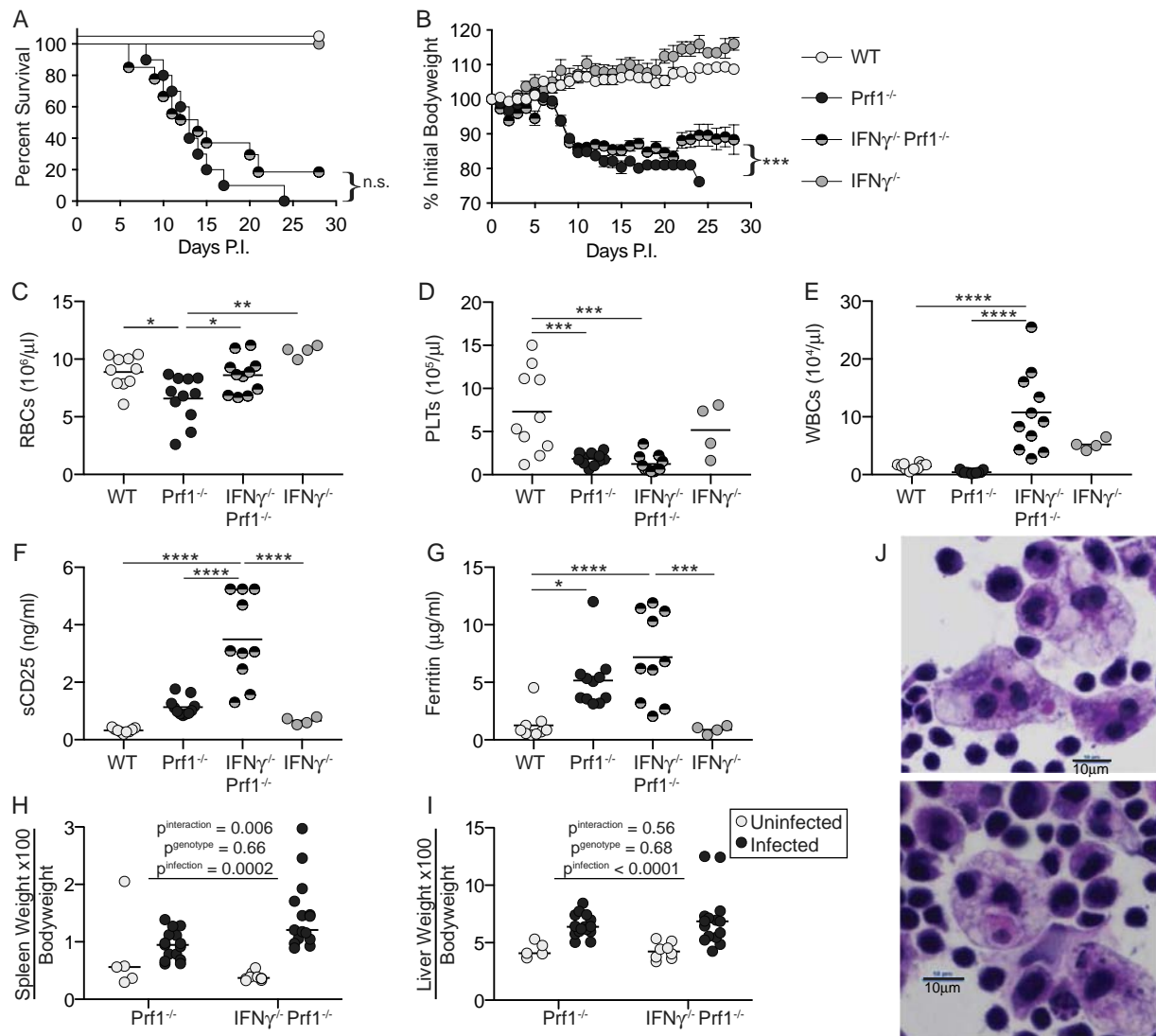
Figure 1. Hemophagocytic lymphohistiocytosis–like disease in IFNγ−/−Prf1−/− mice. **A** and **B**, Survival (**A**) and weight loss (**B**) in wild-type (WT) mice (n = 8), Prf1−/− mice (n = 10), IFNγ−/−Prf1−/− mice (n = 27), and IFNγ−/− mice (n = 5) infected with lymphocytic choriomeningitis virus (LCMV) (Armstrong strain). Results are shown for the indicated days postinfection (PI). Data were combined from 2 independent experiments. Values are the mean ± SEM. Survival curves in **A** were analyzed by log rank (Mantel-Cox) test. Weight loss in **B** was analyzed with a linear mixed-effects model to allow for missing data due to mouse mortality. Treatment and body weight were modeled as fixed effects, and individual mice were treated as a random effect to account for baseline variability between animals (e.g., intercept only). *** = $P < 0.001$. NS = not significant. **C–E**, Numbers of red blood cells (RBCs) (**C**), platelets (PLTs) (**D**), and white blood cells (WBCs) (**E**) in a complete blood cell count in the indicated mouse strains 10 days after infection with LCMV. **F** and **G**, Serum levels of soluble CD25 (sCD25) (**F**) and ferritin (**G**) in the indicated mouse strains 10 days after infection, measured by enzyme-linked immunosorbent assay. In **C–G**, data were combined from 2 independent experiments. Symbols represent individual mice; horizontal lines show the mean. * = $P < 0.05$; ** = $P < 0.01$; *** = $P < 0.001$; **** = $P < 0.0001$, by one-way analysis of variance (ANOVA) with Tukey's honest significant difference post test. **H** and **I**, Weight of spleen (**H**) and liver (**I**) from mice 10 days after infection or uninfected controls. Weights were normalized to body weight preinfection. Symbols represent individual mice; horizontal lines show the mean. P values were determined by two-way ANOVA. **J**, Hematoxylin and eosin–stained splenic touch preparations from IFNγ−/−Prf1−/− mice 10 days after infection, showing the presence of hemophagocytes. Original magnification × 600. Color figure can be viewed in the online issue, which is available at http://onlinelibrary.wiley.com/doi/10.1002/art.41076/abstract.

the presence of mature neutrophils as determined by observation of ringed/multilobed nuclei (Figure 2D). Neutrophils were not observed in any significant quantity in Prf1−/− mouse livers. Additionally, liver histology showed that while Prf1−/− mice had extensive hepatosteatosis (Figure 2D), this finding was absent in IFNγ−/−Prf1−/− mice, suggesting an IFNγ-dependent phenomenon. IFNγ−/−Prf1−/− mice also had large amounts of periportal inflammation, surpassing that of Prf1−/− mice. Taken together, these findings indicate that extensive neutrophilia is a predominant feature of HLH in the absence of IFNγ.
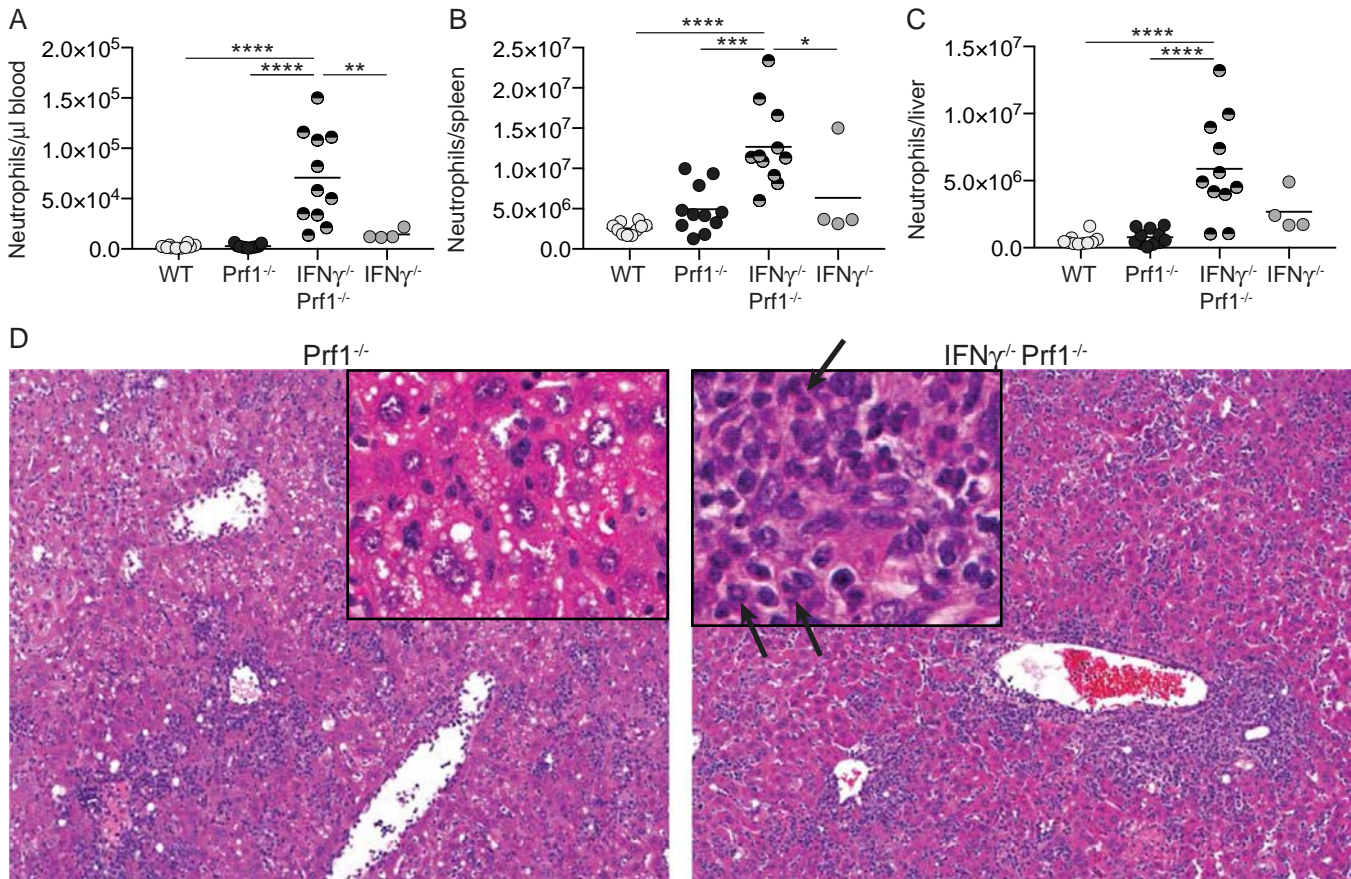
Figure 2. Elevated neutrophil counts in IFNγ⁻/⁻Prf1⁻/⁻ mice. **A–C**, Quantification of neutrophils in the blood (**A**), spleen (**B**), and liver (**C**) in wild-type (WT), Prf1⁻/⁻, IFNγ⁻/⁻Prf1⁻/⁻, and IFNγ⁻/⁻ mice 10 days after infection with lymphocytic choriomeningitis virus, determined by flow cytometry. Neutrophils were designated as live, singlets, CD90.2–, CD19–, CD11b+, or Ly6G+ (see Supplementary Figure 3, available on the *Arthritis & Rheumatology* web site at http://onlinelibrary.wiley.com/doi/10.1002/art.41076/abstract, for gating strategy). Data were combined from 2 independent experiments. Symbols represent individual mice; horizontal lines show the mean. * = $P < 0.05$; ** = $P < 0.01$; *** = $P < 0.001$; **** = $P < 0.0001$, by one-way analysis of variance with Tukey's honest significant difference post test. **D**, Representative hematoxylin and eosin–stained liver sections from a Prf1⁻/⁻ mouse (left) and an IFNγ⁻/⁻Prf1⁻/⁻ mouse (right) 10 days after infection. **Insets**, Higher-magnification views. **Arrows** indicate ringed/multilobed nuclei typical of murine neutrophils. Original magnification × 100; original magnification in **insets** × 200. Color figure can be viewed in the online issue, which is available at http://onlinelibrary.wiley.com/doi/10.1002/art.41076/abstract.

Comparison of altered cytokine milieu in IFNγ⁻/⁻Prf1⁻/⁻ mice with cytokine expression in human HLH patients. Serum IL-6, GM-CSF, and IL-1β levels were all significantly elevated in IFNγ⁻/⁻Prf1⁻/⁻ mice compared to Prf1⁻/⁻ mice and control mice (Figures 3A–C), while Prf1⁻/⁻ mice had extremely high levels of serum IFNγ (Figure 3D). Individual blockade of IL-6, IL-1β, or GM-CSF did not provide major protection against disease in IFNγ⁻/⁻Prf1⁻/⁻ mice (Supplementary Figure 4, available on the *Arthritis & Rheumatology* web site at http://onlinelibrary.wiley.com/doi/10.1002/art.41076/abstract) despite dosing of blocking antibodies that was equivalent to that used in other settings (23–25).

We next made use of a publicly available data set that profiled gene expression from peripheral blood mononuclear cells (PBMCs) of patients with active HLH to compare their cytokine profiles to this mouse model (19). This data set included both HLH patients with identified perforin mutations or no identified genetic cause and

healthy controls (Figure 3E). While it was previously reported that this data set did not show a significant difference in expression of IFNγ-induced transcripts between HLH patients and controls, we were curious to examine whether such an IFNγ signature could be used to discriminate between patients and controls, and the extent to which patients might have differing IFNγ signatures. To do this, we filtered on IFNγ-stimulated genes (MSigDB; Broad Institute) and performed unsupervised hierarchical clustering (Figure 3E). It was clear that HLH patients clustered separately from controls, something not interpretable in gene set enrichment analyses.

In addition, the HLH patients separated into 2 major groups, cluster i, which has a high IFNγ signature, and cluster ii, which has a lower IFNγ signature. Cluster i is a clear and closely related cluster, while cluster ii is more diverse and probably best described as "other." These 2 major clusters are defined by 3 main groups of genes. Group a shows high expression in both
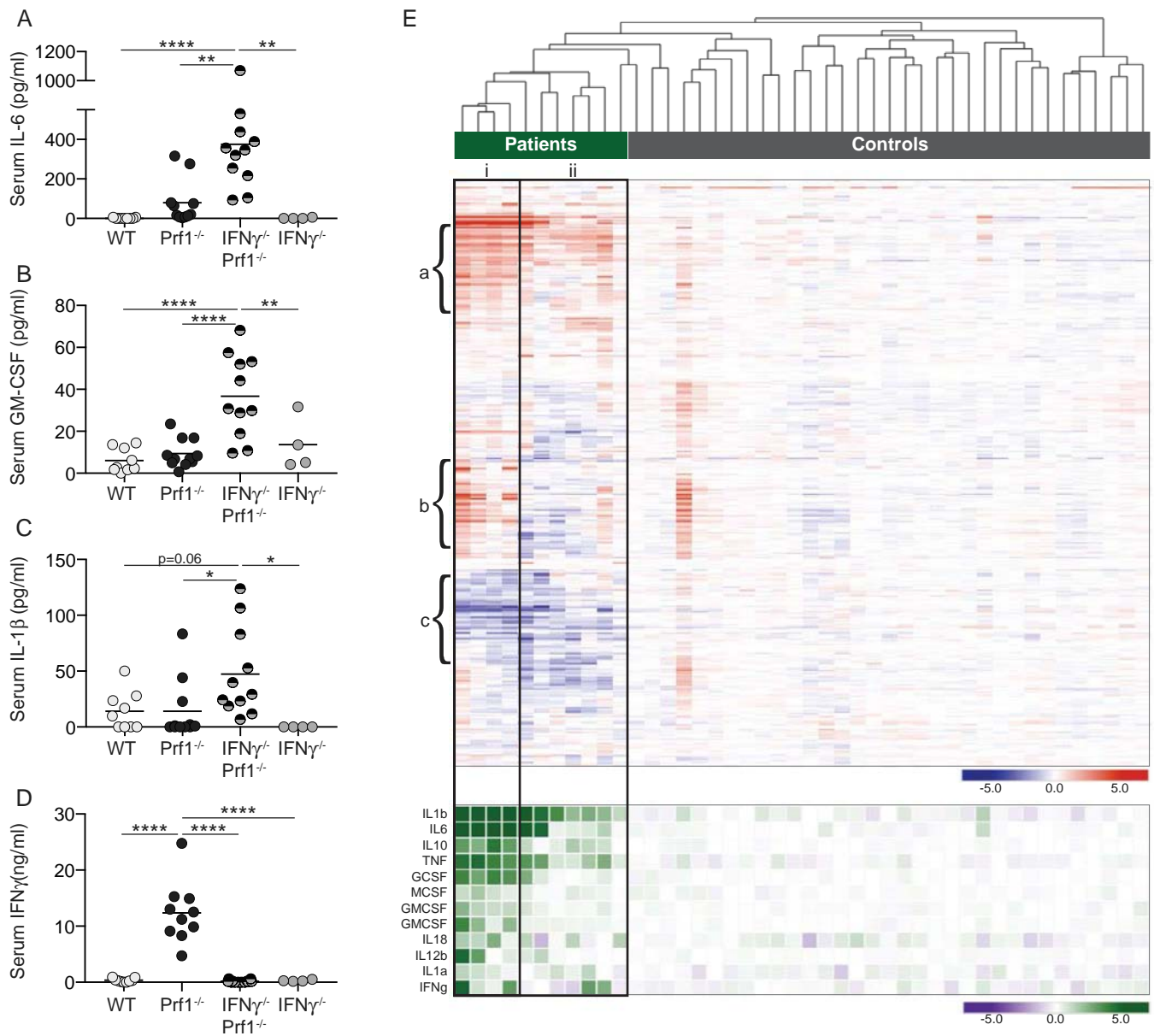
Figure 3. Altered cytokine milieu in IFNγ⁻/⁻Prf1⁻/⁻ mice corresponding with cytokine expression in human patients with hemophagocytic lymphohistiocytosis (HLH). **A–D**, Serum interleukin-6 (IL-6) (**A**), granulocyte–macrophage colony-stimulating factor (GM-CSF) (**B**), IL-1β (**C**), and interferon-γ (IFNγ) (**D**) levels in wild-type (WT), Prf1⁻/⁻, IFNγ⁻/⁻Prf1⁻/⁻, and IFNγ⁻/⁻ mice 10 days after infection with lymphocytic choriomeningitis virus, measured by enzyme-linked immunosorbent assay. Data were combined from 2 independent experiments. Symbols represent individual mice; horizontal lines show the mean. * = $P < 0.05$; ** = $P < 0.01$; **** = $P < 0.0001$, by one-way analysis of variance with Tukey's honest significant difference post test. **E**, Top, Unsupervised hierarchical clustering of gene expression data set from patients with HLH and controls (GEO accession no. GSE26050 [19]) filtered on the curated IFNγ gene set (Molecular Signatures Database; Broad Institute). Bottom, Expression of additional selected cytokines shown according to clustering based on the IFNγ gene set. Columns represent individual patients. TNF = tumor necrosis factor; G-CSF = granulocyte colony-stimulating factor; M-CSF = macrophage colony-stimulating factor.

patient clusters and includes *IL6*, *TNFAIP6*, *TNFAIP3*, *SOCS3*, and *STAT3*, which are up-regulated by a number of cytokines including IL-6 and tumor necrosis factor. Group b shows elevated expression in patient cluster i, depression in cluster ii, and includes the genes *STAT1*, *CXCL10*, *IFIT3*, and *MX1*, which are classic IFNγ response genes. Finally, group c indicates genes depressed in both patient clusters. Group c includes *BANK1*, suggesting

selective absence of B cells from the PBMCs of all patients, and *CIITA*, indicating down-regulation of MHCII or absence of B cells or other antigen-presenting cells. Overall, these findings are consistent with a previous study suggesting the absence of a strong IFNγ signature among HLH patients (19), yet the present analysis makes it clear that the gene expression changes are more complicated than a wholesale absence of an IFNγ response. It may

rather highlight that some patients may have very strong IFNγ signatures, and others may have weaker signatures. It is important to note that perforin-deficient patients did not cluster separately from patients with no identified mutation.

We then examined the expression of other cytokines. Patients falling within the high IFNγ signature cluster tended to have higher expression of other cytokines (Figure 3E), but expression of key cytokines such as IL-1β, TNF, and IL6- remained elevated in all
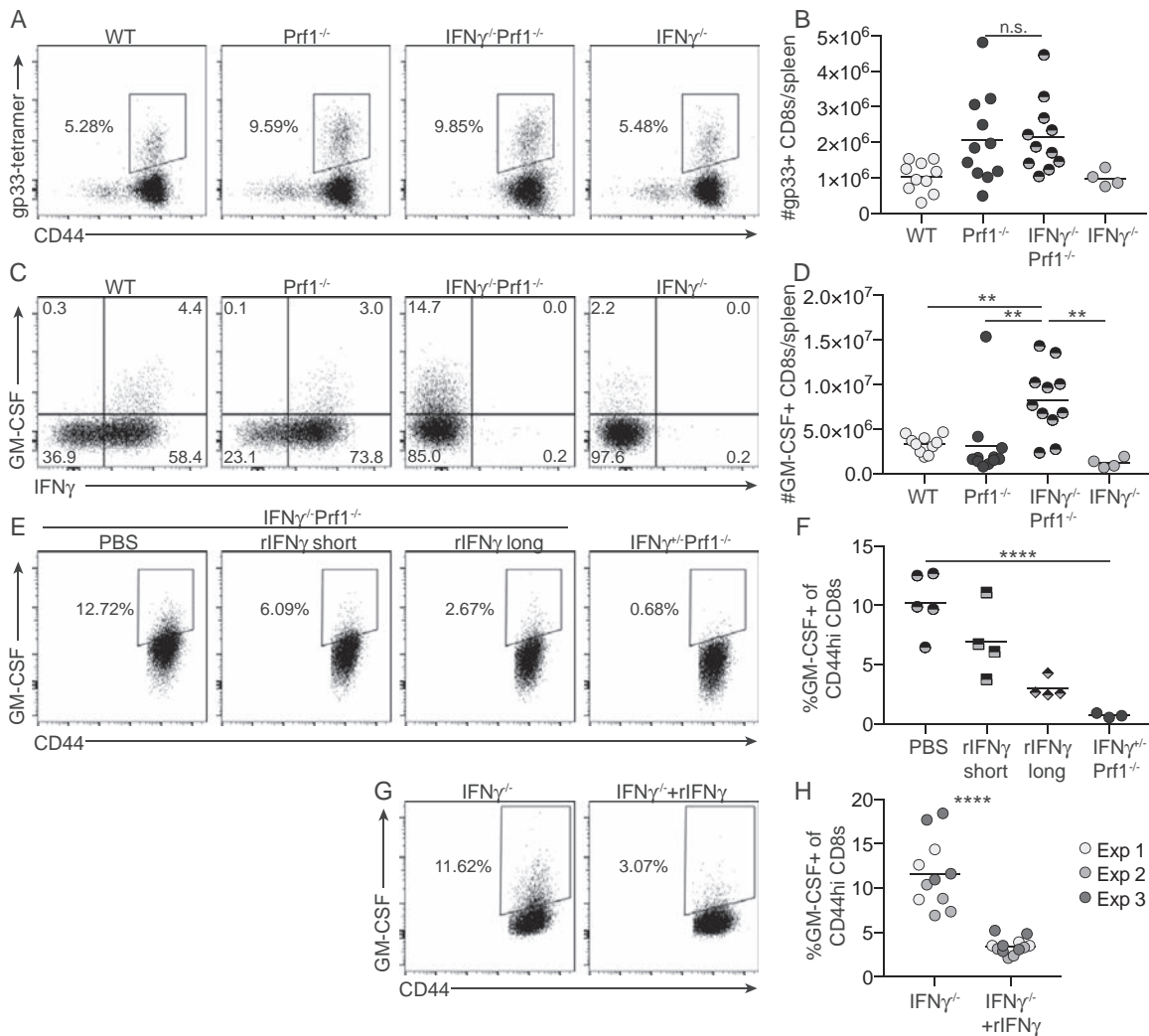

Figure 4. Elevated expression of granulocyte–macrophage colony-stimulating factor (GM-CSF), regulated by interferon-γ (IFNγ), in CD8+ T cells (CD8s) from IFNγ$^{-/-}$Prf1–/– mice. **A**, Representative flow cytometry plots of live, singlet, CD90.2+, CD8+ cells in wild-type (WT), Prf1$^{-/-}$, IFNγ$^{-/-}$Prf1$^{-/-}$, and IFNγ$^{-/-}$ mice 10 days after infection with lymphocytic choriomeningitis virus (LCMV). LCMV-specific CD8+ T cells were identified by H-2D^b-gp33 tetramer staining. **B**, Total number of H-2D^b-gp33+CD44+CD8+ T cells in the spleens of mice 10 days after infection. Data were combined from 2 independent experiments. **C**, Representative flow cytometry plots of live, singlet, CD90.2+, CD8+, CD44^{high} cells in the splenocytes of mice 10 days after infection. Mouse splenocytes were stimulated with phorbol myristate acetate and ionomycin, and IFNγ and GM-CSF expression were analyzed as described in Materials and Methods. (See Supplementary Figure 4, available on the *Arthritis & Rheumatology* web site at http://onlinelibrary.wiley.com/doi/10.1002/art.41076/abstract, for gating strategy.) **D**, Total GM-CSF+CD44^{high}CD8+ T cells in the spleens of mice 10 days after infection. Data were combined from 2 independent experiments. **E**, Representative flow cytometry plots of live, singlet, CD90.2+, CD8+, CD44^{high} cells in IFNγ$^{-/-}$Prf1$^{-/-}$ mice and IFNγ$^{+/-}$Prf1$^{-/-}$ littermate controls infected with LCMV. IFNγ$^{-/-}$Prf1$^{-/-}$ mice were treated with either phosphate buffered saline (PBS), recombinant IFNγ beginning on day 6 (rIFNγ short), or recombinant IFNγ beginning on day 0 (rIFNγ long) by intraperitoneal injection every other day. Mice were killed 10 days after infection, and GM-CSF expression was analyzed as described in Materials and Methods. **F**, Frequency of GM-CSF–expressing CD44^{high}CD8+ T cells in mice treated as indicated in the IFNγ give-back experiment. **G**, Representative flow cytometry plots of live, singlet, CD90.2+, CD8+, CD44^{high} cells among naive CD8+ T cells from uninfected IFNγ$^{-/-}$ mice (purity >90%) cultured in vitro in the presence or absence of rIFNγ for 5 days and then analyzed for GM-CSF expression as described in Materials and Methods. **H**, Frequency of GM-CSF+CD44^{high}CD8+ T cells. Data were combined from 3 independent experiments (Exp). In **B**, **D**, **F**, and **H**, symbols represent individual mice; horizontal lines show the mean. ** = $P < 0.01$; **** = $P < 0.0001$, by one-way analysis of variance (ANOVA) with Tukey's honest significant difference post test in **B** and **D**, by ANOVA with test for linear trend in **F**, and by Student's unpaired 2-tailed *t*-test in **H**. NS = not significant.

patients compared to controls despite partially divergent IFNγ signatures among patients. Thus, there exist a set of patients with weak IFNγ signatures, but overexpression of non-IFNγ cytokines, consistent with the idea of non-IFNγ HLH.

Exogenous IFNγ regulation of elevated GM-CSF expression by CD8+ T cells from IFNγ$^{-/-}$Prf1$^{-/-}$ mice. CD8+ T cells are appreciated to be central mediators of pathology in other murine models of HLH, including the Prf1$^{-/-}$ model (3). We asked whether CD8+ T cells were expanded in LCMV-infected IFNγ$^{-/-}$Prf1$^{-/-}$ mice using H-2D^b-gp33 tetramers to examine the expansion of LCMV-specific CD8+ T cells. Virus-specific IFNγ$^{-/-}$Prf1$^{-/-}$ CD8+ T cells expanded to frequencies and total numbers in the spleen equivalent to those in Prf1$^{-/-}$ mice (Figures 4A and B).

Because of the elevated serum levels of GM-CSF observed in the IFNγ$^{-/-}$Prf1$^{-/-}$ mice, the expansion of IFNγ$^{-/-}$Prf1$^{-/-}$ CD8+ T cells, and the fact that CD8+ T cells are known to make GM-CSF in other settings (26,27), we asked whether CD8+ T cells made GM-CSF in LCMV-infected IFNγ$^{-/-}$Prf1$^{-/-}$ mice. We observed that GM-CSF–producing CD8+ T cells were elevated in both frequency and number in LCMV-infected IFNγ$^{-/-}$Prf1$^{-/-}$ mice compared to wild-type, Prf1$^{-/-}$, and IFNγ$^{-/-}$ mice (Figures 4C and D and Supplementary Figure 5, available on the *Arthritis & Rheumatology* web site at http://onlinelibrary.wiley.com/doi/10.1002/art.41076/abstract). Similar trends were seen for CD4+ T cells; however, CD8+ T cells in LCMV-infected IFNγ$^{-/-}$Prf1$^{-/-}$ mice outnumbered CD4+ T cells by 10 fold (data not shown).

Given these findings, we hypothesized that IFNγ negatively regulates the expression of GM-CSF by CD8+ T cells. We therefore infected IFNγ$^{-/-}$Prf1$^{-/-}$ mice with LCMV and provided exogenous, recombinant IFNγ to these mice every other day from either day 6 postinfection (rIFNγ short) or for the entirety of the 10-day experiment (rIFNγ long) and compared the expression of GM-CSF in CD8+ T cells from these mice to LCMV-infected IFNγ$^{+/-}$Prf1$^{-/-}$ littermate controls. The addition of rIFNγ was sufficient to restore systemic IFNγ signaling, as the IFNγ-stimulated gene, MHCII, was induced on inflammatory monocytes in IFNγ$^{-/-}$Prf1$^{-/-}$ mice treated with rIFNγ (Supplementary Figure 6, available on the *Arthritis & Rheumatology* web site at http://onlinelibrary.wiley.com/doi/10.1002/art.41076/abstract). Consistent with our hypothesis, rIFNγ inhibited the expression of GM-CSF by CD8+ T cells in a dose-dependent manner (Figures 4E and F). Additionally, we cultured naive IFNγ$^{-/-}$ CD8+ T cells in vitro for 5 days with or without the addition of exogenous IFNγ and showed that CD8+ T cells exposed to IFNγ have decreased GM-CSF expression (Figures 4G and H). These data support the notion that IFNγ negatively regulates the expression of GM-CSF by CD8+ T cells.

Regulation of neutrophilia by neutrophil-intrinsic IFNγ signaling through enhanced cell death. In many HLH patients where IFNγ is thought to drive disease, neutropenia correlates with disease severity (28), contrasting with the extensive neutrophilia observed in IFNγ$^{-/-}$Prf1$^{-/-}$ mice. This led us to question whether IFNγ has a direct effect on neutrophilia. First, we asked if restoration of recombinant IFNγ to IFNγ$^{-/-}$Prf1$^{-/-}$ mice would blunt neutrophilia during LCMV infection. IFNγ$^{-/-}$Prf1$^{-/-}$ mice were infected with LCMV and recombinant IFNγ was given every other day for the full 10-day infection (rIFNγ long) or beginning on day 6 after infection (rIFNγ short), and blood neutrophil counts were compared to those in controls. Blood neutrophil counts were decreased in a dose-dependent manner when IFNγ was restored, suggesting that IFNγ suppresses neutrophilia in LCMV-infected IFNγ$^{-/-}$Prf1$^{-/-}$ mice (Figure 5A).

To determine whether this effect was a neutrophil-intrinsic phenomenon, we made IFNγR$^{-/-}$Prf1$^{-/-}$:IFNγR$^{+/+}$Prf1$^{-/-}$ mixed bone marrow chimeras and subsequently infected them with LCMV. The ratio of IFNγR$^{-/-}$Prf1$^{-/-}$ to IFNγR$^{+/+}$Prf1$^{-/-}$ leukocyte populations was determined, and we showed that IFNγ-unresponsive T cells, neutrophils, and inflammatory monocytes outcompeted IFNγ-responsive cells (Figures 5B–D and Supplementary Figure 7, available on the *Arthritis & Rheumatology* web site at http://onlinelibrary.wiley.com/doi/10.1002/art.41076/abstract). IFNγR$^{-/-}$Prf1$^{-/-}$ B cells outcompeted IFNγ-responsive cells in the spleen and blood, but interestingly not in the bone marrow. The most profound effects occurred on the myeloid-derived cell population, suggesting that the IFNγ-mediated suppression of neutrophilia occurs in a myeloid cell–intrinsic manner. Accordingly, common myeloid progenitors, granulocyte–monocyte progenitors, and monocyte–dendritic cell progenitors all were selectively enriched in the IFNγR$^{-/-}$ genotype (Supplementary Figures 8A and B, available on the *Arthritis & Rheumatology* web site at http://onlinelibrary.wiley.com/doi/10.1002/art.41076/abstract). Staining with the proliferation marker Ki-67 indicated no difference in the proliferation of myeloid precursors between donor genotypes (Supplemental Figure 8C).

Neutrophils are typically a short-lived cell type, with a lifespan in mice of ~12.5 hours (29). Therefore, alterations in the lifespan of neutrophils can have profound downstream effects on their accumulation. We sought to determine whether neutrophil-intrinsic IFNγ signaling impacted the survival of neutrophils. Bone marrow from IFNγR$^{-/-}$Prf1$^{-/-}$:IFNγR$^{+/+}$Prf1$^{-/-}$ mixed bone marrow chimeras 10 days after infection was assayed for active caspase 3/7 and plasma membrane permeability directly ex vivo (at 0 hours), or after 6 or 24 hours in vitro. Neutrophils unable to respond to IFNγ displayed notable protection against apoptosis (Figures 5E and F), suggesting that IFNγ limits the lifespan and therefore total accumulation of mature neutrophils in a cell-intrinsic manner.

CD8+ T cells and IL-33 signaling as pathologic drivers of disease in the absence of IFNγ. Hyperactivation of CD8+ T cells is closely linked to HLH immunopathology in IFNγ-sufficient murine models of disease (3,21). To determine whether CD8+ T cells are necessary for disease in the absence of IFNγ, IFNγ$^{-/-}$Prf1$^{-/-}$ mice were infected with LCMV before CD8 depletion
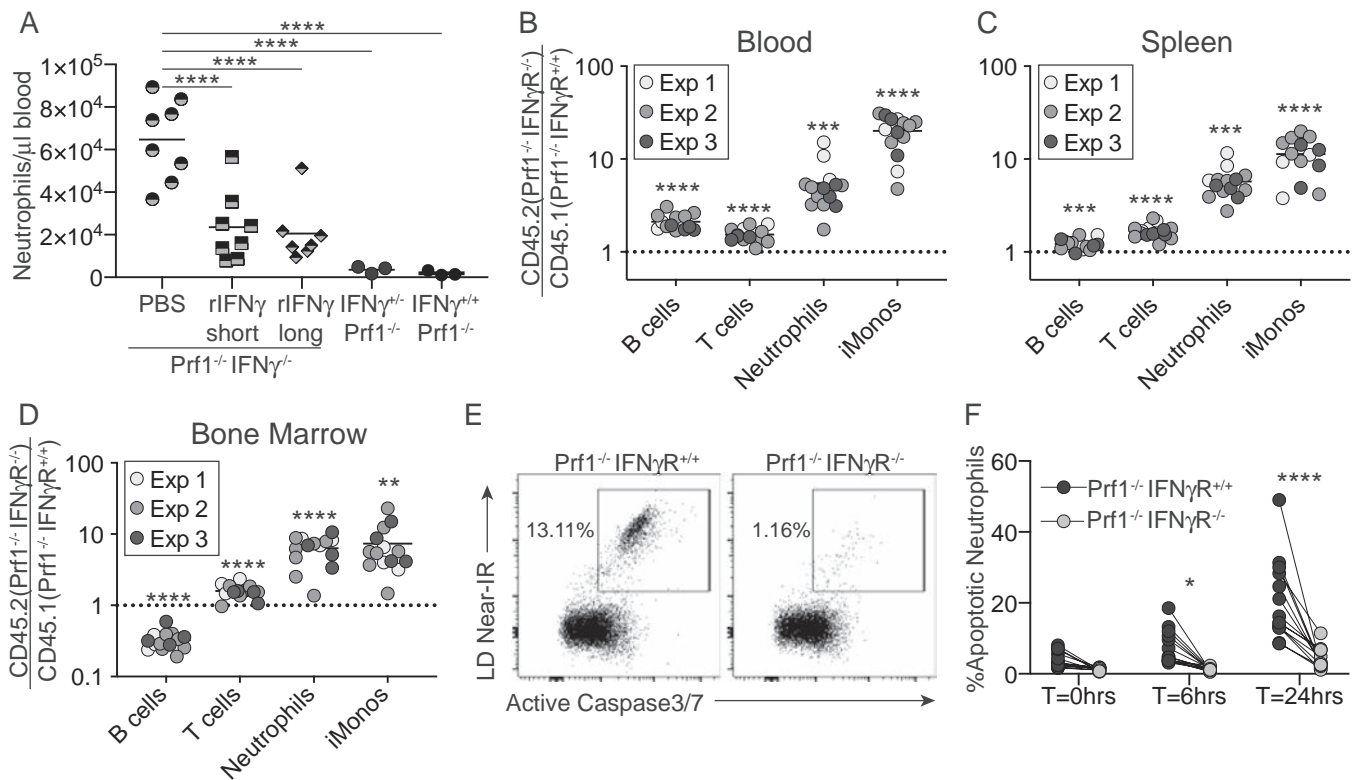
Figure 5. Neutrophil-intrinsic interferon-γ (IFNγ) signaling through enhanced cell death in the regulation of neutrophilia. **A**, Quantification of neutrophils by flow cytometry in IFNγ$^{-/-}$Prf1$^{-/-}$ mice and IFNγ$^{+/-}$Prf1$^{-/-}$ and IFNγ$^{+/+}$Prf1$^{-/-}$ littermate controls 10 days after infection with lymphocytic choriomeningitis virus (LCMV). IFNγ$^{-/-}$Prf1$^{-/-}$ mice were administered either phosphate buffered saline (PBS), recombinant IFNγ beginning on day 6 (rIFNγ short), or recombinant IFNγ beginning on day 0 (rIFNγ long) by intraperitoneal injection every other day. Data were combined from 2 independent experiments. **B–D**, Bone chimeras reconstituted from a 50:50 ratio of Prf1$^{-/-}$IFNγR$^{+/+}$ to Prf1$^{-/-}$IFNγR$^{-/-}$ donor bone marrow were generated. Chimeras were infected with LCMV and killed 10 days after infection. The ratio of specific cell types derived from Prf1$^{-/-}$IFNγR$^{-/-}$CD45.2+ versus Prf1$^{-/-}$IFNγR$^{+/+}$CD45.1+ donor bone marrow was determined and normalized to preinfection ratios in the blood (**B**), spleen (**C**) and bone marrow (**D**). Data were combined from 3 independent experiments (Exp). **E** and **F**, Bone marrow from chimeras on day 10 postinfection was cultured ex vivo and measured for cell permeability and active caspase 3/7 in neutrophils cultured for the indicated times. **E**, Representative flow cytometry plots of neutrophils from Prf1$^{-/-}$IFNγR$^{+/+}$ (left) or Prf1$^{-/-}$IFNγR$^{-/-}$ (right) donors from the same chimeric mouse, cultured for 24 hours. **F**, Percent apoptotic neutrophils at the indicated time points. Lines connect cells from the same chimeric mouse. In **A–D**, symbols represent individual mice; horizontal lines show the mean. Broken lines in **B–D** represent the null ratio of 1. * = $P < 0.05$; ** = $P < 0.01$; *** = $P < 0.001$; **** = $P < 0.0001$, by one-way analysis of variance (ANOVA) with Tukey's honest significant difference post test in **A**, Student's 1-sample t-test in **B–D**, and two-way repeated-measures ANOVA with Sidak's multiple comparison post test in **F**. iMonos = inflammatory monocytes; LD = Live/Dead; IR = infrared.

was initiated beginning on day 3 after infection. IFNγ$^{-/-}$Prf1$^{-/-}$ mice depleted of CD8+ T cells were protected against death (Figure 6A) and weight loss (Figure 6B) compared to isotype-treated controls. CD8+ T cell depletion also resulted in protection against neutrophilia (Figure 6C), suggesting that IFNγ$^{-/-}$Prf1$^{-/-}$ CD8+ T cells provide a signal that enhances neutrophil differentiation, survival, and/or persistence in the bloodstream.

Given our previous work showing that the IL-33/ST2 axis is a crucial upstream mediator of CD8+ T cell effector function leading to their pathologic role in LCMV-infected Prf1$^{-/-}$ mice (7,21), we sought to determine whether IL-33 is required for HLH in the absence of IFNγ. IFNγ$^{-/-}$Prf1$^{-/-}$ mice were infected with LCMV, and ST2 was blocked beginning day 3 postinfection. ST2 blockade remained effective in IFNγ$^{-/-}$Prf1$^{-/-}$ mice, providing significant protection against weight loss (Figure 6D);

increasing survival, by chi-square analysis of total survival on day 10 after infection (7 of 12 mice that received isotype control versus 11 of 11 mice that received anti-ST2 blockade survived; $P = 0.037$ by Fisher's exact test); as well as reducing serum sCD25 levels (Figure 6E) and serum ferritin levels (Figure 6F). The frequency of effector phenotype CD8+ T cells correlated with the total weight loss observed in mice that received ST2 blockade and mice that received isotype control, suggesting a link between decreased CD8+ T cell activation and disease activity (Figure 6G and Supplementary Figure 9, available on the *Arthritis & Rheumatology* web site at http://onlinelibrary.wiley.com/doi/10.1002/art.41076/abstract). Given the role of CD8+ T cells in driving disease in IFNγ$^{-/-}$Prf1$^{-/-}$ mice, we speculate that IL-33/ST2 signaling drives effector differentiation of IFNγ$^{-/-}$Prf1$^{-/-}$ CD8+ T cells and that this differentiation is essential for driving
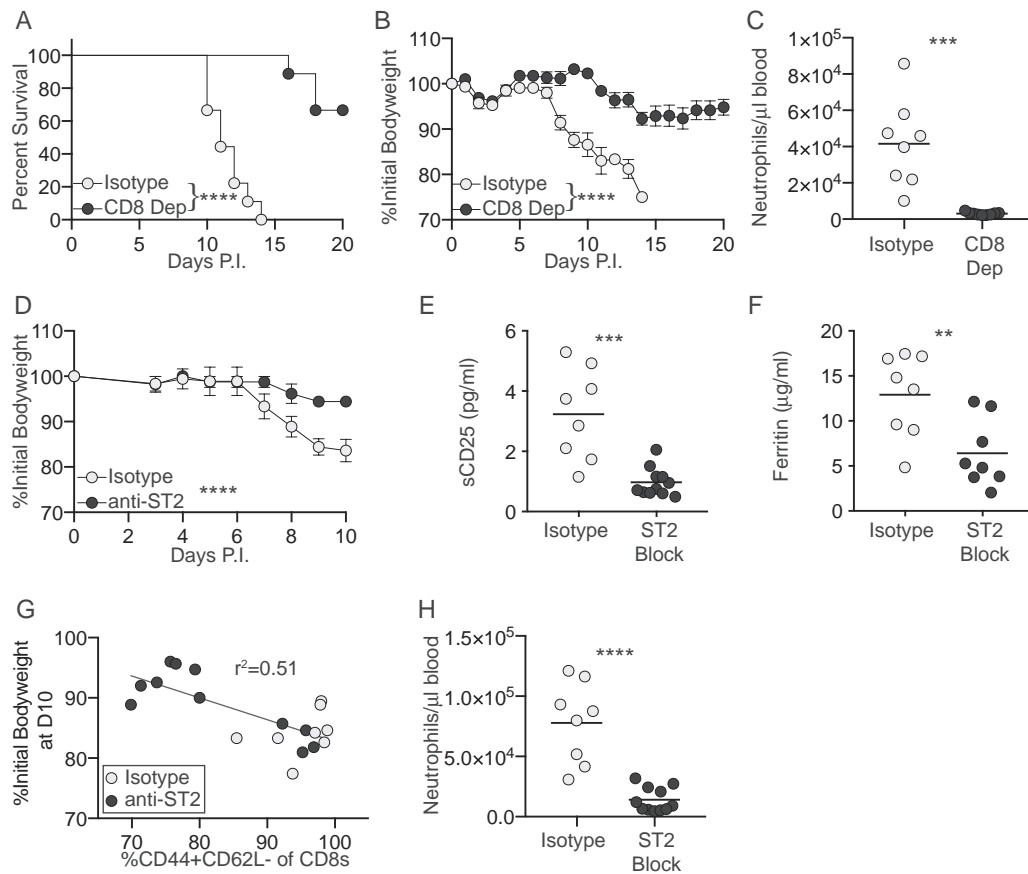
Figure 6. Role of CD8+ T cells (CD8s) and interleukin-33 (IL-33) signaling in driving disease in the absence of interferon-γ (IFNγ). **A** and **B**, Survival (**A**) and weight loss (**B**) in IFNγ$^{-/-}$Prf1$^{-/-}$ mice infected with lymphocytic choriomeningitis virus (LCMV) and administered isotype control or CD8-depleting antibody (CD8 Dep) every other day beginning on day 3 postinfection (PI). **C**, Quantification of neutrophils in the blood 10 days after infection in IFNγ$^{-/-}$Prf1$^{-/-}$ mice administered isotype control or CD8-depleting antibody. Data were combined from 2 independent experiments. **D–F**, Weight loss (**D**), serum soluble CD25 (sCD25) level (**E**), and serum ferritin level (**F**) in IFNγ$^{-/-}$Prf1$^{-/-}$ mice infected with LCMV and administered isotype control or ST2 blocking antibody (anti-ST2) beginning on day 3 after infection and every other day thereafter. Serum sCD25 and ferritin were measured 10 days after infection. In **D**, representative data from 1 of 3 experiments are shown. In **E** and **F**, data were combined from 3 independent experiments. **G**, Frequency of CD44+CD62L–CD8+ T cells (live, singlets, CD90.2+, CD8+) (see Supplementary Figure 8, available on the *Arthritis & Rheumatology* web site at http://onlinelibrary.wiley.com/doi/10.1002/art.41076/abstract, for gating strategy) plotted against total weight loss 10 days after infection. Data were combined from 3 independent experiments. **H**, Quantification of neutrophils in the blood 10 days after infection in IFNγ$^{-/-}$Prf1$^{-/-}$ mice administered isotype control or anti-ST2. Data were combined from 3 independent experiments. ** = $P < 0.01$; *** = $P < 0.001$; **** = $P < 0.0001$, by log-rank (Mantel-Cox) test in **A**, linear mixed-effects model in **B** and **D**, Student's unpaired 2-tailed t-test in **C**, **E**, **F**, and **H**, and linear regression using a single curve for all data sets in **G**. In **B** and **D** values are the mean ± SEM (n = 9 mice per group in **B** and 4 mice per group in **D**). In **C**, **E**, **F**, and **H** symbols represent individual mice; horizontal lines show the mean.

disease. In addition, ST2 blockade completely ameliorated neutrophilia in IFNγ$^{-/-}$Prf1$^{-/-}$ mice (Figure 6H). We hypothesize that this is due to reduced CD8+ T cell activation, which we know is needed for neutrophilia; yet it is also known that IL-33 signaling can act directly on neutrophils to exacerbate inflammation (30). Overall, these data show that IFNγ is not necessary for development of a CD8-driven HLH-like disease in a novel murine model.

DISCUSSION

While much effort has been exerted in targeting the effects of IFNγ signaling in treating HLH/FHLH, a growing body of literature suggests that HLH is a diverse disease triggered by various

agents, under many genetic and pathologic conditions, with a range of mortality-inducing end-stage effectors. We now provide additional support to this notion by showing that HLH-like pathogenesis can occur in the genetic absence of IFNγ. Our study of doubly deficient IFNγ$^{-/-}$Prf1$^{-/-}$ mice showed that IFNγ is not absolutely necessary for disease, identified IFNγ-dependent facets of HLH, and allowed important observations of the regulatory roles of IFNγ in the regulation of neutrophil survival and CD8+ T cell responses to viral infection.

We showed that HLH can develop in the genetic absence of IFNγ. Consistent with our data, infection of IFNγ$^{-/-}$Prf1$^{-/-}$ mice on a mixed B6/129SV background with LCMV (Traub strain) (16) and infection of IFNγ$^{-/-}$Prf1$^{-/-}$ mice with murine γ-herpesvirus 68

caused significant mortality (31). In a model of secondary HLH, BALB/c mice infected with cytomegalovirus succumbed to HLH-like disease, and genetic absence of IFNγ enhanced disease severity (32). Multiple studies have shown a suppressive role of IFNγ in a murine model of systemic JIA, a disease well known to be prone to MAS (17,33). Additionally, the findings of a recent study investigating mechanisms of HLH in IFNγR$^{-/-}$Prf1$^{-/-}$ mice are consistent with our findings and showed development of HLH-like disease in the absence of IFNγ signaling. Interestingly, that study detailed the role of CD25 signaling in the propagation of disease, and showed that IFNγR$^{-/-}$Prf1$^{-/-}$ mice had higher serum levels of sCD25 than Prf1$^{-/-}$ mice (34). This difference in sCD25 levels may be a result of the increased activation state of the CD8+ T cells in the absence of IFNγ (data not shown) (34). Thus, our data contribute to a growing body of literature indicating that IFNγ is not absolutely required for HLH disease manifestation. This study is the first complete description of primary HLH disease in the genetic absence of IFNγ and advances the clinical description of IFNγ-independent HLH pathology. Importantly, diagnostic and clinical features of HLH, such as hepatosplenomegaly, thrombocytopenia, elevated serum ferritin levels, elevated sCD25 levels, hemophagocytosis, and hepatitis remained present despite the absence of IFNγ, highlighting the need to expand the model of pathogenesis beyond this cytokine.

While Prf1$^{-/-}$ and IFNγ$^{-/-}$Prf1$^{-/-}$ mice do not present with identical disease, the most important indicators of mortality and morbidity are not different. Of note, anemia is not a significant problem in the IFNγ$^{-/-}$Prf1$^{-/-}$ mice, supporting the notion that anemia is absolutely driven by IFNγ in HLH. This is consistent with other work from our laboratory showing that in a murine model of the related disease MAS, IFNγ is absolutely required for anemia (35), previous work using LCMV infection of IFNγ$^{-/-}$Prf1$^{-/-}$ mice showing anemia is IFNγ dependent (36), and a study showing that IFNγ signaling is also required for anemia in IFNγR$^{-/-}$Prf1$^{-/-}$ mice (34). No other features of HLH were reported on in IFNγ$^{-/-}$Prf1$^{-/-}$ mice by Zoller et al (36). The mechanism of how IFNγ causes anemia remains elusive. It has been established that anemia and hemophagocytes can be concurrently induced by administration of IFNγ (36), yet we showed here that IFNγ is not *required* for the induction of hemophagocytes, consistent with our previous findings in a different model (35), and the study by Humblet-Baron et al (34). These findings suggest that while excessive IFNγ is sufficient to induce hemophagocytosis, it is not necessary.

Why antibody-mediated blockade of IFNγ protects against HLH disease features, yet genetic absence exacerbates them in some cases is an interesting conundrum. Multiple studies have shown that blockade of IFNγ in murine models of HLH is extremely effective in protecting mice against disease (3,5). We have also reproduced those findings in our laboratory (data not shown). Taken together, these studies provide significant support for the investigation of IFNγ blockade as a treatment for patients with

active HLH, yet it seems contradictory that patients lacking the ability to respond to IFNγ can develop disease. We showed that IFNγ blockade is not 100% efficient in preventing IFNγ signaling, suggesting that low levels of IFNγ signaling constrain alternative pathologic responses, and therefore absolute blockade could be detrimental to outcomes.

While we showed that CD8+ T cells remain important in the manifestation of disease in LCMV-infected IFNγ$^{-/-}$Prf1$^{-/-}$ mice, specific effector cytokines that mediate the downstream immunopathology are the subject of continued investigation. Interestingly, we showed that an alternative cytokine signature predominates when IFNγ is absent. IL-6, IL-1β, and GM-CSF were all elevated in the absence of IFNγ, suggesting IFNγ regulation of either production, and/or accumulation of cell types that produce these cytokines. Individual blockade of these cytokines did not yield significant protection against immunopathology. It remains possible that these cytokines do not act in isolation, and that combination blockade may be effective.

Given the differences between IFNγ-sufficient and -deficient immunopathology, this model allowed the identification of some important IFNγ-driven immunoregulatory networks. The elevated GM-CSF was of particular interest to us given the extensive neutrophilia, the role of CD8+ T cells in driving disease, and the fact that GM-CSF is made by CD8+ T cells (26,37). Indeed, we showed that IFNγ$^{-/-}$Prf1$^{-/-}$ mouse CD8+ T cells expressed elevated levels of GM-CSF, and that exogenous administration of IFNγ regulated this production. Given the paucity of data on GM-CSF regulation in T cells, and the fact that T cell–derived GM-CSF plays an important role in other inflammatory conditions such as multiple sclerosis (MS), and the murine model of MS, experimental autoimmune encephalitis (26,38), there remains a need for a better understanding of this regulation. There are 2 major possibilities as to how IFNγ regulates the expression of GM-CSF: either GM-CSF production by CD8+ T cells is a default state in the absence of IFNγ signaling, or other compensatory signaling pathways that promote GM-CSF production are up-regulated in the absence of IFNγ. Interestingly, there have been case reports of patients who, while receiving myeloablative chemotherapy, had been administered recombinant GM-CSF or the related granulocyte colony-stimulating factor and developed HLH (39–41), suggesting a possible causative role of myeloid-specifying cytokines in the pathogenesis of some subsets of HLH patients.

Our study demonstrated that HLH features can occur independent of IFNγ in a murine model, challenging the dogma that HLH pathogenesis requires IFNγ to drive disease. While IFNγ blockade may be effective in treating many cases of HLH, our study suggests that clinicians should be cognizant that HLH can occur independent of IFNγ, particularly rheumatologists who may see more of the nonclassical familial forms. Differences in therapeutic response in HLH/MAS patients are likely, since HLH/MAS can be initiated by diverse triggers, on heterogenous genetic backgrounds, resulting in various downstream mediators

of disease. This is consistent with a recent study in which whole-exome sequencing of HLH patients revealed a diverse set of potential disease-associated genes (42). IFNγ signatures are not always present in patients with active HLH (19), and we have shown that distinct groups of patients exist that can be divided based on the presence or absence of a robust IFNγ signature. Cytokines such as IL-1β and IL-6 remain up-regulated in both patients with a high IFNγ signature and those with a low IFNγ signature, and in the IFNγ-independent murine model of HLH presented in this study. It is intriguing to note that while not effective in the murine system presented here, IL-1β blockade has been reported to be effective in other human forms of HLH/MAS (43). Clearly, the central cytokines controlling MAS/HLH vary in different scenarios, with continued work needed to dissect all of these nuances.

Even in the absence of IFNγ, we showed that CD8+ T cells remain critically important for disease. This suggests that modulators of CD8+ T cell activation such as IL-33/ST2 (21), rather than blockade of downstream effector molecules, may be a more universally effective way to treat HLH. The effectiveness of this blockade in other models (7), including the IFNγ⁻/⁻Prf1⁻/⁻ mouse model used in this study, suggests that this may be an effective treatment for HLH patients, and warrants further investigation. Taken together, the findings of this study demonstrate that HLH can occur independently of IFNγ, offering insights into potential alternative disease mechanisms and alternative treatment strategies that may be effective in clinical scenarios when IFNγ blockade is insufficient to ameliorate clinical manifestations of life-threatening HLH.

ACKNOWLEDGMENT

AUTHOR CONTRIBUTIONS

All authors were involved in drafting the article or revising it critically for important intellectual content, and all authors approved the final version to be published. Dr. Behrens had full access to all of the data in the study and takes responsibility for the integrity of the data and the accuracy of the data analysis.
Study conception and design. Burn, Weaver, Rood, Behrens.
Acquisition of data. Burn, Weaver, Rood, Chu, Bodansky, Behrens.
Analysis and interpretation of data. Burn, Weaver, Rood, Kreiger, Behrens.

REFERENCES

1. Brisse E, Wouters CH, Matthys P. Hemophagocytic lymphohistiocytosis (HLH): a heterogeneous spectrum of cytokine-driven immune disorders. Cytokine Growth Factor Rev 2015;26:263–80.

2. Stepp SE, Dufourcq-Lagelouse R, Le Deist F, Bhawan S, Certain S, Mathew PA, et al. Perforin gene defects in familial hemophagocytic lymphohistiocytosis. Science 1999;286:1957–9.

3. Jordan MB, Hildeman D, Kappler J, Marrack P. An animal model of hemophagocytic lymphohistiocytosis (HLH): CD8+ T cells and interferon γ are essential for the disorder. Blood 2004;104:735–43.

4. Jenkins MR, Rudd-Schmidt JA, Lopez JA, Ramsbottom KM, Mannering SI, Andrews DM, et al. Failed CTL/NK cell killing and cytokine hypersecretion are directly linked through prolonged synapse time. J Exp Med 2015;212:307–17.

5. Pachlopnik Schmid J, Ho CH, Chrétien F, Lefebvre JM, Pivert G, Kosco-Vilbois M, et al. Neutralization of IFNγ defeats haemophagocytosis in LCMV-infected perforin- and Rab27a-deficient mice. EMBO Mol Med 2009;1:112–24.

6. Rood JE, Rao S, Paessler M, Kreiger PA, Chu N, Stelekati E, et al. ST2 contributes to T-cell hyperactivation and fatal hemophagocytic lymphohistiocytosis in mice. Blood 2016;127:426–35.

7. Taylor MD, Burn TN, Wherry EJ, Behrens EM. CD8 T cell memory increases immunopathology in the perforin-deficient model of hemophagocytic lymphohistiocytosis secondary to TNF-α. Immunohorizons 2018;2:67–73.

8. Jordan M, Locatelli F, Allen C, De Benedetti F, Grom AA, Ballabio M, et al. A novel targeted approach to the treatment of hemophagocytic lymphohistiocytosis (HLH) with an anti–interferon γ (IFNγ) monoclonal antibody (mAb), NI-0501: first results from a pilot phase 2 study in children with primary HLH [abstract]. Blood 2015;126:LBA3.

9. Henter JI, Horne A, AricÓ M, Egeler RM, Filipovich AH, Imashuku S, et al. HLH-2004: diagnostic and therapeutic guidelines for hemophagocytic lymphohistiocytosis [review]. Pediatr Blood Cancer 2007; 48:124–31.

10. Brisse E, Imbrechts M, Mitera T, Vandenhaute J, Berghmans N, Boon L, et al. Lymphocyte-independent pathways underlie the pathogenesis of murine cytomegalovirus-associated secondary haemophagocytic lymphohistiocytosis. Clin Exp Immunol 2018;192:104–19.

11. Van Dommelen S, Sumaria N, Schreiber RD, Scalzo AA, Smyth MJ, Degli-Esposti MA. Perforin and granzymes have distinct roles in defensive immunity and immunopathology. Immunity 2006;25:835–48.

12. Tesi B, Sieni E, Neves C, Romano F, Cetica V, Cordeiro AI, et al. Hemophagocytic lymphohistiocytosis in 2 patients with underlying IFN-γ receptor deficiency. J Allergy Clin Immunol 2015;135: 1638–41.

13. Staines-Boone AT, Deswarte C, Venegas Montoya E, Sánchez-Sánchez LM, García Campos JA, Muñiz-Ronquillo T, et al. Multifocal recurrent osteomyelitis and hemophagocytic lymphohistiocytosis in a boy with partial dominant IFN-γR1 deficiency: case report and review of the literature. Front Pediatr 2017;5:75.

14. Burns C, Cheung A, Stark Z, Choo S, Downie L, White S, et al. A novel presentation of homozygous loss-of-function STAT-1 mutation in an infant with hyperinflammation—a case report and review of the literature. J Allergy Clin Immunol Pract 2016;4:777–9.

15. Krebs P, Crozat K, Popkin D, Oldstone MB, Beutler B. Disruption of MyD88 signaling suppresses hemophagocytic lymphohistiocytosis in mice. Blood 2011;117:6582–8.

16. Nansen A, Jensen T, Christensen JP, Andreasen SØ, Röpke C, Marker O, et al. Compromised virus control and augmented perforin-mediated immunopathology in IFN-γ-deficient mice infected with lymphocytic choriomeningitis virus. J Immunol 1999; 163:6114–22.

17. Avau A, Mitera T, Put S, Put K, Brisse E, Filtjens J, et al. Systemic juvenile idiopathic arthritis–like syndrome in mice following stimulation of the immune system with Freund's complete adjuvant: regulation by interferon-γ. Arthritis Rheumatol 2014;66:1340–51.

18. Ahmed R, Salmi A, Butler LD, Chiller JM, Oldstone MB. Selection of genetic variants of lymphocytic choriomeningitis virus in spleens of

persistently infected mice: role in suppression of cytotoxic T lymphocyte response and viral persistance. J Exp Med 1984;160:521–40.

19. Sumegi J, Barnes MG, Nestheide SV, Molleran-Lee S, Villanueva J, Zhang K, et al. Gene expression profiling of peripheral blood mononuclear cells from children with active hemophagocytic lymphohistiocytosis. Blood 2011;117:e151–60.

20. Palmer G, Talabot-Ayer D, Lamacchia C, Toy D, Seemayer CA, Viatte S, et al. Inhibition of interleukin-33 signaling attenuates the severity of experimental arthritis. Arthritis Rheum 2009;60:738–49.

21. Rood JE, Rao S, Paessler M, Kreiger PA, Chu N, Stelekati E, et al. ST2 contributes to T-cell hyperactivation and fatal hemophagocytic lymphohistiocytosis in mice. Blood 2016;127:426–35.

22. Badovinac VP, Tvinnereim AR, Harty JT. Regulation of antigen-specific CD8+ T cell homeostasis by perforin and interferon-γ. Science 2000;290:1354–8.

23. Copenhaver AM, Casson CN, Nguyen HT, Duda MM, Shin S. IL-1R signaling enables bystander cells to overcome bacterial blockade of host protein synthesis. Proc Natl Acad Sci U S A 2015;112:7557–62.

24. Barber DL, Andrade BB, McBerry C, Sereti I, Sher A. Role of IL-6 in Mycobacterium avium: associated immune reconstitution inflammatory syndrome. J Immunol 2014;192:676–82.

25. Samavedam UK, Iwata H, Müller S, Schulze FS, Recke A, Schmidt E, et al. GM-CSF modulates autoantibody production and skin blistering in experimental epidermolysis bullosa acquisita. J Immunol 2014;192:559–71.

26. Rasouli J, Ciric B, Imitola J, Gonnella P, Hwang D, Mahajan K, et al. Expression of GM-CSF in T cells is increased in multiple sclerosis and suppressed by IFN-β therapy. J Immunol 2015;194:5085–93.

27. Al-Mossawi M, Chen L, Fang H, Ridley A, de Wit J, Yager N, et al. Unique transcriptome signatures and GM-CSF expression in lymphocytes from patients with spondyloarthritis. Nat Commun 2017;8:1510.

28. Lehmberg K, Pink I, Eulenburg C, Beutel K, Maul-Pavicic A, Janka G. Differentiating macrophage activation syndrome in systemic juvenile idiopathic arthritis from other forms of hemophagocytic lymphohistiocytosis. J Pediatr 2013;162:1245–51.

29. Pillay J, den Braber I, Vrisekoop N, Kwast LM, de Boer RJ, Borghans JA, et al. In vivo labeling with ^{2}H$_2$O reveals a human neutrophil lifespan of 5.4 days. Blood 2010;116:625–7.

30. Yazdani HO, Chen HW, Tohme S, Tai S, van der Windt DJ, Loughran P, et al. IL-33 exacerbates liver sterile inflammation by amplifying neutrophil extracellular trap formation. J Hepatol 2018;68:130–9.

31. Bartholdy C, Høgh-Petersen M, Storm P, Holst P, Ørskov C, Christensen JP, et al. IFNγ and perforin cooperate to control infection and prevent fatal pathology during persistent γherpesvirus infection in mice. Scand J Immunol 2014;79:395–403.

32. Brisse E, Imbrechts M, Put K, Avau A, Mitera T, Berghmans N, et al. Mouse cytomegalovirus infection in BALB/c mice resembles virus-associated secondary hemophagocytic lymphohistiocytosis and shows a pathogenesis distinct from primary hemophagocytic lymphohistiocytosis. J Immunol 2016;196:3124–34.

33. Put K, Brisse E, Avau A, Imbrechts M, Mitera T, Janssens R, et al. IDO1 deficiency does not affect disease in mouse models of systemic juvenile idiopathic arthritis and secondary hemophagocytic lymphohistiocytosis. PLoS One 2016;11:e0150075.

34. Humblet-Baron S, Franckaert D, Dooley J, Ailal F, Bousfiha A, Deswarte C, et al. IFN-γ and CD25 drive distinct pathologic features during hemophagocytic lymphohistiocytosis. J Allergy Clin Immunol 2019;143:2215–26.

35. Canna SW, Wrobel J, Chu N, Kreiger PA, Paessler M, Behrens EM. Interferon-γ mediates anemia but is dispensable for fulminant Toll-like receptor 9–induced macrophage activation syndrome and hemophagocytosis in mice. Arthritis Rheum 2013;65:1764–75.

36. Zoller EE, Lykens JE, Terrell CE, Aliberti J, Filipovich AH, Henson PM, et al. Hemophagocytosis causes a consumptive anemia of inflammation. J Exp Med 2011;208:1203–14.

37. Rothchild AC, Stowell B, Goyal G, Nunes-Alves C, Yang Q, Papavinasasundaram K, et al. Role of granulocyte-macrophage colony-stimulating factor production by T cells during Mycobacterium tuberculosis infection. MBio 2017;8:e01514–17.

38. Croxford AL, Lanzinger M, Hartmann FJ, Schreiner B, Mair F, Pelczar P, et al. The cytokine GM-CSF drives the inflammatory signature of CCR38+ monocytes and licenses autoimmunity. Immunity 2015;43:502–14.

39. Wang S, Degar BA, Zieske A, Shafi NQ, Rose MG. Hemophagocytosis exacerbated by G-CSF/GM-CSF treatment in a patient with myelodysplasia. Am J Hematol 2004;77:391–6.

40. Glasser L, LeGolvan M, Horwitz HM. Florid histiocytic hemophagocytosis following therapy with long acting G-CSF (pegfilgrastim). Am J Hematol 2007;82:753–7.

41. Padhi S, Varghese RG, Ramdas A, Phansalkar MD, Sarangi R. Hemophagocytic lymphohistiocytosis: critical reappraisal of a potentially under-recognized condition. Front Med 2013;7:492–8.

42. Chinn IK, Eckstein OS, Peckham-Gregory EC, Goldberg BR, Forbes LR, Nicholas SK, et al. Genetic and mechanistic diversity in pediatric hemophagocytic lymphohistiocytosis. Blood 2018;132:89–100.

43. Miettunen PM, Narendran A, Jayanthan A, Behrens EM, Cron RQ. Successful treatment of severe paediatric rheumatic disease-associated macrophage activation syndrome with interleukin-1 inhibition following conventional immunosuppressive therapy: case series with 12 patients. Rheumatology (Oxford) 2011;50:417–9.

American College
of Rheumatology
Empowering Rheumatology Professionals

Neutrophil Extracellular Traps in Tissue and Periphery in Juvenile Dermatomyositis

Bhargavi Duvvuri,[1] Lauren M. Pachman,[2] Gabrielle Morgan,[2] Amer M. Khojah,[2] Marisa Klein-Gitelman,[3] Megan L. Curran,[4] Stephen Doty,[5] and Christian Lood[1]

Objective. Neutrophils are key immune cells participating in host defense through several mechanisms, including the formation of neutrophil extracellular traps (NETs). This study was undertaken to investigate the role of neutrophils in juvenile dermatomyositis (JDM).

Methods. Electron microscopy was used to identify neutrophils in tissue. NETs were also imaged using fluorescence microscopy and quantified using a myeloperoxidase-DNA enzyme-linked immunosorbent assay (ELISA) in plasma obtained from healthy children (n = 20), disease controls (n = 29), JDM patients (n = 66), and JDM patients with history of calcifications (n = 20). Clinical data included disease activity scores and complement C4 levels. Levels of immune complexes (ICs) and calprotectin were analyzed using ELISA.

Results. Using electron microscopy, neutrophils were found to infiltrate affected muscle tissue, engulfing deposited calcium crystals. Uptake of the crystals led to neutrophil activation ($P < 0.01$) and subsequent phosphatidylinositol 3-kinase– and NADPH oxidase–dependent but peptidylarginine deiminase 4–independent formation of NETs, which contained mitochondrial DNA ($P < 0.05$), as confirmed in vivo ($P < 0.001$) and in vitro ($P < 0.01$). Peripheral NET levels were associated with calcinosis ($P = 0.01$), ICs ($P = 0.008$), and interleukin-8 levels ($P = 0.004$). Children with JDM had impaired NET clearance ($P = 0.01$), associated with autoantibody profiles including melanoma differentiation–associated protein 5 ($P = 0.005$), and depressed complement C4 levels ($r = -0.72$, $P = 0.002$). Furthermore, children with JDM showed evidence of neutrophil activation, with elevated levels of peroxidase activity ($P = 0.02$) and calprotectin ($P < 0.01$), which were associated with disease activity ($P = 0.007$), and dyslipidemia (odds ratio 4.7, $P < 0.05$).

Conclusion. We found novel mechanisms of both calcium crystal–mediated neutrophil activation and cell death in JDM pathophysiology. Targeting this pathway may reduce the frequency and extent of calcinosis, as well as prevent long-term development of comorbidities, including atherosclerosis.

INTRODUCTION

Juvenile dermatomyositis (JDM) is a rare vasculopathic disease with an incidence of 3.2 cases per million children each year in the United States (1). Our lack of knowledge concerning disease pathophysiology is accompanied by adverse outcomes: adults who have had JDM in childhood have evidence of premature cardiovascular damage (2). One debilitating manifestation of chronic JDM is calcinosis, the formation of calcium deposits/crystals in soft tissue, which occurs in ~30%

of children with JDM (3). Of note, calcifications are most likely to be present in children who experienced a delay in the initiation of therapy and/or cutaneous inflammation, which suggests a critical association between chronic inflammation and calcifications (4).

Neutrophils are key immune cells participating in host defense through several mechanisms, including the formation of neutrophil extracellular traps (NETs), a cell death process in which DNA is extruded together with cytoplasmic and granular content to trap and eliminate extracellular pathogens.

Although beneficial from the perspective of host–pathogen interaction, exaggerated neutrophil activation and NET formation have been linked to inflammation, cardiovascular disease, and autoimmunity, including rheumatic diseases (5–9). It was recently found that immune complexes (ICs), commonly found in autoimmune conditions, induce NET formation (5). NETs are inflammatory, and they induce interferon (IFN) production through the cyclic GMP-AMP synthase/stimulator of IFN genes (cGAS/STING) pathway and propagate disease in lupus-prone mice (5,10). IFNs are clearly involved in JDM (11), but the potential role of NETs has yet to be determined.

Neutrophils have received very little attention in JDM pathogenesis, likely due to the lack of their identification in JDM muscle biopsies, despite careful scrutiny (12). However, a recent proteomics study showed a "tumor necrosis factor hub" present in JDM neutrophils as compared to those in healthy children, suggesting that neutrophils are affected by the inflammatory environment (13). Further, elevated levels of the neutrophil-derived alarmin calprotectin have been reported in JDM (14). Cell-free DNA has been seen in adult DM in association with interstitial lung disease, though it is not known whether this corresponds to NETs (15,16). Furthermore, whether children with JDM have elevated levels of NETs has not been investigated.

Inasmuch as calcinosis (e.g., calcium crystals) are involved in the pathophysiology of JDM, it is noteworthy to recognize that other crystals, including cholesterol and monosodium urate monohydrate (MSU) crystals, have the capacity to induce NETosis (17,18), and foster the development of atherosclerosis and gout, respectively. Whether calcium crystals could activate neutrophils to undergo NETosis is not known.

In this report, we describe the presence of calcium crystal–mediated NETosis in children with JDM. Briefly, tissue-infiltrating neutrophils engulfed deposited crystals, triggering a phosphatidylinositol 3-kinase (PI3K)– and reactive oxygen species (ROS)–dependent but peptidylarginine deiminase 4 (PAD4)–independent cell death process leading to NETosis. Evidence of neutrophil activation and cell death was also present in the circulation, particularly in patients with calcinosis, and they were associated with markers of disease activity and dyslipidemia. Our results show several novel mechanisms through which neutrophils may contribute to JDM pathogenesis, suggesting possible new therapeutic targets, as well as biomarkers to monitor and potentially predict the development of severe disease outcomes.

PATIENTS AND METHODS

Patients. Children with JDM (n = 66), healthy children (n = 20), and age-matched disease controls (n = 29) were included in the study after age-appropriate informed consent was obtained (Institutional Review Board #2008-13457 and #2001-11715). For patient characteristics, see Supplementary Tables 1–2, available on the *Arthritis & Rheumatology* web site at http://onlinelibrary.wiley.com/doi/10.1002/art.41078/abstract. Myositis-specific autoantibodies (MSAs) were assessed at the Oklahoma Medical Research Foundation Clinical Immunology Laboratory. Calcifications were confirmed by radiography or computed tomography (19). Calcifications were removed surgically and stored at –80°C after removal of adherent connective tissue. Disease activity scores (DAS) (20) were obtained at the time of the physical examination. Neopterin levels were measured as previously described (21). Fasting lipid levels were measured by an enzymatic method using a Cobas instrument.

Electron microscopy. Tissue samples were preserved in 2% paraformaldehyde and 0.5% glutaraldehyde in $0.05M$ cacodylate buffer (pH 7.4) at 4°C for 4–18 hours. Following fixation, the tissues were treated with reduced osmium tetroxide followed by dehydration in ethyl alcohol. The Spurr's resin (Electron Microscopy Sciences) was prepared and mixed 1:1 with propylene oxide and incubated overnight on a rotator. A change of Spurr's resin:propylene oxide at 3:1 was made, and samples were infiltrated overnight. The final embedding was completed in pure Spurr's resin (hard mixture) for 12–18 hours and polymerized at 60°C. Embedded samples were thin-sectioned (60–80 nm thickness) for electron microscopy using a diamond knife (Diatome) on a Reichert Ultracut E and analyzed using a Philips CM-12 transmission electron microscope at 80 kV accelerating voltage. Mineral crystal size and arrangement were studied by tilting the specimen stage through 0–20 degrees of tilt and/or by darkfield imaging (22). Individual crystals could be measured in the darkfield mode and by using the 002 diffraction line from selected-area diffraction.

Neutrophil biomarker assays. Peroxidase activity was analyzed as previously described (5). Levels of calprotectin (S100A8/A9) were analyzed in plasma using a commercial enzyme-linked immunosorbent assay (ELISA) kit according to the instructions of the manufacturer (R&D Systems).

NET assays. Human neutrophils were isolated from heparinized blood using PolymorphPrep, according to the instructions of the manufacturer (Axis-Shield). Isolated neutrophils (1×10^6 cells/ml) were incubated in poly-L-lysine–coated tissue culture plates with or without the following inhibitors: diphenyleneiodonium (25 μM; Sigma), thenoyltrifluoroacetone (1 μM; Sigma), LY294002 (10 μM; Invitrogen), cytochalasin B (5 μM; Sigma), and Cl-amidine (200 μM; Calbiochem). They were incubated for 1 hour prior to addition of the stimuli, e.g., calcium crystals and phorbol myristate acetate (PMA) (20 nm). After incubation with agonist for 4 hours, NETs were detached with micrococcal nuclease (0.3 units/ml; Fisher Scientific) diluted in nuclease buffer containing 10 mM TrisHCl (pH 7.5), 10 mM MgCl$_2$, 2 mM CaCl$_2$, and 50 mM NaCl.

Detached NETs were quantified by Sytox green staining (Life Technologies). In addition, NETs were quantified using a myeloperoxidase (MPO)–DNA ELISA, as described previously (5). For fluorescence microscopy, cells were fixed with 4% paraformaldehyde, permeabilized with saponin (Alfa Aesar), and blocked with 1% bovine serum albumin (BSA) in phosphate buffered saline (PBS), prior to staining with detection antibodies. DNA was detected using Sytox green, whereas neutrophil elastase was detected using a polyclonal rabbit antibody (ab21595; Abcam) followed by a secondary Cy5-conjugated goat anti-rabbit antibody (Jackson ImmunoResearch). The cells were visualized using an EVOS cell imaging system (Life Technologies).

NET degradation. To detect NET degradation (23), PMA-induced NETs were stained with Sytox green and subsequently incubated with serum (10%) in nuclease buffer for 60 minutes at 37°C. Varying concentrations of micrococcal nuclease were used as positive controls. NETs were washed between each step. NET degradation was calculated as the relative loss of NETs (Sytox green signal) in each well, using the standard curve as a reference.

Calcium crystals. Basic calcium phosphate (BCP) crystals were synthesized according to published protocols (24). Briefly, 15 ml 0.2M NaH$_2$PO$_4$ was mixed with 12.5 ml 0.2M CaCl$_2$ for 1 hour to form calcium precipitates. The precipitates were washed in water with low-speed centrifugation, followed by incubation overnight with 0.5N HCl at a final pH of 9.0 overnight. The precipitates were washed with water 4 times, followed by 70% ethanol and additional water washes. The crystals were resuspended in water and stored at 4°C until used. The surgically removed calcium crystals were fragmented using a mortar and pestle and then washed in water and ethanol, as described above, prior to use.

ELISAs for interleukin-8 (IL-8) and ICs. A 96-well microtiter plate (Corning Clear Polystyrene flat-bottomed, medium binding) was coated with 100 µl of capture antibody (4 µg/ml anti-human IL-8; BioLegend) diluted in PBS and incubated overnight at 4°C. After blocking (1% BSA in PBS), samples were added and incubated overnight at 4°C. For detection, plates were incubated with biotinylated detection antibody (1 µg/ml in blocking buffer), followed by the addition of horseradish peroxidase–streptavidin (BioLegend) for an additional 2 hours at room temperature. The reaction was visualized by the addition of tetramethylbenzidine. The reaction was stopped by addition of 2N sulfuric acid, and absorbance at 450 nm was measured with a plate reader. Wells were washed thoroughly 2 times in PBS–Tween between every step. Levels of ICs were assessed using a MicroVue CIC-C1q ELISA according to the instructions of the manufacturer (Quidel).

Mitochondrial and nuclear DNA analysis. DNA was isolated from cell culture supernatants using a Plasma/Serum Cell-Free Circulating DNA Purification Micro Kit (Thorold). The StepOnePlus Real-Time PCR System was used to perform quantitative polymerase chain reaction (PCR). Primer sequences for nuclear gene targets (ribosomal protein lateral stalk subunit P0 [RPLP0]: forward 5'-GGAATGTGGGCTTTGTGTTC-3', reverse 5'-CCCAATTGTCCCCTTACCTT-3') and mitochondrial gene targets (cytochrome c oxidase subunit 2, cytochrome c oxidase subunit II [COXII]: forward 5'-CCCCACATTAGGCTT AAAAACAGAT-3′, reverse 5′-TATACCCCCGGTCGTGTAGC-3′) were reported previously (25). All components of PCR except for primers were provided in Power SYBR Green PCR Master Mix (ThermoFisher). PCR was set up in a volume of 20 µl that had a 1× final concentration of Power SYBR Green PCR Master Mix, 1 pair of primers directed against nuclear or mitochondrial genes at a final concentration of 100 nM, 5 µl of DNA, and 3 µl of PCR-grade water. Each PCR was set up using the following thermoprofile: incubation for 2 minutes at 50°C followed by a first denaturation step of 10 minutes at 95°C, and 40 cycles of 95°C for 15 seconds, 55°C (COXII) or 60°C (RPLP0) for 1 minute, and then 60°C for 1 minute. Absolute quantification of gene targets is derived from standard curves built by serial dilution of synthesized nuclear and mitochondrial genes.

Statistical analysis. The Mann-Whitney U test and Spearman's correlation test were used when applicable. For comparisons of frequencies, a chi-square test was used. P values less than 0.05 were considered significant. The Bonferroni-Holm correction for multiple comparisons was applied when required.

RESULTS

Neutrophil infiltration in JDM tissue. We readily observed infiltrating neutrophils in inflamed JDM tissue, in particular adjacent to calcified muscle tissue (Figures 1A and B), which suggests chemotactic recruitment to the site of calcification. The neutrophils contained phagocytosed crystals within intracellular vesicles (Figure 1C), as did other infiltrating phagocytes, including macrophages (Figure 1D). The crystalized minerals were fairly homogeneous, 80–120 nm in size, similar to the bone components described previously (26), although the tissue-deposited crystals also formed larger aggregates of considerable size (Figures 1A and B).

NETosis induction by calcium crystals through a ROS- and PI3K-dependent pathway. Given that neutrophils were seen phagocytosing calcium crystals in vivo (Figures 1C and D), we investigated whether such crystals could activate neutrophils to undergo NETosis. Assessing cell surface levels of CD66b, a known neutrophil activation marker, experiments demonstrated the capacity of BCP crystals to activate
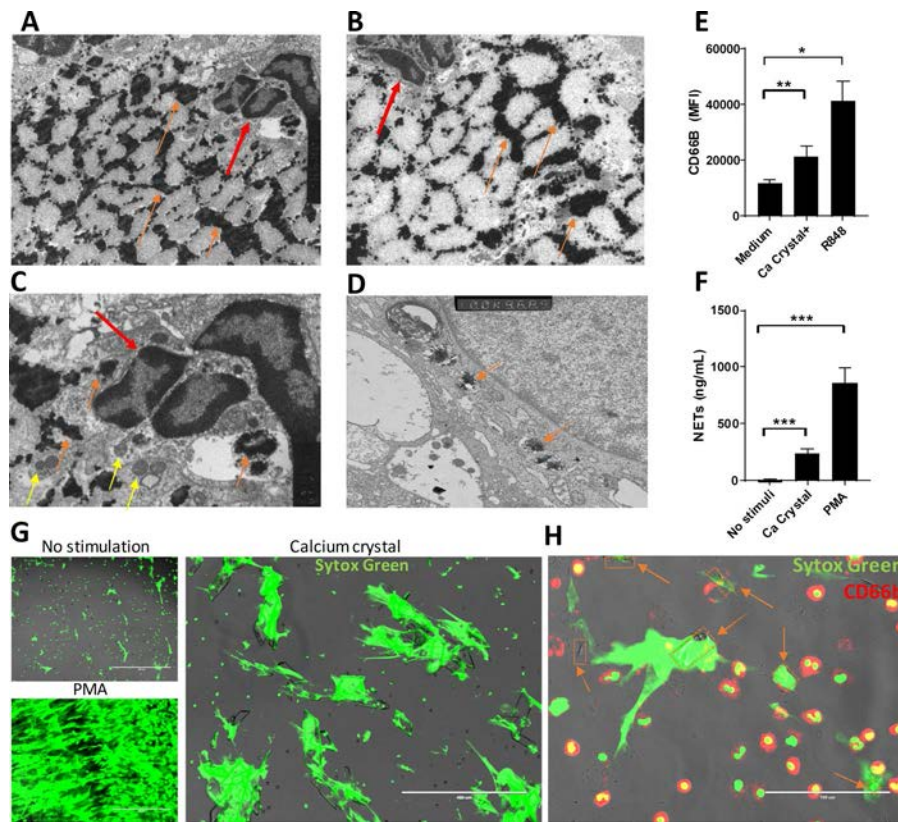
Figure 1. Neutrophil infiltration in the tissue of patients with juvenile dermatomyositis (JDM). **A** and **B**, Muscle tissue (from 2 children with JDM) illustrating calcium deposits (**orange arrows**) and infiltrating neutrophils (**red arrows**). Original magnification × 5,000. **C** and **D**, High-magnification views of a neutrophil engulfing individual and aggregated crystals (magnified view of a portion of **A**) (**C**) and of a macrophage with mineral crystals within vacuoles (**D**). Original magnification × 10,000. **Red arrows** indicate neutrophil lobulated nucleus, **yellow arrows** indicate neutrophil granules, and **orange arrows** indicate calcium crystals. Results are representative of >3 independent experiments. **E** and **F**, Surface expression of CD66b analyzed by flow cytometry (n = 4–6) (**E**) and neutrophil extracellular trap (NET) formation analyzed by fluorimetry (n = 13–15) (**F**). Human primary neutrophils were incubated with synthetic calcium crystals (Ca crystal), Toll-like receptor 7 (TLR-7)/TLR-8 agonist R848, or phorbol myristate acetate (PMA). Bars show the mean ± SEM. **G** and **H**, Fluorescence microscopy staining for DNA using Sytox green (**G**) and CD66b (**H**). Calcium crystals are illustrated with orange boxes and **arrows**. Results are representative of 3 experiments. Bars = 100 μm. * = $P < 0.05$; ** = $P < 0.01$; *** = $P < 0.001$. MFI = mean fluorescence intensity.

neutrophils ($P < 0.01$; Figure 1E). R848, a Toll-like receptor 7 (TLR-7)/TLR-8 agonist, was used as a positive control. To determine whether neutrophil activation proceeded to cell death, we quantified the DNA release using a fluorimetry assay (5,6,10). BCP crystals induced DNA release ($P < 0.001$; Figure 1F), and NETs were apparent when using fluorescence microscopy (Figures 1G and H). Interestingly, only neutrophils in close proximity to the calcium crystals underwent NETosis, whereas neutrophils further away retained a nonactivated phenotype (Figures 1G and H).

NETs can be induced through several distinct signaling pathways, including generation of ROS- and PAD-mediated citrullination of histone H3. PI3K-mediated signaling has previously been shown to be essential in NET formation, acting upstream of NADPH oxidase in generating ROS (10). To investigate the signaling requirements for BCP-mediated NETosis, neutrophils were preincubated with inhibitors blocking pathways known to be involved in NET formation, including PAD2/PAD4, ROS,

PI3K signaling, or actin polymerization. Calcium crystal–mediated NETosis was insensitive to PAD inhibition, though PI3K-mediated ROS production was required. This is similar to what has been described for ICs (10), in contrast to neutrophil activation via MSU crystals (found in adult gout patients), which also required PAD activity to induce NET formation (27). Furthermore, neutrophils required actin cytoskeleton activity to undergo calcium crystal–mediated NETosis (Figure 2A). It has recently been shown that NETs contain inflammatory mitochondrial DNA (5,6), which can activate type I IFNs. To determine if calcium crystals induced extrusion of mitochondrial DNA, we analyzed the content of NETs using a quantitative PCR method that assessed levels of nuclear (RPLP0) and mitochondrial (COXII) DNA. Calcium crystals induced the release of both genomic and mitochondrial DNA in a ROS- and PI3K-dependent process ($P < 0.05$; Figures 2B and C). Selective inhibition of mitochondrial ROS reduced mitochondrial DNA release but not that of nuclear DNA (Figures 2B and C). Thus, calcium crystals induced NETosis with
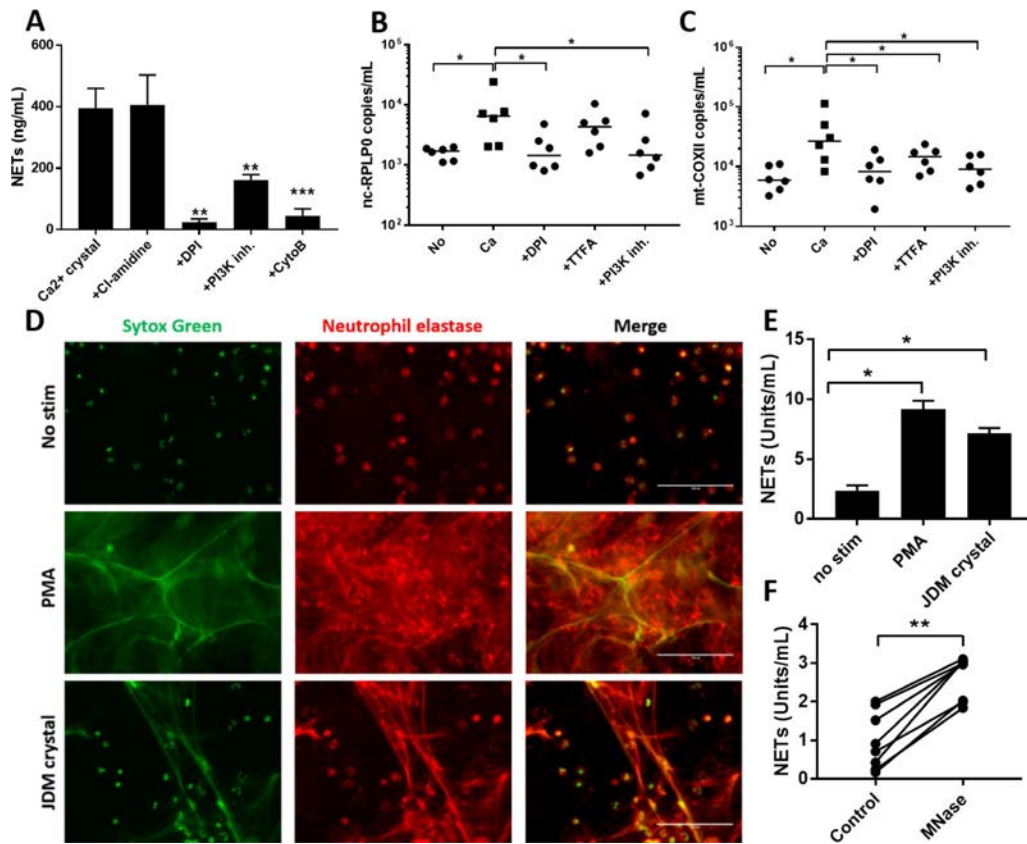
Figure 2. Calcium crystal–mediated NETosis. **A**, Neutrophils were preincubated with inhibitors (inh.) of peptidylarginine deiminase 2 (PAD2)/PAD4 (Cl-amidine; n = 6), reactive oxygen species (ROS) (diphenyleneiodonium [DPI]; n = 8), phosphatidylinositol 3-kinase (PI3K) (n = 8), and cytoskeleton (cytochalasin B [CytoB]; n = 8), prior to addition of calcium crystals and assessment of NETosis by fluorimetry. Bars show the mean ± SEM. ** = $P < 0.01$; *** = $P < 0.001$ versus Ca2+ crystals with no inhibitor added, by Mann-Whitney U test. **B** and **C**, Nuclear ribosomal protein lateral stalk subunit P0 (nc-RPLP0) (**B**) and mitochondrial cytochrome c oxidase subunit II (mt-COXII) (**C**) DNA release, upon calcium crystal–mediated NETosis in the presence of inhibitors targeting ROS (DPI), mitochondrial ROS (thenoyltrifluoroacetone [TTFA]), and the PI3K signaling pathway (n = 6), was assessed by quantitative polymerase chain reaction analysis. Symbols represent individual samples. Bars show the median. **D**, Human primary neutrophils were incubated with crystals that were surgically removed from juvenile dermatomyositis (JDM) patients and analyzed for NETosis by fluorescence microscopy. As a positive control, neutrophils were activated with phorbol myristate acetate (PMA). Results are representative of 3 independent experiments. Bars = 100 μm. **E**, Neutrophils were incubated with crystals that were surgically removed from JDM patients and analyzed for the release of myeloperoxidase (MPO)–DNA (neutrophil extracellular trap [NET]) complexes (n = 6). Bars show the mean ± SEM. **F**, Crystals from JDM patients were either left untreated or treated with micrococcal nuclease (MNase) and analyzed for the release of MPO–DNA complexes by enzyme-linked immunosorbent assay (n = 8). In **B**, **C**, **E**, and **F**, * = $P < 0.05$; ** = $P < 0.01$, by Mann-Whitney U test. No stim = no stimulation.

the release of both mitochondrial and nuclear DNA, in a ROS- and PI3K-dependent but PAD4-independent process.

Crystals isolated from JDM patients are potent NET inducers and contain NET remnants. Given that the BCP crystals could induce NETs in vitro, we next investigated whether tissue-deposited calcium crystals isolated from JDM patients were capable of inducing NETosis. Similar to the BCP crystals, JDM-derived crystals from surgically removed deposits induced NETosis, as was evident by the release of DNA colocalized with neutrophil elastase, as well as MPO–DNA complexes (Figures 2D and E). We then explored whether JDM crystals also induced NETosis in vivo. However, given the difficulty of processing calcified material for immunohistochemistry, we were unable to ana-

lyze the crystals by microscopy. Thus, in an attempt to answer this question, purified JDM crystals were treated with micrococcal nuclease to release crystal-bound NETs. As evident in Figure 2F, MPO–DNA complexes were released upon nuclease treatment ($P < 0.01$), which supports the hypothesis that JDM patients developed crystal-bound NETs in vivo.

No evidence of NETosis in the periphery in children with JDM. We examined whether children with JDM showed evidence of NETs in the circulation or in tissues. To investigate this, we analyzed plasma levels of MPO–DNA complexes, a well-established marker of NETosis, in children with JDM and in controls. Though levels of NETs were increased in patients with pediatric systemic lupus erythematosus (SLE) ($P = 0.007$), none
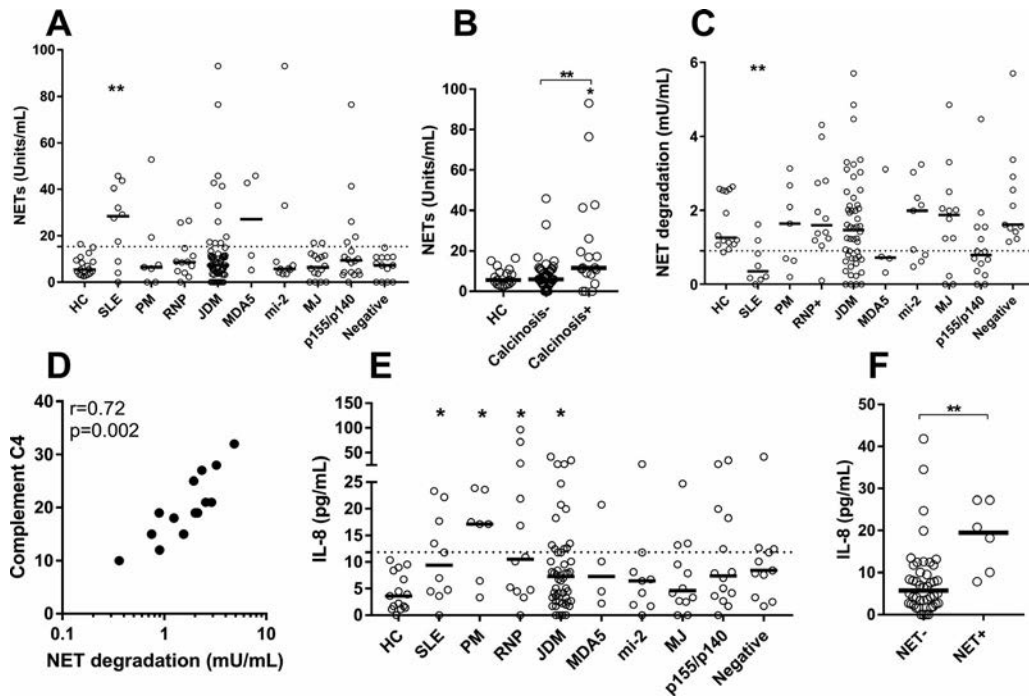
Figure 3. Association of NETosis with calcinosis in JDM. **A**, MPO–DNA complexes (NETs) were measured in different patient groups and compared to the values in healthy children (HC). **B**, NET levels were analyzed in patients without calcinosis (n = 43), patients with calcinosis (n = 18), and healthy children. **C**, NET degradation was assessed in all subjects by in vitro enzymatic assay. **D**, Correlation between levels of complement component C4 and NET degradation (n = 17) was determined using Spearman's correlation test. **E**, Levels of interleukin-8 (IL-8) in all subjects were analyzed by enzyme-linked immunosorbent assay. **F**, IL-8 levels were assessed in patients without circulating NETs (n = 44) and patients with circulating NETs (n = 6). In **A**–**C**, **E**, and **F**, symbols represent individual samples. Bars show the median. The dotted line in **A** represents the 90th percentile of the relevant levels in healthy children, and in **C** and **E**, the dotted lines represent the 10th percentile of these levels. * = $P < 0.05$; ** = $P < 0.01$ versus healthy children or as indicated, by Mann-Whitney U test. SLE = systemic lupus erythematosus; PM = polymyositis; RNP = RNP+ polymyositis; MDA-5 = melanoma differentiation–associated protein 5 (see Figure 2 for other definitions).

of the juvenile myositis groups had elevated levels of NETs (Figure 3A). Given the large variability in NET levels, we investigated whether NETs were associated with certain disease features, including calcinosis. We found that patients with calcinosis had increased levels of NETs compared to JDM patients without calcinosis ($P = 0.009$) and compared to healthy children ($P = 0.02$; Figure 3B).

It was previously shown that SLE patients have reduced degradation of NETs due to low DNase I activity (28). In the present study, there was also a marked impairment in degrading NETs in patients with pediatric SLE ($P = 0.003$; Figure 3C). Similarly, using the 10th percentile of NET degradation in healthy controls as a cutoff, we found that nearly one-third of the JDM patients had an impaired capacity to degrade NETs ($P = 0.01$), particularly patients with MDA-5 and p155/140 MSAs ($P = 0.025$ and $P = 0.024$, respectively, by chi-square test). NET-degrading capacity correlated with complement C4 levels (r = 0.72, $P = 0.002$; Figure 3D). Surprisingly, NET degradation did not correlate with levels of NETs ($P = 0.17$). To investigate whether NETs may contribute to inflammation in JDM, we analyzed levels of the neutrophil chemoattractant IL-8. Levels of IL-8 were elevated in all inflammatory conditions, including pediatric SLE ($P = 0.03$),

polymyositis ($P = 0.01$), RNP+ myositis ($P = 0.02$), and JDM ($P = 0.03$; Figure 3E). Importantly, patients with JDM who displayed NETosis had even higher levels of IL-8 ($P = 0.004$; Figure 3F). These data provide evidence that a subgroup of patients with severe JDM have impaired degradation of NETs accompanied by increased circulating levels of NETs, in the presence of ongoing inflammation and calcinosis.

Association of circulating NET levels with ICs. Children with JDM had increased levels of ICs compared to healthy individuals ($P = 0.006$; Figure 4A). Given the well-known contribution of ICs to NET formation in adult SLE, we examined whether levels of ICs correlated with NET levels in pediatric lupus. IC levels correlated strongly with NET levels in pediatric SLE (r = 0.80, $P = 0.01$; Figure 4B), suggesting that similar mechanisms may operate in pediatric and adult SLE. IC levels also correlated with NET levels in JDM patients (r = 0.31, $P = 0.02$; Figure 4C), with NET levels particularly elevated in patients with evidence of circulating ICs ($P = 0.008$; Figure 4D). Patients with JDM, similar to those with pediatric SLE, had circulating ICs that appeared to contribute to heightened NET levels, as observed in a subgroup of the JDM patients.
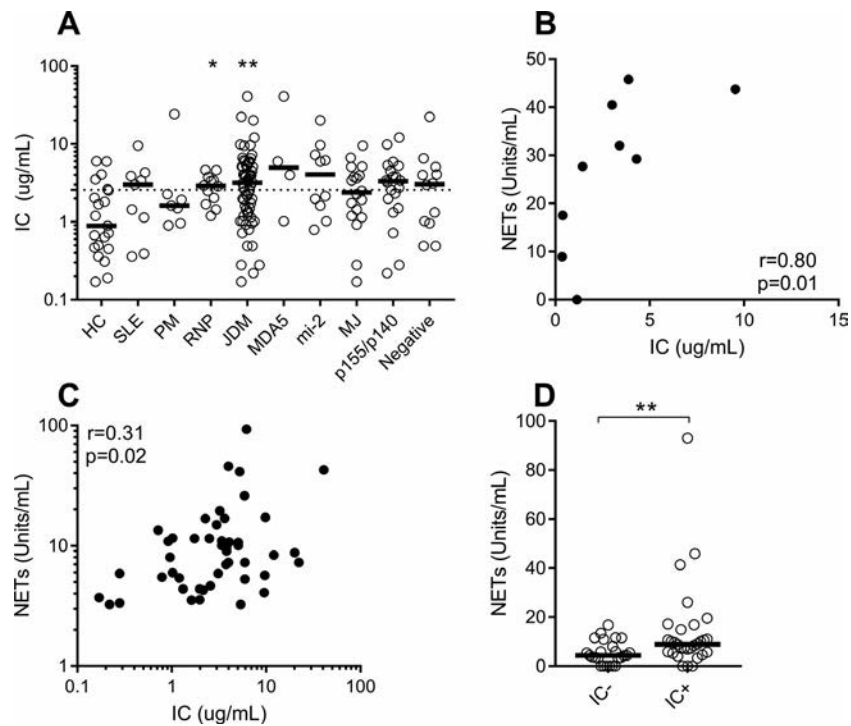
Figure 4. Immune complex (IC) levels in juvenile dermatomyositis (JDM). **A**, IC levels were analyzed by enzyme-linked immunosorbent assay and grouped according to diagnosis and myositis-specific antibodies. The dotted line represents the 75th percentile of the levels in healthy children. * = $P < 0.05$; ** = $P < 0.01$ versus healthy children, by Mann-Whitney U test. **B** and **C**, Correlation between IC levels and neutrophil extracellular trap (NET) levels in pediatric SLE patients (n = 9) (**B**) and JDM patients (n = 55) (**C**) was determined using Spearman's correlation test. **D**, Circulating NET levels were assessed in patients with low levels of ICs (n = 25) and patients with high levels of ICs (n = 30). * = $P < 0.05$; ** = $P < 0.01$, by Mann-Whitney U test. Symbols represent individual samples. Bars show the median. See Figure 3 for other definitions.

Increased neutrophil activation related to disease activity in JDM patients. Given the finding that a subgroup of children with calcinosis demonstrated neutrophil cell death in peripheral blood, we explored whether these children also had evidence of neutrophil activation. To investigate this, we analyzed 2 markers of neutrophil activation in plasma: calprotectin (S100A8/A9) and peroxidase activity. In contrast to previous findings in adult SLE (5), patients with pediatric SLE did not show elevated peroxidase activity (Figure 5A). However, patients with RNP+ myositis and those with JDM showed increased peroxidase activity ($P = 0.01$ and $P = 0.04$, respectively; Figure 5A). Elevated peroxidase activity was observed in patients with high disease activity ($P = 0.02$; Figure 5B) and correlated with markers of inflammation, including the macrophage-derived molecule neopterin (r = 0.45, $P = 0.0007$; Figures 5C and D).

Elevated S100A8/A9 levels in JDM but not in pediatric SLE. It has been reported that serum S100A8/A9 levels are elevated in JDM and associated with disease activity (14). However, S100A8/A9 is released by activated platelets during the clotting process (29,30), which is why serum levels of S100A8/A9 do not reflect physiologic levels of S100A8/A9. In the current study, by using rapidly processed and frozen plasma

samples to assess true levels of S100A8/A9 in patient circulation, we found that calprotectin levels were not elevated in patients with pediatric SLE (Figure 5E), even though clearly elevated levels have been demonstrated in adult SLE (31). These data suggest that children may not behave physiologically as young adults and may have a different disease pathophysiology, at least in SLE. In contrast to SLE, pediatric patients with polymyositis, RNP+ myositis, and JDM all showed elevated levels of S100A8/A9 in the circulation ($P < 0.001$, $P = 0.006$, and $P < 0.01$, respectively; Figure 5E). Levels of S100A8/A9 were inversely associated with Childhood Myositis Assessment Scale scores ($P = 0.007$; Figure 5F), suggesting that S100A8/A9 could be a marker of disease activity in JDM. In contrast to neutrophil activation markers, levels of NETs (e.g., neutrophil cell death) were not associated with disease activity in JDM patients (data not shown). Our data demonstrate that JDM patients have ongoing systemic neutrophil activation that is associated with elevated indicators of inflammation and disease activity.

Association of neutrophil activation with dyslipidemia. Neutrophil activation is instrumental in the development of endothelial damage and subsequent atherosclerosis, with elevated levels of S100A8/A9 associated with cardiovascular disease, including in SLE (29,31,32). In the present study,
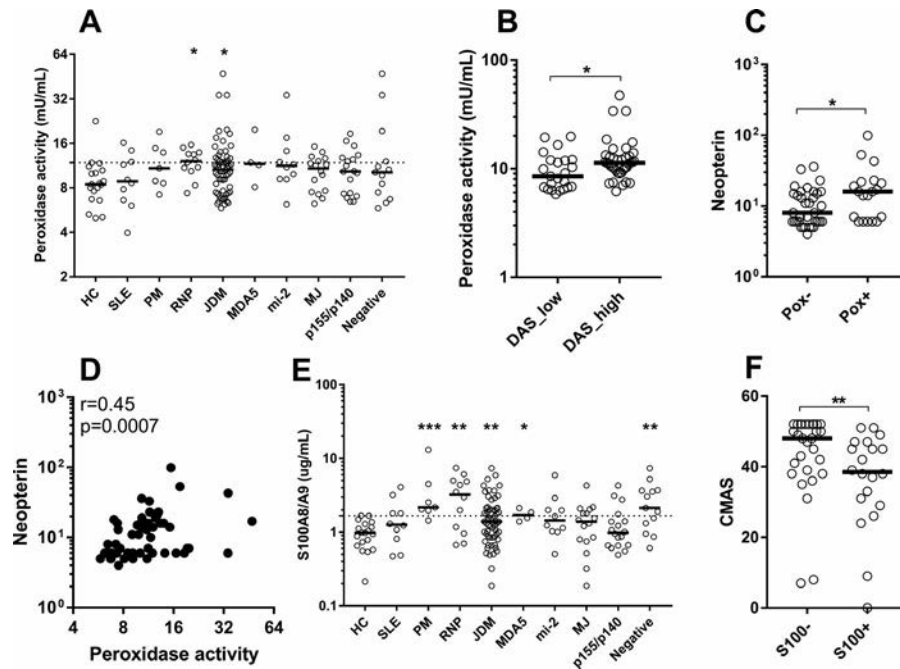
Figure 5. Neutrophil activation markers in juvenile dermatomyositis (JDM). **A**, The neutrophil activation marker peroxidase activity was analyzed in plasma samples from healthy children and from patients with pediatric SLE, PM, RNP, and JDM overall, and JDM subgroups based on myositis-specific antibody positivity. **B**, Peroxidase activity was assessed in plasma samples from JDM patients with low disease activity scores (DAS) (n = 23) and patients with high DAS (n = 38). **C**, Levels of the inflammation marker neopterin were assessed in plasma samples from patients with low peroxidase (Pox) activity and patients with high peroxidase activity. **D**, Correlation between peroxidase activity and neopterin levels in JDM patients (n = 54) was determined using Spearman's correlation test. **E**, The neutrophil activation marker S100A8/A9 was analyzed in plasma samples from all subjects. **F**, The Childhood Myositis Assessment Scale (CMAS) score was determined in JDM patients with low levels of S100A8/A9 (n = 29) and patients with high levels of S100A8/A9 (n = 20). Symbols represent individual samples. Bars show the median. In **A** and **E**, the dotted line represents the 90th percentile of the relevant levels in healthy children. * = $P < 0.05$; ** = $P < 0.01$; *** = $P < 0.001$ versus healthy children or as indicated, by Mann-Whitney U test. See Figure 3 for other definitions.

consistent with prior findings (2,33), JDM patients had low levels of high-density lipoprotein (HDL), with 9 of 23 patients (39%) having dyslipidemia. Furthermore, we observed lipid droplet accumulation in endothelial cells adjacent to muscle fiber, as assessed by electron microscopy. Similar to observations in diabetes mellitus (34), levels of HDL were inversely correlated with calprotectin levels (r = −0.56, $P = 0.01$; Figure 6A) and decreased in children with elevated calprotectin levels ($P = 0.01$; Figure 6B). Finally, elevated levels of calprotectin were associated with dyslipidemia (odds ratio 4.7, $P < 0.05$).

NETs are known to be prothrombotic (35–37), with MPO promoting oxidative modification of HDL and rendering it proatherogenic (38). We found that peroxidase activity, which reflects levels of the main circulating peroxidase, MPO, were inversely correlated with HDL levels (r = −0.44, $P < 0.05$; Figure 6C). Children with high peroxidase activity consistently showed markedly decreased HDL levels ($P = 0.02$; Figure 6D). None of the other markers of disease activity and inflammation (e.g., IC, neopterin, C4, or IL-8 levels) correlated with HDL levels (data not shown), which suggests selectivity in the neutrophil activation markers. Our results indicate that neutrophil

activation is associated with a proatherogenic environment in children with JDM.

DISCUSSION

Neutrophils are frontline immune cells that are recruited immediately upon insult through chemotactic signals, which forces them to leave the circulation and migrate into tissue to combat the pathogen. Similar processes occur in sterile inflammation, including rheumatic disease, wherein insults of varying kinds (e.g., IC deposition) result in recruitment of neutrophils into tissue and cause inflammation and organ damage. In this report, we describe the novel finding that neutrophils are present in affected tissue of JDM patients, particularly adjacent to calcified tissue, suggesting that calcinosis-mediated inflammation contributes to chemotactic signaling. Neutrophils and other phagocytes were involved in clearance of the mineral crystals, as demonstrated by endocytosed crystals. The presence of infiltrating neutrophils is novel in JDM; in prior studies, neutrophils were not identified in diagnostic muscle biopsies from children with JDM (12). This discrepancy may
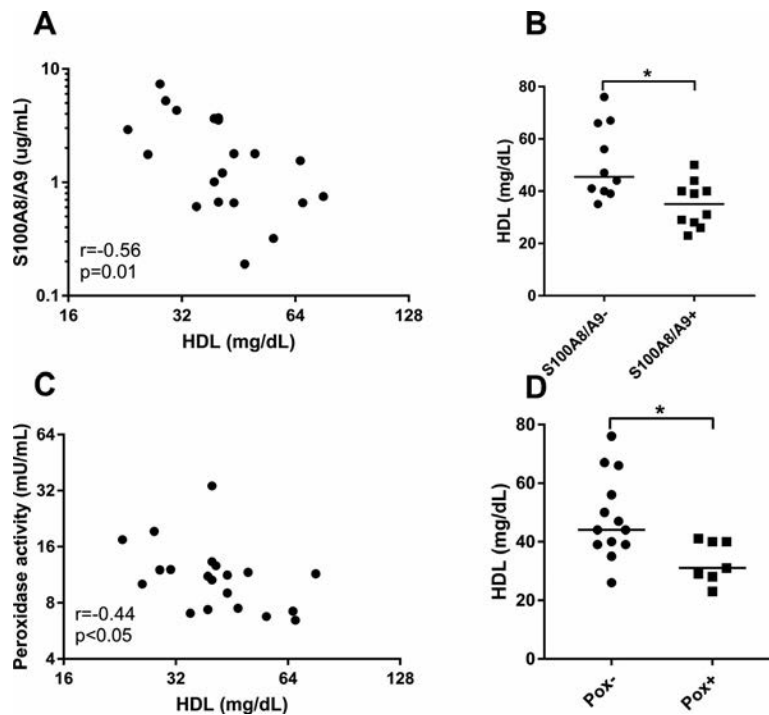
Figure 6. Neutrophil activation markers are associated with dyslipidemia in juvenile dermatomyositis (JDM). **A**, Correlation between levels of calprotectin (S100A8/A9) and fasting levels of high-density lipoprotein (HDL) in JDM patients (n = 20) was determined using Spearman's correlation test. **B**, HDL levels were assessed in patients with high S100A8/A9 levels (n = 10) and patients with low S100A8/A9 levels (n = 10). **C**, Correlation between levels of peroxidase (Pox) activity and fasting levels of HDL in JDM patients (n = 20) was determined using Spearman's correlation test. **D**, HDL levels were assessed in patients with high peroxidase activity (n = 7) and patients with low peroxidase activity (n = 13). In **B** and **D**, bars show the median. * = P < 0.05 by Mann-Whitney U test.

be explained by the selection of our patients (e.g., those with calcinosis), but it may also relate to the rapid turnover of neutrophils. Consistent with our findings and similar to what has been observed in SLE and psoriasis (8,39), neutrophils succumb to cell death upon engaging calcium crystal, leaving only remnants of NETs in the tissue.

Interestingly, tissue-infiltrating neutrophils were found to engulf seemingly indigestible crystals in JDM. The interactions of neutrophils with a wide range of crystals, including cocaine crystals, uric acid crystals, mineralo-organic particles, and cholesterol crystals, have been previously described (6,17,18,40). In accordance with findings from prior investigations, we were able to demonstrate that calcium crystals, either BCP or patient-derived crystals, had the capacity to engage neutrophils to induce a process referred to as "frustrated phagocytosis" and subsequent NET formation. Briefly, as elegantly demonstrated by Branzk and colleagues, once the target is beyond the size of being engulfed, the neutrophil will become frustrated and undergo NETosis (41). Similar mechanisms also seem to apply to crystalline size (40). Though most crystals induce NET formation, the underlying signaling requirements are somewhat distinct. Consistent with many previous findings (6,17,18,40), calcium crystals induced NETs in a ROS-dependent process. In contrast, calcium pyrophosphate

dehydrate crystals, which are involved in pseudogout, induced NETs in a PI3K-dependent but ROS-independent manner (42). The dependency on PAD-mediated citrullination only applies to MSU and cocaine crystals, whereas cholesterol and calcium crystals induced NETs in a citrullination-independent manner (6,17,18,40).

Further studies are needed to characterize both the common and selective signaling pathways involved in crystal-mediated NET formation. Though neutrophil activation (particularly NETosis) can be targeted pharmaceutically—which has been done successfully in other autoimmune rheumatic diseases such as lupus (5)—understanding mechanisms that act upstream of NETosis (e.g., calcinosis development) would be beneficial in identifying a more attractive drug target that could potentially lead to reduction of general inflammation and not just the neutrophil-dependent component.

Though our experimental data support the hypothesis of calcium crystal–mediated NET formation in the tissue in vivo, low levels of NETs were found in the circulation of JDM patients. These findings indicate that the cell death–inducing component (e.g., calcium crystal) is primarily found in tissue and that NET release is restricted to the site of neutrophil activation. Additionally, calcium crystals may be efficiently neutralized by serum components, reducing their NET-inducing capacity (43). What could then be the source

of peripheral NETs? It has previously been demonstrated that ICs induce NET formation in an Fcγ receptor IIa– and TLR-dependent manner in SLE (5,10). Consistent with those findings, we observed that children with pediatric SLE also had highly elevated levels of NETs, which strongly correlated with IC levels. Notably, elevated levels of ICs were also present in JDM patients and were associated with NET levels. Thus, it is likely that ICs may contribute to activation and death of neutrophils in JDM as well. Though most JDM patients did not have elevated levels of NETs in the periphery, impaired degradation, as described in our study, may still affect the persistence of NETs by promoting inflammation and damaging the vasculature (37,44). In accordance with this hypothesis, NET levels and the capacity to degrade NETs were associated with markers of inflammation, in particular IL-6 levels, in JDM patients. It has previously been demonstrated that NETs (specifically NET-derived mitochondrial DNA) were interferogenic and that they signaled through the DNA-sensing cGAS-STING pathway to induce type I IFNs (5). It is therefore likely that NETs may contribute to the prominent type I IFN signature present in JDM patients (11).

Neutrophil activation, with elevated levels of calprotectin, has been described as occurring in the sera of JDM patients and is associated with disease activity (14). However, given the activation of neutrophils and platelets during the coagulation process that results in the release of calprotectin (29,30), serum levels of calprotectin do not reflect physiologic levels of calprotectin. Our investigation is the first to assess true levels of calprotectin in patient circulation using rapidly processed plasma samples, thereby avoiding the influence of coagulation on immune cell activation. Importantly, we found that calprotectin and peroxidase levels were increased in JDM patients and were associated with markers of disease activity, implicating an important role of neutrophils in JDM pathogenesis and their potential utility as biomarkers to monitor disease progression. Furthermore, neutrophil activation (including NETosis) is detrimental in the development of endothelial damage and subsequent atherosclerosis (35–37), with elevated levels of calprotectin associated with cardiovascular disease (29,31,32), likely through facilitating extravasation and receptor for advanced glycation end products–mediated inflammation (45–47).

JDM patients experience pronounced dyslipidemia early in their disease, as demonstrated in this study, with development of atherosclerosis and increased intima-media thickness occurring during progression into adulthood (2,33). However, the role of neutrophils in the atherosclerotic process of JDM had not previously been addressed. Similar to findings in diabetes mellitus and spondyloarthritis (34,48), we observed that neutrophil activation was associated with dyslipidemia in JDM, which suggests the potential involvement of neutrophils in lipid modulation in JDM. Consistent with this interpretation is the notion that neutrophil-derived MPO promotes oxidative modification of HDL, rendering it proatherogenic (38). Further research, including longitudinal studies, is warranted in order to determine the potential contribution

and prognostic value of neutrophil activation and NET formation in dyslipidemia and endothelial dysfunction in JDM.

In conclusion, we have reported on novel mechanisms of calcium crystal–mediated neutrophil activation and cell death in JDM pathogenesis. Targeting this pathway may reduce the disabling consequences of calcinosis and prevent long-term development of comorbidities, including atherosclerosis.

AUTHOR CONTRIBUTIONS

All authors were involved in drafting the article or revising it critically for important intellectual content, and all authors approved the final version to be published. Dr. Lood had full access to all of the data in the study and takes responsibility for the integrity of the data and the accuracy of the data analysis.
Study conception and design. Pachman, Lood.
Acquisition of data. Duvvuri, Morgan, Khojah, Klein-Gitelman, Curran, Doty, Lood.
Analysis and interpretation of data. Duvvuri, Pachman, Lood.

REFERENCES

1. Mendez EP, Lipton R, Ramsey-Goldman R, Roettcher P, Bowyer S, Dyer A, et al, for the NIAMS Juvenile DM Registry Physician Referral Group. US incidence of juvenile dermatomyositis, 1995–1998: results from the National Institute of Arthritis and Musculoskeletal and Skin Diseases Registry. Arthritis Rheum 2003;49:300–5.

2. Eimer MJ, Brickman WJ, Seshadri R, Ramsey-Goldman R, McPherson DD, Smulevitz B, et al. Clinical status and cardiovascular risk profile of adults with a history of juvenile dermatomyositis. J Pediatr 2011;159:795–801.

3. Rider LG, Nistala K. The juvenile idiopathic inflammatory myopathies: pathogenesis, clinical and autoantibody phenotypes, and outcomes. J Intern Med 2016;280:24–38.

4. Pachman LM, Abbott K, Sinacore JM, Amoruso L, Dyer A, Lipton R, et al. Duration of illness is an important variable for untreated children with juvenile dermatomyositis. J Pediatr 2006;148:247–53.

5. Lood C, Blanco LP, Purmalek MM, Carmona-Rivera C, De Ravin SS, Smith CK, et al. Neutrophil extracellular traps enriched in oxidized mitochondrial DNA are interferogenic and contribute to lupus-like disease. Nat Med 2016;22:146–53.

6. Lood C, Hughes GC. Neutrophil extracellular traps as a potential source of autoantigen in cocaine-associated autoimmunity. Rheumatology (Oxford) 2017;56:638–43.

7. Garcia-Romo GS, Caielli S, Vega B, Connolly J, Allantaz F, Xu Z, et al. Netting neutrophils are major inducers of type I IFN production in pediatric systemic lupus erythematosus. Sci Transl Med 2011;3: 73ra20.

8. Villanueva E, Yalavarthi S, Berthier CC, Hodgin JB, Khandpur R, Lin AM, et al. Netting neutrophils induce endothelial damage, infiltrate tissues, and expose immunostimulatory molecules in systemic lupus erythematosus. J Immunol 2011;187:538–52.

9. Khandpur R, Carmona-Rivera C, Vivekanandan-Giri A, Gizinski A, Yalavarthi S, Knight JS, et al. NETs are a source of citrullinated autoantigens and stimulate inflammatory responses in rheumatoid arthritis. Sci Transl Med 2013;5:178ra140.

10. Lood C, Arve S, Ledbetter J, Elkon KB. TLR7/8 activation in neutrophils impairs immune complex phagocytosis through shedding of FcgRIIA. J Exp Med 2017;214:2103–19.

11. Baechler EC, Bilgic H, Reed AM. Type I interferon pathway in adult and juvenile dermatomyositis [review]. Arthritis Res Ther 2011;13:249.

12. Wu Q, Wedderburn LR, McCann LJ. Juvenile dermatomyositis: latest advances. Best Pract Res Clin Rheumatol 2017;31:535–57.

13. Frank MB, Wang S, Aggarwal A, Knowlton N, Jiang K, Chen Y, et al. Disease-associated pathophysiologic structures in pediatric rheumatic diseases show characteristics of scale-free networks seen in physiologic systems: implications for pathogenesis and treatment. BMC Med Genomics 2009;2:9.

14. Nistala K, Varsani H, Wittkowski H, Vogl T, Krol P, Shah V, et al. Myeloid related protein induces muscle derived inflammatory mediators in juvenile dermatomyositis. Arthritis Res Ther 2013;15:R131.

15. Peng Y, Zhang S, Zhao Y, Liu Y, Yan B. Neutrophil extracellular traps may contribute to interstitial lung disease associated with anti-MDA5 autoantibody positive dermatomyositis. Clin Rheumatol 2018;37:107–15.

16. Zhang S, Shu X, Tian X, Chen F, Lu X, Wang G. Enhanced formation and impaired degradation of neutrophil extracellular traps in dermatomyositis and polymyositis: a potential contributor to interstitial lung disease complications. Clin Exp Immunol 2014;177:134–41.

17. Warnatsch A, Ioannou M, Wang Q, Papayannopoulos V. Inflammation: neutrophil extracellular traps license macrophages for cytokine production in atherosclerosis. Science 2015;349:316–20.

18. Schauer C, Janko C, Munoz LE, Zhao Y, Kienhöfer D, Frey B, et al. Aggregated neutrophil extracellular traps limit inflammation by degrading cytokines and chemokines. Nat Med 2014;20:511–7.

19. Ibarra M, Rigsby C, Morgan GA, Sammet CL, Huang CC, Xu D, et al. Monitoring change in volume of calcifications in juvenile idiopathic inflammatory myopathy: a pilot study using low dose computed tomography. Pediatr Rheumatol Online J 2016;14:64.

20. Bode RK, Klein-Gitelman MS, Miller ML, Lechman TS, Pachman LM. Disease activity score for children with juvenile dermatomyositis: reliability and validity evidence. Arthritis Rheum 2003;49:7–15.

21. Ibarra MF, Klein-Gitelman M, Morgan E, Proytcheva M, Sullivan C, Morgan G, et al. Serum neopterin levels as a diagnostic marker of hemophagocytic lymphohistiocytosis syndrome. Clin Vaccine Immunol 2011;18:609–14.

22. Bocciarelli DS. Morphology of crystallites in bone. Calcif Tissue Res 1970;5:261–9.

23. Leffler J, Gullstrand B, Jönsen A, Nilsson JÅ, Martin M, Blom AM, et al. Degradation of neutrophil extracellular traps co-varies with disease activity in patients with systemic lupus erythematosus. Arthritis Res Ther 2013;15:R84.

24. McCarthy GM, Cheung HS, Abel SM, Ryan LM. Basic calcium phosphate crystal-induced collagenase production: role of intracellular crystal dissolution. Osteoarthritis Cartilage 1998;6:205–13.

25. Davis MA, Fairgrieve MR, Den Hartigh A, Yakovenko O, Duvvuri B, Lood C, et al. Calpain drives pyroptotic vimentin cleavage, intermediate filament loss, and cell rupture that mediates immunostimulation. Proc Natl Acad Sci U S A 2019;116:5061–70.

26. Eppell SJ, Tong W, Katz JL, Kuhn L, Glimcher MJ. Shape and size of isolated bone mineralites measured using atomic force microscopy. J Orthop Res 2001;19:1027–34.

27. Sabbione F, Keitelman IA, Iula L, Ferrero M, Giordano MN, Baldi P, et al. Neutrophil extracellular traps stimulate proinflammatory responses in human airway epithelial cells. J Innate Immun 2017;9:387–402.

28. Leffler J, Martin M, Gullstrand B, Tydén H, Lood C, Truedsson L, et al. Neutrophil extracellular traps that are not degraded in systemic lupus erythematosus activate complement exacerbating the disease. J Immunol 2012;188:3522–31.

29. Lood C, Tydén H, Gullstrand B, Jönsen A, Källberg E, Mörgelin M, et al. Platelet-derived S100A8/A9 and cardiovascular disease in systemic lupus erythematosus. Arthritis Rheumatol 2016;68:1970–80.

30. Wang Y, Fang C, Gao H, Bilodeau ML, Zhang Z, Croce K, et al. Platelet-derived S100 family member myeloid-related protein-14 regulates thrombosis. J Clin Invest 2014;124:2160–71.

31. Tydén H, Lood C, Gullstrand B, Jönsen A, Nived O, Sturfelt G, et al. Increased serum levels of S100A8/A9 and S100A12 are associated with cardiovascular disease in patients with inactive systemic lupus erythematosus. Rheumatology (Oxford) 2013;52:2048–55.

32. Katashima T, Naruko T, Terasaki F, Fujita M, Otsuka K, Murakami S, et al. Enhanced expression of the S100A8/A9 complex in acute myocardial infarction patients. Circ J 2010;74:741–8.

33. Kozu KT, Silva CA, Bonfá E, Sallum AM, Pereira RM, Viana VS, et al. Dyslipidaemia in juvenile dermatomyositis: the role of disease activity. Clin Exp Rheumatol 2013;31:638–44.

34. Pedersen L, Nybo M, Poulsen MK, Henriksen JE, Dahl J, Rasmussen LM. Plasma calprotectin and its association with cardiovascular disease manifestations, obesity and the metabolic syndrome in type 2 diabetes mellitus patients. BMC Cardiovasc Disord 2014;14:196.

35. Carlucci PM, Purmalek MM, Dey AK, Temesgen-Oyelakin Y, Sakhardande S, Joshi AA, et al. Neutrophil subsets and their gene signature associate with vascular inflammation and coronary atherosclerosis in lupus. JCI Insight 2018;3:99276.

36. Carmona-Rivera C, Zhao W, Yalavarthi S, Kaplan MJ. Neutrophil extracellular traps induce endothelial dysfunction in systemic lupus erythematosus through the activation of matrix metalloproteinase-2. Ann Rheum Dis 2015;74:1417–24.

37. Knight JS, Luo W, O'Dell AA, Yalavarthi S, Zhao W, Subramanian V, et al. Peptidylarginine deiminase inhibition reduces vascular damage and modulates innate immune responses in murine models of atherosclerosis. Circ Res 2014;114:947–56.

38. Smith CK, Vivekanandan-Giri A, Tang C, Knight JS, Mathew A, Padilla RL, et al. Neutrophil extracellular trap–derived enzymes oxidize high-density lipoprotein: an additional proatherogenic mechanism in systemic lupus erythematosus. Arthritis Rheumatol 2014;66:2532–44.

39. Hu SC, Yu HS, Yen FL, Lin CL, Chen GS, Lan CC. Neutrophil extracellular trap formation is increased in psoriasis and induces human β-defensin-2 production in epidermal keratinocytes. Sci Rep 2016;6:31119.

40. Peng HH, Liu YJ, Ojcius DM, Lee CM, Chen RH, Huang PR, et al. Mineral particles stimulate innate immunity through neutrophil extracellular traps containing HMGB1. Sci Rep 2017;7:16628.

41. Branzk N, Lubojemska A, Hardison SE, Wang Q, Gutierrez MG, Brown GD, et al. Neutrophils sense microbe size and selectively release neutrophil extracellular traps in response to large pathogens. Nat Immunol 2014;15:1017–25.

42. Pang L, Hayes CP, Buac K, Yoo DG, Rada B. Pseudogout-associated inflammatory calcium pyrophosphate dihydrate microcrystals induce formation of neutrophil extracellular traps. J Immunol 2013;190:6488–500.

43. Terkeltaub RA, Santoro DA, Mandel G, Mandel N. Serum and plasma inhibit neutrophil stimulation by hydroxyapatite crystals: evidence that serum α_2-HS glycoprotein is a potent and specific crystal-bound inhibitor. Arthritis Rheum 1988;31:1081–9.

44. Knight JS, Subramanian V, O'Dell AA, Yalavarthi S, Zhao W, Smith CK, et al. Peptidylarginine deiminase inhibition disrupts NET formation and protects against kidney, skin and vascular disease in lupus-prone MRL/lpr mice. Ann Rheum Dis 2015;74:2199–206.

45. Ehlermann P, Eggers K, Bierhaus A, Most P, Weichenhan D, Greten J, et al. Increased proinflammatory endothelial response to S100A8/A9 after preactivation through advanced glycation end products. Cardiovasc Diabetol 2006;5:6.

46. Harja E, Bu DX, Hudson BI, Chang JS, Shen X, Hallam K, et al. Vascular and inflammatory stresses mediate atherosclerosis via RAGE and its ligands in apoE$^{-/-}$ mice. J Clin Invest 2008;118:183–94.

47. Hofmann MA, Drury S, Fu C, Qu W, Taguchi A, Lu Y, et al. RAGE mediates a novel proinflammatory axis: a central cell surface receptor for S100/calgranulin polypeptides. Cell 1999;97:889–901.

48. Genre F, Rueda-Gotor J, Remuzgo-Martínez S, Corrales A, Mijares V, Expósito R, et al. Association of circulating calprotectin with lipid profile in axial spondyloarthritis. Sci Rep 2018;8:13728.

AMERICAN COLLEGE
of RHEUMATOLOGY
Empowering Rheumatology Professionals

Role of Interferon-γ–Producing Th1 Cells in a Murine Model of Type I Interferon–Independent Autoinflammation Resulting From DNase II Deficiency

Sudesh Pawaria,[1] Kerstin Nündel,[1] Kevin M. Gao,[1] Stephanie Moses,[1] Patricia Busto,[1] Kevin Holt,[1] Rohit B. Sharma,[1] Michael A. Brehm,[1] Ellen M. Gravallese,[1] Merav Socolovsky,[1] Anette Christ,[2] and Ann Marshak-Rothstein[1] iD

Objective. Patients with hypomorphic mutations in DNase II develop a severe and debilitating autoinflammatory disease. This study was undertaken to compare the disease parameters in these patients to those in a murine model of DNase II deficiency, and to evaluate the role of specific nucleic acid sensors and identify the cell types responsible for driving the autoinflammatory response.

Methods. To avoid embryonic death, $Dnase2^{-/-}$ mice were intercrossed with mice that lacked the type I interferon (IFN) receptor ($Ifnar^{-/-}$). The hematologic changes and immune status of these mice were evaluated using complete blood cell counts, flow cytometry, serum cytokine enzyme-linked immunosorbent assays, and liver histology. Effector cell activity was determined by transferring T cells from $Dnase2^{-/-} \times Ifnar^{-/-}$ double-knockout (DKO) mice into $Rag1^{-/-}$ mice, and 4 weeks after cell transfer, induced changes were assessed in the recipient mice.

Results. In $Dnase2^{-/-} \times Ifnar^{-/-}$ DKO mice, many of the disease features found in DNase II–deficient patients were recapitulated, including cytopenia, extramedullary hematopoiesis, and liver fibrosis. $Dnase2^{+/+} \times Rag1^{-/-}$ mice (n > 22) developed a hematologic disorder that was attributed to the transfer of an unusual IFNγ-producing T cell subset from the spleens of donor $Dnase2^{-/-} \times Ifnar^{-/-}$ DKO mice. Autoinflammation in this murine model did not depend on the stimulator of IFN genes (STING) pathway but was highly dependent on the chaperone protein Unc93B1.

Conclusion. $Dnase2^{-/-} \times Ifnar^{-/-}$ DKO mice may be a valid model for exploring the innate and adaptive immune mechanisms responsible for the autoinflammation similar to that seen in $DNASE2$-hypomorphic patients. In this murine model, IFNγ is required for T cell activation and the development of clinical manifestations. The role of IFNγ in $DNASE2$-deficient patient populations remains to be determined, but the ability of $Dnase2^{-/-}$ mouse T cells to transfer disease to $Rag1^{-/-}$ mice suggests that T cells may be a relevant therapeutic target in patients with IFN-related systemic autoinflammatory diseases.

INTRODUCTION

The excessive accumulation of nucleic acid debris can lead to the activation of endosomal and/or cytosolic nucleic acid sensors and the subsequent development of autoimmune and autoinflammatory diseases (1,2). Debris can accumulate as a result of inadequate scavenger cell activity, and numerous scavenger receptor defects have been associated with systemic lupus erythematosus (SLE) (3). Importantly, appropriate removal of DNA also depends on DNases located extracellularly or within specific cellular compartments. For example, loss-of-function mutations in an extracellular DNase, DNase IL3, have been associated with SLE both in patient populations and in murine models (4,5), while loss-of-function mutations in the cytosolic enzyme Trex1 leads to neuroinflammation in patients with Aicardi-Goutières syndrome (6), and to myositis and other organ damage in a murine model of autoinflammatory disease (7).

The loss of a lysosomal DNase, DNase II, has also been linked to autoinflammation. In mice, DNase II deficiency results in an embryonically lethal anemia that is caused by the massive accumulation of

undegraded DNA in phagocytic compartments (8). This anemia is linked to the excessive production of interferon-β (IFNβ), since mice deficient in both DNase II and the type I IFN receptor (IFNαR) survive as relatively healthy pups. This IFN production is downstream of the cytosolic DNA–detecting cyclic GMP-AMP synthase (cGAS) pathway, since both stimulator of IFN genes (STING)–deficient and cGAS-deficient mice are protected from embryonic death (9–11). DNA may access the cytosol as a result of lysosome instability, defects in autophagosome formation, or the accrual of self DNA in the cytosol following DNA damage or replication (12–14). However, excessive cell debris, cleared via scavenger receptors, must also accumulate in phagolysosomes, and in this way appear to gain access to nucleic acid–sensing Toll-like receptors (TLRs).

Despite surviving to adulthood, $Dnase2^{-/-} \times Ifnar^{-/-}$ double-knockout (DKO) mice nevertheless develop immune system abnormalities. These include a well-described inflammatory arthritis that results in severely swollen joints by ages 6–10 months (15,16). This late-onset arthritis depends on the cGAS/STING pathway as well as on another cytosolic DNA sensor, absent in melanoma 2 (AIM2) (10,17,18). These DKO mice also develop early onset of splenomegaly and extramedullary hematopoiesis as well as the production of antinuclear antibodies (ANAs), all of which are disease manifestations commonly found in murine models of SLE, especially those driven by TLR-7. In contrast to models of arthritis in which embryonic death occurs, the disease in these DKO mice is not STING dependent, but is dependent on Unc93B1 (19,20), a chaperone protein required for TLR trafficking from the endoplasmic reticulum to endosomal/lysosomal compartments (21); the pathologic mechanisms in these mice are therefore likely to involve endosomal TLRs.

Crow and colleagues have recently identified hypomorphic mutations of DNase II in patients with an uncharacterized interferonopathy (22). These patients develop a spectrum of clinical features that includes severe nonregenerative anemia and thrombocytopenia at birth, splenomegaly, ANA production, glomerulonephritis, liver fibrosis, and deforming arthropathies. Based on the similar characteristics in other patients with a strong IFN signature, it has been assumed that these disease manifestations are predominantly driven by the STING-dependent production of type I IFNs. Intriguingly, we have now shown that many of these disorders develop in DKO mice in the absence of conventional type I IFN signaling and are dependent on the endosomal TLR chaperone Unc93B1. It follows that a better understanding of the mechanisms responsible for the nonarthritic disease parameters in DKO mice might be highly relevant to human disease.

In this study, we identified a major role for a novel IFNγ-producing T cell subset in the propagation of the erythrocyte and lymphocyte developmental defects characteristic of autoinflammation in $Dnase2^{-/-} \times Ifnar^{-/-}$ DKO mice. Our findings suggest that Th1-like cells could be an appropriate therapeutic target in patients with systemic autoimmune diseases associated with IFN signatures.

MATERIALS AND METHODS

Mice. DNase II gene–targeted mice were kindly provided by Dr. S. Nagata (Osaka University, Osaka, Japan) and obtained through the Riken Institute. The mouse strains $Dnase2^{+/-} \times Ifnar^{-/-}$ (heterozygote), $Dnase2^{-/-} \times Ifnar^{-/-}$ (DKO), $Dnase2^{-/-} \times Ifnar^{-/-} \times Unc93B1^{3d/3d}$ (Unc93B1 triple-knockout [TKO]), and $Dnase2^{-/-} \times Ifnar^{-/-} \times Tmem173^{-/-}$ (STING TKO) have been described previously (17,19,20). $Ifngr^{-/-}$ mice, obtained from The Jackson Laboratory, and both $Tlr3^{-/-}$ and $Tlr7^{-/-}$ C57BL/6 mice, kindly provided by Dr. D. Golenbock (University of Massachusetts Medical School, Worcester), were intercrossed with DKO mice to generate the corresponding TKO lines. B6 $Rag1^{-/-}$ mice (The Jackson Laboratory) were intercrossed with $Ifngr^{-/-}$ mice to generate $Rag1^{-/-} \times Ifngr^{-/-}$ mice.

Complete blood cell counts in the mice were carried out at the University of Massachusetts Medical School Animal Medicine Core. All animal procedures were approved by and performed in accordance with the Institutional Animal Care and Use Committee at the University of Massachusetts Medical School.

Flow cytometry. Cell suspensions were analyzed by flow cytometry, as described previously (19). Spleen and bone marrow single-cell suspensions were incubated in Fc block 2.4G2 supernatant (2.4G2 hybridoma; ATCC) before staining. The following fluorochrome-labeled antibodies were obtained: allophycocyanin (APC)–conjugated Ter119, Pacific Blue (PB)–conjugated anti-CD19 (1D3), phycoerythrin (PE)–conjugated CD4 (RM4-5), APC-conjugated CD8 (SK1), PB-conjugated CD45R/B220 (RA3-6B2), PB-conjugated CD11b (M1/70) (all from Tonbo BioSciences), APC-conjugated Ly6C (1A8), fluorescein isothiocyanate–conjugated Ly6G (RB6-8C5), PE–Cy7–conjugated CD71 (RI7217), PB-conjugated CD69 (H1.2F3), PerCP–Cy5.5–conjugated CD62L (MEL-14), APC–Cy7–conjugated CD44 (IM7), APC-conjugated CD93 (AA4.1), and APC-conjugated CD45.1 (A20) (all from BioLegend). Samples were analyzed with an LSR II flow cytometer (BD Biosciences), and results were analyzed using FlowJo software version 9.7.6 (Tree Star).

Flow cytometry data were analyzed by Mann-Whitney non-parametric t-test, using GraphPad Prism software (version 7.0). P values less than or equal to 0.05 were considered significant.

Magnetic bead–based cell purification. BD Biosciences IMag anti-mouse magnetic particles were used for depletion or purification of CD45R/B220 cells (catalog no. 552311), CD4+ T cells (catalog no. 551539), or CD8+ T cells (catalog no. 551516). CD3+ T cells were purified using biotin anti-mouse CD3e (145-2C11) (catalog no. 30-0031; Tonbo Biosciences) and BD Biosciences IMag Streptavidin Particles Plus-DM (catalog no. 557812).

Histology. Mouse liver sections were formalin-fixed and stained with trichrome. Histologic analyses of the liver sections were carried out at Applied Pathology Systems in Worcester, Massachusetts.

Measurement of ANAs. Serum levels of ANAs were determined in a manner as previously described (19). The mouse serum, diluted 1:50, was incubated on HEp-2 antigen substrate slides (MBL International), and bound antibodies were detected with DyLight 488–coupled goat anti-mouse IgG antibodies (Poly4053; BioLegend).

Gene expression analysis. Gene expression was quantified with a Nanodrop ND-1000 spectrophotometer (Thermo Fisher Scientific) using a NanoString nCounter Immune Panel (catalog no. XT-CSO-MIM1-12; NanoString Technologies) according to the manufacturer's protocol. The data were normalized to the values for a set of 6 internal positive controls and 8 internal negative controls, and then to the values for 20 housekeeping genes. Gene expression values above the threshold (defined as the mean + 2SD of values in negative controls) were considered for analysis. Normalized log$_2$-transformed values were analyzed using nSolverTM analysis software (version 3.0), and unbiased hierarchical clustering was used to generate a heatmap in the open-source R-based software, as described previously (23). Relative gene expression levels were compared using Morpheus software (https://software.broadinstitute.org/morpheus).

Determination of cytokine titers. Serum cytokine titers were determined by multiplex enzyme-linked immunosorbent assays (Procarta-plex bead assay; Thermo Fisher Scientific). The assays were conducted on a MAGPIX instrument with Luminex xMAP Technology.

Spleen fragment transplantation. Mouse spleen fragments were transplanted under the kidney capsule of *Rag1*$^{-/-}$ C57BL/6 mice using established procedures (24). Briefly, spleens isolated from 4–10-day-old neonatal mice were cut into 1-mm^3 fragments with a scalpel. Mice were first injected subcutaneously with 0.1 ml of a cefazolin–gentamicin antibiotic mixture and then were anesthetized by intraperitoneal injection of a ketamine–xylazine solution (150 mg/kg ketamine and 10 mg/kg xylazine). The kidney of recipient mice was exposed through an abdominal incision, and a 1–2-mm cut was made in the capsule. The spleen fragment was then inserted under the capsule using a surgical trocar. The kidney was returned to the abdominal cavity, the cavity wall was sutured, and the skin incision was closed with autoclips.

T cell adoptive transfer. Red blood cell (RBC)–depleted total spleen cells (10^7), T or B cell–depleted spleen cells (10^7), or 3–10 × 10^6 magnetic bead–purified CD4+, CD8+, or CD3+ T cells were injected intravenously into *Rag1*$^{-/-}$ mice. The mice were euthanized, and tissue samples were collected for analysis at 4 weeks postinjection. Th1 cells were generated using standard Th1-skewing conditions (25).

RESULTS

Similarity of hematologic abnormalities between DKO mice and human DNase II–deficient patients, and dependency on Unc93B1. To determine the extent of cytopenia in DKO mice relative to DNase II–sufficient control mice, complete blood cell counts in young *Dnase2*$^{-/-}$ × *Ifnar*$^{-/-}$ DKO mice were compared to those in DNase II heterozygotes (*Dnase*$^{+/-}$ × *Ifnar*$^{-/-}$). Similar to DNase II–deficient patients, young DKO mice showed a significant reduction in the total white blood cell, lymphocyte, platelet, and RBC counts, as well as increased numbers of immature erythrocytes and an increased frequency of granulocytes and monocytes, compared to the other 2 groups of mice (Figure 1A; further details available from the corresponding author upon request). They also developed dramatically enlarged spleens, even as early as age 4 weeks, as well as elevated serum concentrations of erythropoietin and a reduced hematocrit level (Figure 1A). This evidence of extramedullary hematopoiesis was consistent with the increased number and percentage of splenic Ter119+ erythroid lineage cells (19), proerythrocytes (CD71^{high}Ter119^{intermediate}), and erythroblasts (CD71^{high}Ter119^{high}) at the basophilic stage (EryA) and later stages (EryB) of erythrocyte differentiation (26) in the spleens of DKO mice compared to heterozygote controls (Figure 1B).

We also included Unc93 TKO mice (*Dnase2*$^{-/-}$ × *Ifnar*$^{-/-}$ × *Unc93b1*$^{3d/3d}$ TKO) in these analyses, and found that most of the aforementioned abnormalities were reversed in Unc93B1-deficient mice. However, compared to heterozygote controls, the percentage of both EryA and EryB erythroblasts remained high in Unc93 TKO mice, even though the total spleen weight and cell numbers were significantly lower than those found in littermate DKO mice.

Splenomegaly in the DKO mice was associated with a corresponding defect in bone marrow erythropoiesis, as indicated by low numbers of EryB erythrocytes (Figure 1C) (further details available from the corresponding author upon request). These type I IFN–independent defects also showed a dependency on Unc93B1. Based on these findings, we conclude that *Dnase2*$^{-/-}$ × *Ifnar*$^{-/-}$ DKO mice have ineffective erythropoiesis, and that anemia stimulates erythropoietin production which, in turn, drives expansion of erythropoietic precursors, but nevertheless fails to generate a normal number of circulating erythrocytes.

Additional changes in the lymphocyte and myeloid cell compartments in the spleen and bone marrow of DKO mice. Early-onset extramedullary hematopoiesis was associated with additional shifts in the myeloid and lymphocyte compartment in the spleen and bone marrow, which was clearly apparent in the DKO mice by age 10 weeks. The percentage of B cells in the DKO mouse spleens after RBC depletion was significantly lower than in either the heterozygote or Unc93B1 TKO mouse spleens (19). This decrease in the proportion of splenic B cells reflected a disruption in B cell development in the bone

marrow, in which the DKO mice had comparable numbers of total B220+ cells but had a much lower proportion of AA4.1[negative] mature B cells when compared to the other 2 groups (Figure 2A).

The percentage of splenic T cells was also reduced in DKO mice, and residual T cells were highly activated, as shown by the increased frequency of CD69^{high} T cells and T cells expressing the effector memory phenotype CD44^{high}CD62^{low} (Figure 2B). There was a corresponding increase in the percentage and/or number of CD11b+ cells in both the spleen and bone marrow of DKO mice, concomitant with a dramatic increase in the percentage of neutrophils in the spleen (Figure 2C).

Hereinafter, these observed hematopoietic defects are referred to as the "DKO phenotype." Such a phenotype can be readily assessed by the presence of the following features: increased spleen weight, increased frequency of Ter119+Cd11b+ cells, and granulocytes in the spleen, decreased percentage of total B cells in the spleen and mature B cells in the bone marrow, increased percentage of CD11b+ cells in the bone marrow, and ineffective erythropoiesis in the bone marrow.

Production of proinflammatory cytokines and development of liver fibrosis in DKO mice. DNase II–deficient patients show elevated serum titers of IFNγ and IFN-induced cytokines and chemokines, as well as IFN-independent cytokines (22). Similarly, titers of IFNγ and IFNλ/interleukin-28 (IL-28), IFN-inducible cytokines and chemokines (e.g., IL-12, CXCL10/IFNγ-inducible protein 10), IFN-independent cytokines (e.g., tumor necrosis factor, IL-6), chemokines associated with the recruitment of myeloid cells (CCL5/RANTES, CCL3/macrophage inflammatory protein 1α, and CXCL1/keratinocyte chemoattractant), and immunoregulatory type 2 cytokines (IL-10 and IL-19) (27) were significantly elevated in the serum of DKO mice compared to the serum of heterozygote and Unc93B1 TKO control mice (Figure 3A). Therefore, even cytokine/chemokine production seems to be dependent on Unc93B1, raising the possibility that cytokine production is downstream of TLR signaling.

DNase II–deficient patients also develop liver fibrosis. In our studies, the DKO mice again reflected DNase II–deficient patient populations, since the livers of 6-month-old DKO mice, but not those of heterozygote or Unc93B1 TKO control mice, showed extensive periportal trichrome staining for liver fibrosis (Figure 3B).

Induction of the DKO phenotype by transplantation of DKO neonatal mouse spleen fragments into *Dnase2^{+/+} × Rag1^{-/-}* recipients. It has been generally assumed that the failure to clear apoptotic debris has a major impact on hematopoietic cells, as opposed to stromal cell subsets. However, in previous radiation chimera studies, we found that the DKO phenotype depended on DNase II deficiency in both the stem cell donor and the recipient (20), suggesting that stromal elements might contribute to the splenic abnormalities. To address this possibility, we transplanted spleen fragments from CD45.1 DKO or heterozygote mice into
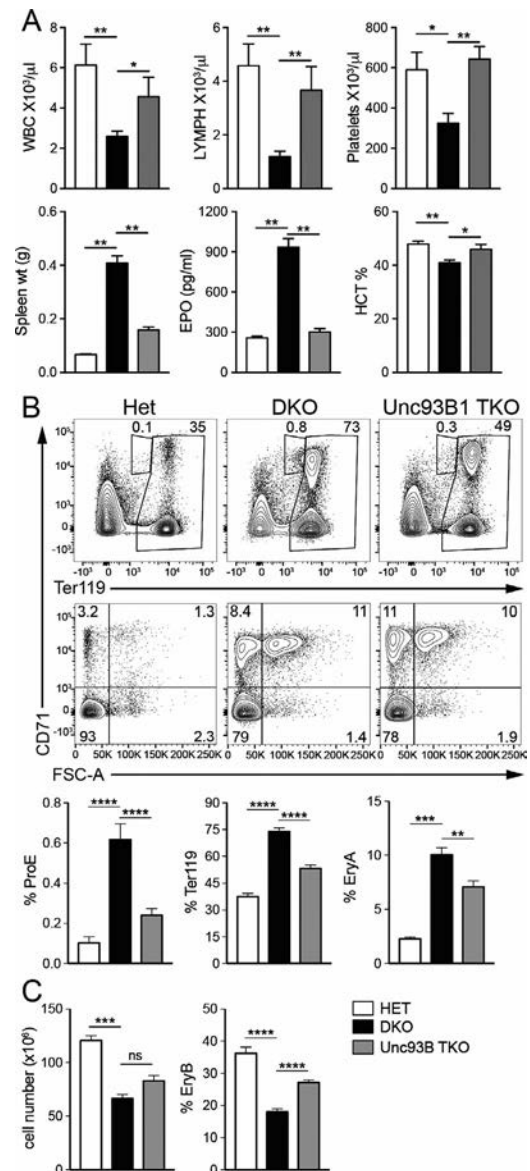

Figure 1. Unc93B1-dependent, type I interferon–independent hematologic defects in *Dnase2^{-/-}* mice. **A**, Blood samples were collected from heterozygote (Het), *Dnase2^{-/-} × Ifnar^{-/-}* double-knockout (DKO), and Unc93B1 triple-knockout (TKO) mice. Total white blood cell (WBC) counts, lymphocyte (LYMPH) counts, platelet counts, and hematocrit (Hct) levels were determined in 5–7-week-old mice (n = 6 per group), spleen weight (Wt) was determined in 4-week-old mice (n = 12–19 per group), and serum erythropoietin (EPO) levels were determined in 10-week-old mice (n = 4–6 per group). **B**, Total spleens from 10-week-old mice were assessed by fluorescence-activated cell sorting to identify the proportions of erythroid progenitors (proE) (CD71+Ter119^{low}; n = 12–14 per group), erythroid lineage cells (Ter119^{high}; n = 13–16 per group), and EryA erythroblasts (Ter119+CD71+FSC-A[high]; n = 12–14 per group). **C**, The number of cells recovered from 4 leg bones per mouse and number of EryB erythroblasts (Ter119+CD71+FSC-A[low]) in total bone marrow were determined in 10-week-old mice (n = 7–16 per group). Results are the mean ± SEM. * = P < 0.05; ** = P < 0.01; *** = P < 0.001; **** = P < 0.0001. NS = not significant.
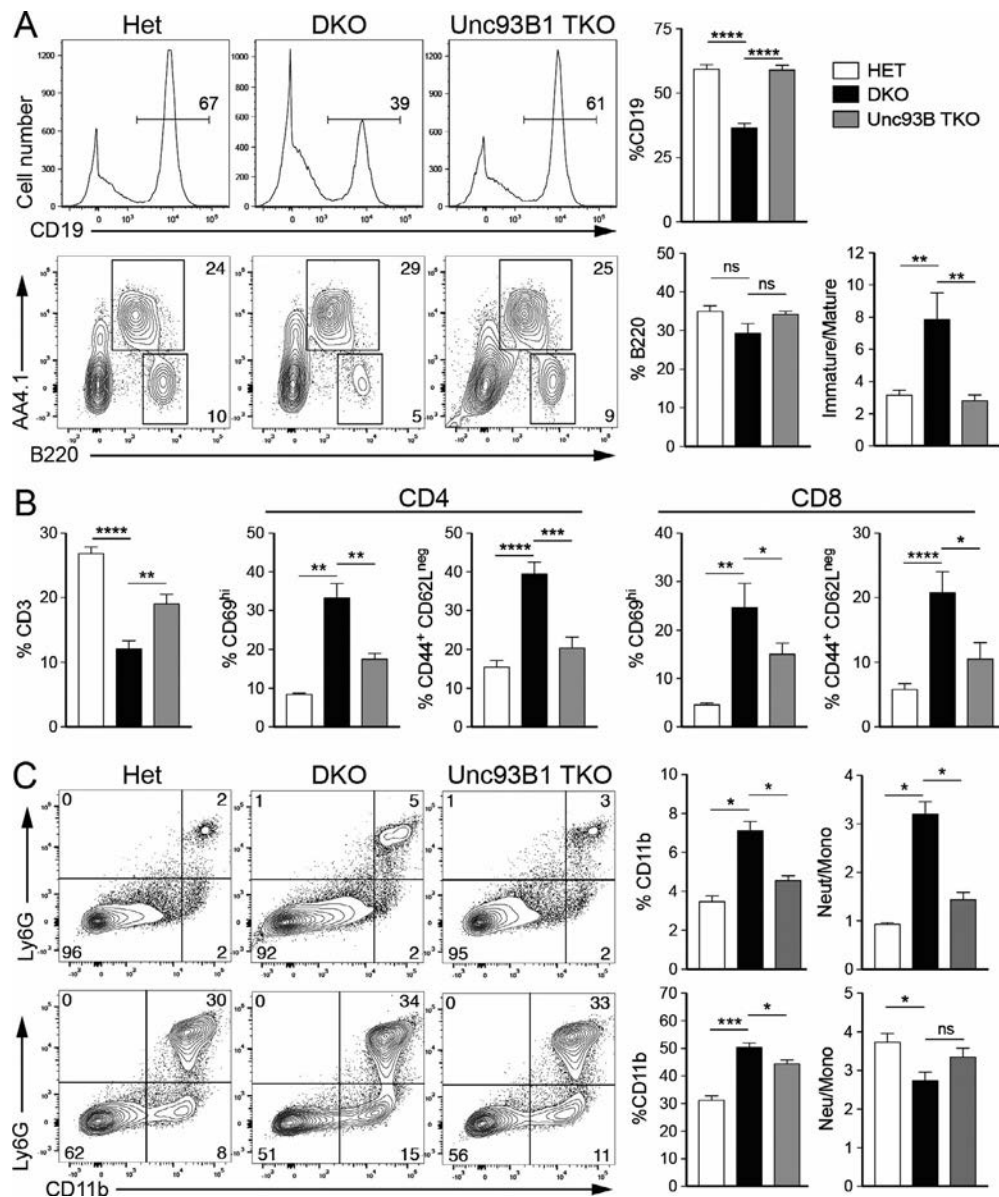
Figure 2. Lymphocyte and myeloid cell abnormalities in DKO mice. **A**, Fluorescence-activated cell sorter analysis was used to determine the percentage of Ter119^{negative} spleen cells stained for the B cell marker CD19, and total bone marrow cells stained for B220 and AA4.1 to identify immature (AA4.1^{high}) and mature (AA4.1^{low}) B cells, in heterozygote, DKO, and Unc93B TKO mice. **B**, Ter119^{negative} spleen cells were stained for CD3, CD4, CD8, CD69 (activated T cells), and effector memory T cell subsets (CD44+CD62L^{negative}). **C**, Ter119^{negative} spleen cells were analyzed to identify myeloid cells (CD11b+) and neutrophils (Neut) (CD11b+Ly-6G+) in the spleen (top) and bone marrow (bottom). Results are the mean ± SEM of 5–22 10-week-old mice per group in 5 independent experiments. Mono = monocytes (see Figure 1 for other definitions). * = $P < 0.05$; ** = $P < 0.01$; *** = $P < 0.001$; **** = $P < 0.0001$.

CD45.2 *Rag1*⁻/⁻ mice by insertion of the fragments under the kidney capsule. We assumed that if splenic stromal cells promote the DKO phenotype by producing proinflammatory chemokines, we would see more severe hematologic abnormalities in the transplanted DKO mouse spleen than in the host spleen.

The mice were analyzed 5 months posttransplantation. We found that spleen fragments from 8 of 9 heterozygote mice had visibly engrafted, but residual subcapsular spleen fragments could not be found in any of the 9 mice that had been transplanted with DKO mouse spleen fragments. However, closer examination

revealed that the spleens of the host *Rag1*⁻/⁻ mice were significantly enlarged when initially transplanted with DKO mouse spleen fragments, in contrast to that seen in host mice transplanted with heterozygote mouse spleen fragments. These enlarged spleens had a significant increase in the percentage of erythroblasts as compared to heterozygote fragment–transplanted or untransplanted *Rag1*⁻/⁻ control mice (Figure 4A).

In addition, the bone marrow of the DKO mouse spleen fragment–transplanted mice was also abnormal, as shown by a decreased percentage of erythroblasts and an increased
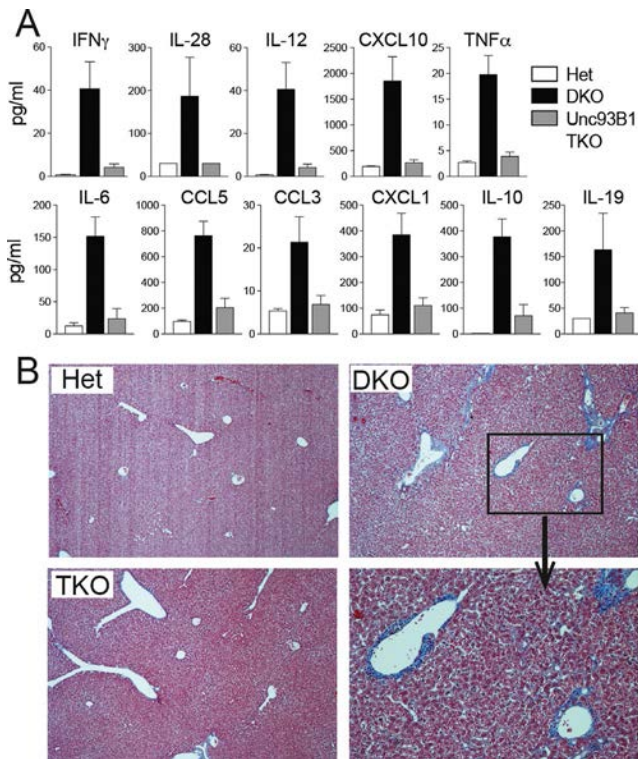
Figure 3. Proinflammatory cytokine production and liver fibrosis in DKO mice. **A**, Cytokine levels were assessed in the serum of 8-week-old heterozygote, DKO, and Unc93B1 TKO mice. Results are the mean ± SEM of 5 mice per group. **B**, Liver sections from representative 6-month-old mice were stained with trichrome to identify histologic features of fibrosis. Top and bottom left, original magnification × 40. Bottom right, original magnification × 100. IFNγ = interferon-γ; IL-28 = interleukin-28; TNF = tumor necrosis factor (see Figure 1 for other definitions).

percentage of CD11b+ cells. Importantly, >99% of the CD11b+ cells were CD45.1^{negative} (data not shown), and therefore were derived from recipient stem cells (Figure 4A). These data indicate that hematopoietic cells present in the spleens of DKO mice, but not those present in the spleens of heterozygote mice, could induce aberrant development of DNase II–sufficient cells and the ensuing DKO-associated splenic and bone marrow abnormalities in the recipient $Rag1^{-/-}$ mice.

Induction of the DKO phenotype by transfer of DKO mouse hematopoietic cells into $Dnase2^{+/+} \times Rag1^{-/-}$ mice.
To determine whether a DKO mouse spleen cell suspension alone was sufficient to induce the DKO phenotype, 10^7 spleen cells isolated from CD45.1 DKO mice or heterozygote mice were injected intravenously into CD45.2 B6 $Rag1^{-/-}$ mice, and the recipient mice were analyzed 4 weeks later. Compared to uninjected mice or mice injected with heterozygote or Unc93B1 TKO mouse spleen cells, erythropoiesis was disrupted in mice injected with either DKO or STING TKO mouse spleen cells, as shown by an increased percentage of Ter119+ erythroblasts in the spleens and corresponding development of splenomegaly (Figure 4B).

The DKO and STING TKO mouse spleen cell–injected mice also had fewer erythroblasts and more CD11b+ cells in the bone marrow; almost all of the CD11b+ cells were CD45.1^{negative}/CD45.2+, indicating that they were derived from $Rag1^{-/-}$ mouse progenitor cells (Figure 4B; further details available from the corresponding author upon request). Early B cell development in the bone marrow was also abnormal in these mice. In $Rag1^{-/-}$ mice, B cells normally proceed to the pro–B cell stage of B cell development (IgM–/–CD19+AA4.1+) (28). This early step in B cell differentiation was impaired in the DKO mouse splenocyte–injected mice, and B lineage cells failed to move into the pro–B cell compartment (IgM^{negative}CD19^{negative}B220^{negative}AA4.1+) (Figure 4B; further details available from the corresponding author upon
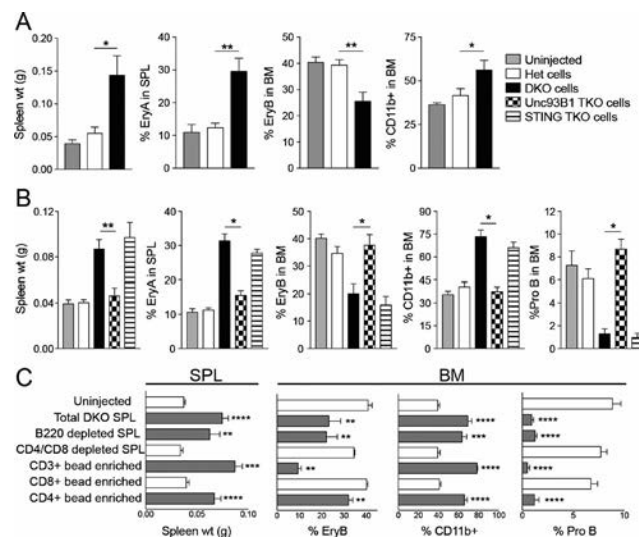

Figure 4. Induction of autoinflammation in $Rag1^{-/-}$ mice. **A**, $Rag1^{-/-}$ mice were transplanted under the kidney capsule with spleen (SPL) fragments from heterozygote or DKO mice, and tissue samples were collected from the host mice 5 months posttransplantation. Spleen weight was assessed, and the percentage of erythroblasts and myeloid cells in the spleens and bone marrow (BM) was determined by flow cytometry. Results are the mean ± SEM of 5–9 mice per group. **B**, $Rag1^{-/-}$ mice were injected intravenously (IV) with 10^7 red blood cell (RBC)–depleted spleen cells from heterozygote, DKO, Unc93B1 TKO, or stimulator of interferon genes (STING) TKO mice, and tissue samples were collected from the host mice 4 weeks postinjection. Spleen weight was assessed, and the percentage of erythroblasts, myeloid cells, and pro–B cells in the spleens and bone marrow was determined. Results are the mean ± SEM of 4–5 experiments (n = 3–13 mice per group). **C**, $Rag1^{-/-}$ mice were injected IV with 10^7 total RBC–depleted DKO mouse spleen cells, B220-depleted DKO mouse spleen cells, CD4/CD8-depleted DKO mouse spleen cells, or 3×10^6 bead-purified spleen cells, and tissue samples were collected from the host mice 4 weeks postinjection. Spleen weight was assessed, and the percentage of erythroblasts, myeloid cells, and pro–B cells in the bone marrow was determined. Results are the mean ± SEM of 4–5 experiments (n = 18 mice for depleted cells, and n = 3–14 mice for purified cells). Uninjected $Rag1^{-/-}$ mice were used as controls. * = $P < 0.05$; ** = $P < 0.01$; *** = $P < 0.001$; **** = $P < 0.0001$. See Figure 1 for other definitions.

request). Consistent with the phenotype of the parental strains, Unc93B1 TKO mouse cells did not transfer these defects, while transfer of STING TKO mouse T cells elicited the same outcome as that with DKO mouse T cells.

Induction of the DKO phenotype by adoptive transfer of DKO mouse CD4+ T cells into *Dnase2*^{+/+} × *Rag1*^{−/−} recipients. Previous studies have documented the presence of activated thymocytes in neonatal DKO mice (8), which is consistent with our own data on splenic T cells (Figure 2B). To determine whether T cells or B cells could be responsible for inducing the DKO phenotype, the DKO mouse spleen cell suspension was depleted of B cells or both CD4+ and CD8+ T cells and then injected into B6 *Rag1*^{−/−} mice. CD4+/CD8+ T cell depletion, but

not B cell depletion, abrogated the ability of the DKO mouse spleen cells to transfer the DKO phenotype (Figure 4C).

To confirm that the relevant cells were T cells and not CD4+ or CD8+ dendritic cells, we used magnetic beads to isolate CD3+ T cells and injected 3×10^6 cells/mouse into *Rag1*^{−/−} host mice. These CD3+ T cells could transfer the DKO phenotype as effectively as total DKO mouse spleen cells. Magnetic bead–enriched CD4+ T cells, but not enriched CD8+ cells, also transferred autoinflammation into the *Rag1*^{−/−} hosts (Figure 4C).

To better define the autoinflammation elicited by DKO mouse CD4+ T cells, we further compared *Rag1*^{−/−} mice injected with magnetic bead–enriched DKO mouse CD4+ T cells to mice injected with comparably isolated cells from littermate
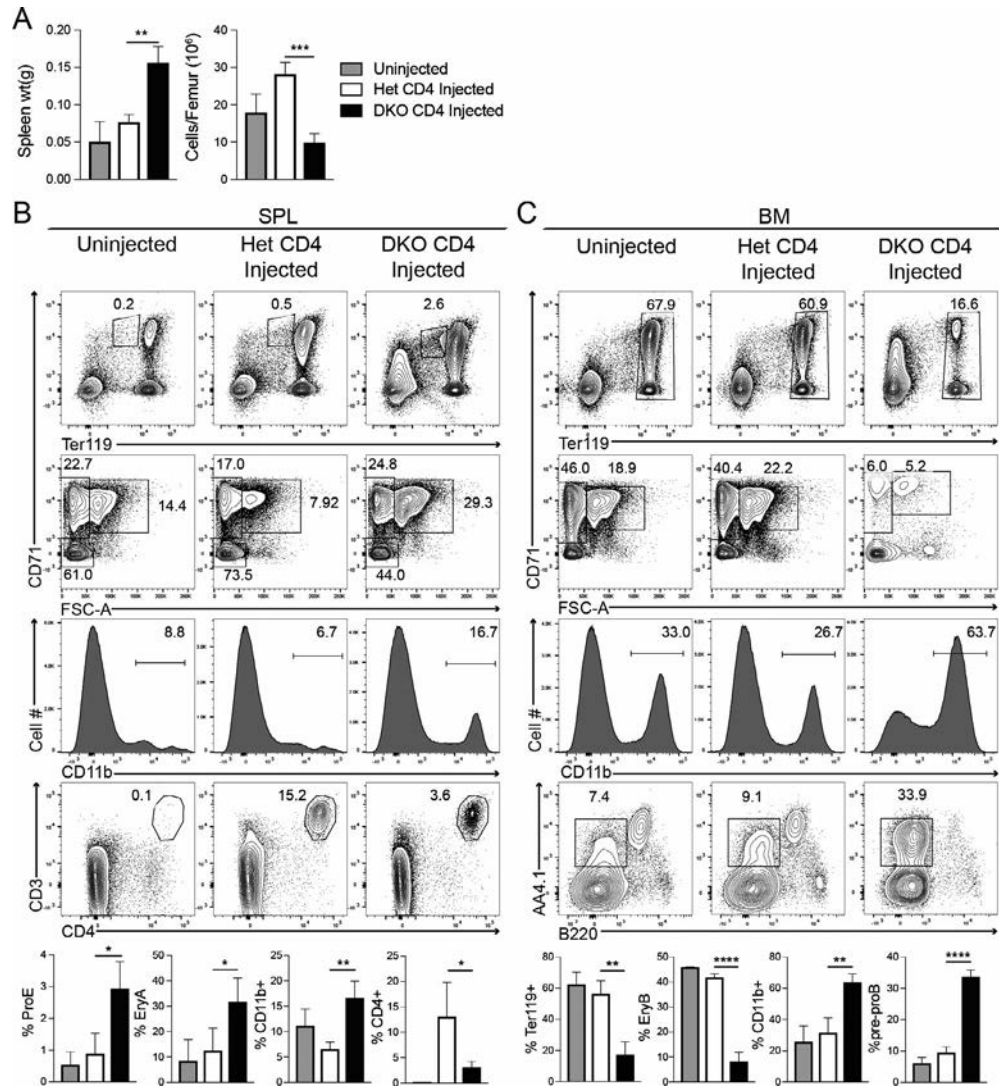
Figure 5. Induction of autoinflammation by transfer of DKO mouse CD4+ T cells into *Rag1*^{−/−} mice. **A**, *Rag1*^{−/−} mice were injected with 10⁷ magnetic bead–purified CD4+ T cells isolated from either heterozygote or DKO mice, and the spleen (SPL) weight and number of cells per femur bone obtained from euthanized mice were assessed 4 weeks later. Tissue from uninjected *Rag1*^{−/−} mice was used as controls. **B** and **C**, Spleen (**B**) and bone marrow (BM) (**C**) cell suspensions isolated from the same mice were analyzed by flow cytometry for the percentage of different cell populations. Bottom panels summarize the flow cytometry data. Results are the mean ± SEM of 3–5 mice per group. * = $P < 0.05$; ** = $P < 0.01$; *** = $P < 0.001$; **** = $P < 0.0001$. See Figure 1 for other definitions.

heterozygote controls. By 4 weeks post–T cell transfer, only the DKO mouse T cell–injected mice, but not the mice injected with heterozygote mouse T cells, exhibited extramedullary hemato-poiesis, as demonstrated by the development of splenomegaly and an increased frequency of proerythrocytes as well as both EryA and EryB erythroblasts. In addition, mice injected with DKO mouse T cells showed an increased percentage of CD11b+ cells in the spleen, consistent with features of myeloid cell activation. This outcome could not be attributed to a failure of the hete-rozygote mouse T cells to engraft, since the mice injected with heterozygote mouse CD4+ T cells had a much higher percentage of T cells compared to the other groups (Figures 5A and B).

Furthermore, the DKO mouse CD4+ T cell recipients exhib-ited bone marrow hyperplasia, which was not seen in the het-erozygote mouse CD4+ T cell recipients. This was clearly evident in the findings indicating an overall reduced cellularity and fewer RBCs in DKO mouse CD4+ T cell recipients (Figure 5A; further details available from the corresponding author upon request). The bone marrow of the DKO mouse CD4+ T cell–injected mice also contained fewer Ter119+ cells, a reduced percentage of EryA and EryB erythroblasts within the Ter119 cell subset, and an increased percentage of CD11b+ cells (Figure 5C). Pro–B cell differentiation was also suppressed, as shown by the accumulation of B lineage cells in the AA4.1+B220^{negative} compartment.

Taken together, these data show that DKO mouse CD4+ T cells can induce developmental abnormalities in both the bone marrow and spleen of DNase II–sufficient mice, and that low num-bers of DKO mouse CD4+ T cells can disrupt the bone marrow niche responsible for development of erythroid lineage cells and B cells, in a manner independent of the production of cytokines by erythroid island macrophages (or any other cells) present in the bone marrow of DNase II–deficient mice.

Role of Unc93B1-dependent TLRs in the inflammatory response. Exactly how Unc93B1 contributes to the inflammatory response in DKO mice is not clear. TLR-9 has been proposed to play a T cell–intrinsic role in the generation of Treg cells (29), and it is very possible that the DKO phenotype reflects an absence of Treg cells in DKO mice that would normally limit the inflammatory response. However, 2 separate studies have found that TLR-9 cannot detect natural DNA ligands in DKO mice, presumably due to the fact that double-stranded DNA will not degrade into frag-ments that could be detectable by TLR-9 in DNase II–deficient mice (19,30).

TLR-7 has been shown to contribute to autoantibody pro-duction in numerous models of SLE. To assess the role of TLR-7 in DKO mice, we generated $Dnase2^{-/-} \times Ifnar^{-/-} \times Tlr7^{-/-}$ TKO mice. These TLR-7 TKO mice lost the ability to make the autoantibodies normally detected in DKO mouse serum, but they still developed splenomegaly and autoinflammation (Figure 6A).

To further explore the role of RNA-sensing TLRs, we also generated TLR-3 TKO mice. However, TLR-3 deficiency in these

mice had no effect on autoantibody production or the develop-ment of splenomegaly (Figure 6A).

A strong IFNγ signature in DKO mouse T cells. CD4+ T cells obtained from heterozygote, DKO, and Unc93B1 TKO mouse spleens were evaluated for gene expression using the Nanostring immune code set. The isolated cells were mainly CD4+ T cells, but also included 5% CD4+CD11c+ dendritic cells (more details available from the corresponding author upon request). Genes associated with the Th1 cell subset were uniquely up-regulated in the DKO mice. Examples include the transcription factor Tbet (Tbx21), the canonical IFNγ cytokine Th1 chemokine receptors CXCR3 and CCR5, Th1 chemok-ine receptor ligands CXCL9 and CXCL10, IL-12 cytokine and receptor subunits, and other genes known to be induced by IFNγ (Figure 6B).

The increased production of IFNγ by the DKO mouse CD4+ T cells was confirmed by cytoplasmic staining (results avail-able from the corresponding author upon request). CXCL9 and CXCL10 are produced by dendritic cells and not T cells, and most likely made by CD11c+CD4+ T cells, which are included in the magnetic bead purification of CD4+ T cells. A number of inflammatory chemokines (CCL3, CCL4, CCL5, CCL2, CCL8, CCL19), cytotoxic molecules (Ctsg, Gzmb, Camp), and comple-ment components were up-regulated 10–100-fold in DKO mice as compared to heterozygote mice. Additional highly up-regulated genes included the RAGE ligands S100A and S100B and several caspases, further pointing to a general state of inflammation. The majority of these genes were not up-regulated in the Unc93B1 TKO mice (the complete data set is available from the correspond-ing author upon request). These data further support an important role of Unc93B1, and therefore endosomal TLRs, in the inflamma-tory response in DKO mice.

No requirement for IFNγ signaling in the transfer of the DKO phenotype. To determine whether IFNγ is required for the development of the DKO phenotype, we intercrossed DKO mice with mice lacking an IFNγR. Splenomegaly was reduced and the frequency of Ter119+ cells in the spleen was lower in IFNγR TKO mice compared to DKO mice (Figure 6A). Furthermore, the percentage and activation status of splenic T cells in IFNγR TKO mice returned to the normal range, as reflected by the mean flu-orescence intensity of CD69+ cells (Figure 6C). In contrast, the bone marrow of IFNγR TKO mice was still disrupted. Thus, IFNγ is required for the generation of the effector Th1 cell subset in DKO mice, but not for DKO-associated bone marrow abnormalities. These bone marrow abnormalities in $Dnase2^{-/-}$ mice can occur in the absence of activated T cells.

The absence of IFNγ signaling did not impact the TLR-independent development of inflammatory arthritis. Clinical dis-ease scores of IFNγR TKO mice were comparable to those in age-matched DKO mice (results available from the corresponding
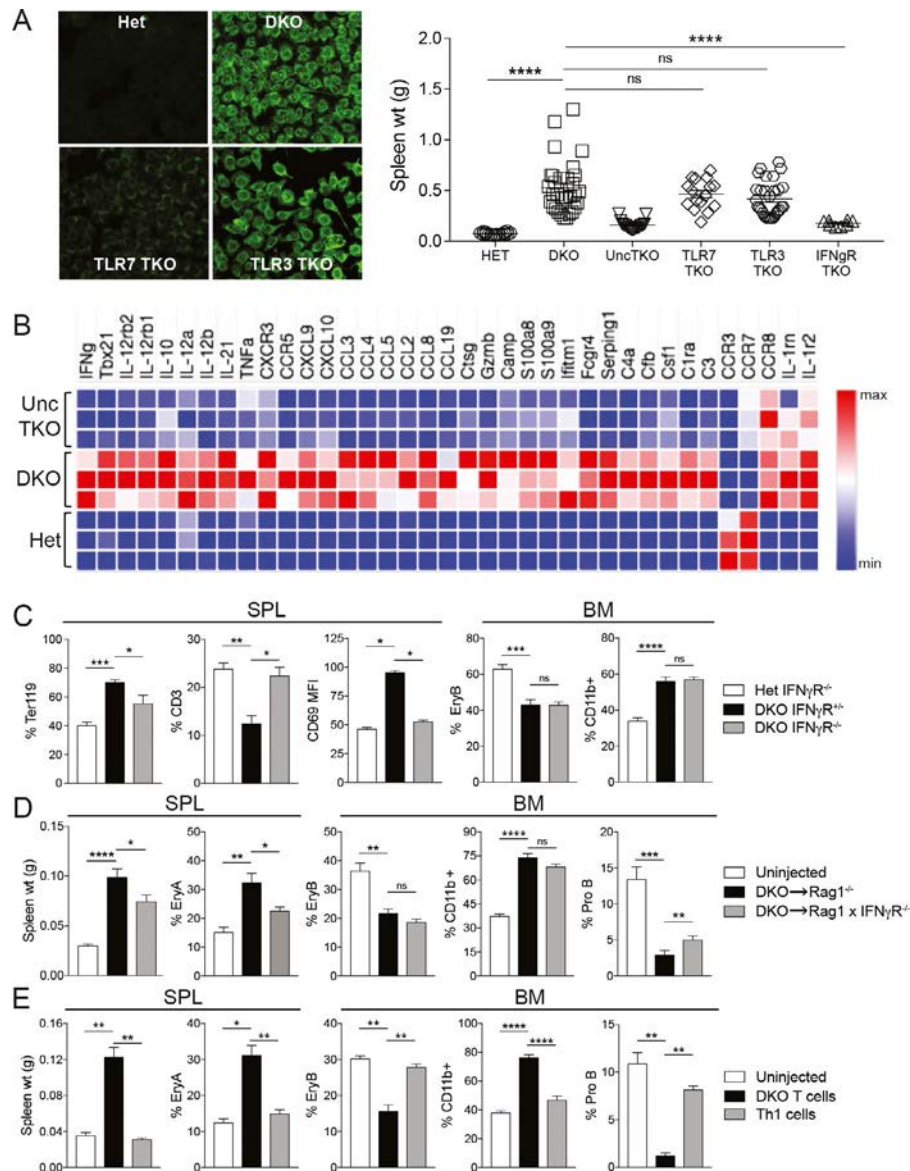
Figure 6. Role of Toll-like receptors and interferon-γ (IFNγ) in autoinflammation. **A**, Left, Immunofluorescence analyses were used to stain HEp-2 cells for antinuclear antibodies in the serum of 4–5-month-old mice of the indicated strains. Right, Spleen (SPL) weights were compared in 4–10-week-old mice of the indicated strains (n = 8–31 mice per group). Symbols represent individual mice; horizontal lines indicate the mean. **B**, RNA was extracted from bead-purified CD4+ T cells obtained from heterozygote, DKO, and Unc93B1 TKO mice, and gene expression levels were quantified using the Nanostring Immune Code Set. Morpheus software was used to generate heatmaps of Th1-related genes and additional genes that were up-regulated 10–100-fold in DKO mice compared to heterozygotes (n = 3 mice per group). **C**, Percentages of Ter119+, CD3+, EryB, and CD11b+ cells and mean fluorescence intensity (MFI) of CD69 expression in the spleens and bone marrow (BM) were compared in 5-week-old mice of the indicated strains (n = 3–10 mice per group). **D** and **E**, Spleen weight and percentages of EryA, EryB, CD11b+, and pro–B cells in the spleens and bone marrow were compared between uninjected *Rag1*^{-/-} mice and either *Rag1*^{-/-} or *Rag1*^{-/-} × *Ifngr*^{-/-} mice injected with DKO mouse spleen cells (n = 3–19 mice per group) (**D**) or either *Rag1*^{-/-} mice injected with DKO mouse T cells or *Rag1*^{-/-} × *Ifngr*^{-/-} mice injected with in vitro–generated Th1 cells (n = 3–17 mice per group) (**E**). Results in **C–E** are the mean ± SEM. * = P < 0.05; ** = P < 0.01; *** = P < 0.001; **** = P < 0.0001. See Figure 1 for other definitions. Color figure can be viewed in the online issue, which is available at http://onlinelibrary.wiley.com/doi/10.1002/art.41090/abstract.

author upon request), consistent with the development of inflammatory arthritis in *Rag2*^{-/-} TKO mice (16).

The next question to address was whether IFNγ or some other factor made by the DKO mouse T cells was responsible for the ability of adoptively transferred, activated DKO mouse CD4+ T cells to induce the DKO phenotype in *Rag1*^{-/-} mice. IFNγR is expressed

on most hematopoietic progenitors, including hematopoietic stem cells, multipotent progenitors, common myeloid progenitors, granulocyte-monocyte progenitors, megakaryocyte-erythroid progenitors, and common lymphoid progenitors, and IFNγ can have a direct stimulatory or inhibitory impact on hematopoiesis (31). To assess the role of IFNγR expression in the *Rag1*^{-/-} recipient

mice, we generated $Rag1^{-/-} \times Ifngr^{-/-}$ mice and injected these mice with DKO mouse spleen cells. The loss of IFNγR in recipient mice had only a modest impact on the ability of these mice to acquire the DKO phenotype (Figure 6D). Taken together, these data demonstrate that T cell production of IFNγ is required for the development/expansion of activated DKO mouse T cells and for the occurrence of splenomegaly, but cannot completely account for the capacity of DKO mouse T cells to elicit bone marrow–associated inflammation.

We also attempted to transfer the DKO phenotype into mice using Th1 cells that had been generated in vitro. These Th1 cells did not transfer the DKO phenotype, despite the successful engraftment of T cells producing copious amounts of IFNγ (Figure 6E). These findings suggest that DKO mouse CD4+ T cells have a function that is independent of IFNγ production in mediating the transfer of autoinflammation.

DISCUSSION

Autoinflammation due to DNase II deficiency falls in the category of type I interferonopathy as defined by increased expression of IFN-inducible genes, elevated serum IFNα titers, and increased phosphorylation of STAT1 and STAT3 (22). We show herein that in the DKO mouse model, many of the features of DNase II–deficient patients are recapitulated, including splenomegaly, lymphopenia, thrombocytopenia, anemia, elevated serum titers of non–IFN-induced inflammatory cytokines, and liver inflammation/fibrosis. Moreover, DNase II–deficient mice develop deforming arthropathies remarkably similar to that seen in patients with type I interferonopathies (15). Autoinflammation in these mice is independent of type I IFN and at least partially dependent on Unc93B1 expression. Therefore, autoinflammation in the DNase II–deficient patient population may be more dependent on type II IFN (or type III IFN) than type I IFN. Recent studies have shown that gene-targeted mice expressing gain-of-function mutations in STING also develop an inflammatory disease through type I IFN–independent mechanisms (32,33). These STING mutations were originally identified in children who developed an autoinflammatory syndrome referred to as STING-associated vasculitis of infancy (or SAVI). Thus, a better understanding of the interplay between aberrant activation of nucleic acid–sensing receptors and activation of the adaptive immune system is needed.

Results of the adoptive transfer studies in the current study reveal an unanticipated capacity of DKO mouse T cells to induce autoinflammation upon adoptive transfer into $Rag1^{-/-}$ mice. Although the percentage of splenic T cells was reduced in DKO mice, the persisting T cells were highly activated, as indicated by elevated levels of CD44 and CD69. Gene expression analysis of a spleen cell fraction, highly enriched for T cells, revealed a strong Th1/IFNγ signature, consistent with the high levels of IFNγ detected in the serum, both in the murine model and in patient popula-

tions. According to the Nanostring data, the DKO mouse CD4+ T cells also produced IL-21, and IFNγ/IL-21 double-producing CD4+ T cells have been shown to promote IL-12 production in the context of inflammation and infections (34,35). It is also possible that a distinct subset of IL-21–producing CD4+ T cells contributes to the activation of autoreactive B cells.

DKO mouse T cell activation depended on IFNγR, as IFNγR TKO mouse T cells did not up-regulate the expression of either CD69 or CD44, and splenomegaly and extramedullary hematopoiesis were dramatically reduced in the IFNγR TKO mice when compared to DKO mice. T cell transfer of DKO mouse CD4+ T cells, and not CD4+ T cells from heterozygotes, into naive $Dnase2^{+/+} \times Rag1^{-/-}$ recipients resulted in disrupted erythropoiesis and B cell development in the bone marrow, even though the recipient cells all expressed DNase II. Both recipient mice and the T cell donor mice were on a C57BL/6 background, and the DKO and heterozygote mouse T cell donors were littermates, and therefore the outcome was not likely to be attributable to a graft-versus-host response. Nevertheless, IFNγR TKO mice still developed bone marrow abnormalities despite the lack of activated T cells, suggesting that loss of DNase II in non–T cells contributed to the development of autoinflammation.

Limitations of this study include a minimal understanding of the conditions that drive the activation of CD4+ T cells in DKO mice and the mechanisms by which T cells induce autoinflammatory defects in B6 $Rag1^{-/-}$ mice. The absence of autoinflammation in Unc93B1 TKO mice, and the minimal impact of STING deficiency, implicates nucleic acid–sensing TLRs in these events. Since prior studies had shown that TLR-9–deficient cells could not respond to double-stranded DNA (19,30), we reasoned that the excessive accumulation of cell debris in DKO mice, as the result of an inability to degrade DNA, could provide a source of RNA that in turn engaged one of the RNA-sensing TLRs. This premise was consistent with our previous data showing that DKO mice produce autoantibodies that frequently stain HEp-2 cells with a nucleolar staining pattern (19). We found that TLR-7 deficiency in mice prevented autoantibody production but not other features of autoinflammation. Moreover, TLR-3 deficiency appeared to have no impact on either autoantibody production or autoinflammation. Therefore, we assume that the RNA-sensing TLRs are redundant, and that the combined deletion of TLR-3, TLR-7, and TLR-8 will be needed to ameliorate disease; so far, we have been unable to generate these conditions in mice. Alternatively, it will be necessary to re-explore the role of TLR-9 in the context of the DKO mouse model.

Importantly, endosomal TLRs have been shown to act synergistically in the induction of type III IFN expression, particularly in dendritic cell subsets and epithelial cells (36–38). Therefore, IL-28 activity may account for DKO mouse dendritic cell production of IFN-induced chemokines (as shown in Figure 6B). Type III IFNs have been further linked to chemokine production and renal injury in SLE patient populations (39,40). In renal sections

obtained from patients with severe lupus nephritis, the presence of IFNλ was associated with crescent formation, thereby connecting type III IFN production with fibrosis (40). Type III IFNs are also produced by liver cells, and in vivo administration of IFNλ specifically reduced the viral load in a murine model of herpes simplex virus 2 infection (41). Whether type III IFN contributes to the liver fibrosis exhibited by DKO mice is a question that warrants further study and could be addressed in DKO mice that fail to express the type III IFN receptor.

Overall, we believe that the current data are consistent with the concept of a biphasic disease process in which DNase II deficiency initially leads to excessive accumulation of cell debris and the subsequent Unc93B1-dependent activation of antigen-presenting cells that, in turn, induce the IFNγ-dependent development of an unusual Th1 cell subset. Once these T cells develop, they have the capacity to promote autoantibody production and to mediate tissue damage. They can also independently maintain an "autoinflammatory state" and induce inflammation in *DNase2*-sufficient mice (further details available from the corresponding author upon request). If validated, this framework could have important implications for the treatment of patients with autoinflammatory conditions, in that it will be important to block both the initiating innate stimuli that lead to T cell activation and the T cells that can then independently promote hematopoietic and immune cell abnormalities.

AUTHOR CONTRIBUTIONS

All authors were involved in drafting the article or revising it critically for important intellectual content, and all authors approved the final version to be published. Dr. Marshak-Rothstein had full access to all of the data in the study and takes responsibility for the integrity of the data and the accuracy of the data analysis.
Study conception and design. Pawaria, Nündel, Gao, Brehm, Socolovsky, Marshak-Rothstein.
Acquisition of data. Pawaria, Nündel, Gao, Moses, Busto, Holt, Sharma, Brehm, Gravallese, Socolovsky, Christ, Marshak-Rothstein.
Analysis and interpretation of data. Pawaria, Nündel, Gao, Gravallese, Socolovsky, Marshak-Rothstein.

REFERENCES

1. Nagata S, Hanayama R, Kawane K. Autoimmunity and the clearance of dead cells [review]. Cell 2010;140:619–30.

2. Elliott MR, Ravichandran KS. Clearance of apoptotic cells: implications in health and disease. J Cell Biol 2010;189:1059–70.

3. Mahajan A, Herrmann M, Muñoz LE. Clearance deficiency and cell death pathways: a model for the pathogenesis of SLE [review]. Front Immunol 2016;7:35.

4. Al-Mayouf SM, Sunker A, Abdwani R, Abrawi SA, Almurshedi F, Al-hashmi N, et al. Loss-of-function variant in DNASE1L3 causes a familial form of systemic lupus erythematosus. Nat Genet 2011;43:1186–8.

5. Sisirak V, Ganguly D, Lewis KL, Couillault C, Tanaka L, Bolland S, et al. Genetic evidence for the role of plasmacytoid dendritic cells in systemic lupus erythematosus. J Exp Med 2014;211:1969–76.

6. Crow YJ, Hayward BE, Parmar R, Robins P, Leitch A, Ali M, et al. Mutations in the gene encoding the 3'-5' DNA exonuclease TREX1 cause Aicardi-Goutières syndrome at the AGS1 locus. Nat Genet 2006;38:917–20.

7. Stetson DB, Ko JS, Heidmann T, Medzhitov R. Trex1 prevents cell-intrinsic initiation of autoimmunity. Cell 2008;134:587–98.

8. Yoshida H, Okabe Y, Kawane K, Fukuyama H, Nagata S. Lethal anemia caused by interferon-β produced in mouse embryos carrying undigested DNA. Nat Immunol 2005;6:49–56.

9. Ahn J, Gutman D, Saijo S, Barber GN. STING manifests self DNA-dependent inflammatory disease. Proc Natl Acad Sci U S A 2012; 109:19386–91.

10. Gao D, Li T, Li XD, Chen X, Li QZ, Wight-Carter M, et al. Activation of cyclic GMP-AMP synthase by self-DNA causes autoimmune diseases. Proc Natl Acad Sci U S A 2015;112:E5699–705.

11. Okabe Y, Kawane K, Akira S, Taniguchi T, Nagata S. Toll-like receptor-independent gene induction program activated by mammalian DNA escaped from apoptotic DNA degradation. J Exp Med 2005;202:1333–9.

12. Terman A, Kurz T, Gustafsson B, Brunk UT. Lysosomal labilization. IUBMB Life 2006;58:531–9.

13. Lan YY, Londoño D, Bouley R, Rooney MS, Hacohen N. Dnase2a deficiency uncovers lysosomal clearance of damaged nuclear DNA via autophagy. Cell Rep 2014;9:180–92.

14. Ahn J, Ruiz P, Barber GN. Intrinsic self-DNA triggers inflammatory disease dependent on STING. J Immunol 2014;193:4634–42.

15. Kawane K, Ohtani M, Miwa K, Kizawa T, Kanbara Y, Yoshioka Y, et al. Chronic polyarthritis caused by mammalian DNA that escapes from degradation in macrophages. Nature 2006;443:998–1002.

16. Kawane K, Tanaka H, Kitahara Y, Shimaoka S, Nagata S. Cytokine-dependent but acquired immunity-independent arthritis caused by DNA escaped from degradation. Proc Natl Acad Sci U S A 2010;107:19432–7.

17. Baum R, Sharma S, Carpenter S, Li QZ, Busto P, Fitzgerald KA, et al. Cutting edge: AIM2 and endosomal TLRs differentially regulate arthritis and autoantibody production in DNase II-deficient mice. J Immunol 2015;194:873–7.

18. Jakobs C, Perner S, Hornung V. AIM2 drives joint inflammation in a self-DNA triggered model of chronic polyarthritis. PLoS One 2015;10:e0131702.

19. Pawaria S, Moody K, Busto P, Nündel K, Choi CH, Ghayur T, et al. Cutting edge: DNase II deficiency prevents activation of autoreactive B cells by double-stranded DNA endogenous ligands. J Immunol 2015;194:1403–7.

20. Baum R, Nündel K, Pawaria S, Sharma S, Busto P, Fitzgerald KA, et al. Synergy between hematopoietic and radioresistant stromal cells is required for autoimmune manifestations of DNase II–/– IFNaR–/– mice. J Immunol 2016;196:1348–54.

21. Brinkmann MM, Spooner E, Hoebe K, Beutler B, Ploegh HL, Kim YM. The interaction between the ER membrane protein UNC93B and TLR3, 7, and 9 is crucial for TLR signaling. J Cell Biol 2007;177: 265–75.

22. Rodero MP, Tesser A, Bartok E, Rice GI, Della Mina E, Depp M, et al. Type I interferon-mediated autoinflammation due to DNase II deficiency. Nat Commun 2017;8:2176.

23. Mande P, Zirak B, Ko WC, Taravati K, Bride KL, Brodeur TY, et al. Fas ligand promotes an inducible TLR-dependent model of cutaneous lupus-like inflammation. J Clin Invest 2018;128:2966–78.

24. Aryee KE, Shultz LD, Brehm MA. Immunodeficient mouse model for human hematopoietic stem cell engraftment and immune system development. Methods Mol Biol 2014;1185:267–78.

25. Pawaria S, Ramani K, Maers K, Liu Y, Kane LP, Levesque MC, et al. Complement component C5a permits the coexistence of pathogenic Th17 cells and type I IFN in lupus. J Immunol 2014;193: 3288–95.

26. Liu Y, Pop R, Sadegh C, Brugnara C, Haase VH, Socolovsky M. Suppression of Fas-FasL coexpression by erythropoietin mediates erythroblast expansion during the erythropoietic stress response in vivo. Blood 2006;108:123–33.

27. Pestka S, Krause CD, Sarkar D, Walter MR, Shi Y, Fisher PB. Interleukin-10 and related cytokines and receptors. Annu Rev Immunol 2004;22:929–79.

28. Miller JP, Izon D, DeMuth W, Gerstein R, Bhandoola A, Allman D. The earliest step in B lineage differentiation from common lymphoid progenitors is critically dependent upon interleukin 7. J Exp Med 2002;196:705–11.

29. Alikhan MA, Summers SA, Gan PY, Chan AJ, Khouri MB, Ooi JD, et al. Endogenous Toll-like receptor 9 regulates AKI by promoting regulatory T cell recruitment. J Am Soc Nephrol 2016;27:706–14.

30. Chan MP, Onji M, Fukui R, Kawane K, Shibata T, Saitoh S, et al. DNase II-dependent DNA digestion is required for DNA sensing by TLR9. Nat Commun 2015;6:5853.

31. De Bruin AM, Voermans C, Nolte MA. Impact of interferon-γ on hematopoiesis. Blood 2014;124:2479–86.

32. Bouis D, Kirstetter P, Arbogast F, Lamon D, Delgado V, Jung S, et al. Severe combined immunodeficiency in stimulator of interferon genes (STING) V154M/wild-type mice. J Allergy Clin Immunol 2019;143:712–25.

33. Motwani M, Pawaria S, Bernier J, Moses S, Henry K, Fang T, et al. Hierarchy of clinical manifestations in SAVI N153S and V154M mouse models. Proc Natl Acad Sci U S A 2019;116:7941–50.

34. Xiao L, Jia L, Zhang Y, Yu S, Wu X, Yang B, et al. Human IL-21+IFN-γ+CD4+ T cells in nasal polyps are regulated by IL-12. Sci Rep 2015;5:12781.

35. Li L, Jiang Y, Lao S, Yang B, Yu S, Zhang Y, et al. Mycobacterium tuberculosis-specific IL-21+IFN-γ+CD4+ T cells are regulated by IL-12. PLoS One 2016;11:e0147356.

36. Mäkelä SM, Österlund P, Julkunen I. TLR ligands induce synergistic interferon-β and interferon-λ1 gene expression in human monocyte-derived dendritic cells. Mol Immunol 2011;48:505–15.

37. Coccia EM, Severa M, Giacomini E, Monneron D, Remoli ME, Julkunen I, et al. Viral infection and Toll-like receptor agonists induce a differential expression of type I and λ interferons in human plasmacytoid and monocyte-derived dendritic cells. Eur J Immunol 2004;34:796–805.

38. Ank N, Iversen MB, Bartholdy C, Staeheli P, Hartmann R, Jensen UB, et al. An important role for type III interferon (IFN-λ/IL-28) in TLR-induced antiviral activity. J Immunol 2008;180:2474–85.

39. Wu Q, Yang Q, Lourenco E, Sun H, Zhang Y. Interferon-λ1 induces peripheral blood mononuclear cell-derived chemokines secretion in patients with systemic lupus erythematosus: its correlation with disease activity. Arthritis Res Ther 2011;13:R88.

40. Zickert A, Oke V, Parodis I, Svenungsson E, Sundström Y, Gunnarsson I. Interferon (IFN)-λ is a potential mediator in lupus nephritis. Lupus Sci Med 2016;3:e000170.

41. Ank N, West H, Bartholdy C, Eriksson K, Thomsen AR, Paludan SR. λ interferon (IFN-λ), a type III IFN, is induced by viruses and IFNs and displays potent antiviral activity against select virus infections in vivo. J Virol 2006;80:4501–9.

AMERICAN COLLEGE
of RHEUMATOLOGY
Empowering Rheumatology Professionals

LETTERS

Unresolved questions on the relationship between EZH2 and lupus: comment on the article by Rohraff et al

To the Editor:

Systemic lupus erythematosus (SLE) is a systemic autoimmune disorder characterized by a range of manifestations, such as kidney, bone, and skin damage and impairment of immune system regulation. Cumulative evidence has shown that both genetic and environmental factors lead to an imbalance in autoimmunity, which contributes to SLE pathogenesis (1).

EZH2 is a catalytic subunit of polycomb repressive complex 2 and can catalyze trimethylation of histone H3 at lysine 27 to silence its target genes (2). EZH2 has been demonstrated to play a critical role in T cell response as well as in the function of dendritic cells and macrophages. We read with great interest the recent report by Rohraff et al (3), describing a study in which they showed that EZH2 expression was elevated in neutrophils, monocytes, B cells, and CD4+ T cells from SLE patients compared to those from controls. Interestingly, suppression of EZH2 improved survival of lupus-prone mice and down-regulated generation of anti–double-stranded DNA (anti-dsDNA) antibody production in these mice. Inhibition of EZH2 reduced splenomegaly, lymphadenopathy, and lymphoproliferation and decreased production of inflammatory cytokines such as tumor necrosis factor (TNF) and interleukin-10 (IL-10) (3). Rohraff and colleagues' findings suggest that EZH2 is increased in SLE patients and that targeting EZH2 has potential as a therapeutic option in SLE.

However, based on current findings about EZH2 in patients with lupus, this notion is considered too preliminary, and several questions still need to be discussed. Tsou et al reported that EZH2 levels were up-regulated in CD4+ T cells in SLE patients compared to those in healthy volunteers (4), and that overexpression of EZH2 in CD4+ T cells led to DNA methylation changes and promoted CD4+ T cell adhesion, whereas blocking of EZH2 down-regulated the capacity of CD4+ T cells to adhere to endothelial cells in lupus patients (4). In contrast, Hu and colleagues observed that levels of EZH2 were significantly decreased in CD4+ T cells in patients with active lupus compared to patients with inactive lupus and healthy controls (5). The relationship between EZH2 and lupus is unclear, and questions remain on whether EZH2 expression is increased in lupus (and if so, if this contributes to lupus development), or, conversely, if EZH2 expression is reduced in lupus and negatively related to disease pathogenesis. Whether EZH2 can be used as a disease marker for lupus is also still unresolved. Though

Rohraff et al demonstrated that inhibition of EZH2 led to reduced expression of TNF and IL-10, both the interaction between EZH2 and TNF/IL-10 and the manner in which EZH2 expression results in down-regulation of these inflammatory cytokines remain unclear. Further, it is also not yet known whether there is any signaling pathway via which EZH2 regulates these cytokines, therefore inhibiting lupus development. These questions also require clarification in future studies.

Wang-Dong Xu, MD
Department of Evidence-Based Medicine
Southwest Medical University
An-Fang Huang, MD iD
Department of Rheumatology and Immunology
Affiliated Hospital of Southwest Medical University
Sichuan, China

1. Xu WD, Fu L, Liu XY, Wang JM, Yuan ZC, Su LC, et al. Association between TL1A gene polymorphisms and systemic lupus erythematosus in a Chinese Han population. J Cell Physiol 2019;234:22543–53.
2. Emran AA, Chatterjee A, Rodger EJ, Tiffen JC, Gallagher SJ, Eccles MR, et al. Targeting DNA methylation and EZH2 activity to overcome melanoma resistance to immunotherapy. Trends Immunol 2019;40:328–44.
3. Rohraff DM, He Y, Farkash EA, Schonfeld M, Tsou PS, Sawalha AH. Inhibition of EZH2 ameliorates lupus-like disease in MRL/lpr mice. Arthritis Rheumatol 2019;71:1681–90.
4. Tsou PS, Coit P, Kilian NC, Sawalha AH. EZH2 modulates the DNA methylome and controls T cell adhesion through junctional adhesion molecule A in lupus patients. Arthritis Rheumatol 2018;70:98–108.
5. Hu N, Qiu X, Luo Y, Yuan J, Li Y, Lei W, et al. Abnormal histone modification patterns in lupus CD4+ T cells. J Rheumatol 2008;35:804–10.

EZH2 inhibition in B cell subsets: comment on the article by Rohraff et al

To the Editor:

Rohraff and colleagues' study demonstrates the value of targeting EZH2 using the inhibitor 3′-deazaneplanocin (DZNep) in systemic lupus erythematosus (SLE) and assessing its effects on the prevention and treatment of SLE in a preclinical model (Rohraff DM, He Y, Farkash EA, Schonfeld M, Tsou PS, Sawalha AH. Inhibition of EZH2 ameliorates lupus-like disease in MRL/*lpr* mice. Arthritis Rheumatol 2019;71;1681–90). The modulation of
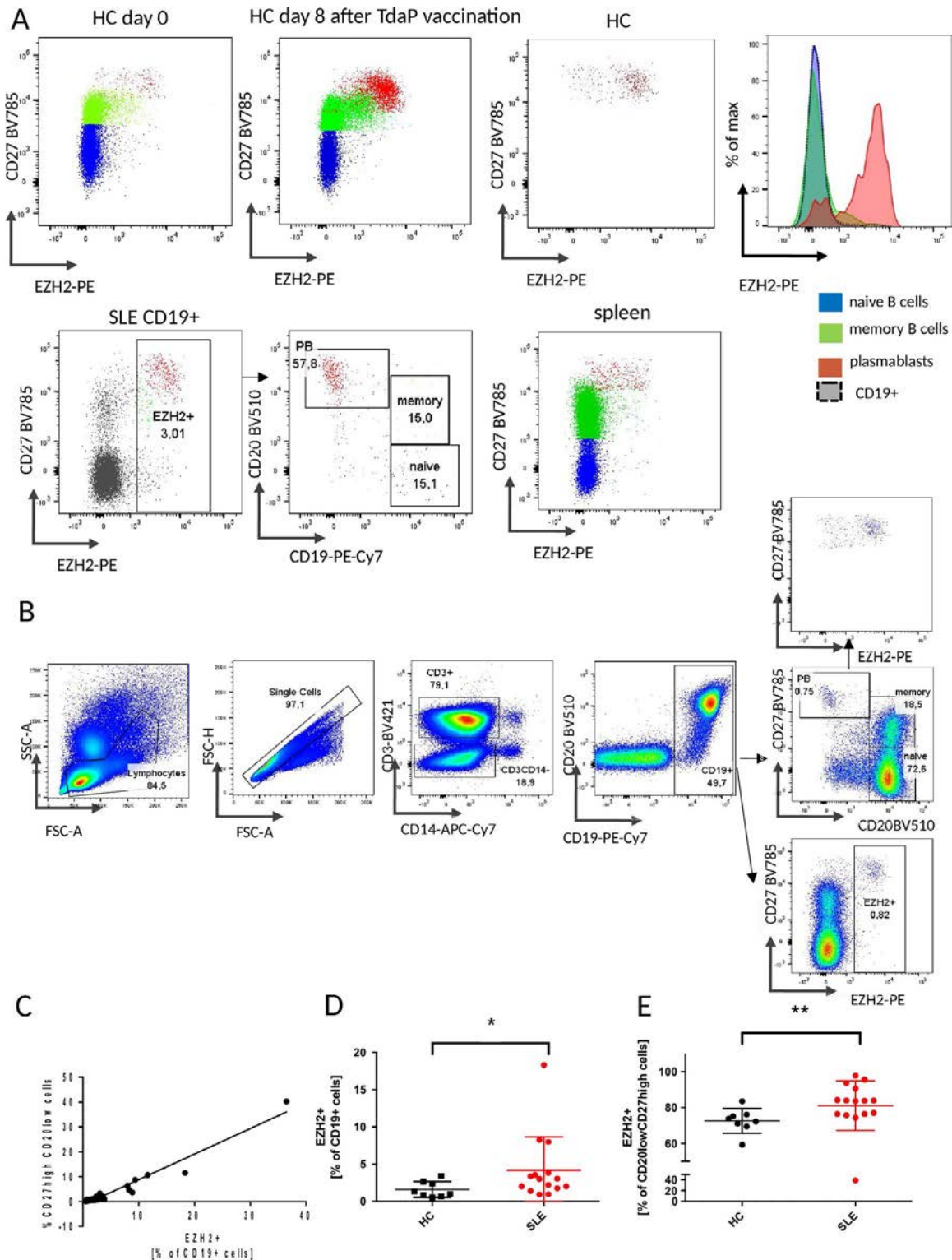
Figure 1. A, Dot plots and histogram of naive B cells (CD20+CD27−), memory B cells (CD20+CD27+), and plasmablasts (CD27highCD20low) in peripheral blood (PB) mononuclear cells from healthy controls (HCs), patients with systemic lupus erythematosus (SLE), and a healthy control after receiving the Tdap vaccine against tetanus, diphtheria, and pertussis, and in the spleen. PE = phycoerythrin. **B**, Gating strategy. APC = allophycocyanin. **C**, Correlation plot of plasmablasts with frequencies of CD19+EZH2+ cells ($r^2 = 0.96$, $P < 0.001$). **D** and **E**, Frequencies of CD19+EZH2+ cells (**D**) and CD27highCD20lowEZH2+ cells (**E**) in 8 healthy controls and 15 SLE patients. Each symbol represents an individual subject; bars show the mean ± SEM. * = $P < 0.05$; ** = $P < 0.01$.

epigenetic changes is of interest. They found EZH2 to be significantly up-regulated in monocytes, neutrophils, and CD19+ B cells from lupus patients, whereas in studies at our laboratory, EZH2 levels were increased almost exclusively in plasmablasts, but not in memory and naive B cells. As such, plasmablasts require particular consideration with regard to their elevated EZH2 expression. Moreover, CD19+ cells carry both EZH2-positive and EZH2-negative populations, which makes the use of mean fluorescence intensity (MFI) as experimental measure inferior to the use of frequency. This also applies to plasmablasts containing EZH2-positive and EZH2-negative fractions (Figure 1A). In our experience, EZH2+ cells from SLE patients are mainly plasmablasts (Figure 1B). Also, after receipt of the Tdap vaccine to protect against tetanus, diphtheria, and pertussis, the frequency of EZH2+ cells increases, and they consist of mainly plasmablasts (Figure 1A). This observation applies not only to peripheral blood, but also to tissue-resident cells in the spleen (Figures 1A and B).

Notably, the relationship between the frequency of peripheral plasmablasts and the frequency of CD19+EZH2+ cells was significant (r^2 = 0.96), whereas the relationship between CD19+EZH2+ cells and MFI was not. In our data set consisting of 15 lupus patients and 8 healthy controls, the frequencies of CD19+EZH2+ cells and CD27^{high}CD20^{low}EZH2+ cells demonstrated the most pronounced differences between SLE patients and healthy controls (Figures 1D and E).

These data indicate that an increase of EZH2 in B-lineage cells can be largely attributed to plasmablasts and appears to be independent of the underlying disease, including known disturbances of peripheral B cell homeostasis in SLE (Jacobi AM, Mei H, Hoyer BF, Mumtaz IM, Thiele K, Radbruch A, et al. HLA-DR^{high}CD27^{high} plasmablasts indicate active disease in patients with systemic lupus erythematosus. Ann Rheum Dis 2010;69:305–8). Thus, if overexpression of EZH2 in B-lineage cells is involved, it seems to be likely related to an elevated plasmablast population. Alternatively, the observed effects on EZH2 inhibition in the MRL/lpr lupus mouse model described by Rohraff et al might have an impact on T cell–, monocyte-, or neutrophil-mediated effects, while methotrexate treatment would potentially be useful in assessing the effects of EZH2.

Eva Schrezenmeier, MD [iD]
Charité Universitätsmedizin Berlin
  and Berlin Institute of Health
Andreia C. Lino, PhD [iD]
Deutsches Rheumaforschungszentrum Berlin
Tobias Alexander, MD
Thomas Dörner, MD
Deutsches Rheumaforschungszentrum Berlin
  and Charité Universitätsmedizin Berlin
Berlin, Germany

Reply

To the Editor:

I thank Dr. Xu et al for their interest in my group's work examining the role of EZH2 in lupus. We have previously reported changes in T cell DNA methylation patterns that are associated with increased disease activity in lupus patients and have identified a possible role of EZH2 in the induction of these proinflammatory epigenetic changes (1,2). We followed these findings with mechanistic investigations in vitro that resulted in the identification of junctional adhesion molecule A as a novel important target gene that is dysregulated by EZH2 in lupus T cells (3). Subsequently, in the study currently being commented on, we demonstrated a robust effect of an EZH2 inhibitor in improving survival and abrogating lupus-like disease in MRL/lpr mice. We have observed overexpression of EZH2 in lupus CD4+ T cells compared to cells from healthy matched controls at both the messenger RNA and protein levels (3). Furthermore, the level of H3K27me3 (which is catalyzed by the enzymatic activity of EZH2) was increased in lupus CD4+ T cells compared to control cells, and 2 microRNAs (miRNAs) that regulate EZH2 in T cells (miR-101 and miR-26a) were both down-regulated in lupus CD4+ T cells (3). Increased CD4+ T cell expression of EZH2 in lupus was also supported by analysis of publicly available gene expression data described in the current study. Therefore, our in vitro and complementary in vivo investigations demonstrate a role of increased EZH2 expression in lupus pathogenesis.

Although previous findings by Ding and colleagues have suggested reduced EZH2 expression in lupus CD4+ T cells (4), more recent work from the same group demonstrated a pathogenic role of EZH2 in lupus via the induction of H3K27me3 and suppression of miR-142–3p/5p, which results in T cell activation and B cell hyperstimulation in lupus patients (5,6). The rationale for using a systemic EZH2 inhibitor approach in our in vivo studies was to facilitate and prioritize possible repurposing of EZH2 inhibitors that are currently being used in clinical trials to treat cancer, for use in lupus patients. Indeed, the data we obtained suggest that increased EZH2 expression and activity is pathogenic and that a clinical trial for EZH2 inhibition in lupus patients is warranted. As we discussed in our current report, systemic inhibition of EZH2 in vivo does not allow for detailed mechanistic characterization of the therapeutic effects observed. Therefore, we suggested that careful mechanistic and functional studies are warranted to understand the effect of EZH2 inhibition in vivo on specific cell subsets. For example, cell-specific EZH2 deletion using genetic approaches in lupus-prone mice would be a reasonable next step for study.

I also thank Dr. Schrezenmeier and colleagues for their follow-up on our work investigating EZH2 in lupus. Further
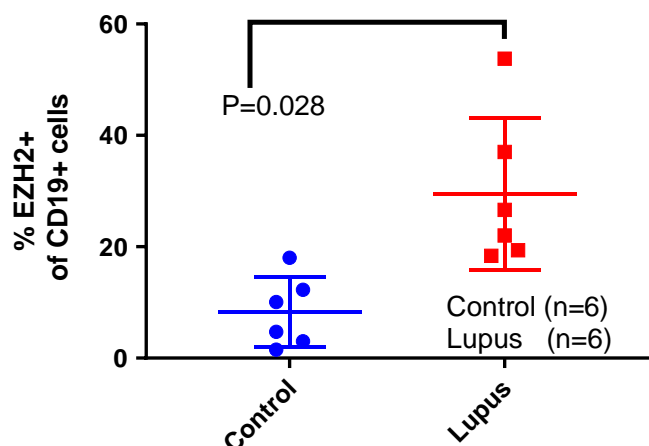
Figure 1. Percentage of EZH2+ cells in CD19+ cells in the peripheral blood of patients with lupus compared to age-, sex-, and race-matched healthy controls. Each symbol represents an individual subject; bars show the mean ± SD.

study examining expression patterns of EZH2 in different immune cell subpopulations is certainly of interest, as we noted above. However, we are puzzled by Schrezenmeier and colleagues' comment that their findings on the expression of EZH2 by B-lineage cells are not consistent with our report of EZH2 being significantly up-regulated in monocytes, neutrophils, and CD19+ B cells in lupus patients. They show no data on monocytes or neutrophils and do indeed show data that suggest a higher frequency of CD19+EZH2+ cells in lupus patients compared to healthy controls (Figure 1D in their letter), which contradicts their statement and is consistent with our published data. We used MFI to estimate levels of EZH2 expression in different cell types, and examination of the percentage of EZH2+CD19+ cells revealed consistent results in our data set (Figure 1).

Amr H. Sawalha, MD iD
Children's Hospital of Pittsburgh
University of Pittsburgh School of Medicine
and Lupus Center of Excellence
Pittsburgh, PA

1. Coit P, Dozmorov MG, Merrill JT, McCune WJ, Maksimowicz-McKinnon K, Wren JD, et al. Epigenetic reprogramming in naive CD4+ T cells favoring T cell activation and non-Th1 effector T cell immune response as an early event in lupus flares. Arthritis Rheumatol 2016;68:2200–9.
2. Weeding E, Sawalha AH. Deoxyribonucleic acid methylation in systemic lupus erythematosus: implications for future clinical practice [review]. Front Immunol 2018;9:875.
3. Tsou PS, Coit P, Kilian NC, Sawalha AH. EZH2 modulates the DNA methylome and controls T cell adhesion through junctional adhesion molecule A in lupus patients. Arthritis Rheumatol 2018;70:98–108.
4. Ding S, Liang Y, Zhao M, Liang G, Long H, Zhao S, et al. Decreased microRNA-142-3p/5p expression causes CD4+ T cell activation and B cell hyperstimulation in systemic lupus erythematosus. Arthritis Rheum 2012;64:2953–63.
5. Ding S, Zhang Q, Luo S, Gao L, Huang J, Lu J, et al. BCL-6 suppresses miR-142-3p/5p expression in SLE CD4+ T cells by modulating histone methylation and acetylation of the miR-142 promoter [editorial]. Cell Mol Immunol 2019. E-pub ahead of print.
6. Sawalha AH. BCL-6 and EZH2 cooperate to epigenetically repress anti-inflammatory miR-142-3p/5p in lupus CD4+T cells [editorial]. Cell Mol Immunol 2019. E-pub ahead of print.

Reactivity of IgG with the p40 protein encoded by the long interspersed nuclear element 1 retroelement: comment on the article by Carter et al

To the Editor:

The nature and specificity of self antigens targeted by autoantibodies, which is characteristic of systemic autoimmune diseases, can suggest clues to mechanisms initiating disease. In systemic lupus erythematosus (SLE), anti–double-stranded DNA (anti-dsDNA) autoantibodies are features of active disease and are particularly associated with lupus nephritis, and the identity of the self or foreign antigens that "break tolerance" (leading to anti-dsDNA and other autoantibody specificities) has been a topic of extensive study. In that context, the study described by Carter et al (1), in which they identified reactivity of sera from SLE patients using the 40-kd protein product of the first open-reading frame (ORF) of the human long interspersed nuclear element 1 (LINE-1) retroelement, is of great interest.

Carter and colleagues studied the reactivity of sera from SLE patients, disease control patients with systemic sclerosis, and healthy donors with purified LINE-1 p40 using both immunoblotting and enzyme-linked immunosorbent assay (ELISA) techniques. Several striking observations were noted. Sera from both SLE patients and from healthy donors reacted with p40 by immunoblotting. Several patient and control samples were then tested by ELISA using the same purified p40 protein as antigen. The ELISA data largely supported the immunoblotting results, with sera from SLE patients showing significantly higher levels of IgG reactive with LINE-1 p40 compared to sera from healthy donors.

Data generated by investigators at my laboratory support the results reported by Carter et al (Crow MK, et al: unpublished observations). A His-tagged, LINE-1, ORF-1 p40 protein was expressed, purified, and used in immunoblot and ELISA studies. The immunoblot in Figure 1A demonstrates analysis of sera from 7 healthy donors and 7 SLE patients. Six of the 7 SLE sera showed bands (some of which were strong) corresponding to 42 kd, which has been demonstrated in previous studies to identify our p40 fusion protein (2). Surprisingly, all sera from healthy donors also reacted with the electrophoresed p40 protein, although in most cases the bands were less strong than those identified in SLE sera. We developed an antigen-antibody capture ELISA using the recombinant LINE-1 p40 protein. Like the results reported by

Carter and colleagues, we found significantly higher expression of IgG reactive with LINE-1 p40 in sera from SLE patients than in sera from healthy donors (Figure 1B). Together, these immunoblot and ELISA results are highly similar to those described by Carter et al, showing reactivity of SLE and healthy donor sera with purified LINE-1 p40 protein by immunoblotting as well as significantly higher levels of IgG anti-p40 in SLE patient sera compared to healthy donor sera.

What is particularly striking in the study by Carter and colleagues, and not addressed in our experiments, is the relationship between the presence of anti-p40 antibodies in patient sera and clinical and serologic features of active disease. High levels of anti-p40 were associated with higher Systemic Lupus Erythematosus Disease Activity Index scores (3) and lupus nephritis. The most notable observation was the highly significant association of p40 level with the presence of anti-DNA antibodies as well as anti-C1q autoantibodies and low C3 levels. These significant associations raise the question of whether detected anti-p40 reactivity in fact reflects reactivity with DNA. Our group has demonstrated that both RNA and DNA are associated with RNP particles containing LINE-1 p40 and that the p40 protein is released from the particles following a 30-minute incubation with RNase or DNase (Crow MK, et al: unpublished observations). Detailed analyses by others have demonstrated that the LINE-1 p40 monomer forms a coiled-coil–mediated trimer that binds DNA nonspecifically with high affinity (4). Carter et al considered the potential for IgG to bind DNA in their test sera and supported the specificity of SLE IgG for LINE-1 p40 by inhibiting reactivity in their ELISA with a 10-fold excess of

soluble p40 (we noted a similar result with the same approach). They also included DNase in the ELISA procedure without reducing the level of IgG reactivity. However, the DNase was added to the adsorbed p40 at the same time as patient serum.

Further investigation of the contribution of DNA to the p40 reactivity is needed in order to fully interpret the presented results. As noted by Carter and colleagues, anti-DNA antibodies are frequently detected in sera from healthy donors, which again raises the possibility that DNA reactivity could be contributing to the reactivity of IgG from healthy donors and SLE patients with LINE-1 p40 in the studies performed by Carter et al and those at our laboratory.

The potential for genomic retroelements to contribute to the induction or amplification of systemic autoimmune disease has been raised by many investigators. Those elements, with sequence and genomic structure similar to retroviruses, are abundant in our genome. LINE-1 is of particular interest in SLE (5), with a number of "active" transposable LINE-1s in the human genome. LINE-1 transcription and translation are usually rigorously controlled through genome methylation and mechanisms implemented by members of the apolipoprotein B messenger RNA–editing enzyme catalytic polypeptide family, endogenous nucleases, and other enzymes that edit potentially stimulatory nucleic acids, yet our previous studies demonstrated that LINE-1 RNA transcripts and LINE-1 p40 protein can be expressed in the involved renal and salivary gland tissue of patients with SLE or Sjögren's syndrome, respectively (2). In addition, LINE-1 nucleic acid can induce
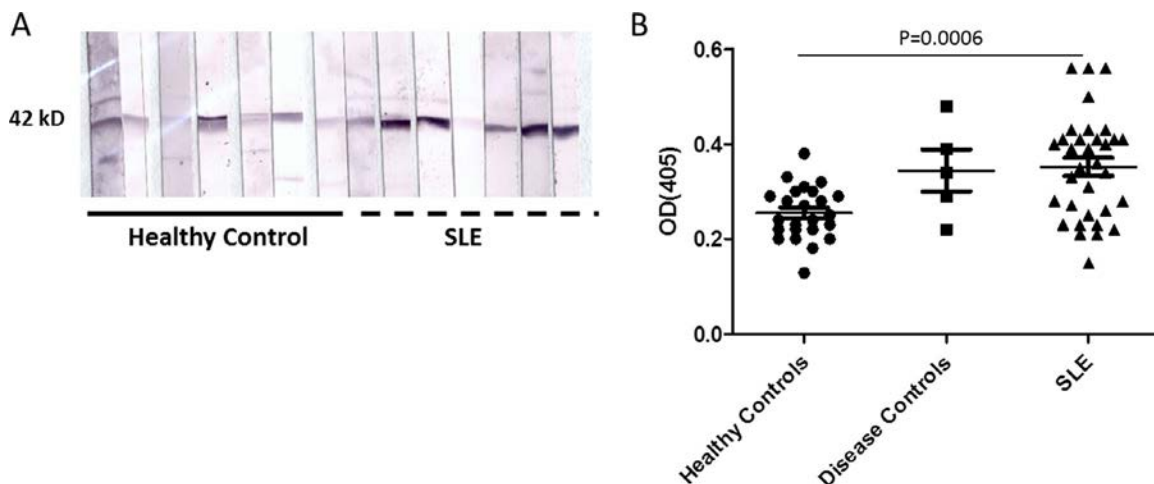

Figure 1. Reactivity of systemic lupus erythematosus (SLE) and healthy donor IgG with long interspersed nuclear element 1 (LINE-1) p40 fusion protein. A human LINE-1 open-reading frame 1 sequence subcloned from the embryonal carcinoma NTERA-2 clone D1 cell line was cloned into a pQE-30 expression vector. *Escherichia coli* bacteria were transformed, and p40 protein expressed and purified with a histidine tag. **A**, In an immunoblot assay, p40 fusion protein (700 ng/ml per lane) was electrophoresed and transferred to PVDF membranes, cut into strips, immunoblotted with 1:100 sera from SLE patients or healthy donors, and developed with anti-human IgG. **B**, Microwells were coated with 500 ng/well LINE-1 p40 fusion protein, blocked with 5% milk, and incubated overnight with a 1:50 dilution of SLE or healthy donor sera. In addition, 5 samples from patients with other autoimmune rheumatic diseases (3 with polymyositis, 1 with Sjögren's syndrome, and 1 with psoriatic arthritis) were assayed. After washing, alkaline phosphatase–labeled goat anti-human IgG was added, and the color reaction measured at 405 nm absorbance. Each symbol represents an individual subject; bars show the mean ± SD.

type I interferon (IFN), a key pathogenic mediator in SLE (2). In that regard, the data from Carter and colleagues' study support the notion of a relationship between high levels of IgG anti-p40 and a high type I IFN score (1). The RNP particles that contain LINE-1 p40, associated LINE-1 RNA, and DNA, as well as a multitude of proteins that have been implicated as autoantigens in systemic autoimmune diseases (6), should be priority targets for detailed study of the mechanisms through which the viral remnants in our genomes might act as initiators of autoimmunity.

Mary K. Crow, MD
Hospital for Special Surgery
New York, NY

1. Carter V, LaCava J, Taylor MS, Liang SY, Mustelin C, Ukadike KC, et al. High prevalence and disease correlation of autoantibodies against p40 encoded by long interspersed nuclear elements (LINE-1) in systemic lupus erythematosus. Arthritis Rheumatol 2020;72:89–99.

2. Mavragani CP, Sagalovskiy I, Guo Q, Nezos A, Kapsogeorgou EK, Lu P, et al. Expression of long interspersed nuclear element 1 retroelements and induction of type I interferon in patients with systemic autoimmune disease. Arthritis Rheumatol 2016;68:2686–96.

3. Bombardier C, Gladman DD, Urowitz MB, Caron D, Chang DH, and the Committee on Prognosis Studies in SLE. Derivation of the SLEDAI: a disease activity index for lupus patients. Arthritis Rheum 1992;35:630–40.

4. Naufer MN, Furano AV, Williams MC. Protein-nucleic acid interactions of LINE-1 ORF1p [review]. Semin Cell Dev Biol 2019;86:140–9.

5. Crow MK. Long interspersed nuclear elements (LINE-1): potential triggers of systemic autoimmune disease. Autoimmunity 2010;43:7–16.

6. Goodier JL, Cheung LE, Kazazian HH Jr. Mapping the LINE1 ORF1 protein interactome reveals associated inhibitors of human retrotransposition. Nucleic Acids Res 2013;41:7401–19.

DOI 10.1002/art.41104

Reply

To the Editor:

We are delighted that our discovery of autoantibodies directed against LINE-1 retroelement–encoded p40/ORF1p in SLE patients has been so rapidly replicated, and we thank Dr. Crow for her excellent summary of our findings. Her laboratory's detection of LINE-1 messenger RNA (mRNA) and immunoreactive p40 protein in salivary gland specimens from patients with primary Sjögren's syndrome and kidney specimens from SLE patients (1) was an important impetus for our study. We also agree with Dr. Crow that anti–LINE-1 immunity is indicative of a poten-

tial role of LINE-1 in SLE pathogenesis. Besides the presence of autoantibodies against p40, the literature suggests at least 2 additional reasons to suspect this hypothesis: 1) LINE-1–encoded proteins are physically associated with Ro 60 and other well-recognized autoantigens in SLE, together with LINE-1 mRNA or short RNA species such as Alu and YRNA transcripts and 2) the other LINE-1–encoded protein, p145/ORF2p, is a reverse transcriptase that uses p40-bound RNA as a template for DNA synthesis. The presence of autoantibodies against p40 therefore suggests that the autoimmune reaction in the SLE patient is targeting a protein–RNA complex that may also include DNA newly synthesized by reverse transcription, which has been shown to trigger the GMP-AMP synthase (cGAS)/stimulator of IFN genes (STING) pathway to induce type I IFN production in senescent cells (2). Indeed, Dr. Crow's group has shown that introduction of full-length LINE-1 can induce type I IFN production in transfected cells (1). Furthermore, it has also been reported that activation of cGAS does occur in a subset of SLE patients (3).

The fact that LINE-1 p40/ORF1p is an RNA binding protein and that bound RNA can be reverse-transcribed into DNA by p145/ORF2p makes the question of autoantibody specificity particularly important. Additionally, p40 can also bind single-stranded DNA (ssDNA), single-stranded RNA (ssRNA), and DNA heteroduplexes (LaCava J, et al: unpublished observations) but not dsDNA (4). The binding of RNA and ssDNA requires properly folded trimeric p40. Denatured p40 protein run on a sodium dodecyl sulfate gel and visualized as a 40-kDa band must be devoid of any bound DNA or RNA, yet was recognized by patient IgG in our experiments. Furthermore, our p40 preparation was extensively treated with RNase as part of its purification from *Escherichia coli*. The purification protocol also included ultraviolet spectroscopy, which shows the presence of protein but not DNA or RNA. Nevertheless, we considered it important to exclude the possibility that, for example, DNA from SLE patient sera might bind p40 and then be recognized by patient autoantibodies, particularly in the ELISAs. As addressed by Dr. Crow, we included DNase (which was present for at least 2 hours) or competing free DNA, minimizing the risk of any significant signal contribution by anti-dsDNA or anti-ssDNA antibodies.

We continue this line of research to better understand the contribution of LINE-1 proteins and bound nucleic acids to autoimmunity and, potentially, SLE pathogenesis. We are also analyzing additional diseases, particularly those that are often associated with a type I IFN gene signature, for the presence of anti-p40 autoantibodies.

Tomas Mustelin, MD, PhD
Kennedy Ukadike, MD
University of Washington
Seattle, WA

John LaCava, PhD iD
Rockefeller University
New York, NY
Marty Taylor, MD, PhD
Massachusetts General Hospital
Boston, MA

1. Mavragani CP, Sagalovskiy I, Guo Q, Nezos A, Kapsogeorgou EK, Lu P, et al. Expression of long interspersed nuclear element 1 retroelements and induction of type I interferon in patients with systemic autoimmune disease. Arthritis Rheumatol 2016;68:2686–96.
2. De Cecco M, Ito T, Petrashen AP, Elias AE, Skvir NJ, Criscione SW, et al. L1 drives IFN in senescent cells and promotes age-associated inflammation. Nature 2019;566:73–8.
3. An J, Durcan L, Karr RM, Briggs TA, Rice GI, Teale TH, et al. Expression of cyclic GMP-AMP in patients with systemic lupus erythematosus. Arthritis Rheumatol 2017;69:800–7.
4. Khazina E, Truffault V, Buttner R, Schmidt S, Coles M, Weichenrieder O. Trimeric structure and flexibility of the L1ORF1 protein in human L1 retrotransposition. Nat Struct Mol Biol 2011;18:1006–14.

Gout management as part of secondary cardiovascular prevention: comment on the article by Stamp et al

To the Editor:

The article by Stamp and colleagues (1) contributes to confirming the deleterious role of gout in patients with established cardiovascular (CV) disease. In this study, patients with gout were shown to have a shorter time to readmission, mainly for heart failure, though an increased risk of subsequent myocardial infarction, CV-related death and all-cause death has also been reported (2). Of interest, these poor outcomes occurred despite appropriate CV management. Gout is a disease with variable levels of inflammation (3), driven by the deposition of monosodium urate crystals. Therefore, its negative impact on atherosclerotic disease highlights the potential of managing inflammation as a part of secondary CV prevention, as also suggested by the results of the Canakinumab Antiinflammatory Thrombosis Outcome Study (4).

Some issues about Stamp and colleagues' study should be addressed. The primary explanatory variables—gout and serum urate (SU) levels—were recorded only at baseline, so how gout was managed during follow-up is unknown. The authors remarked that almost all participants classified as having gout were receiving allopurinol, impeding any insights into the CV effects of the drug. Despite this therapy, the mean SU level at baseline was 0.42 mmoles/liter, and 69.4% of patients had SU levels of >0.36 mmoles/liter, the target recommended by the American College of Rheumatology (5). Thus, in the majority of participants with gout in this cohort, the SU level was not at even the most conservative target. Allopurinol doses were not specified in the report, but they appear to not be optimal. In the whole sample, having a lower baseline

SU level was significantly associated with reduced mortality and readmissions. No subgroup analysis was performed, probably due to size concerns, even though having the data on those with gout might be informative.

Normalizing SU levels in gout leads to the removal of urate crystals (6,7) and reduction of systemic inflammation (8), which could contribute to secondary (4)—and likely primary—CV prevention. Further studies on CV outcomes in gout patients should aim to include patients receiving proper gout management.

Dr. Andrés has received consulting fees, speaking fees, and/or honoraria from Menarini, Horizon, Grünenthal, and AstraZeneca (less than $10,000 each). No other disclosures relevant to this letter were reported.

Mariano Andrés, MD, PhD iD
Hospital General Universitario de Alicante (ISABIAL)
and Universidad Miguel Hernández
Irene Calabuig, MD iD
Hospital General Universitario de Alicante (ISABIAL)
Alicante, Spain

1. Stamp LK, Frampton C, Drake J, Doughty RN, Troughton RW, Richards AM. Associations of gout and baseline serum urate level with cardiovascular outcomes: analysis of the Coronary Disease Cohort Study. Arthritis Rheumatol 2019;71:1733–8.
2. Pagidipati NJ, Clare RM, Keenan RT, Chiswell K, Roe MT, Hess CN. Association of gout with long-term cardiovascular outcomes among patients with obstructive coronary artery disease. J Am Heart Assoc 2018;7:e009328.
3. Terkeltaub R. What makes gouty inflammation so variable? BMC Med 2017;15:158.
4. Ridker PM, Everett BM, Thuren T, MacFadyen JG, Chang WH, Ballantyne C, et al. Antiinflammatory therapy with canakinumab for atherosclerotic disease. N Engl J Med 2017;377:1119–31.
5. Khanna D, Fitzgerald JD, Khanna PP, Bae S, Singh MK, Neogi T, et al. 2012 American College of Rheumatology guidelines for management of gout. Part 1. Systematic nonpharmacologic and pharmacologic therapeutic approaches to hyperuricemia. Arthritis Care Res (Hoboken) 2012;64:1431–46.
6. Li-Yu J, Clayburne G, Sieck M, Beutler A, Rull M, Eisner E, et al. Treatment of chronic gout. Can we determine when urate stores are depleted enough to prevent attacks of gout? J Rheumatol 2001;28:577–80.
7. Pascual E, Sivera F. Time required for disappearance of urate crystals from synovial fluid after successful hypouricaemic treatment relates to the duration of gout. Ann Rheum Dis 2007;66:1056–8.
8. Okuda C, Koyama H, Tsutsumi Z, Yamamoto A, Kurajoh M, Moriwaki Y, et al. Serum CRP in patients with gout and effects of benzbromarone. Int J Clin Pharmacol Ther 2011;49:191–7.

Georgia abortion law and our commitment to patients

To the Editor:

On May 7, 2019, Georgia, the home of the American College of Rheumatology (ACR), enacted a law that effectively bans abortion in the state. Kentucky, Mississippi, Ohio, Louisiana, Alabama, and Missouri recently passed similar laws.

These laws conflict directly with the most fundamental principles of medical practice in a free society—respect for our patients, responsibility to practice evidence-based medicine in their best interests, and the freedom to do so without political interference. The laws not only challenge and disrespect the autonomy of patients and their physicians, they also threaten patients and physicians with criminal prosecution, up to and including prosecution for murder. Among its provisions, the Georgia law even allows the state to investigate women who miscarry to determine whether their personal behavior contributed to the miscarriage, in which case they may be prosecuted.

In opposing these laws, we are keenly aware that health care professionals, like the rest of the country, have diverse personal beliefs regarding abortion. However, those personal beliefs need not undermine a principle that should be common to all of us—that politicians should not interfere in medical decision-making and certainly should not threaten physicians and patients who do not align with their partisan political agenda. There should be no doubt about that principle, no matter which end of the political spectrum is involved.

Rheumatologists are trained for, and trusted with, providing expert care of women impacted by disorders of the immune system, including some that are particularly notable for complications during pregnancy. These complications typically occur well past the 6-week time frame defined by these so-called heartbeat laws. Patients with autoimmune rheumatologic disorders require vigilance and shared decision-making among patient, rheumatologist, and obstetrician when complications arise, often acutely and requiring immediate decisions on management in the best interest of the patient.

When we embarked on careers in medicine, we committed to honor patient well-being as the first principle that must guide our actions. We believe that this oath obligates us not only to serve our patients, but also to publicly oppose any law or regulation that would interfere with our ability to do so. We are aware that the ACR has acknowledged the recent anti-abortion legislation and released a general statement of principle (Advocacy News: ACR and Anti-Abortion Legislation; https://www.rheumatology.org/Advocacy/Advocacy-News). However, the ACR Board of Directors did not directly express opposition to these laws, including the law in Georgia, where the ACR resides. We hope that the ACR will reconsider that decision, and, in the future, will publicly oppose all laws that allow politics to interfere in the practice of medicine.

Joseph E. Craft, MD
Yale University
New Haven, CT
Mary K. Crow, MD (iD)
Michael D. Lockshin, MD
Jane E. Salmon, MD (iD)
Hospital for Special Surgery
New York, NY
Betty Diamond, MD
Feinstein Institute
Manhasset, NY
Keith B. Elkon, MD
University of Washington
Seattle, WA
Joseph Flood, MD
Ohio State University Medical Center
Columbus, OH
David A. Fox, MD
University of Michigan
Ann Arbor, MI
Sherine E. Gabriel, MD, MSc
Rush University
Chicago, IL
Gary S. Gilkeson, MD
Medical University of South Carolina
Charleston, SC
Bevra H. Hahn, MD
University of California Los Angeles Medical Center
John Hardin, MD
Montefiore Hospital and Medical Center
Bronx, NY
William J. Koopman, MD
University of Alabama at Birmingham
William E. Seaman, MD
David Wofsy, MD
University of California San Francisco
John S. Sergent, MD
Vanderbilt University Medical Center
Nashville, TN
Audrey B. Uknis, MD
Temple University School of Medicine
Philadelphia, PA
Michael E. Weinblatt, MD
Brigham and Women's Hospital
Boston, MA

ACR Announcements

AMERICAN COLLEGE OF RHEUMATOLOGY
2200 Lake Boulevard NE, Atlanta, Georgia 30319-5312
www.rheumatology.org

ACR Meetings

State-of-the-Art Clinical Symposium
March 27–29, 2020, New Orleans

Pediatric Rheumatology Symposium
April 29–May 2, 2020, New Orleans

For additional information, contact the ACR office.

ACR 2020 State-of-the-Art Clinical Symposium

Join the ACR in New Orleans for rheumatology's premier weekend symposium, complete with cutting-edge clinical best practices and emerging trends, without taking time from work! What's new in 2020? The first full day of the 2020 meeting kicks off with a wellness yoga session to help you avoid physician burnout and get a healthy jumpstart to the weekend. Cap off the day in New Orleans style with Cocktails & Cases, an event designed to encourage discussion and networking. You'll also be able to participate in a lively panel discussion after each group session. Experience the exceptional educational programs yourself, March 27–29 in New Orleans, LA. Advance registration ends March 11. After March 11, you may register on-site. To take advantage of special housing rates, reserve your room by March 6. Visit rheumatology.org/Learning-Center/Educational-Activities to learn more and register.

ACR 2020 Pediatric Rheumatology Symposium

Join your pediatric colleagues from across the country at the Pediatric Rheumatology Symposium (PRSYM), a scientific meeting dedicated exclusively to pediatric rheumatology. In 2020, PRSYM is being held in New Orleans for the first time ever! The most cutting-edge pediatric rheumatology research will be on display in the poster hall, where a variety of abstracts will provide enlightening content to bring back to your team. Get an interactive learning experience with panel discussions, as well as several key networking opportunities. Take part in the exciting educational programs, April 29–May 2 in New Orleans. Register by March 4 for early-bird rates or by April 15 for advance registration rates, or register on-site. Reserve your room early to take advantage of special rates (until April 8). Visit rheumatology.org/Learning-Center/Educational-Activities to learn more and register.

Education Programs

6th Systemic Sclerosis World Congress. March 5–7, 2020, Prague, Czech Republic. The Systemic Sclerosis World Congress boasts an eclectic mix of interactive opportunities for attendees, including hands-on workshops; lectures, and discussions between physicians, medical staff, and patients; oral presentations; and satellite sessions. Lectures will be given in English but will be translated into major audience languages, and some topics will be covered in different languages in smaller groups. The broad scope of the Congress includes, among other topics, developments in scleroderma treatments, an update on major research projects, and how to treat pain in digital ulcers. Smaller groups will examine more specific topics, including juvenile scleroderma and the impact of scleroderma on sexual life. Registration fees are €760 (December 3–February 17) and €830 (February 18–onsite) for physicians; €300 (December 3–February 17) and €365 (February 18–onsite) for fellows, basic scientists, and health professionals; and €180 (December 3–February 17), and €240 (February 18–onsite) for students. For additional information, e-mail worldsclerodermafoundation@gmail.com or visit the web site http://worldsclerofound.org/systemic-sclerosis-world-congress/.

Precision Medicine in Autoimmunity. March 11–13, 2020, Denver, CO. Expert speakers will present scientific and clinical advances related to precision medicine in rheumatoid arthritis, juvenile inflammatory arthritis, systemic lupus erythematosus, psoriasis and psoriatic arthritis, ankylosing spondylitis, inflammatory bowel disease, myositis, and scleroderma, and on checkpoint inhibitors and immune-related adverse events, influence of lifestyle factors on autoimmunity, and patient-reported outcomes. Registration fee is $475. For additional information, visit the web site www.precisionmedicineautoimmunity.org.